(NASA-CR-129947) CSM SPACECRAFT OPERATIONAL DATA BOOK. VOLUME 2: LM DATA BOOK, PART 1 (Grumman Aerospace Corp.) 29 Jan. 1971 410 p

X73-70331

Unclas

00/99 37145

Volume II LM Data Book
Subsystem Performance Data - RCS

TABLE OF CONTENTS

TABLE OF CONTENTS (Continued)

4.8 REACTION CONTROL SUBSYSTEM (RCS)

4.8.1 Propellant Usage

RCS propellant is used to perform rotations and small ΔV maneuvers, to control the effects of moment unbalance during periods of main engine thrusting and to stabilize the vehicle under a variety of conditions.

The procedure for calculation of propellant use varies with the method of use and may further depend on the control system in use (PGNS or AGS), the mode of vehicle control (attitude hold or automatic) and the vehicle mass, inertia and center of gravity.

RCS maneuvers must be broken down to a sequence of activities, each of which has a particular procedure for calculating consumption, as detailed below. Consumption is calculated for each activity and summed to provide total usage.

The following will further aid in the use of the instructions detailed:

- During a period of main engine thrusting, the RCS propellant required for moment control and for rotations, if any, are determined independently and summed.
- RCS firings for main engine tank settling are synonymous with RCS translation maneuvers in calculating usage.
- Certain sequences, such as docking and landing, are too involved to permit simplified manual calculating of consumption. The usage (based on simulation data) is therefore specifically given below.
- Vehicle weight must be given.

4.8.1.1 Rotations

The propellant consumed for rotations under AGS control is shown in Figures 4.8-21 thru 4.8-24.

1. Rates

In the undocked configuration, manual rotations (Rate Command/Attitude Hold) are performed in PGNS at a maximum rate of 20.0°/sec with a fully deflected hand controller on the high scale setting and 4.0°/sec on the low scale setting. In the docked configuration, the maximum rates for high and low scaling are 2.0°/sec and 0.4°/sec respectively.

4.8.1.1 (Continued)

The propellant consumed for undocked rotations using the rate command/attitude-hold mode is shown in Figures 4.8-1 and 4.8-2 (without RCS plume deflectors) and 4.8-3 (with plume deflectors). These figures assume the c.g. location varies with LM inertia. Figures 4.8-3.1 through 4.8-3.4 show the propellant consumed for rotations using the PGNS rate command/attitude-hold mode in the docked configuration (with plume deflectors) assuming constant c.g. locations with varying vehicle inertia. For consistency with AGS RCS propellant consumption curves, they are given in terms of the body reference system.

Automatic rotations in each axis, for PGNS, are crew selectable to limits of 0.2, 0.5, 2.0 and 10.0°/sec for maneuvers during unpowered flight and 10.0°/sec automatically selected during powered flight. These rates are stored in the LGC and are selected via the DSKY. The propellant consumed for rotations in the automatic mode, including the effects of jet impingement in the descent and docked configurations, may be obtained in the following manner:

Single axis maneuvers may be handled similarly to manual rotations. Knowing the maneuver rate, propellant consumed can be obtained from Figures 4.8-4 and 4.8-5 (without RCS plume deflectors) or 4.8-6 (with deflectors). The curves shown for the automatic mode are for 0.2, 0.5, 2.0 and 10.0°/sec. For other rates, interpolation can be used. Figures 4.8-3.1 through 4.8-3.4 show the propellant consumed for rotations using PGNS automatic rates of 0.5 and 2.0°/sec in the docked configuration (with plume deflectors) assuming constant c.g. locations with varying vehicle inertia.

For multi-axis (combined) maneuvers, knowing the selected total vector rate (ω°/sec) the vehicle body axis rates (P, Q and R°/sec) may be determined. (Ref. LMO 500-711). Once they are known, the corresponding RCS propellant consumption (W_p, W_q and W_r lbs) is obtained from Figures 4.8-4, 4.8-5, and 4.8-6. The total propellant for the maneuver is then W_p plus the maximum of W_q or W_r.

To all rotational (manual or automatic) maneuver propellant consumption calculations, the limit cycling propellant to hold the desired rate about each axis, must be added. Curves of limit cycling propellant consumption rates in lbs/min as a function of deadband and moment of inertia are given in Figures 4.8-7 to 4.8-10. The limiting cycling time for rotational maneuver is the maximum value of $\Delta\,\theta/Q$, $\Delta\,\psi/R$, or $\Delta\,\phi/P$, where $\Delta\,\theta$, $\Delta\,\psi$, and $\Delta\,\phi$ (degrees) are the changes in the vehicle's orientation angles in pitch, roll and yaw.

4.8.1.1 (Continued)

For automatic rotations in AGS, the vehicle seeks to attain a rate dependent on commanded angle and angular acceleration (which is a function of inertia). This maximum rate for various typical accelerations is shown in Figure 4.8-11 as a function of commanded angle. The actual vehicle rate will be this maximum or the applicable rate limit, whichever is smaller.

For rotations with AGS: four jets are always commanded for rotations about the X axis, four jets are commanded for Y and Z axis rotations in powered flight, and two jets in unpowered flight.

2. Simultaneous Maneuvers

For preliminary planning it should be assumed that all rotational maneuvers require rotations about two axes unless it is fairly evident that this is not required. For example, pitchover for visibility at high gate requires only a pitch rotation; orientation for IMU alignment may require pitch and yaw rotations.

The total consumption for simultaneous maneuvers is the sum of that required for yaw and the larger of that required for pitch or roll commanded maneuver.

When maneuvers are performed during powered flight the total propellant used by the RCS is the sum of that used for the maneuver and that used for moment control.

4.8.1.2 Coasting

When the vehicle is not maneuvering, its attitude is maintained within certain angular limits in a limit cycle operation. There are four angular limits, known as deadbands, used as follows:

Attitude Hold Mode		Automatic Mode		
Wide	±5°	Wide	±5°	(Undocked)
Narrow	±0.3°	Narrow	±1.4°	(Docked case only)
		Narrow	±1.0°	(PGNS; prior to undocked engine burn only)
		Narrow	±0.3°	(Undocked)

In PGNS mode the deadbands are stated about the (X, U, V) axes and in AGS mode the deadbands are stated about the (X, Y, Z) axes. The following equation is supplied to allow for the transforming of moments of inertia from the (X, Y, Z) axes to the (X, U, V) axes.

$$I_{eff_{(uu,vv)}} = \frac{2IyyIzz}{Iyy+Izz}$$

The rate of propellant consumption per axis as a function of deadband and inertia is determined using the following equation (Ref. LMO-500-352):

$$\dot{W} = \frac{0.25\,(\text{Min. Imp. x } N_{jet})^2\, r_c}{Isp_m\, D\, I}$$

4.8.1.2 (Continued)

where

$\dot{W}$ = Propellant consumption per unit time (lb/sec)

Min. Imp. = That impulse which is obtained from the shortest electrical "on" and "off" command (Ref. Figure 4.8-41 at 70°F).

Docked Min. Imp. = 9.7 lb-sec

Undocked Min. Imp. = 0.8 lb-sec

N_{jet} = Number of jets commanded; depends on the axis commanded, and the mode that the LM is in.

DAP

N_{jet} (X-axis) = 2

N_{jet} (U-and V-axes) = 1 (Note: In docked configuration, N_{jet} = 2)

AGS

N_{jet} (X-axis) = 4

N_{jet} (Y-and Z-axes) = 2

r_c = Moment arm; depends on which axis a rotation is made about.

r_c (X-axis) = 5 ft

r_c (Y-and Z-axes) = 5.5 ft

r_c (U-and V-axes) = 7.8 ft

Isp_m = That specific impulse which is obtained from the shortest electrical "on" and "off" command (Ref. Figure 4.8-42 at 70°F).

Docked Isp_m = 260 sec

Undocked Isp_m = 165 sec

D = Deadband commanded, in radians: 5°/57.3, 1.4°/57.3, 1°/57.3, or 0.3°/57.3

I = Moment of inertia per axis (slug-ft^2)

The resulting Figures 4.8-7 to 4.8-10 and 4.8-12 to 4.8-15 show propellant consumption per unit time. Total consumption is obtained by summing the per-axis rates and multiplying by the duration of the coasting period. It should be noted that the curves supplied represent minimum theoretical values, and may

4.8.1.2 (Continued)

not be characteristic of real mission coasts. Disturbing torques such as LM venting, atmospheric drag or any other vehicle perturbations are not considered in the derivation of the equation.

Where atmospheric drag effects are significant, no consumption rate lower than 2.0 lbs per hour can be assumed.

4.8.1.3 Translation

The propellant required for a steady state RCS burn for a given time is 0.367 lbs per second per jet, based on a minimum I_{sp} of 273 sec and a thrust per jet of 100 lbs.

RCS propellant to provide a given ΔV (ft/second) exclusive of propellant required for moment control is determined from:

$$\left.\begin{array}{l} W_R = W_V \times \Delta V/8780 \\ W_R = \text{RCS propellant (lbs)} \\ W_V = \text{Vehicle weight (lbs)} \end{array}\right\} \text{Y and Z axes}$$

For X axis:

$$W_R = [W_V \times \Delta V/8780]1.12$$

1.12 = plume impingement correction factor

4.8.1.4 Moment Control

1. X-, Y- or Z-Axis Translation

Propellant required for moment control during X-axis translation is negligible.

Translation maneuvers along the Y- or Z-axis create significant moments (roll and pitch, respectively) when the center of gravity is not in the plane of the thrusters.

Propellant consumption per unit ΔV as a function of vehicle weight can be determined using Figure 4.8-16. The propellant consumption given in Figure 4.8-16 is the total of that required for both moment control and translation.

2. Descent Engine Thrusting - PGNS

During descent engine firings, RCS moment control in PGNS operation is required during the following:

a) descent engine start-up

b) descent engine throttling (due to mount compliance)

c) sudden attitude change required during descent engine operation

The RCS propellant required during the above descent engine operations can be determined from the following equations:

$$W_{rcs} = \frac{\text{Max}\left(|M_{y_{avg.}}|, |M_{z_{avg.}}|\right) \text{Max}\left(|t_1|, |t_2|\right)}{R_o I_{sp}} \qquad \text{Eq. (A)}$$

4.8.1.4 (Continued)

where the first factor is the larger of either $|M_{y_{avg.}}|$ or $|M_{z_{avg.}}|$, and is multiplied by the second factor, the larger of either $|t_1|$, or $|t_2|$ and;

$$M_{y_{avg.}} = T\left(\left|\left[c.g._{zo} + E_y \Delta x + |\Delta T| K_t \Delta x\right]\right| - 0.5\, W_o \Delta x t_1\right)$$

$$M_{z_{avg.}} = T\left(\left|\left[c.g._{yo} + E_z \Delta x - |\Delta T| K_t \Delta x\right]\right| - 0.5\, W_o \Delta x t_2\right)$$

$$t_1 = \frac{\left|\left[c.g._{zo} + E_y \Delta x + |\Delta T| K_t \Delta x\right]\right|}{W_o \Delta x}$$

$$t_2 = \frac{\left|\left[c.g._{yo} + E_z \Delta x - |\Delta T| K_t \Delta x\right]\right|}{W_o \Delta x}$$

$$M_T = \sqrt{M_{y_{avg.}}^{\ 2} + M_{z_{avg.}}^{\ 2}}$$

and where:

W_{rcs} = RCS propellant consumption (lbs)

T = descent engine final thrust level per maneuver (lbs)

$c.g._{yo}$ = Displacement of the thrust vector from the center of gravity on Y-axis (ft.)
= 0 (during engine throttling phase)

$c.g._{zo}$ = Displacement of the thrust vector from the center of gravity on Z-axis (ft.)
= 0 (during engine throttling phase)

W_o = gimbal drive rate (0.2°/57.3)rad./sec.

E_y = uncertainty in position of pitch gimbal angle (0.655/57.3)rad.
= 0 (during engine throttling phase)

E_z = uncertainty in position of initial roll gimbal angle (0.655/57.3)rad.
= 0 (during engine throttling phase)

4.8.1.4 (Continued)

Δx = difference between location of center of gravity on X-axis and gimbal pivot point

$= \frac{(Xc.g. - 154")}{12}$ (ft)

Xc.g. = location of center of gravity on X-axis (in)

ΔT = change in thrust level (note: during start-up $T_{initial} = 0$, so $\Delta T = T$)

K_t = gimbal mount compliance factor $(0.46/57.3) \times 10^{-4}$ rad/lb. per axis

R_o = moment arm for control in pitch and roll maneuvers (5.5 ft)

$M_{y_{avg.}}$ = time average moment unbalance about Y-axis (ft-lbs)

$M_{z_{avg.}}$ = time average moment unbalance about Z-axis (ft-lbs)

I_{sp} = f (M_T) (See Figure 4.8-17.)

Prior to engine throttling, and after the initial start transient, the thrust vector passes through the c.g. Thus in calculating $M_{y_{avg.}}$, $M_{z_{avg.}}$, t_1, and t_2 for the RCS propellant used during descent engine throttling, due to mount compliance, the terms $c.g._{yo}$, $c.g._{zo}$, $E_y \Delta x$ and $E_z \Delta x$ are set equal to zero.

Figures 4.8-18, 4.8-19, and 4.8-20 are the result of a compilation of data from a computer program using Equation (A). From this program we establish the following equation:

$$W_{rcs} = (P_F KCT) \times 10^{-3} \qquad \text{Eq. (B)}$$

where

W_{rcs} = RCS propellant consumption (lbs)

P_F = propellant factor (Figure 4.8-18)

4.8.1.4 (Continued)

Notes:

a) for descent engine start-up, P_F is determined from the gimbal angle displacement from the nominal gimbal angle (including mount compliance)

b) for descent engine throttling, gimbal angle displacement from the nominal gimbal angle is determined from

$$\delta = K_t \Delta T \qquad \text{(either } \delta\Theta \text{ or } \delta\psi\text{)}$$

K = thrust correction factor (determined from ΔT magnitude; note using correct assumptions for ΔT and Figure 4.8-19)

C = $X_{c.g.}$ location correction factor (determined from vehicle $X_{c.g.}$ position; Figure 4.8-20)

It should be noted that if the descent burn is accomplished docked, where the RCS jets are inhibited, there is no RCS propellant consumption. Also, when an attitude change is required, propellant consumption should be determined from the supplied rotation curves (Figures 4.8-11 and 4.8-21 to 4.8-24). Now, the RCS propellant consumption during descent engine burns can be computed using Equation (B) and Figures 4.8-18, 4.8-19, and 4.8-20.

After the transient period is over, i.e., during descent engine throttling (due to mount compliance), and after large attitude changes during descent engine operation, then vehicle attitude stabilization is maintained by control of the gimbal drive actuators. While the gimbal drive actuators are in control there is no RCS propellant consumption.

3. Descent Engine Thrusting - AGS

In addition to control during transients, noted in Para. 4.8.1.4 Part 2, moment control during non-maneuvering descent engine thrusting using AGS will be in the form of a combined RCS/gimbal drive actuator limit cycle operation and will consume RCS propellant at a rate of 4.2 lbs/minute.

4.8.1.4 (Continued)

4. Ascent Engine Thrusting - Canted Engine

Nominally, during ascent engine burns the APS/RCS interconnect will be manually opened after the ullage maneuver has been completed and will be closed prior to ascent engine cutoff. For ascent from the lunar surface the interconnect is opened prior to lift off. Figure 4.8-25 gives the nominal LM control boundaries for ascent engine firing. Figure 4.8-26 gives the reduction in the nominal LM control boundaries due to RCS and APS thrust vector location, and thrust magnitude uncertainties vs X C.G. location.

Figures 4.8-27 to 4.8-30 show the RCS propellant flow rate, the delta APS/RCS specific impulse (i.e. the difference between the APS alone and APS/RCS specific impulse), the delta APS/RCS mixture ratio (i.e. difference between APS alone and APS/RCS mixture ratio) and effective RCS thrust during moment control. These are shown as functions of the Yc.g. and Zc.g. of the manned dry vehicle (i.e. no tanked RCS or APS propellant), where the dry vehicle weight =5308 lbs. The data presented in the figures are for a rotated ascent engine (pitch cant angle of -1.5° and a Z-axis offset of +3.75 in. with the DAP in control), a burnout delta velocity of 6050 ft/sec, and the following lunar mission expected nominal ascent engine characteristics:

Thrust = 3515 lbs
Specific Impulse = 308.9 sec
Mixture Ratio = 1.593

The RCS propellant remaining at lunar liftoff is 511.6 lbs. C.G. locations where no data is provided indicate that the maximum available RCS restoration capability of 1100 ft-lbs has been exceeded. The APS and RCS thrust vectors location and magnitude are nominal. The total propellant consumption and burn time may be calculated using the following equations.

1. $$\ln\left[\frac{\text{Initial Vehicle Weight}}{\text{Final Vehicle}}\right] = \frac{\Delta V}{32.174\,(\text{APS Isp} - \Delta\text{APS/RCS Isp})}$$

where
ΔAPS/RCS Isp is obtained from Figure 4.8-107

Δ V = 6050 fps
Initial Vehicle Weight = 11046.7 lbs
APS Isp = 308.9 sec

APS total propellant consumption = Initial Vehicle Weight - Final Vehicle Weight

4.8.1.4 (Continued)

2. Burn Time $= \dfrac{\text{Propellant Consumption}}{\dot{W}_{APS} + \dot{W}_{RCS}}$

where

$$\dot{W}_{APS} = \frac{F_A}{Isp_{APS}} = \frac{3515}{308.9}\ \frac{\text{lbs}}{\text{sec}},$$

and

$\dot{W}_{RCS}$ is obtained from Figure 4.8-27

The RCS propellant flow rate and APS/RCS integrated specific impulse during moment control, with PGNS or AGS, may be calculated as a function of instantaneous $Y_{c.g.}$ & $Z_{c.g.}$ using Figures 4.8-31 through 4.8-34 and the following equations.

1) $$XM = \frac{F_A}{12}\left[\delta\psi(Z_{c.g.} - Z_B) + \delta\theta(Y_{c.g.} - Y_B)\right]^*$$

2) $$YM = \frac{F_A}{12}\left[-Z_{c.g.} - \delta\theta(X_{STA} - X_A) + Z_B\right]$$

$$= 291.6\left[-Z_{c.g.} - \delta\theta(X_{STA} - X_A) + Z_B\right]$$

3) $$ZM = \frac{F_A}{12}\left[Y_{c.g.} - \delta\psi(X_{STA} - X_A) - Y_B\right]^*$$

* $\delta\psi = Y_B = 0$ nominally

4) $MU_H = XM$

5) $$MU_U = \frac{ZM}{\sqrt{2}} + \frac{YM}{\sqrt{2}}$$

$$MU_V = \frac{ZM}{\sqrt{2}} - \frac{YM}{\sqrt{2}}$$

Using MU_H, enter Figures 4.8-31 and 4.8-32 and read $\dot{W}_H$ and O/F_H.

4.8.1.4 (Continued)

6) $$\dot{W}_{OH} = \frac{\dot{W}_H\,(O/F_H)}{(1 + O/F_H)}$$

$$\dot{W}_{FH} = \frac{\dot{W}_H}{(1 + O/F_H)}$$

For AGS Control

6A) For $MU_U > 0$ $$D_U = \left| \frac{MU_U}{100\left[5.5\sqrt{2} - \frac{Ycg}{12\sqrt{2}} + \frac{Zcg}{12\sqrt{2}}\right]} \right|$$

For $MU_U < 0$ $$D_U = \left| \frac{MU_U}{100\left[5.5\sqrt{2} + \frac{Ycg}{12\sqrt{2}}\right] - \frac{Zcg}{12\sqrt{2}}\Big]} \right|$$

For $MU_V > 0$ $$D_V = \left| \frac{MU_V}{100\left[5.5\sqrt{2} - \frac{Ycg}{12\sqrt{2}} - \frac{Zcg}{12\sqrt{2}}\right]} \right|$$

For $MU_V < 0$ $$D_V = \left| \frac{MU_V}{100\left[5.5\sqrt{2} + \frac{Ycg}{12\sqrt{2}} + \frac{Zcg}{12\sqrt{2}}\right]} \right|$$

6B) $$FS_U = \frac{D_U}{0.013}\left(1 - \frac{D_U}{D_U + 0.3 - 0.3\,D_U}\right)$$

$$FS_V = \frac{D_V}{0.013}\left(1 - \frac{D_V}{D_V + 0.3 - 0.3\,D_V}\right)$$

6C) $$F_U = \begin{cases} FS_U & \text{for } D_U \leq 0.182 \\ \left[S_1\,(D_U - 0.182) + 1\right] FS_U & \text{for } 0.182 < D_U \leq 0.575 \\ \left[S_2\,(D_U - 0.85) + B_1\right] FS_U & \text{for } D_U > 0.85 \\ B_1\ FS_U & \text{for } 0.575 < D_U \leq 0.85 \end{cases}$$

4.8.1.4 (Continued)

$$6C)\quad F_V = \begin{cases} FS_V & \text{for } D_V \leq 0.182 \\ \left[S_1 \ (D_V - 0.182) + 1\right] FS_V & \text{for } 0.182 < D_V \leq 0.575 \\ \left[S_2 \ (D_V - 0.85) + B_1\right] FS_V & \text{for } D_V > 0.85 \\ B_1 \ FS_V & \text{for } 0.575 < D_V \leq 0.85 \end{cases}$$

$$\text{where } B_1 = \frac{0.2 \text{ (Vehicle Weight, lbs) } + 1900}{5{,}000}$$

$$S_1 = \frac{B_1 - 1}{0.393}$$

$$S_2 = \frac{1 - B_1}{0.15}$$

$$6D)\quad TW_U = \frac{D_U}{F_U} \qquad \text{for } F_U > 0$$

$$TW_V = \frac{D_V}{F_V} \qquad \text{for } F_V > 0$$

For PGNS Control

Using MU_U and MU_V along with the effective diagonal axis inertia

$\left(I_{eff} = \frac{2Iyy\ Izz}{Iyy + Izz}\right)$ enter Figures 4.8-33 and 4.8-34. Read TW_U and TW_V, and F_U and F_V, respectively.

The following equations are applicable both for AGS and for PGNS control:

$$7)\quad \dot{W}_{OX} = \dot{W}_{OH} + (0.24892\ TW_U - 0.00011)\ F_U + (0.24892\ TW_V - 0.00011)\ F_V$$

$$\dot{W}_{FUEL} = \dot{W}_{FH} + (0.12043\ TW_U + 0.00033)\ F_U + (0.12043\ TW_V + 0.00033)\ F_V$$

4.8.1.4 (Continued)

$$\dot{W}_{RCS} = \dot{W}_{OX} + \dot{W}_{FUEL}$$

8) $F_R = 100\ (F_U \times TW_U + F_V \times TW_V)$

9) $\dot{W}_{TOTAL} = \dot{W}_{RCS} + \dot{W}_{APS}$ = Total Flow Rate

10) $F_T = F_R + F_A \cos \delta\theta \cos \delta\psi$

11) $I_{sp} = \dfrac{F_T}{\dot{W}_{TOTAL}}$

where

$\left.\begin{matrix} XM \\ YM \\ ZM \end{matrix}\right\}$ = Moment unbalance about the center of gravity of the vehicle, ft-lbs

X_{STA} = X center of gravity with reference to the LM X_E coordinate system

$\left.\begin{matrix} Z_{c.g.} \\ Y_{c.g.} \end{matrix}\right\}$ = Center of gravity in inches with reference to the dry vehicle (i.e., no tanked RCS or APS propellant)

X_A = The distance from the nozzle throat to the LM X_E coordinate system. Nominally 232.96 inches

F_A = Ascent Engine Thrust = 3500 lbs nominally

$\delta\theta$ = Pitch cant angle, radians = − 0.02617 rad

$\delta\psi$ = Roll cant angle, radians = 0

$\left.\begin{matrix} Z_B = 3.75 \text{ inches} \\ Y_B = 0\text{, nominally} \end{matrix}\right\}$ lateral displacement of Ascent Engine

$\dot{W}_H$ = RCS propellant flow rate (lb/sec) caused by horizontal jet firings

4.8.1.4 (Continued)

$\dot{W}_{TV}$ = RCS propellant flow rate (lb/sec) caused by vertical jet firings

$\dot{W}_{OH}$ = RCS oxidizer flow rate (lb/sec) caused by horizontal jet firings

$\dot{W}_{FH}$ = RCS fuel flow rate (lb/sec) caused by horizontal jet firings

$\dot{W}_{OX}$ = Total RCS oxidizer flow rate (lb/sec)

$\dot{W}_{FUEL}$ = Total RCS fuel flow rate (lb/sec)

$\dot{W}_{RCS}$ = Total RCS propellant flow rate, (lb/sec)

$\dot{W}_{APS}$ = Total APS flow rate = 11.43 lb/sec nominally

F_R = Effective RCS force along X axis, lbs

TW_U = RCS jet pulse width, for the U-axis (sec)

TW_V = RCS jet pulse width, for the V-axis (sec)

F = RCS jet frequency, Hz

MU_H = Moment unbalance, horizontal

MU_{TV} = Moment unbalance, total vertical

$\left.\begin{array}{l} MU_U \\ MU_V \end{array}\right\}$ = Moment Unbalance about U and V axes

F_U = RCS jet frequency for the U-axis (Hz)

F_V = RCS jet frequency for the V-axis (Hz)

Δ APS/RCS Isp = Isp of APS with interconnect open, less time-integrated Isp of APS, RCS combination using APS fuel.

4.8.1.4 (Continued)

D_U, D_V = Jet duty factor required to compensate for MU_U, MU_V

FS = RCS jet static frequency corresponding to fixed input to the Abort Control System Pulse Ratio Modulators

$\left.\begin{matrix} B_1 \\ S_1 \\ S_2 \end{matrix}\right\}$ = Conversion factors to convert static frequency to dynamic frequency (F)

APS/RCS = Denotes RCS using APS propellant.

O/F_H = RCS oxidizer-to-fuel ratio for horizontal jet firings.

For a nominal inflight FITH, 0.81 lbs are used. With off nominal pre-staging conditions of roll and pitch attitudes and rates this may vary from 0.52 to 2.61 lbs.

For a nominal FITH from the lunar surface with 0^o tilt angles 1.4 lbs of fuel are used. For other values of tilt angles up to $\pm 40^o$ this varies from 0.95 to 2.47 lbs.

5. Yaw Moments

The propellant used for yaw moment control is insignificant for most purposes. Usage rate as a function of yaw unbalance is shown in Figure 4.8-35.

4.8.1.5 Control Limits

4.8.1.5.1 Descent Engine: LM Docked or Undocked

4.8.1.5.1.1 2 or 4 Jet Rotational Control

Using equation

$$\Delta CG = \left| Ycg + CG\ (\delta\psi) \right| + \left| Zcg + CG\ (\delta\Theta) \right|$$

where

ΔCG = Maximum controllable CG location within the RCS thruster capability (Figure 4.8-36)

4.8.1.5.1.1 (Continued)

Ycg = Y axis CG location

Zcg = Z axis CG location

$CG(\delta\psi \text{ or } \delta\Theta)$ = Effective CG in the Y-Z plane; i.e., that CG controllable by the descent engine thrust vector (Figure 4.8-37).

the LM controllability can be determined using the following procedure:

1- Find ΔCG from Figure 4.8-36, where ΔCG depends on whether the controlling RCS moment is 2-jet or 4-jet, and upon the magnitude of the descent engine thrust level.

2- Determine $CG(\delta\Theta)$ and $CG(\delta\psi)$ from Figure 4.8-37 where the Xcg location is known and the descent engine thrust vector angle is assumed.

3- Substituting the determined values for ΔCG, $CG(\delta\Theta)$, $CG(\delta\psi)$ and the known values for Ycg and Zcg in the above equation, it can be determined whether the LM is controllable by the following:

$$\text{if } \Delta CG \geq \left| Ycg + CG(\delta\psi) \right| + \left| Zcg + CG(\delta\Theta) \right|$$

the LM is controllable,

$$\text{if } \Delta CG < \left| Ycg + CG(\delta\psi) \right| + \left| Zcg + CG(\delta\Theta) \right|$$

the LM is not controllable.

4.8.1.5.1.2 + X and - X Firing Jets Inhibited

With both + X and -X jet firing inhibited, the nominal control boundary of the LM is a function of the descent engine thrust vector angle. Therefore, given the LM CG location, the control boundary is determined by using Figure 4.8-37 and the following logic:

if $CG(\delta\psi, \delta\Theta) \geq$ Ycg or Zcg respectively,
then LM is controllable,

if $CG(\delta\psi, \delta\Theta) <$ Ycg or Zcg respectively,
then the LM can not be controlled.

4.8.1.5.2 Ascent Engine

Figure 4.8-25 gives the nominal LM control boundaries for ascent engine firing. Figure 4.8-26 gives the reduction in the nominal LM control boundaries due to RCS and APS thrust vector location and thrust magnitude uncertainties vs X CG location.

4.8.1.6 Docking

The propellant required for docking, obtained from six degrees of freedom simulations of a staged LM, together with the mass properties and initial conditions is shown in Table 4.8-1.

4.8.1.7 Landing

The propellant consumption for landing varies with takeover altitude, landing site selection, mass properties, and mode of operation. The LM modes of operation for landing are:

Automatic: ullage, descent engine ignition, throttle and spacecraft attitude controlled automatically beginning at 50,000 feet.

Landing Site Redesignation: begin at 50,000 feet; at 8,000 feet new landing site is selected and manual pitch and/or yaw commands are made.

Manual Rate of Descent: takeover manual control of spacecraft's rate of descent at 500 feet.

Manual Throttle Control: takeover at 1,000 feet to 100 feet - manual throttle selected.

The propellant used for landing, as obtained from simulation studies is shown in Table 4.8-2.

4.8.1.8 Pulse Mode

The rate of propellant usage in the pulse mode with PGNS is 0.0100 lb per pulse in each axis being pulsed, for a pulse width of 14 milliseconds. With the PGNS in control, undocked, the minimum RCS pulse width is 14.60 $\pm$0.85 milliseconds. If docked, the minimum pulse width is 60 milliseconds (Q,R axes).

The rate of propellant usage in the pulse mode with AGS in control is 0.0655 lb/sec in pitch or roll (4.64 pulses per second) and 0.125 lb/sec in yaw (4.45 pulses per second). With AGS, the minimum RCS pulse width is 13.68 $\pm$1.5 milliseconds.

4.8.1.9 Manual Override Modes

In direct or hardover modes the rate of propellant usage is 0.367 lb per second per jet.

4.8.2 Ullage Settling Time

Prior to initiation of all main engine burns, except for FITH with the DPS on, and APS lift-off from the lunar surface, two or four +X RCS thrusters must be fired to provide an acceleration which will settle the Main Propulsion Subsystem propellants. Propellant settling times (ideal) for the unstaged and staged LM are determined using Figures 4.8-38 and 4.8-39, respectively. However, the propellant settling times obtained from Figures 4.8-38 and 4.8-39 must be corrected for the effective loss in RCS thrust due to plume impingement (unstaged configuration only) and control system inefficiency (AGS only). The Plume Impingement Correction Factors are obtained from Table 4.8-3 (or for a specific spacecraft from the appropriate spacecraft appendix), and the Control System Efficiency Correction Factors are obtained from Table 4.8-4 (unstaged or docked) or Table 4.8-5 (staged).

The required propellant settling time in the docked or unstaged configuration is then obtained by multiplying the propellant settling time from Figure 4.8-38 by the Correction Factor obtained for Table 4.8-3 (or the equivalent table in a specific spacecraft appendix) in the PGNS mode, and Table 4.8-3 and Table 4.8-4 in the AGS mode. In the staged configuration the required propellant settling time obtained from Figure 4.8-39 is multiplied by the Efficiency Correction Factors (Table 4.8-5) in the AGS mode. The PGNS mode requires no correction for control system inefficiency in either the staged or unstaged configuration. The settling time obtained as described above should be increased to the nearest 0.5 second and an additional 0.5 second should be added for engine start overlap.

4.8.3 Mass Properties

Detailed data for discrete vehicle conditions, including transferred equipment, consumables, and propellant allocations for APS, DPS, and RCS are given in Volume III, Mass Properties Data Book.

4.8.4 RCS Engine Characteristics

Figures 4.8-40 through 4.8-47, and Tables 4.8-6 through 4.8-9 (Ref. LMO-310-335), give the latest data on RCS engine performance.

4.8.4 (Continued)

The following is data pertaining to buildup and decay statistics on the RCS engines.

Condition	Time,sec
Buildup: ON signal to 90% steady-state thrust	0.021
Decay: OFF signal to ≈0% thrust	0.060
Time delay between ON-commands and actual start of thrust buildup	0.008
Time delay between OFF-commands and actual start of thrust decay	0.0065

Typical curves of thrust buildup and decay are shown in Figures 4.8-48 to 4.8-61 (Results of RCS Engine Supplemental Qualification Test Program, LMO-310-335).

It should be noted that there are no particular inflight environmental characteristics that may cause an engine to operate drastically different from nominal. Nominal variations in inlet conditions due to propellant sloshing, vehicle spinning, or interactions of other pulsing jets cause no significant deviation in engine performance.

Figure 4.8-62 defines the region of safe RCS engine operation, which is given in terms of 1) the number of heaters in operation, 2) the number of pulses and the OFF time between pulses to reach a redline injector head temperature of 108°F. Engine operation in the unsafe region shown in Figure 4.8-62 could cause engine malfunction. The mission operating envelope is far removed from the unsafe region of engine operation, and during a nominal mission there is no possibility of entering this region when in automatic mode. Note that the data supplied in Figure 4.8-62 was at the minimum voltage for the duty cycle, and therefore the redline represents the worst case, lowest redline (i.e., any change of assumed conditions can only result in decreasing the unsafe regions of Figure 4.8-62).

The dribble volumes of the Marquardt R4D engine are as follows: fuel side 0.04425 in.^{3}, oxidizer side 0.03574 in.^{3}. The dribble volume is defined as the volume in the injector from the propellant shutoff valve (when closed) to the exit from the injector into the combustion chamber.

4.8.5 Electrical Power Requirements for the RCS Thrusters

The power requirement per pound of propellant consumed for operation of the thruster valves is 0.077 watt-hours for the primary coils and 0.019 watt-hours for the secondary coils.

4.8.6 RCS Plume Impingement of the LM

Due to plume impingement on the LM, continuous LM RCS jet firings are limited as indicated in Operational Limitation RCS-5.

4.8.6.1 RCS Plume Impingement Heating Effects - for Contingency Situations Only.

4.8.6.1.1 RCS +X Engines, LM Unstaged

Figure 4.8-106 shows the plume impingement limits of the +X RCS thrusters in terms of allowable thruster activity at various duty cycles as a function of elapsed time. The primary +X firing constraint is the allowable plume impingement capabilities. The plume deflector constraint shown is based on analysis and the firing times are far in excess of any flight or test experience. Figure 4.8-106 should only be used in contingency situations and not for nominal mission planning. The maximum nominal firing remains 40 seconds. Also shown are the constraints for the scientific equipment bay, quad III stowage, quad IV MESA insulation, and the ladder rung.

The effects of exceeding the +X RCS plume impingement constraint will probably result in plume deflector failure. The deflector configuration after failure is undefined and heating rates obtained are unknown. Assuming these rates to be equal to plume heating without deflectors, the following thermal and structural problems will occur:

- D/S quad thermal blankets would be severely degraded (approaching an uninsulated configuration). Lunar stay and lifeboat mission could not be accomplished.

- The hardware (screws, washers, standoffs) used to retain A/S and D/S plume shields and insulation blankets could be over temperatured, causing these shields and blankets to fall free of the LM due to "g" loads and vibrations. This would cause loss of micrometeroid protection for A/S and D/S tanks.

- Plume impingement on interstage area would cause damage to the A/S FITH insulation, leading to overtemperature and subsequent failure of the A/S FITH shield during FITH abort. Possibly loose D/S FITH blankets could be blown off and block the vent areas increasing A/S and D/S pressures during FITH burns.

- The higher heating would severely degrade the landing gear insulation, and would cause landing gear structural temperatures to exceed acceptable limits for adequate strength. In this condition, a lunar landing could not be accomplished.

- Failure of the plume deflector could result in impact with the RCS thruster and possible failure of the thruster.

It can be seen from Figure 4.8-106 that it is possible to exceed the LM-10 ladder, quad III stowage, quad IV MESA, and the scientific equipment bay insulation constraints without exceeding the plume deflector constraints. These situations will not constrain landing but may alter mission operations as explained below:

- If ladder plume-impingement constraints are exceeded without exceeding the plume deflector limits, it may be required to abort the EVA. Evaluation of the landing conditions to determine the severity of FUT heating, and sun orientation could be evaluated after touchdown and the ladder constraints could be reviewed before EVA.

- If the scientific equipment bay limits are exceeded without exceeding the deflector limit, there will be a loss of the Mylar portion of the two SEQ bay blankets. Nine layers of the h-film will remain on the top of the SEQ bay, and five layers of h-film will remain on the side of the SEQ bay. Degraded thermal insulation reduces the capability of the LM to perform thermally severe missions and new timeline and procedural changes may be required to ensure mission success. During lunar stay with sun on quad II, the degraded blankets would cause ALSEP to run hot. The ALSEP would have to be removed soon after touchdown. In addition, the temperature of the water line inlet to PLSS could exceed its temperature limit. If quad II were in shadow, it is possible that the D/S waterline will freeze. The degraded quad II blankets during a lifeboat mission would require that quad II experience limited sun or cold holds.

- Exceeding the quad III stowage area limit will result in the loss of the Mylar portion of the insulation blanket covering the top of the center pallet of the quad III stowage area. This will leave 18 layers of h-film intact. Firing of the engine to the plume deflector limit would produce shrinkage of the remaining h-film layers, but no additional damage. The quad III stowage area is thermally isolated from the descent stage and degradation of the stowage area blanket will not affect the descent stage thermal performance. Degradation of the insulation blanket will increase the stowage area temperature excursions for extreme hot or cold landing orientations.

Exceeding the quad IV MESA limit will result in the loss of the Mylar portion of the insulation blanket on the outboard (when stowed) face of the quad IV MESA. Since the MESA is thermally isolated from the D/S, degradation of this blanket will have no effect on the D/S thermal performance. Loss of the Mylar portion of the blanket would leave nine layers of h-film intact, which would provide adequate thermal protection for MESA for a nominal LM orientation on the lunar surface. It is felt that internal MESA heaters can provide enough energy to compensate for any additional heat loss through a degraded blanket. If after landing, the LM is oriented with sun on quad IV, temperatures within MESA could possibly exceed desirable limits. The MESA has three flight temperature sensors which would allow a real-time definition of a thermal problem. Should MESA temperatures exceed desirable limits, the MESA could be deployed, and temperature sensitive equipment could be removed and relocated.

From Figure 4.8-106 the maximum continuous firing of the RCS without exceeding the plume deflector constraint is 140 seconds. This corresponds to the maximum allowable plume deflector strut temperature of 1050°F. (Text continued on next page)

To prevent overtemperature of the plume deflector, a set of working curves is included. From these curves (Figures 4.8-107 through 4.8-110) permissable LM +X RCS continuous firings with the LM unstaged can be derived which will not overtemperature the deflector. Figure 4.8-107 is a plot of increase in deflector strut temperature versus firing time for a range of initial strut temperature. Figure 4.8-108 shows the decrease in temperature versus cooldown time for a range of initial strut temperatures. Figures 4.8-107 and 4.8-108 were cross plotted to produce Figures 4.8-109 and 4.8-110.

Figures 4.8-107 through -110 can be used to determine allowable continuous firings which will not overtemperature the deflector. If, for example, the required total firing time is 200 seconds (60 seconds in excess of the 140 second maximum continuous limit) the following duty cycles could be utilized.

Firing or Cooldown	Time (Sec)	T (initial) °F	ΔT °F	T (Final) °F	Figure Utilized
Firing	40	250	325	575	4.8-107
Cooldown	200	575	-90	485	4.8-110
Firing	60	485	385	870	4.8-109
Cooldown	400	870	-340	530	4.8-110
Firing	71	530	420	950	4.8-109
Cooldown	60	950	-100	850	4.8-108
Firing	29	850	165	1015	4.8-107

Figure 4.8-111 contains a quick method for selecting a specific number of constant duration firings and cooldowns within the 1050°F strut limit. Several examples in the use of Figure 4.8-111 are tabulated below for the 200-second total burn-time:

Firing Time (Sec)	Cooldown Time (Sec)	Number of Firings
100	300	2
66.6	140	3
50	80	4
40	55	5

Figure 4.8-112 contains a firing-plus-cooldown time-optimization plot. For a given total firing time requirement, use of Figure 4.8-112 will allow the user to plan for achieving the total firing time requirement within the minimum total time span. As an example assume 260 seconds of firing time is required.

Solution: (using Figure 4.8-112)

1) 1st firing is always 140 seconds (the maximum allowable single firing from 250°F).

2) Then cooldown for 300 seconds on the cooldown curve. (300 seconds was selected because cooling beyond this point slows down as the slope becomes horizontal).

3) 2nd firing is 92 seconds giving an accumulated firing time of 232 seconds (determined by drawing a horizontal line from the cooldown curve to the firing curve).

4) Required 3rd firing is 28 seconds to achieve the total firing time of 260 seconds. The necessary cooldown for the 3rd firing is obtained by locating the intersection of the 28 second firing on the firing curve and moving horizontally to the cooldown curve. The required cooldown is 50 seconds.

Utilizing these methods to extend firing times has no effect on the ladder whose constraint is exceeded. The side of the SEQ, quad III stowage and quad IV MESA blanket effects will differ. As previously discussed, a small amount of degradation is expected for 140 seconds of firing (which does not exceed the deflector constraints). However, if Figures 4.8-107 through 4.8-112 are used to obtain more firing time, the mylar will be destroyed. This is because the deflector cooldown times are not sufficient to allow the mylar to cool down, resulting in heat accumulation in the blanket. Potentially the quad III stowage blanket, quad IV MESA blanket and the top of the SEQ could be reduced to 8 layers, and the side of the SEQ to 4 layers (all blankets 26 layers original), resulting in very poor insulation performance. To prevent blanket damage for firings greater than the maximum allowable continuous firing for each area, Figures 4.8-113, 4.8-113.1, 4.8-113.2, and 4.8-113.3 are provided. To illustrate the use of Figure 4.8-113.3, the following schedule could be utilized if 200 seconds of firing are required:

1. 100-second initial firing.

2. 1100-second cooldown (Figure 4.8-113.3) for a 70-second firing.

3. 70-second continuous firing.

4. 490-second cooldown for the remaining 30-second firing that is left to total 200 seconds.

5. 30-second continuous firing.

4.8.6.1.2 RCS +X Engines, LM Staged

The quad I RCS engine (B1D) has a 325-second limit for a continuous firing. At this time, degradation of the Mylar portion of the blanket over A/S panel 140 begins. (See Fig. 4.8-120) Since there are only four Mylar layers of a total of 26 layers of insulation, degradation of these four layers would have negligible impact on the A/S thermal performance.

The quad III RCS engine (B3D) has a 140-second limit for a continuous firing, after which degradation of the Mylar portion of the blanket covering A/S panel 129 begins (see Fig. 4.8-120). Complete loss of all of the Mylar would leave 16 intact layers of h-film insulation. The relatively small affected area and large number of remaining layers would cause the loss of the Mylar layers to have a negligible affect on the A/S thermal performance.

The quad II and quad IV RCS engines (A2D, A4D) have an 85-second limit for a continuous firing. The constraining items are the aluminum frames of A/S panels 130 and 137 (see Fig. 4.8-120). Exceeding the firing constraint will cause the frames to exceed their temperature limit of 780°F. Above this temperature, expected vibration loads will exceed the aluminum ultimate strength and failure of the frame will occur. Since the aluminum skin is fastened to the A/S structure through the frame, failure of the frame could allow the entire panel (skin and frame) to fall free of the A/S. This would result in loss of micrometeroid protection for the A/S fuel and oxidizer tanks.

Figures 4.8-114 through 4.8-117 show the heating and cooling times required in order to maintain the frame temperature at or below 780°F during an RCS down-firing cycle.

Figure 4.8-114 presents the increase in temperature of the 130-panel aluminum frame vs. RCS firing time for a range of initial frame temperatures.

Figure 4.8-115 presents the decrease in temperature vs. cooldown time for a range of initial frame temperature.

Figures 4.8-114 and 115 are cross-plotted to produce Figure 4.8-116 which presents increase in temperature vs. initial temperature for a range of firing times and Figure 4.8-117 which presents the decrease in frame temperature vs. initial frame temperature for a range of cooldown times.

Figure 4.8-114 through Figure 4.8-117 can be used to determine allowable duty cycles. If, for example, the required firing time for a particular maneuver is 150 seconds (far in excess of the 85-second maximum continuous limit) the following duty cycles could be utilized.

Example 1

Firing or Cooldown	Time	T (Initial) °F	ΔT °F	T (Final) °F	Figure Utilized
Firing	42.5 sec.	250	330	580	4.8-114
Cooldown	2.8 min.	580	-180	400	4.8-115
Firing	43.0 sec.	400	280	680	4.8-114
Cooldown	1.1 min.	680	-130	550	4.8-115
Firing	33.0 sec.	550	180	730	4.8-114
Cooldown	0.5 min.	730	-80	650	4.8-115
Firing	31.0 sec.	650	128	778	4.8-114

Example 2

Firing or Cooldown	Time	T (Initial) °F	ΔT °F	T (Final) °F	Figure Utilized
Firing	30 sec.	250	240	490	4.8-116
Cooldown	3.0 min.	490	-125	365	4.8-117
Firing	50 sec.	365	330	695	4.8-116
Cooldown	3.0 min.	695	-265	430	4.8-117
Firing	30 sec.	430	205	635	4.8-116
Cooldown	.15 min.	635	-40	595	4.8-115
Firing	40 sec.	595	190	780	4.8-116

Figures 4.8-114 through 117 provide information to determine arbitrary RCS firing schedules which do not result in over-temperatures. These figures were used to derive the cooldown requirements for repetitive firings of the same burn duration. The results are presented in Figure 4.8-118. Use of Figure 4.8-118 is illustrated below, again for 150-seconds total burn-time. Note that all the combinations given below are acceptable The initial temperature for Figure 4.8-118 is 250°F corresponding to solar heat input.

Firing Time (Seconds)	Cooldown Time (Minutes)	Number of Firings
75.0	6.9	2
50.0	1.9	3
37.5	1.1	4
30.0	0.8	5

4.8.6.1.3 RCS -X Engines, LM Unstaged or Staged

Figure 4.8-119 presents the constraints on -X RCS engine firing. The S-band steerable antenna curves constrain engines A3U and B4U. They are based on initial temperatures as read on flight sensor GT 0454T. The firing limits correspond to the antenna qualification temperature limit of 170°F. It is possible that the antenna has a higher temperature limit, but insufficient data is available to determine a higher upper limit.

The EVA antenna curve (Figure 4.8-119) constrains engines A3U and B2U. This antenna may also have additional capability, but insufficient data is available to determine a higher upper limit.

The curve for the A/S upper midsection panels (Figure 4.8-119) constrains all -X RCS engines. This curve represents the limit for the aluminum frames on panels 84 through 89, 91 and 92 (see Figure 4.8-120). Exceeding this limit could result in the aluminum skins falling free of the A/S, and the loss of micrometeroid protection.

4.8.6.1.4 RCS ±Y and ±Z Engines, LM Staged and Unstaged

The -Y thrusters, A3R and A4R, produce the same heating to the S-band steerable antenna as the -X engines, A3U and B4U. These engines therefore have the same constraint (Figure 4.8-119) as the two -X thrusters.

The ±Y and ±Z engines cause insignificant heating to the A/S and D/S insulation panels and the landing gear.

4.8.6.2 Effects of RCS Plume Impingement on Attitude Control

Tables 4.8-13 and 4.8-14 show the attitude control authority of the RCS with the LM equipped with plume deflectors. Since the X-axis location of the center of pressure on the deflectors is approximately X = 222 in. (above the expected vehicle center of gravity only in the heavy descent configuration) the effect of the resulting side forces caused by RCS impingement is an increase in attitude control authority. However, in vehicle configurations where the vehicle center of gravity is above the center of pressure, such as in the docked mode, the control authority is reduced by the actual calculated impingement force components and the associated pitch and roll moments of each thruster in the various LM configurations. The standard LM body axis system is used. It is to be noted that during a pitch or roll maneuver only the downward firing jet(s) contributes an impingement moment.

The forces on the plume deflectors during thrusting can be resolved with respect to both the X-Y-Z body axis system and the X-U-V axis system as shown in Figure 4.8-97. The coordinates at which the forces act, as well as those of the deflectors, are also shown.

4.8.6.3 RCS Plume Impingement Forces During Staging

Figure 4.8-98 shows the pressure distribution on the plume deflector as a function of chord length. These data were determined by using the Grumman Reference (Isentropic) Plume Profile and together with the information given in Figure 4.8-97, which specifies maximum values, should more accurately predict the deflector performance range. Based on these data, Figure 4.8-99 shows the magnitude of the normal force on the plume deflector as a function of rotation of RCS thrusters with respect to the deflectors; Figure 4.8-100 shows the magnitude of the vertical impingement force as a function of engine sideslip along the quad diagonal (U or V axis); Figures 4.8-101 and 4.8-102 show the vertical and the horizontal impingement forces as a function of separation distance; Figure 4.8-103 shows the horizontal impingement force as a function of sideslip and Figures 4.8-104 and 4.8-105 show the distance of the horizontal force from the top deck as a function of rotation, sideslip and separation. It is to be noted that all horizontal forces (forces in the Y-Z plane) act inward along their respective quad diagonals.

4.8.7 Engine Location and Alignment

4.8.7.1 Engine Reference Location

The RCS engine locations for Quad IV follow.

Engine Reference	X Station (Inches)	Y Station (Inches)	Z Station (Inches)
Forward	254.0	61.5	66.35
Up	258.8*	66.1	66.1
Down	248.7*	66.1	66.1
Side (right)	254.0	66.35	61.5

*Point of assumed application of thrust. The RCS thruster location, identification, and geometry are given in Figures 4.8-63 and 4.8-64.

Quads I, II and III have the same X, Y and Z coordinates except for appropriate sign differences.

The error tolerance on these nominal coordinates by specification does not exceed 0.3 inches (3σ). (LSP-370-3A Lunar Module Primary Guidance, Navigation and Control Subsystem Equipment Performance and Interface Specification.)

4.8.7.2 RCS Engine Alignment

Figure 4.8-64.1, RCS Manufacturing and Assembly Uncertainties, shows the results of a study conducted at GAC to determine the uncertainties in the RCS thrust vector due to manufacturing and assembly tolerances.

(Text continued on next page.)

4.8.7.2 (Continued)

The study determined that the alignment of the RCS cluster during vehicle assembly is accurate enough to insure that the thrust vector uncertainties are held within the 3° conical angle control specification (LSP 370-3A, see above).

Figure 4.8-64.2, (RCS Thrust Vector Uncertainties) shows, for a typical X, Y and Z thruster, a section of the possible area that can be swept out by the thrust vector and still be within the control requirements (shown cross hatched). Superimposed on this section is an outline of the profile of the root-sum-square (RSS) of the manufacturing and assembly tolerances.

As a result of the study, it was decided that no measurement of RCS cluster alignment is necessary for LM-5 and subsequent.

In over forty actual measurements on four LM vehicles the largest thrusters misalignment measured about any axis was 0° 28' 45". This indicates that on a 3σ basis the worst case misalignment expected is less than 1.5° about any axis and that the thrusters are being positioned more accurately than predicted in the manufacturing study.

4.8.8 Helium Tank Loading

The RCS helium bottle loading envelope is given in constraint RCS-18 in the spacecraft appendixes, together with the helium tank pressure-temperature limitations.

4.8.9 Propellant Quantity Measuring Device

The RCS tanks have an inflight gauging system with an estimated uncertainty of 5% of full scale deflection. Since the PQMD was defined by the LM-1 RCS propellant load of 616 lb, the cabin display pegs at 100% of this value. However, due to the fact that 25.8 lb of propellant remains trapped in the lines and is therefore unavailable for thrusting, the 100% value is based on a 590.2 lb usable load. The gauging system uncertainty of 5% applies to this load and corresponds to 29.5 lb. Figure 4.8-65 is a correlation of the actual propellant weight remaining in the LM-RCS as a function of displayed PQMD reading. Also shown are: 1) The maximum amount of unexpelled propellant (12.2 lb) due to bladder efficiency of 98%; 2) The maximum O/F uncertainty resulting from an overall mission O/F of 1.88 which leaves an excess of 14.8 lb of oxidizer (equivalent to 12.3 lb of propellant at O/F = 2.00); 3) Nominal, minimum, and maximum loads for LM-4 and subsequent vehicles with a pressurized RCS.

In case of PQMD malfunction, Fig. 4.8-66 would serve as its backup. This figure gives propellant quantity versus helium pressure reduction for several temperatures. (NOTE: Original helium pressure from which the pressure reduction is calculated refers to the nominal pressure for several denoted temperatures.)

In Figure 4.8-67, the ratio of the final to initial temperature of the helium, during high RCS propellant consumption rates, is shown as a function of the pressure ratio. This figure was derived from data taken during high RCS consumption rates on the LM-3 flight and assumes that these periods are typical of duty cycles expected during orientation and MPS burns on subsequent flights. Data applicable to specific vehicles are given in the spacecraft appendices.

4.8.10 Propellant Flow Regulation

4.8.10.1 Regulator Pressures

The following table shows the regulator outlet pressures for helium tank pressures of 500 to 4500 psia. This table is also applicable for helium bottle pressures below 500 psia under the following conditions:

3 engine operation; He tank pressure = 450 psia.
2 engine operation; He tank pressure = 400 psia.
1 engine operation; He tank pressure = 350 psia.

Valve Status	Primary Regulator Outlet Pressure, psi	Secondary Regulator Outlet Pressure, psi
Lockup	178 to 188	182 to 192
Open (He flows up to 100%)	181 ± 3	185 ± 3

4.8.10.2 Manifold Pressures Using APS/RCS Interconnect

The following table shows the propellant pressure in the RCS manifold when the APS/RCS interconnect is open.

Ascent Engine Status	RCS Manifold Pressure, psia
Firing	173 ± 3
Not Firing	178 to 194

4.8.11 Valve Characteristics

4.8.11.1 Engine Valves

There has been no limit established for continuous operation of the engine valves when power is continuously applied to them with propellant flowing. The maximum time duration the engine valves may be activated without propellant is 2 minutes during any 15-minute period for the primary coils and 45 minutes during any 60-minute period for the secondary coils. These values are based on an initial temperature of 80°F and maximum terminal voltages of 15 VDC for a single direct coil and 30 VDC for two direct coils in series.

4.8.12 RCS Propellant Depletion

4.8.12.1 Complete expulsion of RCS propellant is undesirable. For flight safety planning purposes, propellant utilization should be terminated prior to expulsion of the last of the usable propellant. A margin of safety is necessary due to uncertainties in the measuring systems. During emergency situations that require use of the RCS, propellant consumption may be extended, but should be terminated at the first indication of a decrease in manifold pressure.

4.8.12.2 Blowdown Operation

Partial or complete loss of a system's helium due to a leak upstream of the quad check valves limits the operation capability of that system. Following the helium loss, the system can be operated in blowdown mode until the manifold pressure drops to 100 psia. Figure 4.8-67.1 shows the amount of propellant which is available from blowdown operation of a system.

The assumptions made for determining the best case curve, consider maximum tank size, propellant temperature of 40°F, best O/F for complete propellant consumption ≤2.05 and an initial manifold pressure of 184 psia. The worst case assumptions consider a minimum tank size, a propellant temperature of 100°F, an O/F of 1.88 and an initial manifold pressure of 178 psia. The vertical axis in Figure 4.8-67.1 shows exact values for the percentage of propellants remaining. When estimating the amount of propellant available from blowdown operation by using the readings taken just prior to pressurization failure the errors inherent in the measuring system should be taken into account. For example: An indication of 80% just before pressurization system failure, if subjected to an error of ±10% results in 90% propellant remaining and 30 lbs. available from blowdown in the worst case.

4.8.13 RCS Thermal Requirements

4.8.13.1 RCS Heater Duty Cycle

The duty cycle for RCS Quad Heaters for particular missions can be found in the appendices.

4.8.13.2 Parametric Study of RCS Steady Firings

The computer model developed from the latest PRI test (Reference: LMO-510-879 "Test Report - Environmental Testing on a LM-Aft RCS Thruster Cluster", 2 July 1968) was used to analyze the thermal effect of steady firings plus variable thermal inputs on the 1) Down engine ejector, 2) the "D" Ox valve and 3) the quad temperature.

Steady firings were considered for durations of 5 seconds to 120 seconds. Only firings on the "D" engine were considered. The effects of solar input and LM structure temperature during firing and soakback were also considered.

Solar input was determined for the cluster orientation in Figure 4.8-68.

LM structure temperature was set at 30°F & 100°F. These temperatures correspond to the predicted range of LM structure temperature for worst case missions.

The maximum soakback temperatures for the "D" injector, Ox valve, and the quad versus the steady firing time duration are tabulated in Table 4.8-10 for all cases analyzed.

In Figure 4.8-69 are plotted the temperatures for the injector and quad, for cases 1 and 4. These curves show the maximum effect of LM temperature and solar input on peak soakback.

Figures 4.8-70 through 4.8-81 contain the transient response curves for the injector, quad and engine oxidizer valve. Plots are arranged so that, for each case of boundary conditions, the nine incremental firings are shown on the same figure. Injector, quad and Ox valve temperatures rise from steady state condition as prescribed by the particular case to the first incremental burn point (5 seconds) and then proceed along the indicated heavy black line (for 5, 10, 15, 20, 30, 40, 60, 90 & 120 seconds during firing). Soakback curves take off from the heavy, thick line for all of the nine incremental firings. A good estimate can be obtained by using linear interpolation for burn times in-between those plotted.

Other engine injectors and valves in a quad may be expected to respond approximately the same as given for engine "D"; however, the quad response will be slower and have a lower peak.

4.8.13.3 Effects of Orientation on RCS Tank Temperatures

Extended time periods of particular vehicle orientation with respect to the sun can cause the RCS propellant temperature limits, and possibly their upper fracture mechanics limit to be exceeded. These limits are 40°F to 100°F for the propellant. The upper fracture mechanics limits are given in Figure 3.8.1-1 of the appendixes.

Figure 4.8-81.1 shows plots of the temperature change rates for the RCS propellant tank skins as a function of propellant quantity (percentage). These plots are parameterized with respect to H Missions vehicle orientation. Hence, it is possible to calculate tank skin temperatures for any time interval by using the tank start temperature and information contained in Figure 4.8-81.1. The data indicates that for a nominal H Mission, the RCS tanks stay well within their temperature limits.

4.8.14 RCS Performance Limitations as a Result of Gimbal Drive Actuator (±Pitch or ±Roll) Failure During Powered Descent

4.8.14.1 Plume Impingement Constraints due to GDA Failure.

Based on current RCS constraints, the maximum allowable GDA offset angle at failure is limited by RCS plume impingement. Figure 4.8-88 presents the limiting case. In the period of 0 to 600 seconds GDA lockup at offset angles greater than the indicated allowable will eventually fail the S-Band steerable antenna. Likewise, after 600 seconds, lockup at greater than maximum allowable angles will eventually lead to failure of the plume deflectors. However, for the points above the curve, additional hardware damage may result, with the sequence of degradation being unrelated to the item indicated on Figure 4.8-88. The exact sequence of thermal degradation can be determined from the data presented in the appropriate spacecraft appendix.

Since RCS is normally used only for major attitude maneuvers during powered descent, accumulated RCS firing time can be used as an indication of DPS gimbal mistrim due to a failure. Figure 4.8-89 shows the maximum allowable accumulated RCS thruster firing time (+ or -x) as a function of D/E burn time during powered descent. Accumulated firing histories in excess of those shown are indicative of RCS duty cycles which cause excessive plume impingement.

4.8.14.2 Additional RCS Propellant Consumption as a Result of GDA Failure

Nominally the gimballed descent engine tracks the vehicle center of mass and controls the attitude of the vehicle for small maneuvers. Therefore, the RCS jets fire, in nominal operation during the large changes of thrust and large attitude change combined-failure maneuvers. However, if either or both of the GDA's (gimbal drive actuators) fail, the RCS jets would have the additional job of correcting any torque unbalanced created by the descent engine offset from the vehicle center of mass. Thus, the RCS propellant expenditure, if the GDA's fail, is an amount proportional to the engine center-of-mass offset.

Figures 4.8-82 through 4.8-85 present the RCS propellant consumed during powered descent for a locked pitch or roll GDA failure. The RCS propellant consumption calculations assume the engine was locked away from the nominal value at the angular increments given. Although the results presented are for separate pitch and roll failure, they are applicable to a combined failure. The combined-failure propellant usage can be obtained by taking the root - sum - square of the RCS propellant consumption for the individual angle offsets (pitch and roll).

4.8.14.2 Continued:

The RCS has limited torque authority (2200 ft - lbf). The torque authority can be exceeded at various combinations of descent engine offset. Figures 4.8-86 and 4.8-87 show the maximum pitch or roll angle at the time of GDA failure during powered descent firing that will provide sufficient RCS propellant at lunar touchdown to complete the mission or that will not exceed the torque authority of the RCS.

4.8.15 Parametric Study of RCS Pulse Firings

Pulse firings were considered for durations of 50, 100, 200 and 400 seconds, at duty cycles of 10, 25, 50, 100 percent. A 100 percent duty cycle constitutes a steady firing (see Paragraph 4.8.13).

$$\text{Percent Duty Cycle} = \frac{\text{Pulse Width}}{\text{Pulse Width + Off Time}}$$

For each firing LM structure temperature was maintained at 100°F and solar input was determined for the cluster orientation in Figure 4.8-68.

The maximum soakback temperature versus the percent duty cycle for the durations above, for the "D" injector, Quad and Ox valve are presented in Figures 4.8-90, 4.8-91 and 4.8-92 respectively.

Three pulse widths (50, 100, 500 ms) were run for each of the above cases. The results showed that the peak soakback for a given duty cycle is independent of the three pulse widths used. This would hold true for any pulse width greater than 30 ms because 80% of the full I_{sp} is achieved.

The maximum peak soakback temperature for long duration pulsing trains occurs at low duty cycles (about 10%). The reason for this is the interruption of propellant coolant flow thru the injector during the off times. As the duty cycle decreases the off time inbetween each pulse increases, allowing more heat from the combustion chamber to soak back. A point is reached when the duty cycle is just sufficient to maintain significant combustion chamber temperatures and the combustion chamber conducts heat back into the injector due to the temperature gradient. Normally, in a steady burn, this combustion chamber soakback is balanced by the propellant coolant flow in the injector at an injector temperature of 175°F. However, when this coolant flow is interrupted, this balance is ended and soakback works to boost the injector temperature during the off time. For the 10% duty cycle and durations in excess of 200 sec. the injector temperature continues to rise to 211°F at 400 seconds. The post-pulsing soakback results in a peak injector temperature of 263°F.

4.8.16 Parametric Study of RCS Heater Failure

The computer model developed from the latest PR-1 test (LMO-510-879, "Test Report - Environmental Testing On a LM-Aft RCS Thruster Cluster, Par. I - Cold Soak and Heater Warmup Test", dated 2 July 1968) was used to analyze "ON" and "OFF" heater failure modes and the effect of variable thermal inputs. Two heater failures per engine and single heater failures were investigated. The results for the double failures are summarized in Table 4.8-11 and Figures 4.8-93 through 4.8-96. The single failure results are summarized in Table 4.8-12.

The failures considered were two heaters per engine full "ON" or "OFF" and one heater per engine full "ON" or "OFF". Since the cluster heaters are redundant, all two-heater cases considered require a double failure on the same engine. For any single "OFF" failure the normal heater operating temperatures are maintained due to the redundancy feature. In addition, three variables were considered, namely solar input, heater voltage and LM structure temperature.

To study the maximum temperature deviations from normal, the three variable boundary condition values were put in at maximum and minimum levels. Solar input was calculated for the orientation of the cluster as shown in Figure 4.8-68. Heater voltage levels of 24 VDC and 32 VDC were used corresponding to the minimum and maximum inputs from the LM batteries.

LM structure temperature was put in at 30°F or 100°F. These temperatures correspond to the predicted range of LM structure temperature for worst case missions.

For the double failures, the sixteen series shown in Table 4.8-11 represent all the combinations of the six parameters and the two failure modes. Each series was divided into four subseries which correspond to the four engines: Side, Forward, Down and Up (see Figure 4.8-68).

The "initial temperature" (Table 4.8-11) is the steady state temperature for normal heater operation and for the conditions listed in the particular series. The "steady state temperature" is the temperature reached due to a particular heater failure mode on a particular engine for a given set of conditions.

For the "ON" failure mode the 'U' and 'D' engine Ox valves were found to be the most responsive of the four engine Ox valves. From Figures 4.8-93 and 4.8-94 and Table 4.8-11, the following should be noted:

1. The effect of LM structure temperature is small compared to the effect of solar input and maximum voltage on the final steady state temperature.

4.8.16 (Continued)

2. There is no unique correspondence between a particular failure and set of conditions with a particular quad steady state temperature.

NASA reference (NASA MSC TWX EP4-10-68-PP6-T168) states that a minimum combustion chamber flange (CCF) temperature of 120°F is required prior to firing the RCS engines. TMC Margin Testing 1968, unpublished, indicates that for injector temperatures of 100°F-140°F the CCF is approximately 8°F less. Thus for the off failures, any injector whose steady state temperature is below 128°F indicates an unsafe condition. From Table 4.8-11 and Figures 4.8-95 and 4.8-96 the following is noted:

1. Series: II(All); IV(All); VI(All); VIII(All); X (S and F); XIV (S & F); XVI (S and F). All Fail the above criterion.

2. The quad lower temperature limit is 119°F. For the series listed above the quad lower limit is not reached.

3. A voltage of 24 or 32 volts has no effect on the injector or quad in the 'OFF' failure mode. The heaters on the other engine provide the same heat (i.e., they are temperature controlled) in both the 24 volt and 32 volt series, with corresponding parameters, to maintain the same quad and injector temperatures.

For the single failures, three series of "ON" failures are shown in Table 4.8-12. "OFF" failures do not produce any change in cluster temperatures.

TABLE 4.8-1. RCS PROPELLANT USAGE FOR DOCKING[1] (PARA. 4.8.1.6)

Mass Properties				Closing Rate (ft/sec)	Range (feet)	RCS Propellant Used	
Wt (lbs)	I_{xx} (slug-ft^2)	I_{yy} (slug-ft^2)	I_{zz} (slug-ft^2)			Mean (lbs)	Max (lbs)
5210	2746	2648	1460	1.08	327	10.6 trans. 6.9 rot.	
5210	2746	2648	1460	3.54	327	12.9 trans. 7.3 rot.	
5210	2746	2648	1460	5.10	327	14.2 trans. 7.0 rot.	
5434	3002	2728	1757	7.18	495.5	33.3	66.6
10,449	5284	2782	5166	7.28	574	58.2	73.9

[1]These mass properties were used for the purpose of this analysis. Reference should be made to Volume III, Spacecraft Operational Data Book, for current official mass properties data.

TABLE 4.8-2. RCS PROPELLANT USAGE FOR LANDING[1] (PARA. 4.8.1.7)

Mass Properties				Takeover Altitude (feet)	Mode of Operation	RCS Propellant Used	
Wt (lbs)	I_{xx} (slug-ft^2)	I_{yy} (slug-ft^2)	I_{zz} slug-ft^2)			Mean (lbs)	Max (lbs)
16,622	12,402	13,324	15,882	500	Rate of Descent	44.6	57.7
16,622	12,402	13,324	15,882	500	Manual	45.0	56.4
17,400	12,900	13,400	16,000	1,000	Manual	32.1	55.5
17,400	12,900	13,400	16,000	700	Manual	36.2	58.5
17,400	12,900	13,400	16,000	500	Manual	37.9	61.8
17,400	12,900	13,400	16,000	300	Manual	37.7	61.2
17,400	12,900	13,400	16,000	100	Manual	38.2	61.1
33,134	22,804	25,154	25,300	50,000	Automatic	34.6	40.2
33,134	22,804	25,154	25,300	8,000	Landing Site Redesignation	35.4	45.9

[1] These mass properties were used for the purpose of this analysis. Reference should be made to Volume III, Spacecraft Operational Data Book, for current official mass properties data.

Table 4.8-3. Plume Impingement Correction Factor for Ullage Calculations (Para. 4.8.2)

Control Mode	Correction Factor
4 jet	1.15
2-jet (IId and IVd)	1.12
2-jet (Id and IIId)	1.19

Table 4.8-4. Control System Efficiency (Unstaged or Docked) - AGS (Para. 4.8.2)

CONTROL MODE	ULLAGE CORRECTION FACTOR
4-jet primary coils	1.10
4-jet secondary coils	1.00
2-jet primary coils	1.04

Table 4.8-5. Control System Efficiency (Staged) - AGS (Para. 4.8.2)

CONTROL MODE	ASCENT PROP. REMAINING (LBS)	ULLAGE CORRECTION FACTOR*
4-jet primary coils	0	1.06
	5300	1
4-jet secondary coils	0	1.04
	5300	1
2-jet primary coils	0	1
	5300	1

*These numbers can be interpolated for ascent propellant weights between 0 and 5300 lbs.

Table 4.8-6 Engine Performance Test Conditions Using "GREEN" N_2O_4 and Helium - Saturated Propellants (Para. 4.8.4)

CONDITION	PROPELLANT TEMPERATURE, °F	VALVE VOLTAGE, PRIMARY COIL, VOLTS	PROPELLANT PRESSURE CONDITIONS, PSIA[1]
Nominal	70 ± 10	25 ±0.2	170 ± 2.5
Low	40 ± 5	21 ±0.2	170 ± 2.5
High	100 ± 5	29 ±0.2	170 ± 2.5

[1] Pressure is read at engine inlets during steady state firing.

Table 4.8-7, Steady State RCS Engine Vacuum Performance (Para. 4.8.4)

CONDITION (SEE TABLE 4.8-6)	THRUST, LB.	THRUST COEFFICIENT	C* FT/SEC	O/F RATIO	Isp, SEC	3σIsp	NUMBER OF 5-SEC. RUNS
Nominal	100.3	1.776	5096	2.049	281.0	0.90%	20
Low	99.7	1.773	5008	2.058	275.7	0.88%	8
High	100.4	1.775	5204	2.012	286.8	1.59%	8

Table 4.8-8. Average Response Times of RCS Engine Valves Using Primary Coils (Para. 4.8.4)

<table>
<tr><th rowspan="2">VALVE VOLTAGE, VOLTS</th><th colspan="2">TIME FROM ELECTRICAL SIGNAL "ON" TO VALVE FULL OPEN (ALL PULSE WIDTHS), SECONDS</th><th colspan="2">TIME FROM ELECTRICAL SIGNAL "OFF" TO VALVE FULL CLOSE (ALL P.W. EXCEPT .013 SEC), SEC.</th><th colspan="2">TIME FROM ELECTRICAL SIGNAL "OFF" TO VALVE FULL CLOSE (.013 SEC. P.W.), SECONDS</th></tr>
<tr><th>Fuel</th><th>Oxidizer</th><th>Fuel</th><th>Oxidizer</th><th>Fuel</th><th>Oxidizer</th></tr>
<tr><td>21 ± 0.2</td><td>0.0091</td><td>0.0112</td><td>0.0054</td><td>0.0071</td><td>0.0050</td><td>0.0050</td></tr>
<tr><td>25 ± 0.2</td><td>0.0078</td><td>0.0095</td><td rowspan="2">0.0056</td><td rowspan="2">0.0073</td><td rowspan="2">0.0052</td><td rowspan="2">0.0066</td></tr>
<tr><td>29 ± 0.2</td><td>0.0066</td><td>0.0080</td></tr>
</table>

Table 4.8-9. Average Opening Response Times of RCS Engine Valves Using Secondary Coils (Para. 4.8.4)

VALVE VOLTAGE VOLTS	TIME FROM ELECTRICAL SIGNAL "ON" TO VALVE FULL OPEN, SECONDS	
	Fuel	Oxidizer
24 ± 0.2	0.0270	0.0378
27 ± 0.2	0.0232	0.0325

TABLE 4.8-10. PEAK SOAKBACK TEMPERATURE FOR "D" INJECTOR (PARA. 4.8.13.2)

	CASE I LM = 30°F No Solar			CASE II LM = 100°F No Solar			CASE III LM = 30°F Solar			CASE IV LM = 100°F Solar		
Firing Duration (Seconds)	Injector °F	Ox Valve °F	Quad °F	Injector °F	Ox Valve °F	Quad °F	Injector °F	Ox Valve °F	Quad °F	Injector °F	Ox Valve °F	Quad °F
5	185	138	148	187	140	151	189	141	152	191	144	155
10	204	138	155	206	140	155	207	141	157	210	145	161
15	215	137	158	217	139	161	217	140	161	220	145	165
20	220	136	160	223	138	163	223	139	163	226	144	166
30	226	135	162	228	137	165	229	138	164	231	144	168
40	230	135	163	232	136	166	232	137	165	234	142	169
60	233	134	164	235	135	167	235	136	166	236	141	170
90	234	133	164	236	134	167	236	135	167	239	140	171
120	236	132	165	237	134	168	237	134	168	240	139	172
See Figure 4.8-	70	71	72	73	74	75	76	77	78	79	80	81

TABLE 4.8-11. SUMMARY OF HEATER DOUBLE-FAILURE RESULTS (PARA. 4.8.16)

Series	LM Structure Temperature °F	Heater Voltage	Solar	Failure Mode	Temperature °F						Notes
					Injector		Ox Valve		Quad		
					Initial	Steady State	Initial	Steady State	Initial	Steady State	
I S	30	24	NONE	ON	140.0	178	106	126.5	134	142	
F	30	24	NONE	ON	140.0	178	106	124.0	134	142	
D	30	24	NONE	ON	139.0	180	136	158.5	134	150	
U	30	24	NONE	ON	140.0	187	136	162.0	134	138	
II S	30	24	NONE	OFF	140.0	109	106	89	134	127	**
F	30	24	NONE	OFF	140.0	109	106	89	134	127	**
D	30	24	NONE	OFF	139.0	106.15	136	120.5	134	122	**
U	30	24	NONE	OFF	140.0	107.5	136	118.5	134	125	**
III S	100	24	NONE	ON	138.0	184	122	148.5	136	146	
F	100	24	NONE	ON	140.0	184	122	145.0	136	146	
D	100	24	NONE	ON	140.0	186	137	163.0	136	155.5	
U	100	24	NONE	ON	139.0	195	137	167.0	136	142	
IV S	100	24	NONE	OFF	138.0	117	122	111.5	136	131	**
F	100	24	NONE	OFF	140.0	117	122	111.5	136	131	**
D	100	24	NONE	OFF	140.0	119	137	126	136	127.5	**
U	100	24	NONE	OFF	139.0	116	137	124.5	136	133.5	**
V S	30	32	NONE	ON	140.0	230	106	152	134	154	
F	30	32	NONE	ON	140.0	230	106	149.5	134	154	
D	30	32	NONE	ON	139.0	232	136	185.5	134	171	*
U	30	32	NONE	ON	140.0	247	136	191.5	136	145	*
VI S	30	32	NONE	OFF	140.0	110	106	89.0	134	127.5	**
F	30	32	NONE	OFF	140.0	109.5	106	88.5	134	127.5	**
D	30	32	NONE	OFF	139.0	111	136	120.5	134	123.0	**
U	30	32	NONE	OFF	140.0	108	136	119	134	131	**
VII S	100	32	NONE	ON	138.0	241	122	177.5	136	171	•
F	100	32	NONE	ON	140.0	246	122	175.0	136	165.5	*
D	100	32	NONE	ON	140.0	251	137	202	136	190	*
U	100	32	NONE	ON	139.0	262.5	137	205	136	157.5	•
VIII S	100	32	NONE	OFF	138.0	116.5	122	111	136	137.0	**
F	100	32	NONE	OFF	140.0	116.5	122	111.5	136	130.5	**
D	100	32	NONE	OFF	140.0	119.0	137	126.0	136	128.0	**
U	100	32	NONE	OFF	139.0	116	137	124.5	136	133.5	**

Note: Both heaters on the engine shown are failed either off or on as shown.
The heaters on the other engines in the cluster are operating normally.

* On failure where Ox valve steady state temperature exceeds 175°F

** Off failure where C.C.F. steady state temperature is below the 120°F lower limit

TABLE 4.8-11. (Continued)

Series	LM Structure Temperature °F	Heater Voltage	Solar	Failure Mode	Temperature °F						Notes
					Injector		Ox Valve		Quad		
					Initial	Steady State	Initial	Steady State	Initial	Steady State	
IX S	30	24	YES	ON	139	202	108	142.5	135	158	
F	30	24	YES	ON	141	202.5	107	141.0	135	158	
D	30	24	YES	ON	138	205	137	177.0	135	168.5	*
U	30	24	YES	ON	138	213	137	179.5	135	150	*
X S	30	24	YES	OFF	139	127	108	101	135	132	**
F	30	24	YES	OFF	141	127	107	101	135	132	**
D	30	24	YES	OFF	138	130	137	132	135	131	
U	30	24	YES	OFF	138	129	137	131.5	135	134	
XI S	100	24	YES	ON	139	226.5	126	124	138	185	
F	100	24	YES	ON	138	227.0	126	172.5	138	184.5	
D	100	24	YES	ON	140	231	138	202	138	195.0	*
U	100	24	YES	ON	138	237.5	138	204	138	177.5	*
XII S	100	24	YES	OFF	139	133.5	126	123.5	138	136	
F	100	24	YES	OFF	138	134	126	123.5	138	136	
D	100	24	YES	OFF	140	137	138	137	138	136	
U	100	24	YES	OFF	138	137.5	138	137.5	138	137.5	
XIII S	30	32	YES	ON	139	278	108	184	135	203	*
F	30	32	YES	ON	141	278	107	181	135	202	*
D	30	32	YES	ON	138	284	137	232	135	221	*
U	30	32	YES	ON	138	294	137	234	135	189.5	*
XIV S	30	32	YES	OFF	139	126.5	108	101	135	132.5	**
F	30	32	YES	OFF	141	127.5	107	101	135	.133	**
D	30	32	YES	OFF	138	130	137	132	135	131	
U	30	32	YES	OFF	138	129	137	131.5	135	134.5	
XV S	100	32	YES	ON	139	298	126	211	138	225.5	*
F	100	32	YES	ON	138	299	126	208.5	138	225.5	*
D	100	32	YES	ON	140	305	138	252.5	138	243.5	*
U	100	32	YES	ON	138	315.5	138	254.5	138	213.5	*
XVI S	100	32	YES	OFF	139	134	126	123.5	138	136.5	**
F	100	32	YES	OFF	138	134	126	123.5	138	136.5	**
D	100	32	YES	OFF	140	137	138	137	138	137	
U	100	32	YES	OFF	138	137	138	137	138	137	

Note: Both heaters on the engine shown are failed either off or on as shown. The heaters on the other engines in the cluster are operating normally.

* On failure where Ox valve steady state temperature exceeds 175°F

** Off failure where C. C. F. steady state temperature is below the 120°F lower limit

TABLE 4.8-12. SUMMARY OF HEATER SINGLE-FAILURE RESULTS (PARA. 4.8.16)

Series	LM Structure Temperature °F	Heater Voltage	Solar	Failure Mode	Temperature °F						Notes
					Injector		Ox Valve		Quad		
					Initial	Steady State	Initial	Steady State	Initial	Steady State	
VII S	100	32	NONE	ON	138	177	122	143	136	144	
F	100	32	NONE	ON	140	178	122	141	136	144	
U	100	32	NONE	ON	140	187	137	162	136	141	
D	100	32	NONE	ON	139	180	137	159	136	153	
VIII S	30	32	YES	ON	139	192	108	137	135	152	
F	30	32	YES	ON	141	192	107	135	135	152	
U	30	32	YES	ON	138	201	137	172	135	145	
D	30	32	YES	ON	138	195	137	170	135	161	
XV S	100	32	YES	ON	139	217	126	169	138	179	
F	100	32	YES	ON	138	217	126	168	138	179	
U	100	32	YES	ON	140	227	138	195	138	172	*
D	100	32	YES	ON	138	221	138	195	138	186	*

Note: (1) Only one heater on the engine shown has failed on. The other heater on the engine is off. The heaters on the other engines in the cluster are operating normally.

(2) Series shown in this table have parametric inputs similar to those in Table 4.8-10, except these are for single heater failure.

* On failure where Ox valve steady state temperature exceeds 175°F

Table 4.8.13. Forces and Moments due to RCS Plume Impingement (Para. 4.8.6.2)

Engine Quad Number	Impingement Force (lbs)			Pitch and Roll Impingement Moments* (ft-lbs)			
	Fx	Fy	Fz	Beginning of Powered Descent	Lunar Landing	CSM/LM Docked	Reference Thruster Plane (x = 254, y=0 z=0)
Id	-10.4	41.7	-41.7	75.8	-28.4	-378.4	-167.4
IId	-10.4	41.7	41.7	75.8	-28.4	-378.4	-167.4
IIId	-10.4	-41.7	41.7	75.8	-28.4	-378.4	-167.4
IVd	-10.4	-41.7	-41.7	75.8	-28.4	-378.4	-167.4

* Positive moments act in same direction as control torques

Table 4.8.14. Effect of RCS Thruster Plume Impingement on Attitude Control (Para. 4.8.6.2)

Attitude and Transition Control Mode	Mission Phase		
	Beginning Powered Descent c.g. (x=184 in, Y=0 in, z=0 in.)	Lunar Landing c.g. (x=214 in, y=0 in, z=0 in.)	CSM/LM Docked c.g. (x=315 in, Y=0 in, z=0 in.)
2-jet +X Translation force (lbs)	179.2	179.2	179.2
4-jet +X Translation force (lbs)	358.2	358.2	358.2
2-jet Control Torque (ft-lbs) (pitch or roll)	1175.8	1071.6	721.6
4-jet Control Torque (ft-lbs) (pitch or roll)	2351.6	2143.2	1443.2

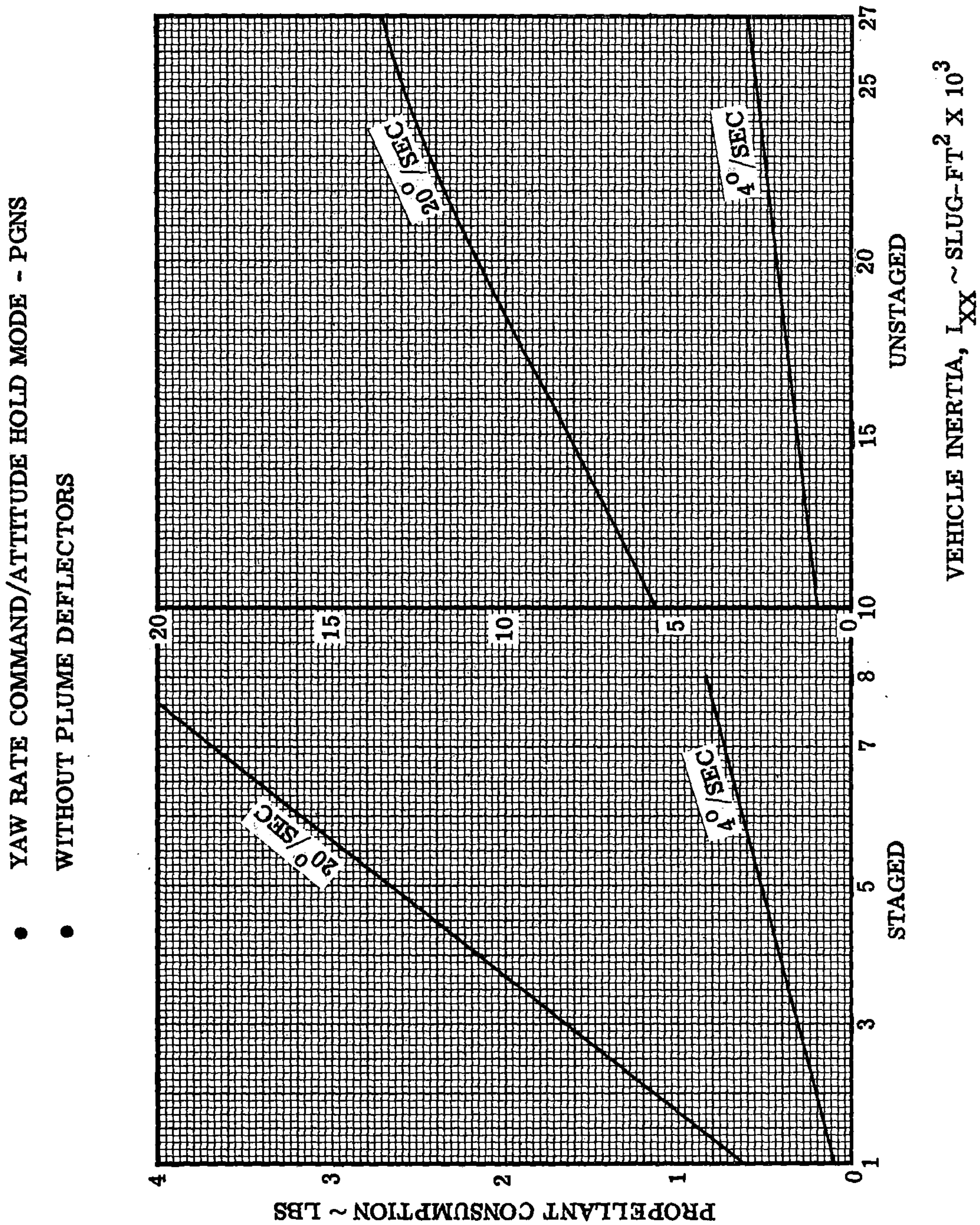

Figure 4.8-1. RCS Propellant for Rotation versus Vehicle Inertia
(See Para. 4.8.1.1)

- PITCH OR ROLL RATE COMMAND/ATTITUDE HOLD MODE - PGNS
- WITHOUT PLUME DEFLECTORS

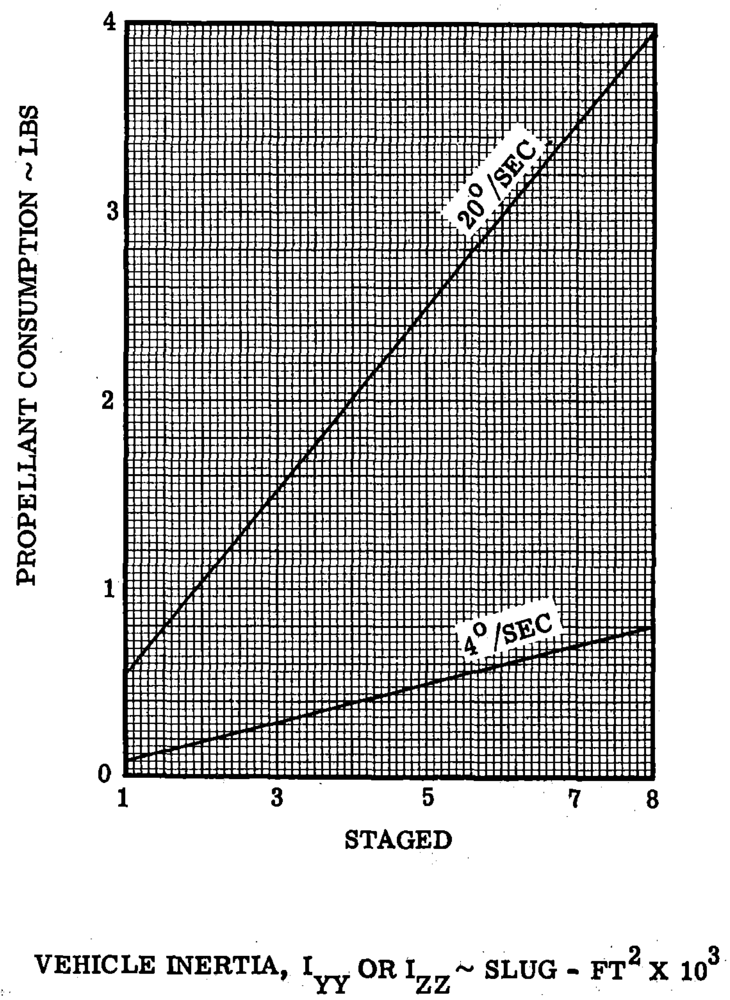

Figure 4.8-2. RCS Propellant for Rotation versus Vehicle Inertia
(See Para. 4.8.1.1)

- PITCH OR ROLL RATE COMMAND/ATTITUDE HOLD MODE - PGNS
- WITH PLUME DEFLECTORS

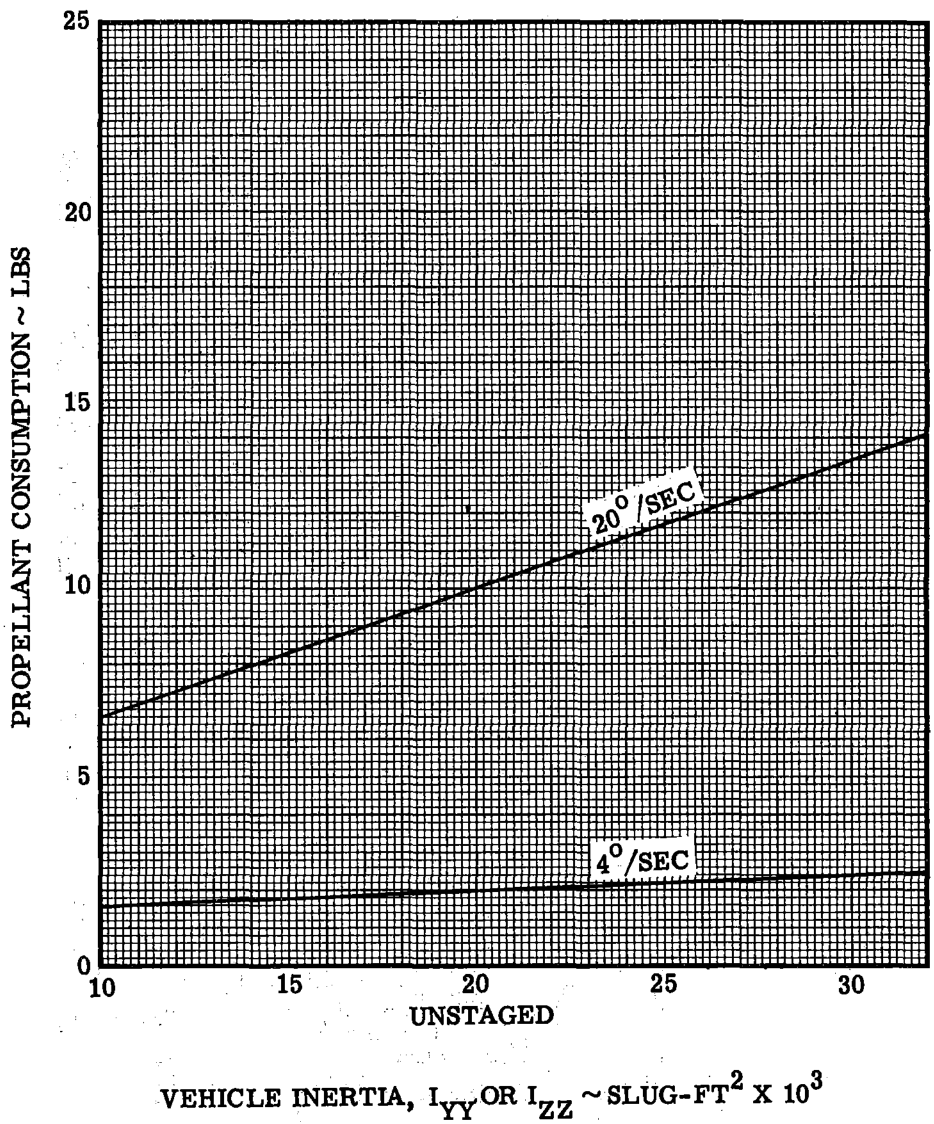

Figure 4. 8-3. RCS Propellant for Rotation versus Vehicle Inertia
(See Para. 4. 8. 1. 1)

- PITCH OR ROLL RATE - .4°/SEC MANUAL; .5°/SEC AUTO
- ATTITUDE HOLD OR AUTOMATIC - PGNS
- WITH PLUME DEFLECTORS
- CSM/LM DOCKED
- X_{CG} LOCATIONS IN LM COORDINATES MEASURED FROM STA. 254
- CONSUMPTION FOR .5°/SEC MULTIPLY ORDINATE READING BY 5/4

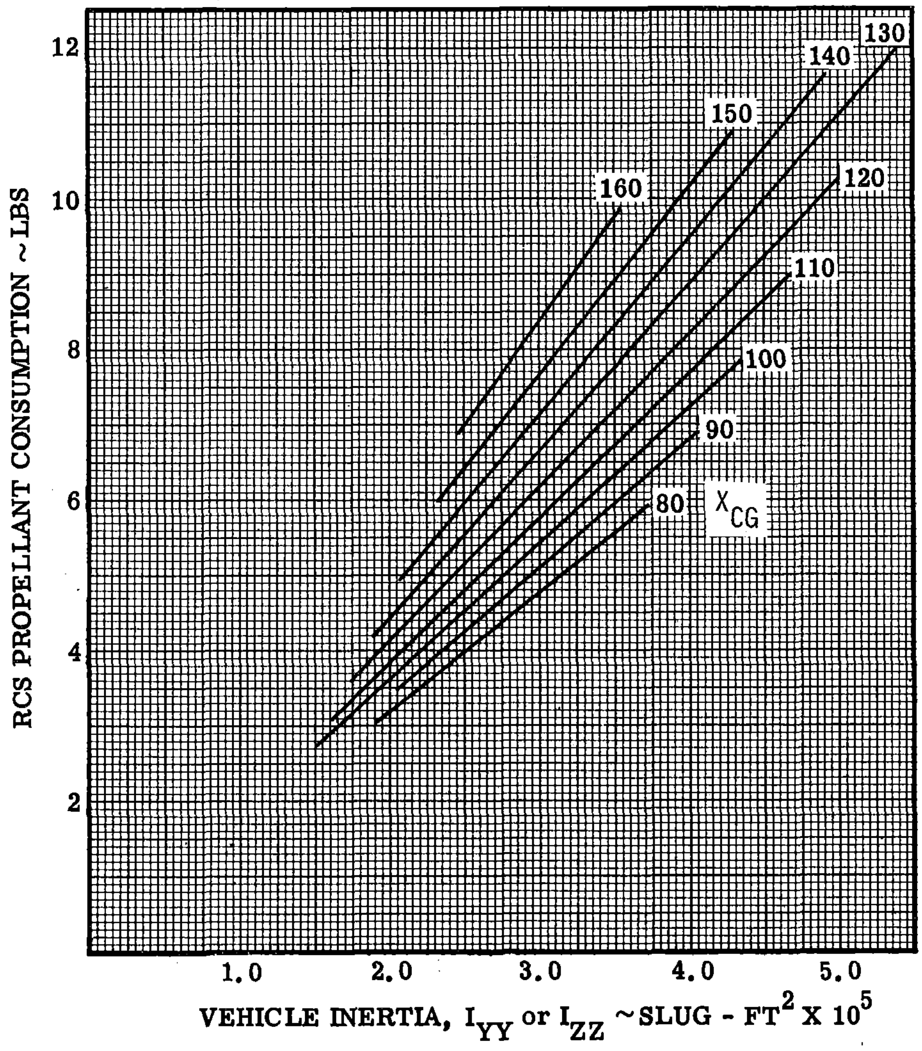

Figure 4.8-3.1. RCS Propellant Consumption for Pitch or Roll Rotations Versus Vehicle Inertia at Constant C.G. (PGNS, Docked). (See Para. 4.8.1.1)

- PITCH OR ROLL RATE - 2.0°/SEC
- ATTITUDE HOLD OR AUTOMATIC - PGNS
- WITH PLUME DEFLECTORS
- CSM/LM DOCKED
- X_{CG} LOCATIONS IN LM COORDINATES MEASURED FROM STA. 254

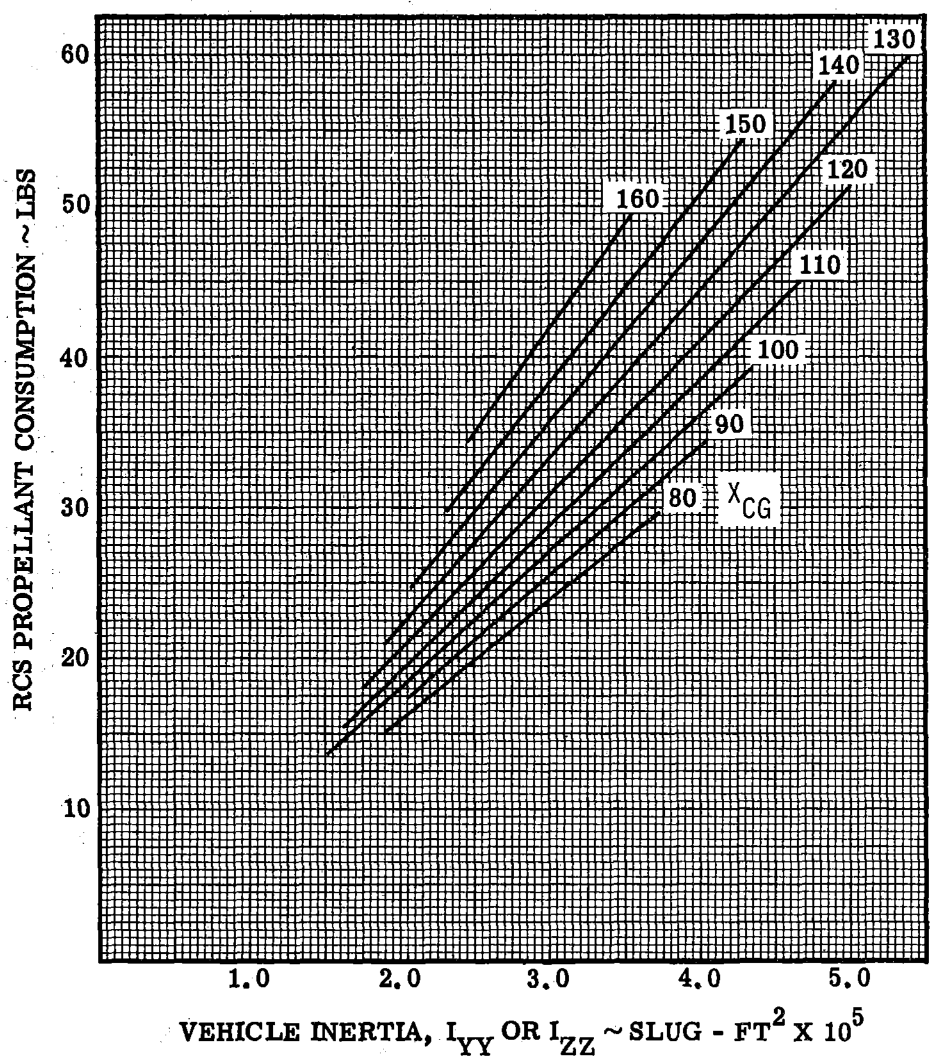

Figure 4.8-3.2. RCS Propellant Consumption for Pitch or Roll Rotations Versus Vehicle Inertia at Constant C. G. (PGNS, Docked). (See Para. 4.8.1.1)

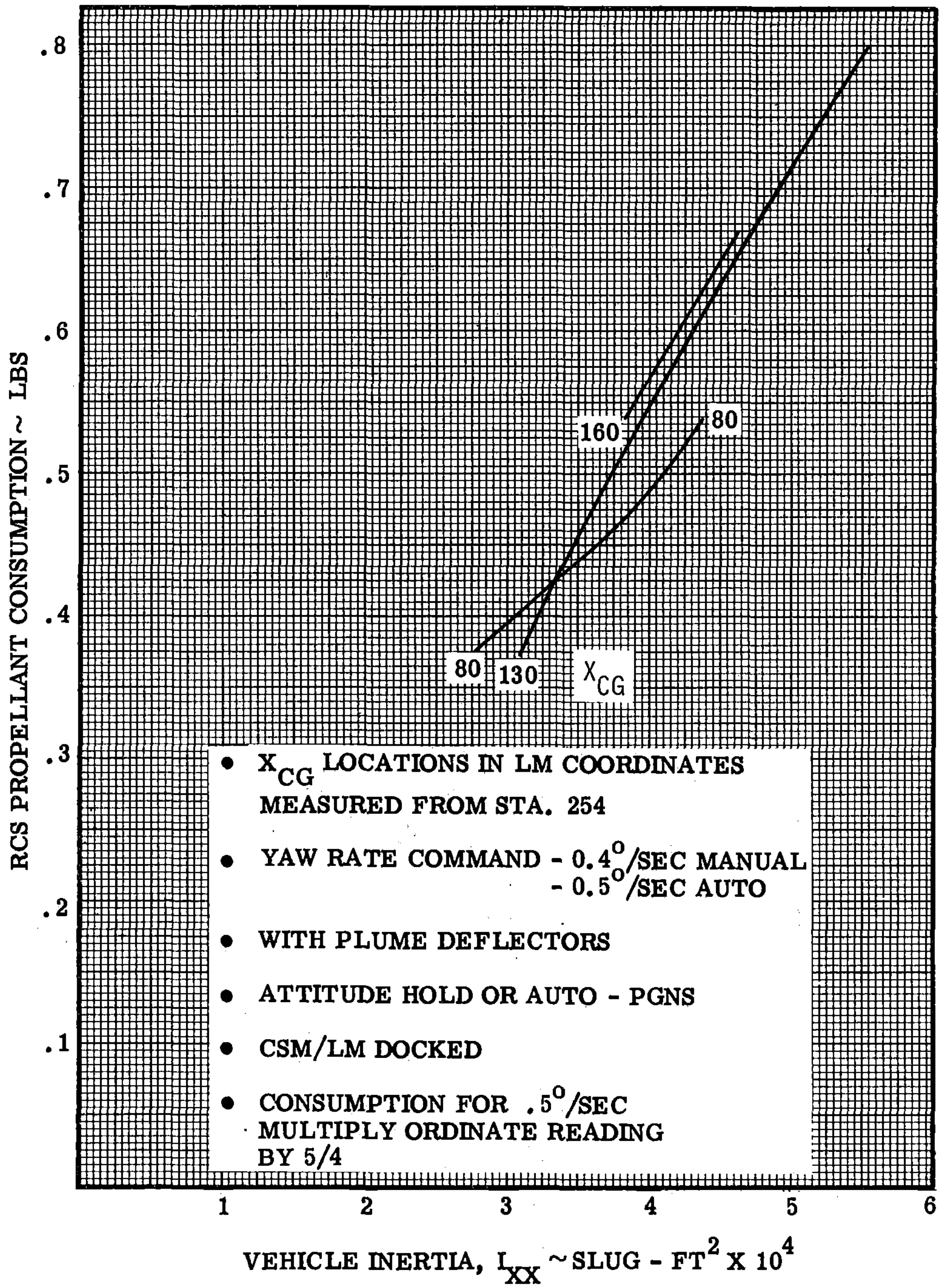

Figure 4. 8-3. 3. RCS Propellant Consumption for Yaw Rotations Versus Vehicle Inertia at Constant C. G. (PGNS, Docked) (See Para. 4. 8. 1. 1)

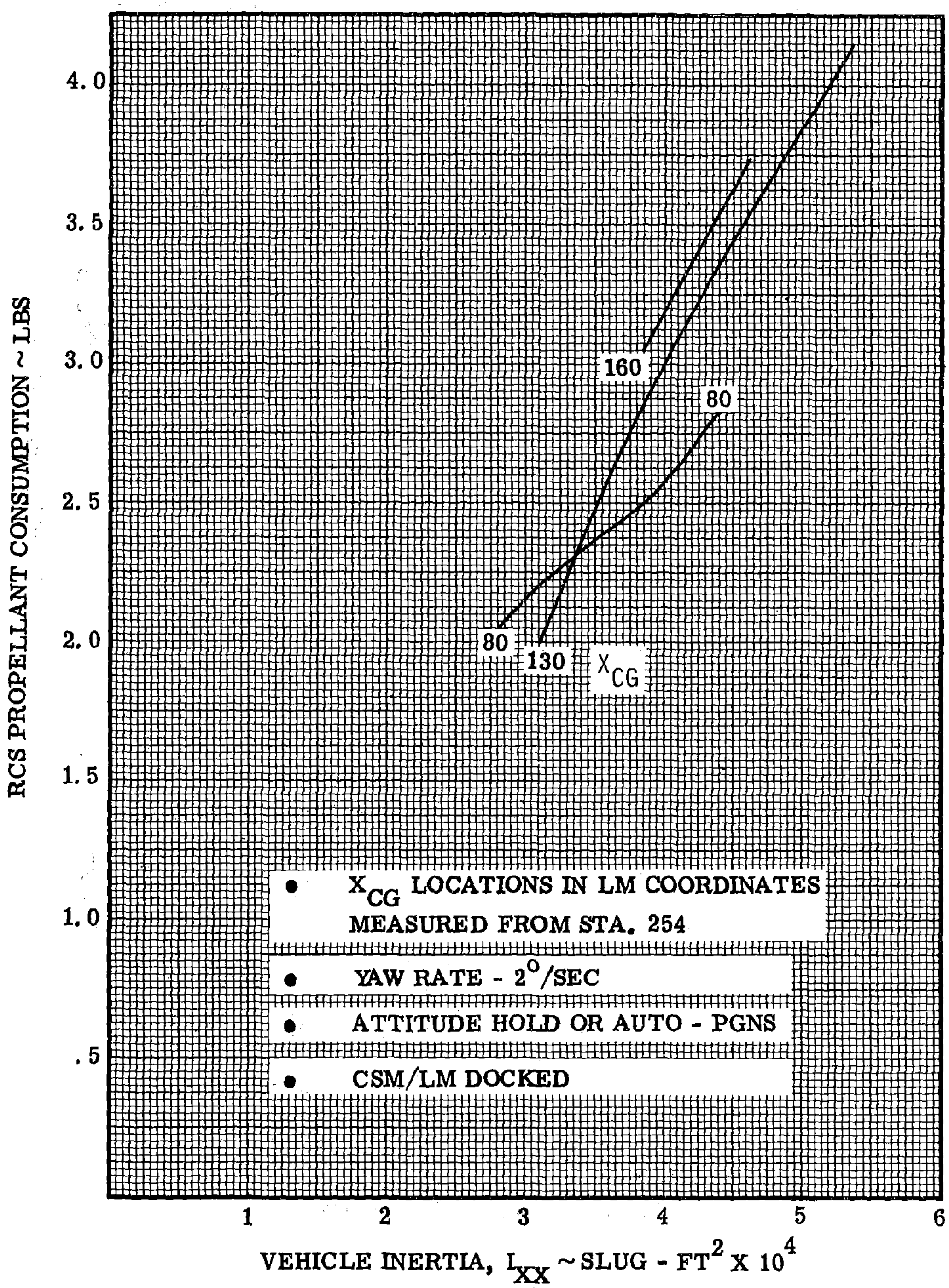

Figure 4.8-3.4. RCS Propellant for Yaw Rotations Versus Vehicle Inertia at Constant C.G. (PGNS, Docked). (See Para. 4.8.1.1)

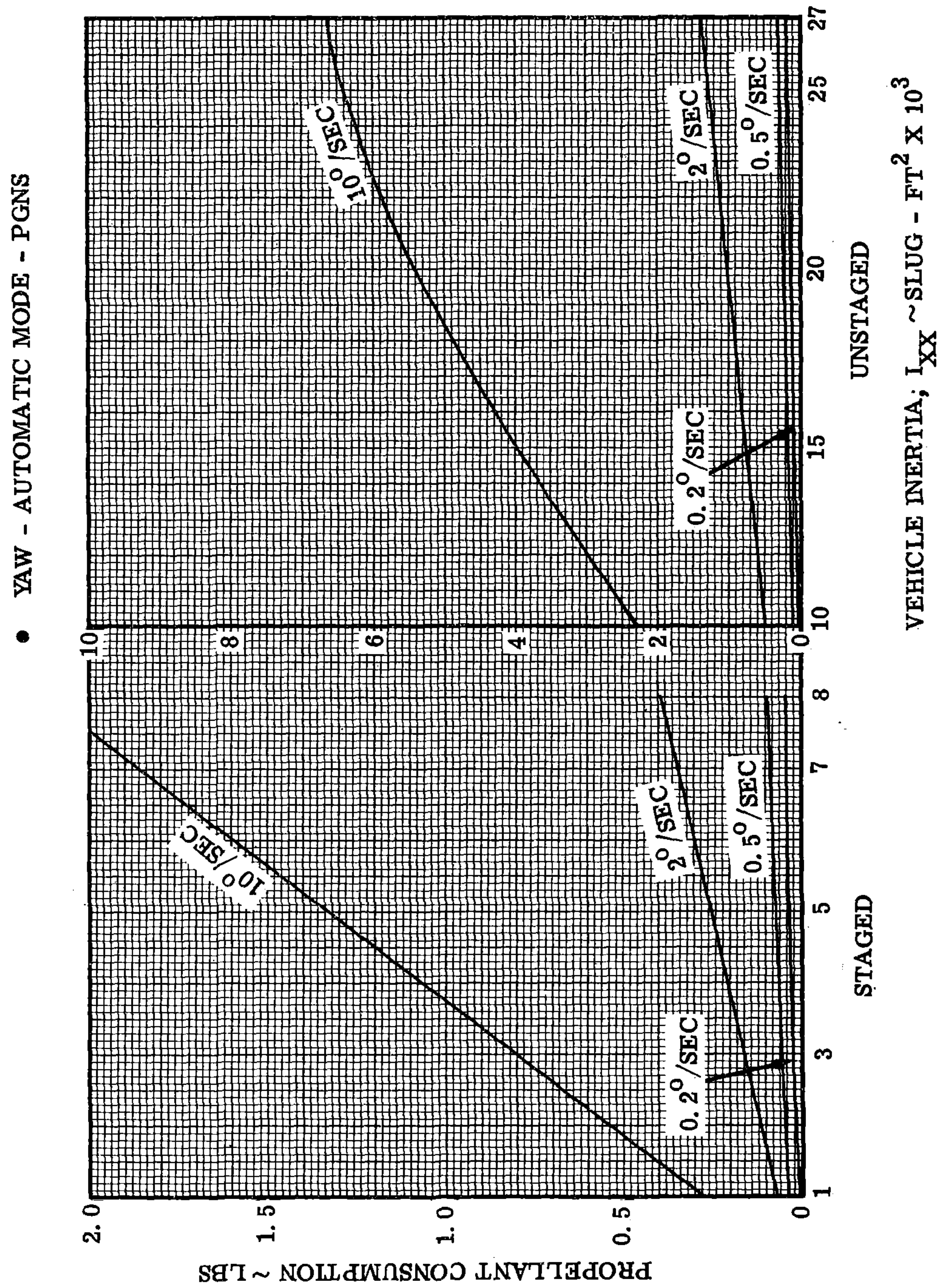

Figure 4. 8-4. RCS Propellant for Rotation versus Vehicle Inertia
(See Para. 4. 8. 1. 1)

- PITCH OR ROLL - AUTOMATIC MODE - PGNS
- WITHOUT PLUME DEFLECTORS

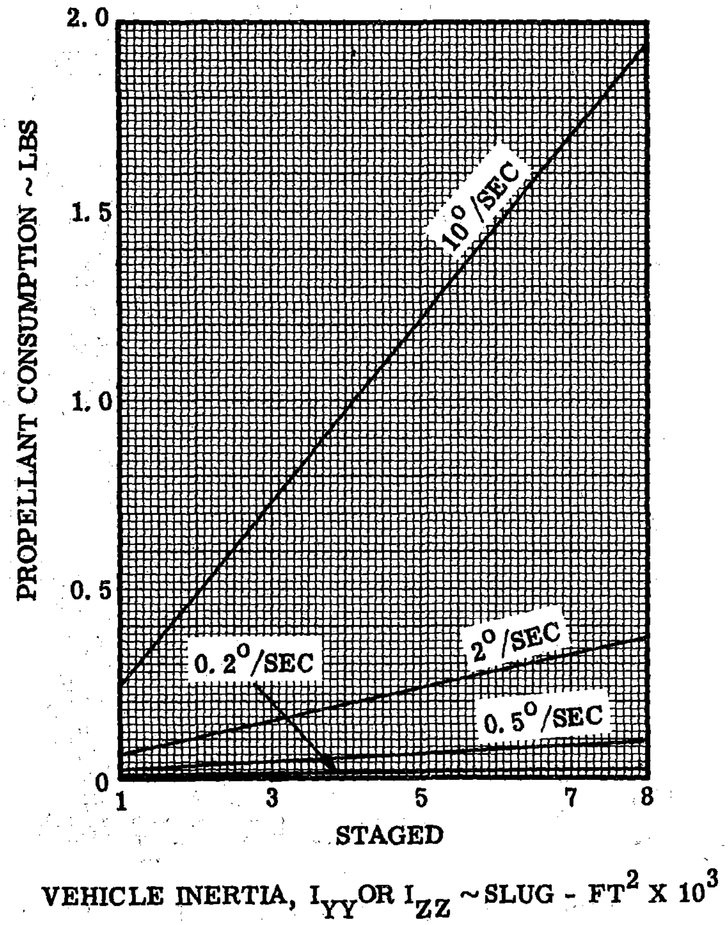

Figure 4.8-5. RCS Propellant for Rotation versus Vehicle Inertia (See Para. 4.8.1.1)

- PITCH OR ROLL - AUTOMATIC MODE - PGNS
- WITH PLUME DEFLECTORS

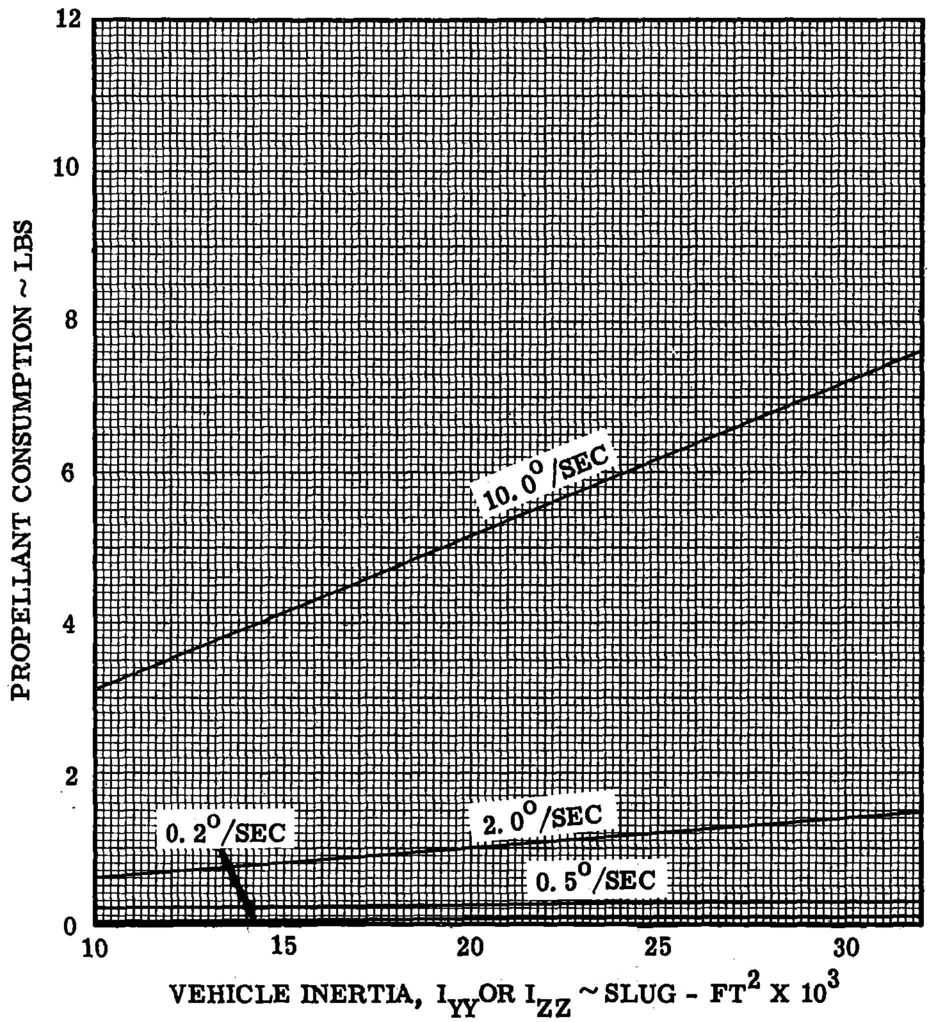

Figure 4.8-6. RCS Propellant for Rotation versus Vehicle Inertia
(See Para. 4.8.1.1)

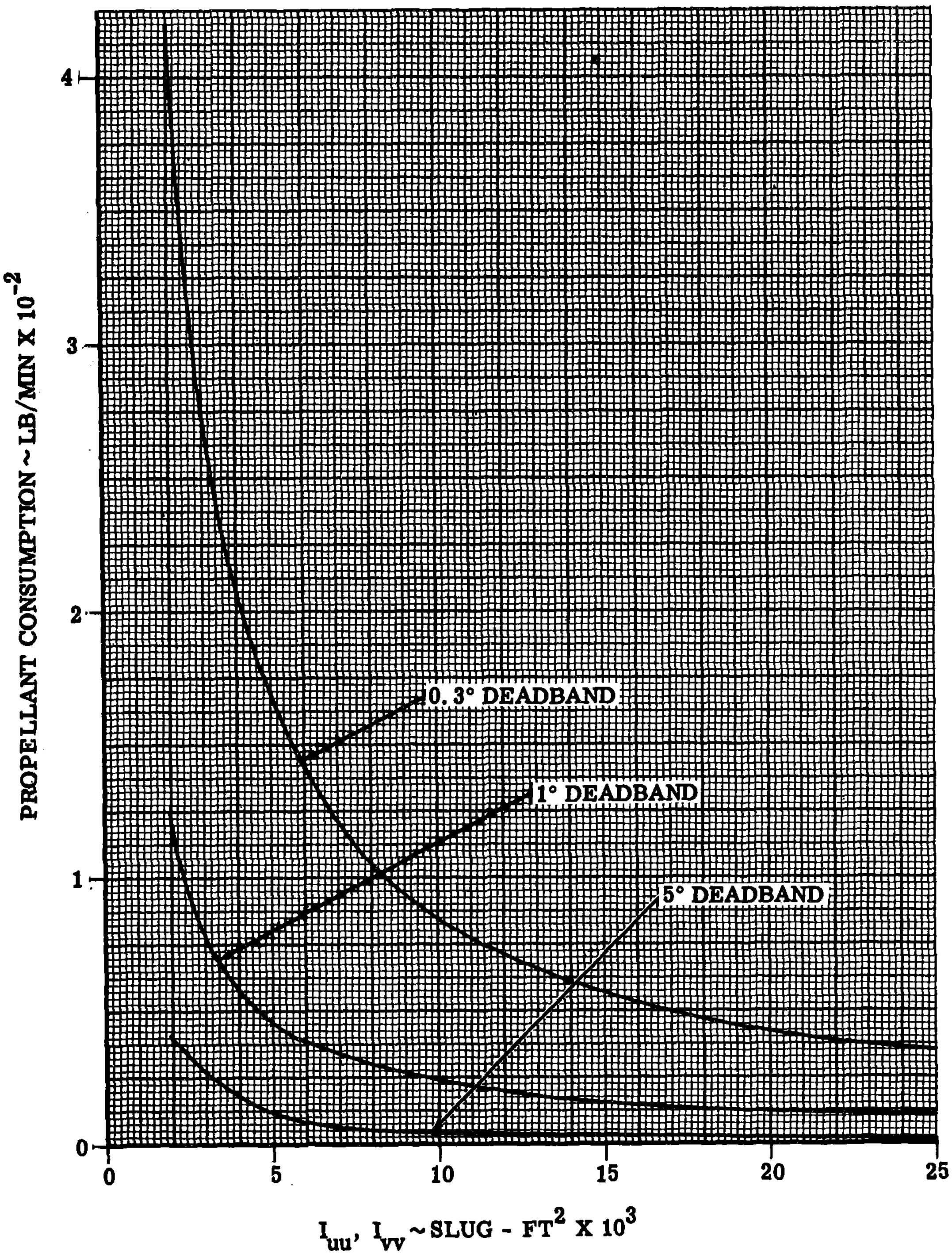

Figure 4.8-7. RCS Propellant Usage, Pitch or Roll - Digital Autopilot Undocked Not compensated for atmospheric drag or other vehicle perturbations (See Paragraphs 4.8.1.1 and 4.8.1.2)

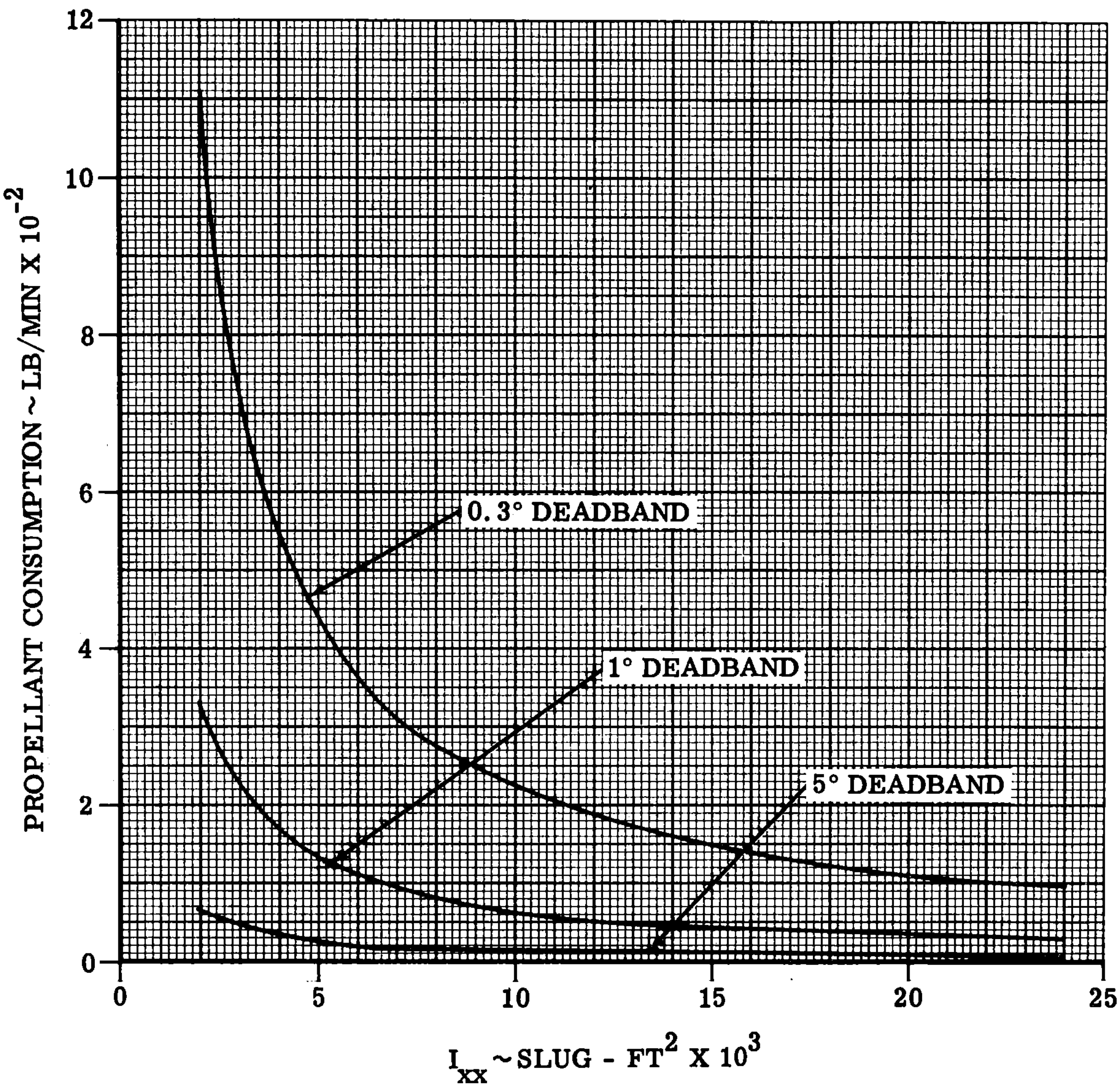

Figure 4.8-8. RCS Propellant Usage, Yaw - Digital Autopilot Undocked
Not compensated for atmospheric drag or other vehicle perturbations (See Paragraphs 4.8.1.1 and 4.8.1.2)

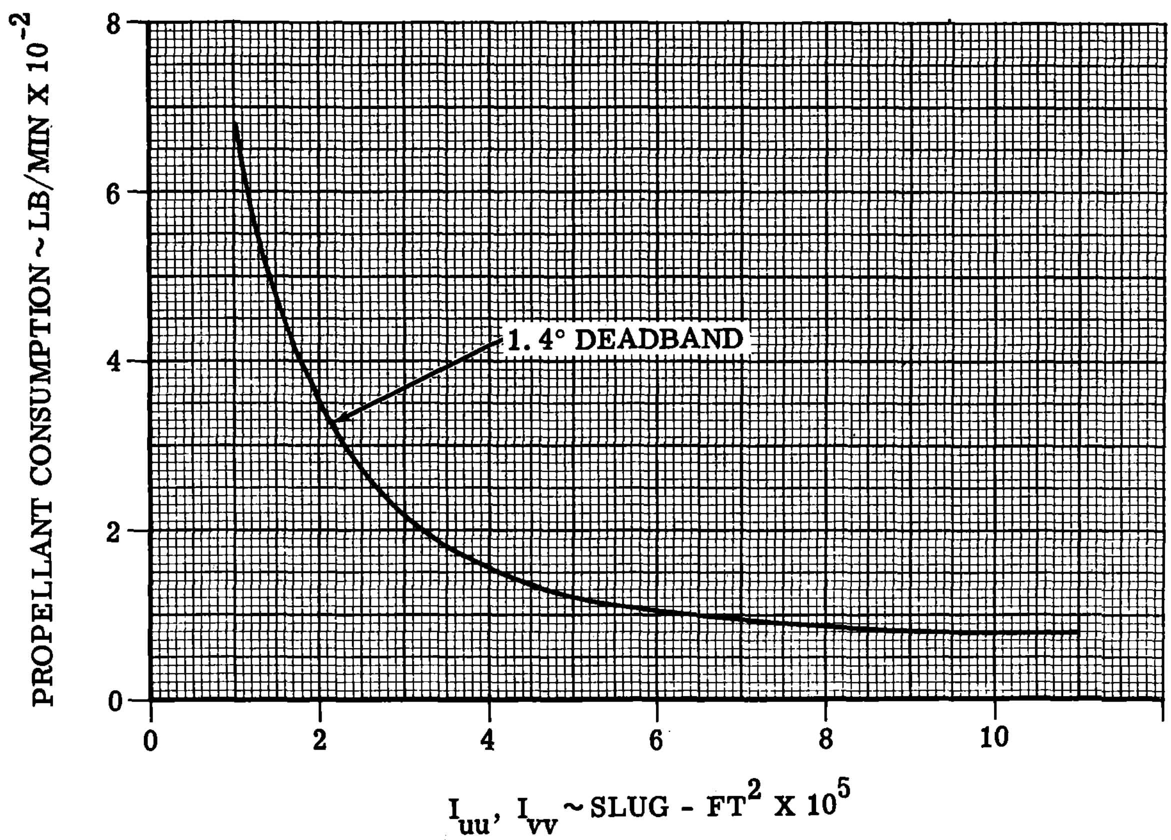

Figure 4.8-9. RCS Propellant Usage, Pitch or Roll - Digital Autopilot Docked
Not compensated for atmospheric drag or other vehicle perturbations (See Paragraphs 4.8.1.1 and 4.8.1.2)

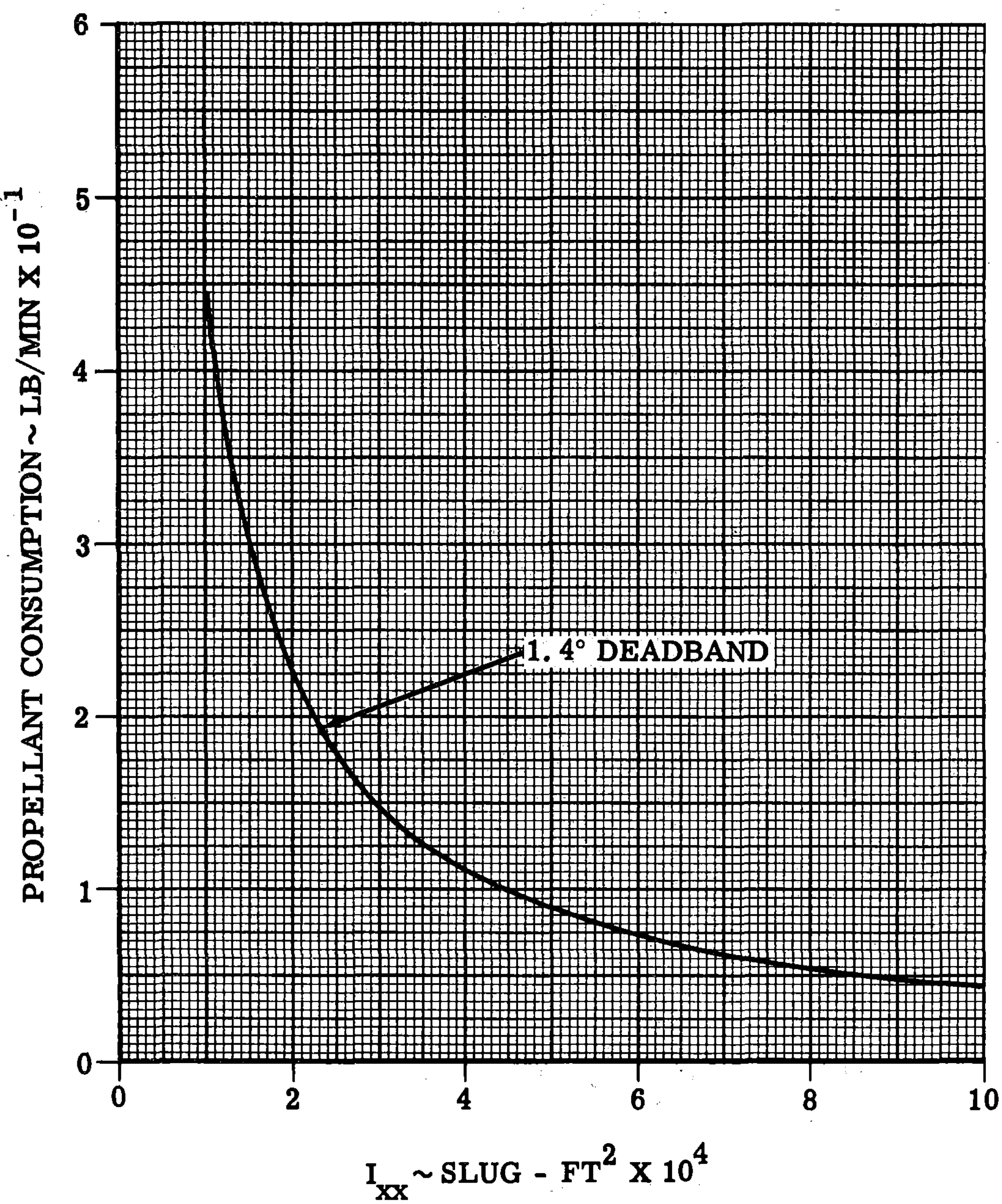

Figure 4.8-10. RCS Propellant Usage, Yaw - Digital Autopilot Docked
Not compensated for atmospheric drag or other vehicle perturbations (See Paragraphs 4.8.1.1 and 4.8.1.2)

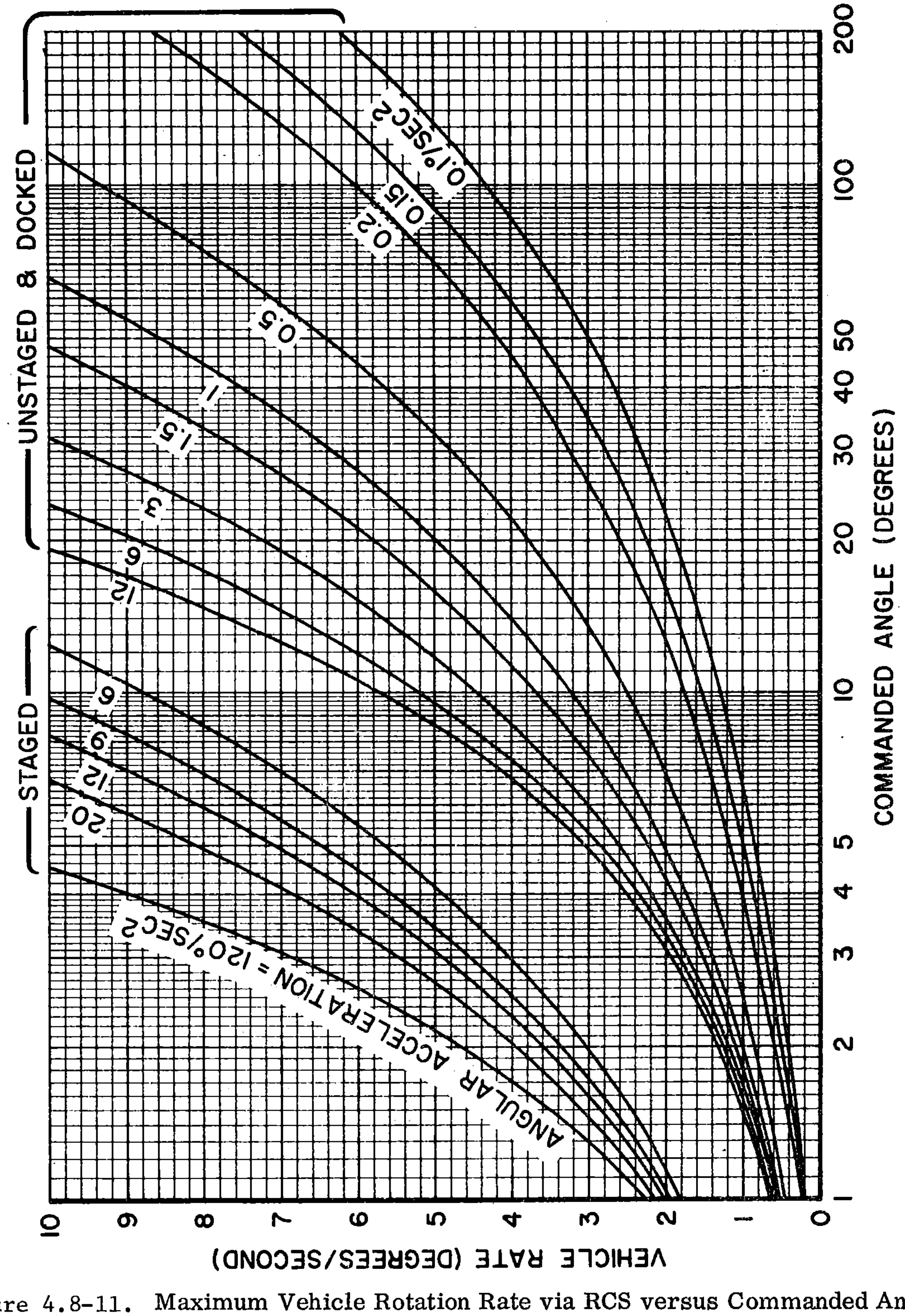

Figure 4.8-11. Maximum Vehicle Rotation Rate via RCS versus Commanded Angle for Typical Angular Acceleration (See Paragraph 4.8.1.1)

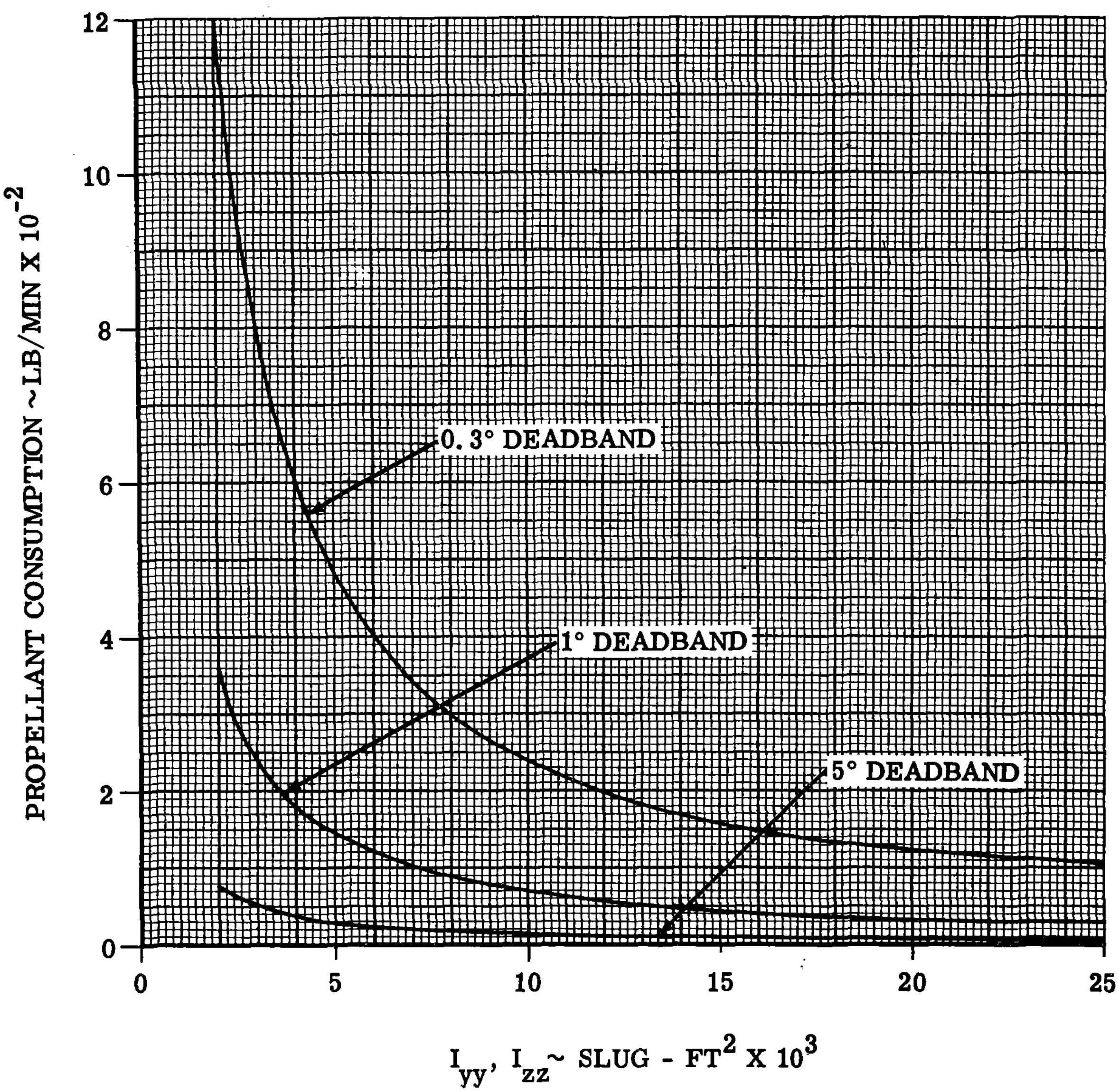

Figure 4.8-12. RCS Propellant Usage, Pitch or Roll - AGS Undocked
Not compensated for atmospheric drag or other
vehicle perturbations (See Paragraph 4.8.1.2)

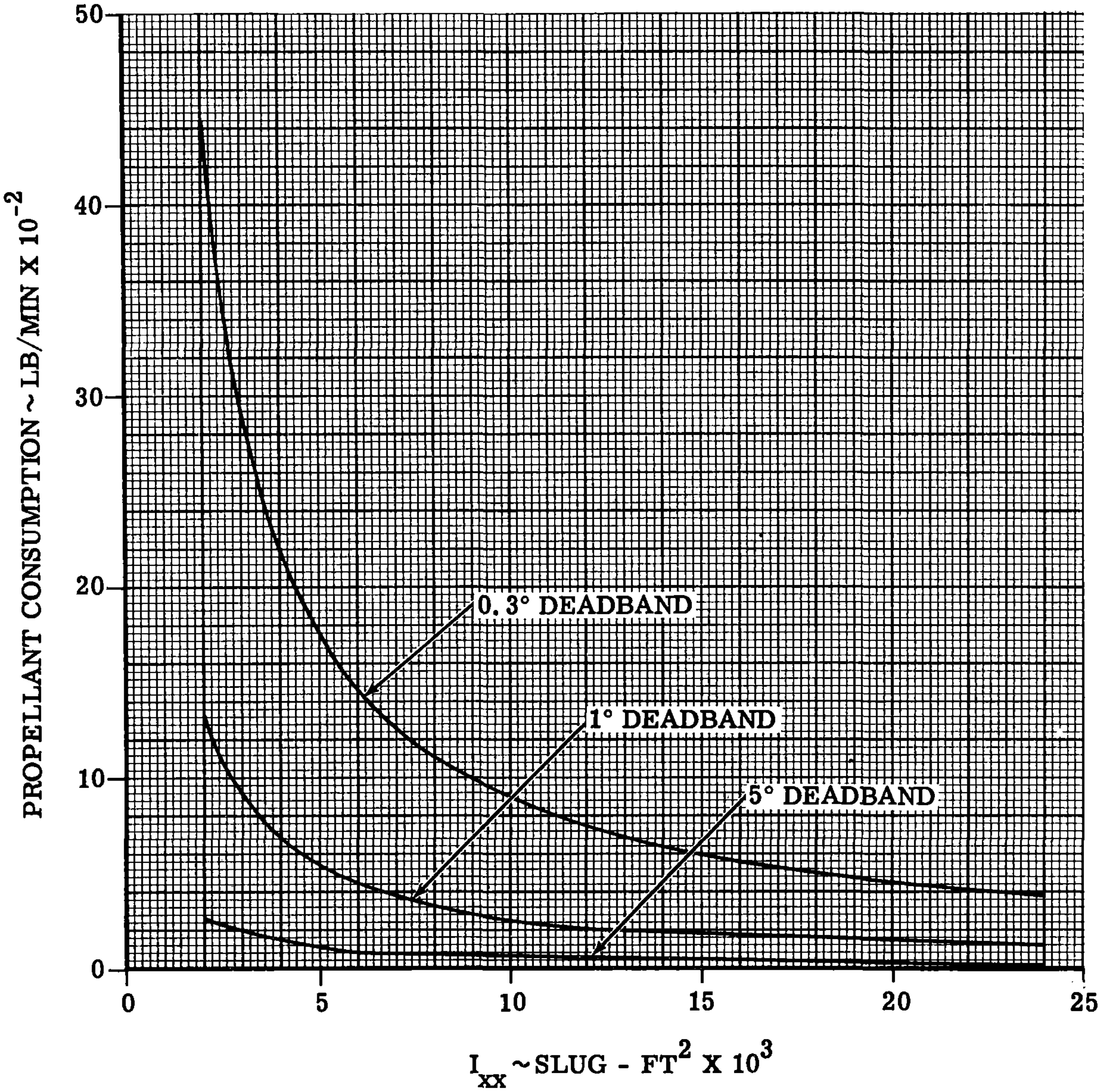

Figure 4.8-13. RCS Propellant Usage, Yaw - AGS Undocked
Not compensated for atmospheric drag or other vehicle perturbations (See Paragraph 4. 8. 1. 2)

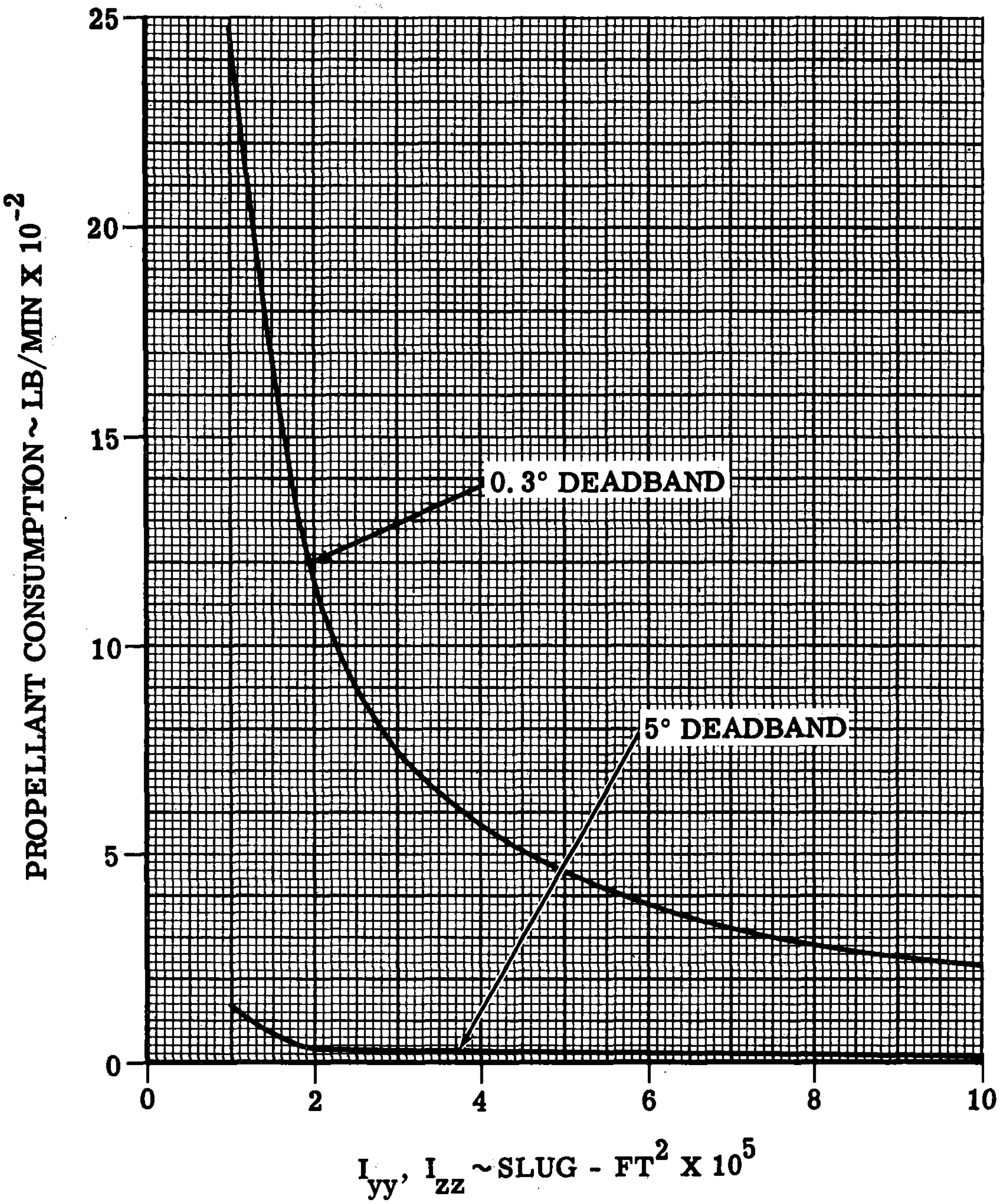

Figure 4.8-14. RCS Propellant Usage, Pitch or Roll - AGS Docked Not compensated for atmospheric drag or other vehicle perturbations (See Paragraph 4.8.1.2)

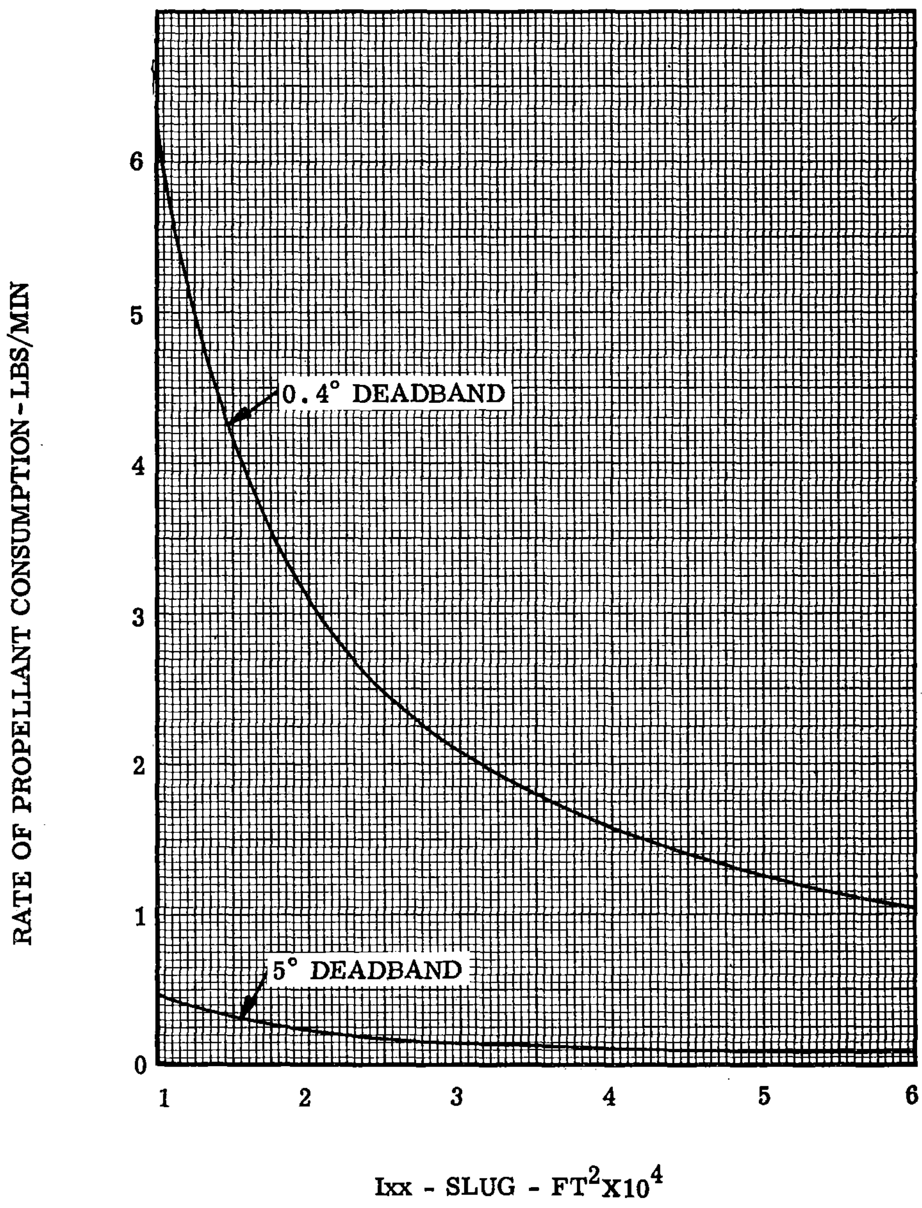

Figure 4.8-15. RCS Propellant Usage YAW-AGS, Docked. Not Compensated for Atmospheric Drag or Other Vehicle Perturbations (See Paragraphs 4.8.1.1 and 4.8.1.2)

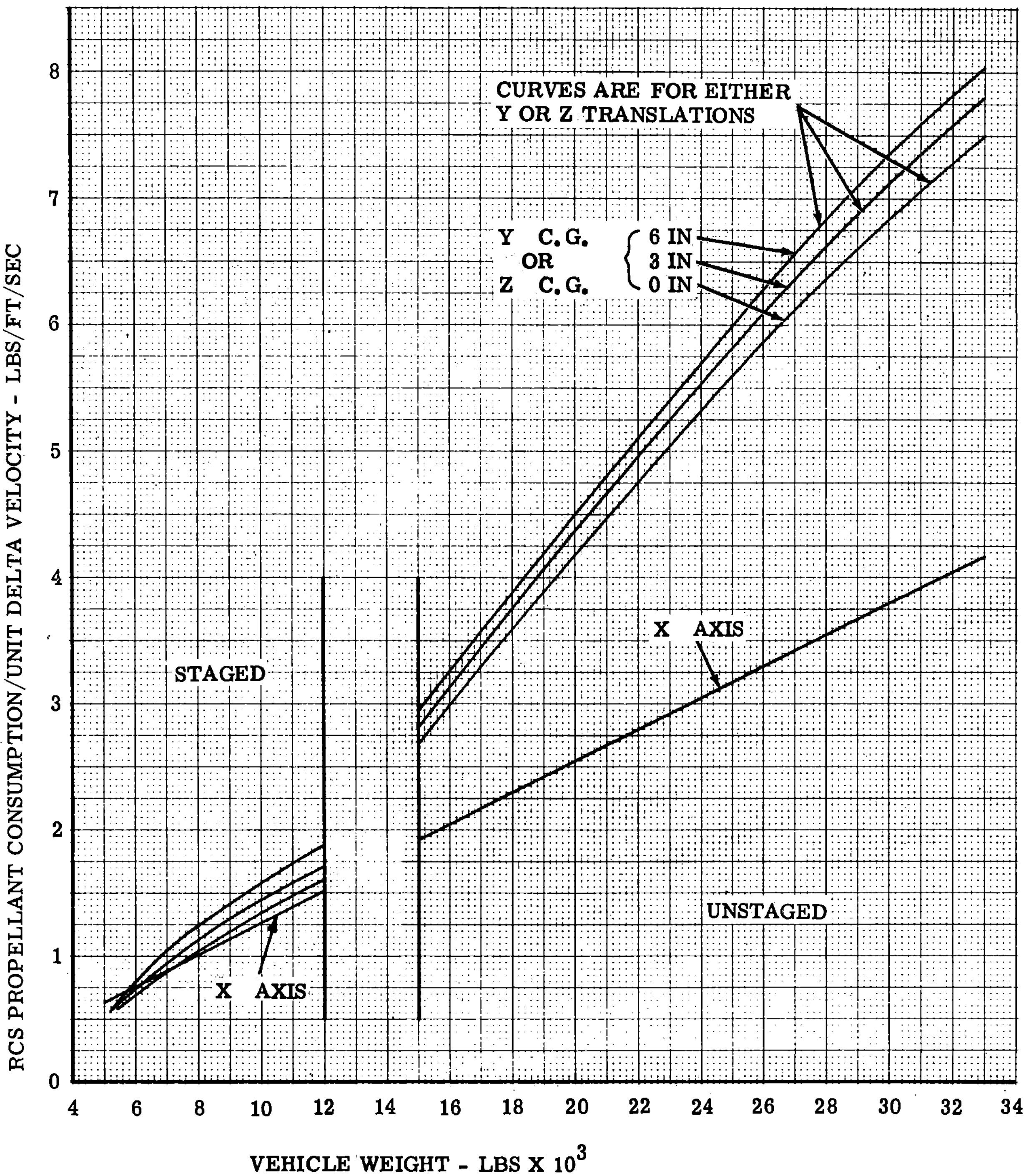

Figure 4.8-16. RCS Propellant Consumption/Unit Delta Velocity versus Vehicle Weight for X, Y, or Z Translation - PGNS or AGS (See Paragraph 4.8.1.4)

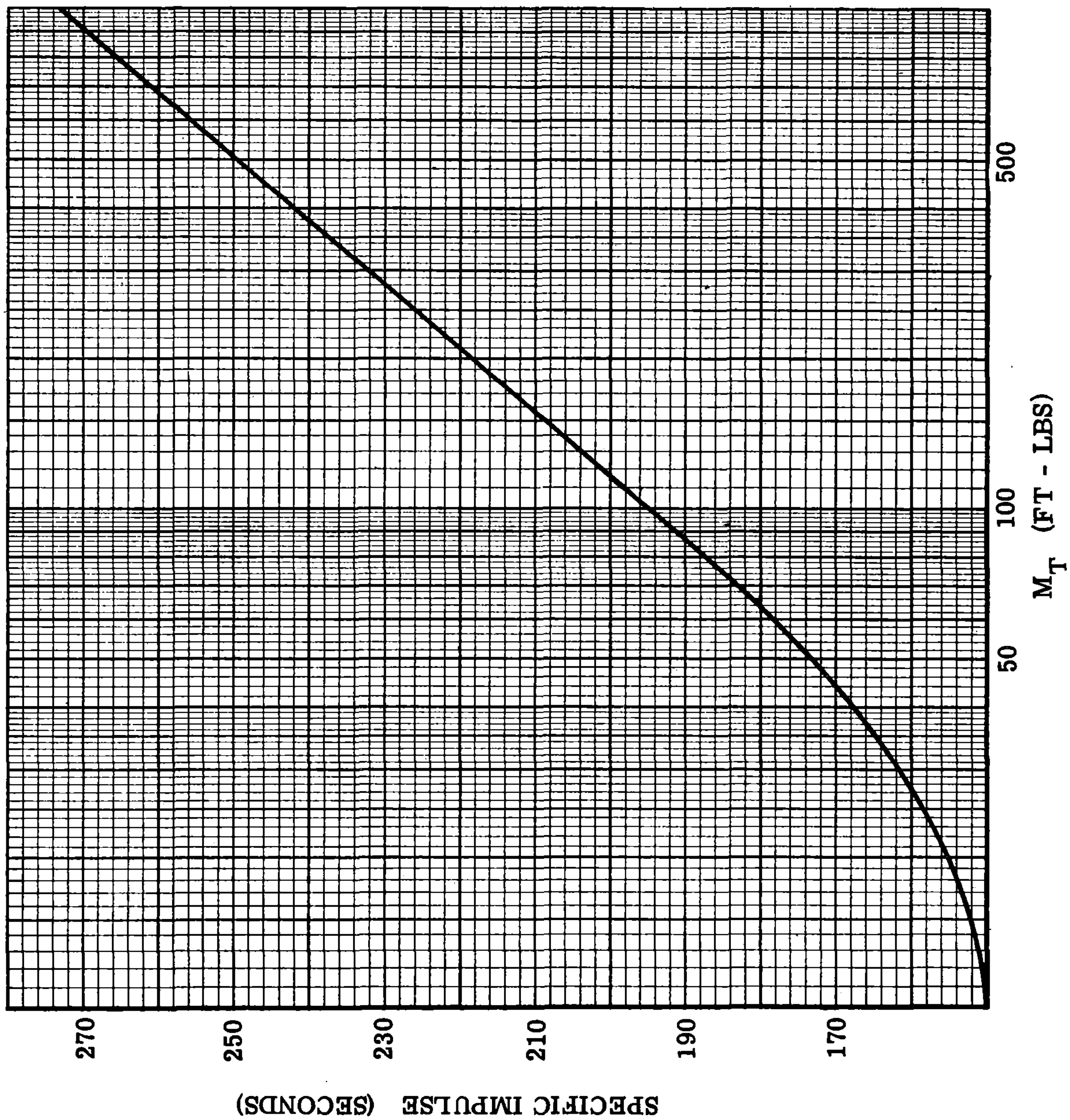

Figure 4.8-17. RCS Specific Impulse vs Descent Engine Moment Unbalance
(See Para. 4.8.1.4)

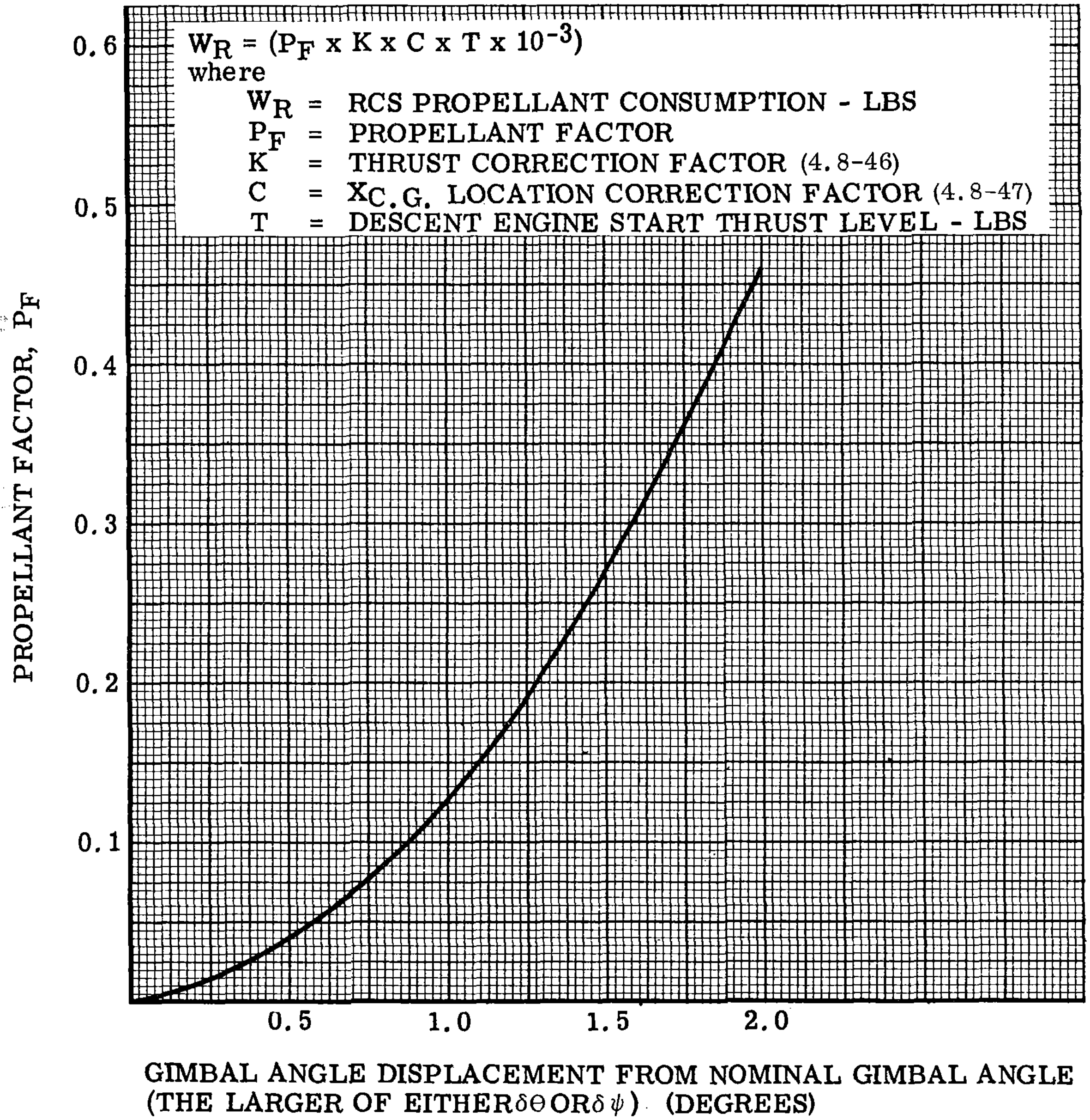

Figure 4.8-18. RCS Propellant Factor vs Gimbal Angle Displacement From Nominal Gimbal Angle For Descent Engine Starts (See Para. 4.8.1.4)

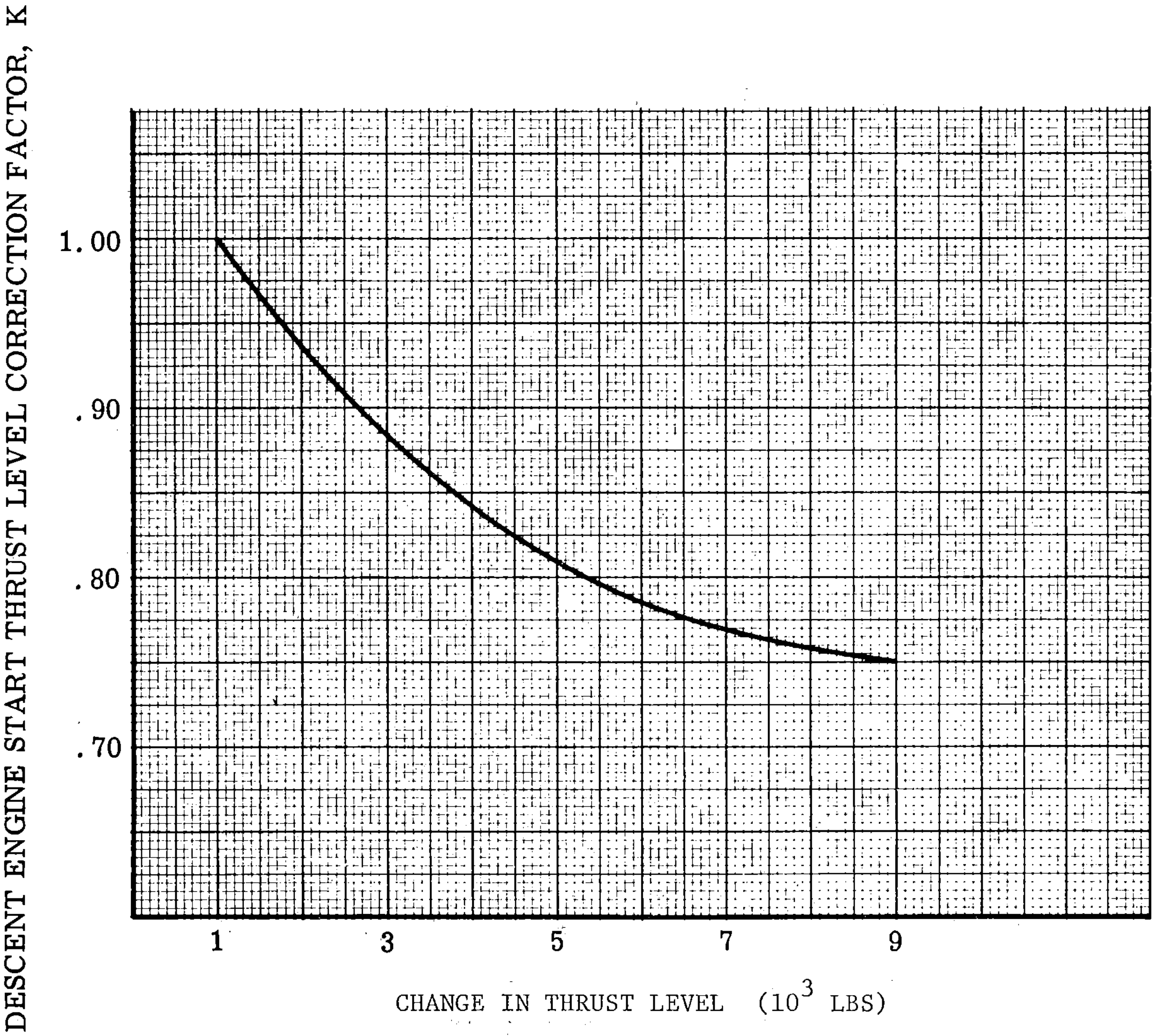

Figure 4.8-19. Thrust Level Correction Factor vs Change In Descent Engine Thrust Level (See Para. 4.8.1.4)

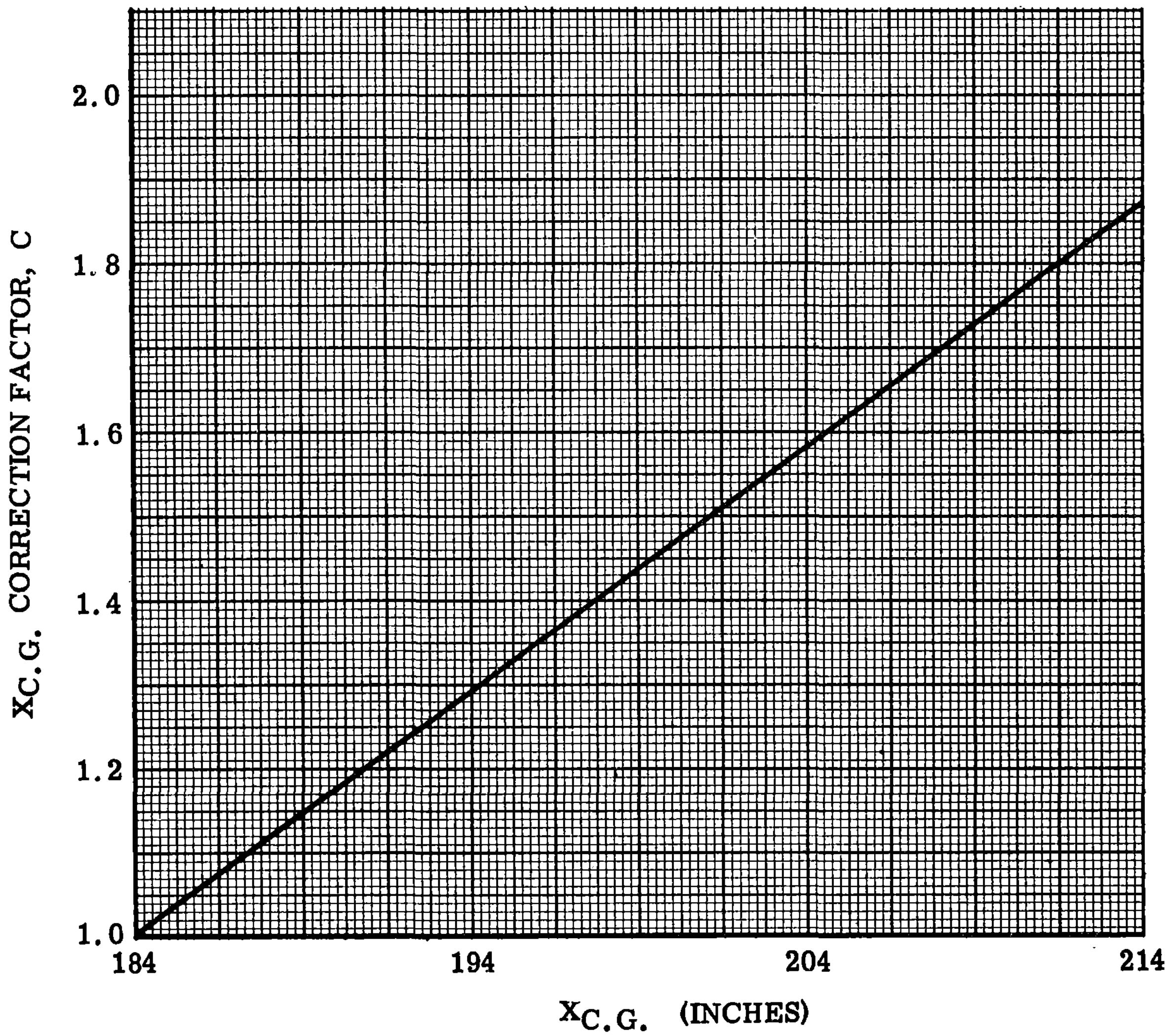

Figure 4.8-20. $X_{c.g.}$ Correction Factor vs X CG Location
(See Para. 4.8.1.4)

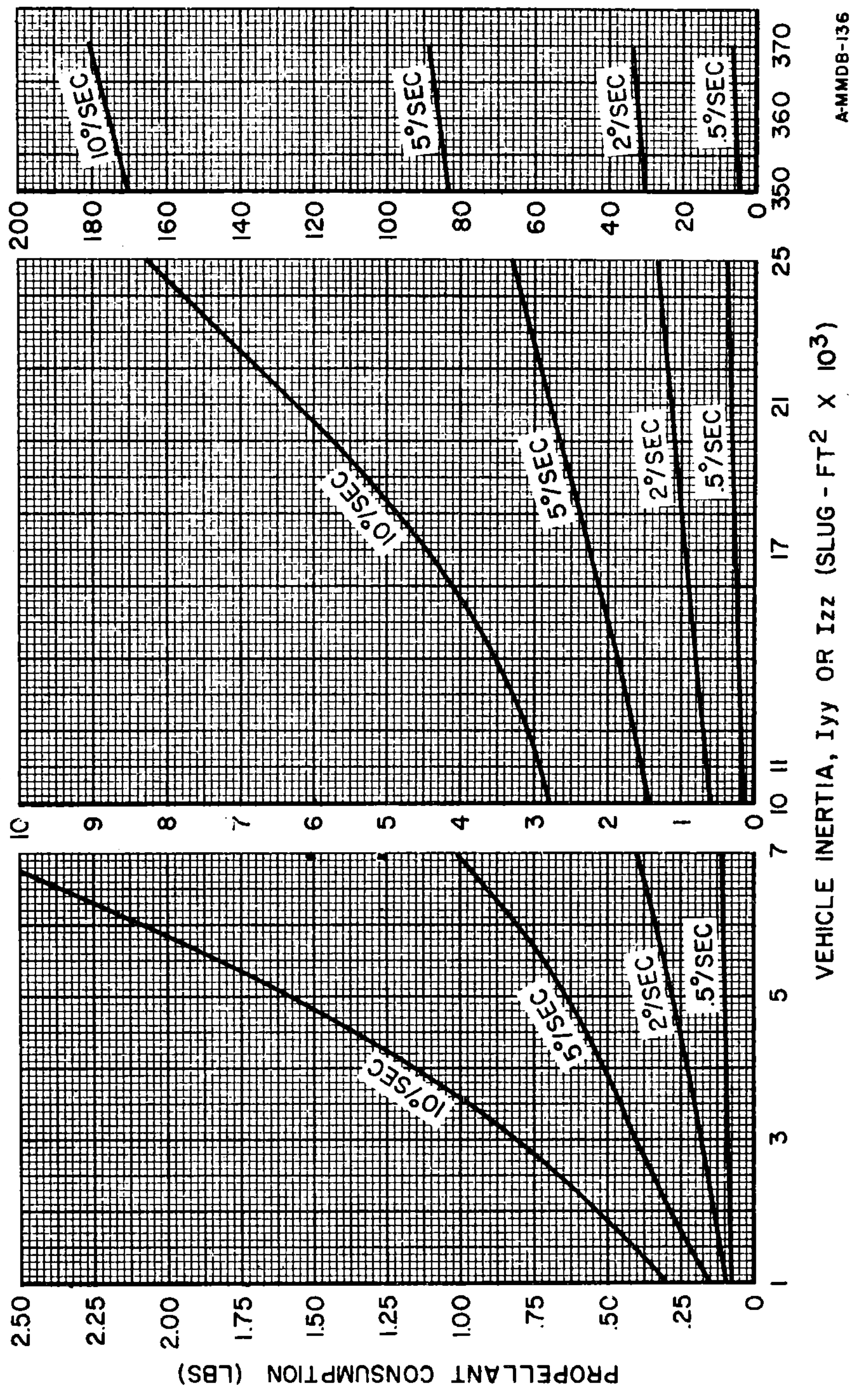

Figure 4.8-21. RCS Propellant for Rotations versus Vehicle Inertia, Pitch or Roll - Automatic Mode - AGS (See Paragraph 4.8.1.4)

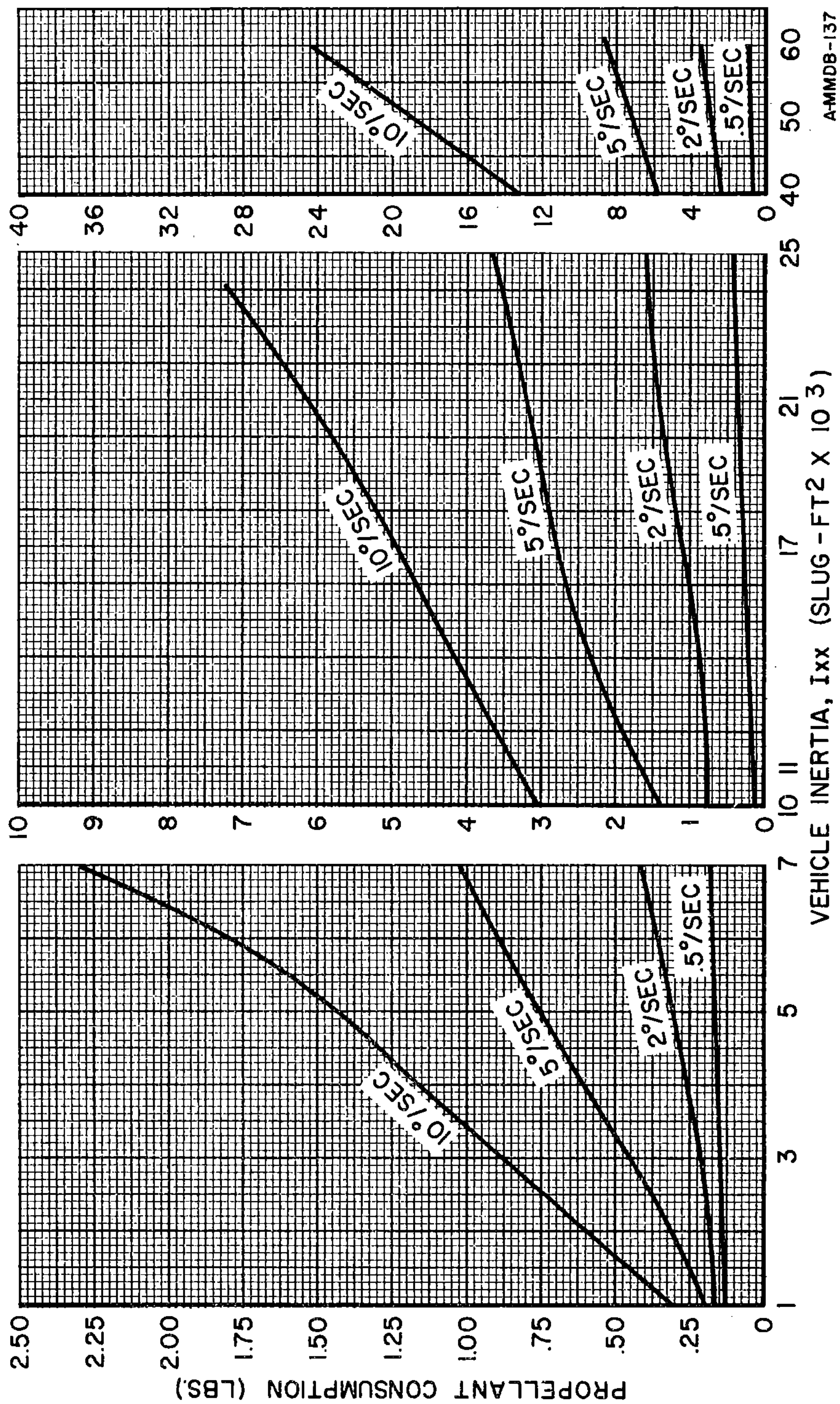

Figure 4.8-22. RCS Propellant for Rotation versus Vehicle Inertia, Yaw-Automatic Mode - AGS (See Paragraph 4.8.1.4)

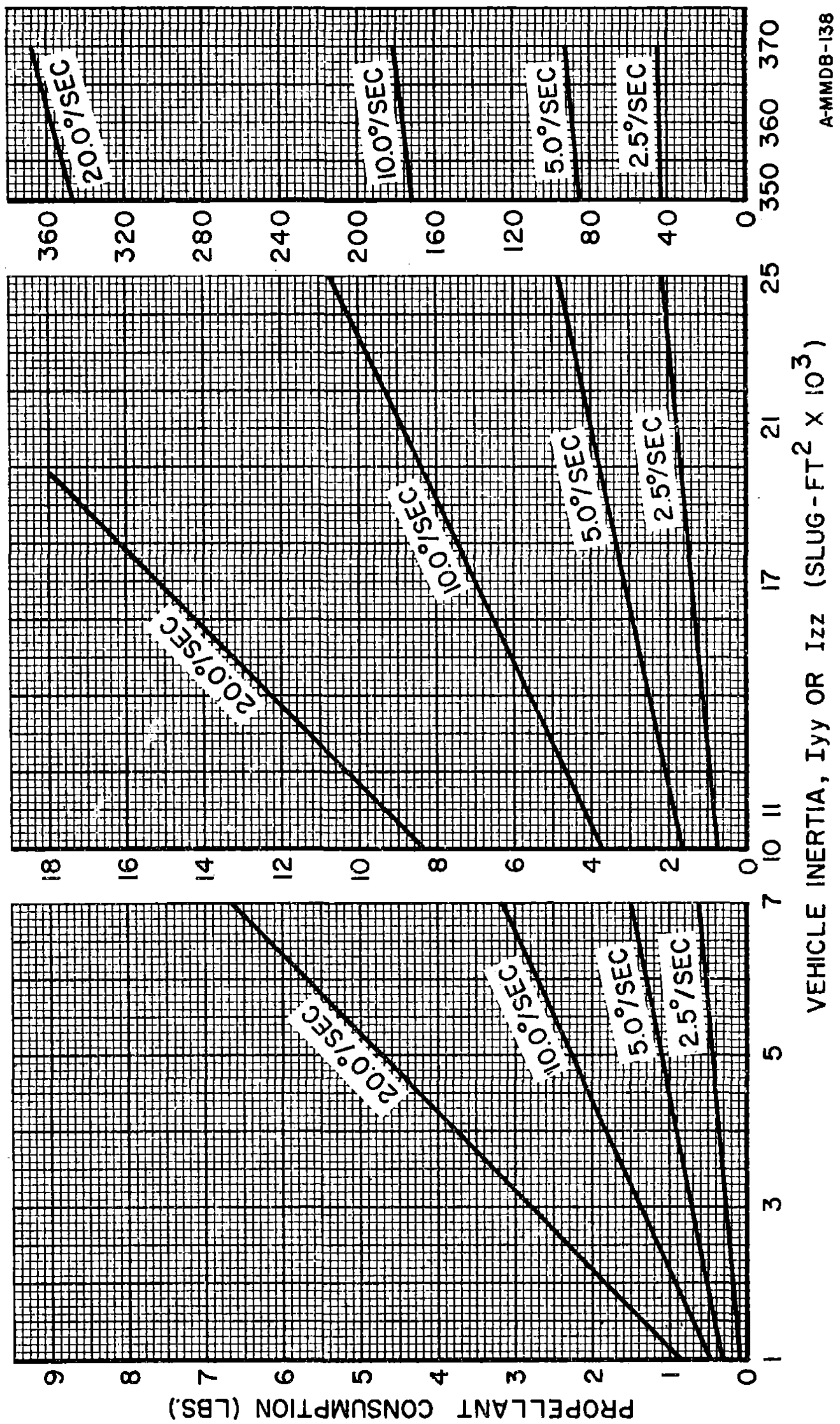

Figure 4.8-23. RCS Propellant for Rotation versus Vehicle Inertia, Pitch or Roll Rate Command/Attitude Hold Mode - AGS (See Paragraph 4.8.1.4)

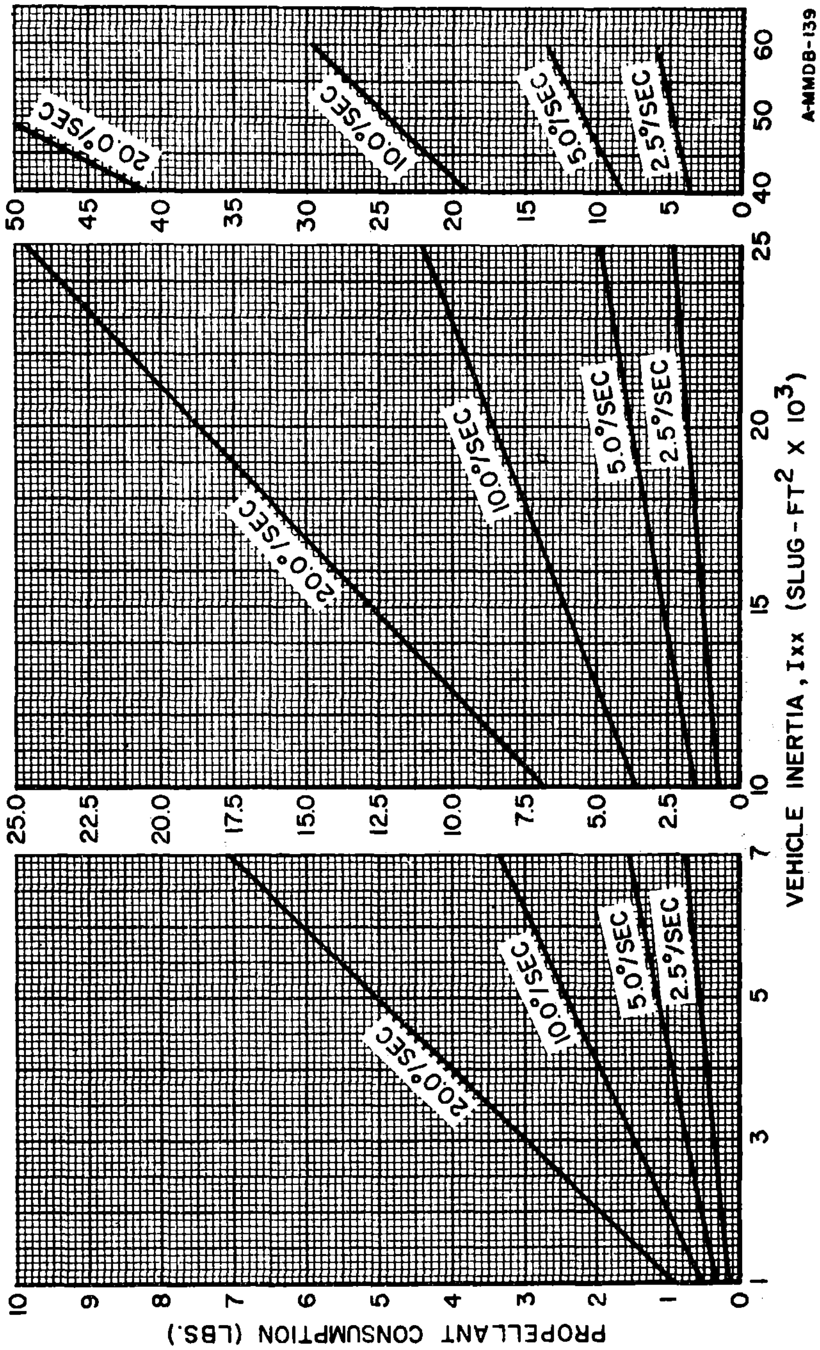

Figure 4.8-24. RCS Propellant for Rotation versus Vehicle Inertia Yaw-Rate Command/Attitude Hold Mode - AGS (See Paragraph 4.8.1.4)

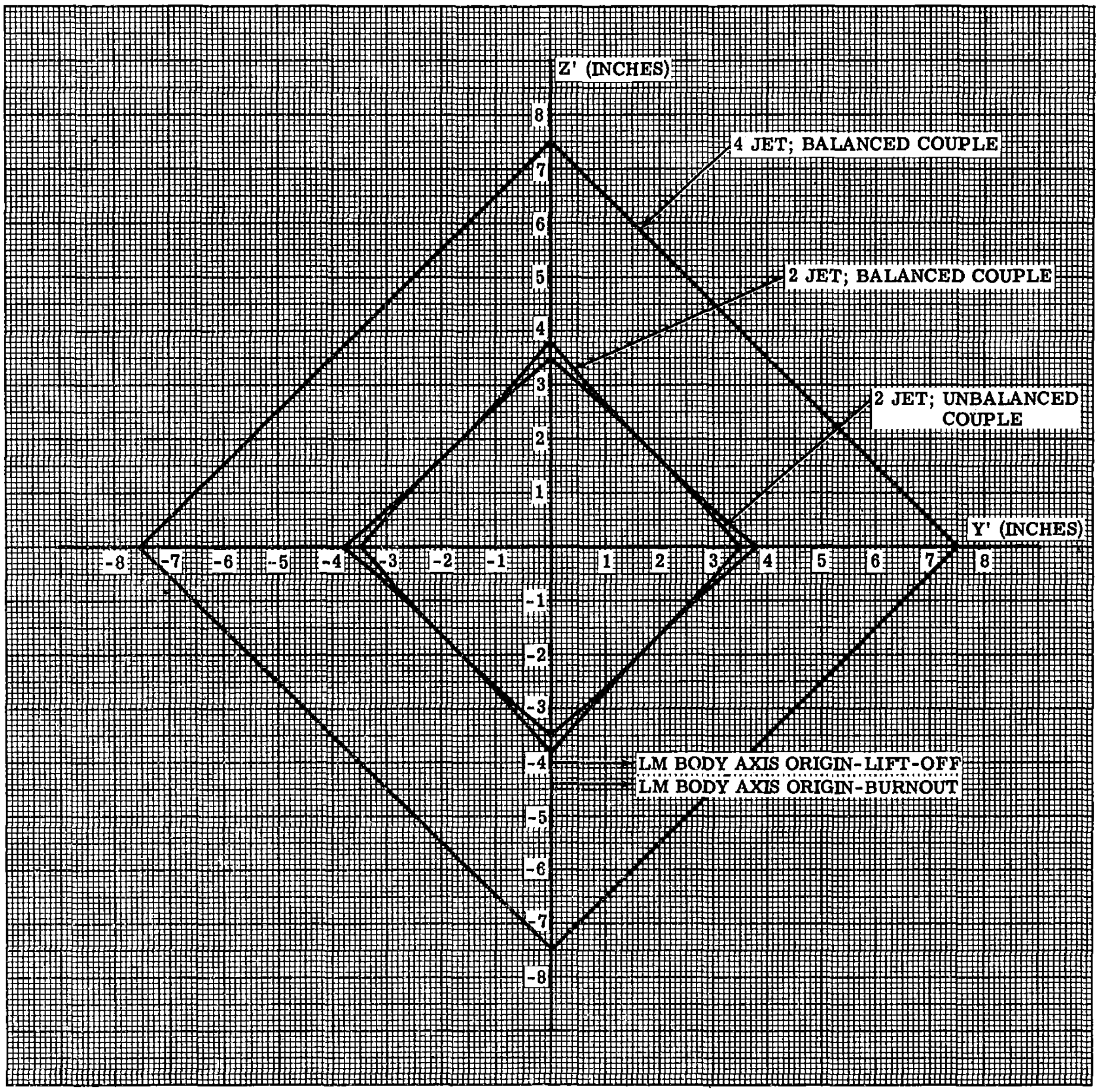

Figure 4.8-25. Nominal Limits on Ascent Y and Z C.G. Location for LM Controllability (Ascent Engine Canted -1.5^{o})
(See Para. 4.8.1.4)

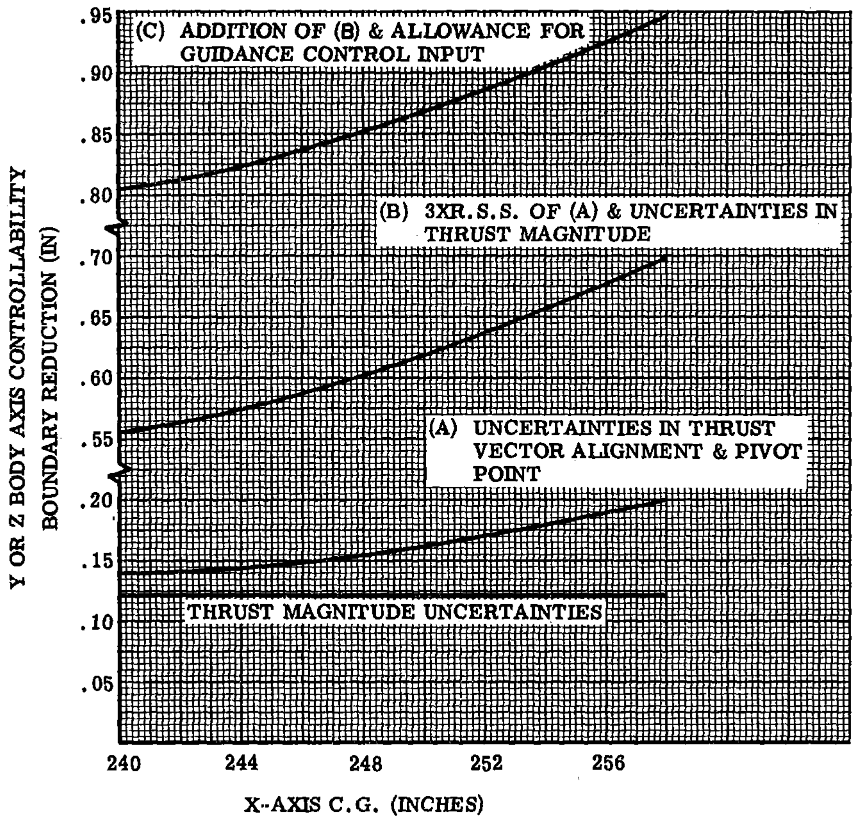

Figure 4.8-26. Reduction in Controllability Boundary Due to RCS and APS Thrust Vector and Alignment Uncertainties vs X C.G. Location (See Para. 4.8.1.4)

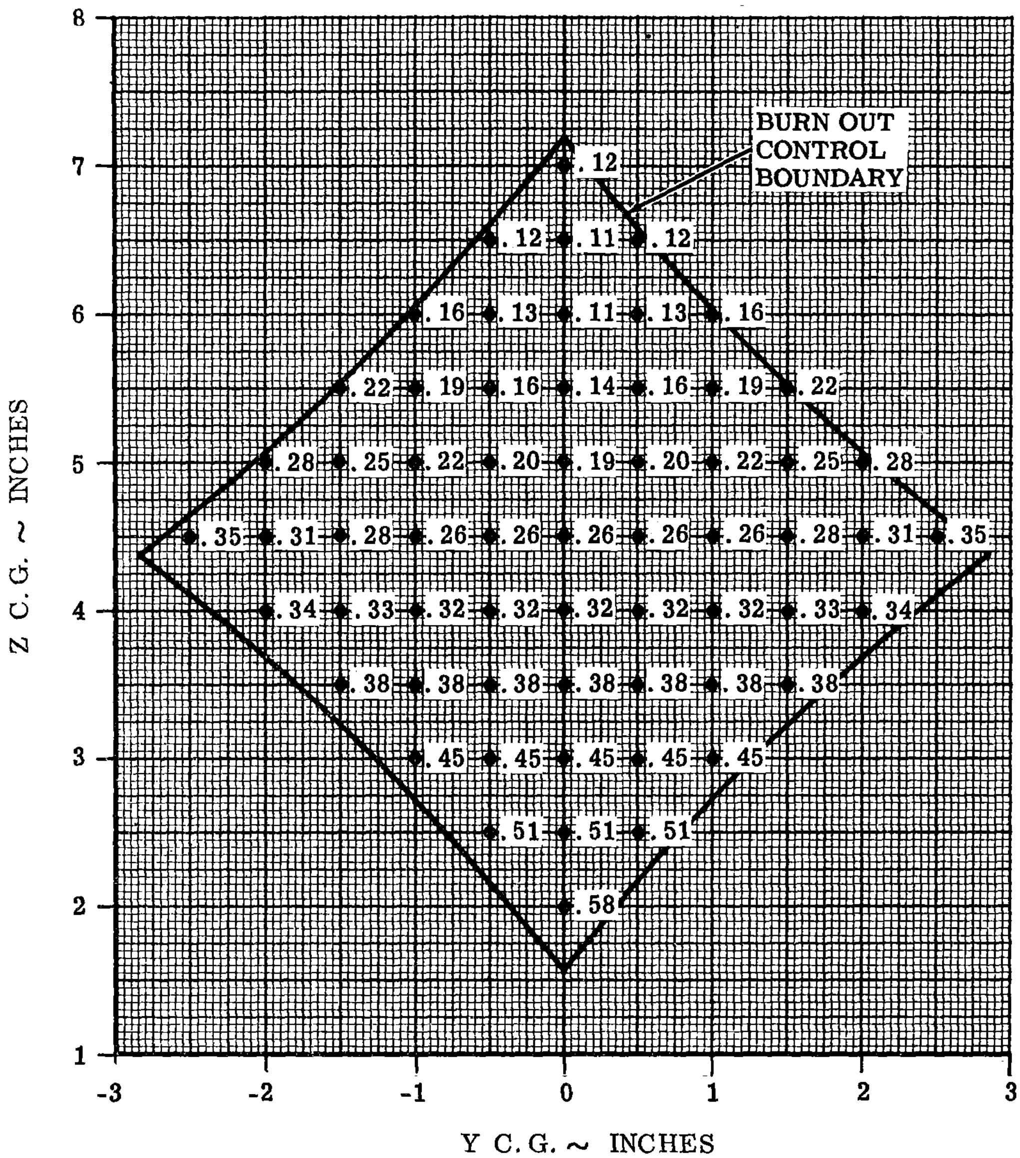

Figure 4.8-27. **RCS Propellant Flow Rate (lb/sec) for Moment Control versus Dry Vehicle C.G.** (See Para. 4.8.1.4)

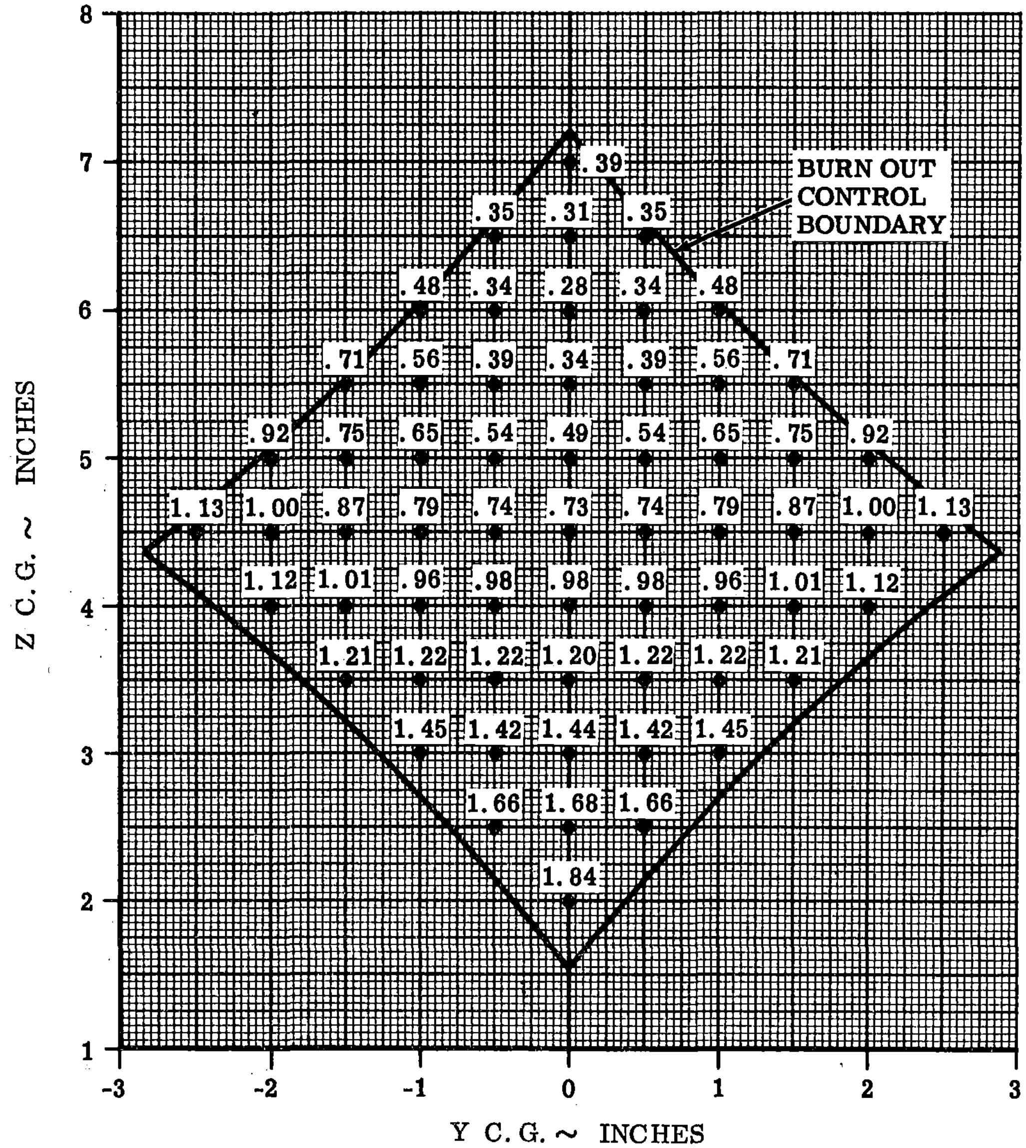

Figure 4.8-28. **Delta APS/RCS Specific Impulse (seconds) During Moment Control versus Dry Vehicle C.G.** (See Para. 4.8.1.4)

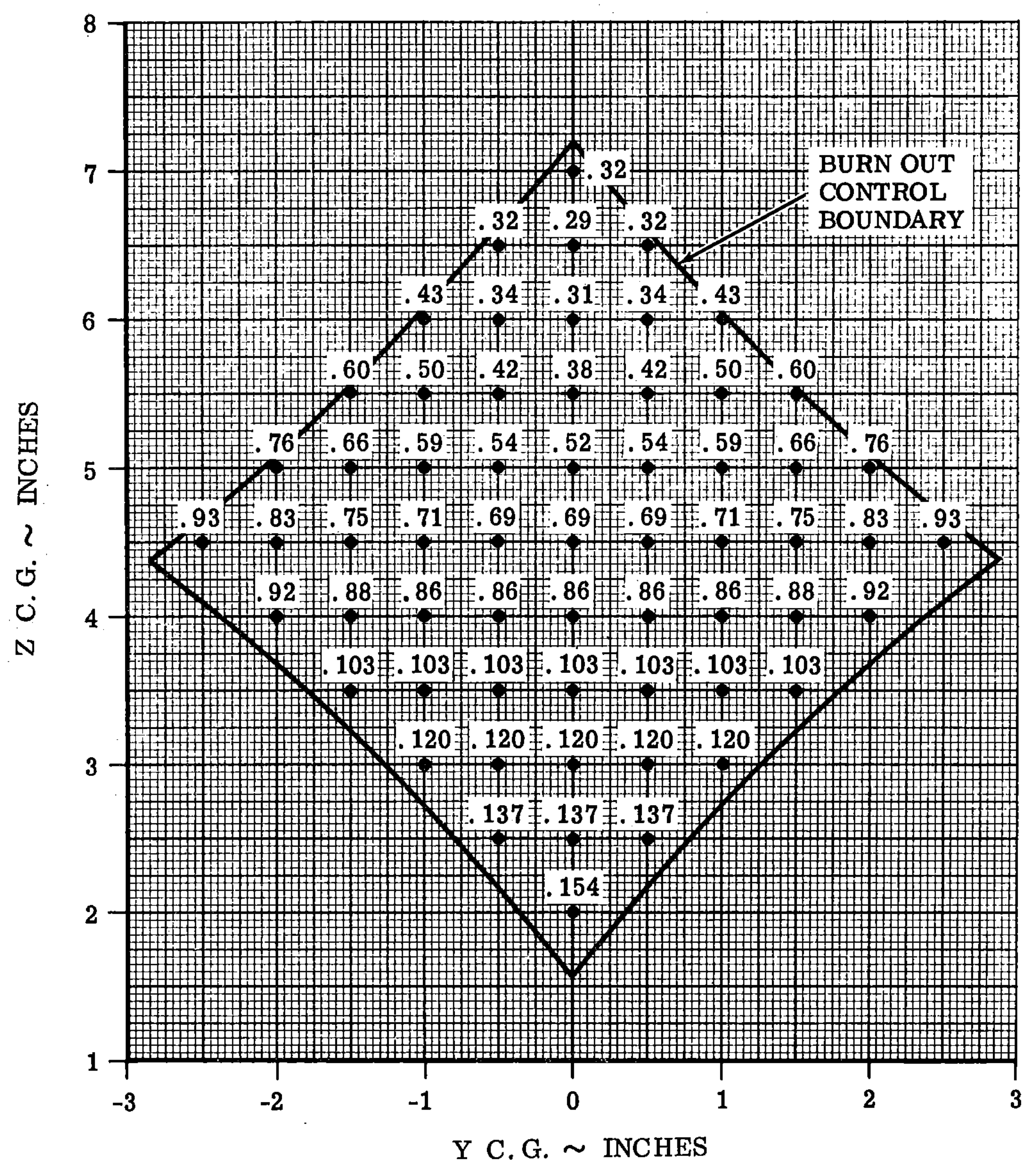

Figure 4.8-29. **Effective RCS Thrust (lbs) During Moment Control versus Dry Vehicle C.G.** (See Para. 4.8.1.4

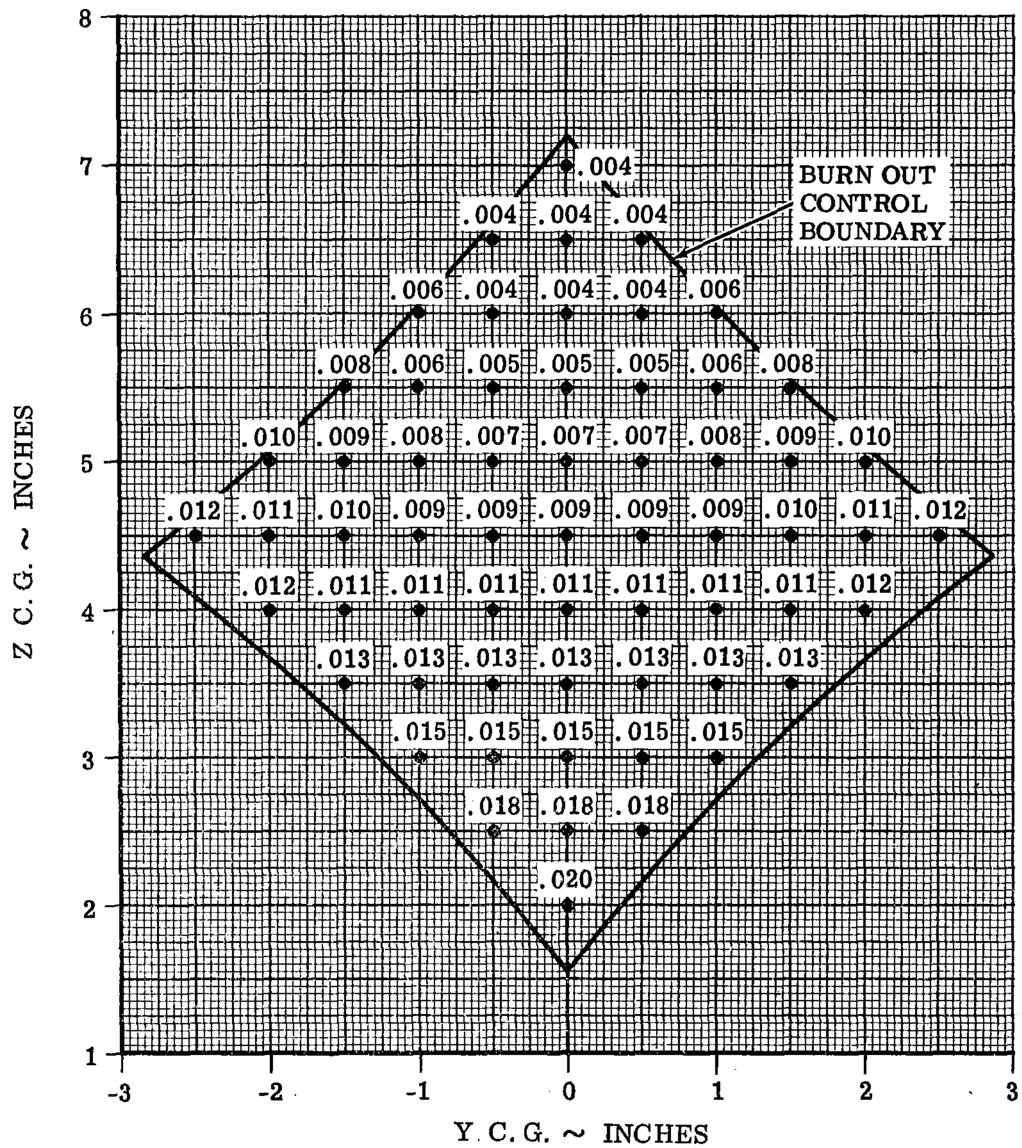

Figure 4.8-30. Delta Integrated APS/RCS Mixture Ratio During Moment Control versus Dry Vehicle C. G. (See Para. 4.8.1.4)

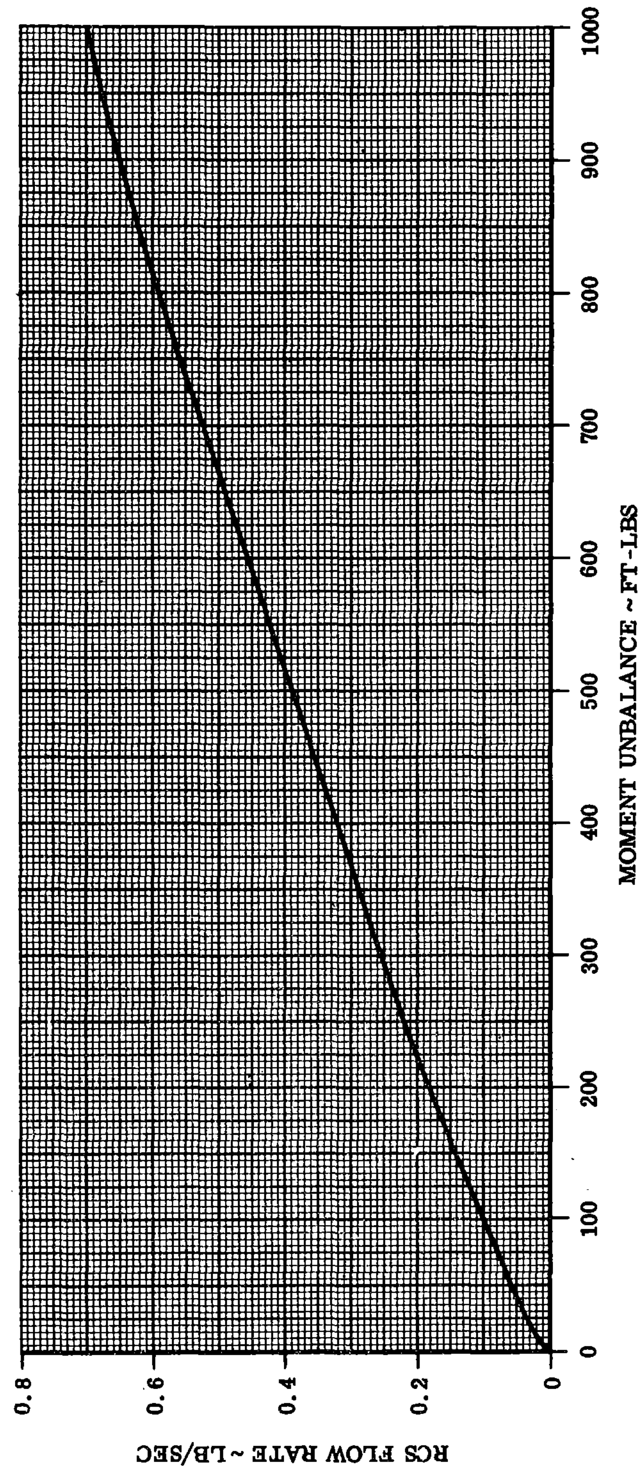

Figure 4.8-31. RCS Flow Rate versus Moment Unbalance
(See Para. 4.8.1.4)

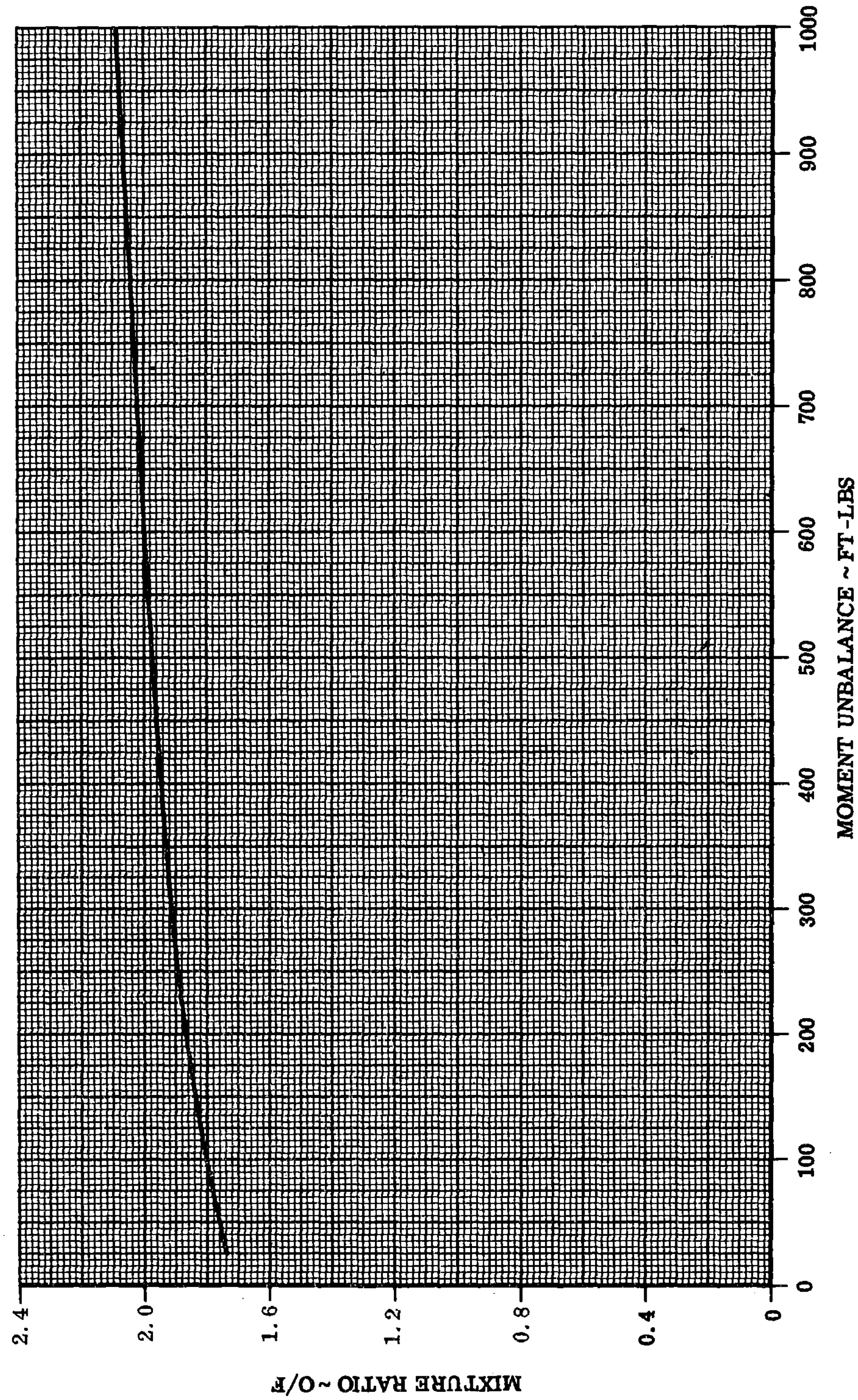

Figure 4.8-32. RCS Mixture Ratio versus Moment Unbalance
(See Para. 4.8.1.4)

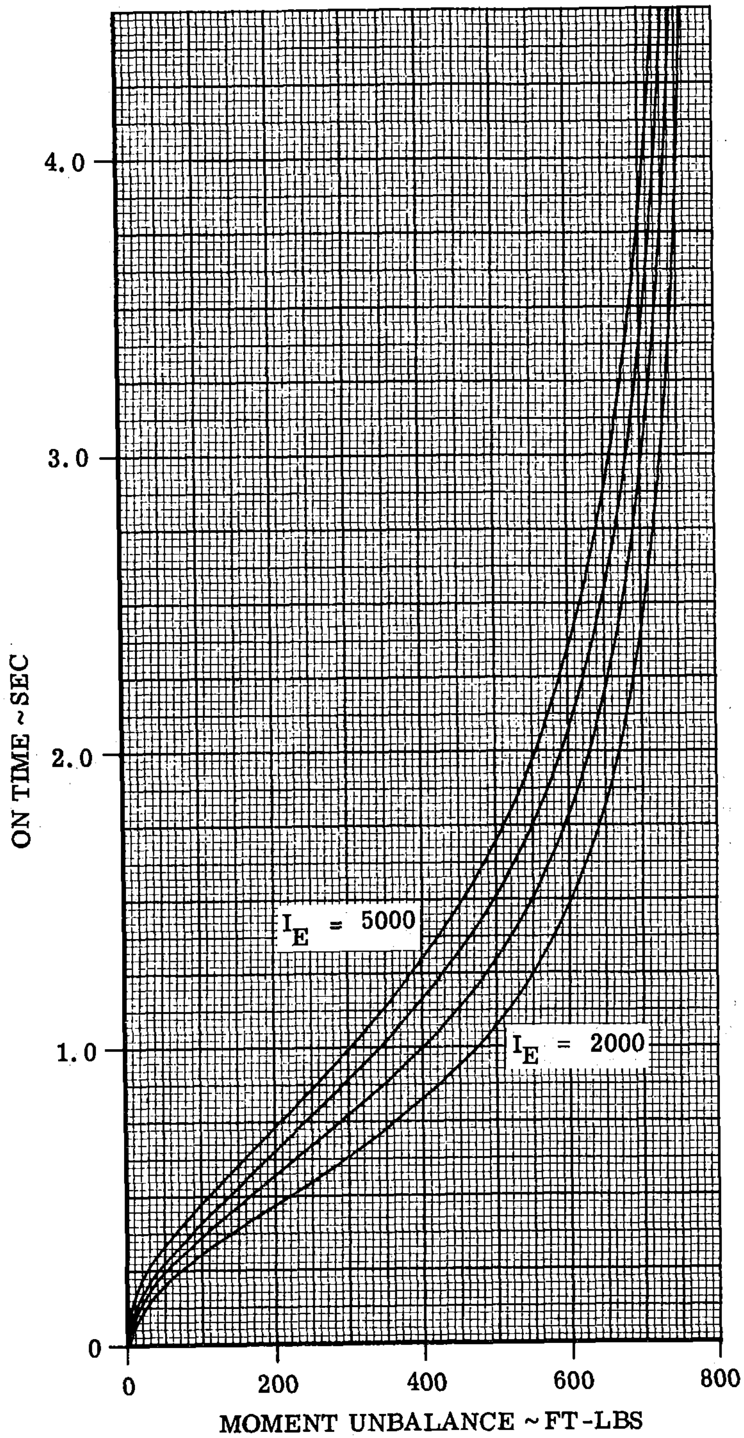

Figure 4.8-33. "On" Time versus Moment Unbalance
(See Para. 4.8.1.4)

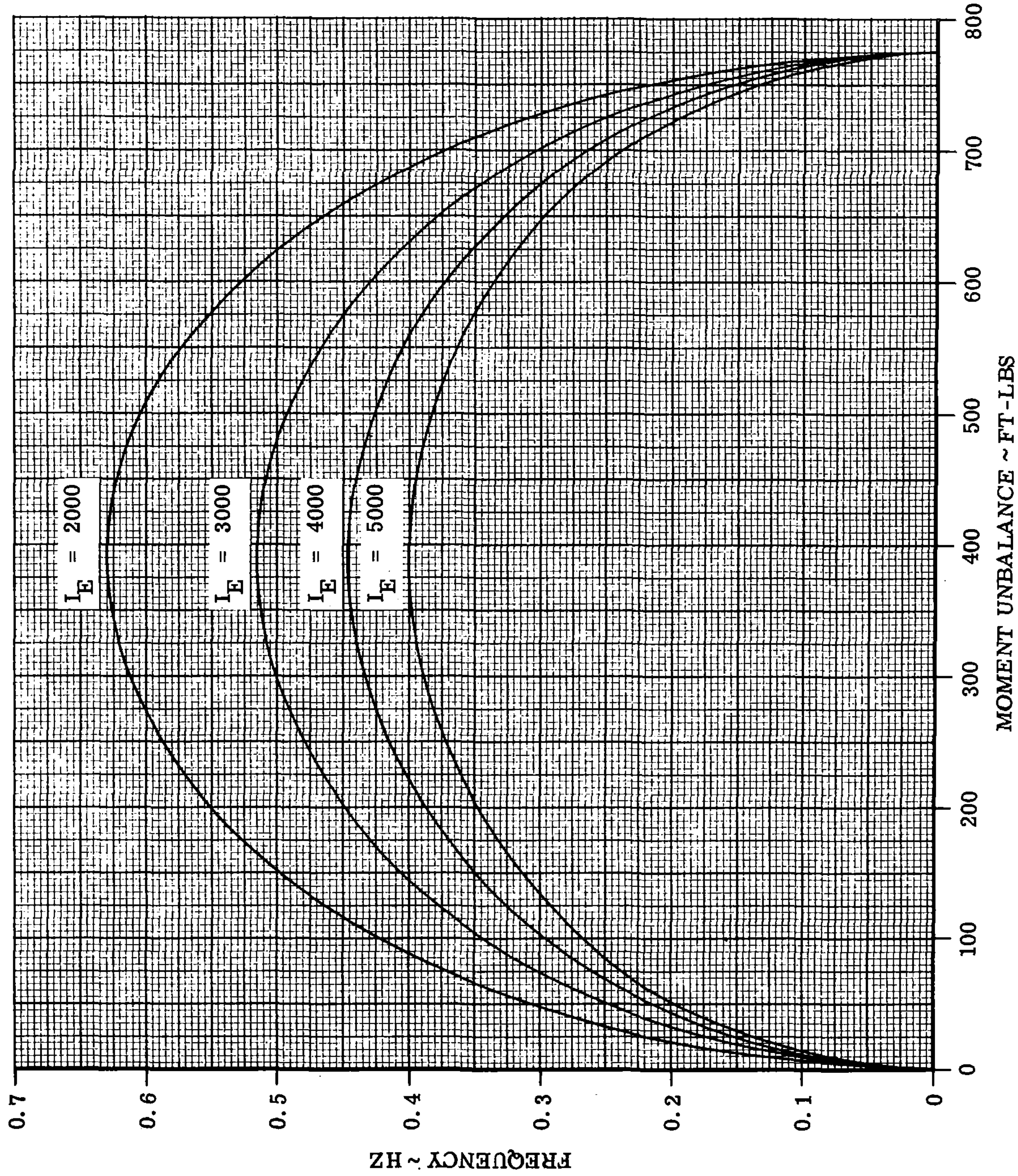

Figure 4.8-34. **Frequency versus Moment Unbalance**
(See Para. 4.8.1.4)

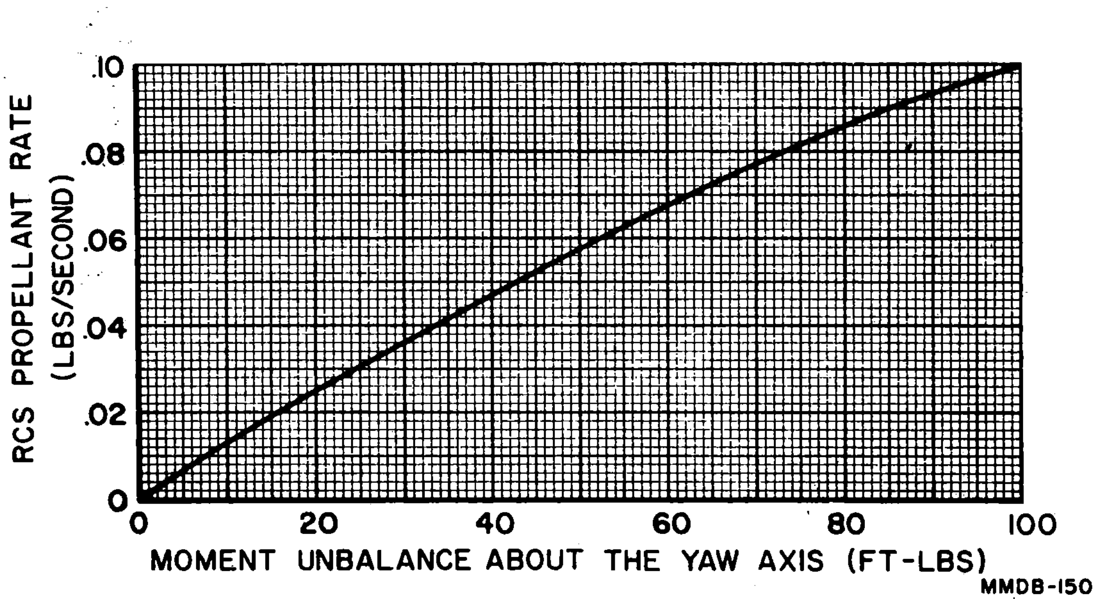

Figure 4.8-35. RCS Propellant Usage versus Yaw Moment Unbalance
(See Paragraph 4.8.1.4)

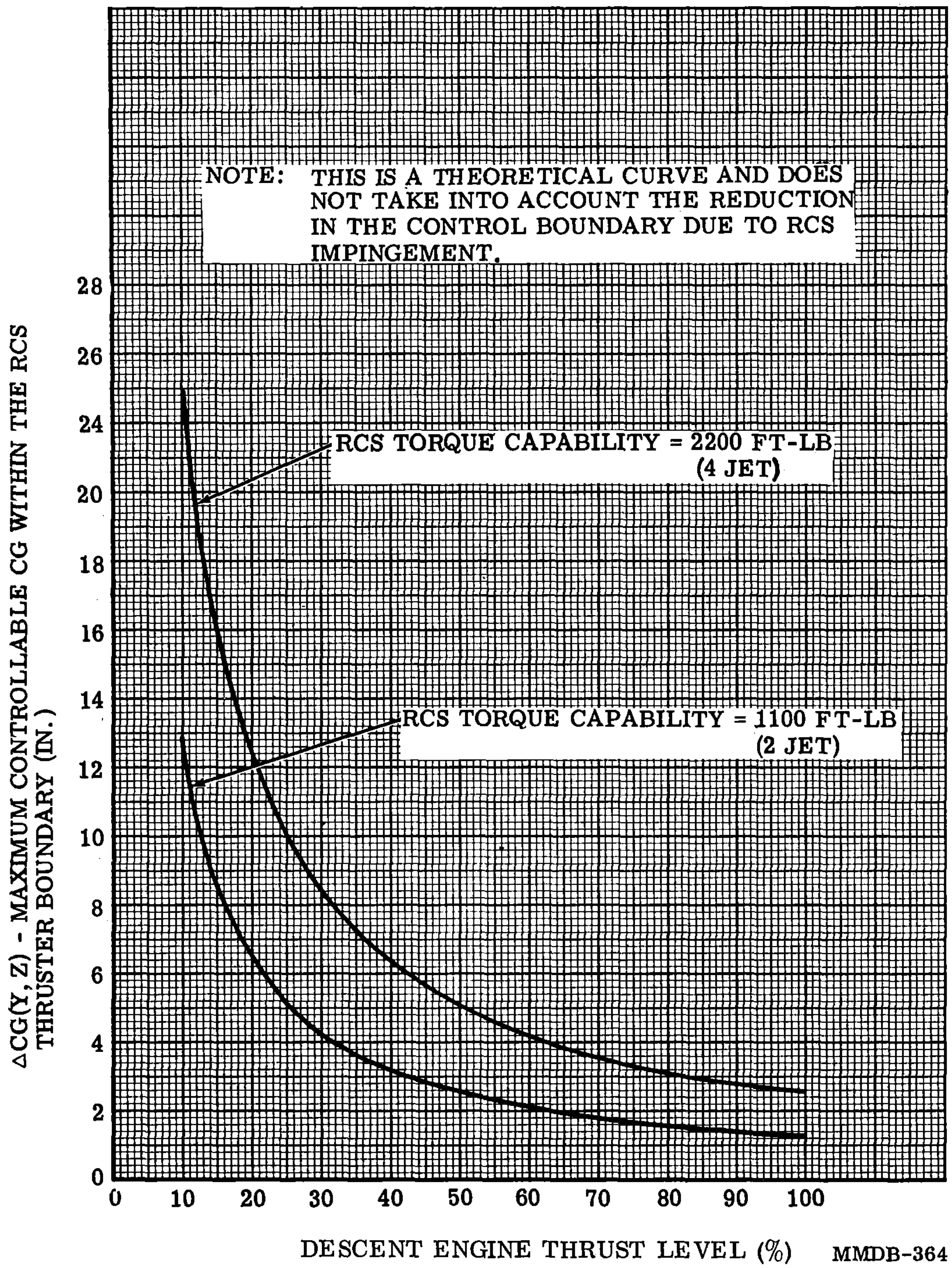

Figure 4.8-36. Maximum Controllable C.G. in the Y-Z Plane vs Descent Engine Thrust Level (2 or 4 Jet Control) (See Para. 4.8.1.5.1.1)

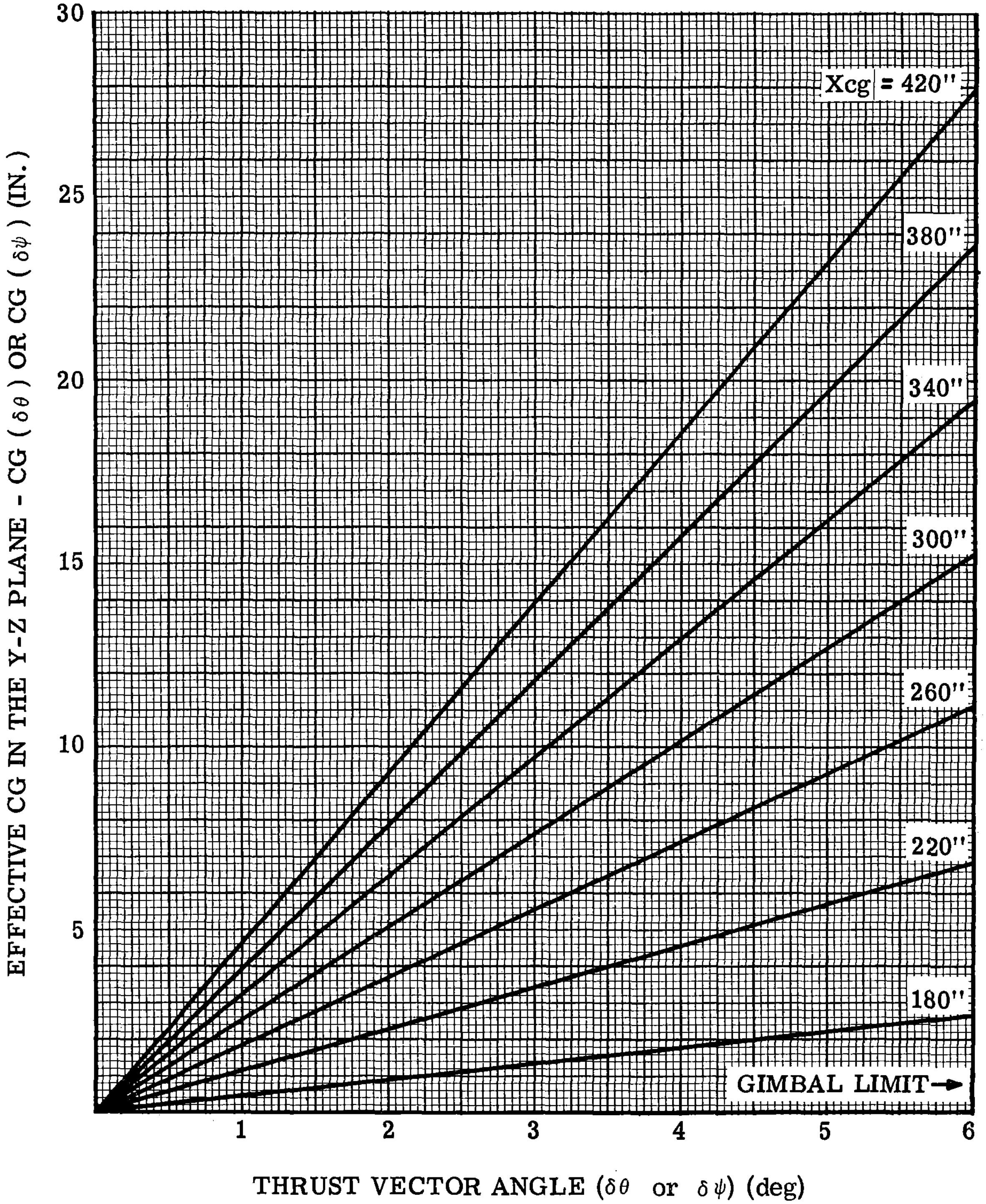

Figure 4.8-37. Effective CG (Y, Z) as a Function of Thrust Vector Angle ($\delta\theta$, $\delta\psi$) at Various Xcg Locations (Unstaged, Docked, Undocked) (See Para. 4.8.1.5.1.1)

$Tu = (U_F \times \sqrt{W_T})$

PLUS 0.5 SEC FOR ENGINE OVERLAP
WHERE -
T_U = PROPELLANT SETTLING TIME ~ SEC
W_T = TOTAL VEHICLE WT ~ LBS
U_F = ULLAGE FACTOR

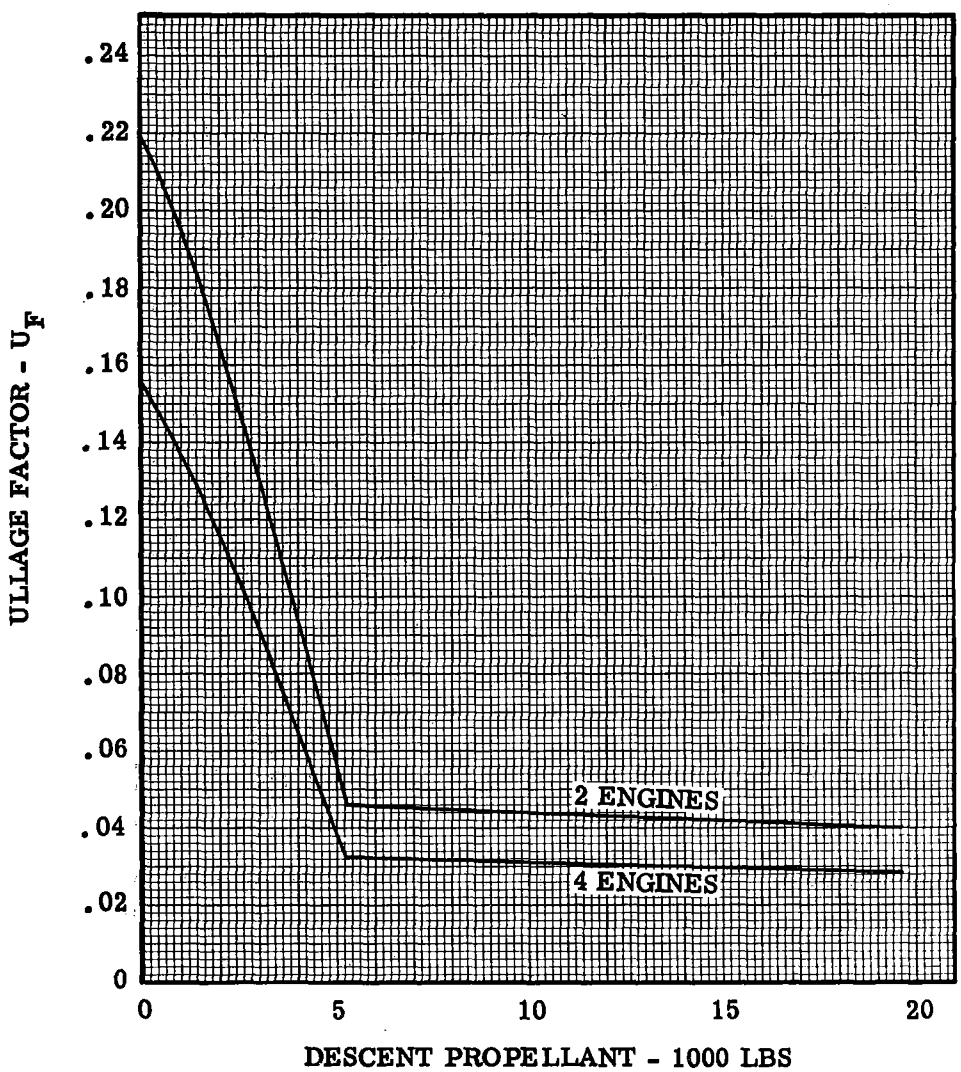

Figure 4.8-38. Descent Propellant Settling Time
(See Para. 4.8.2)

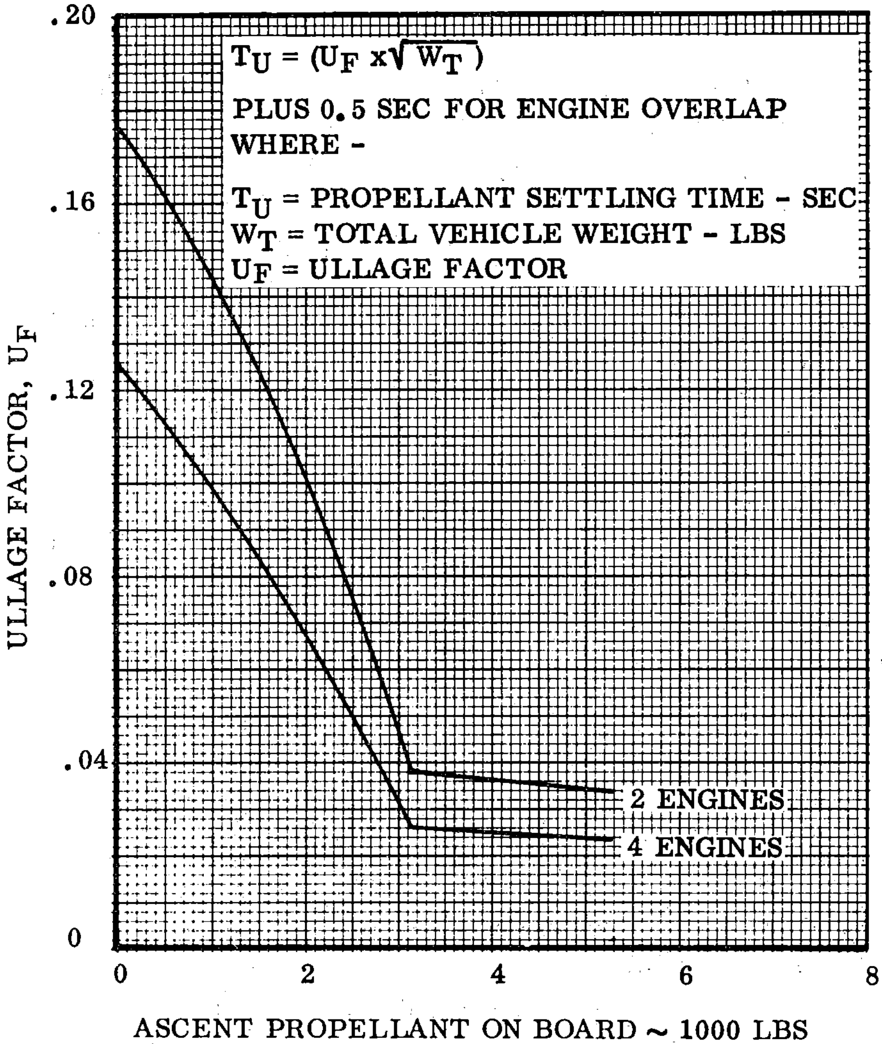

Figure 4.8-39. Ascent Propellant Settling Time Information (See paragraph 4.8.2)

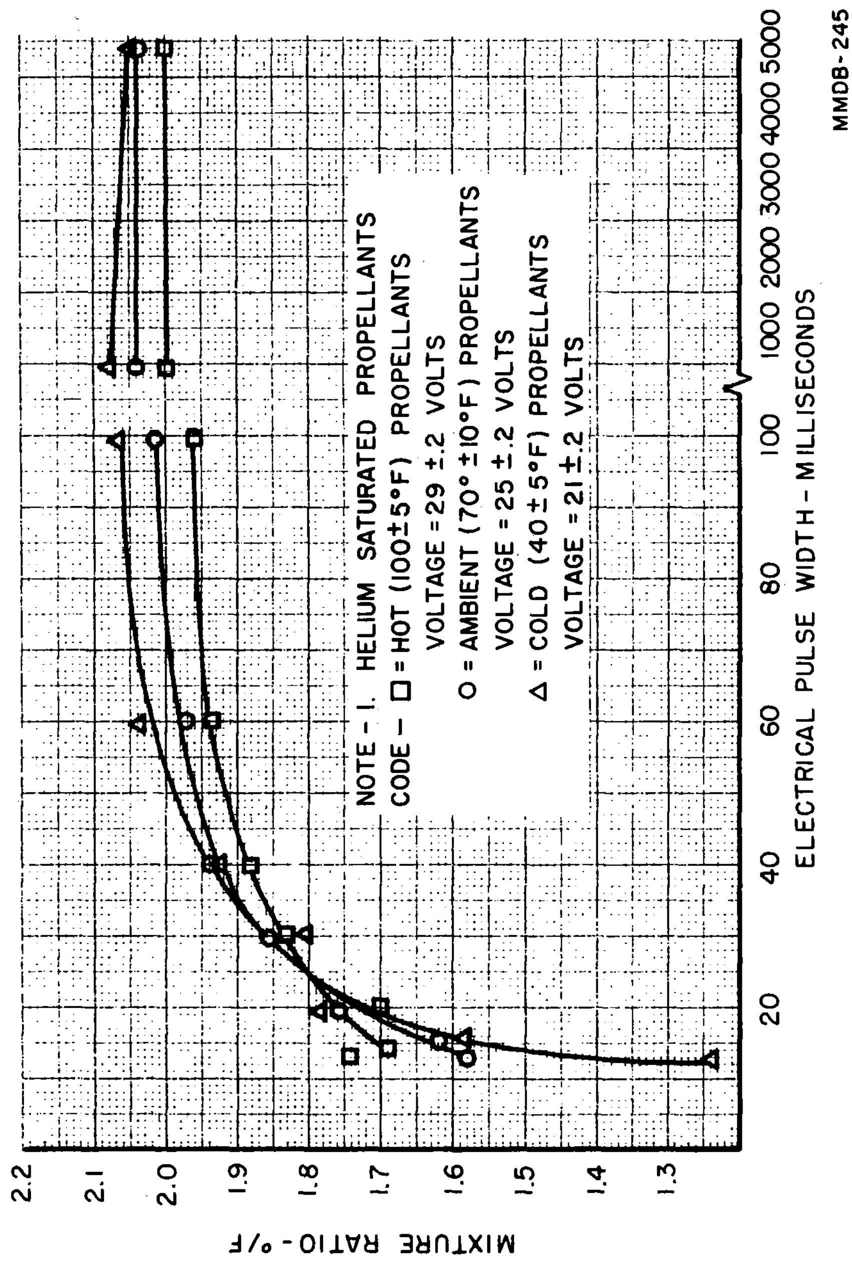

Figure 4.8-40. Reaction Control Jets Mixture Ratio versus Electrical Pulse Width (See Paragraph 4.8.4)

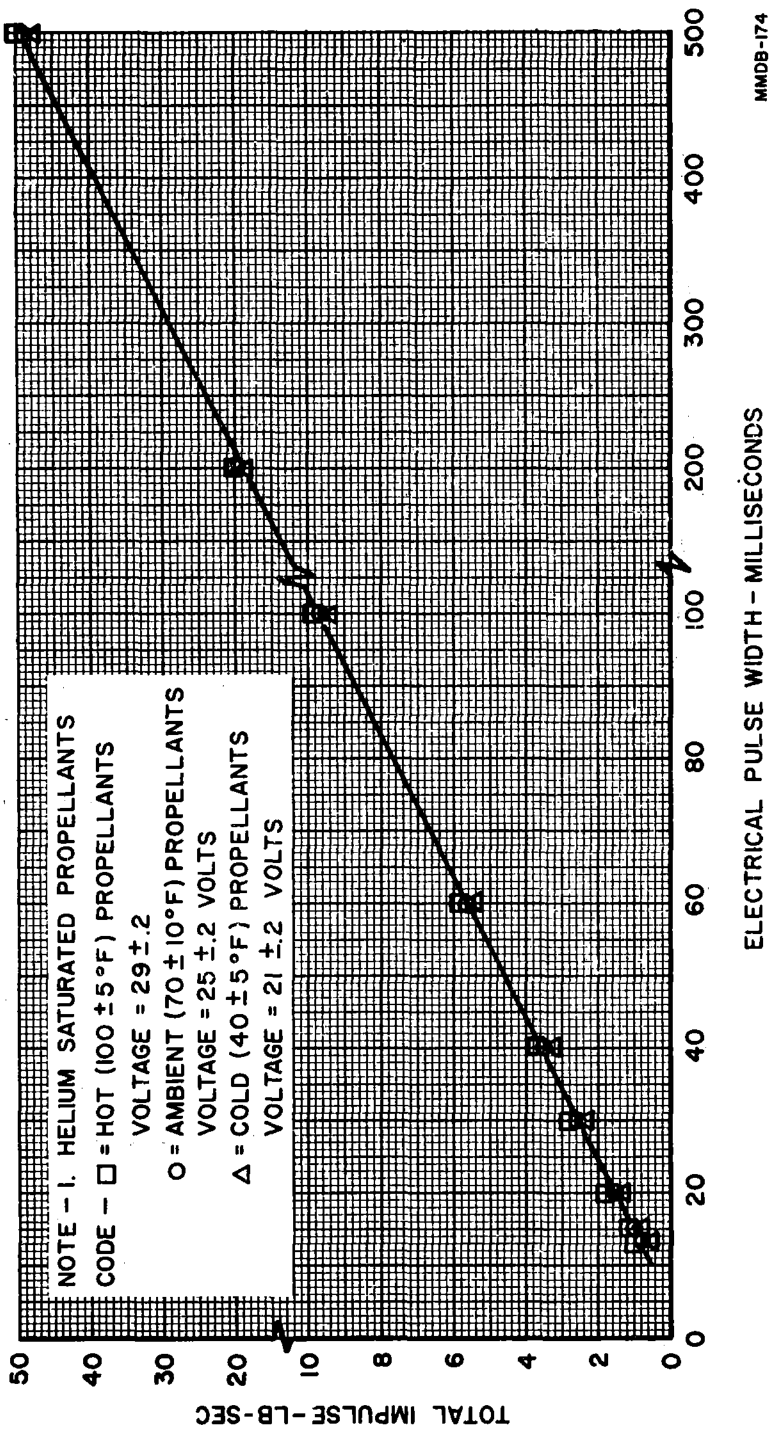

Figure 4.8-41. Reaction Control Jets: Total Impulse versus Electrical Pulse Width (See Paragraph 4.8.4)

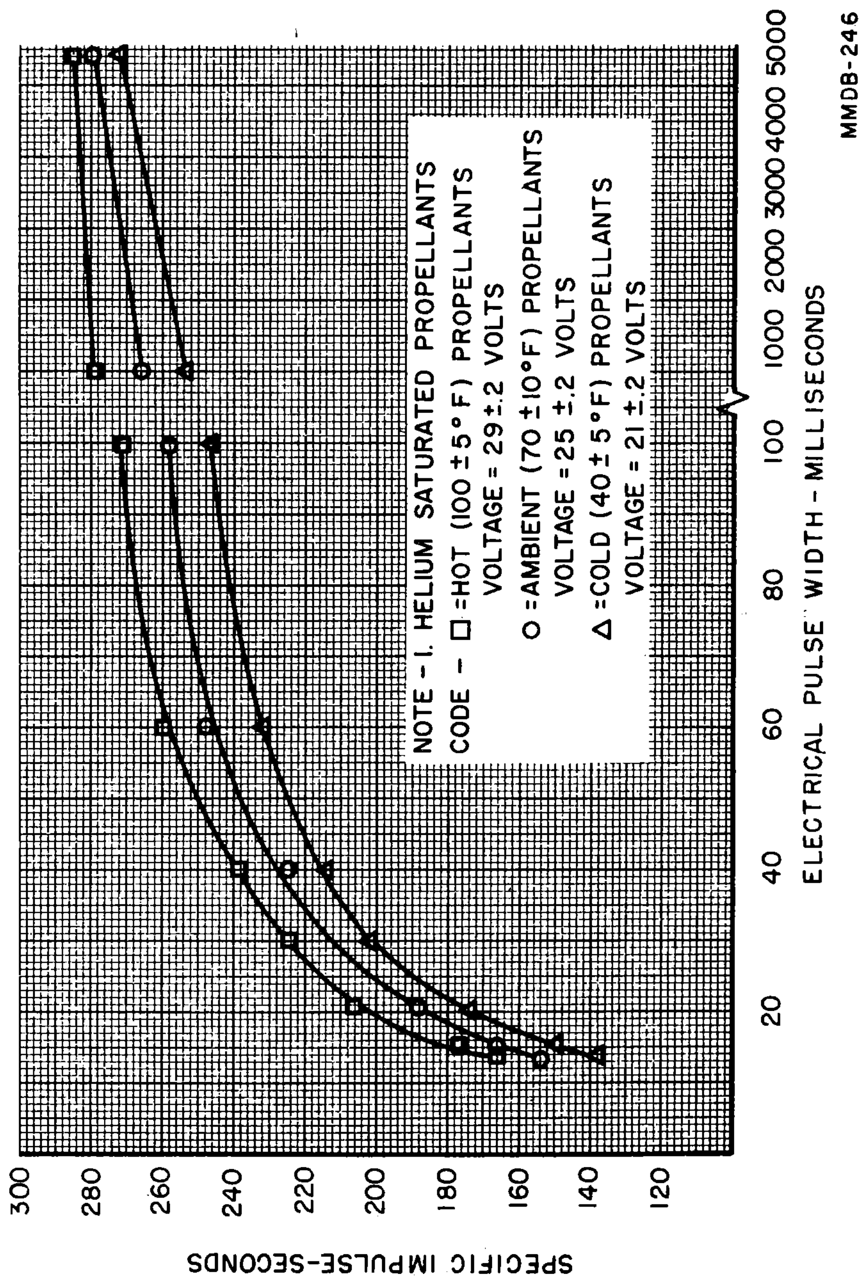

Figure 4.8-42. Reaction Control Jet Specific Impulse versus Electrical Pulse Width (See Paragraph 4.8.4)

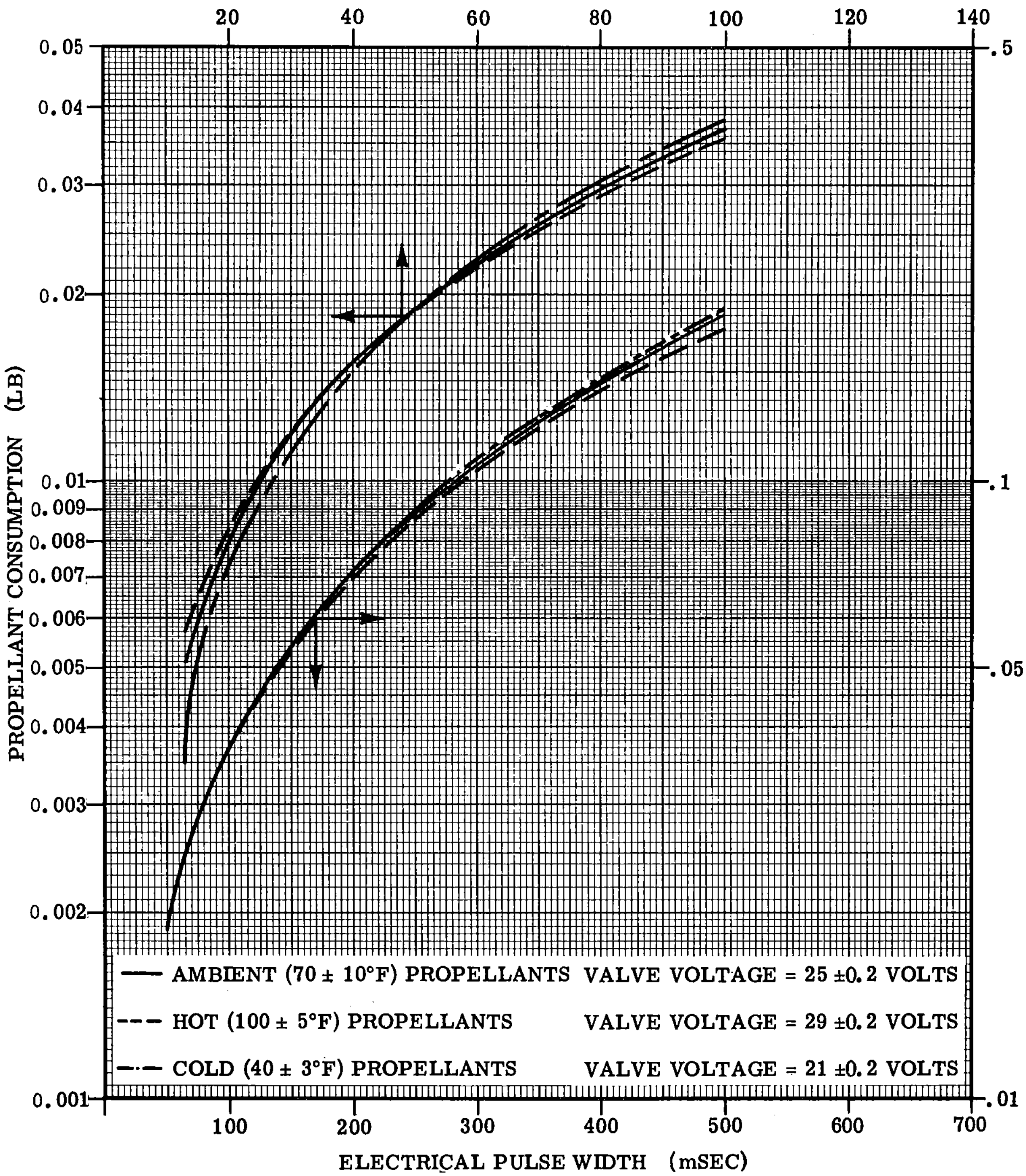

Figure 4.8-43. Propellant Consumption vs Electrical Pulse Width(Helium-Saturated Propellants) (See Para. 4.8.4)

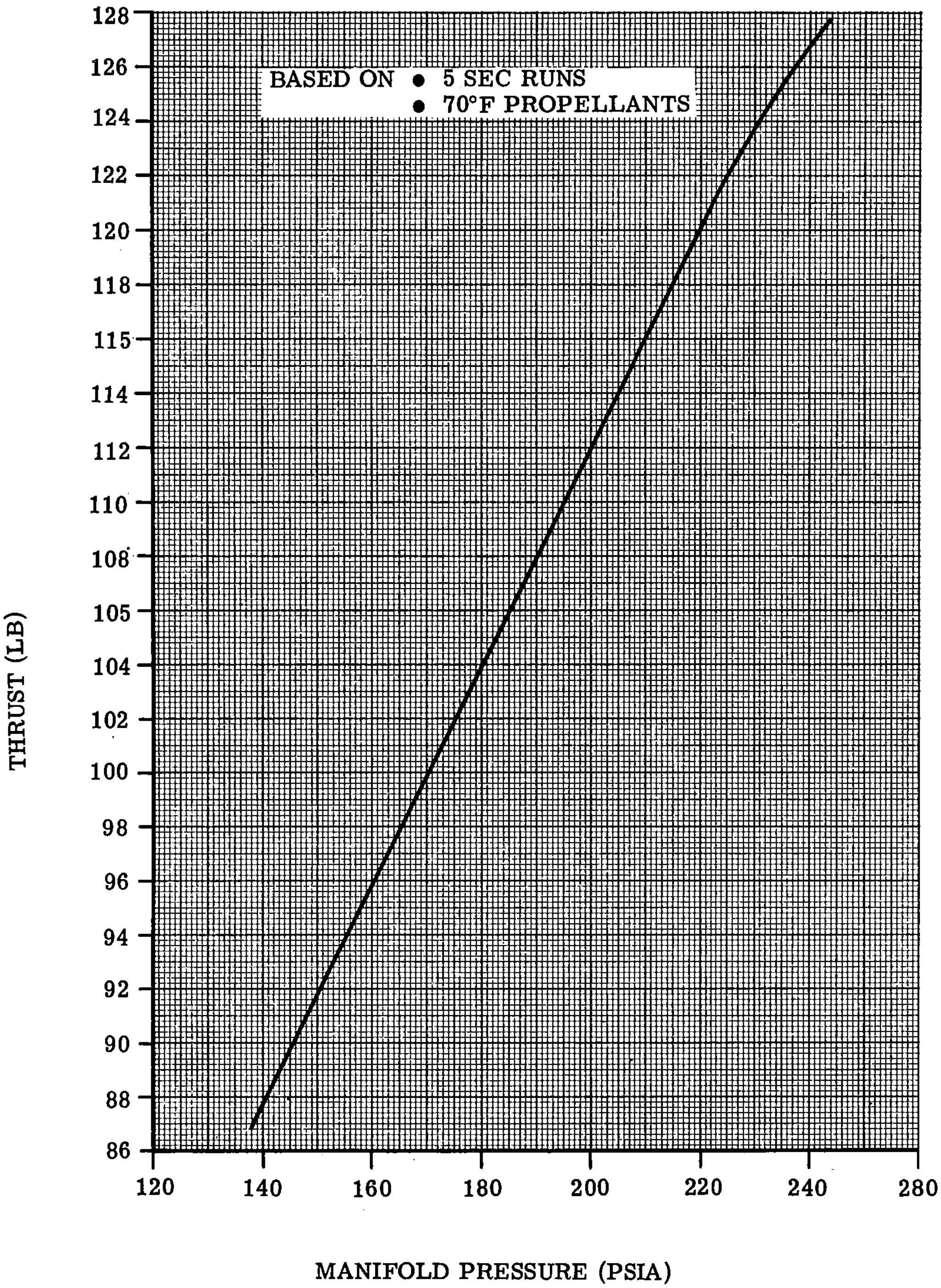

Figure 4.8-44. LM RCS Engine - Thrust vs Manifold Pressure
(See Para. 4.8.4)

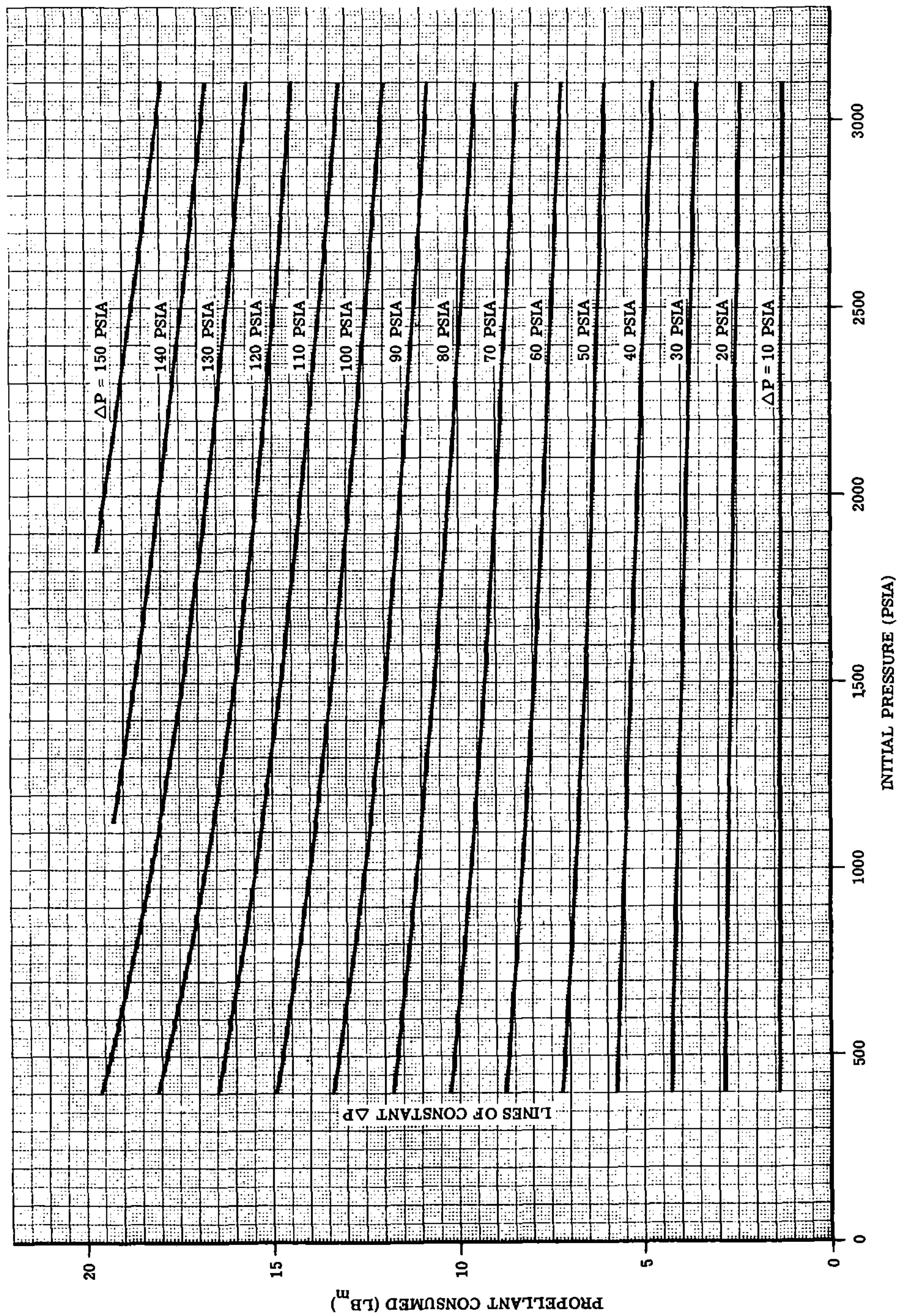

Figure 4.8-45. Effect of Propellant Consumption on Helium Tank ΔP for Selected Initial Helium Tank Pressures and Temperatures (Initial Helium Temperature = 20°F) (See Para. 4.8.4)

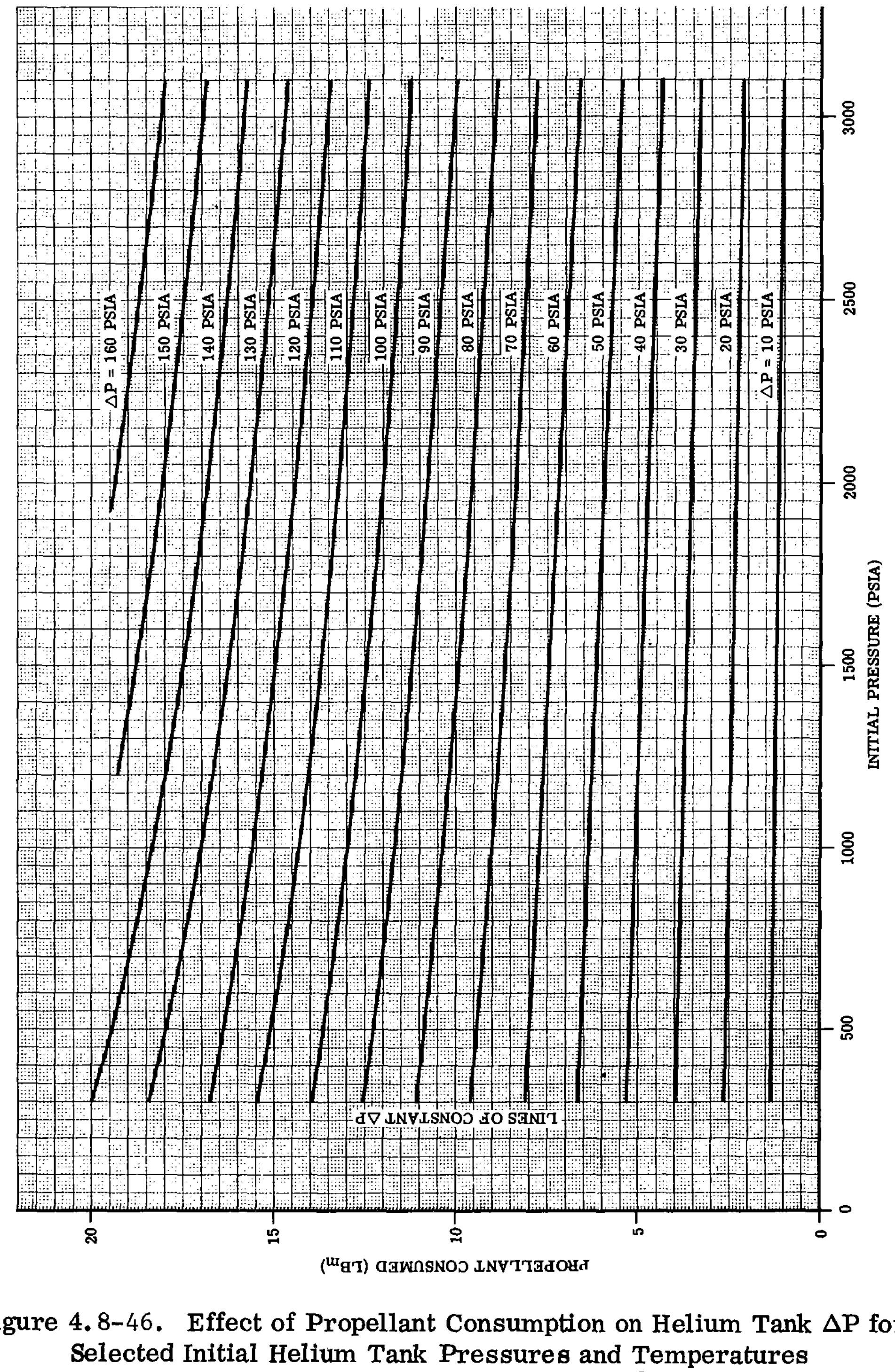

Figure 4.8-46. Effect of Propellant Consumption on Helium Tank ΔP for Selected Initial Helium Tank Pressures and Temperatures (Initial Helium Temperature = $60^{o}F$) (See Para. 4.8.4)

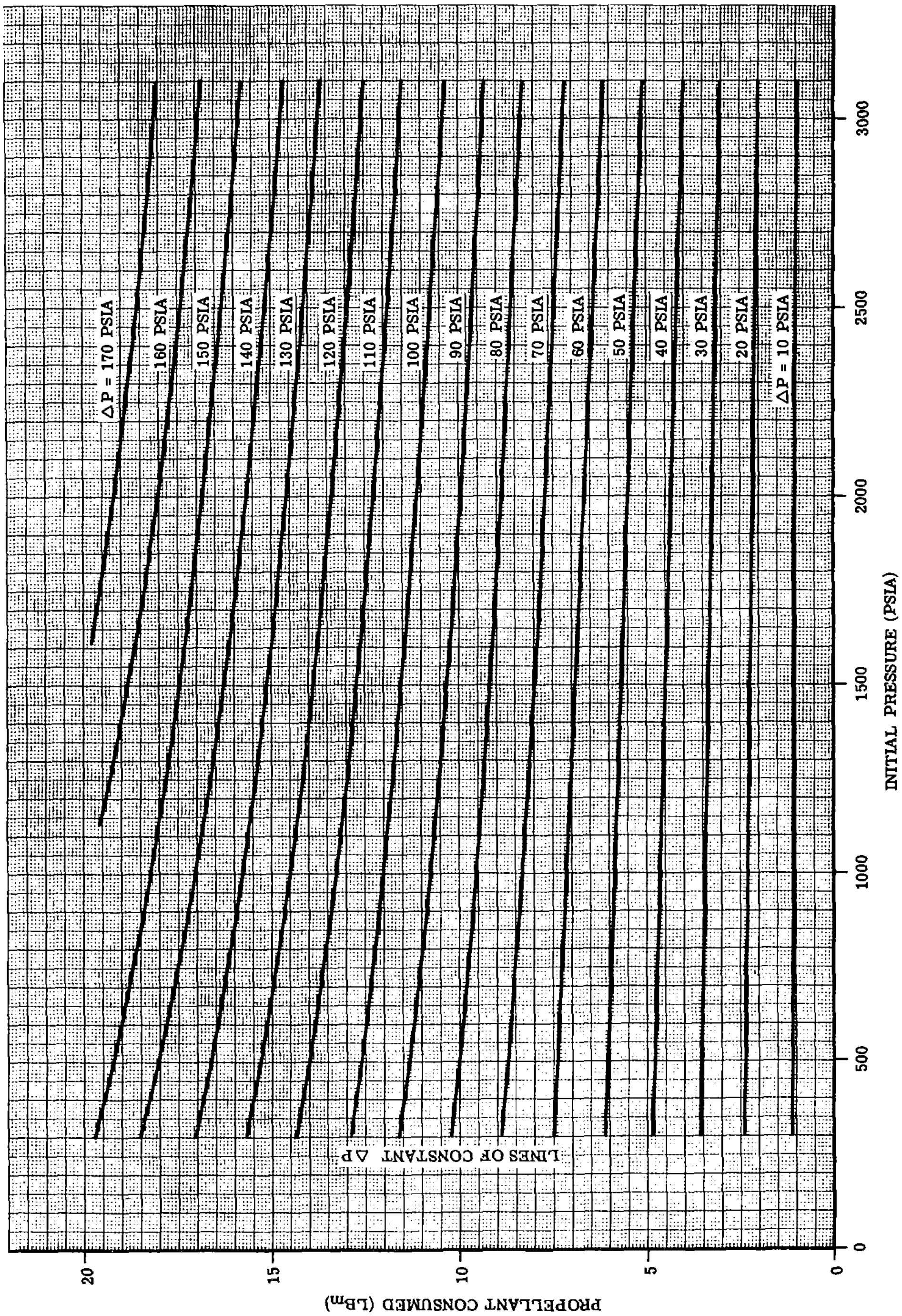

Figure 4.8-47. Effect of Propellant Consumption on Helium Tank ΔP for Selected Initial Helium Tank Pressures and Temperatures (Initial Helium Temperatures = 100°F) (See Para. 4.8.4)

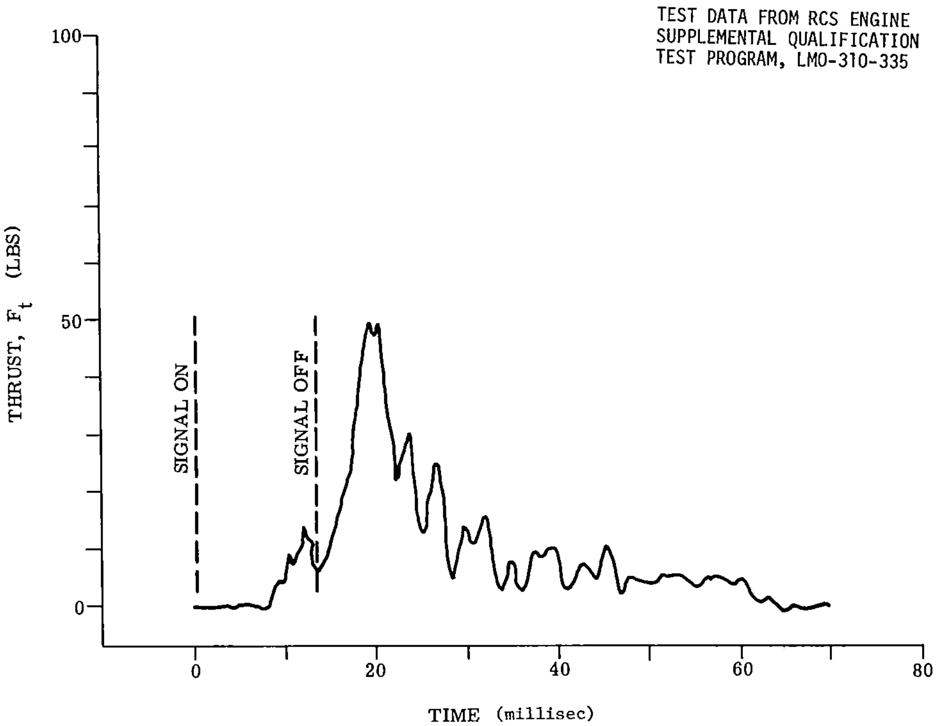

Figure 4.8-48. RCS Engine Thrust Buildup and Decay vs Time (Pulse width: 13 ms; Condition: Ambient, 25 $\pm$ 0.2 volts) (See Para. 4.8.4)

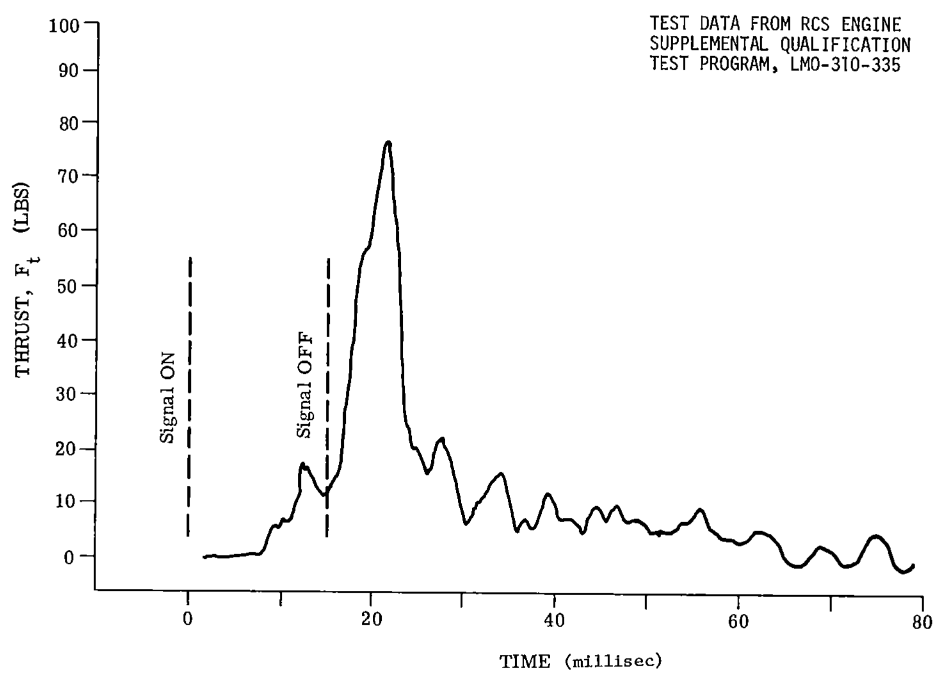

Figure 4.8-49. RCS Engine Thrust Buildup and Decay vs Time (Pulse width: 15 ms; Condition: Ambient, 25 $\pm$ 0.2 volts) (See Para. 4.8.4)

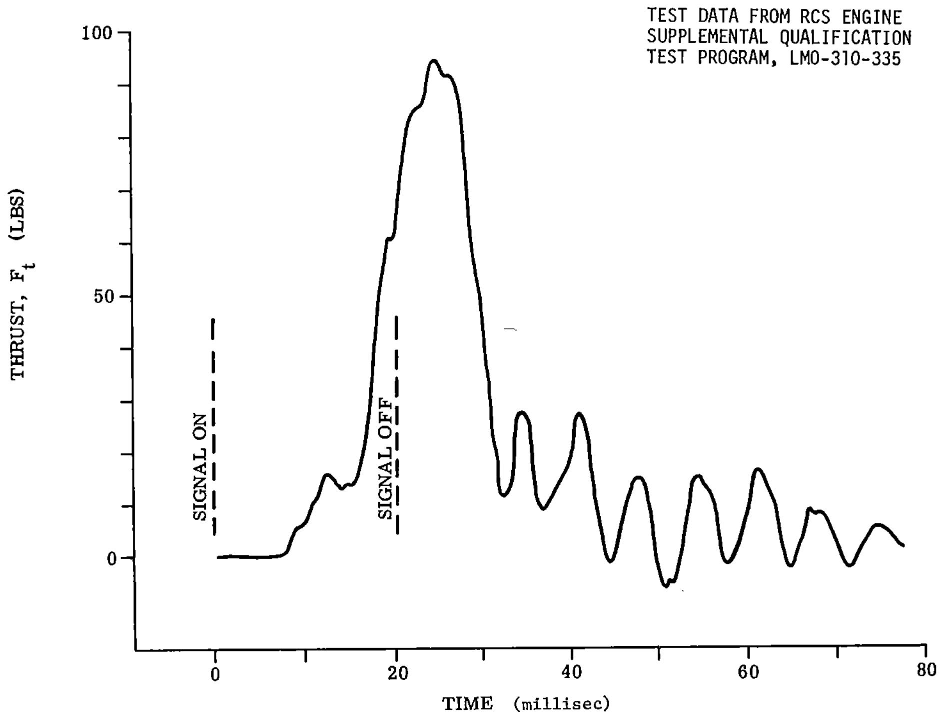

Figure 4.8-50. RCS Engine Thrust Buildup and Decay vs Time (Pulse width: 20 ms; Condition: Ambient, 25 ± 0.2 volts)(See Para. 4.8.4)

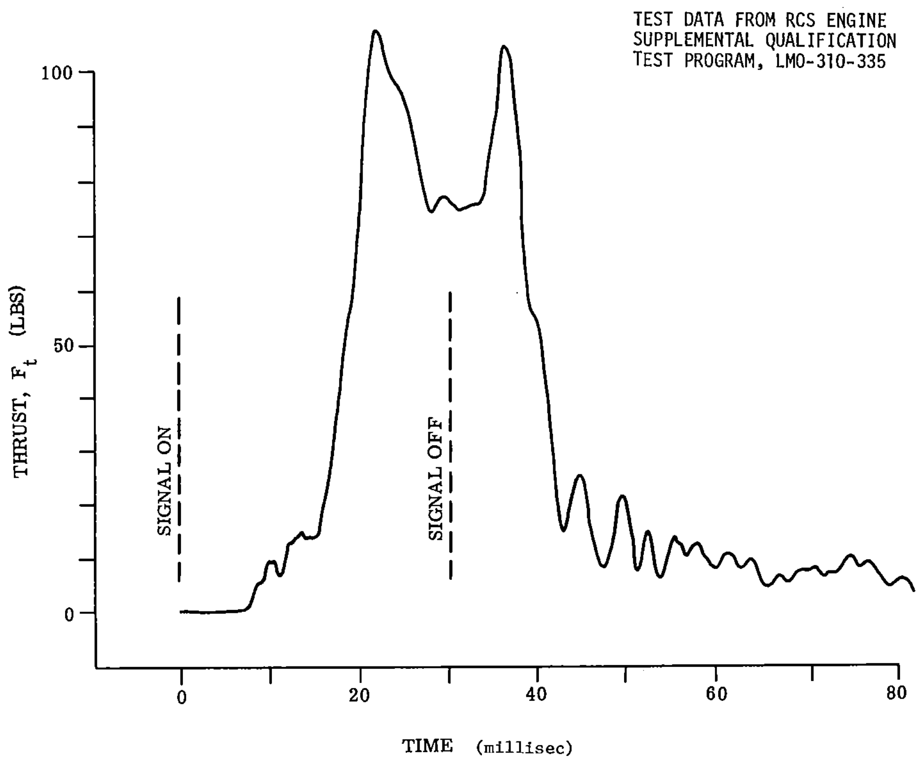

Figure 4.8-51. RCS Engine Thrust Buildup and Decay vs Time (Pulse width: 30 ms; Condition: Ambient, 25 ± 0.2 volts)(See Para. 4.8.4)

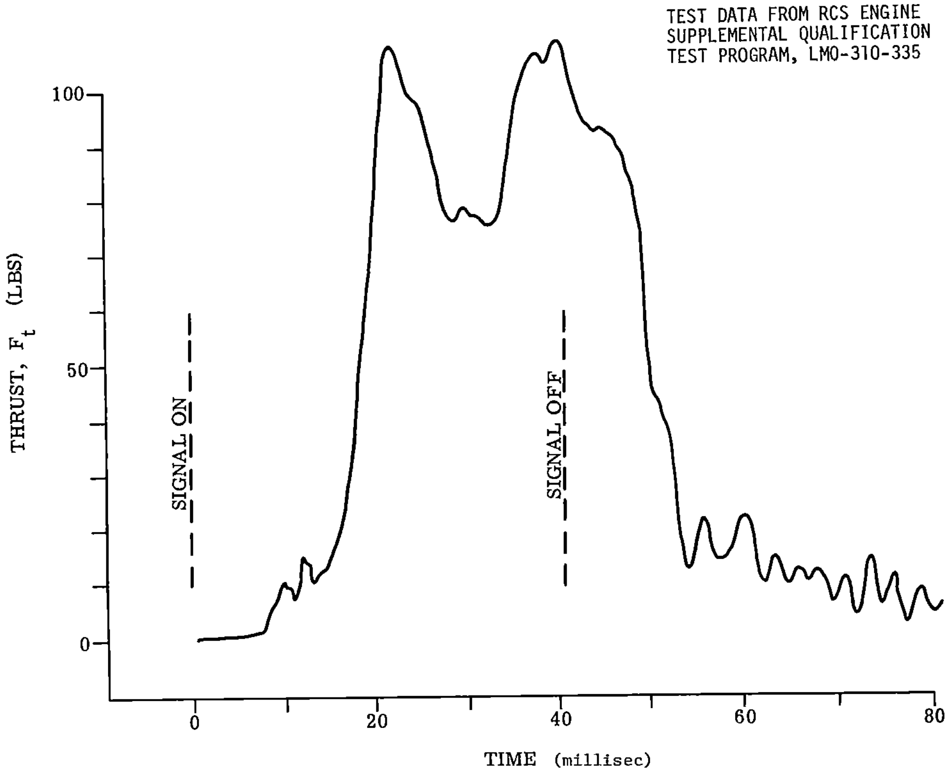

Figure 4.8-52. RCS Engine Thrust Buildup and Decay vs Time (Pulse width: 40 ms; Condition: Ambient, 25 ± 0.2 volts) (See Para. 4.8.4)

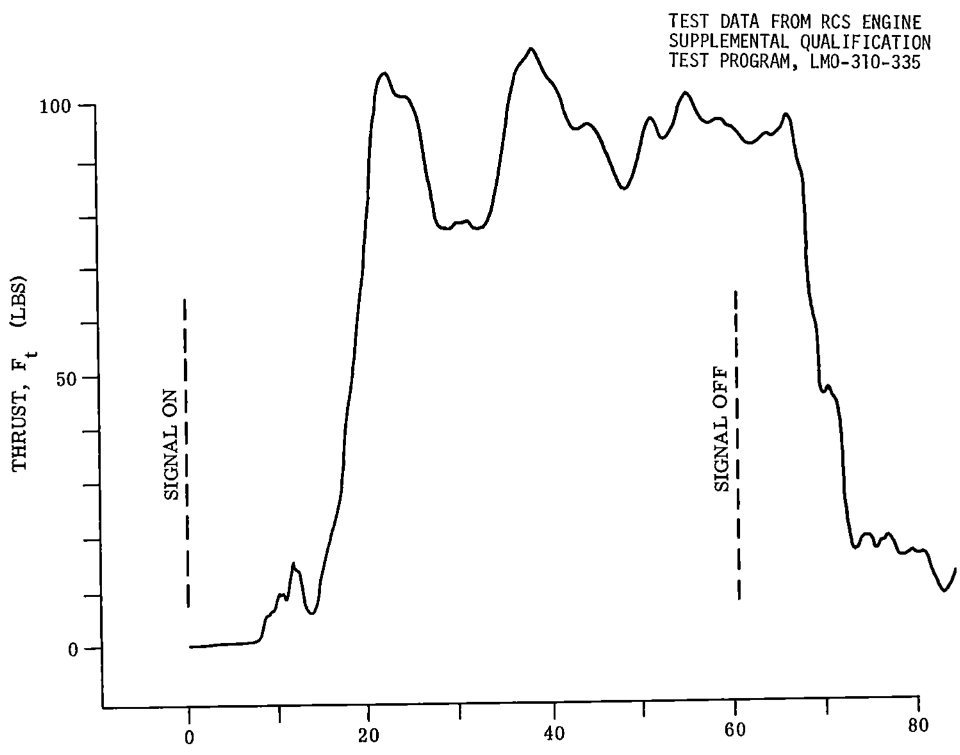

Figure 4.8-53. RCS Engine Thrust Buildup and Decay vs Time (Pulse width: 60 ms; Condition: Ambient, 25 ± 0.2 volts) (See Para. 4.8.4)

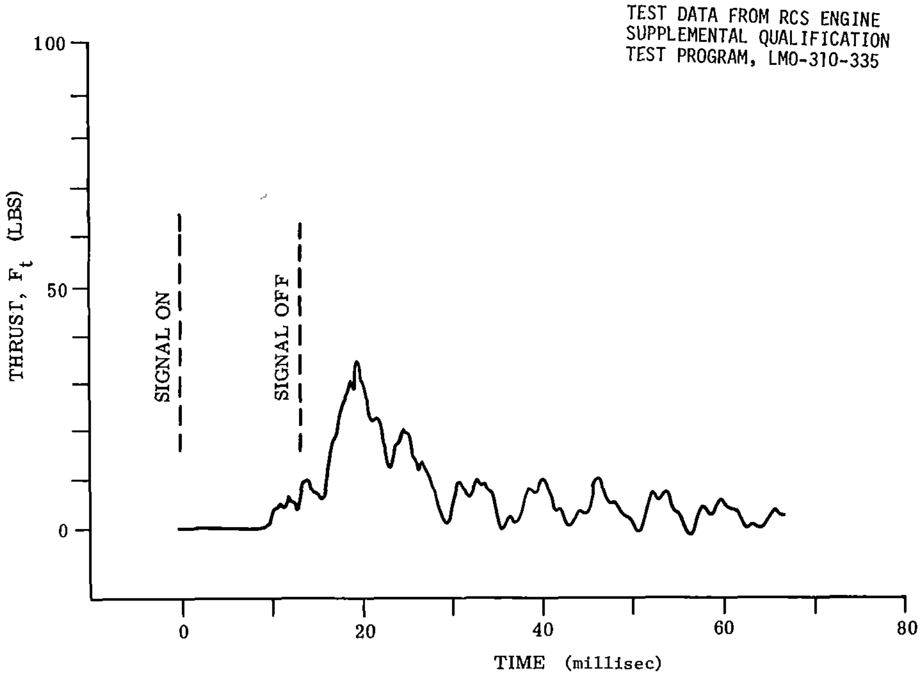

Figure 4.8-54. RCS Engine Thrust Buildup and Decay vs Time (Pulse width: 13 ms; Condition: Cold, 21 $\pm$0.2 volts)(See Para. 4.8.4)

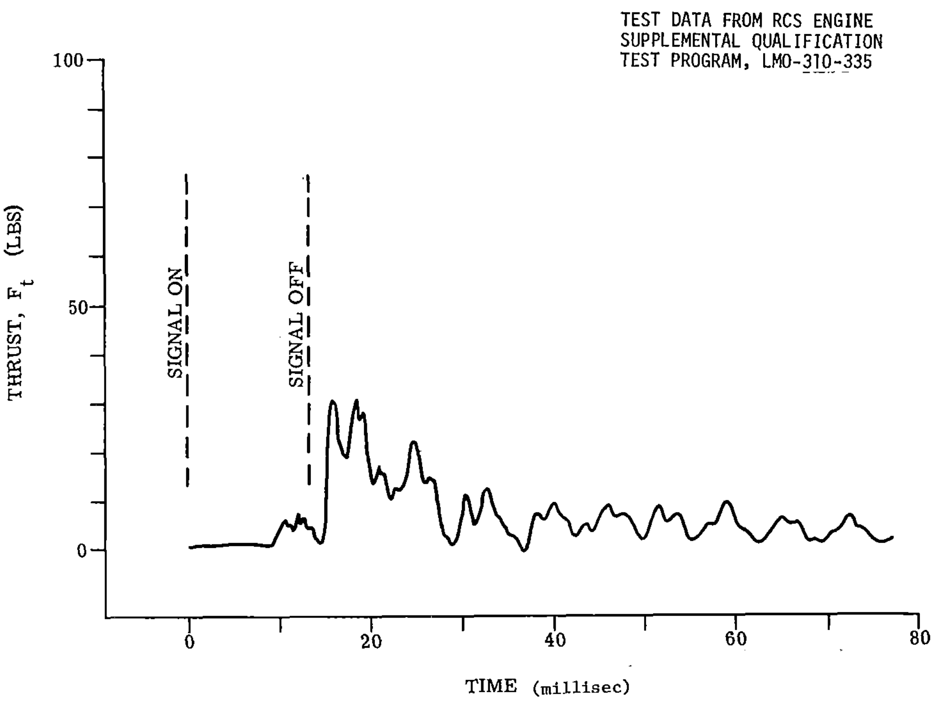

Figure 4.8-55. RCS Engine Thrust Buildup and Decay vs Time (Pulse width: 13 ms; Condition: Cold, 21 $\pm$ 0.2 volts)(See Para. 4.8.4)

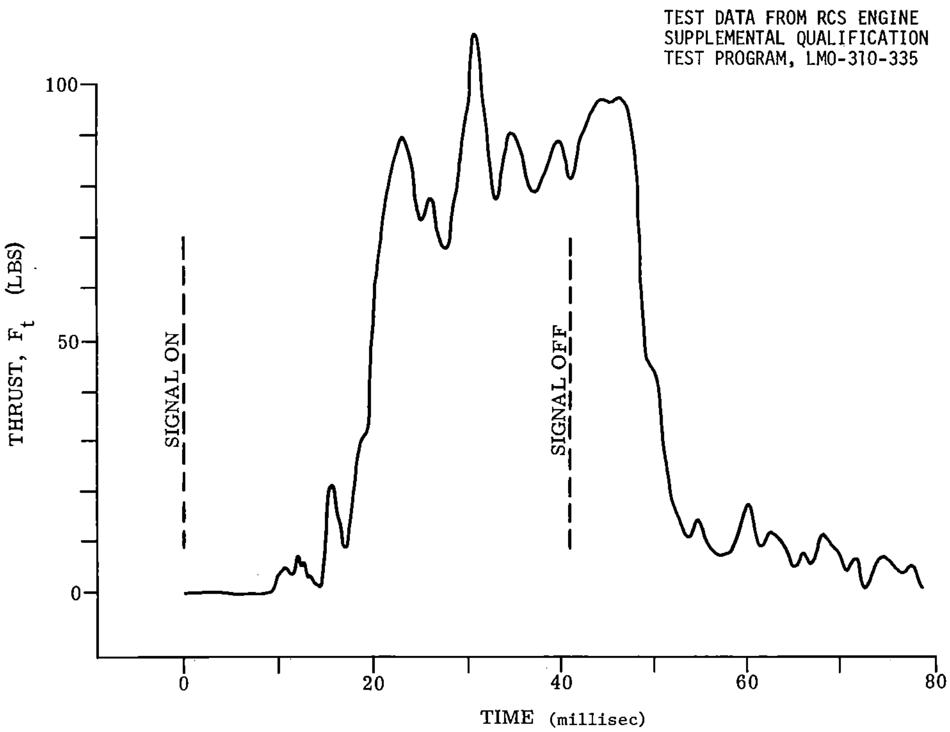

Figure 4.8-56. RCS Engine Thrust Buildup and Decay vs Time (Pulse width: 40 ms; Condition: Cold, 21 ± 0.2 volts)(See Para. 4.8.4)

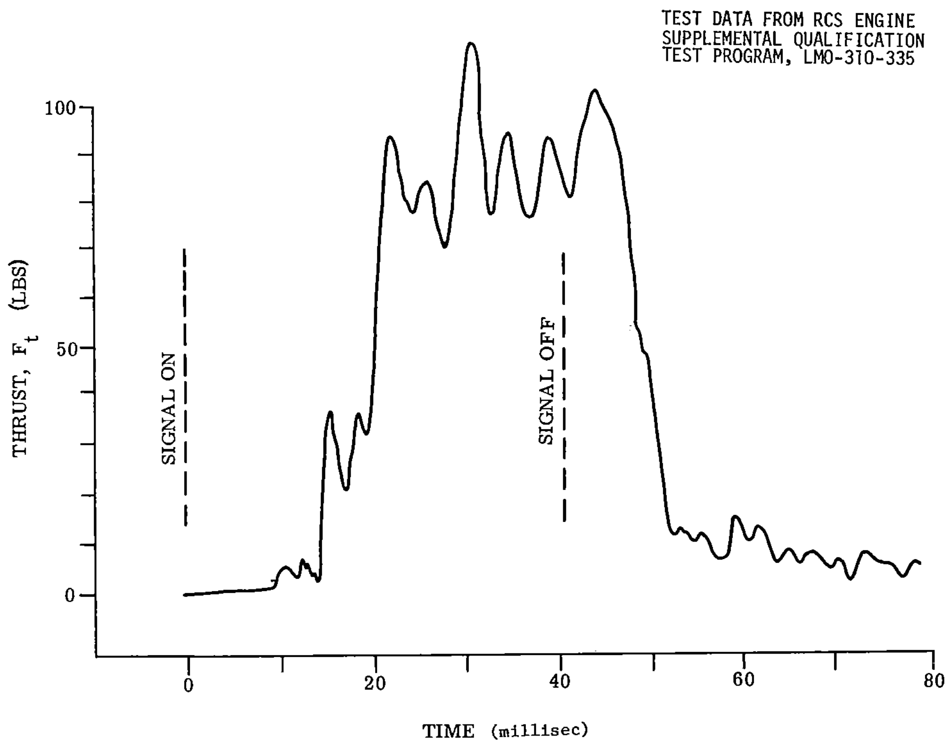

Figure 4.8-57. RCS Engine Thrust Buildup and Decay vs Time (Pulse width: 40 ms; Condition: Cold, 21 ± 0.2 volts) (See Para 4.8.4)

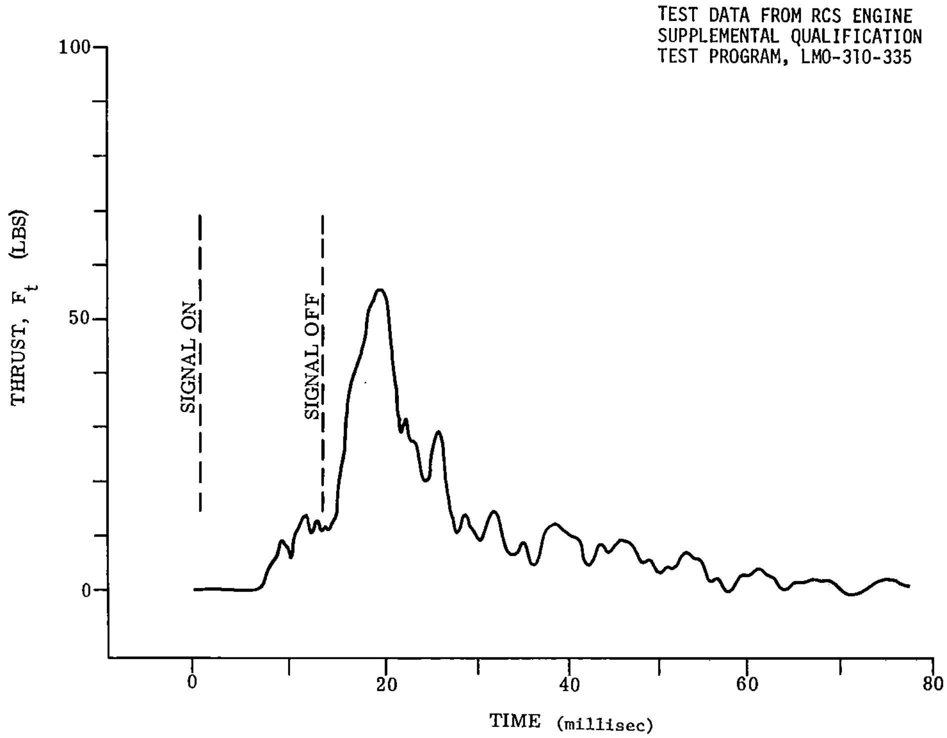

Figure 4.8-58. RCS Engine Thrust Buildup and Decay vs Time (Pulse width: 13 ms; Condition: Hot, 29 ± 0.2 volts) (See Para. 4.8.4)

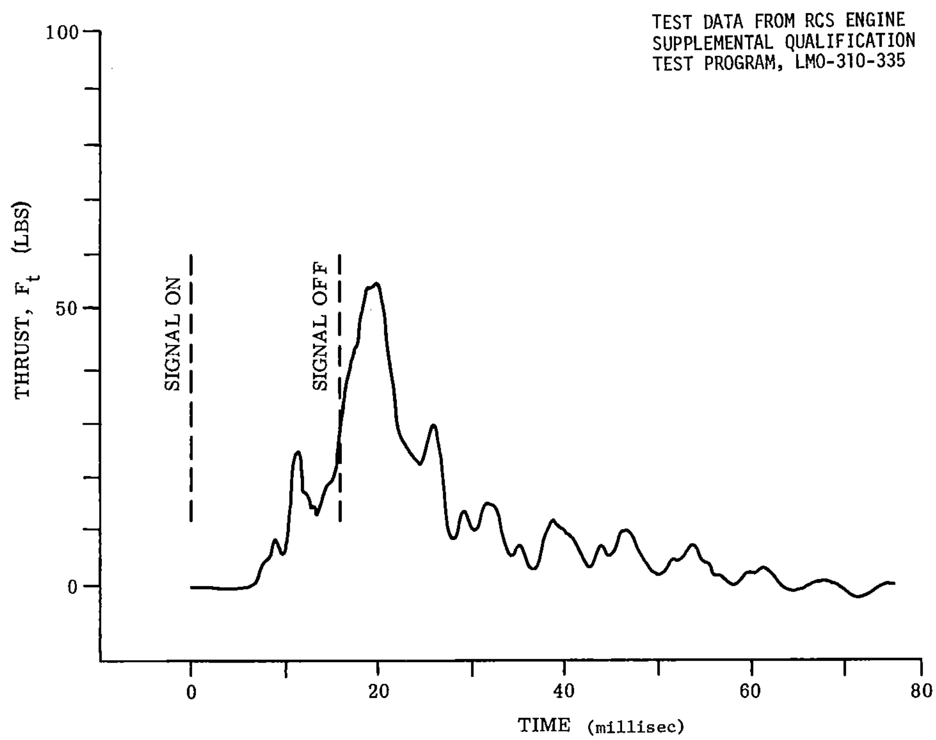

Figure 4.8-59. RCS Engine Thrust Buildup and Decay vs Time (Pulse width: 13 ms; Condition: Hot, 29 ± 0.2 volts) (See Para. 4.8.4)

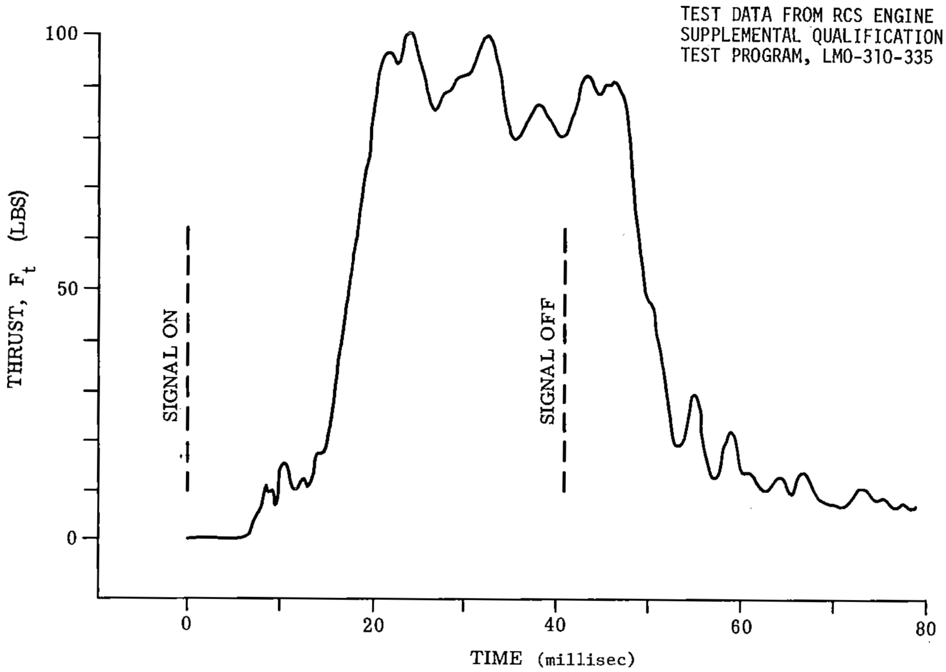

Figure 4.8-60. RCS Engine Thrust Buildup and Decay vs Time (Pulse width: 40 ms; Condition: Hot, 29 ± 0.2 volts) (See Para. 4.8.4)

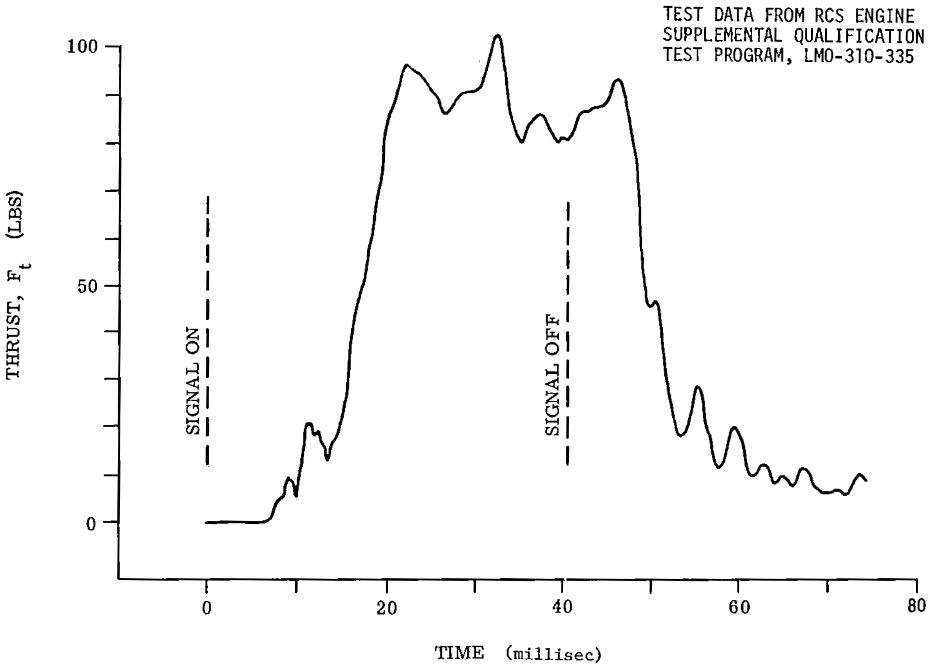

Figure 4.8-61. RCS Engine Thrust Buildup and Decay vs Time (Pulse width: 40 ms; Condition: Hot, 29 ± 0.2 volts) (See Para. 4.8.4)

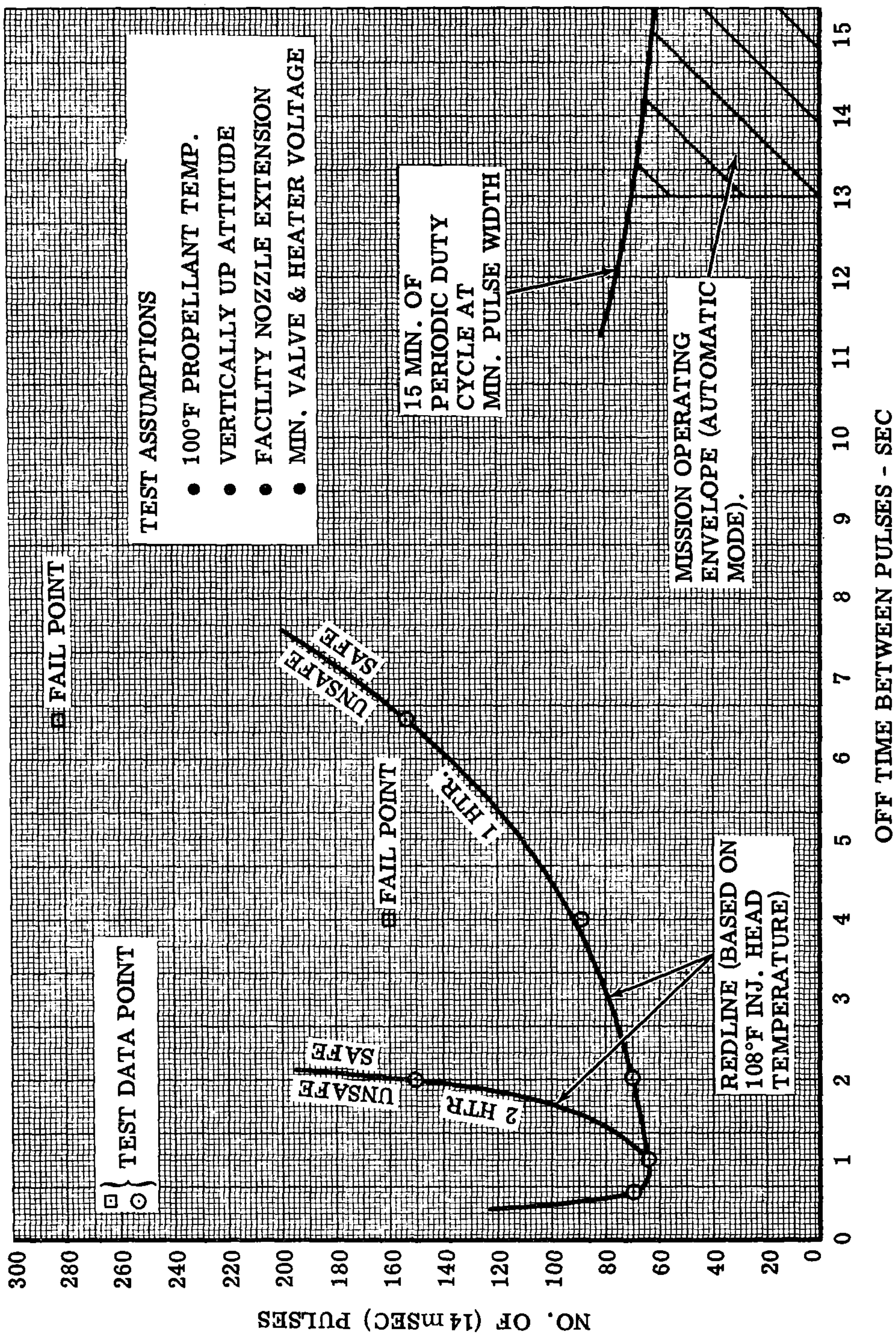

Figure 4.8.62. Map for Safe Operation of RCS Engine (Automatic Mode; Minimum Pulse Width) (See Para. 4.8.4)

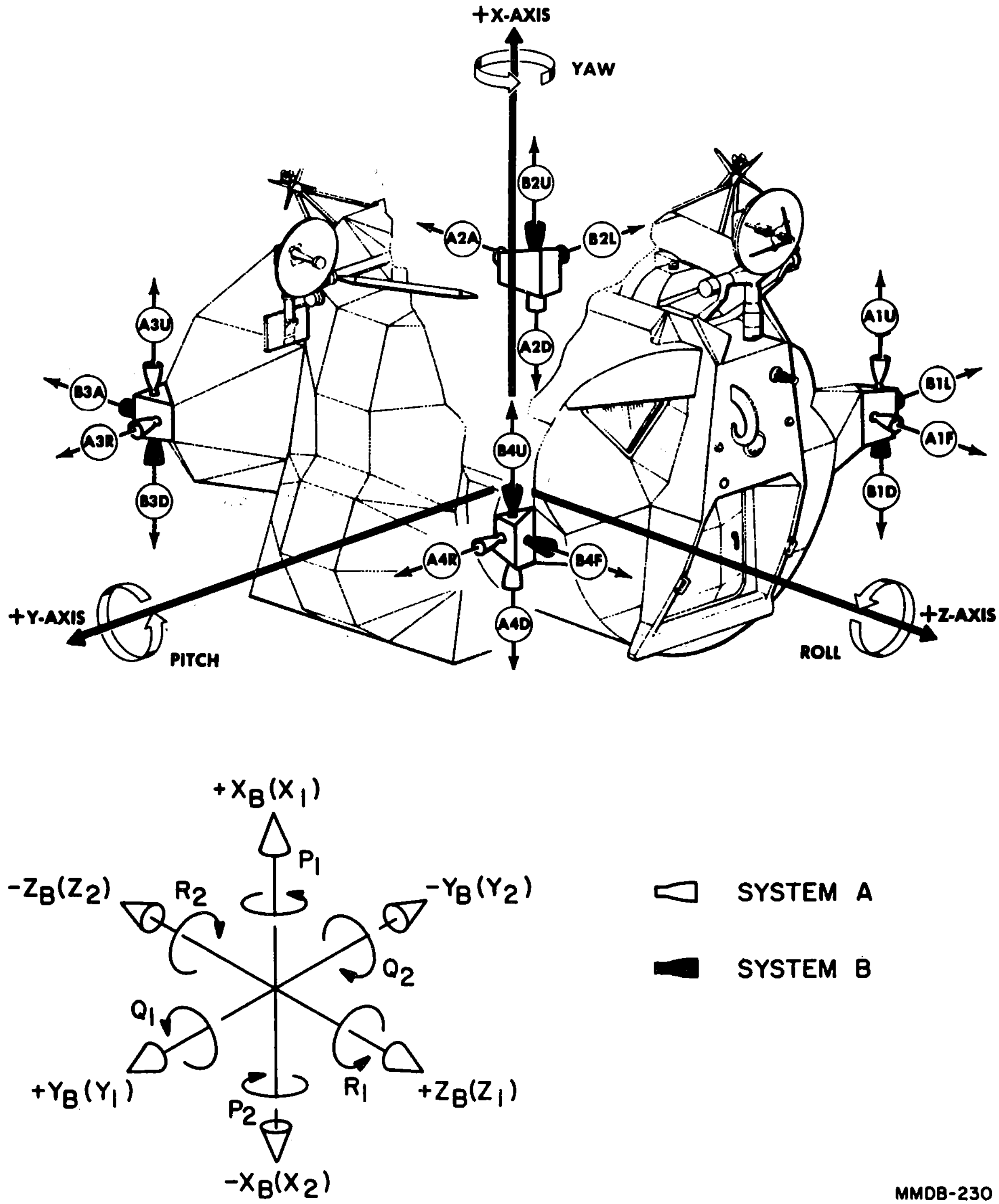

MMDB-230

Figure 4.8-63. RCS Thruster Location and Identification
(See Para. 4.8.7)

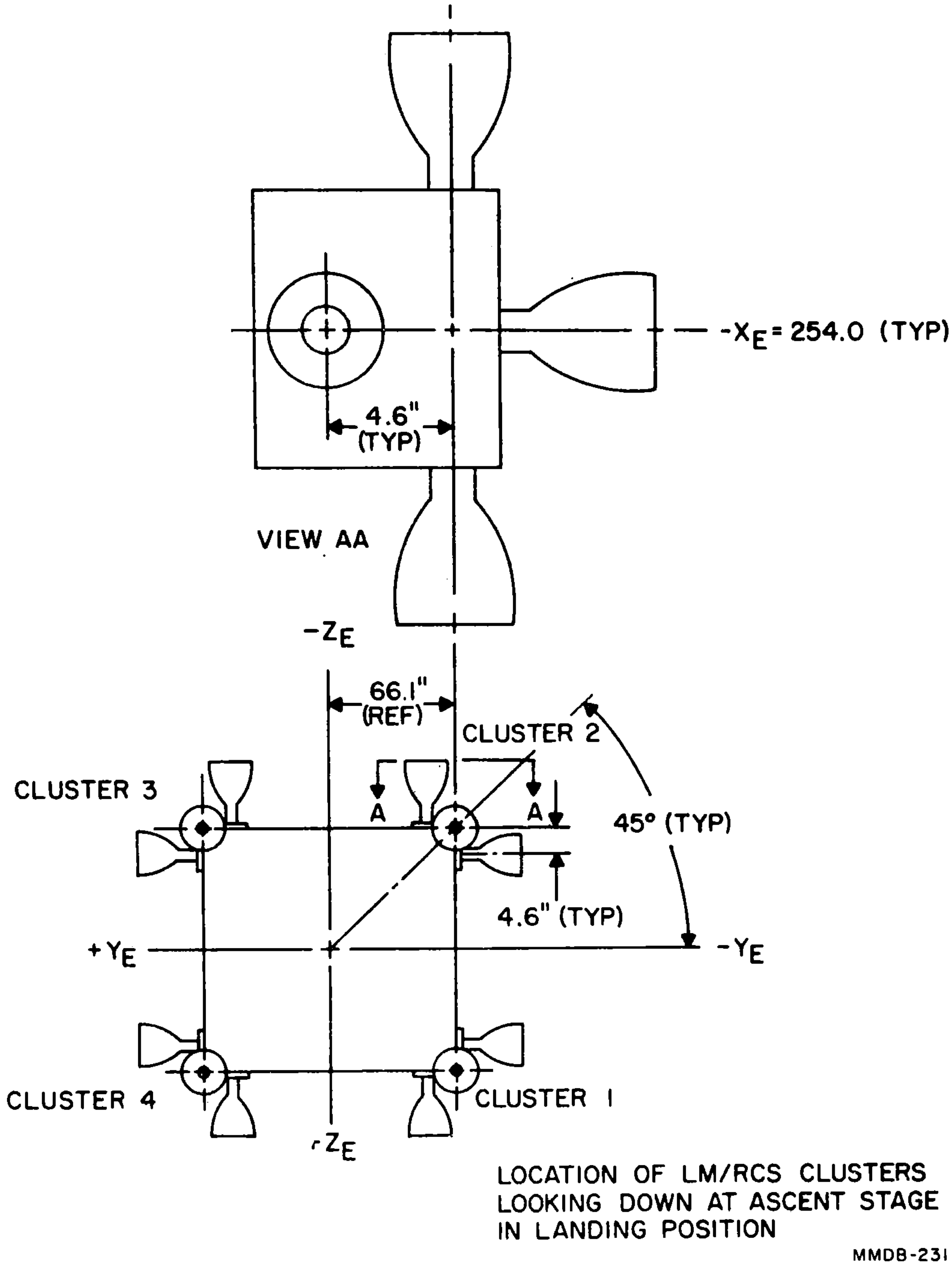

Figure 4.8-64. LM/RCS Thrust Chamber Geometry
(See Para. 4.8.7)

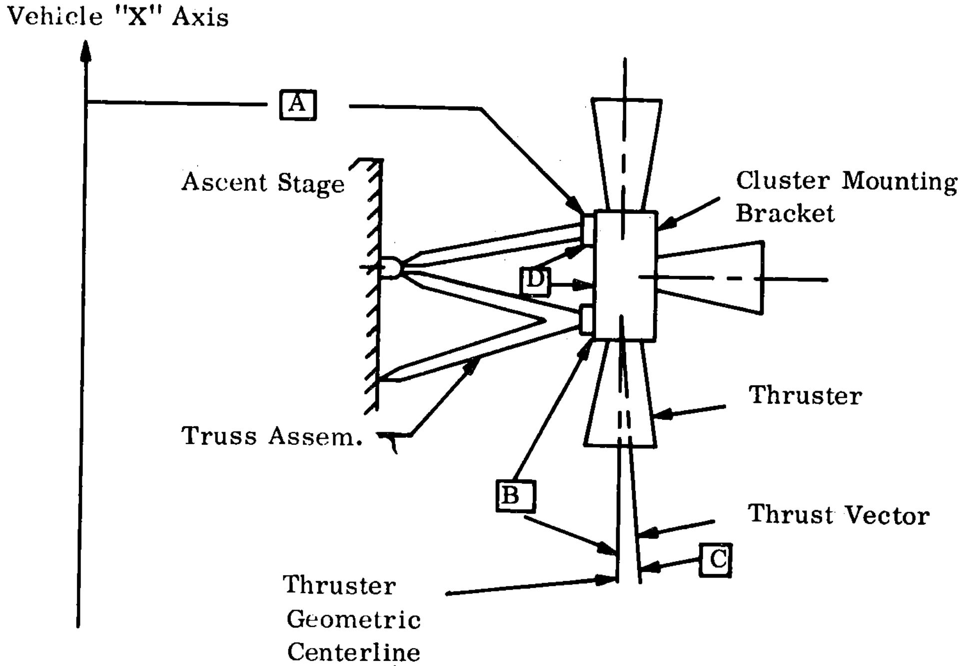

Schematic Of LM With Typical RCS Cluster Installed

Table of Manufacturing and Assembly Uncertainties

Ref.	Description	Uncertainty (Worst Case)
A	Truss Assembly Fitting to Vehicle Axis	±0.5° about Y Axis ±0.25° about Z Axis
B	Thruster Geometric Centerline Relative to cluster mounting bracket	±1.25° Conical Radius (each thruster)
C	Thrust Vector Centerline relative to Thruster Geometric Centerline	±1.0° Conical Radius
D	Cluster mounting bracket relative to Truss Assembly Fitting.	±0.79° about X Axis

NOTE: Sign convention in accordance with right hand rule.

Figure 4.8-64.1 RCS Manufacturing and Assembly Uncertainties
(See Para. 4.8.7.2)

a) Typical Down (-X) and Up (+X) Firing Thrust Vector Uncertainties

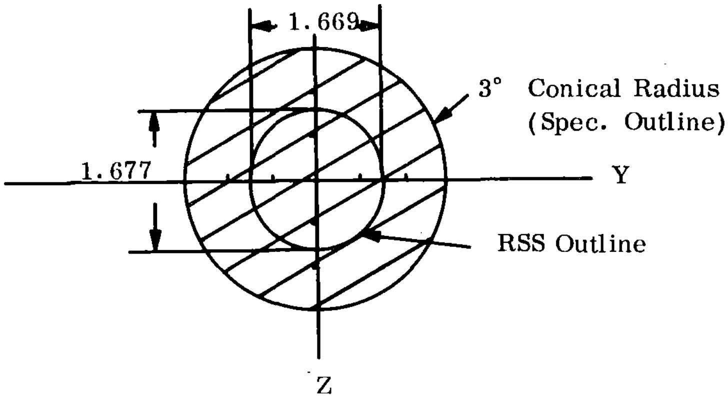

b) Typical Forward (+Z) and AFT (-Z) Thrust Vector Uncertainties

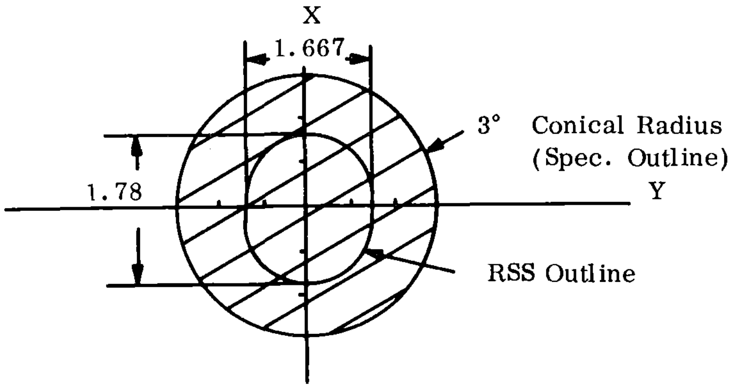

c) Typical Right (+Y) and Left (-Y) Thrust Vector Uncertainties

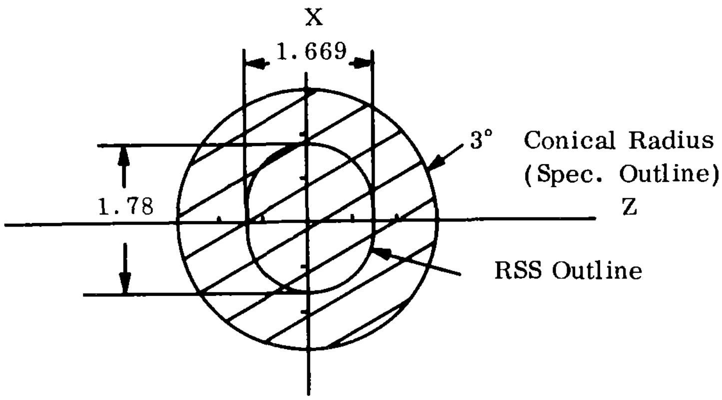

Figure 4.8-64.2 RCS Thrust Vector Uncertainties
(See Paragrah 4.8.7.2)

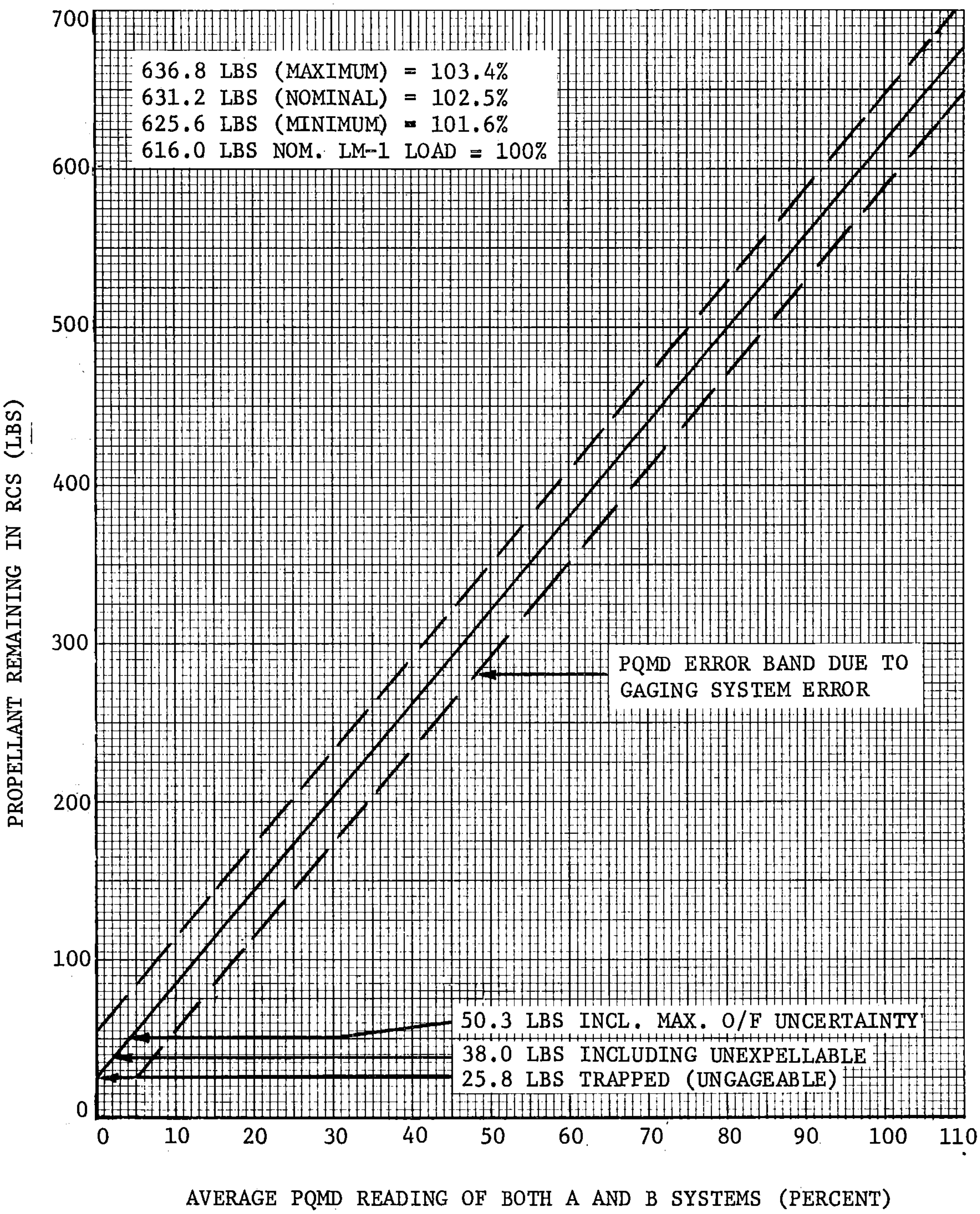

Figure 4.8-65. Correlation of Propellant Quantity Measuring Device (PQMD) Reading with Actual Propellant Quantity Remaining in the LM RCS System (See Para. 4.8.9)

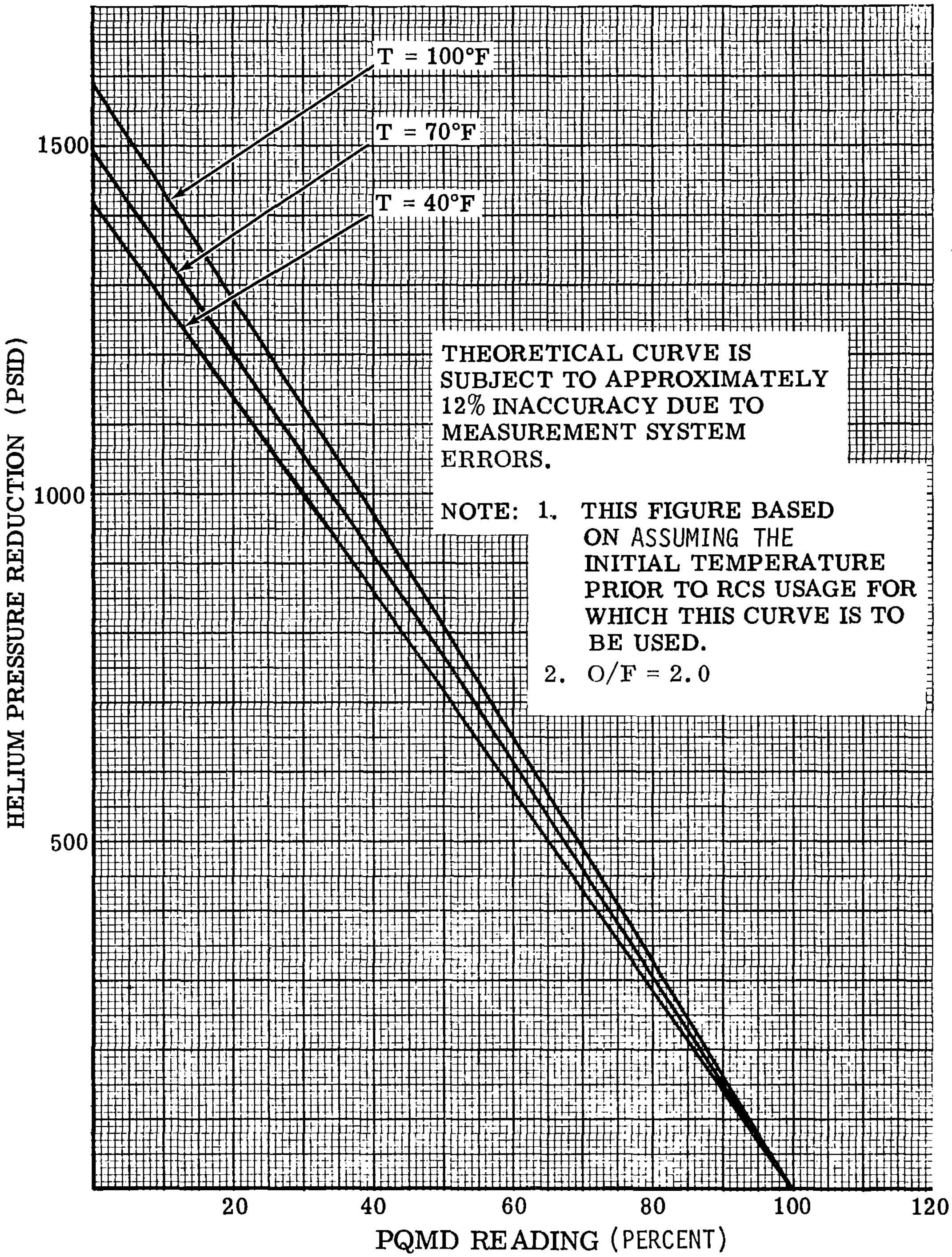

Figure 4.8-66. RCS He Tank Pressure Reduction vs Propellant Quantity Remaining (See Para. 4.8.9)

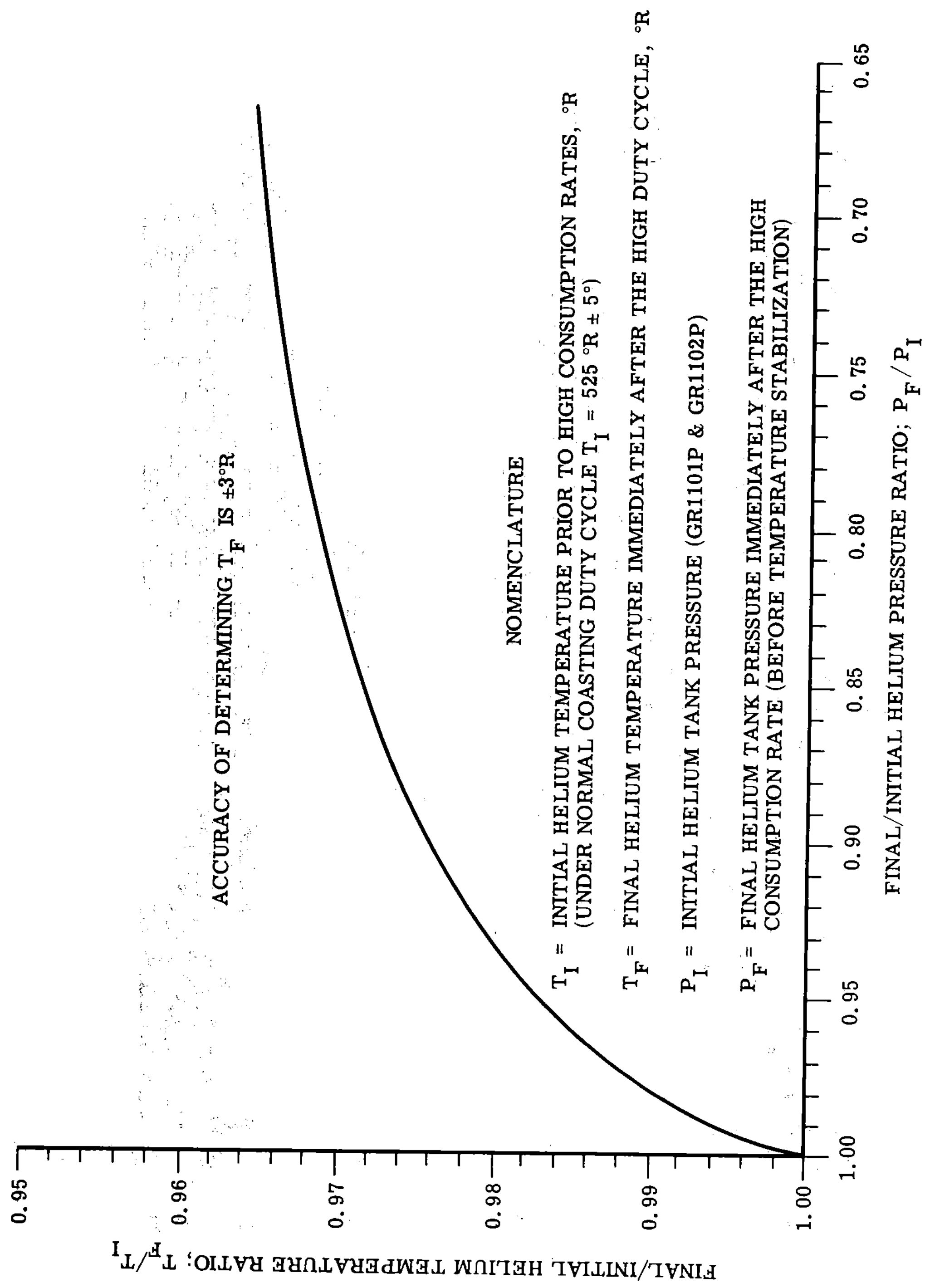

Figure 4.8-67. **Determination of Helium Temperature Change Due to High RCS Propellant Consumption Rates** (See Para. 4.8.9)

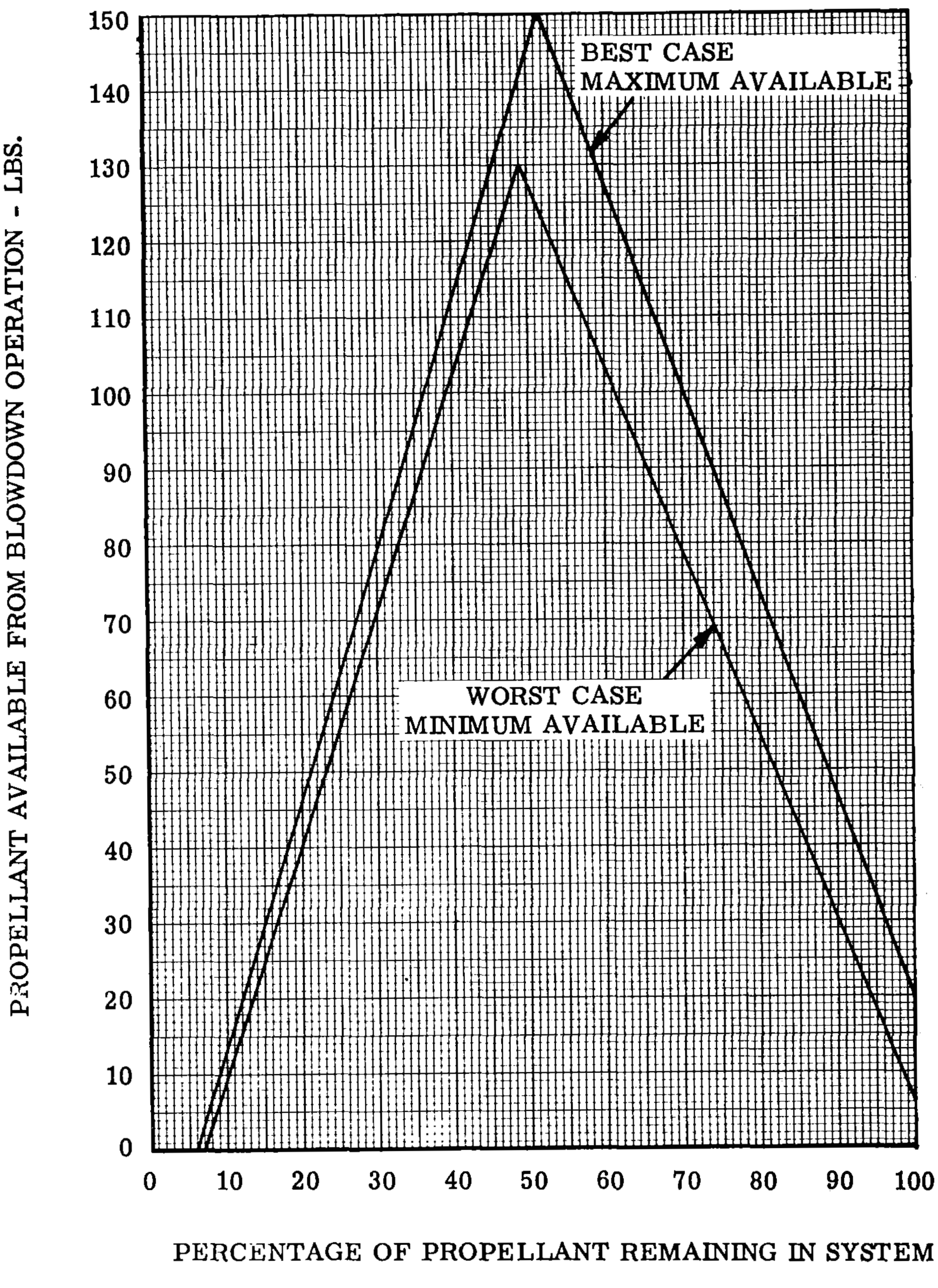

Figure 4.8-67.1 Propellant Available Per System From Blowdown Operation. (See Para. 4.8.12.2)

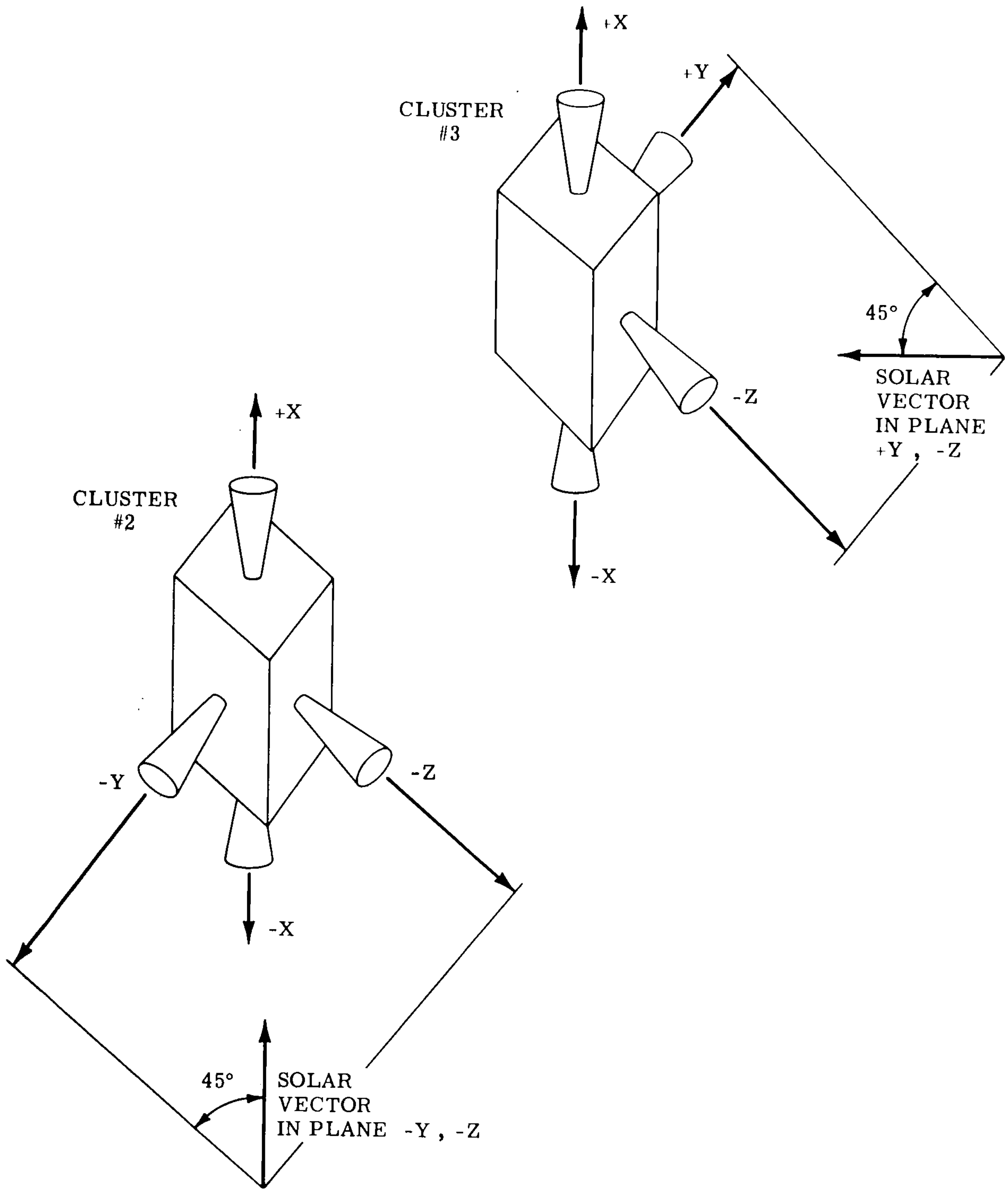

Figure 4.8-68. Orientation of Aft Cluster Toward Sun
(See Para. 4.8.13.2)

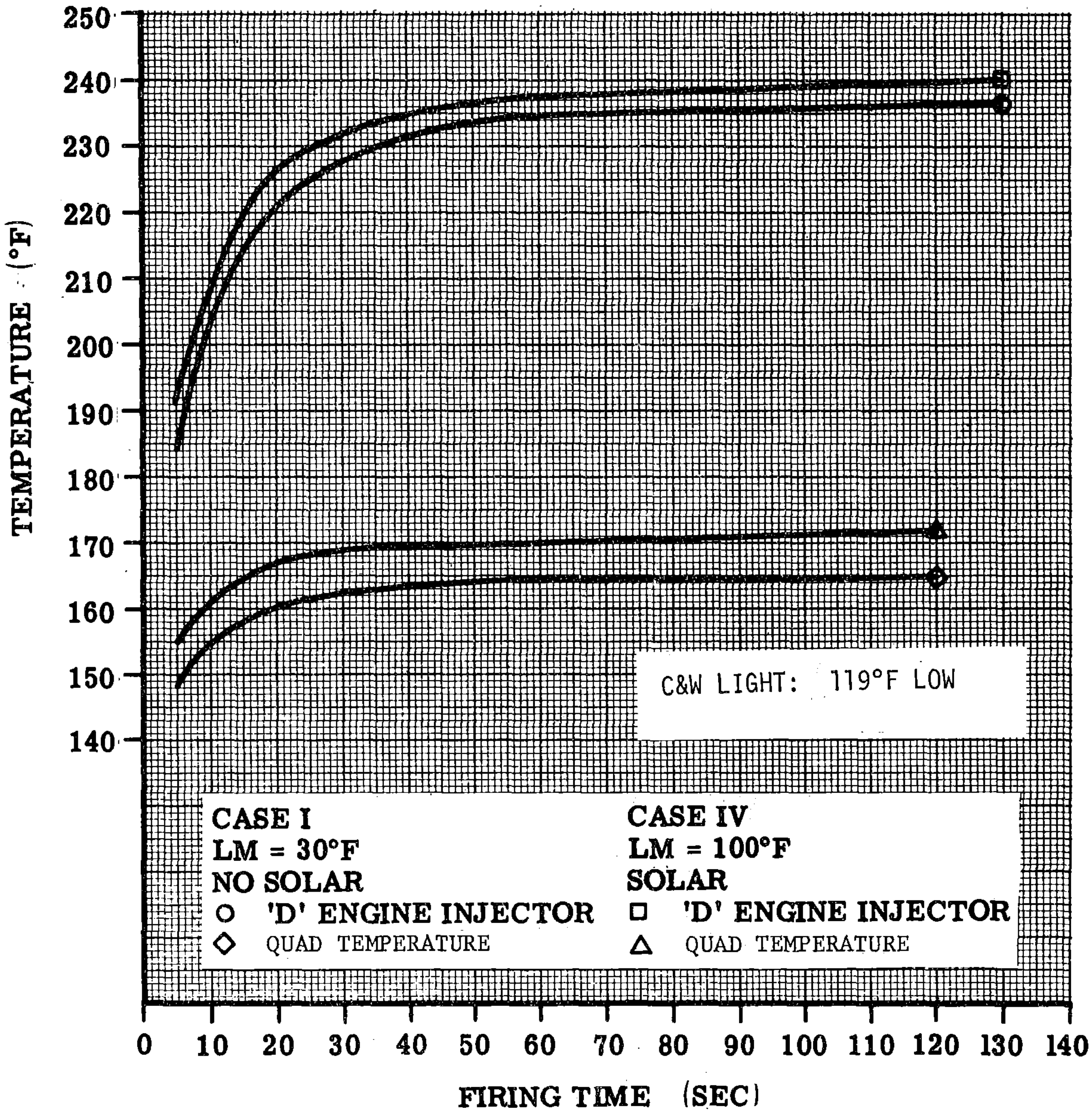

Figure 4.8-69. Peak Soakback Temperature versus Steady Firing Duration (See Para. 4.8.13.2)

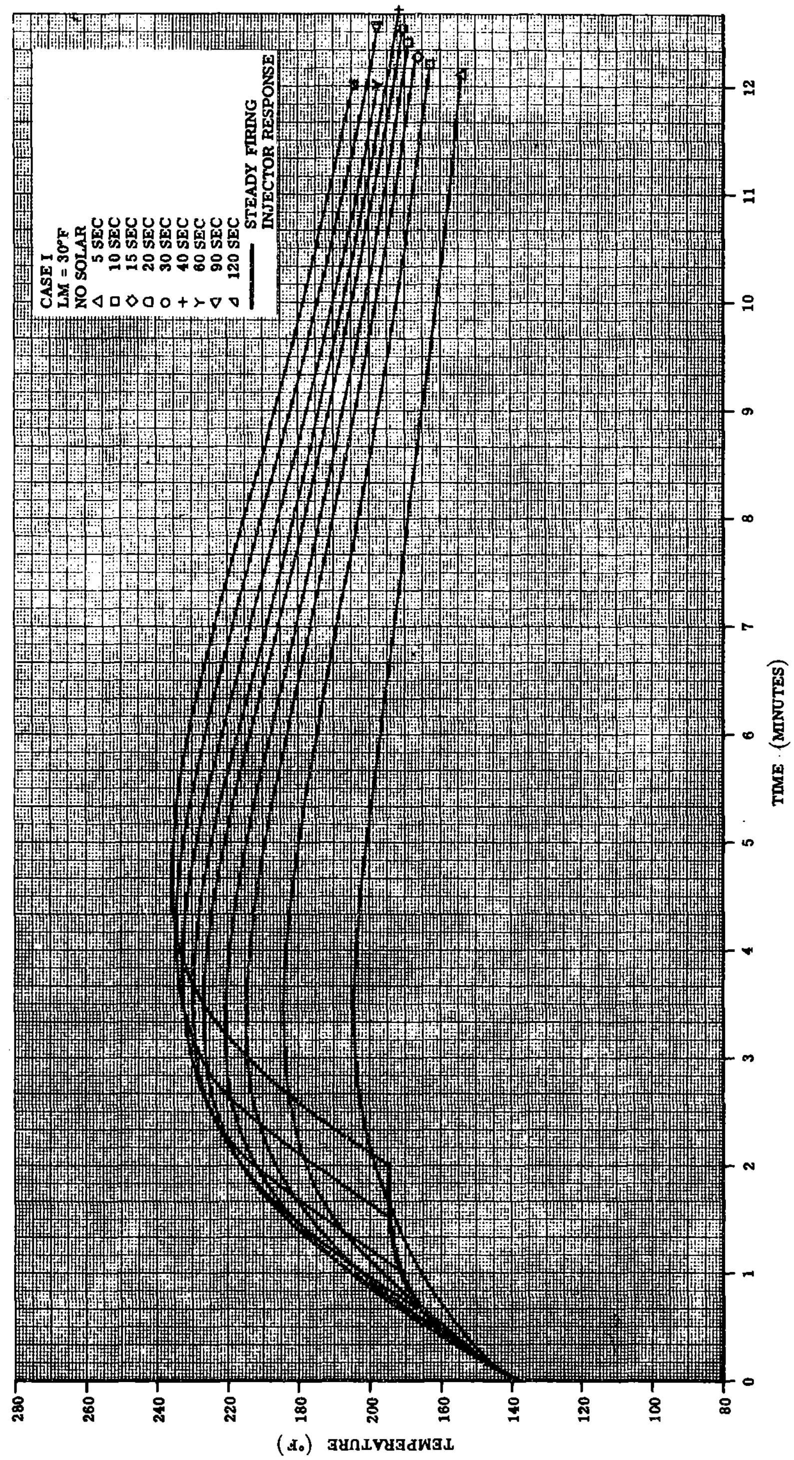

Figure 4.8-70. Steady Firing - Injector Response and Soakback
(See Para. 4.8.13.2)

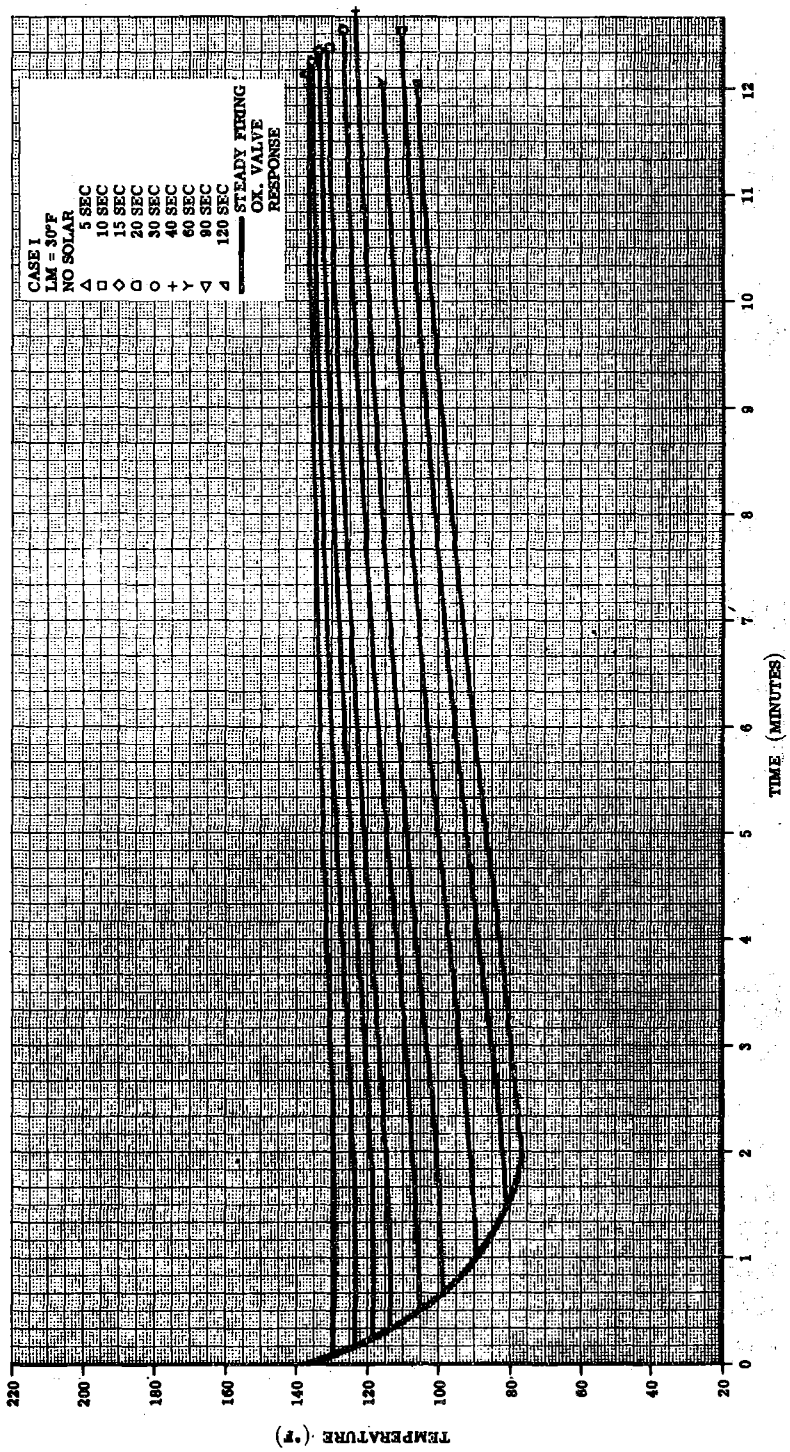

Figure 4.8-71. Steady Firing - Ox. Valve Response and Soakback
(See Para. 4.8.13.2)

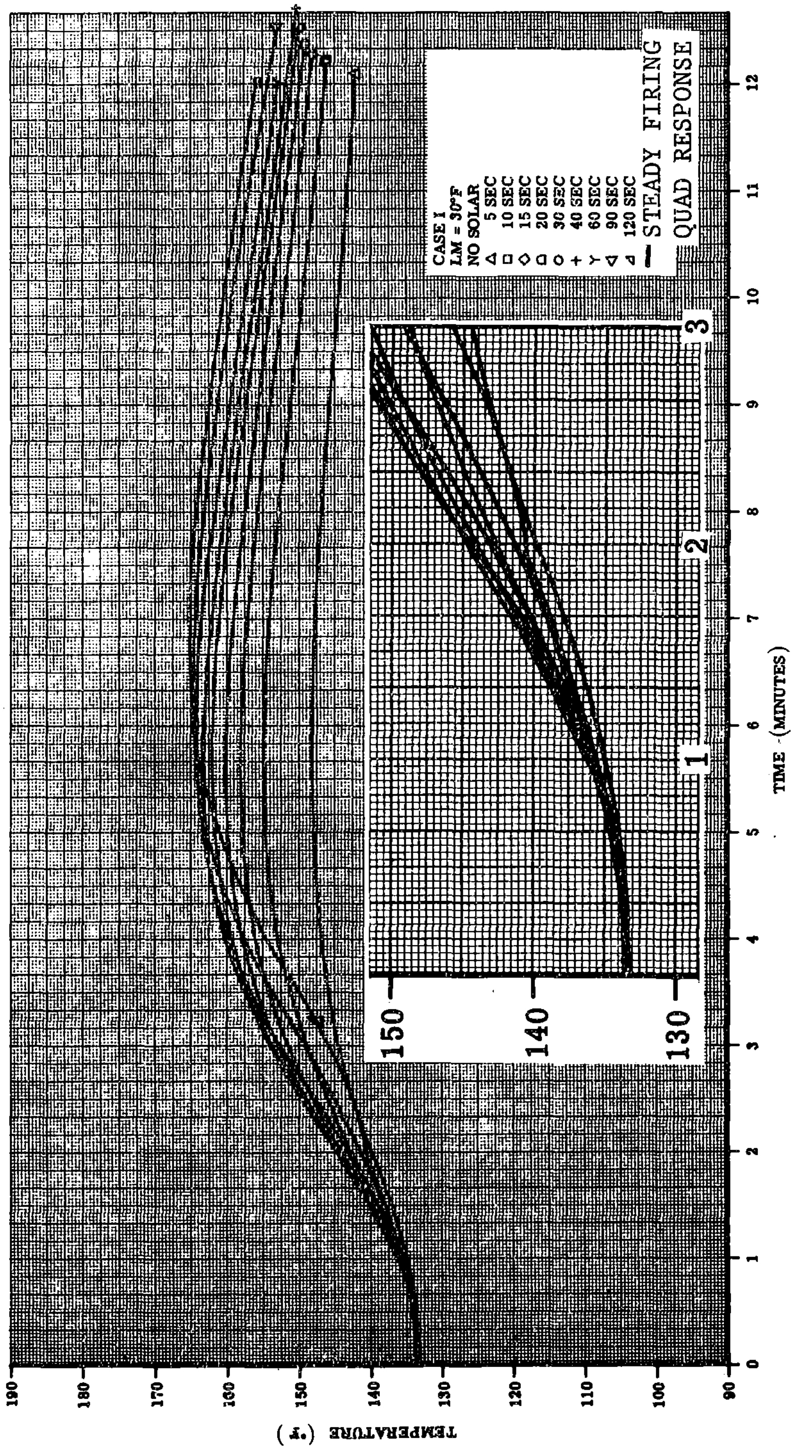

Figure 4.8-72. Steady Firing - Quad Response and Soakback
(See Para. 4.8.13.2)

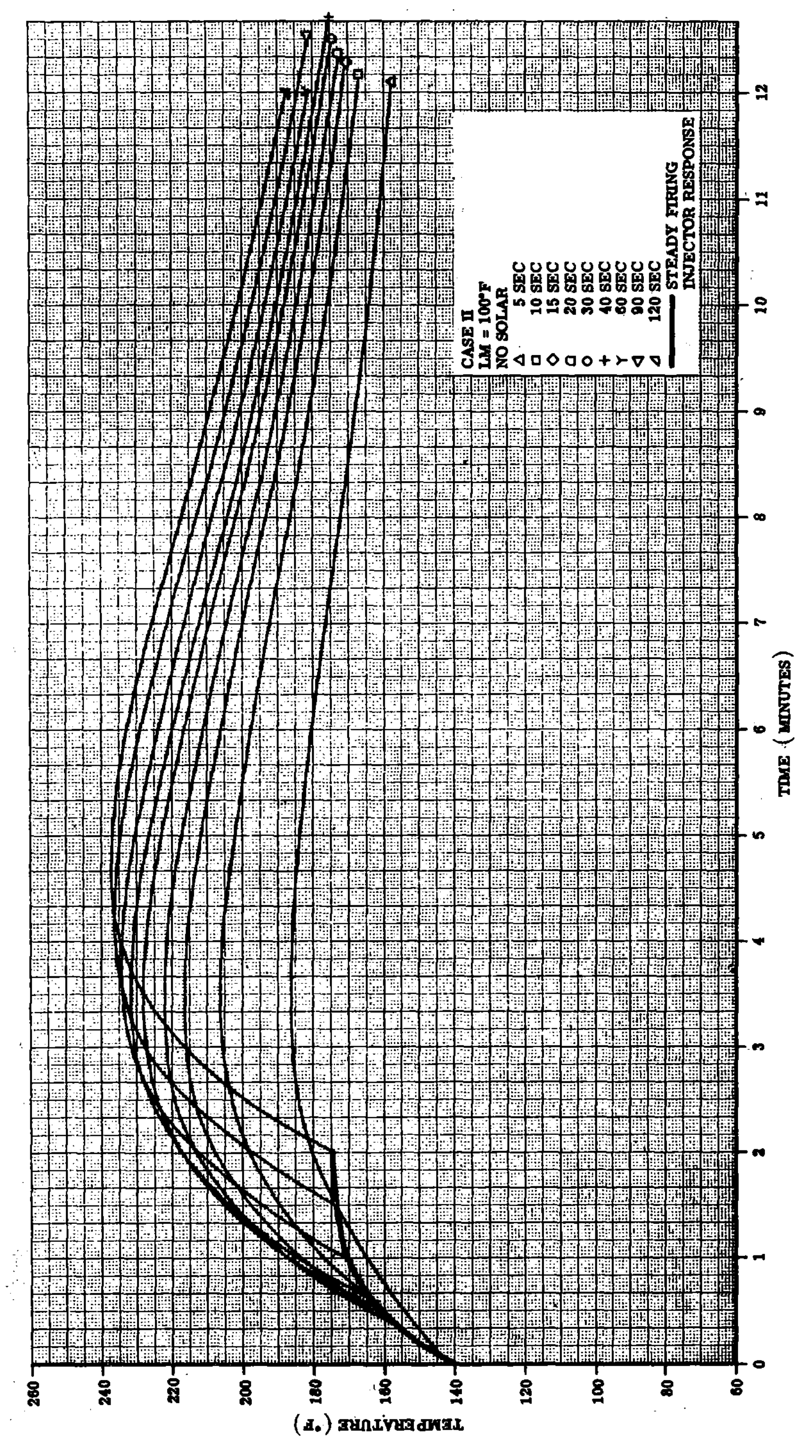

Figure 4.8-73. Steady Firing - Injector Response and Soakback
(See Para. 4.8.13.2)

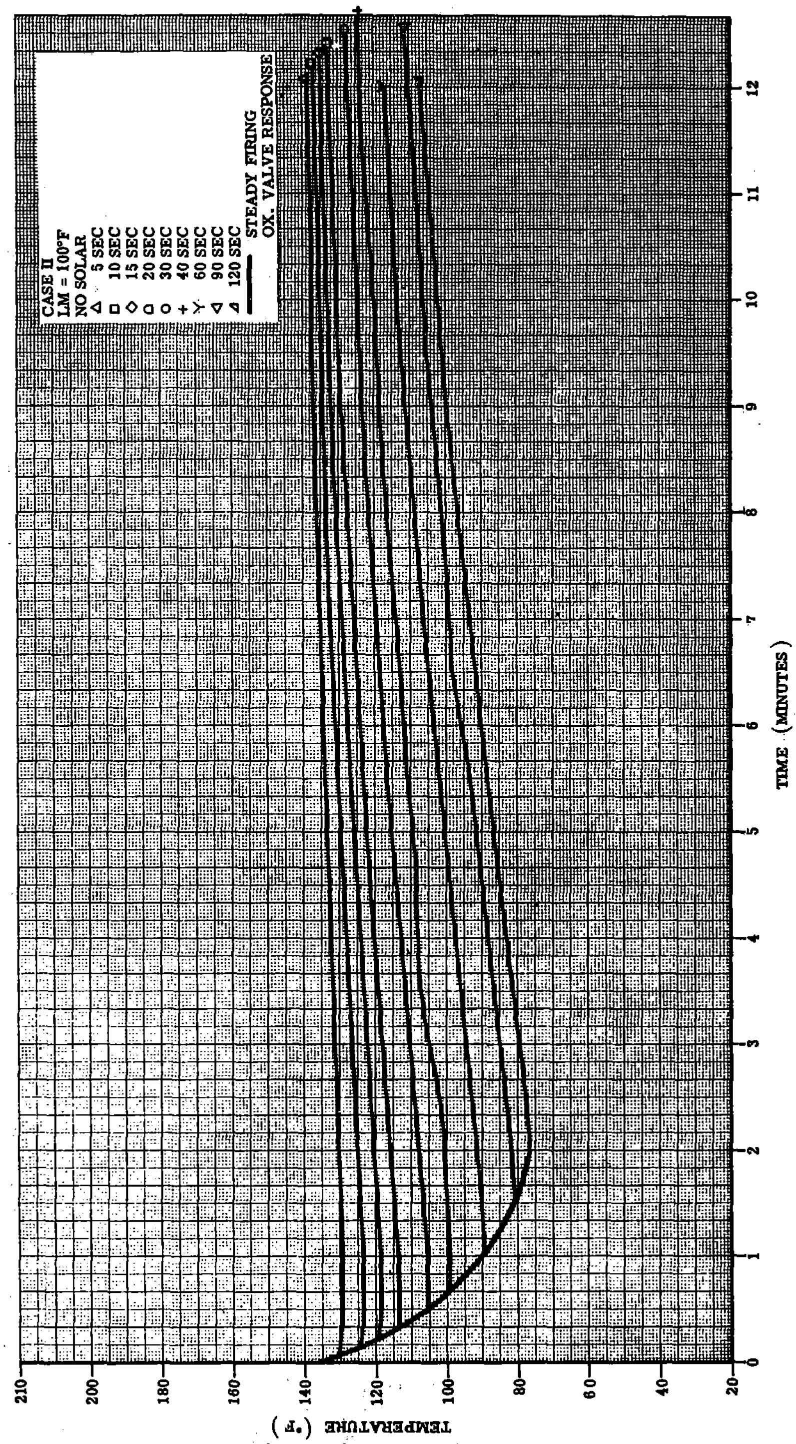

Figure 4.8-74. Steady Firing - Ox. Valve Response and Soakback
(See Para. 4.8.13.2)

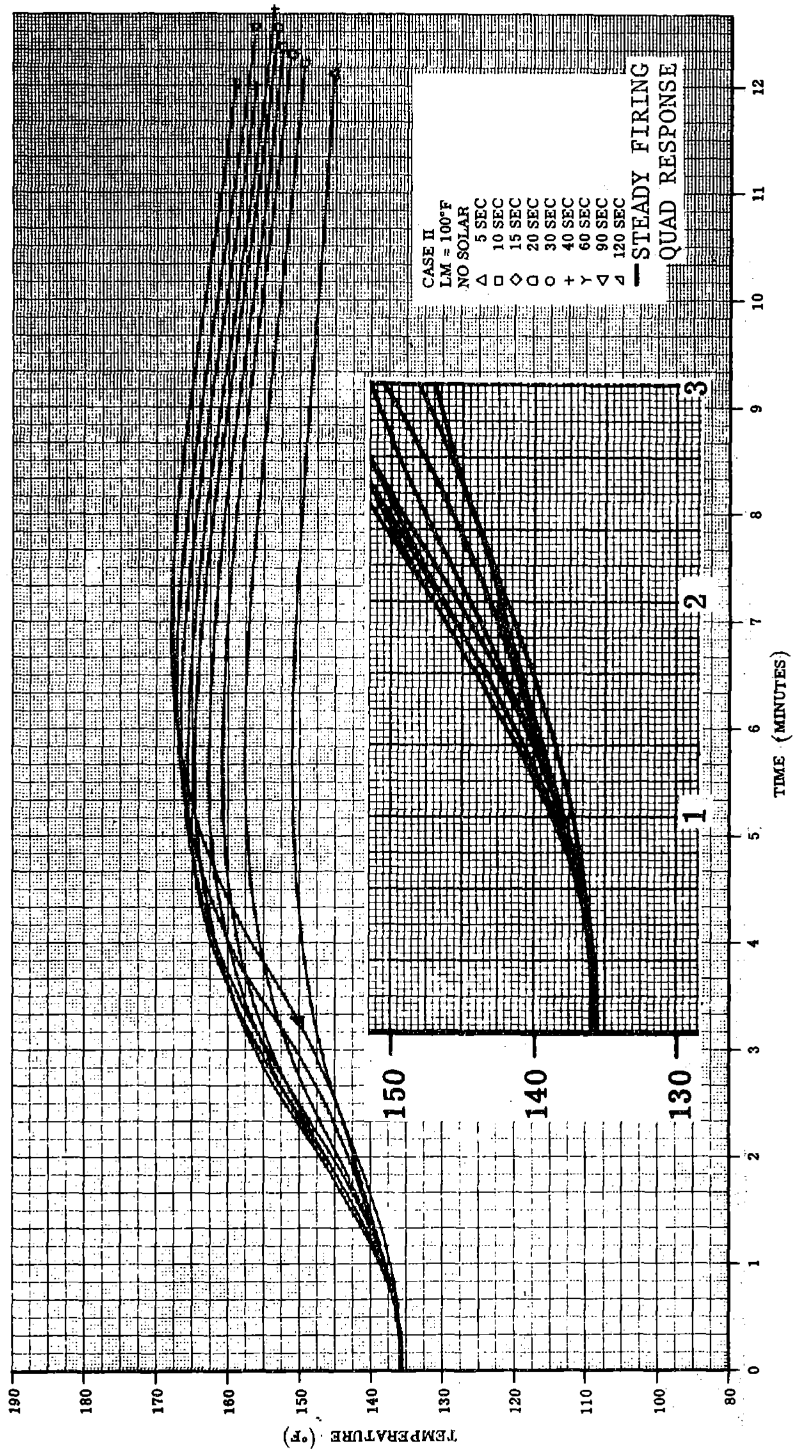

Figure 4.8-75. Steady Firing - Quad Response and Soakback
(See Para. 4.8.13.2)

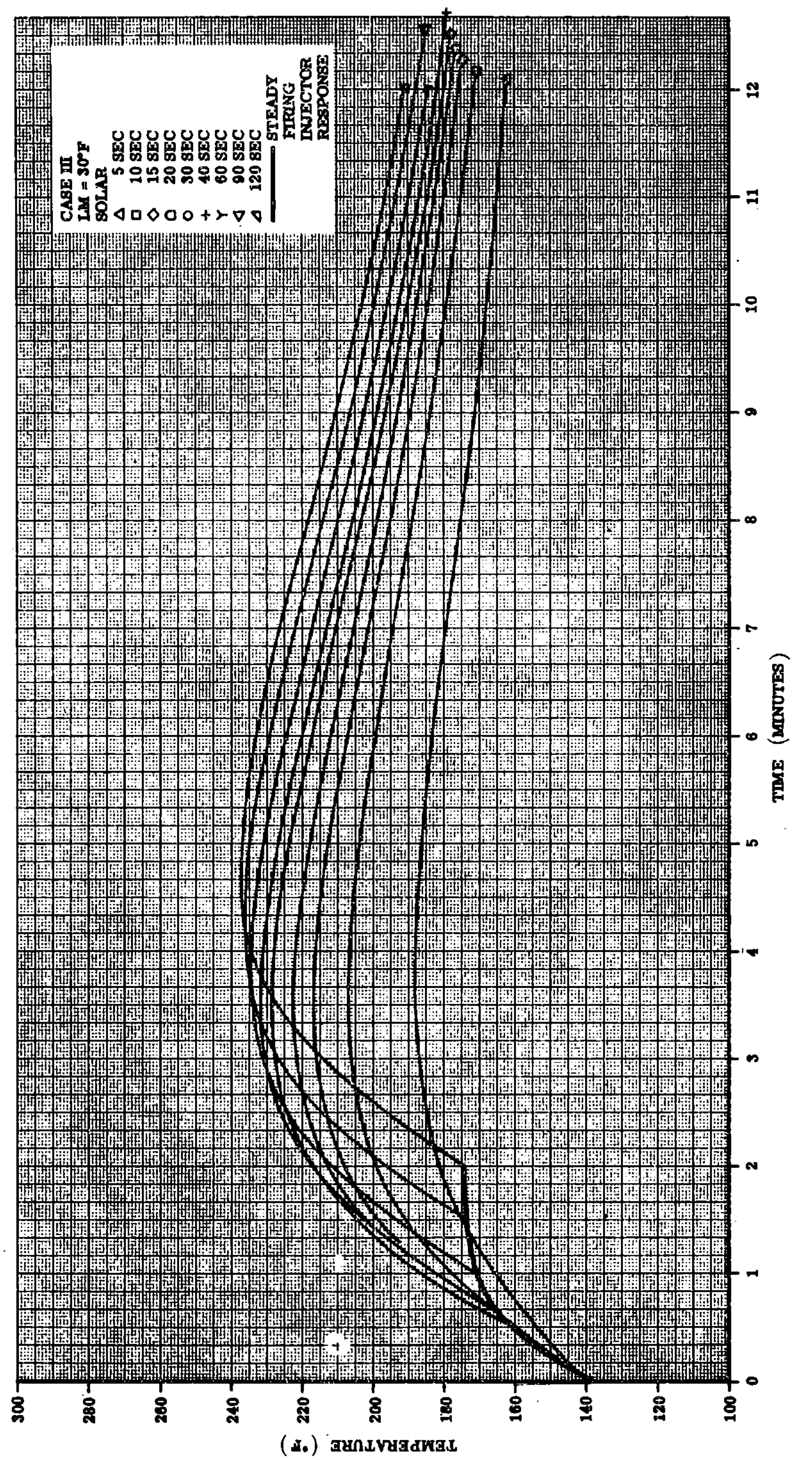

Figure 4.8-76. Steady Firing - Injector Response and Soakback
(See Para. 4.8.13.2)

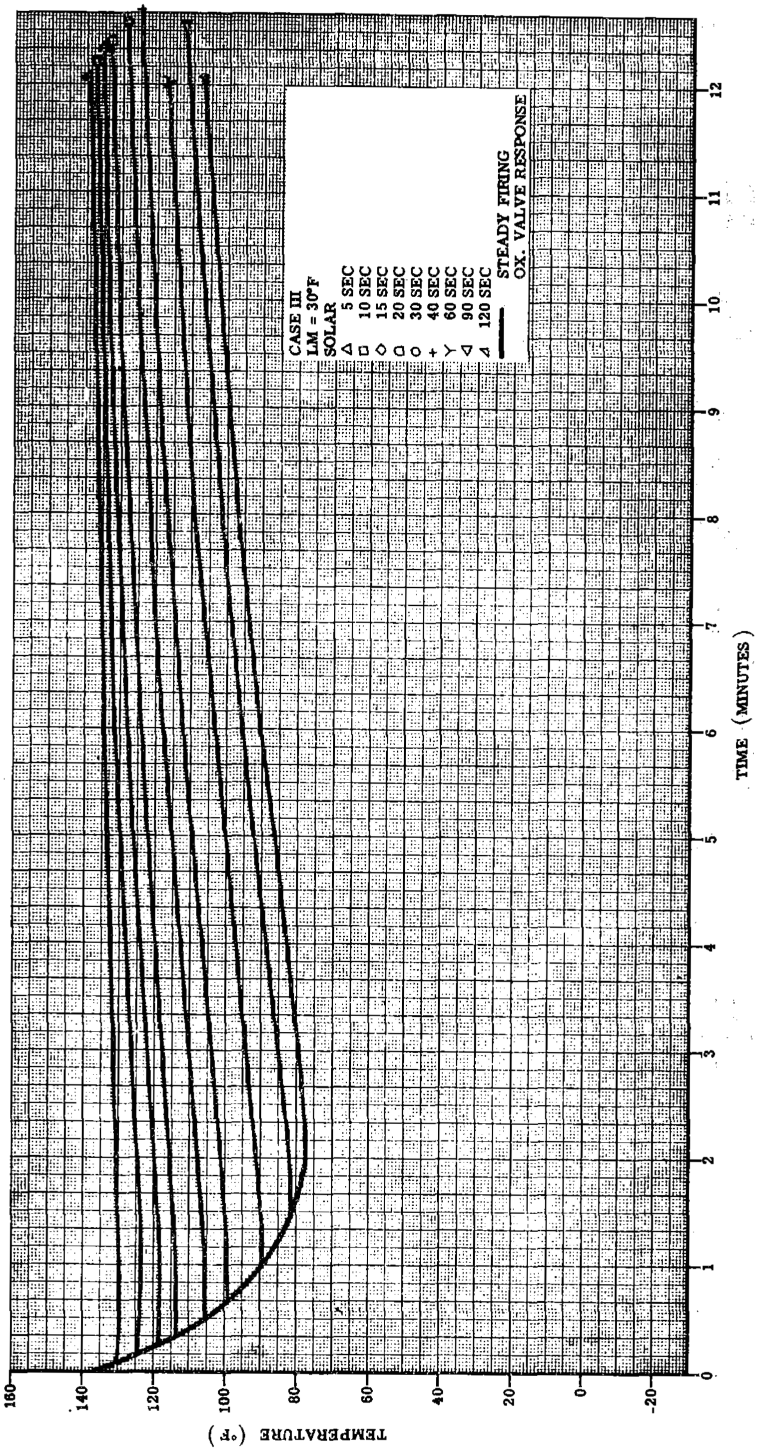

Figure 4.8-77. Steady Firing - Ox. Valve Response and Soakback
(See Para. 4.8.13.2)

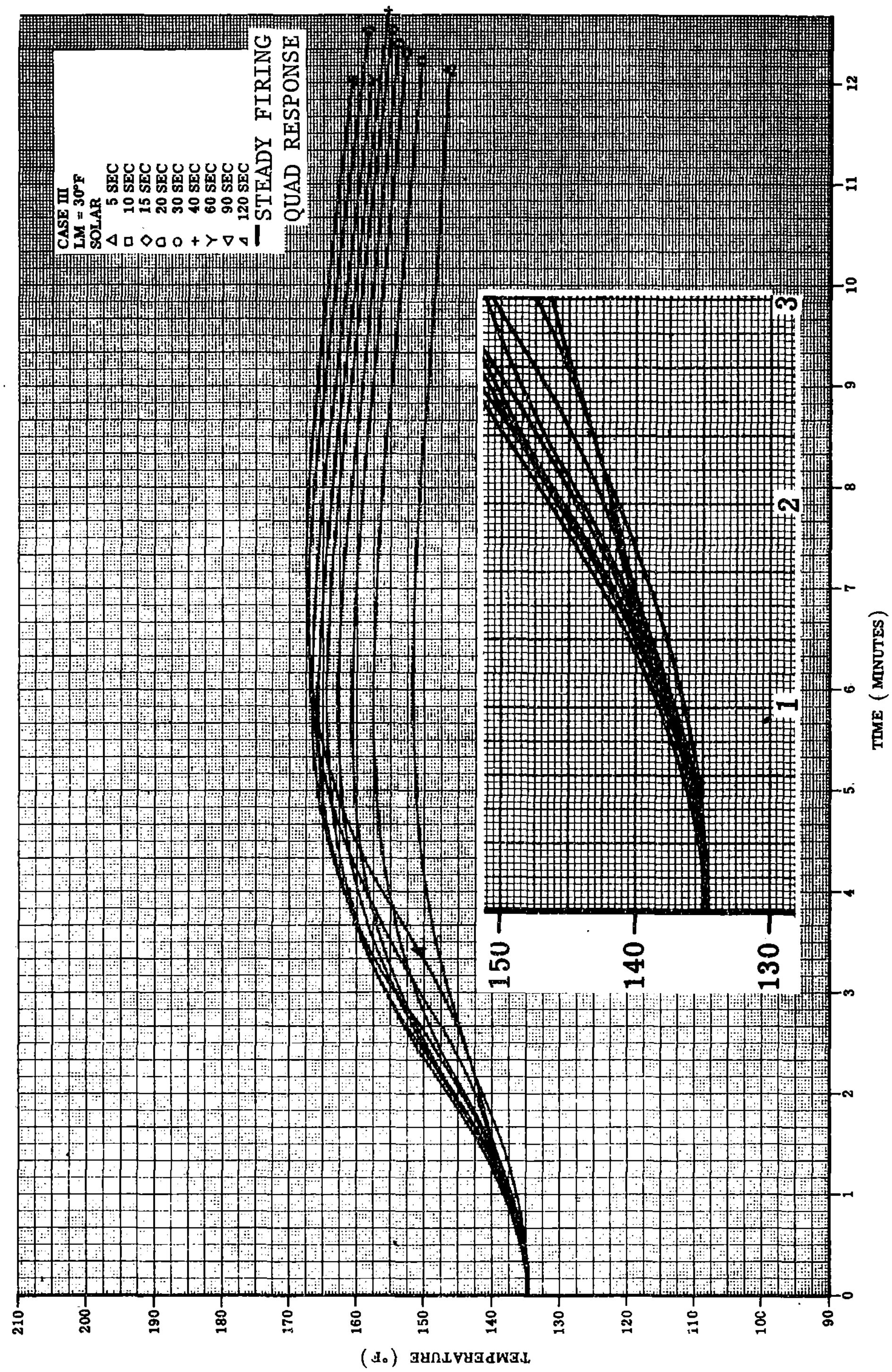

Figure 4.8-78. Steady Firing - Quad Response and Soakback
(See Para. 4.8.13.2)

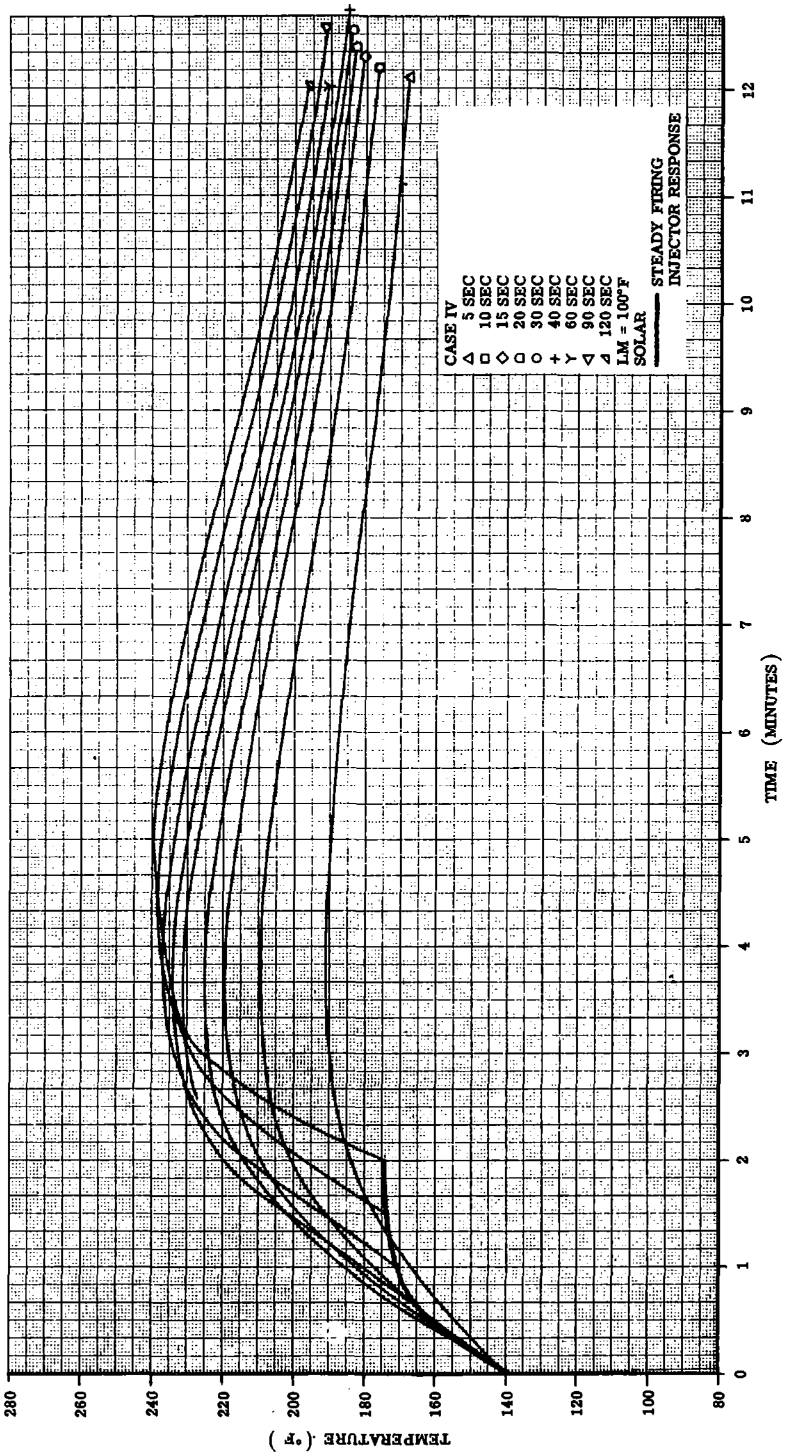

Figure 4.8-79. **Steady Firing - Injector Response and Soakback**
(See Para. 4.8.13.2)

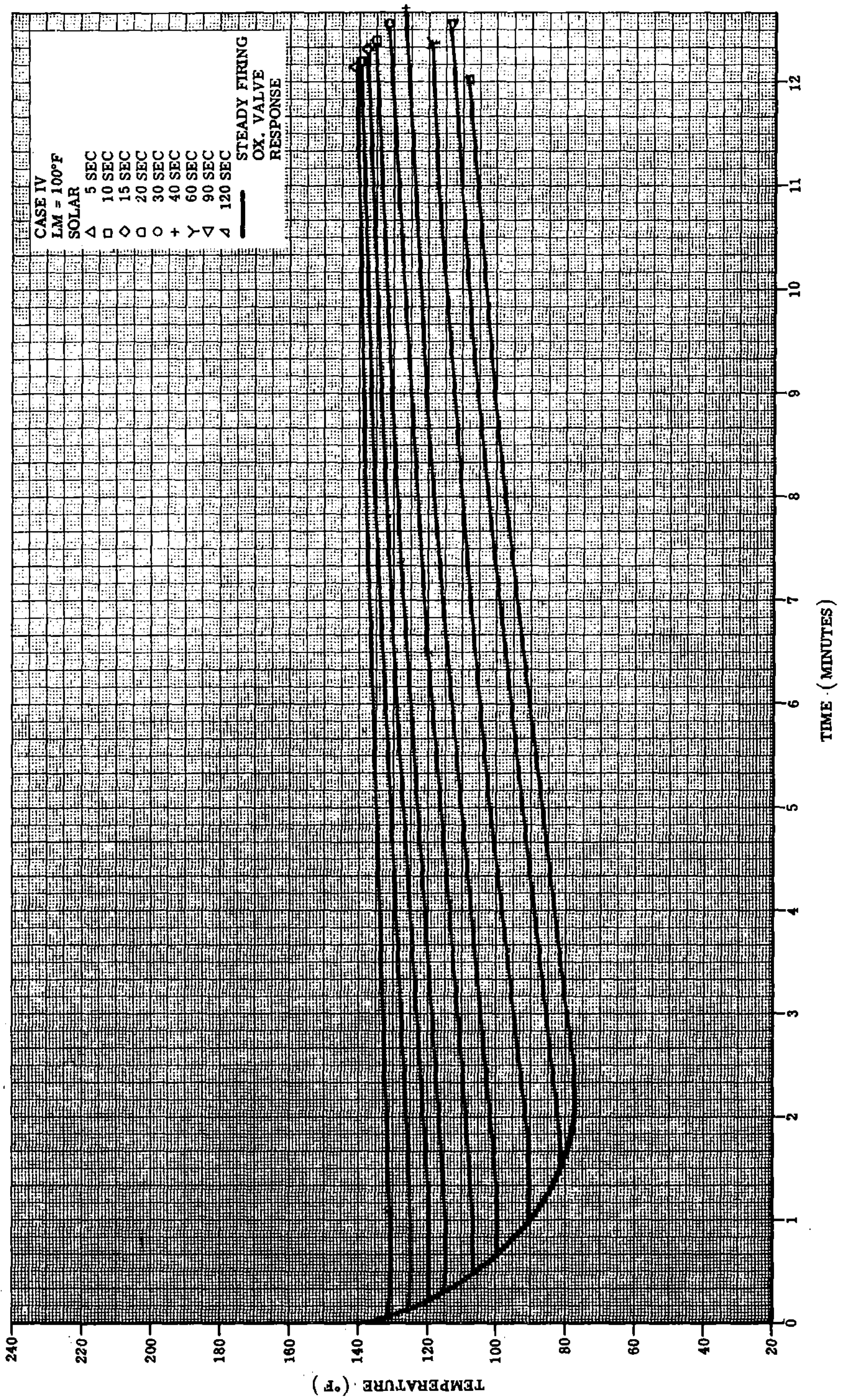

Figure 4.8-80. Steady Firing - Ox. Valve Response and Soakback
(See Para. 4.8.13.2)

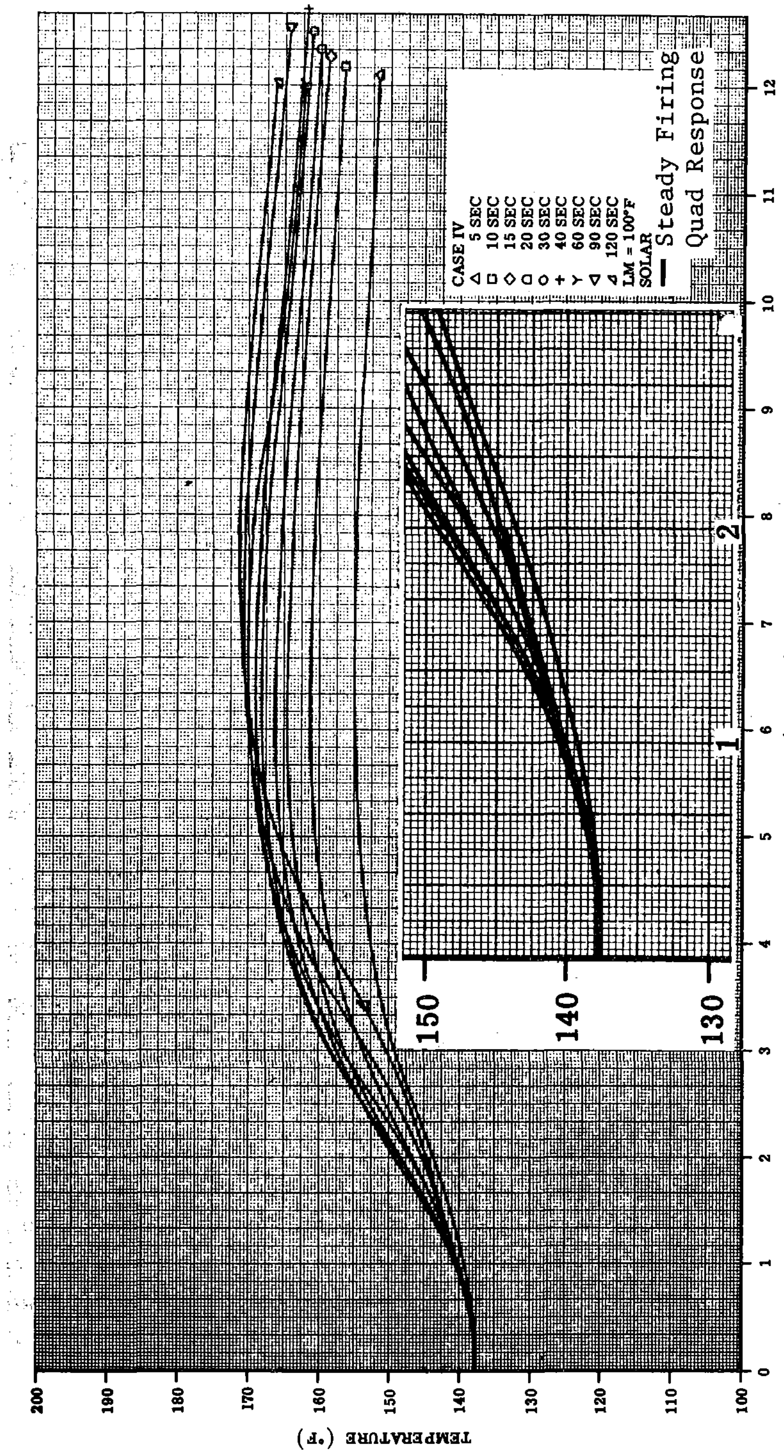

Figure 4.8-81. Steady Firing - Quad Response and Soakback
(See Para. 4.8.13.2)

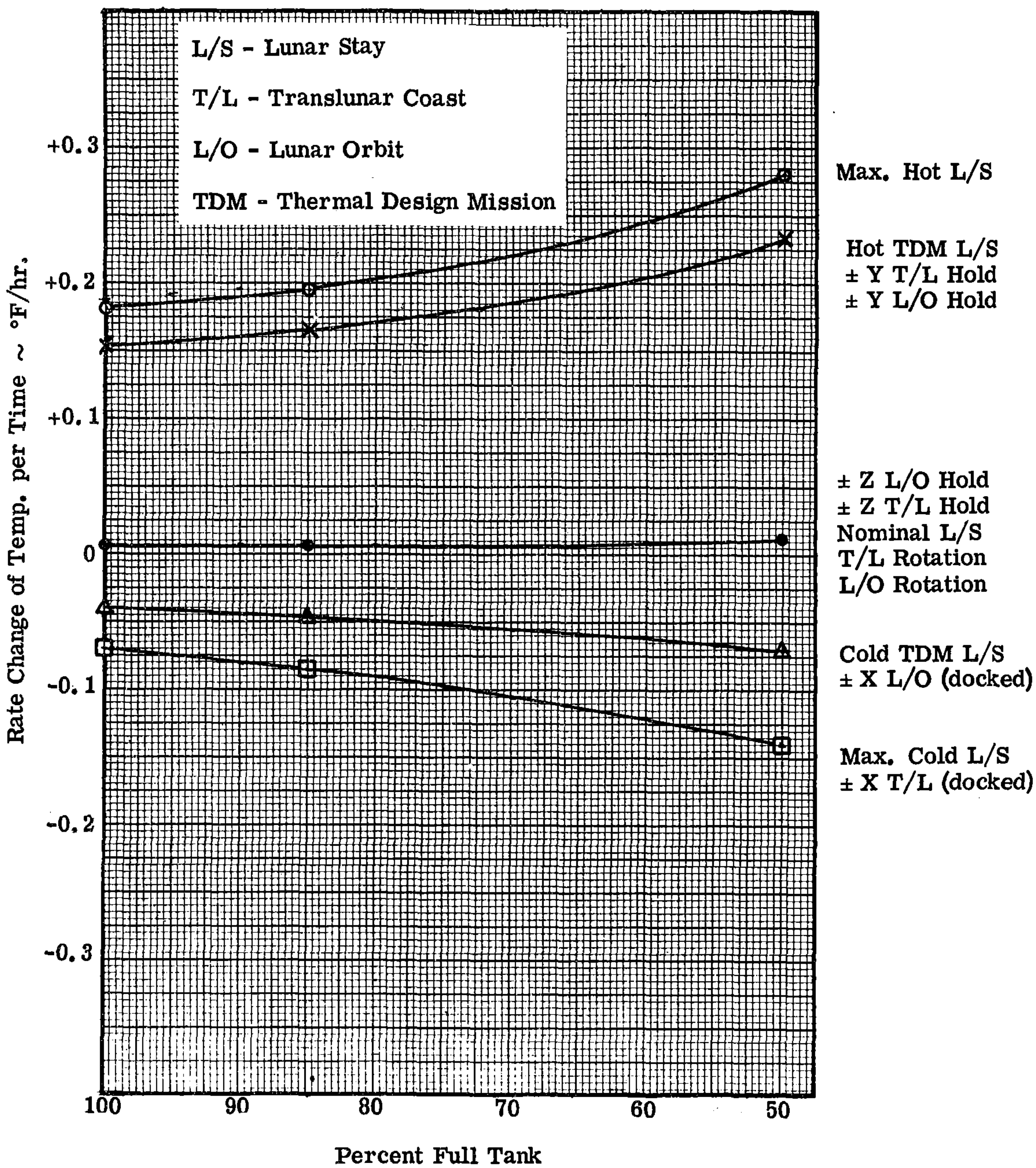

Figure 4.8-81.1 RCS Tank Skin Response vs. Percentage of Tank Propellant Quantity for J Missions

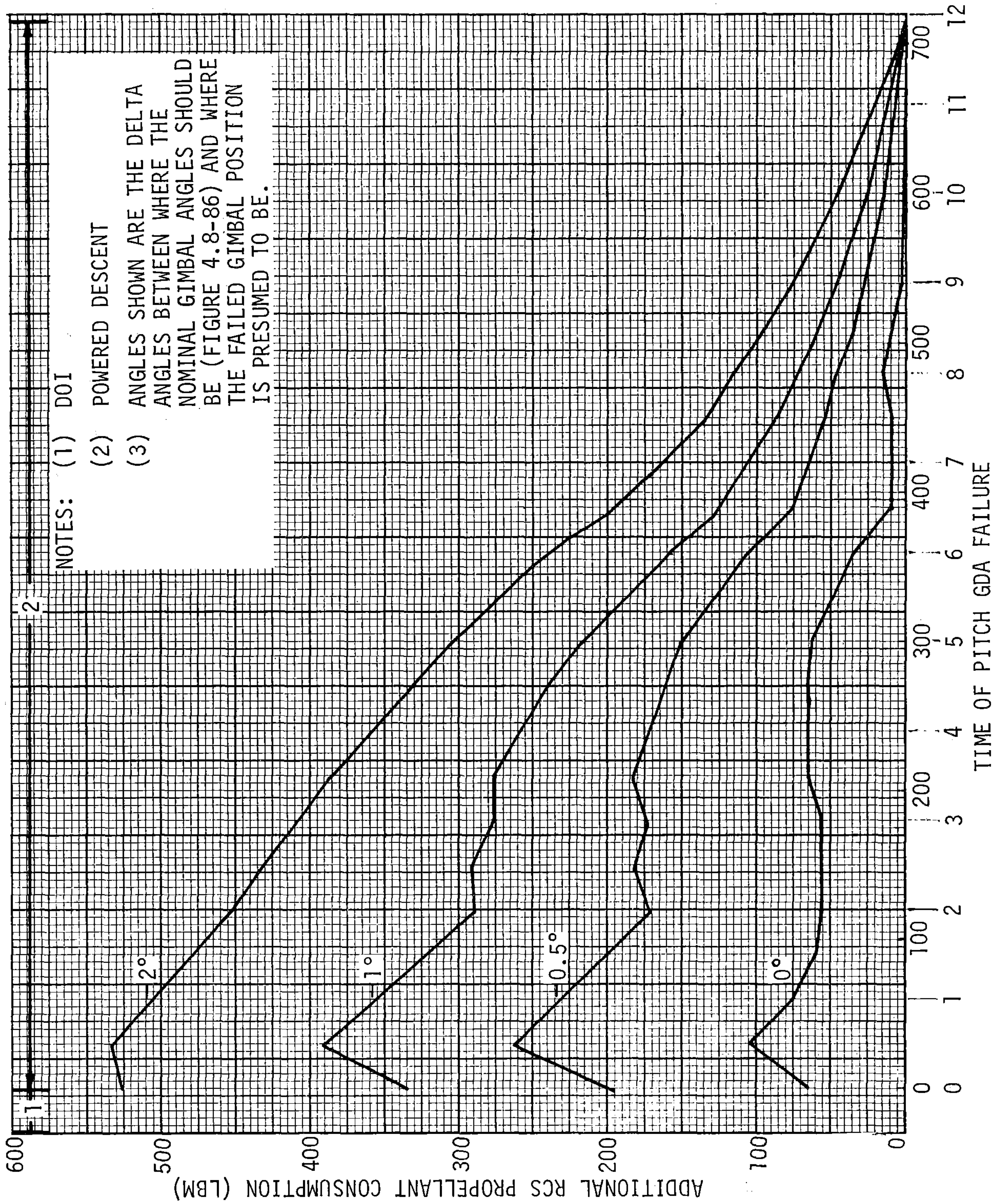

Figure 4.8-83. Additional RCS Consumption as a Result of a - Pitch GDA Failure During a DPS Firing (See Para. 4.8.14)

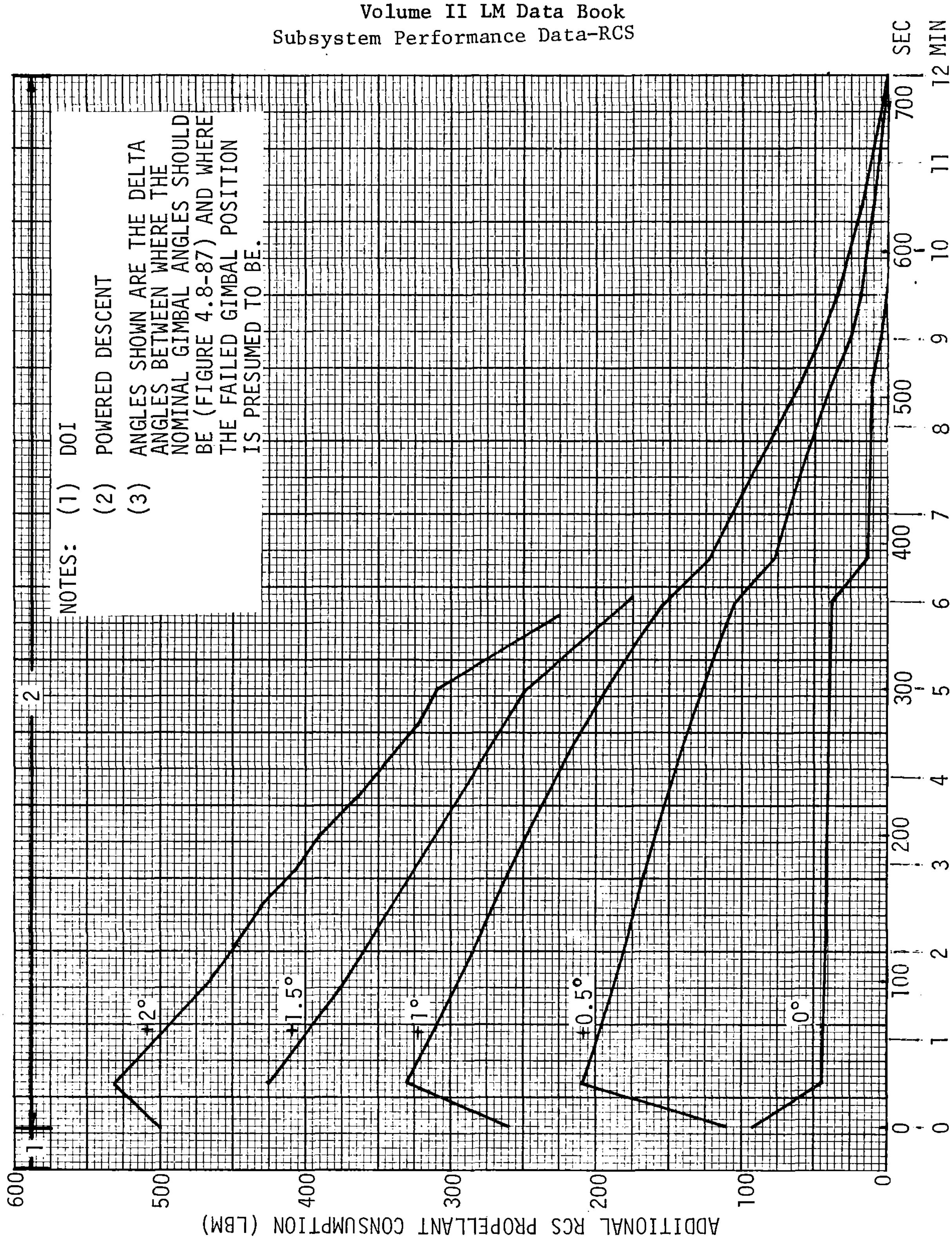

Figure 4.8-84. Additional RCS Consumption as a Result of a + Roll GDA Failure During a DPS Firing (See Para. 4.8.14)

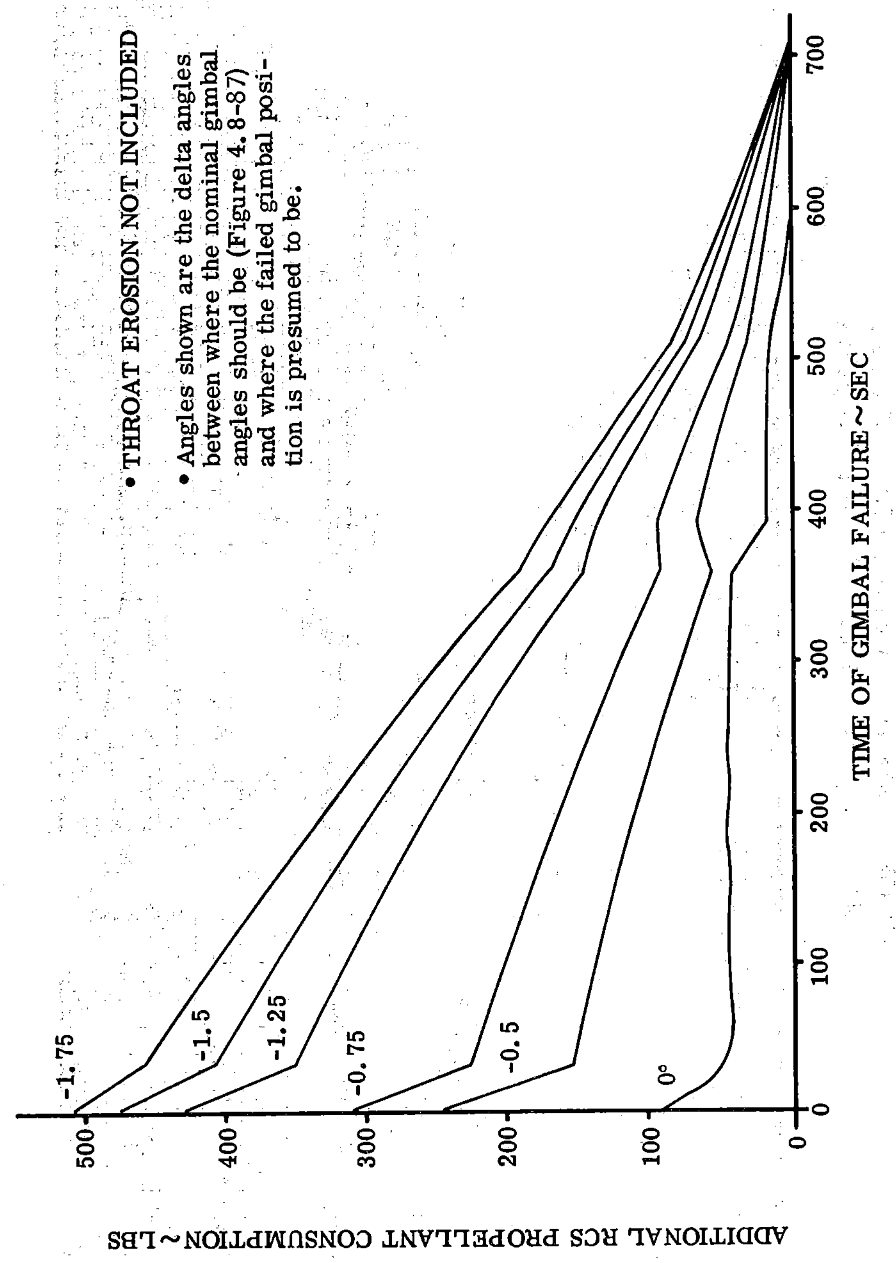

Figure 4.8-85. Additional RCS Propellant Consumption as a Result of a Roll GDA Failure During a DPS Firing (Para 4.8.14)

CURVES BASED ON MAXIMUM ALLOWABLE DEVIATIONS FOR RCS PROPELLANT AND CONTROLLABILITY RED LINES AS A FUNCTION OF ELAPSED BURN TIME

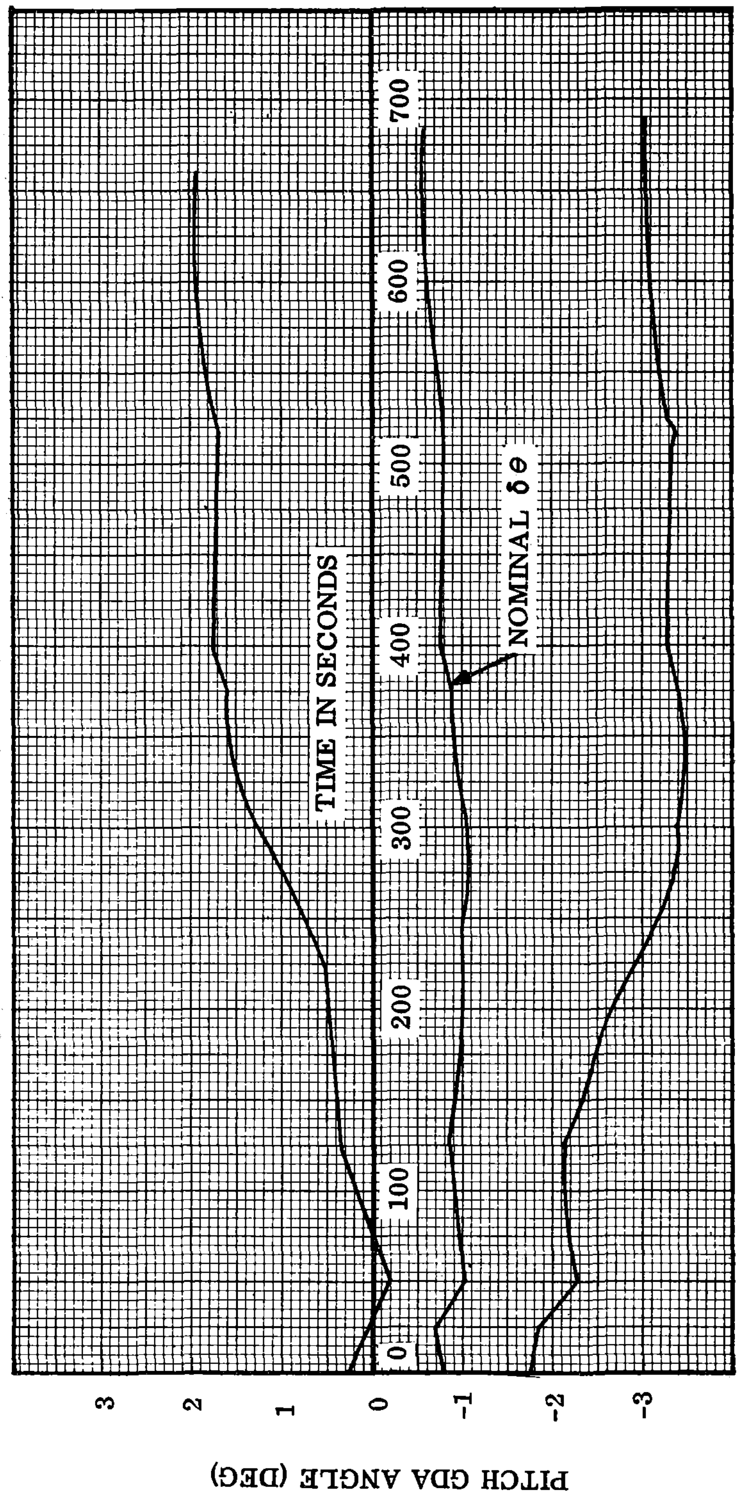

NOTES: (1) ASSUMES 140 LBM RCS PROPELLANT REMAINING AT TOUCHDOWN

(2) THRUST VECTOR CHANGES DUE TO THROAT EROSION NOT INCLUDED

Figure 4.8-86. Maximum Allowable Pitch GDA Failure Angle Vs. Time During Powered Descent (See Para. 4.8.14.2)

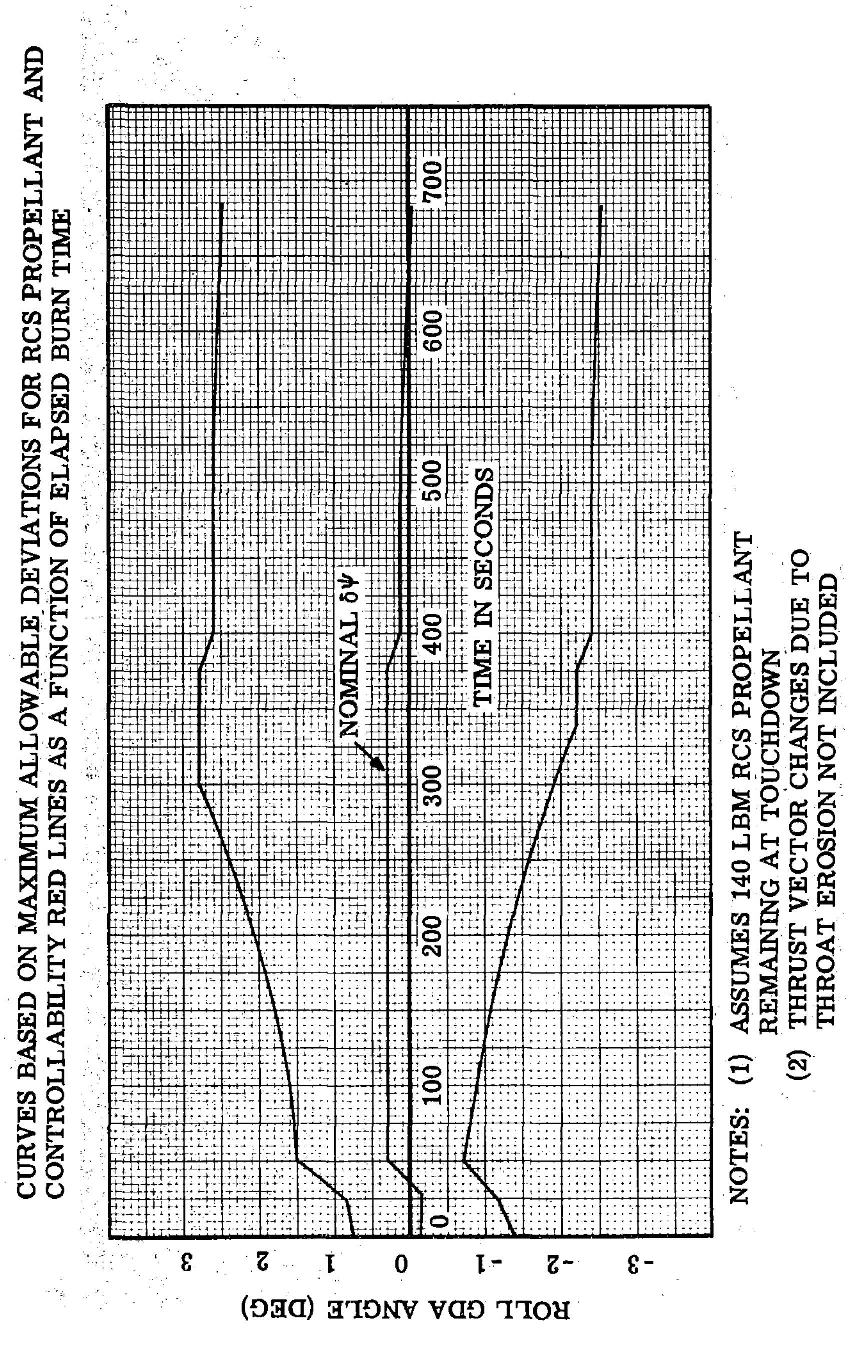

Figure 4.8-87. Maximum Allowable Roll GDA Failure Angle Vs. Time During Powered Descent (See Para. 4.8.14.2)

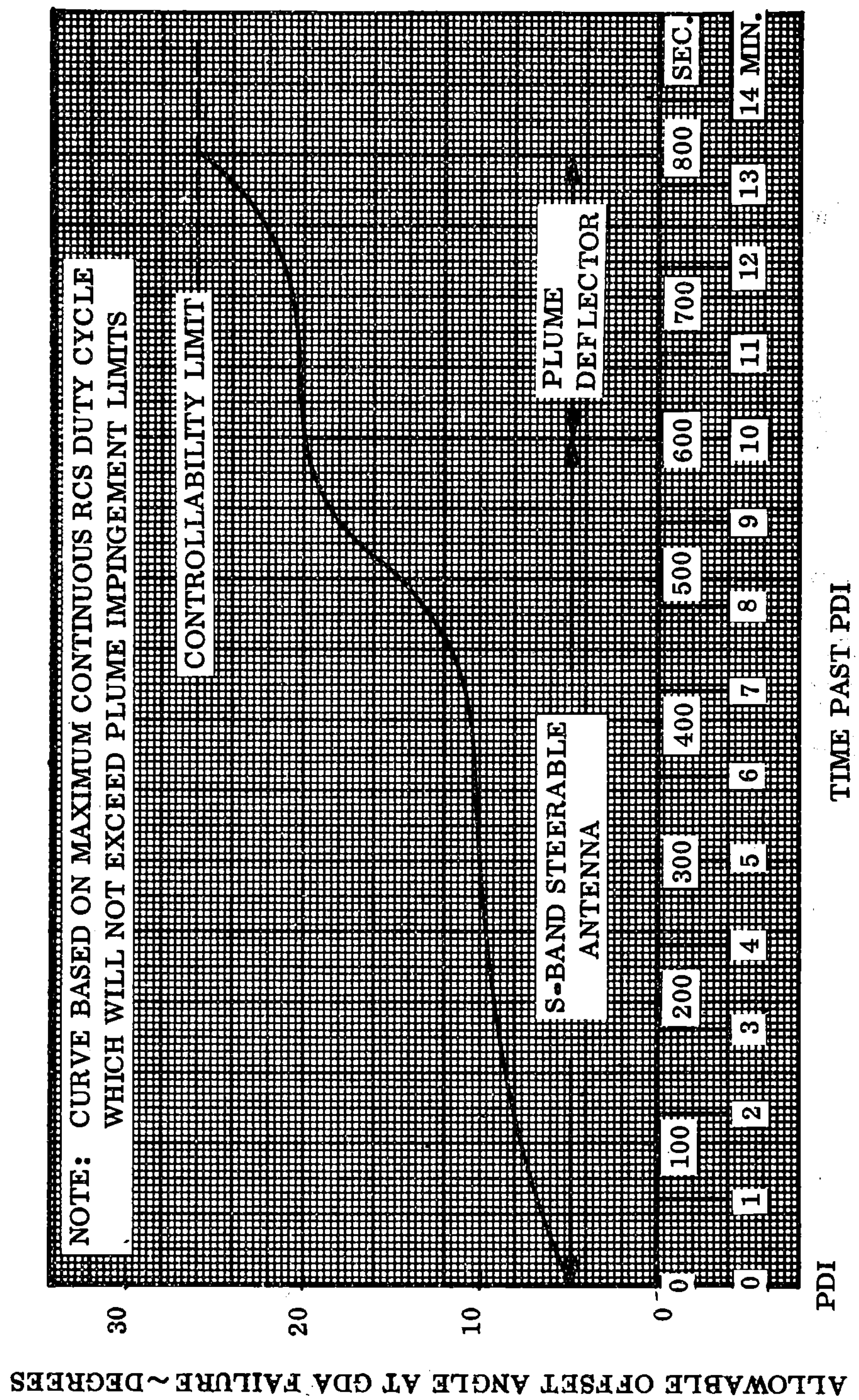

Figure 4.8-88. Maximum Allowable GDA Offset Angle at the Time of GDA Failure vs Time During a DPS Firing (See para. 4.8.14)

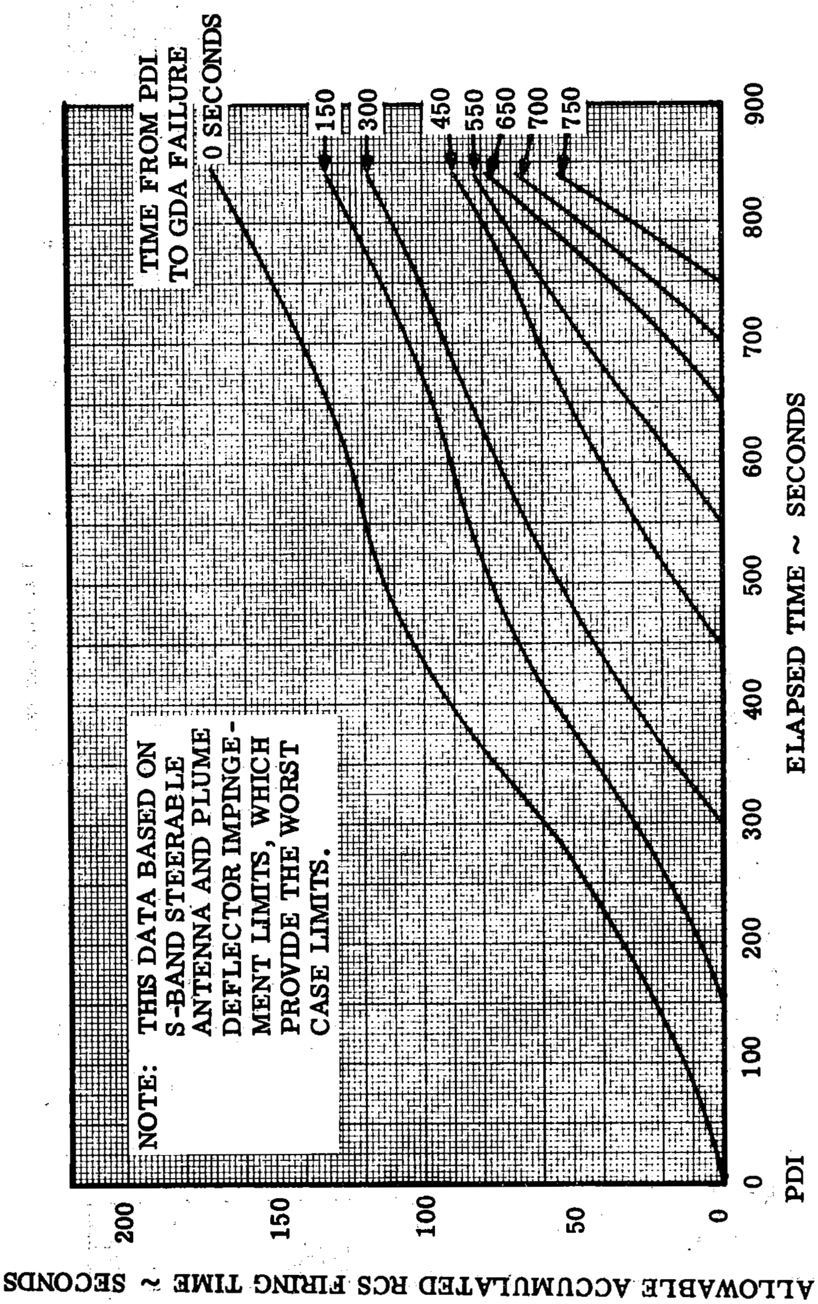

Figure 4.8-89. Allowable RCS (+ or - X) Firing Time vs. Time From PDI With a Failed GDA (See Para. 4.8.14)

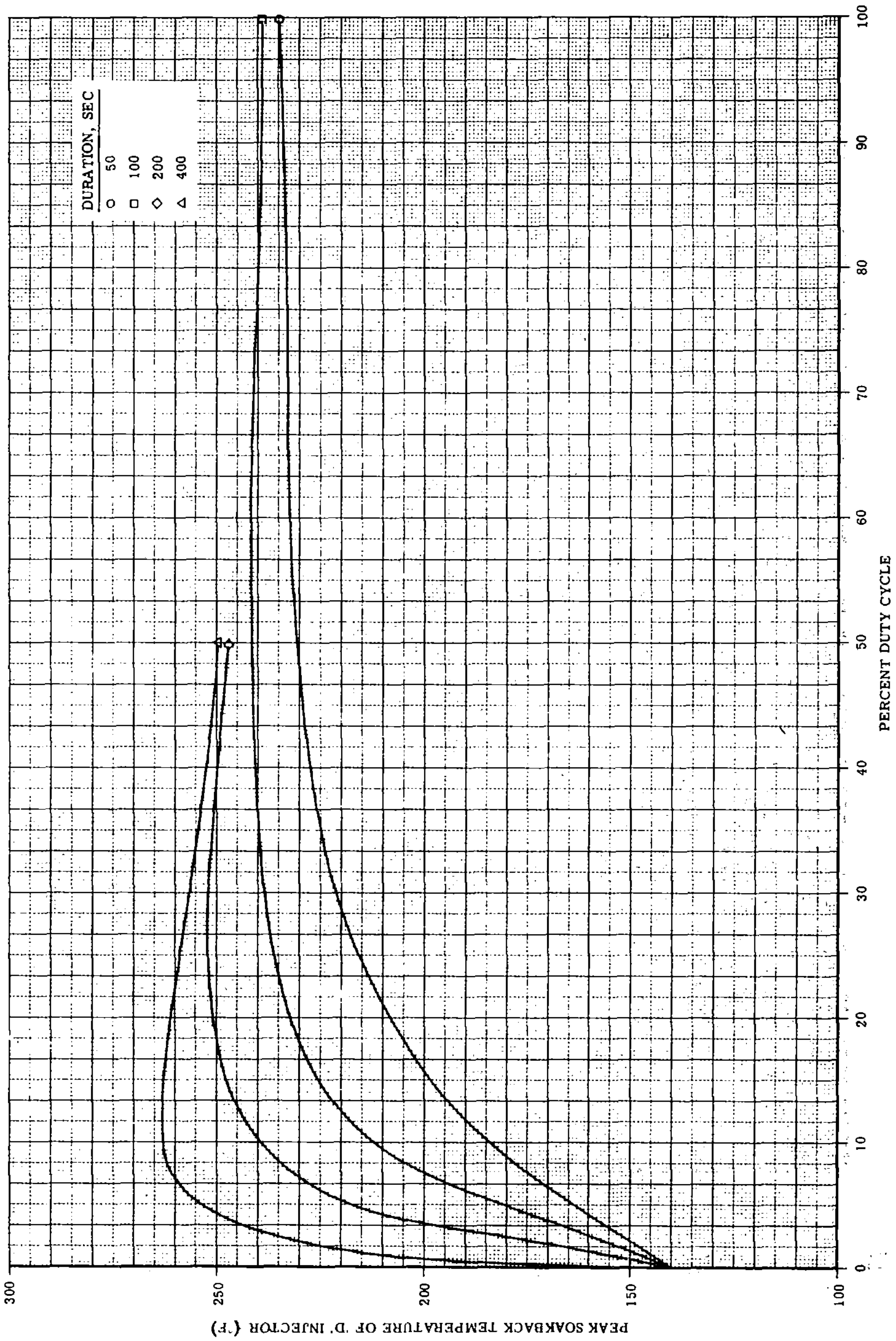

Figure 4.8-90. Peak Soakback Temperature of 'D' Injector versus Percent Duty Cycle
(See Para. 4.8.15)

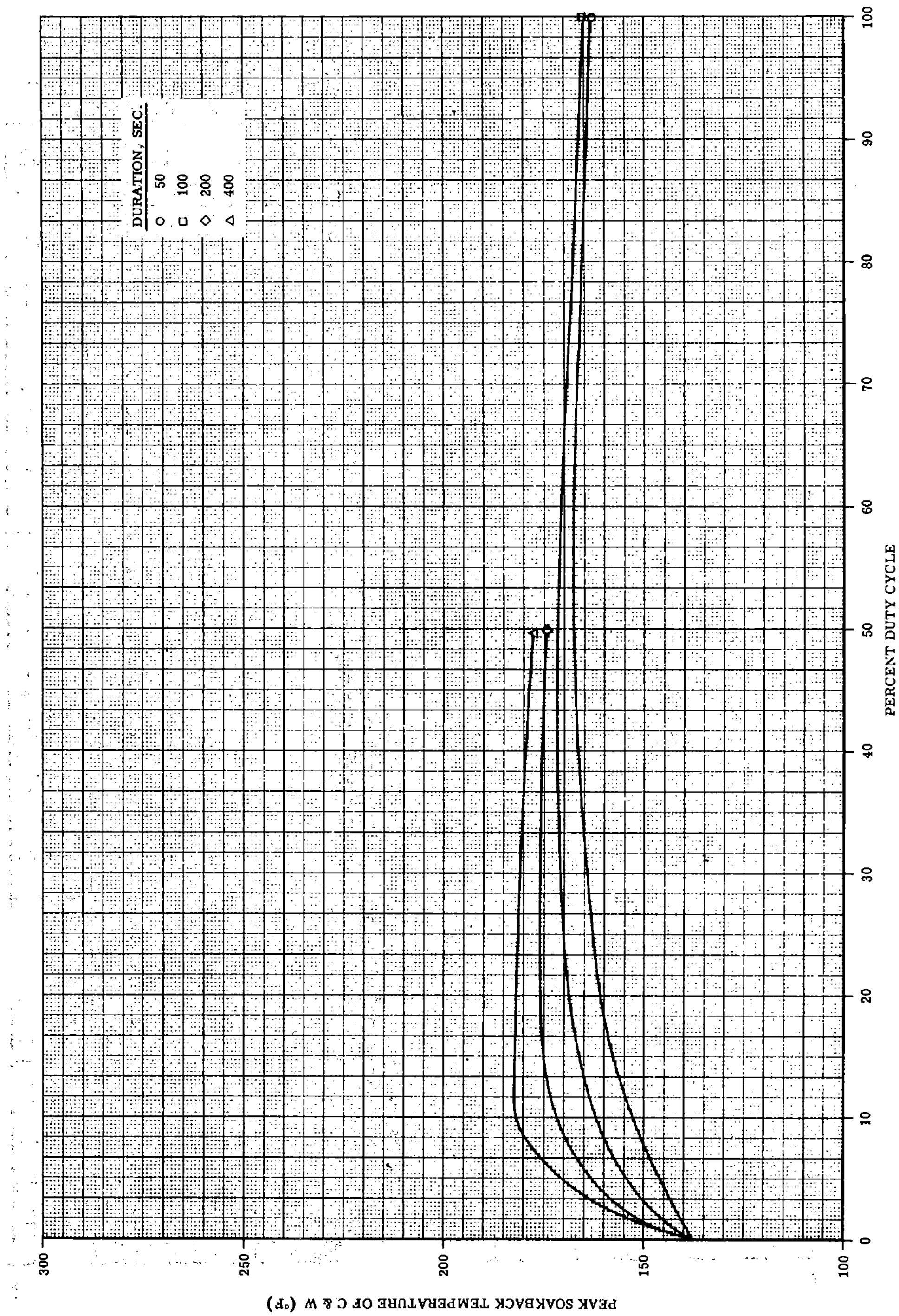

Figure 4.8-91. Peak Soakback Temperature of Quad versus Percent Duty Cycle (See Para. 4.8.15)

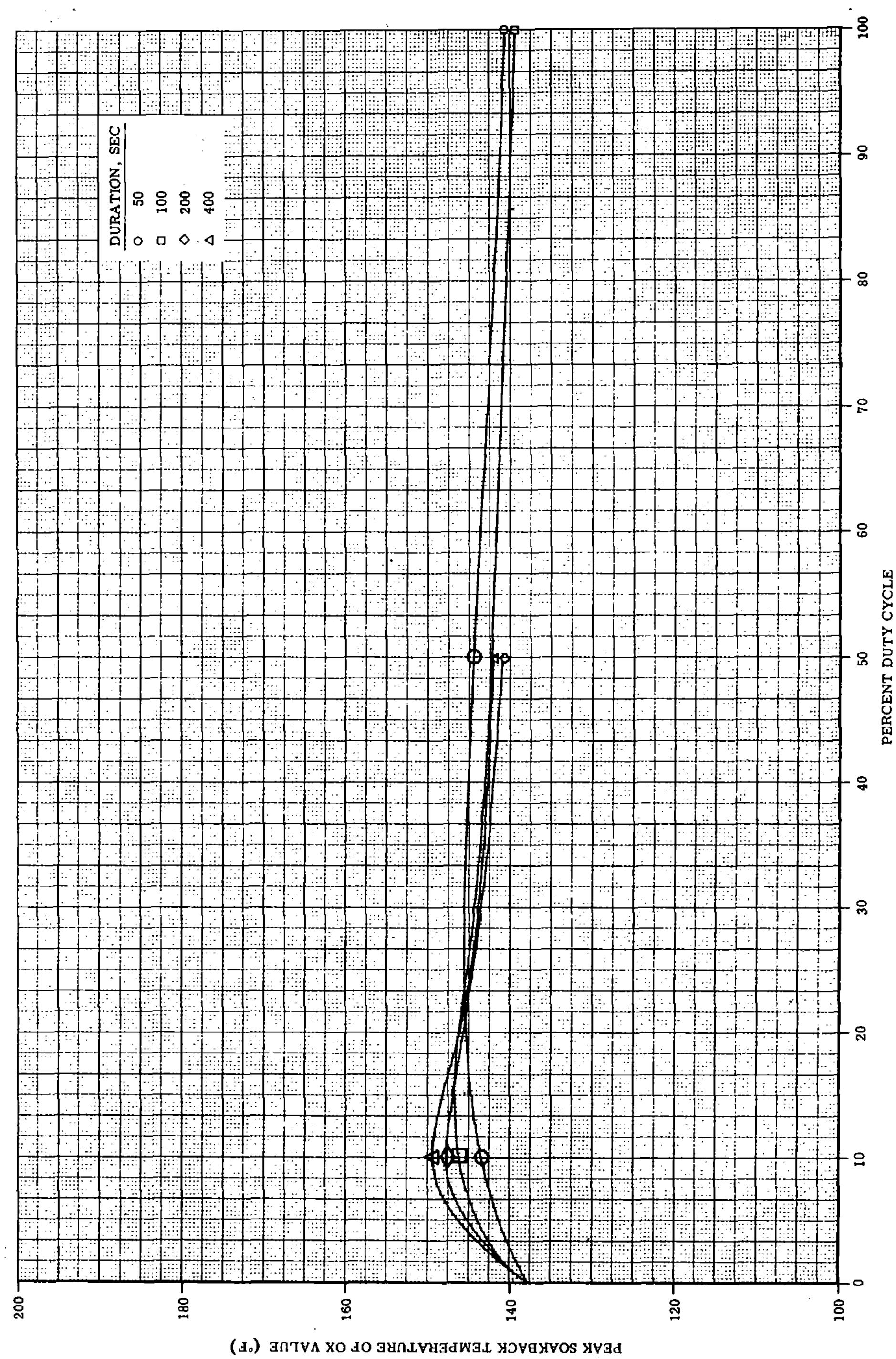

Figure 4.8-92. Peak Soakback Temperature of Ox Valve versus Percent Duty Cycle
(See Para. 4.8.15)

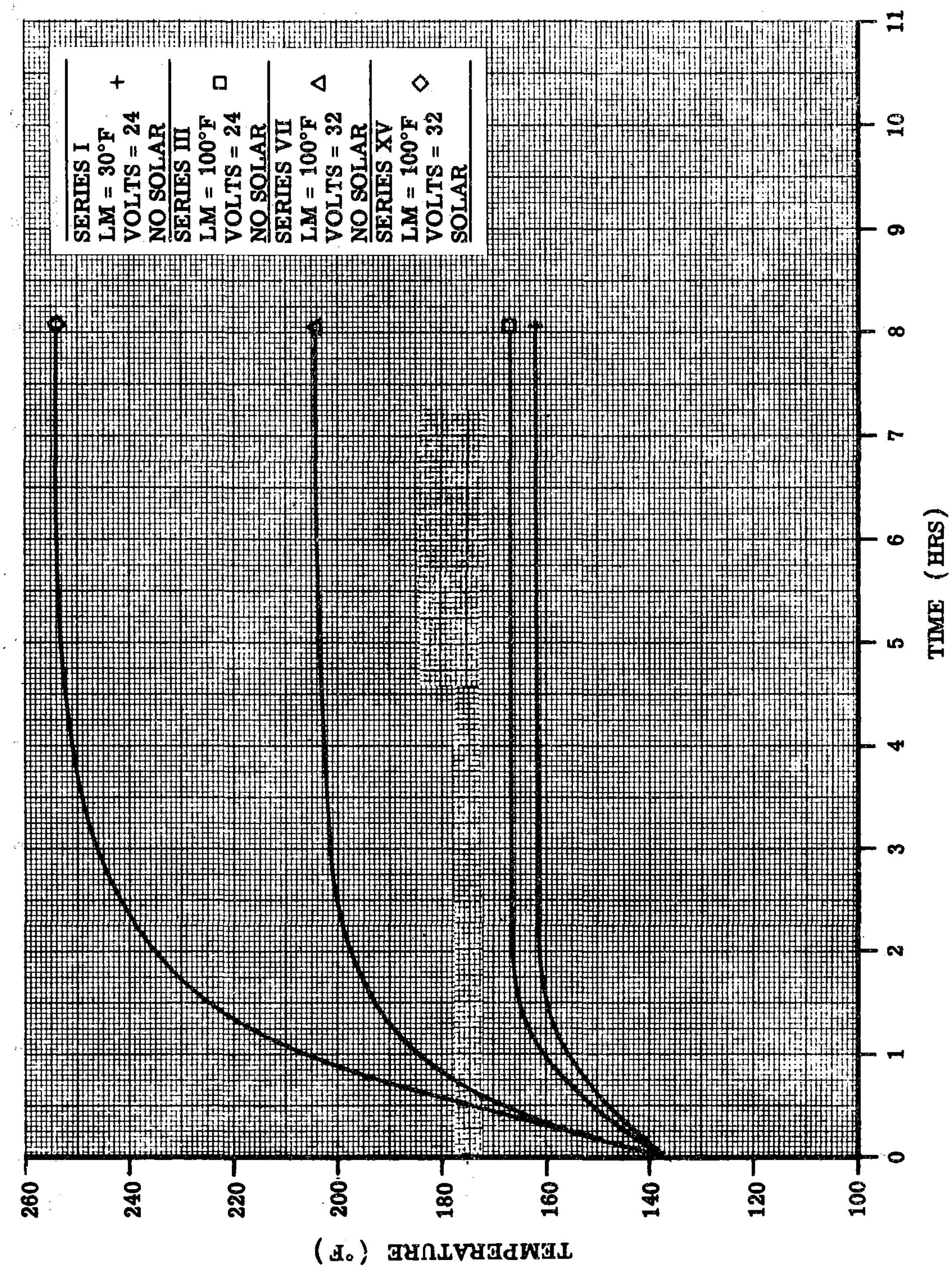

Figure 4.8-93. Comparison of Ox Valve ('U' Engine) Transients for a Spectrum of 'U' Engine Heater-On Failures (See Para. 4.8.16)

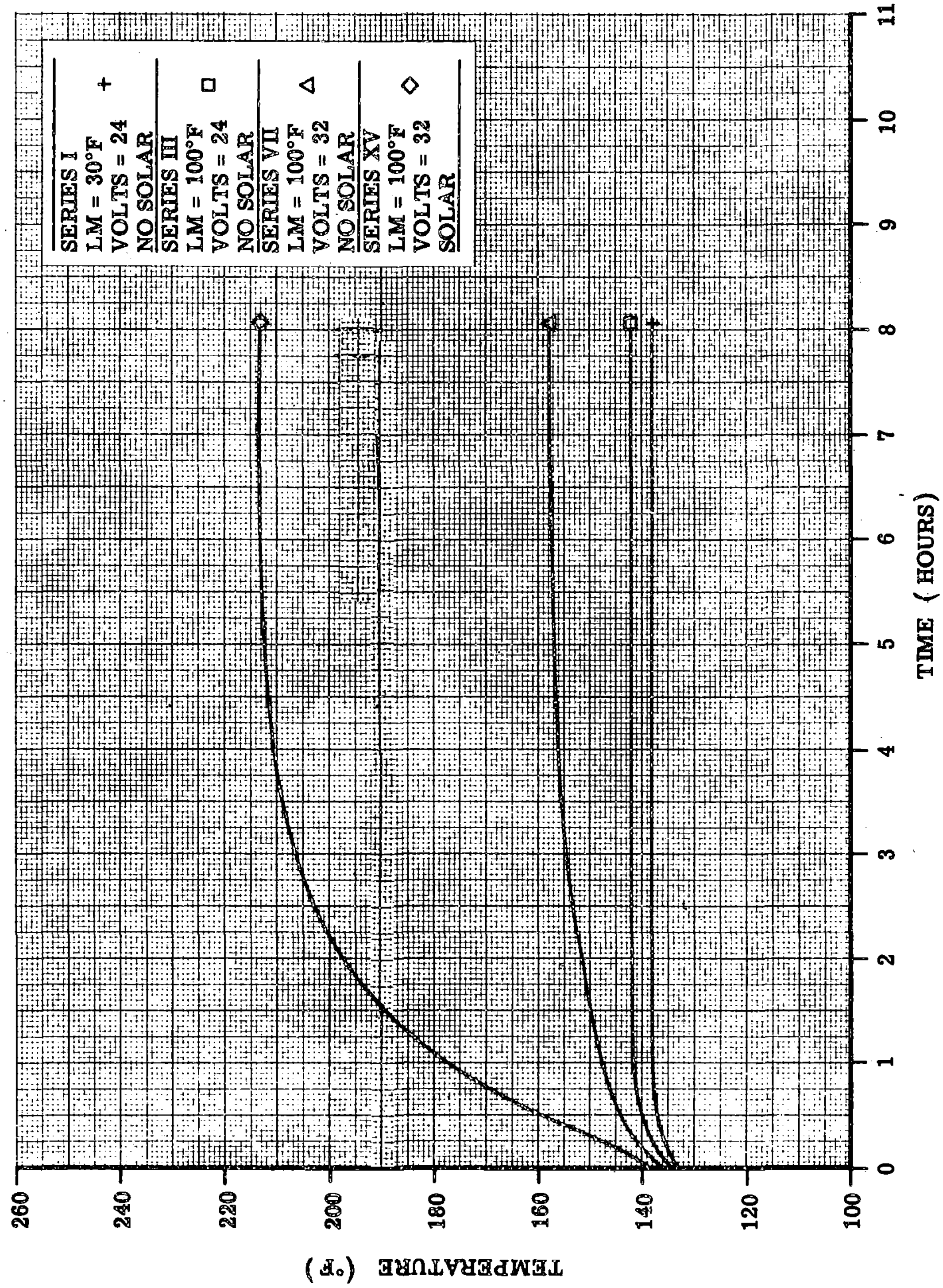

Figure 4.8-94. Comparison of Quad Transients for a Spectrum of 'U' Engine Heater-On Failures (See Para. 4.8.16)

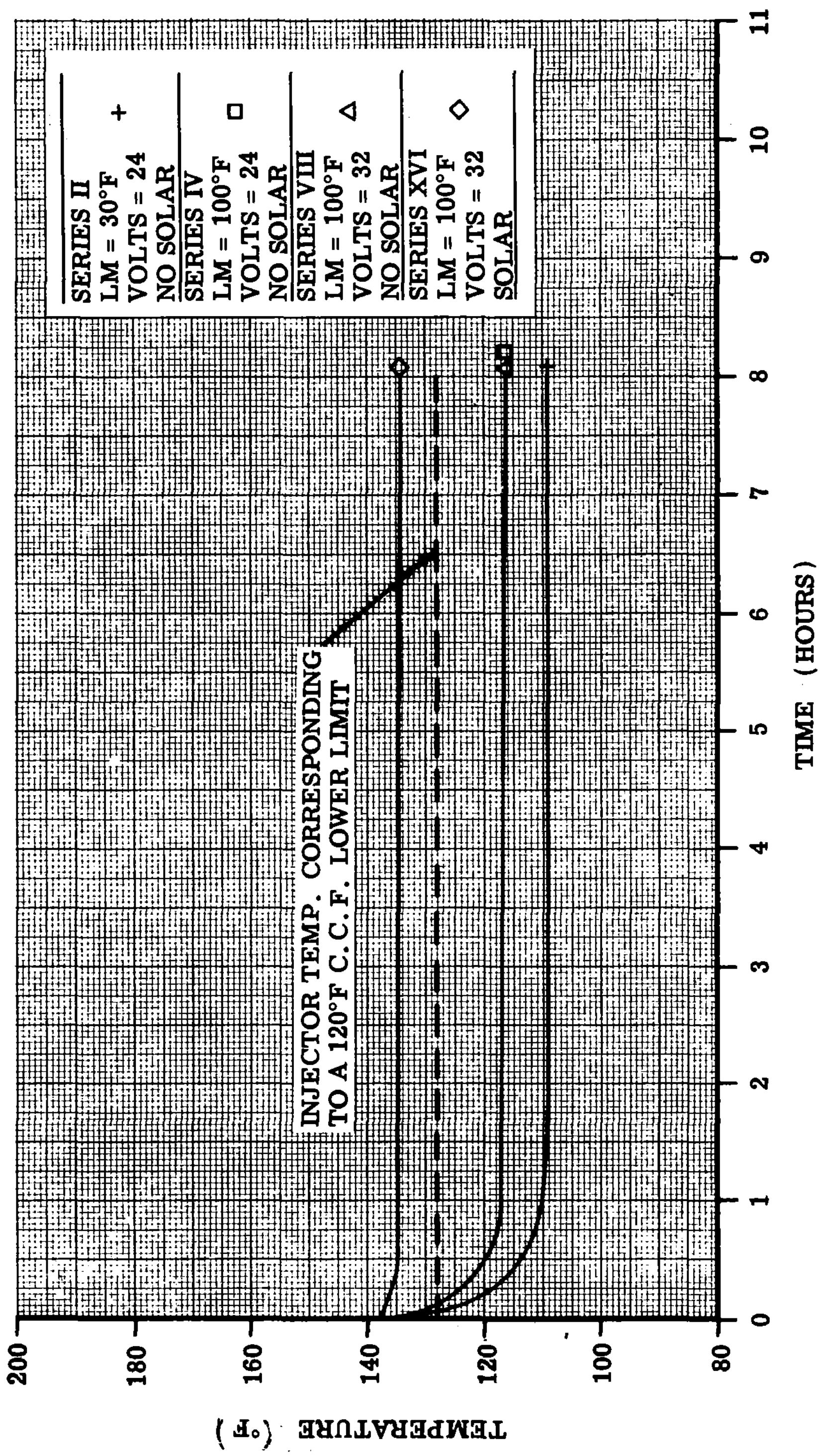

Figure 4.8-95. Comparison of Injector 'F' Engine Transients for a Spectrum of 'F' Engine Heater-Off Failures
(See Para. 4.8.16)

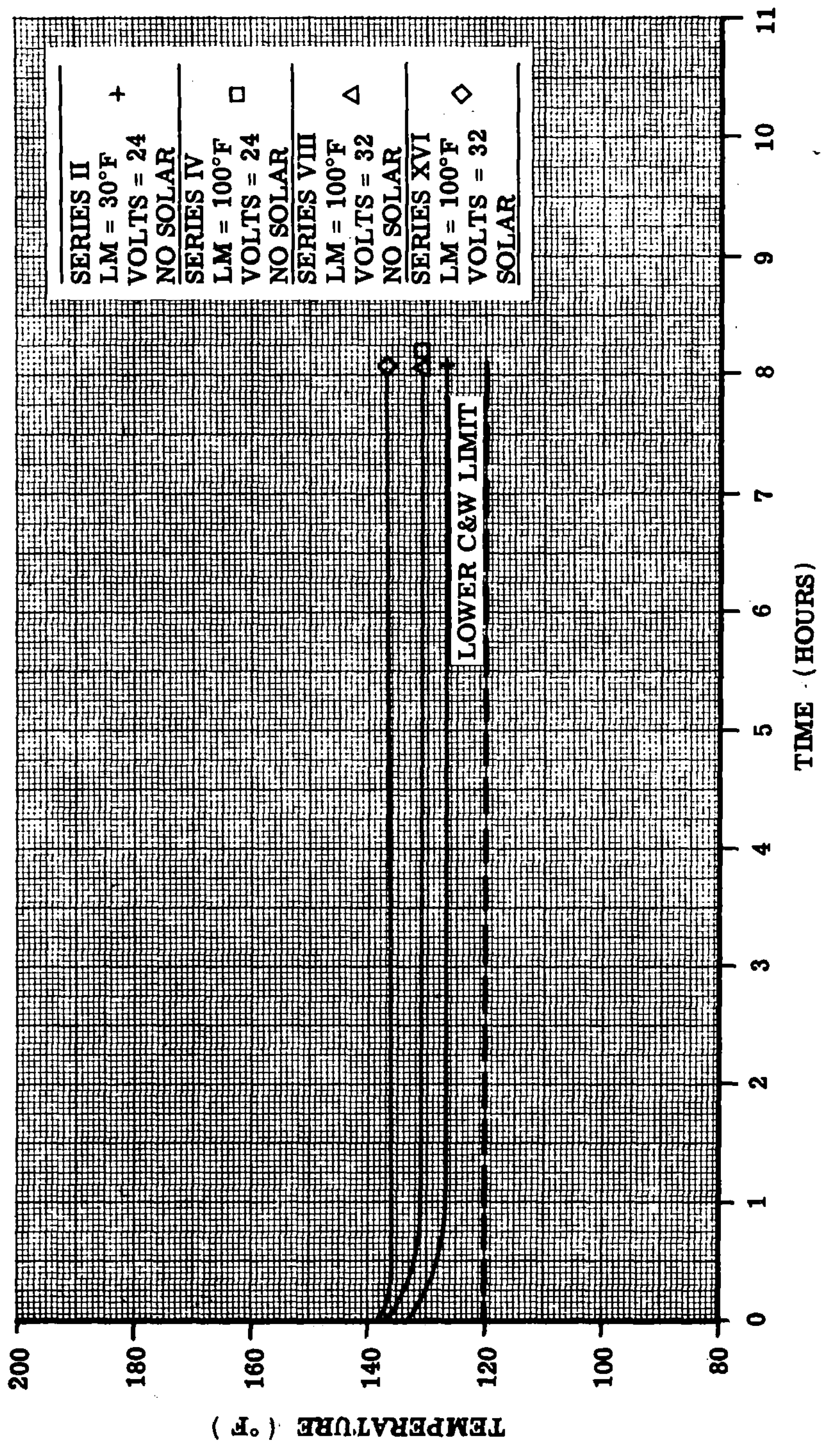

Figure 4.8-96. Comparison of C&W Transients for a Spectrum of 'F' Engine Heater-Off Failures
(See Para. 4.8.16)

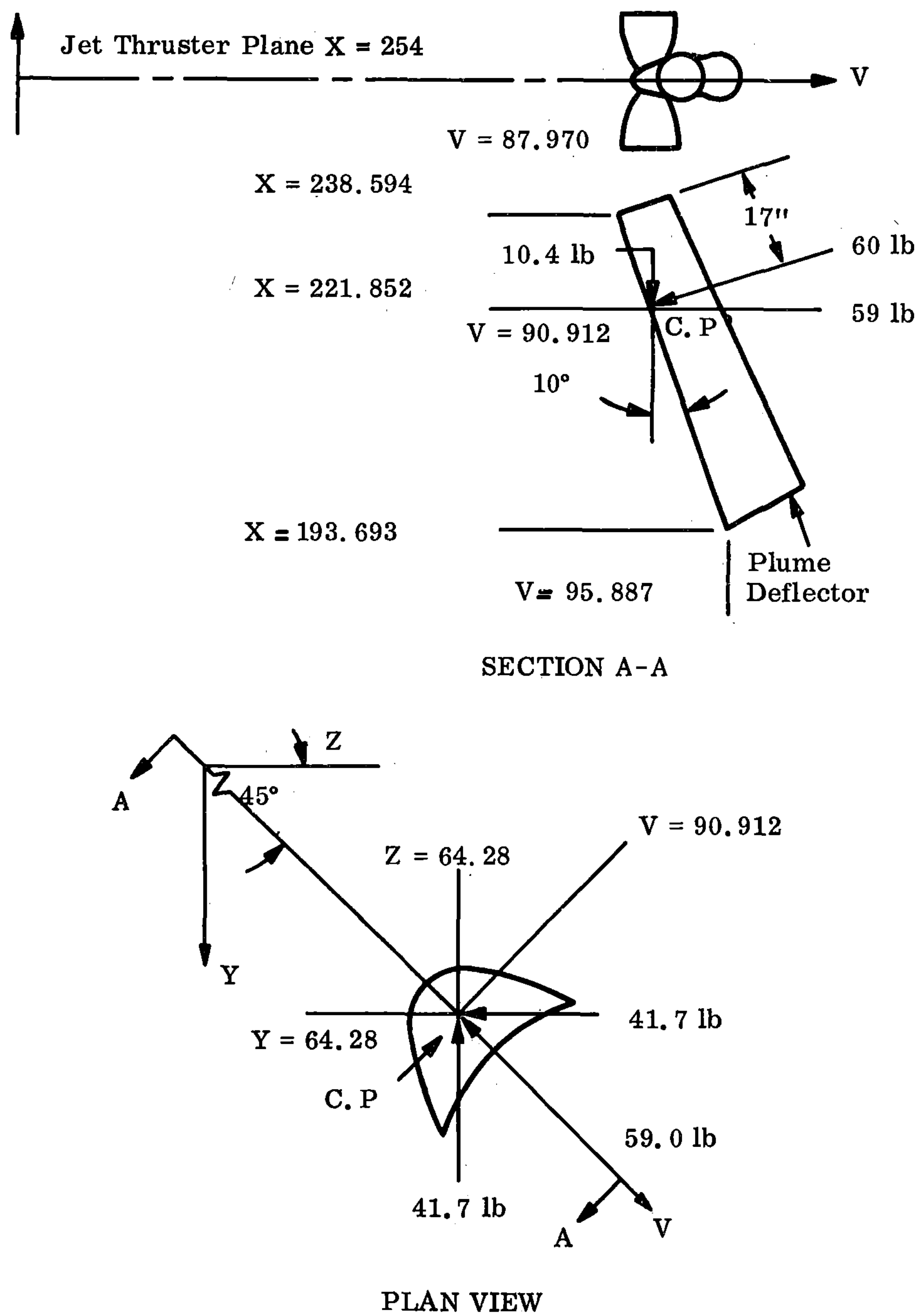

Figure 4.8-97. Location of RCS Plume Deflector and Impingement Forces (Para. 4.8.6.2)

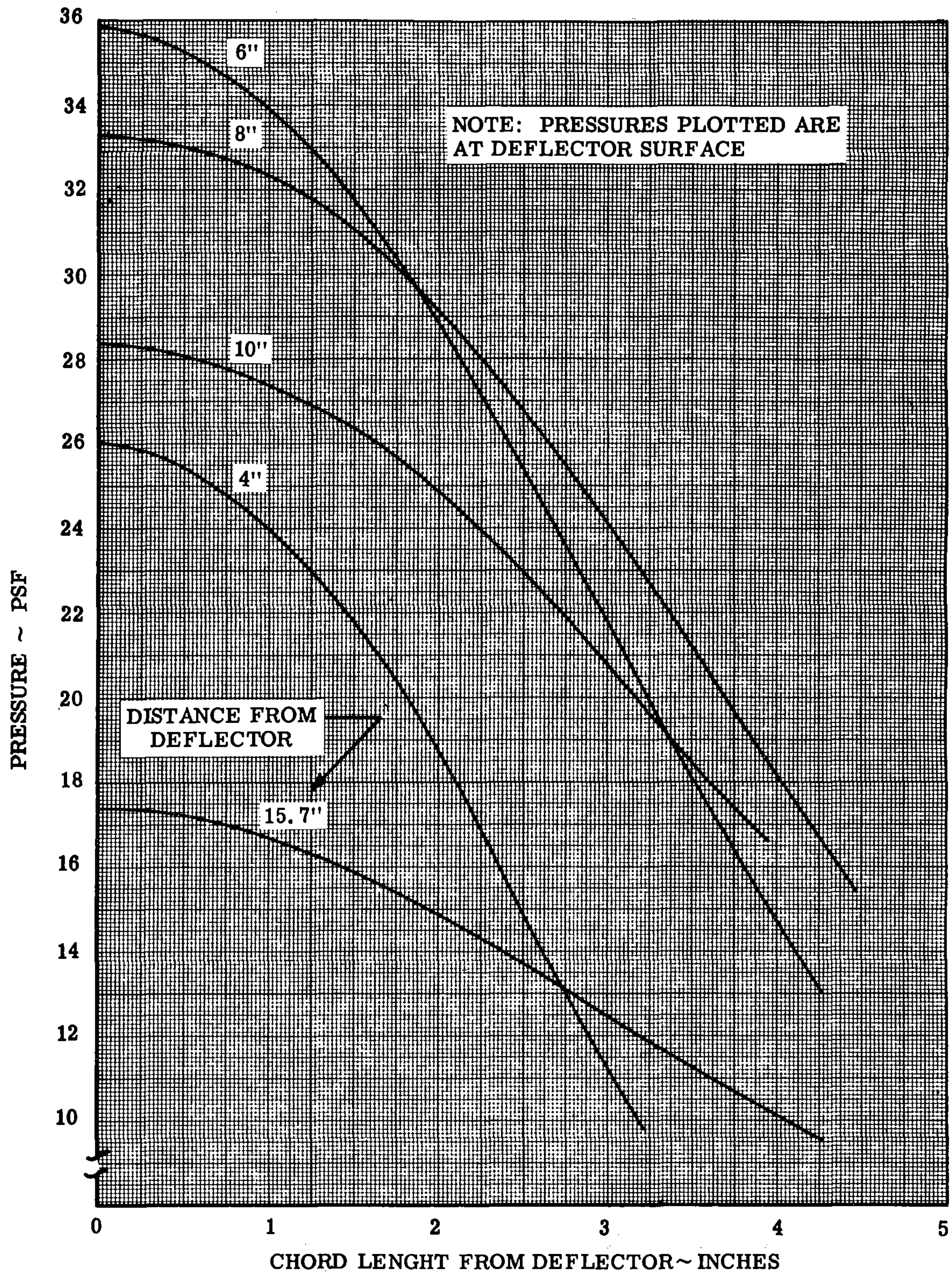

Figure 4.8-98. Deflector Pressure Distribution
(Para. 4.8.6.3)

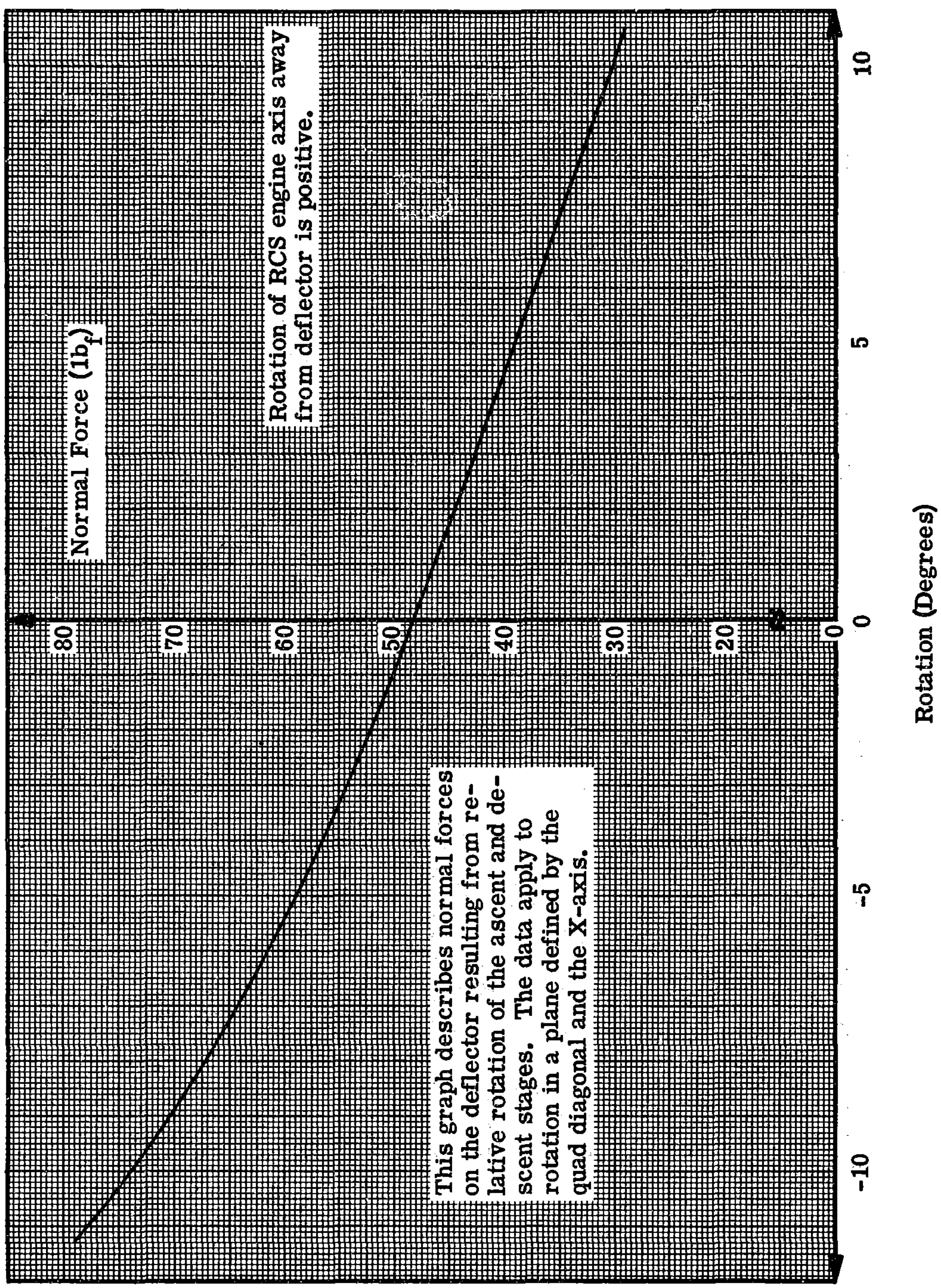

Figure 4.8-99. Normal Force On Deflector Due to **Ascent/Descent Rotation**

(See Para. 4.8.6.3)

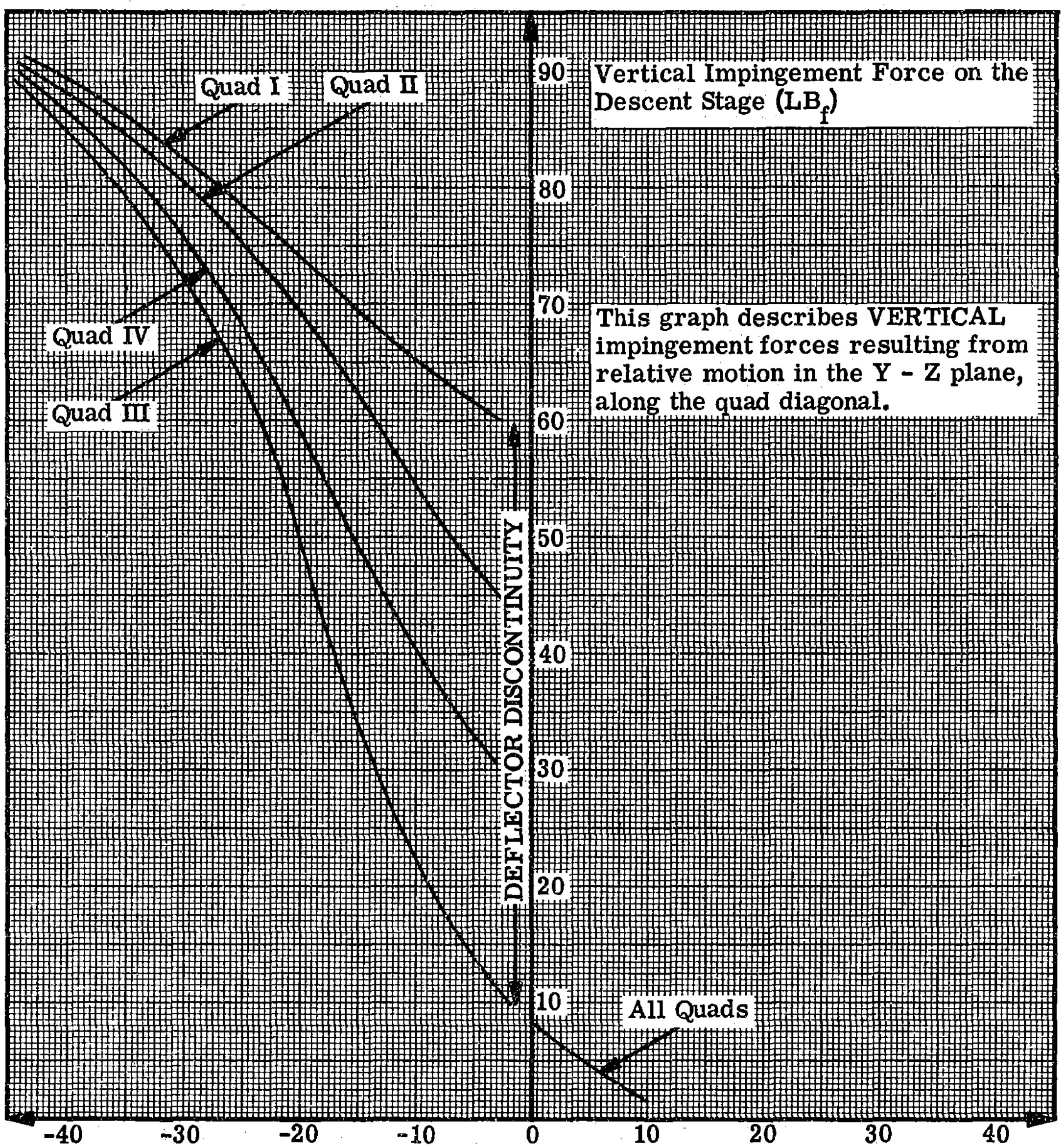

Figure 4.8-100. Vertical Impingement Force vs. Ascent/Descent Stage Side Slip

(See Para. 4.8.6.3)

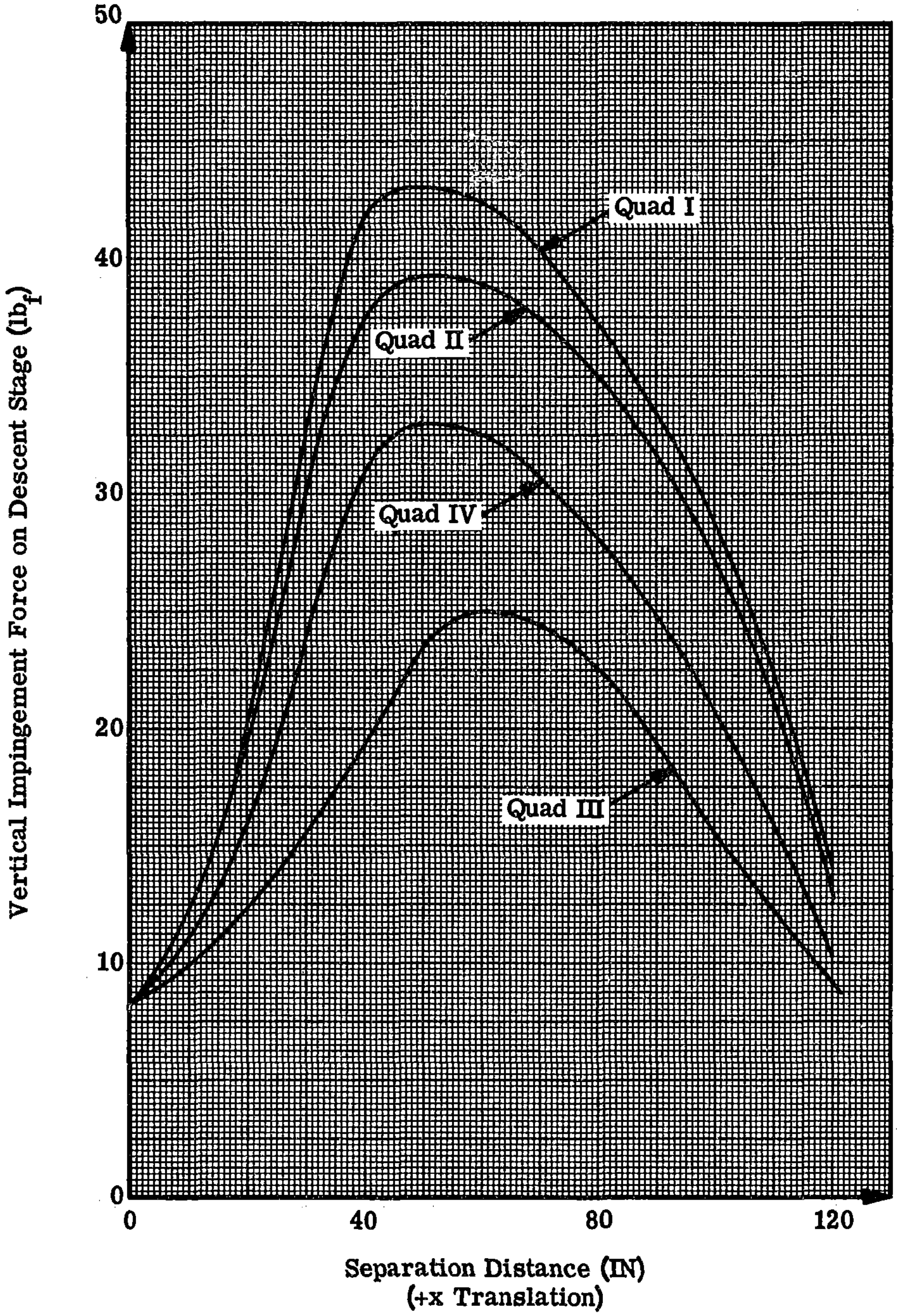

Figure 4.8-101. Vertical Impingement Force vs. Ascent/Descent Stage Separation

(See Para. 4.8.6.3)

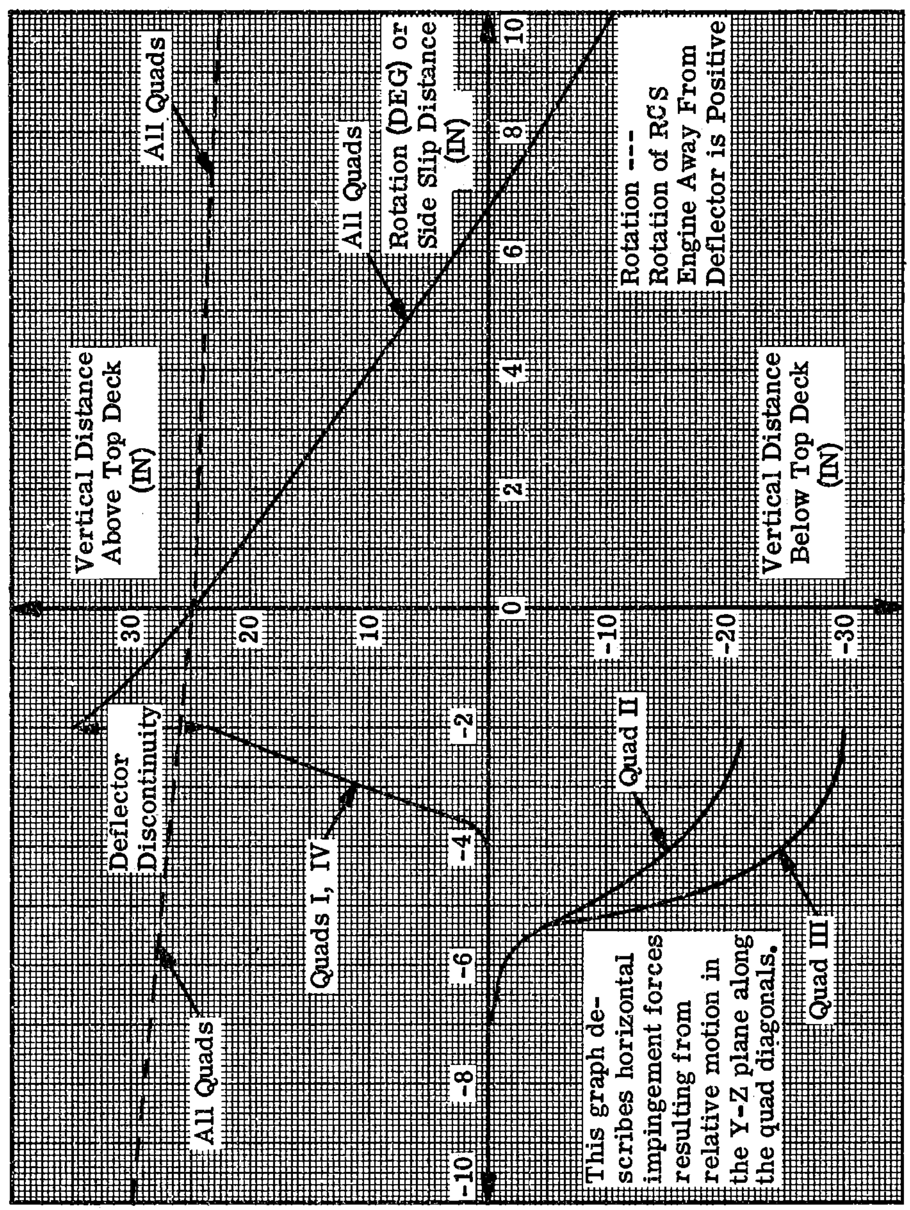

Figure 4.8-102. Vertical Distance From Top Deck (of Descent Stage) of Horizontal Force vs. Ascent/Descent Stage Side Slip and Rotation

(See Para. 4.8.6.3)

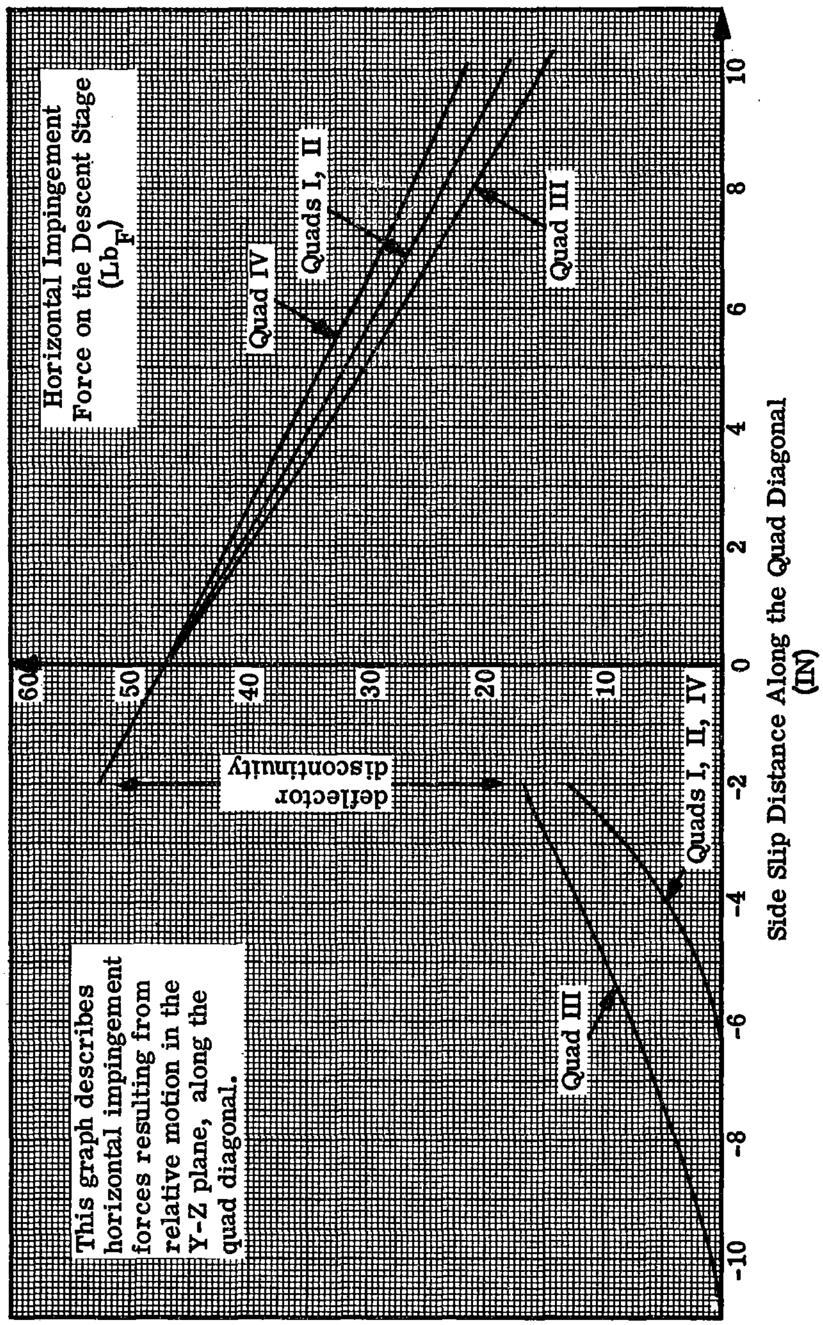

Figure 4.8-103. Horizontal Impingement Force vs. Ascent/Descent Stage Side Slip

(See Para. 4.8.6.3)

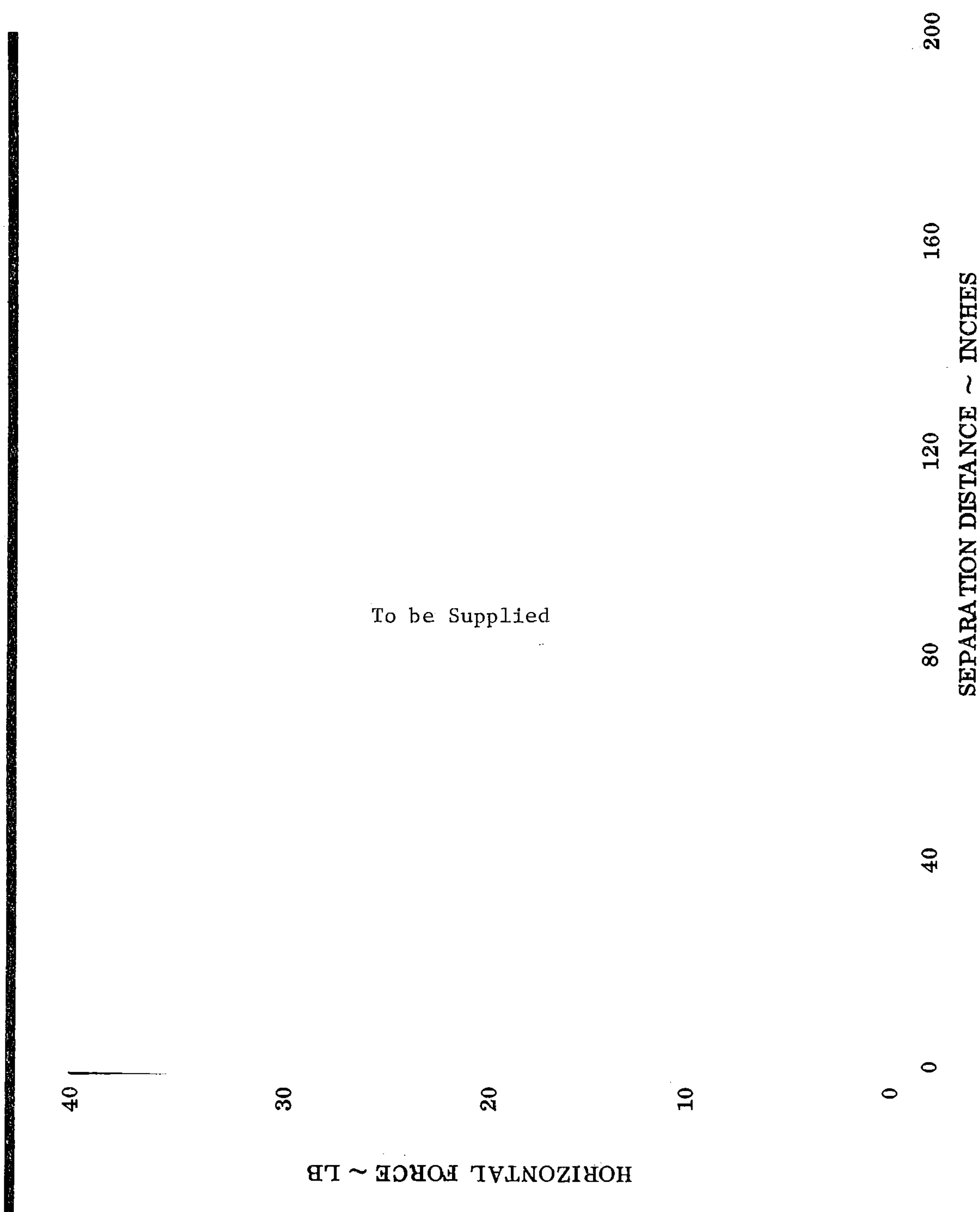

Figure 4.8-104. Horizantal Force vs Separation Distance
(See Para. 4.8.6.3)

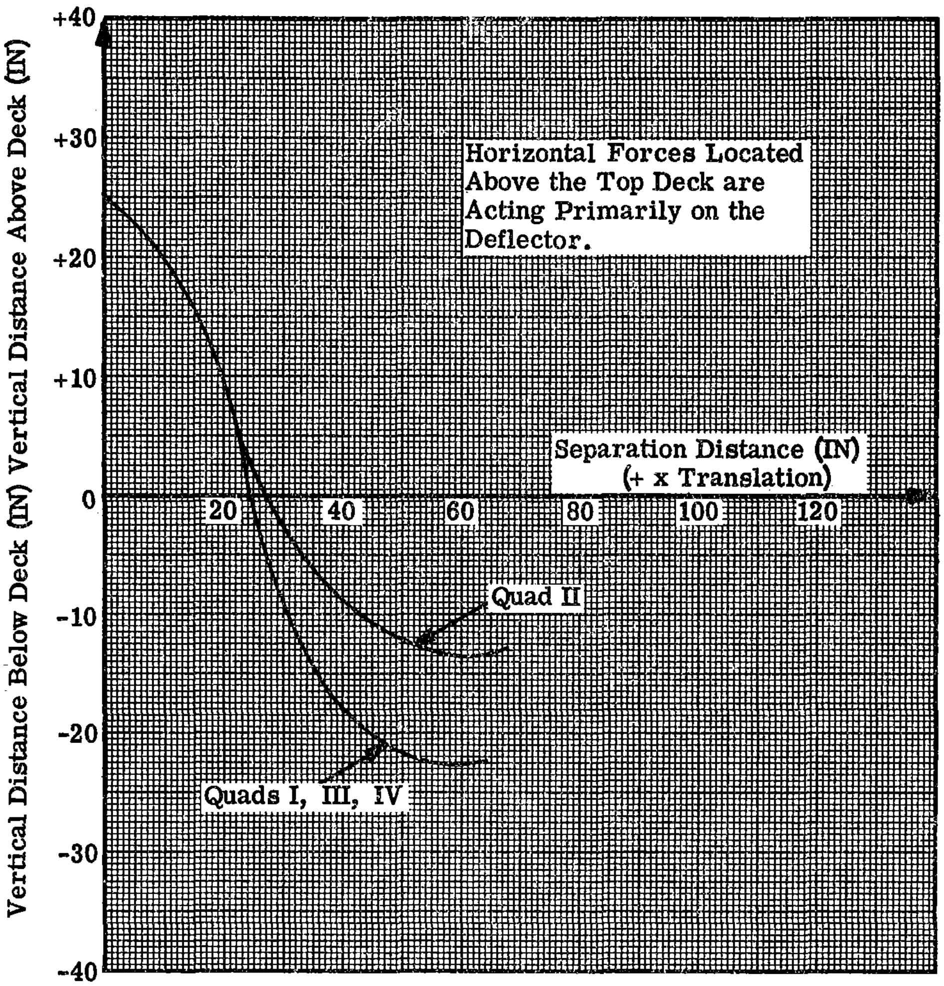

Figure 4.8-105. Vertical Distance From Top Deck of Horizontal Force vs. Ascent/Descent Stage Separation

(See Para. 4.8.6.3)

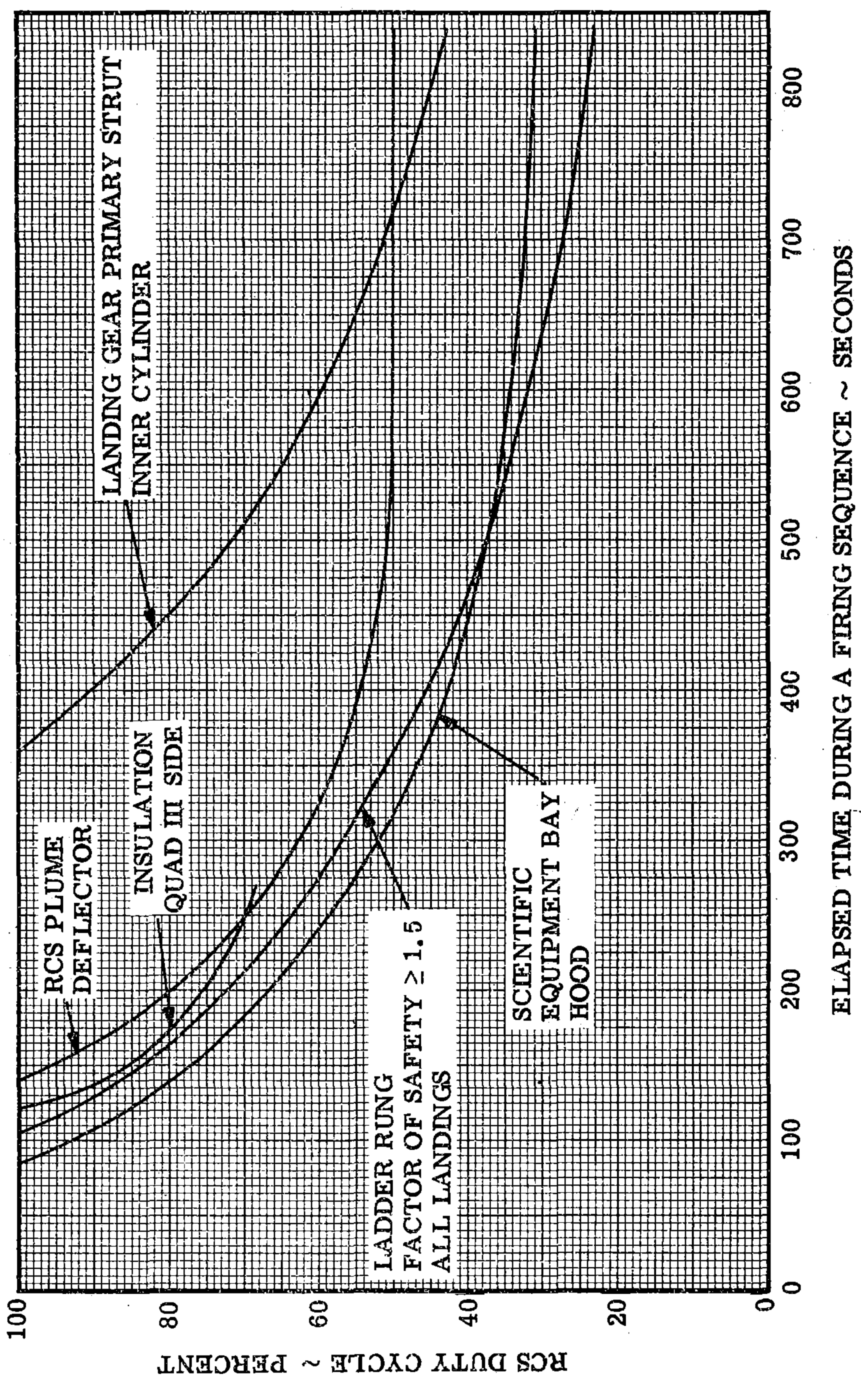

Figure 4.8-106. +X Plume Impingement Capability - Unstaged (See Para. 4.8.6.1)

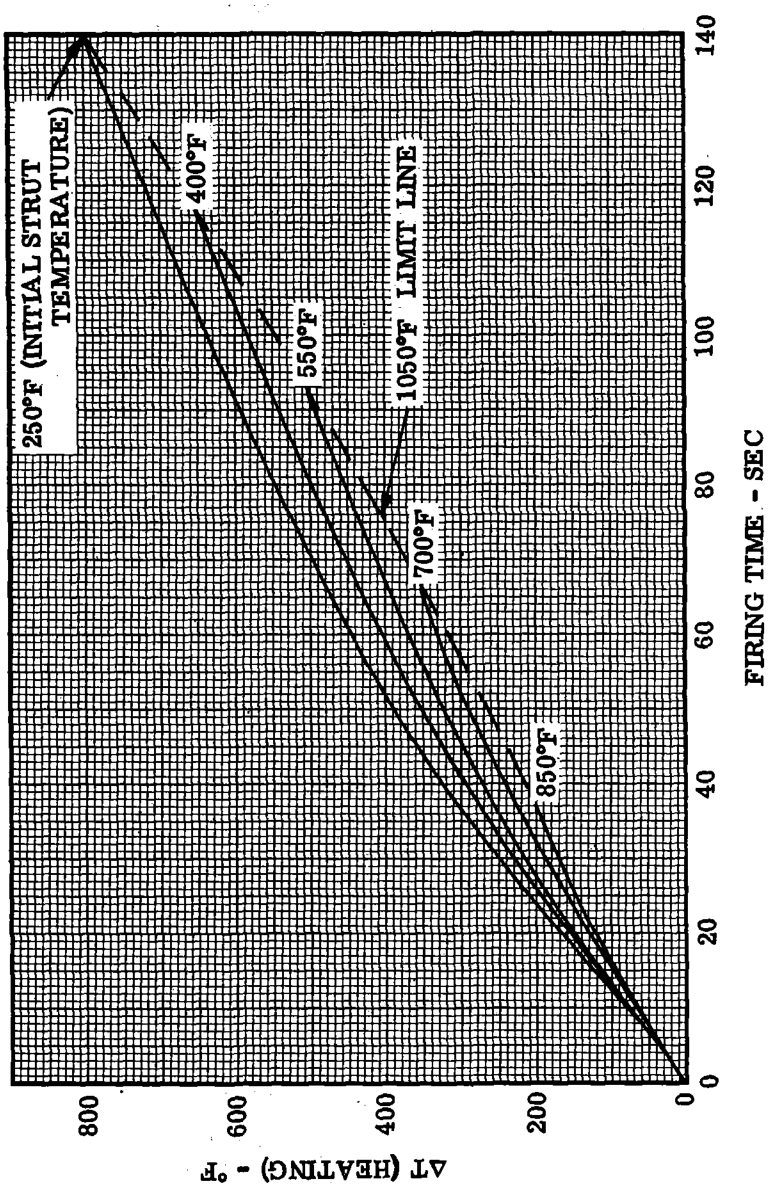

Figure 4.8-107. Temperature Change of Plume Deflector Center Strut During Firing (See Para. 4.8.6.1)

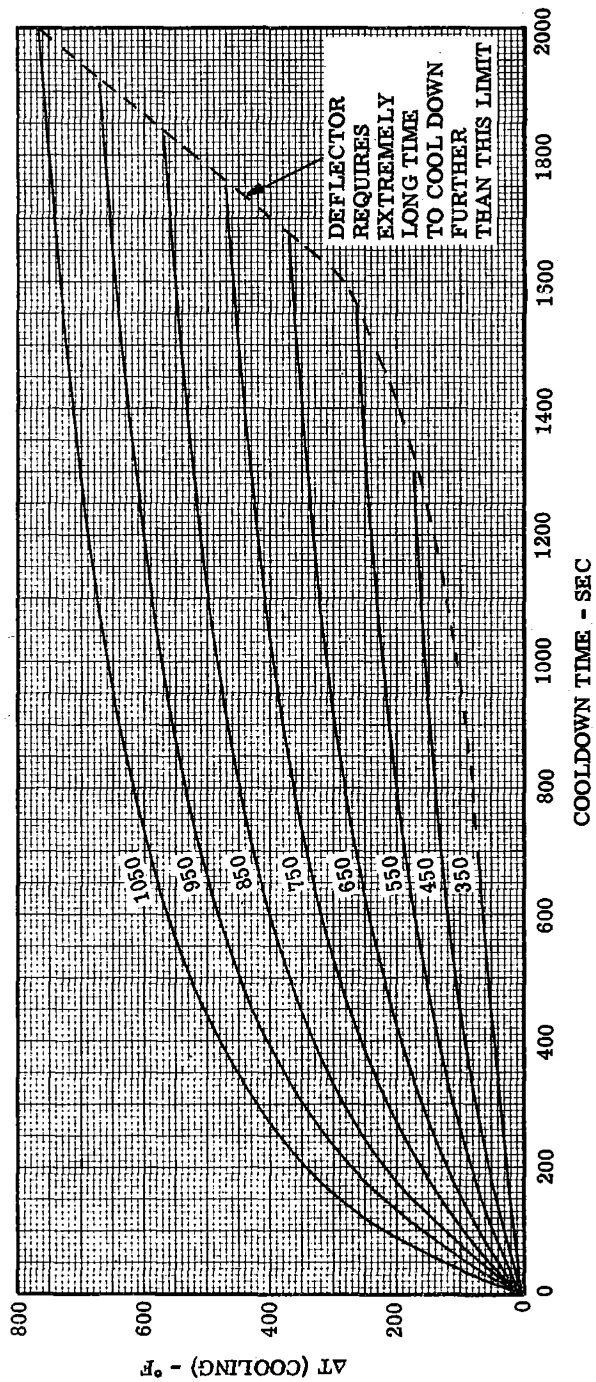

Figure 4.8-108. Temperature Change of Plume Deflector Center Strut During Cooldown (See Para. 4.8.6.1)

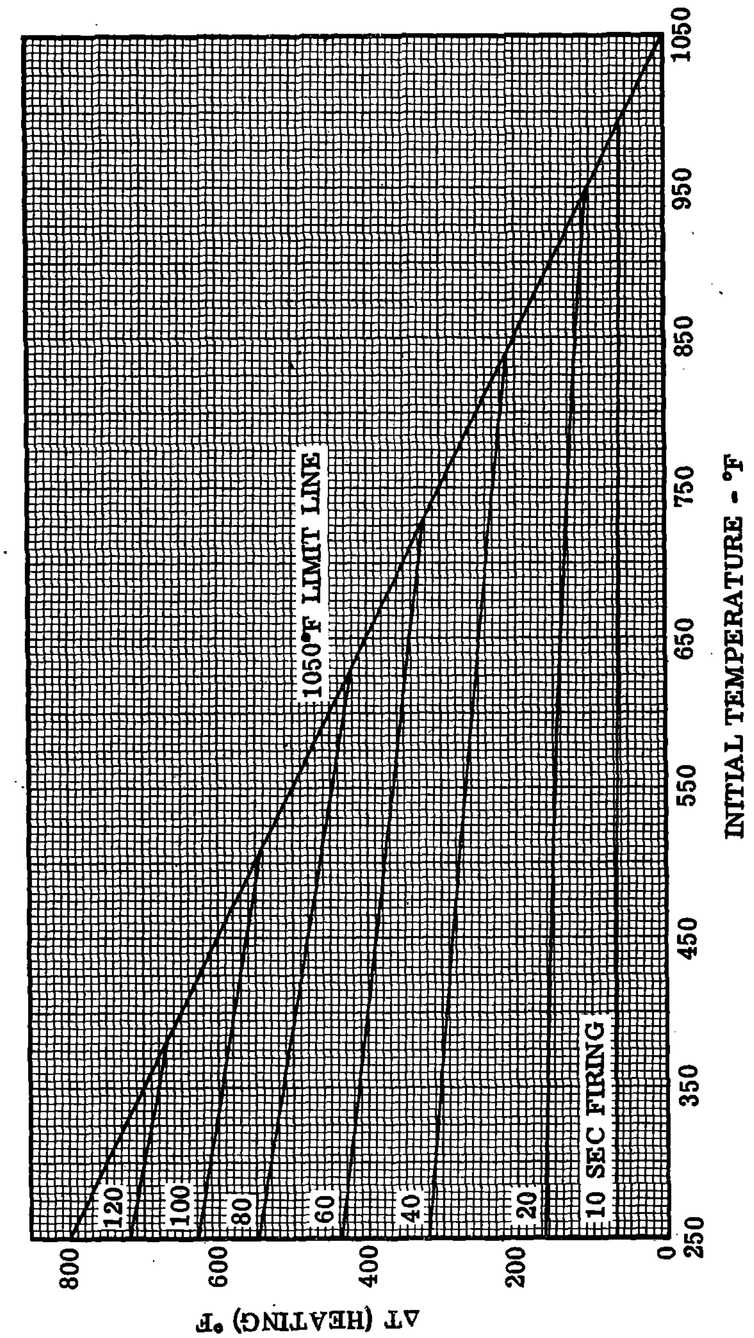

Figure 4.8-109. Temperature Rise Due to Heating of Plume Deflector Strut vs. Initial Strut Temperature For a Range of Firing Times (See Para. 4.8.6.1)

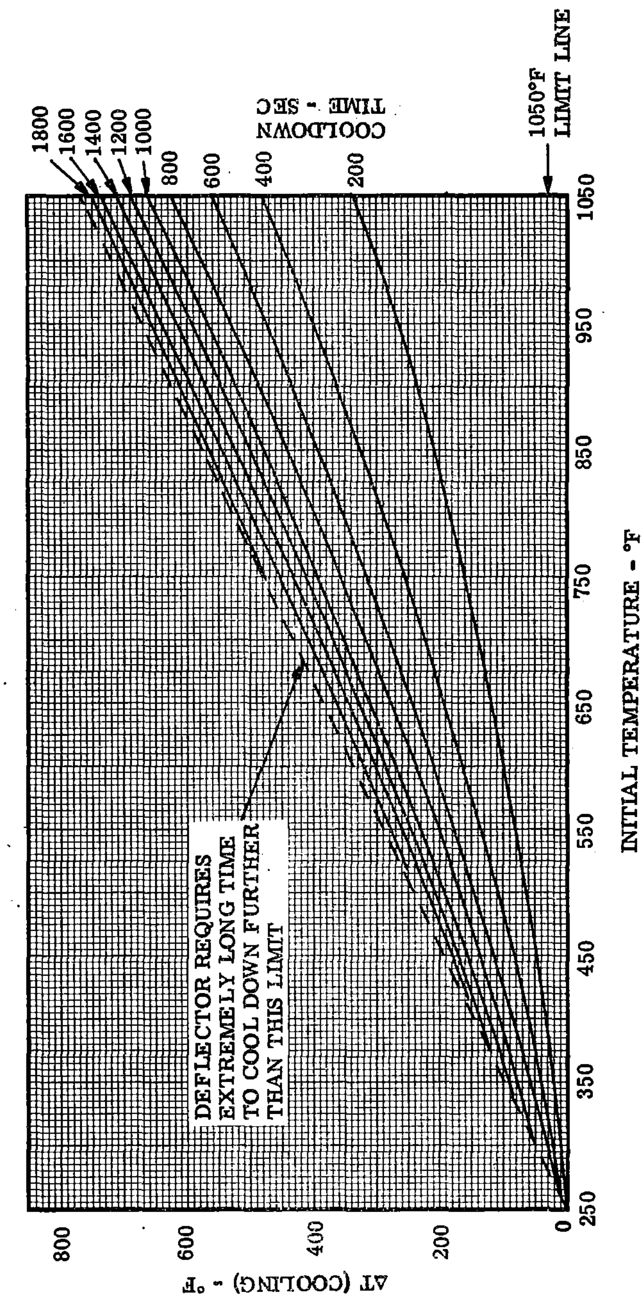

Figure 4.8-110. ΔT (Cooling) of Plume Deflector Center Strut vs. Initial Strut Temperature for a Range of Cooldown Times (See Para. 4.8.6.1)

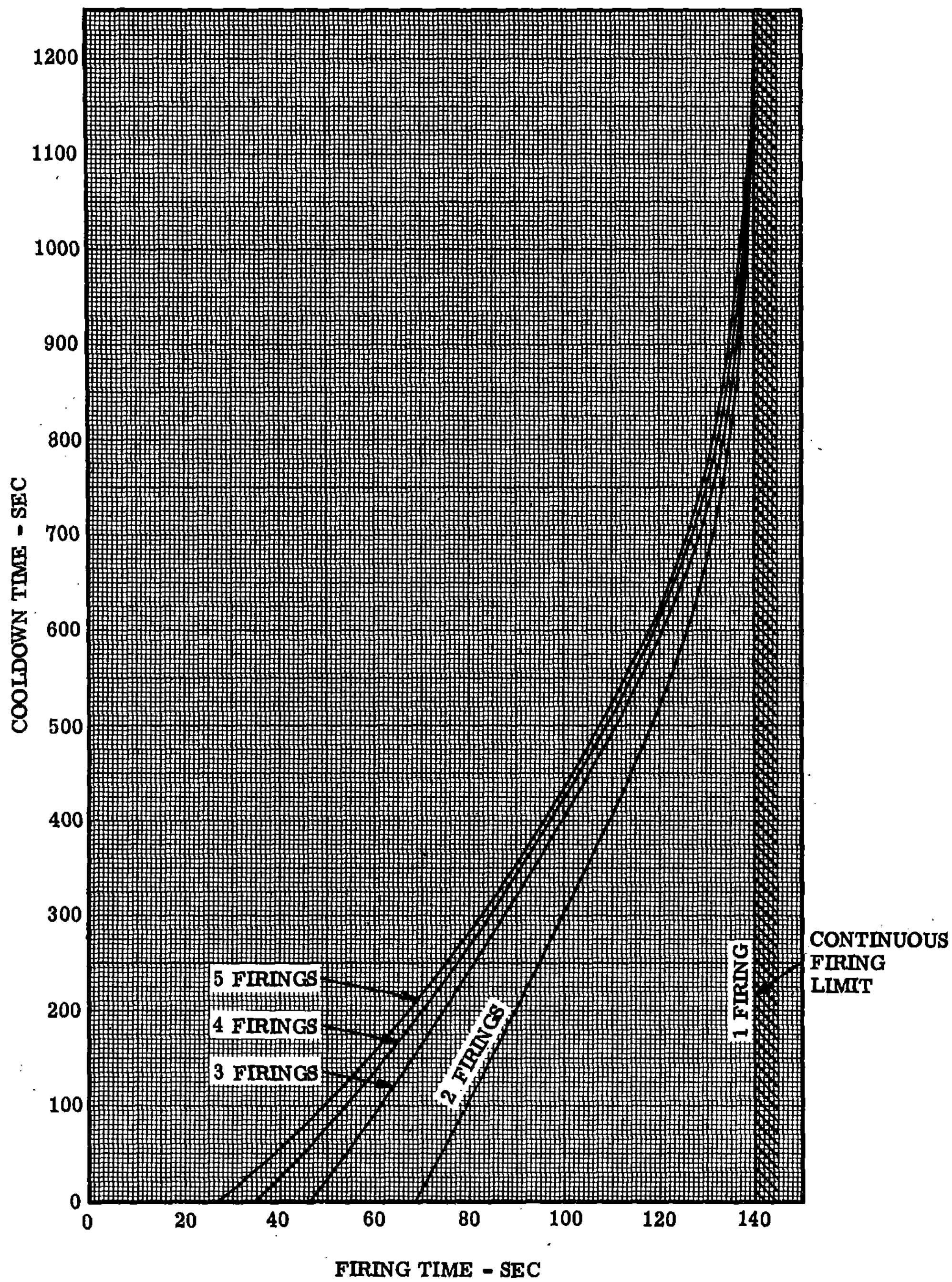

Figure 4.8-111. Cooldown Time Required Between Firings vs. Firing Time for a Range of Total Number of Firings With an Initial Temperature of 250°F (See Para. 4.8.6.1)

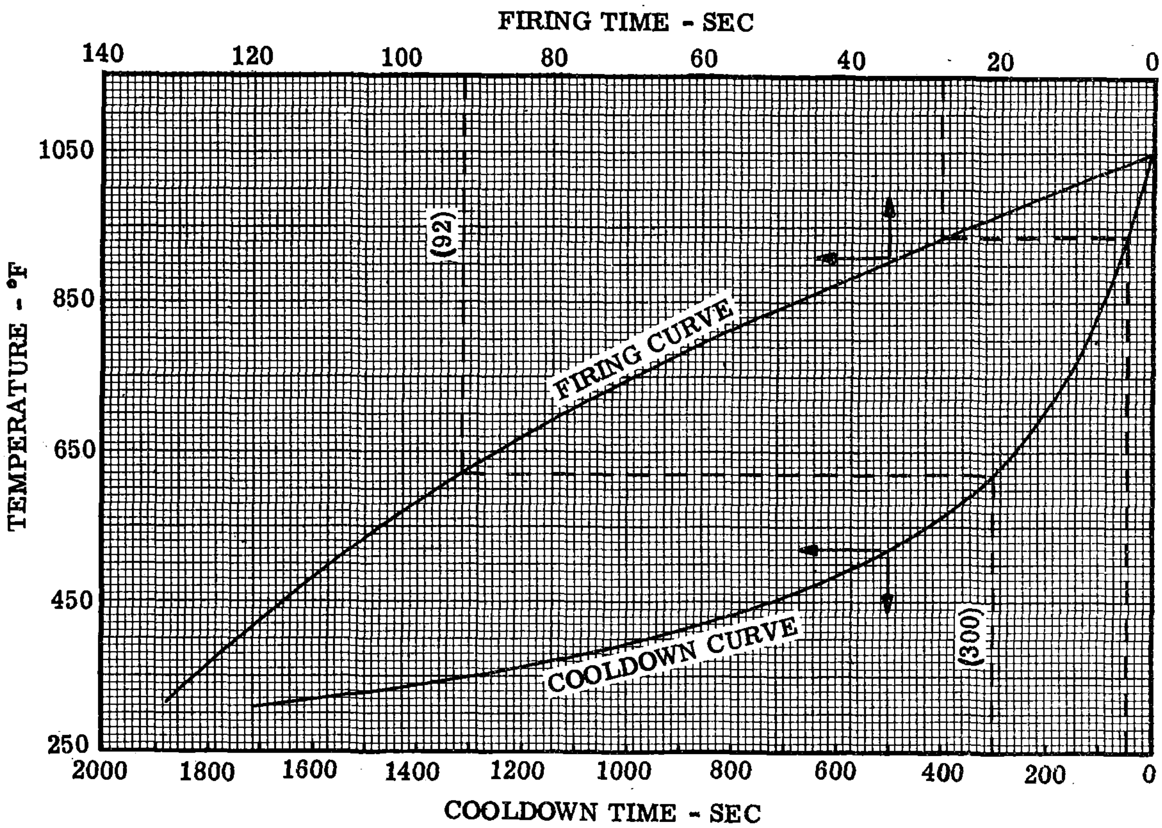

Figure 4.8-112. Firing Plus Cooldown Time Optimization (See Para. 4.8.6.1)

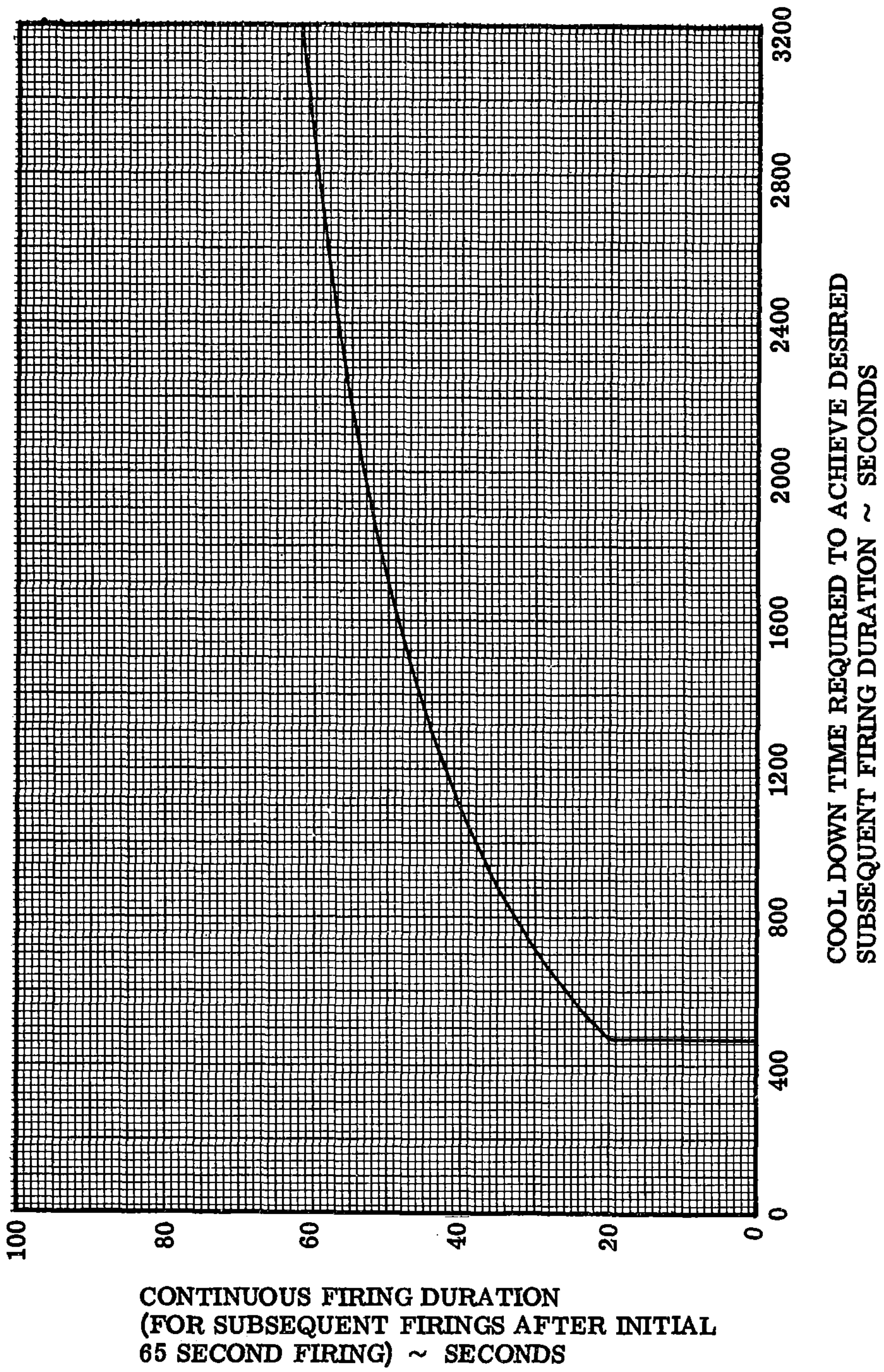

Figure 4.8-113. Cool Down Time Required for Subsequent Firings after 65 Seconds of Firing on the Quad III Stowage Compartment (See Para. 4.8.6.1)

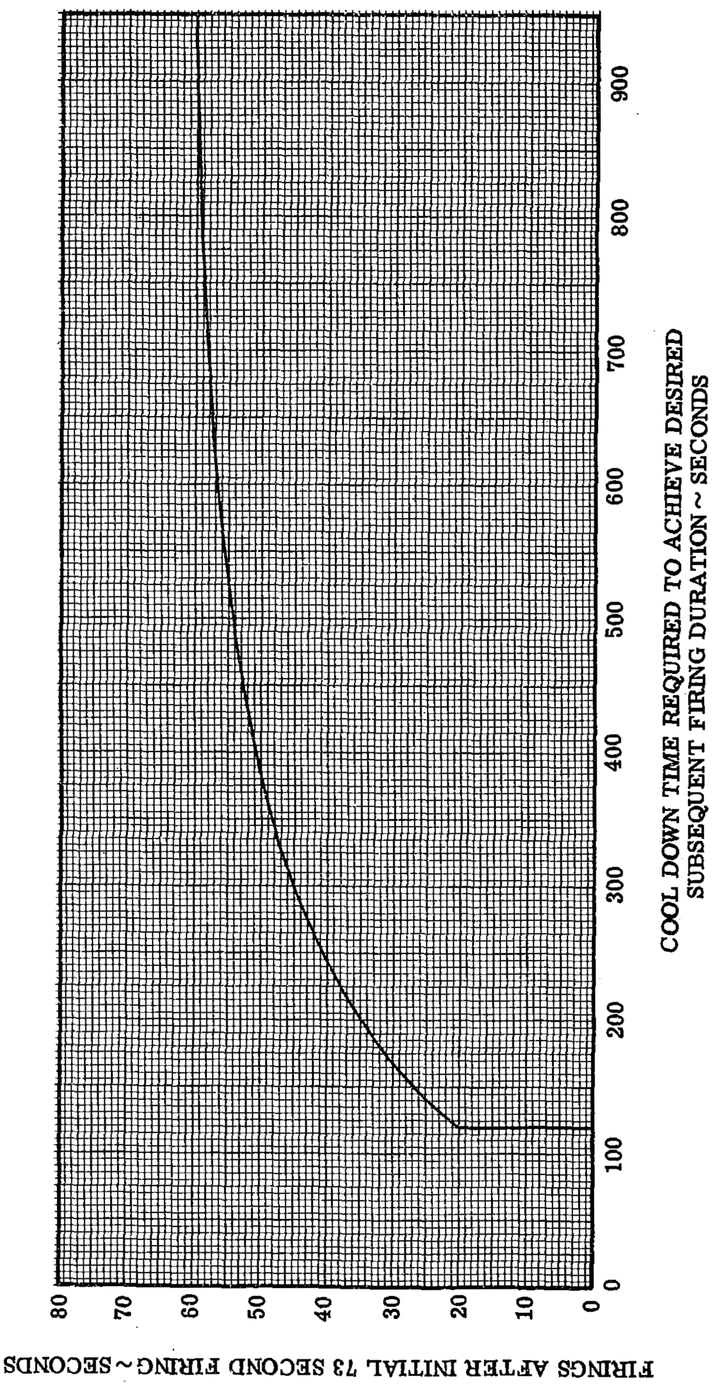

Figure 4.8-113.1. Cool Down Time Required for Subsequent Firings After 73 Seconds of Firing on the MESA (See Para. 4.8.6.1)

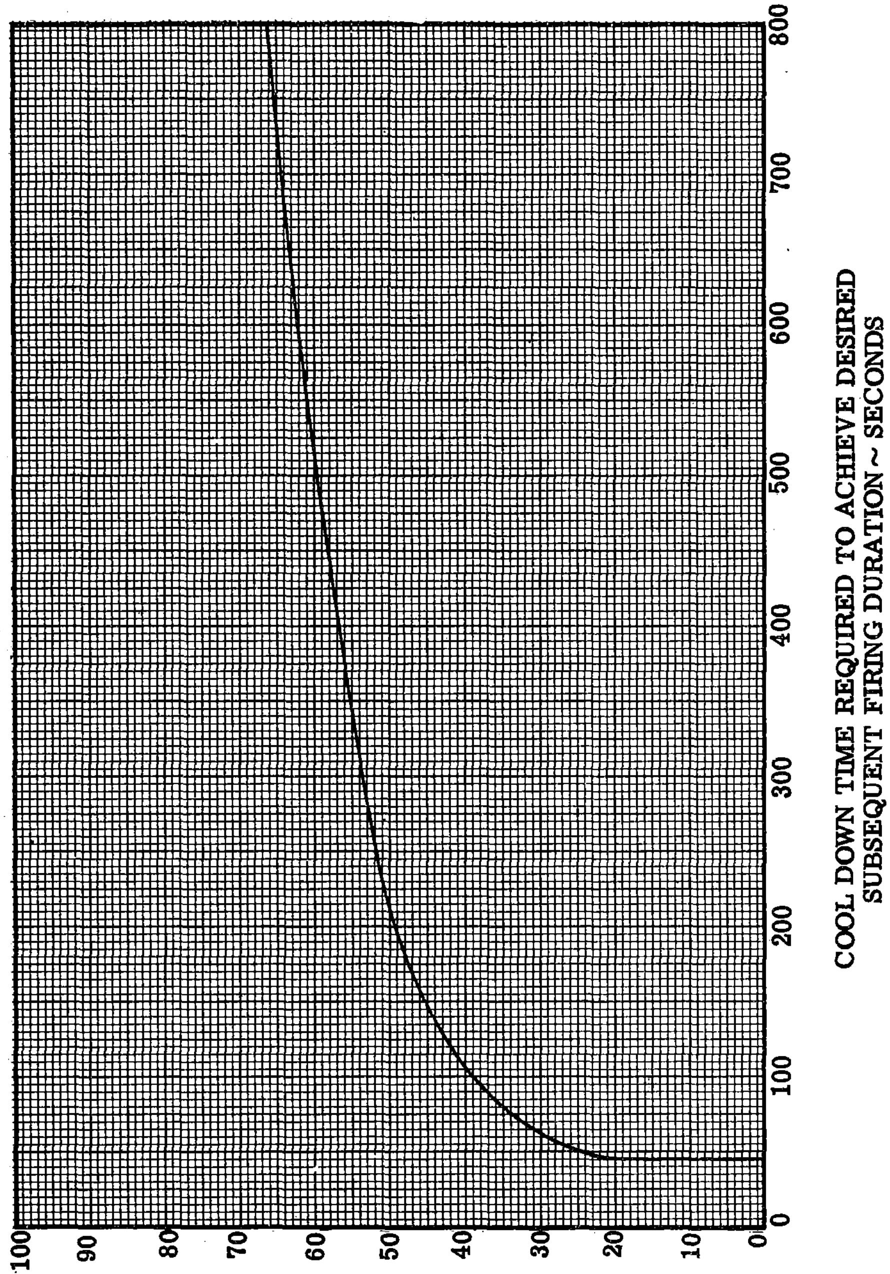

CONTINUOUS FIRING DURATION (FOR SUBSEQUENT FIRINGS AFTER INITIAL 66 SECOND FIRING) ~ SECONDS

Figure 4.8-113.2. Cool Down Time Required for Subsequent Firings after 66 Seconds of Firing on the Side of SEQ (See Para. 4.8.6.1)

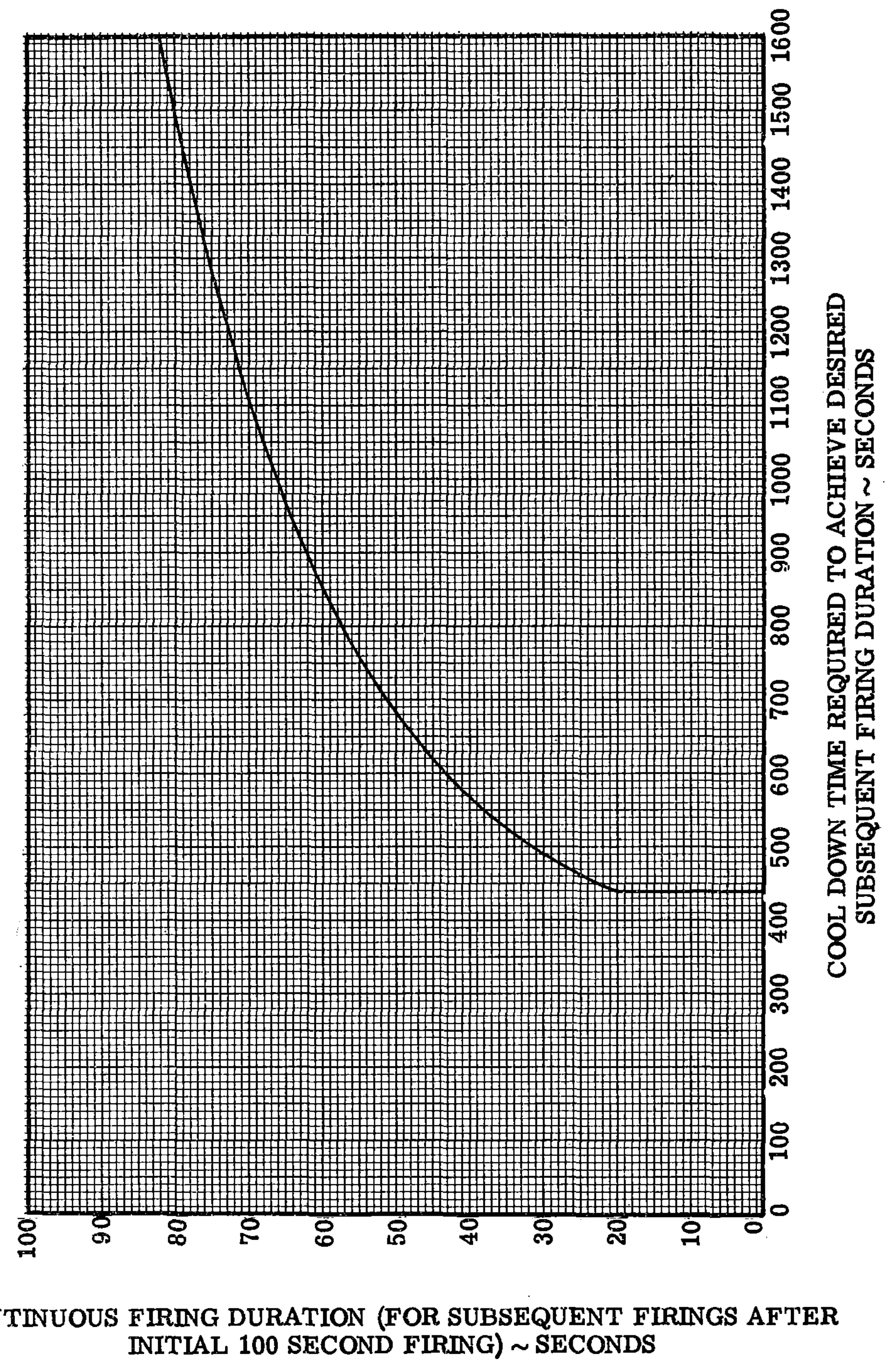

Figure 4.8-113.3 Cool Down Time Required for Subsequent Firings after 100 Seconds of Firing on the Top of SEQ (See Para. 4.8.6.1)

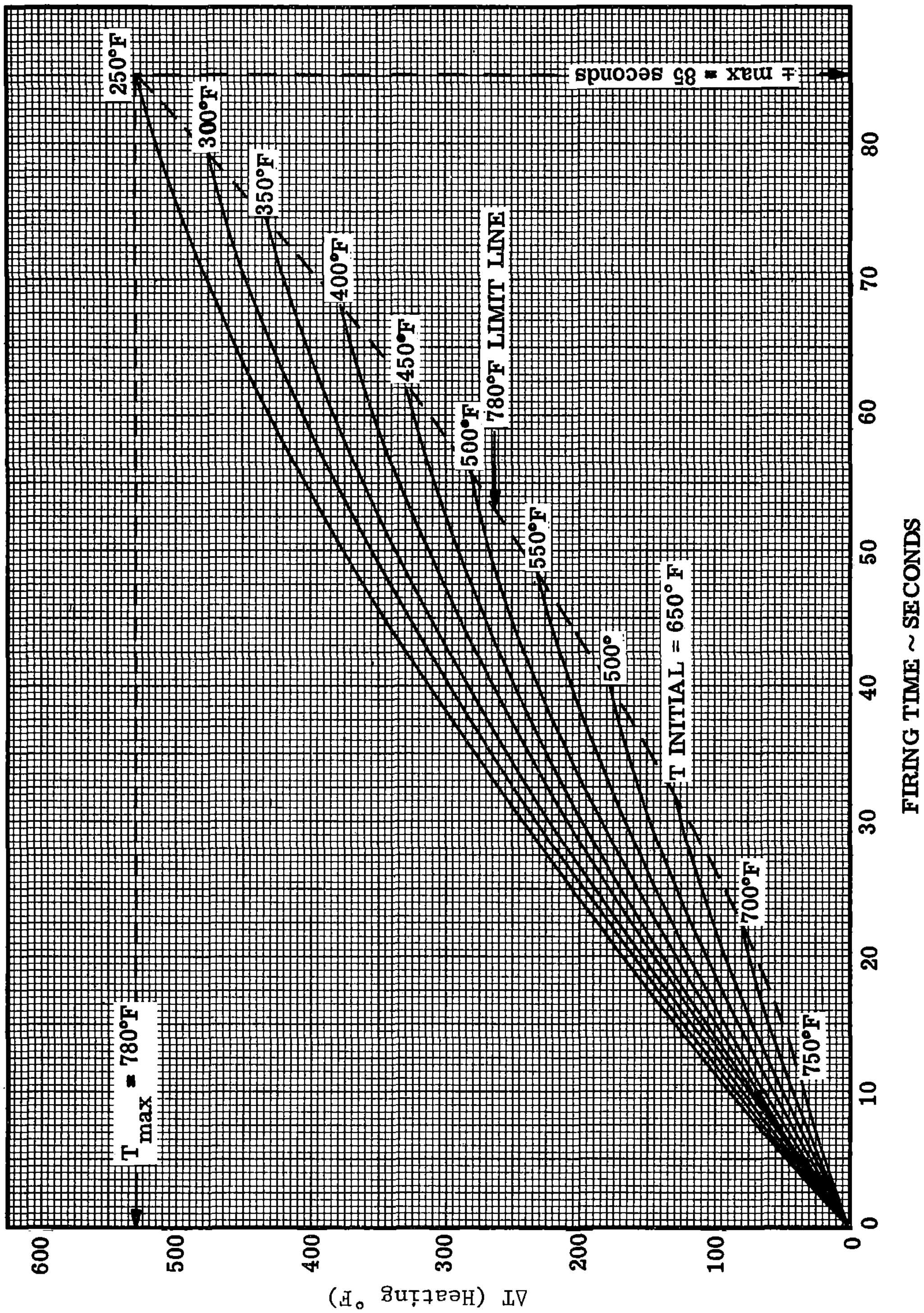

Figure 4.8-114. ΔT(Heating) of 0.032" Aluminum Frame vs. Firing Time for a Range of Initial Frame Temperatures (See Para. 4.8.6.1)

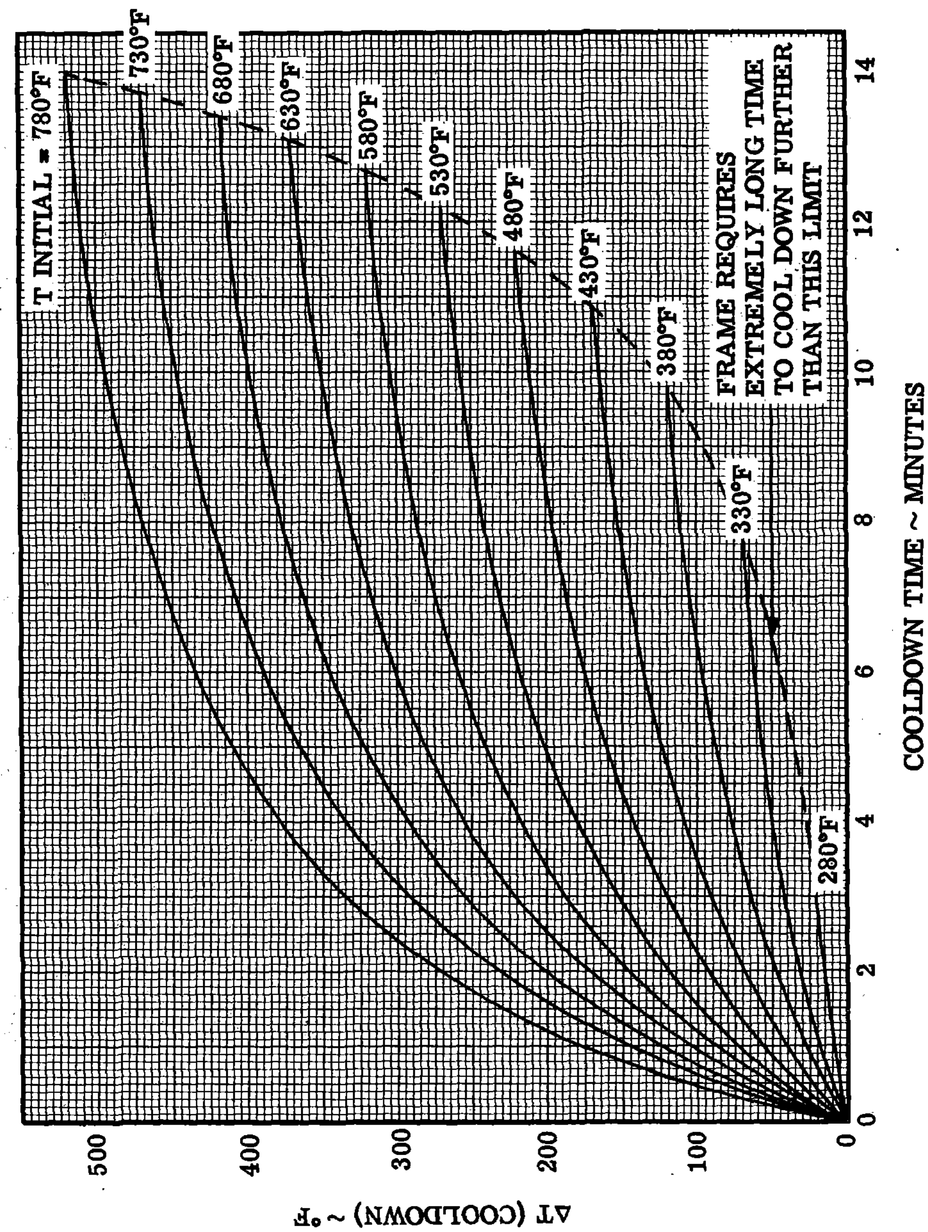

Figure 4.8-115. ΔT (Cooldown) of 0.032" Aluminum Frame vs. Cooldown Time for a Range of Initial Frame Temperatures (See Para. 4.8.6.1)

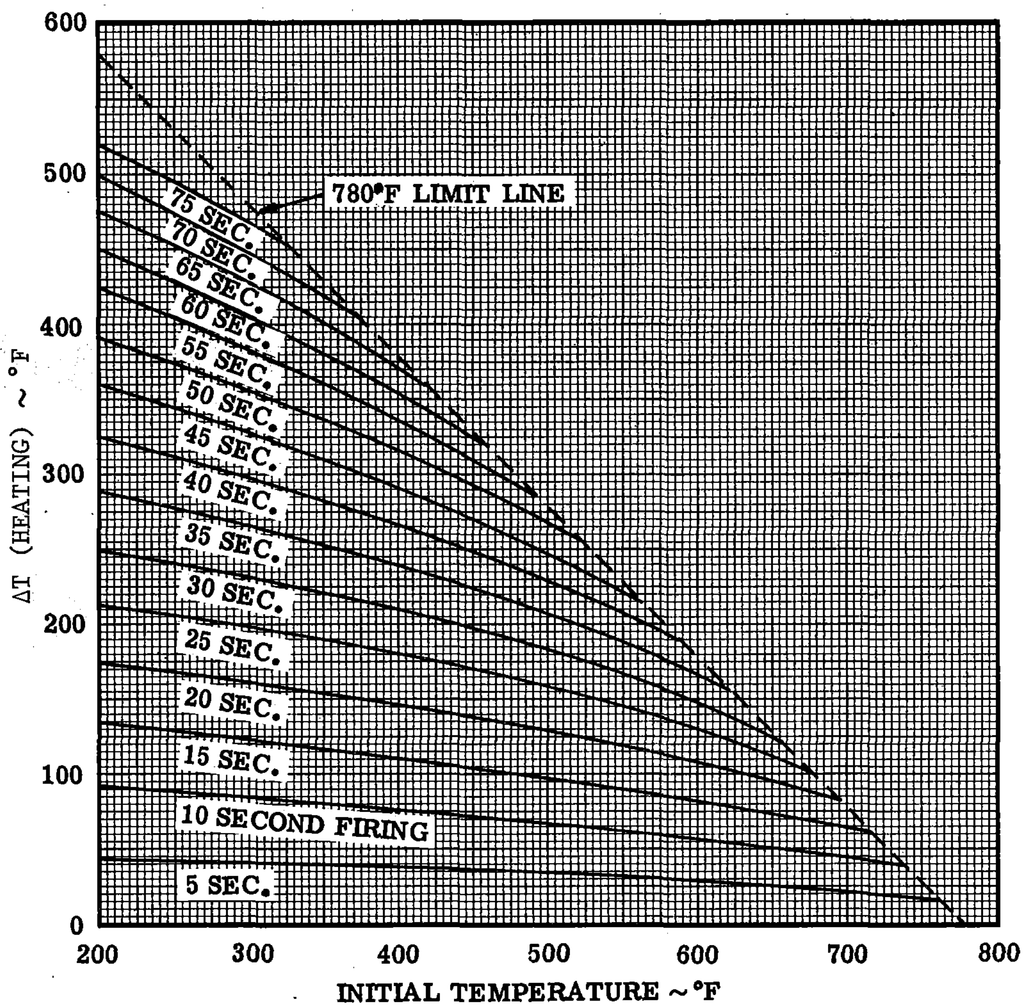

Figure 4.8-116. ΔT (Heating) of .032" Aluminum Frame vs. Initial Frame Temperature for a Range of Firing Times (See Para. 4.8.6.1)

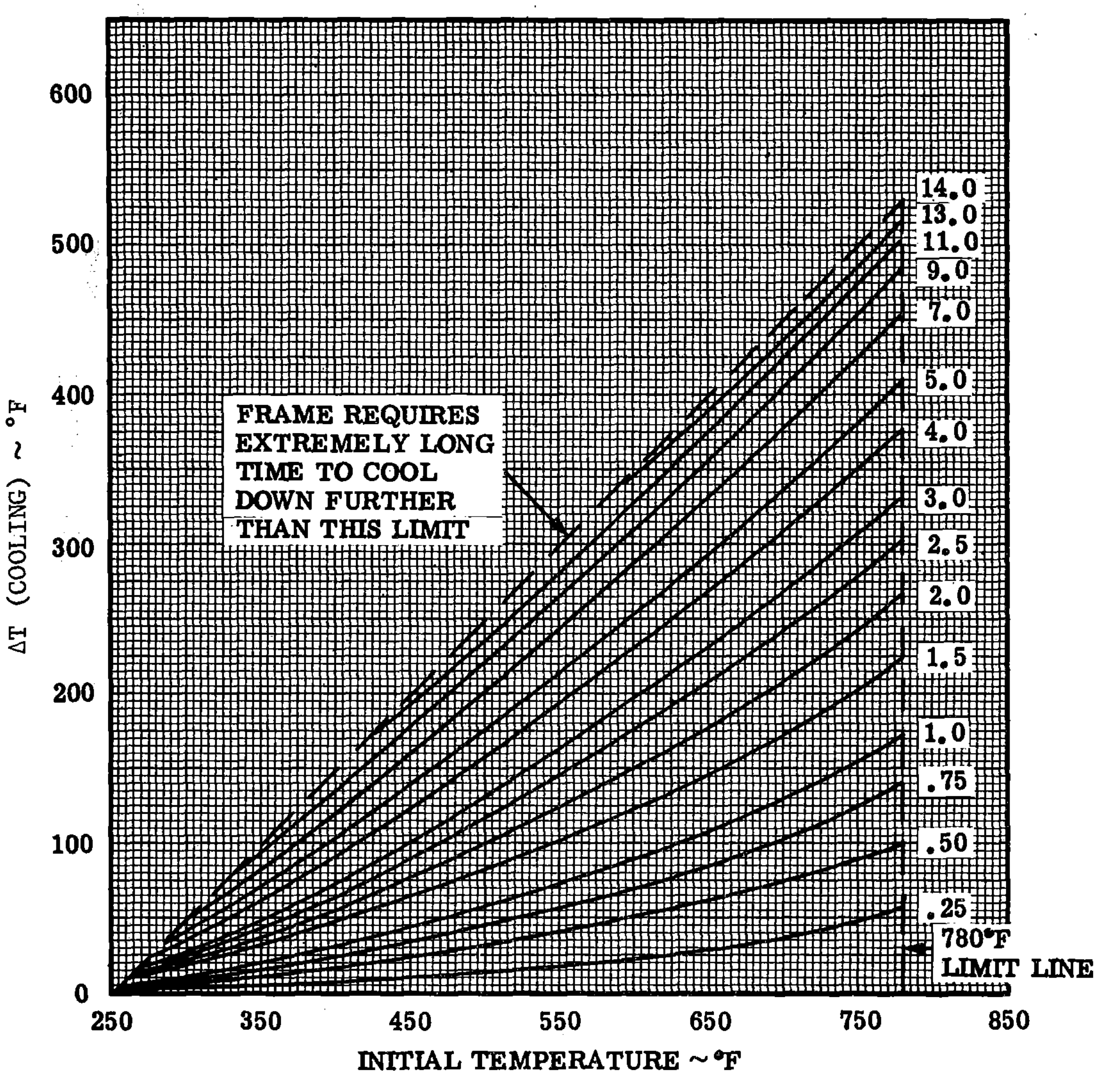

Figure 4.8-117. ΔT (Cooling) of 0.032" Aluminum Frame vs. Initial Frame Temperature for a Range of Cooldown Times (See Para. 4.8.6.1)

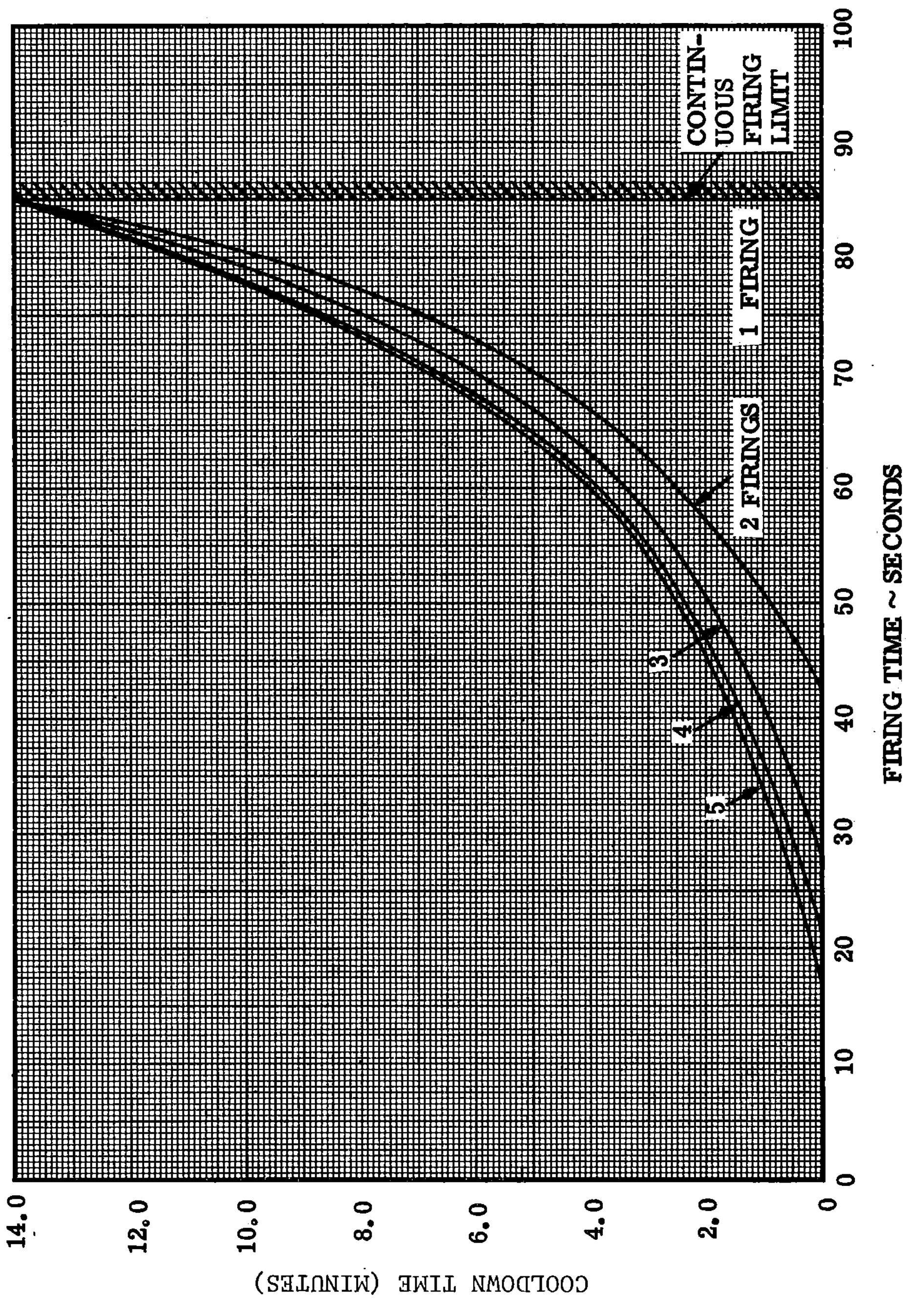

Figure 4.8-118. Cooldown Time Required Between Firings vs. Firing Time for a Range of Total Number of Firings With an Initial Temperature of 250°F (See Para. 4.8.6.1)

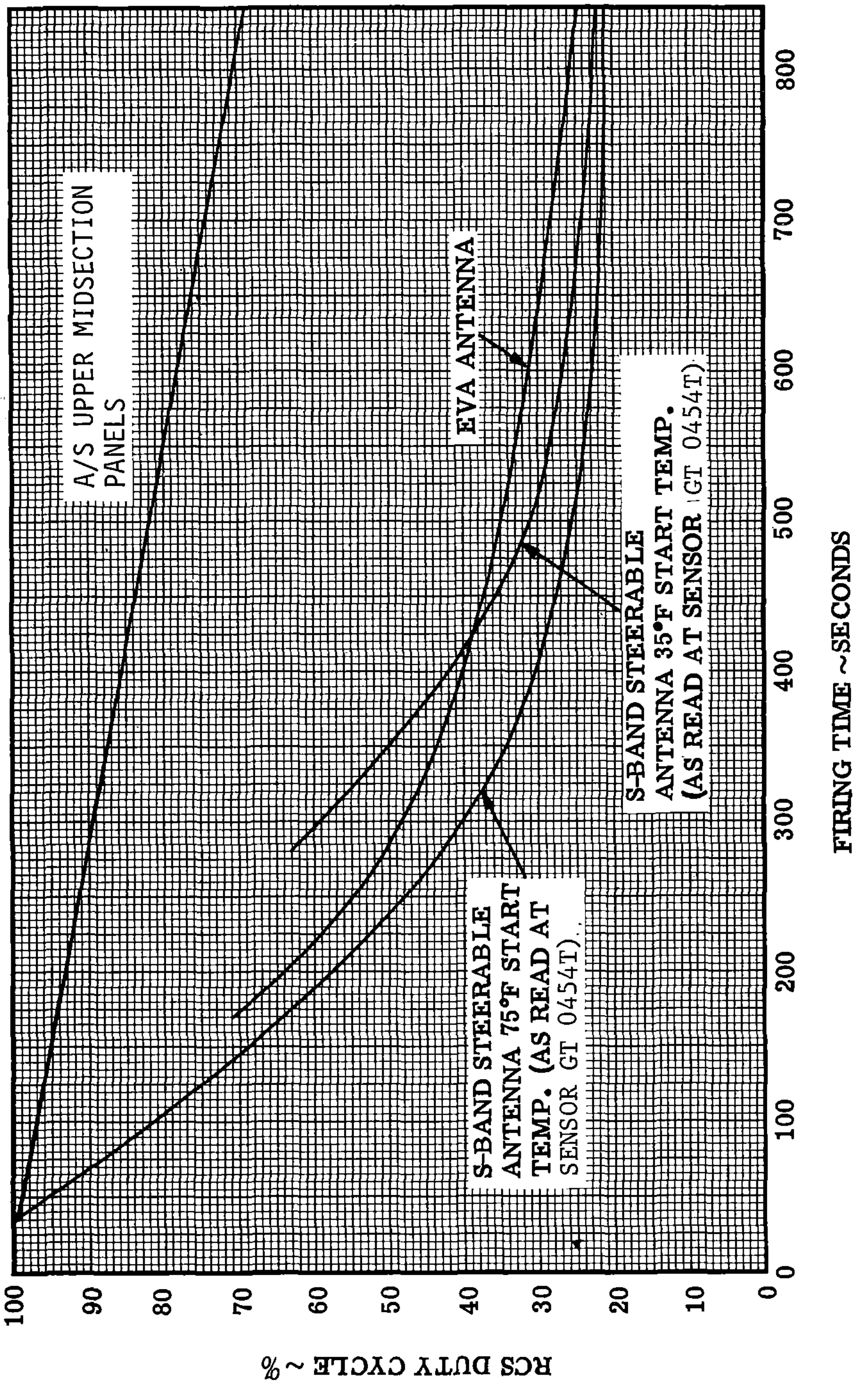

Figure 4.8-119. LM-8 and Subsequent RCS Plume Impingement Capability for Antennas (See Para. 4.8.6.1)

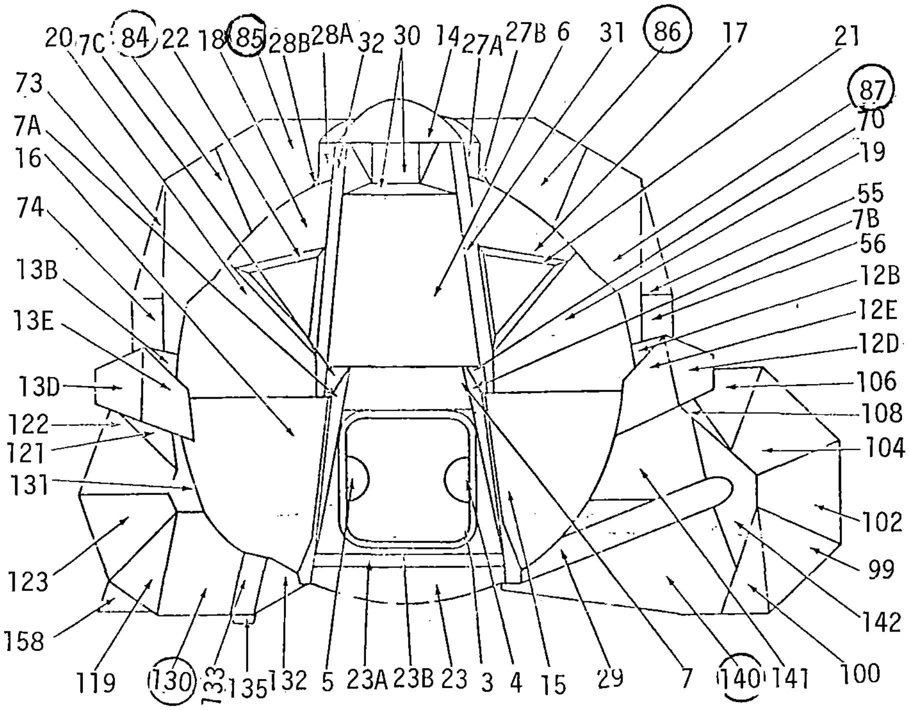

LM PANEL IDENTIFICATION, ASCENT STAGE, FRONT

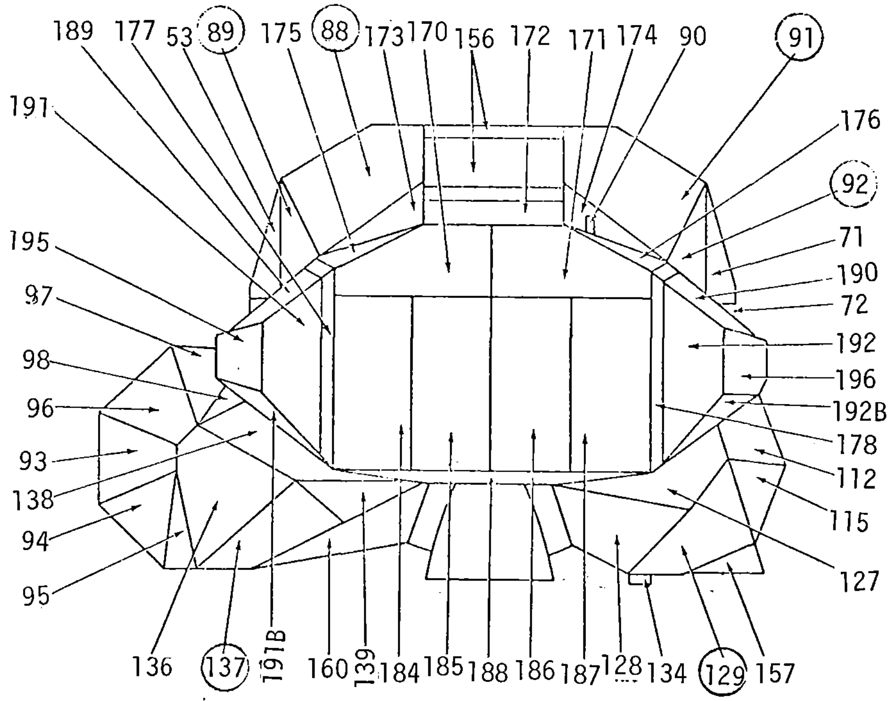

LM PANEL IDENTIFICATION, ASCENT STAGE, REAR

Figure 4.8-120. LM Panel Identification for Thermal Reference (See paragraph 4.8.6.1.2)

Volume II LM Data Book
Subsystem Performance Data - Struc/Mech

TABLE OF CONTENTS

4.9 STRUCTURAL/MECHANICAL

4.9.1 Sample Return Container C. G. and Weight Tolerances

The maximum allowable weight of each loaded Sample Return Container (SRC) is 80 earth lbs. The total combined maximum weight for two SRC's is 160 lbs.

The allowable C. G. positions and tolerances are:

SRC #1	LM X Station	265.90	+0.75 -1.75
	LM Y Station	-20.75	±2.0
	LM Z Station	-6.0	±3.0
SRC #2	LM X Station	257.44	+0.75 -1.75
	LM Y Station	-20.75	±2.0
	LM Z Station	-6.0	±3.0

5.0 AERODYNAMICS (NASA DATA SOURCE)

5.1 Extreme Altitude Aerodynamic Drag Coefficients for the LM and the LM-SIVB

This section presents extreme altitude aerodynamic drag coefficients for the LM-SIVB configuration as shown in Figure 5.1-1, and includes the extreme altitude aerodynamic drag coefficients from Reference 1 for the LM configuration as shown in Figure 5.1-2.

The drag coefficients were calculated using the free molecular flow theory as presented in Reference 2. The drag diffuse reflection equation for a flat plate is as follows:

$$C_D = \frac{2}{S\sqrt{\pi}} \left[e^{-(S \sin \theta)^2} + \sqrt{\pi}\ S \sin \theta \left(1 + \frac{1}{2S^2}\right) \operatorname{erf}(S \sin \theta) + \frac{\pi S}{S_w} \sin^2 \theta \right]$$

where θ is the angle of attack between the surface and the flow direction, and S denotes the molecular speed ratio which can also be expressed in terms of the Mach number, M, and the isentropic exponent γ by

$$S = M\sqrt{\frac{\gamma}{2}}$$

It was assumed that S was equal to 10.0 and equal to S_w, since S_w requires knowledge of the surface temperature, as explained in Reference 2.

It should be noted that the drag coefficients presented in Table 5.1-1 (from Reference 1) and Table 5.1-2 have been calculated using the standard Apollo reference area of 129.4 ft^2. Continuum flow conditions are assumed to be valid only for altitudes below 325,000 feet, while the free molecular flow conditions are assumed to exist above an altitude of 450,000 feet. It is not known, at the present, in what manner or at what altitude the transition from free molecular flow to continuum takes place, but it is assumed to occur between 450,000 feet and 325,000 feet. Therefore, since the dynamic pressure expected by the time altitude has decreased to 300,000 - 325,000 feet is expected to be sufficiently large enough to substantially alter the fragile LM original geometry, no continuum aerodynamic data is included. The free molecular flow data presented should be used for altitudes greater than 300,000 feet.

5.1 Extreme Altitude Aerodynamic Drag Coefficients for the LM and the LM-SIVB (Continued)

Centers of pressure, Table 5.1-3, for the various LM configurations were determined by calculating the centroids of the projected areas for the various vehicle configurations and attitudes. The centers of pressure are defined as station numbers in the standard LM axis system as shown in Section 2.0 of this volume.

References

1. R. S. Morton, Jr., Extreme Altitude Aerodynamic Drag Coefficients for the LM, MSC Memorandum to PM3, March 30, 1967.

2. Howard W. Emmons, Fundamentals of Gas Dynamics, Vol. II, High Speed Aerodynamics and Jet Propulsion, Princeton University Press, 1958, pp. 703-705.

5.1.1 CSM-LM Docked Aerodynamic Coefficients at Extreme Altitude

Drag coefficients for the LM and the CSM (Spacecraft Operational Data Book, Volume I, Section 6.0) were used to calculate drag coefficients at extreme altitude (≥450,000 feet) for the CSM-LM in the docked configuration. Locations of the center of pressure for various attitudes were also calculated.

The free molecular flow drag coefficients for the CSM + Total LM (less landing legs and pads) and the CSM + LM Ascent Stage are given in Table 5.1-4 for various vehicle attitudes. Angles of attack and sideslip are defined in the standard LM axis system as shown in Section 2.0 of this Volume. The centers of pressure, given in Table 5.1-5, were determined by calculating the centroids of the projected areas for the CSM + LM configurations and attitudes, and are defined as station numbers in the standard LM axis system.

Table 5.1-1. LM Free Molecular Flow Drag Coefficients

Reference Area = 129.4 ft^2

Total LM (Less Landing Legs and Pads)

Attitude		C_D
$\alpha = 0°$	$\beta = 0°$	2.60
$\alpha = 90°$	$\beta = 0°$	3.20
$\alpha = 180°$	$\beta = 0°$	2.60
$\alpha = 0°$	$\beta = 90°$	3.34

Ascent Stage

Attitude		C_D
$\alpha = 0°$	$\beta = 0°$	2.11
$\alpha = 90°$	$\beta = 0°$	1.65
$\alpha = 180°$	$\beta = 0°$	2.11
$\alpha = 0°$	$\beta = 90°$	1.83

Descent Stage (Less Landing Legs and Pads)

Attitude		C_D
$\alpha = 0°$	$\beta = 0°$	2.52
$\alpha = 90°$	$\beta = 0°$	1.55
$\alpha = 180°$	$\beta = 0°$	2.52
$\alpha = 0°$	$\beta = 90°$	1.55

Tumbling Drag Coefficient

Total LM*	$C_D = 2.97$
Ascent Stage	$C_D = 1.97$
Descent Stage*	$C_D = 2.04$

*Less landing legs and pads.

Table 5.1-2. LM-SIVB Free Molecular Flow Drag Coefficients

Reference Area = 129.4 ft^2

Attitude		C_D
$\alpha = 0°$	$\beta = 0°$	6.75
$\alpha = 90°$	$\beta = 0°$	23.40
$\alpha = 180°$	$\beta = 0°$	6.75
$\alpha = 0°$	$\beta = 90°$	23.49
Tumbling		16.78

TABLE 5.1-3. LM CENTERS OF PRESSURE FOR DIFFERENT VEHICLE CONFIGURATIONS AND ATTITUDES

Total LM (less landing legs and pads)

Attitude		Center-of-Pressure Location	
$\alpha = 0°$	$\beta = 0°$	$Y_E = 0.3$	$Z_E = 0.7$
$\alpha = 90°$	$\beta = 0°$	$X_E = 202.7$	$Y_E = -3.4$
$\alpha = 180°$	$\beta = 0°$	$Y_E = 0.3$	$Z_E = 0.7$
$\alpha = 0°$	$\beta = 90°$	$X_E = 205.7$	$Z_E = 6.0$

Ascent Stage

Attitude		Center-of-Pressure Location	
$\alpha = 0°$	$\beta = 0°$	$Y_E = 0.3$	$Z_E = 4.1$
$\alpha = 90°$	$\beta = 0°$	$X_E = 251.4$	$Y_E = -6.9$
$\alpha = 180°$	$\beta = 0°$	$Y_E = 0.3$	$Z_E = 4.1$
$\alpha = 0°$	$\beta = 90°$	$X_E = 257.5$	$Z_E = 11.9$

Descent Stage (less landing legs and pads)

Attitude		Center-of-Pressure Location	
$\alpha = 0°$	$\beta = 0°$	$Y_E = 0.0$	$Z_E = 0.0$
$\alpha = 90°$	$\beta = 0°$	$X_E = 154.4$	$Y_E = 0.0$
$\alpha = 180°$	$\beta = 0°$	$Y_E = 0.0$	$Z_E = 0.0$
$\alpha = 0°$	$\beta = 90°$	$X_E = 153.3$	$Z_E = 0.0$

TABLE 5.1-4. DOCKED CSM-LM FREE MOLECULAR FLOW DRAG COEFFICIENTS

Reference Area = 129.4 sq. ft.

CSM + Total LM (less landing legs and pads)

Attitude		C_D
$\alpha = 0°$	$\beta = 0°$	2.60
$\alpha = 90°$	$\beta = 0°$	8.21
$\alpha = 180°$	$\beta = 0°$	2.60
$\alpha = 0°$	$\beta = 90°$	8.35

CSM + Ascent Stage

Attitude		C_D
$\alpha = 0°$	$\beta = 0°$	2.11
$\alpha = 90°$	$\beta = 0°$	6.66
$\alpha = 180°$	$\beta = 0°$	2.41
$\alpha = 0°$	$\beta = 90°$	6.84

Tumbling Drag Coefficient

CSM + Total LM*	$C_D = 6.02$
CSM + Ascent Stage	$C_D = 4.97$

*Less landing legs and pads.

TABLE 5.1-5. DOCKED CSM-LM CENTERS OF PRESSURE

CSM + Total LM (less landing legs and pads)

Attitude		Center-of-Pressure Location	
$\alpha = 0°$	$\beta = 0°$	$Y_E = 0.3$	$Z_E = 0.7$
α 90°	$\beta = 0°$	$X_E = 380.0$	$Y_E = -1.2$
$\alpha = 180°$	$\beta = 0°$	$Y_E = 0.3$	$Z_E = 0.7$
α 0°	$\beta = 90°$	$X_E = 378.8$	$Z_E = 2.2$

CSM + Ascent Stage

Attitude		Center-of-Pressure Location	
$\alpha = 0°$	$\beta = 0°$	$Y_E = 0.3$	$Z_E = 0.9$
$\alpha = 90°$	$\beta = 0°$	$X_E = 430.3$	$Y_E = -1.5$
$\alpha = 180°$	$\beta = 0°$	$Y_E = 0.3$	$Z_E = 0.9$
$\alpha = 0°$	$\beta = 90°$	$X_E = 429.9$	$Z_E = 2.7$

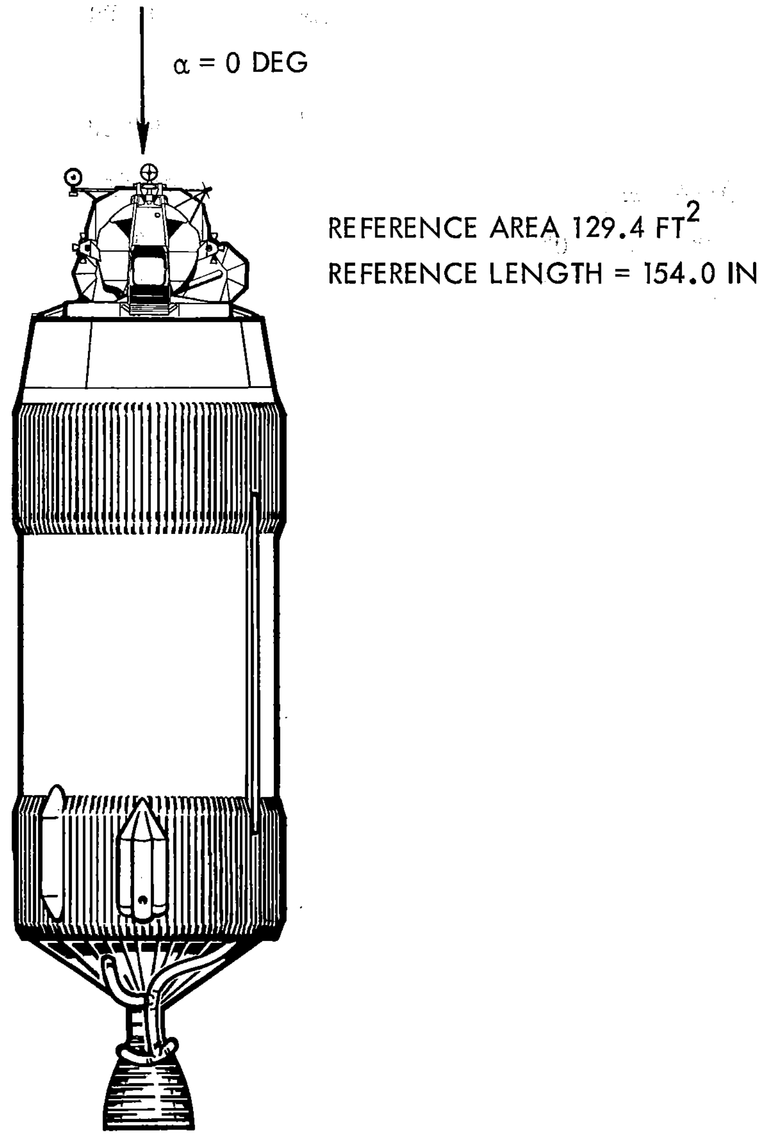

Figure 5.1-1. LM-S-IVB Configuration (See Para. 5.1)

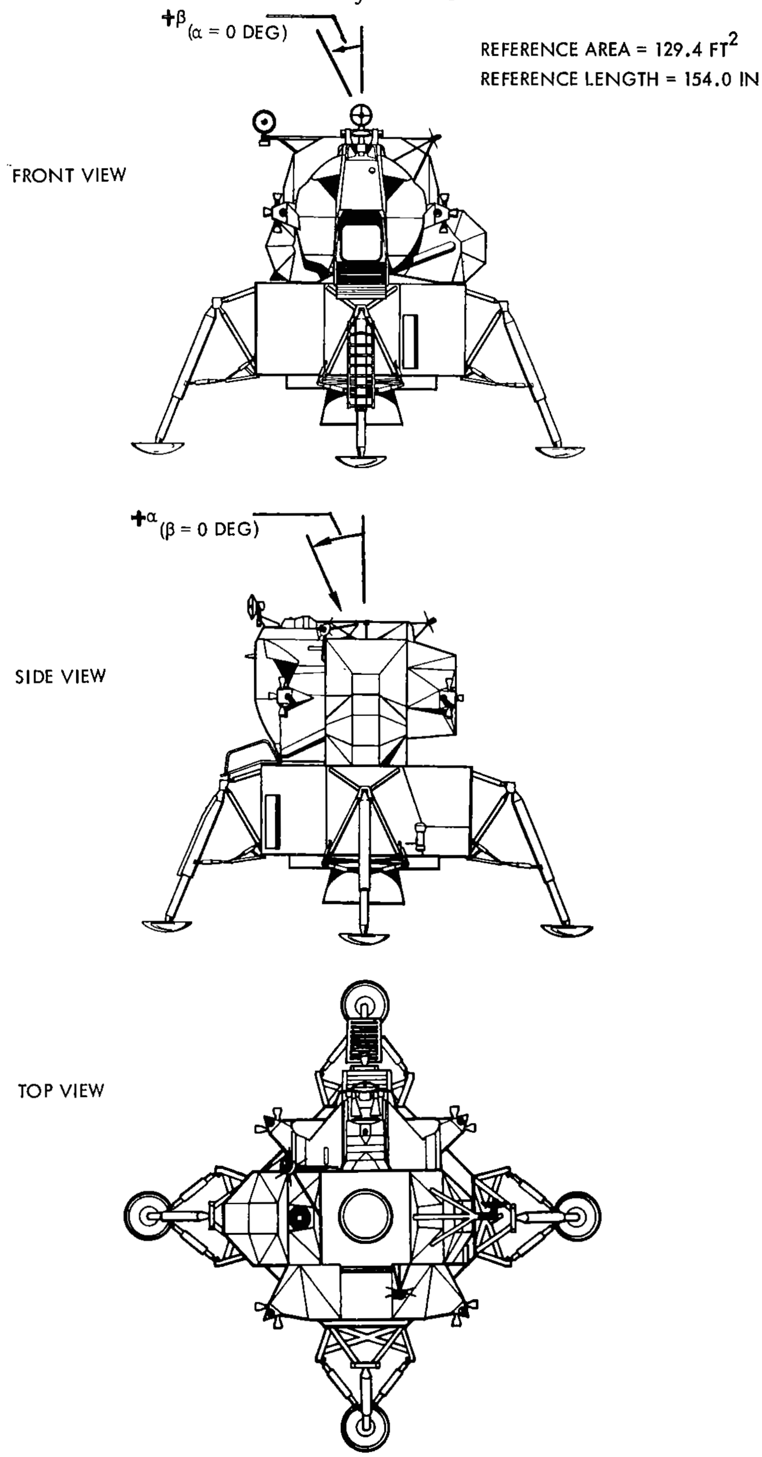

Figure 5.1-2. LM Axis System and Configuration Geometry (See Para. 5.1)

6.0 MISSION EVENT SEQUENCES

6.1 Abort Stage

The time sequences for an abort stage are given in Table 6.1-1 and the associated logic block diagram of Figure 6.1.1. The assumption made is that the Abort-Stage button is depressed during descent engine firing. However, the data can generally be applied with minor modification to other applications of Abort-Stage activation.

TABLE 6.1-1. LM ABORT STAGE SEQUENCE

Event	Elapsed Time (Seconds)		
	Minimum	Nominal	Maximum
INITIATE ABORT STAGE SEQUENCE (T_0)		0.000	
Ascent Engine Press. Relay Pull-In		0.010	
Descent Engine Cut-off Signal		0.012	
Ascent Engine Press. Squib Blows		0.020	
Ascent Stage EPS Batteries Activated		0.046	
Descent Stage EPS Batteries Dead-Faced		0.070	
AGS Supplies Engine ON Signal		0.100	
PGNS Supplies Engine ON Signal		0.150	
Descent Engine Thrust Decays to 10%	0.242	0.312	0.382 (1)
Ascent Engine Arming Signal Activated	0.320	0.400	0.480
APS Engine ON (T_1)	0.324	0.410	0.493
APS Tanks Fully Pressurized (180 psi), He and Propellant	0.430		4.030
Descent Engine Thrust Decays to Zero	3.012	6.62	10.012 (1)
APS ENGINE ON (T_1)		0.000	
Stage Nuts and Bolts and ECI Relays Activated	0.004	0.008	0.011
Stage Nuts and Bolts and ECI Removal Completed	0.006	0.012	0.016
Guillotine Relay Activated		0.090	
Guillotine Severs Umbilical		0.100	
APS Engine Builds Up to 10% Thrust Assuming 180 psi Pre-Pressure	0.30		0.43 (2)
APS Engine Builds Up to 90% Thrust Assuming 180 psi Pre-Pressure	0.325		0.455 (2)
APS Engine Builds up to 10% Thrust Assuming 100 psi Pre-Pressure		0.545 (2)	
APS engine Builds Up to 90% Thrust Assuming 100 psi Pre-Pressure		0.555 (2)	

(1) See Figure 4.7-16, Descent Engine Thrust Decay for Shutdowns.
(2) See Figure 4.6-29, APS Fire in the Hole (FITH) Thrust Build Up.

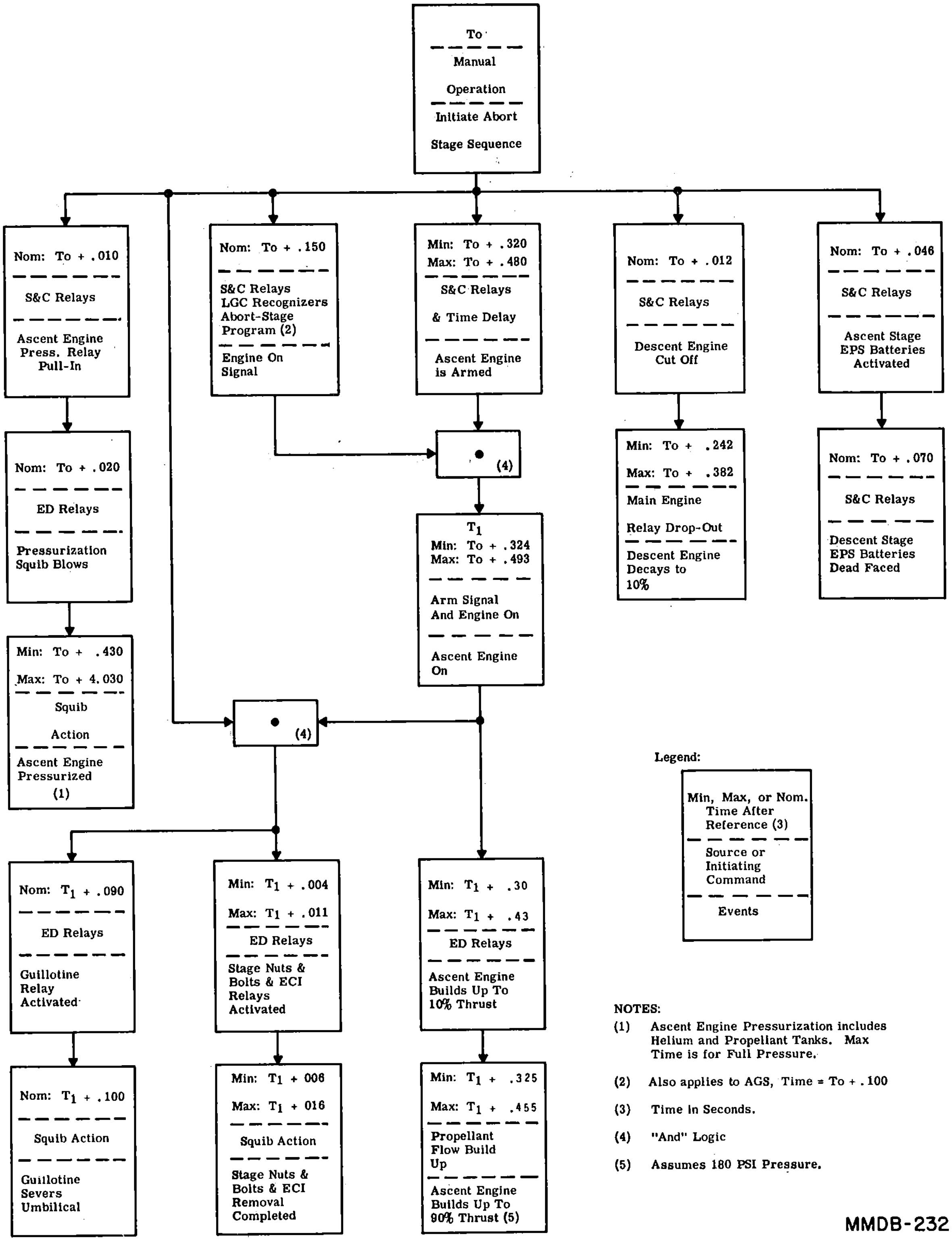

NOTES:

(1) Ascent Engine Pressurization includes Helium and Propellant Tanks. Max Time is for Full Pressure.

(2) Also applies to AGS, Time = To + .100

(3) Time in Seconds.

(4) "And" Logic

(5) Assumes 180 PSI Pressure.

MMDB-232

Figure 6.1-1. Block Diagram of LM Abort Stage Sequence

7.0 SPACECRAFT BENDING MODES

7.1 LM Bending Data

This section presents the Lunar Module (LM) Free-Free Modes for one weight condition with the mated ascent and descent stages, and two conditions of the ascent stage only. These data shown in Tables 7.1-1, 7.1-2 and 7.1-3 were obtained from ground vibration tests of LTA-3. Accuracy on frequency is approximately 10% and up to 50% on amplitudes. Damping values are considered low because the test article did not have some items that contribute to damping.

(Ref: MSC source data memo, "Lunar Module (LM) Free-Free Modes," ES2 to EG23, 9 November 1967)

Volume II LM Data Book
Subsystem Performance Data-Bending Modes
Table 7.1-1. Modal Displacements at Lunar Touchdown Condition

Config: Mated Ascent/Descent Stages Free-Free
Ascent Stage Full, Descent Empty

Mode		1	2	3	4	5	6	7	Units
Frequency		8.06	8.18	10.20	10.210	11.900	12.180	12.500	Hz
Damping	$g = 2\ C/C_c$	.07	.06	.02	.055	.028	.025	.048	
Displ. at RCS's									
Cluster I	X	.20	0.195	0.000	0.105	.100	0.000	0.000	
	Y	.12	.151	-.106	-.105	.350	0.000	.182	n.d.
	Z	.11	.127	-.080	-.100	.520	0.000	.450	
Cluster II	X	.10	0.000	0.000	0.000	.580	-.306	1.000	
	Y	-.25	-.215	.159	.093	-.870	0.000	-.534	n.d.
	Z	.12	.156	-.090	-.136	.800	0.000	-.550	
Cluster III	X	-.14	-.129	0.000	-.098	0.000	-.287	.740	
	Y	-.24	-.210	.154	.096	-.830	0.000	-.542	n.d.
	Z	-.25	-.229	.200	.064	-.530	0.000	-.158	
Cluster IV	X	-.24	-.226	0.000	-.104	-.440	0.000	-.300	
	Y	.18	.190	-.120	-.100	.350	0.000	.170	n.d.
	Z	-.24	-.198	.152	0.000	-.230	0.000	0.000	
Displ. at IMU	X	0.00	0.000	.035	0.000	-.075	0.000	-.027	
	Y	.26	.292	-.062	0.000	.470	0.000	.279	n.d.
	Z	0.00	0.000	0.000	-.024	.340	-.182	.580	
Displ. at Desc. Engine	X	0.000	0.000	-.330	0.000	0.000	0.000	0.000	
	Y	.055	.090	.078	-.022	.190	0.000	.025	n.d.
	Z	0.000	0.000	.462	-.033	.240	0.000	.050	
Rotations at IMU	α_x	0.000	0.000	0.000	.0031	-.0058	-.0018	.0013	
	α_y	0.000	0.000	0.000	.0037	-.0069	-.0022	.0015	rad/in.
	α_z	0.000	0.000	.0045	0.0000	-.0097	0.0000	0.0035	
Rotations at Desc. Engine	α_x	-.010	-.0164	-.0141	.0190	.0027	0.0000	-.0045	
	α_y	0.000	0.0000	.0490	-.0030	.0082	0.0000	.0045	rad/in.
	α_z	0.005	.0082	.0070	-.0095	-.0014	0.0000	.0022	
Generalized Mass		5.237	5.072	2.290	1.948	8.468	1.943	5.998	$\frac{\text{lb-sec}^2}{\text{inch}}$

Note: Modal displacements are normalized to one (1) inch maximum amplitude.

Table 7.1-2. Modal Displacements at Lunar Lift-Off

Config: Ascent Stage Free-Free with Full Tanks

Mode		1	2	3	4	5	6	Units
Frequency		11.08	17.15	18.97	19.82	24.25	27.55	Hz
Damping	$g = 2\ C/C_c$	.062	.020	.058	.013	.032	.015	
Displacements at RCS's								
Cluster I	X	-.3513	.4084	-.0729	.0727	-.0260	-.0358	
	Y	-.0321	-.0725	.0537	-.0866	.9323	.2787	n.d.
	Z	-.5764	.7580	-.1172	.0614	-.5392	-.2268	
Cluster II	X	-.3199	-.8530	.0771	.3762	.4194	2.9640	
	Y	.7270	.6755	-.1200	.1188	.1712	.2785	n.d.
	Z	.0918	-.0408	.1472	-.0319	.0247	-.4564	
Cluster III	X	.4731	.4463	-.3752	.4063	-.2164	-2.8290	
	Y	.7128	.4985	-.1403	.2551	.0357	.0239	n.d.
	Z	-.3226	.1738	-.1402	.0499	.0795	.2272	
Cluster IV	X	-.0183	.0564	-.0060	.0675	-.0384	.3501	
	Y	-.4364	.3631	-.0933	.1850	-.0555	.2678	n.d.
	Z	-.0977	.0068	.0034	-.2103	-.2774	.3036	
Displ. at IMU	X	-.1201	.0140	-.0451	.2089	.0625	.0210	
	Y	-.3417	.2636	-.0408	.0143	.2813	-.0581	n.d.
	Z	-.0347	.1001	.0181	-.1077	.1420	-.0570	
Displ. at Asc. Engine	X	-.0478	.1246	-.0065	-.0466	-.0356	.0802	
	Y	.0183	.0762	.1100	-.1009	.0918	.6722	n.d.
	Z	-.1089	.1965	.0439	-.2320	.0973	-.2100	
Rotations at IMU	α_x	-.0099	.0034	-.0022	.0056	-.0012	-.0026	
	α_y	-.0045	.0035	-.0024	.0065	-.00095	-.0014	rad/in.
	α_z	-.0018	.0065	-.0006	-.00014	.0113	.0080	
Rotation at Asc. Engine	α_x	-.0050	-.00063	-.00023	.00035	-.00038	-.0016	
	α_y	-.0019	.0045	-.0017	.0049	.0063	.0440	rad/in.
	α_z	-.0017	.0038	-.00011	-.0021	-.0030	-.0130	
Generalized Mass		4.3730	2.2500	.9740	1.8140	3.7460	6.0210	$\frac{\text{lb-sec}^2}{\text{inch}}$

Note: Modal displacements are not normalized.

Table 7.1-3. Modal Displacements at Terminal Rendezvous

Config: Ascent Stage Free-Free, Empty Tanks

Mode		1	2	3	4	5	6	Units
Frequency		18.400	19.600	22.500	23.500	25.700	31.900	
Damping $g = 2\ C/C_c$		.062	.020	.058	-.013	.032	.015	Hz
Displacement at RCS's								
	X	0.000	0.000	0.000	-.400	0.290	-.170	
Cluster I	Y	0.000	0.000	0.000	0.730	0.140	0.150	n.d.
	Z	-.140	0.100	0.290	-.870	0.310	0.100	
	X	0.470	-.270	-.910	0.290	-.530	0.940	
Cluster II	Y	-.300	0.150	0.220	-.130	0.150	0.190	n.d.
	Z	0.140	0.000	-.100	0.130	0.000	-.210	
	X	-.590	0.220	0.000	-.200	0.600	-.900	
Cluster III	Y	-.300	0.150	0.000	-.130	0.150	0.150	n.d.
	Z	-.130	0.000	0.000	0.000	0.000	0.100	
	X	0.000	0.000	0.000	0.000	-.140	0.130	
Cluster IV	Y	0.000	0.000	0.000	-.400	0.120	-.190	n.d.
	Z	0.150	-.140	0.000	-.200	-.200	-.160	
Displ. at IMU	X	0.000	0.000	-.250	0.000	0.050	0.000	
	Y	0.000	0.000	0.170	-.070	0.240	-.065	n.d.
	Z	0.000	0.000	0.240	0.070	0.050	0.000	
Displ. at Asc.	X	0.000	0.000	0.290	-.100	0.000	0.000	
Engine	Y	0.100	0.000	0.190	0.000	0.000	1.000	n.d.
	Z	0.000	0.000	0.360	0.110	0.000	-.180	
Rotations at IMU	α_x	0.000	0.000	-.0065	-.0084	0.0064	0.000	
	α_y	0.000	0.000	-.0077	-.0100	0.0077	0.000	rad/in.
	α_z	0.000	0.000	0.0039	0.0000	0.0064	0.000	
Rotations at Asc.	α_x	0.000	0.000	0.0000	0.0000	0.0000	0.0000	
Engine	α_y	0.000	0.000	0.0069	0.0090	-.0096	-.0630	rad/in.
	α_z	0.000	0.000	-.0037	0.0053	0.0000	-.0170	
Generalized Mass		0.7388	0.3263	3.7780	2.0240	1.6680	2.2720	$\frac{\text{lb-sec}^2}{\text{inch}}$

Note: Modal displacements are normalized to one (1) inch maximum amplitude.

8.0 PROPELLANT SLOSH

This section presents the LM tank sloshing data. It is based on the pendulum mechanical analogy to the fluid equations. It is also assumed that the acceleration is in the positive X_E direction.

8.1 Descent Tank Sloshing Data

The fundamental sloshing frequency is given by

$$\omega = \lambda \sqrt{\frac{a}{R}}$$

where a is the acceleration along the vehicle X axis, R is the tank radius, 25.5 inches. Table 8.1-1 presents the slosh functions for (each of) the propellant tanks.

8.1.1 References

LMO-500-721, "Mechanical Model Representation of the LMMP Descent Stage Propellant Sloshing", 1 August 1969.

LMO-500-583, "A Comparison Between a Static and Dynamic Liquid Propellant Method for Calculating LM Mass Properties," 1 June 1967.

8.2 Ascent Tank Sloshing Data

The fundamental sloshing frequency is given by the same expression as is shown in Paragraph 8.1, but in the case of the ascent tanks R is 24.7 inches.

Table 8.2-1 presents the slosh functions for (each of) the propellant tanks.

8.2.1 Reference

LMO-500-168, "Mechanical Model Representations for LM Ascent and Descent Stage Propellant Sloshing," 8 April 1964.

Table 8.1-1. Descent Tank Propellant Slosh Functions

Fraction of Propellant in Tank	Ratio:Slosh Mass to Max Prop. Mass	λ, Frequency Parameter	Support Position*
0.0	0.00	1.00	-0.22
0.1	0.08	1.10	-0.22
0.2	0.14	1.16	-0.22
0.3	0.17	1.22	-0.20
0.4	0.19	1.30	-0.17
0.5	0.20	1.34	-0.13
0.6	0.21	1.35	-0.05
0.7	0.20	1.35	0.02
0.8	0.18	1.36	0.10
0.9	0.15	1.52	0.21
1.0	0.00	2.50	0.22

*Support Position is the ratio of pendulum support distance (x_T measured from the tank center positive toward the top) to the tank diameter.

Table 8.2-1. Ascent Tank Propellant Slosh Functions

Fraction of Propellant in Tank	Ratio: Slosh Mass to Max Prop. Mass	λ, Frequency Parameter	Support Position
0	0	1.00	0 *
0.1	0.08	1.06	0
0.2	0.16	1.10	0
0.3	0.22	1.14	0
0.4	0.27	1.18	0
0.5	0.30	1.22	0
0.6	0.31	1.27	0
0.7	0.30	1.33	0
0.8	0.27	1.43	0
0.9	0.19	1.64	0
1.0	0	2.30	0

*Support position is at center of the tank.

Appendixes for LM-3 thru LM-5 have been removed from Revision 2. Revisions subsequent to the Apollo 11 flight may introduce data into the basic text that conflicts with the data in these appendixes. Maintaining the above listed appendixes in the SODB, Revision 2, is entirely at the option of the user. Copies of these deleted appendixes are also available from ASPO, PD7.

9.0 VENTING IMPULSES

9.1 Disturbing Impulses due to Venting of Gases

In-flight experience has shown that the thrust neutralizers provided for external vents on the LM are less effective than expected and that venting gases through these external vents will produce forces and torques which will disturb the vehicle attitude and motion to a measurable extent.

It has, therefore, been deemed prudent to assume that the thrust neutralizers are totally ineffective when examining the possible effects of venting. The maximum possible forces (which will occur at the start of the venting) and the total impulses thus determined are summarized in Table 9.1-1 and figures 9.1-1 through 9.1-4.

References:

1) LMO-510-1612 "Impulse due to LM Venting", May 22, 1970

9.2 LM Active Docked Control Performance

Table 9.2-1 presents the results of a series of FMES/FCI testing performed to determine the acceptability of various LM control modes for docked operations. The table indicates the various vehicle configurations and the recommended, satisfactory or unsatisfactory, control modes for each configuration. Where data were available, RCS propellant consumption is also indicated. For some vehicle configurations only thrusting maneuvers were listed, since it was assumed that if the higher weight configuration was controllable for coasting, maneuvering and PTC, the lighter configuration would also be controllable in the same modes. (Reference: LTR 500-10130, FMES/FCI LM Docked Contingency Control Modes Test Report, dated Jan. 1971).

Table 9.1-1. Disturbing Impulses due to Venting of Gases

Vent	Location (inches)				F max (Lb_f)	Impulse (Lb_f-sec)
DPS Fuel Drains	(1) x = 110 y = 50 z = -26	(2) 110 50.35 -25.25	(3) 110 51.25 -24.75	(4) 110 51.75 -24.25	Fx = 1.2	Ix = 9.0 Iy = 0 Iz = 0
APS Fuel Drains	(1) x = 219.0 y = 44.7 z = -34.0	(2) 218.32 -42.4 -34.0	(3) 221.35 -42.1 -34.0	(4) 221.95 -36.2 -34.0	Fz = -1.2	Ix = 0 Iy = 0 Iz = -15.5
SHe Tank Burst Disc Rupture (51.8 lbs)	x = 161 y = 82 z = -28				Fx = 0 Fy = -32.8 Fz = 0	Ix = 0 Iy = 1290 Iz = 1290
SHe Vent Through Lunar Dump Valves (51.8 lbs)	(1) x = 197 y = -27 z = -84	(2) 197 -84 -29			Fx = 0 Fy = +13.4 Fz = 13.4	Ix = 0 Iy = 742 Iz = 742
D/S Ullage Venting	(1) x = 197 y = -27 z = -84	(2) 197 -84 -29			Fx = 0 Fy = +15.0 Fz = 15.0	Ix = 0 Iy = 3190 Iz = 3190
APS He Vent (y)	x = 280 y = 46.25 z = -34				Fx = -6.94 Fy = -6.94 Fz = 0	Ix = -64.25 Iy = -64.25 Iz = 0
APS He Vent (-y)	x = 280 y = -46.25 x = -34				Fx = -6.94 Fy = 6.94 Fz = 0	Ix = -64.25 Iy = 64.25 Iz = 0

Table 9.1-1. Disturbing Impulses due to Venting of Gases (Continued)

Vent	Location (inches)	F max (Lb_f)	Impulse (Lb_f-sec)
D/S GOX Burst Disc (Venting into Quad III and out of Quad II, III & IV vents)* (Continued) Forces due to flow induced pressure distribution on side of Quads	Vent #3 (Quad IV) x = 160.45 y = +74.25 z = +33.75	Fx = 4.73 Fy = 0 Fz = 0	Ix = 1410 Iy = 0 Iz = 0
	Vent #1 (Quad II) x = 157.35 y = -76.50 z = -32.25	Fx = 0 Fy = 2.12 Fz = 2.12	Ix = 0 Iy = 630 Iz = 630
	Vent #2 (Quad III) x = 155.20 y = 33.25 z = -76.50	Fx = 0 Fy = -2.12 Fz = +2.12	Ix = 0 Iy = -630 Iz = 630
	Vent #3 (Quad IV) x = 152.45 y = +72.75 z = +32.0	Fx = 0 Fy = -2.12 Fz = -2.12	Ix = 0 Iy = -630 Iz = -630

*Venting impulse due to Quad I vents is negligible because of small size and high flow resistance from Quads II & IV to the Quad I vents.

Table 9.1-1. Disturbing Impulses due to Venting of Gases (Continued)

Vent	Location (inches)				F max (Lb_f)	Impulse (Lb_f-sec)
Primary H_2O Boiler	x = 311.63 y = 9.78 z = -35.00				Fx = -0.091 Fy = -0.007 to +0.004 Fz = +0.027	
Secondary H_2O Boiler	x = 313.25 y = 26.00 z = -29.25				Fx = -0.055 Fy = 0 Fz = +0.013	
Upper Hatch Vent Valve	x = 295.00 y = 7.071 z = 7.071				Fx = -14 Fy = 0 Fz = 0	Ix = -240 Iy = 0 Iz = 0
Forward Hatch Vent Valve	x = 234.725 y = 10.51 z = 65.00				Fx = 0 Fy = 0 Fz = -14	Ix = 0 Iy = 0 Iz = -240
D/S GOX Burst Disc (Venting into Quad III and out of Quad II, III & IV vents)*						
Forces due to flow out of ducts	Vent #1 (Quad II) x = 165.35 y = -78.0 z = -34.0				Fx = 4.73 Fy = 0 Fz = 0	Ix = 1410 Iy = 0 Iz = 0
	Vent #2 (Quad III) x = 163.20 y = +35.0 z = -78.0				Fx = 4.73 Fy = 0 Fz = 0	Ix = 1410 Iy = 0 Iz = 0

Legend to Table 9.2-1 (LM-Active Docked Control Matrix)

PGNS/AGS	P = PGNS A = AGS
Rating	R = Recommended S = Satisfactory U = Unsatisfactory/Unstable (See Reference for detailed information)
Mode Sw.	AH = Attitude Hold Auto = Automatic Auto/AH = Either Automatic or Attitude Hold
DSKY Verb	76 = Pulse 77 = Rate Command/Attitude Hold
U-V Jets	E = Enable D = Disable (V65E)
GDA's	E = Enable Off = Off
DAP DB	1.4 = 1.4° 5 = 5° (All weight in LM via DAP load) 5* = 5° (Weight distributed between LM and CSM via DAP load)
BAL CPL	On = On Off = Off
ATT/TRANS	2 = 2 Jet 4 = 4 Jet
AGS DB	Min = .3° Max = 5.0°
Axis Att Cont	D = Direct P = Pulse M = Mode Control
Control Axis Input	A = ACA T = T/TCA
" - "	= Not applicable or has no effect

* Performed in pulse but known to yield better performance in direct.

** Not performed but known to be satisfactory due to simulations of a similar configuration.

TABLE 9.2-1. LM - ACTIVE DOCKED CONTROL MATRIX

Vehicle Configuration	PGNS/ AGS	Rating	Maneuver	CONTROL CONFIGURATION: Mode Sw.	DSKY Verb	U-V Jets	GDA's	DAP DB	Bal Cpls	Att/ Trans	AGS DB	Att. Axis Cont: Yaw	Pitch	Roll	CONTROL AXIS INPUT: Yaw	Pitch	Roll	Comments
LM (Unstage) CSM (FULL)			Coasting															
	P	R		AH	77	-	-	5	-	-	-	M	M	M	-	-	-	
	P	S		AH	77	-	-	1.4	-	-	-	M	M	M	-	-	-	
	P	U		AH	76	-	-	-	-	-	-	M	M	M	A	A	A	
	A	S		AH	-	-	-	-	ON	-	MIN	P	P	P	A	T	T	
	A	U		AH	-	-	-	-	ON	-	MAX	M	M	M	-	-	-	Unstable
			Maneuvering															
	P	R		AH	76	-	-	-	-	-	-	M	M	M	A	T	T	
	P	S		AH	77	-	-	1.4	-	-	-	M	M	M	A	A	A	Impingement, Cross CPL'G
	A	S		AH	-	-	-	-	ON	-	MIN	P	P	P	A	T	T	Best AGS
	A	S		AH	-	-	-	-	ON	-	MIN	M	M	M	A	A	A	
			Thrusting															
	P	R		Auto/AH	77	D	E	1.4	-	-	-	M	M	M	-	-	-	RCS usage: 1.79 # /min
	A	S		AH	-	-	D	-	OFF	4	MIN	M	P	P	-	T	T	RCS usage: 22 # /min
			PTC															
	P	R	Programmed (1)	AH	76	E	-	-	-	-	-	M	M	M	A	T	T	
	P	S		AH	77	E	-	1.4	-	-	-	M	M	M	-	-	-	RCS usage: DPS full - .965 # /min DPS Empty - 1.032 # /min
	A	S		AH	-	-	-	-	ON	-	MIN	P	P	P	A	T	T	
LM (Unstaged) CSM (3/4 full)			Coasting															
	P	R		AH	77	E	-	5	-	-	-	M	M	M	-	-	-	
	P	S		AH	77	E	-	1.4	-	-	-	M	M	M	-	-	-	
	P	U		AH	76	E	-	-	-	-	-	M	M	M	A	A	A	
	A	S		AH	-	-	-	-	ON	-	MAX	P	P	P	A	T	T	
	A	U		AH	-	-	-	-	ON	-	MAX	M	M	M	-	-	-	Unstable
			Maneuvering															
	P	R		AH	76	E	-	-	-	-	-	M	M	M	A	T	T	
	P	S		AH	77	E	-	1.4	-	-	-	M	M	M	A	A	A	Impingement, Cross-CPL'G
	A	S		AH	-	-	-	-	ON	-	MIN	P	P	P	A	T	T	Best AGS
	A	S		AH	-	-	-	-	ON	-	MIN	M	M	M	A	A	A	
			Thrusting															
	P	R		Auto/AH	77	D	E	1.4	-	-	-	M	M	M	-	-	-	RCS usage: 2.31 # / min
	A	S		AH	-	-	D	-	OFF	4	MIN	M	P	P	-	T	T	RCS usage: 9.45 # / min

(1) The programmed PTC maneuver used a modification of the program that was developed for re-entry spin-up of the CM on Apollo 13. This modification is such as to develop a rotation rate of 0.5°/sec.

Table 9.2-1. LM - Active Docked Control Matrix (Cont)

Vehicle Configuration	PGNS/AGS	Rating	Maneuver	CONTROL CONFIGURATION: Mode Sw.	DSKY Verb	U-V Jets	GDA's	DAP DB	Bal Cpls	Att/Trans	AGS DB	Axis Att. Cont: Yaw	Pitch	Roll	CONTROL AXIS INPUT: Yaw	Pitch	Roll	Comments
LM (Unstaged) CSM (3/4 full) Cont.			PTC															
	P	R	Programmed ①	AH	76	E	-	-	-	-	-	M	M	M	A	T	T	
	P	S		AH	77	E	-	1.4	-	-	-	M	M	M	-	-	-	High RCS prop usage
	A	S		AH	-	-	-	-	ON	-	MIN	P	P	P	A	T	T	
LM (unstaged) CSM (1/2 full)	P	R	Thrusting	Auto	77	D	E	1.4	-	-	-	M	M	M	-	-	-	RCS usage: 2.18 # /min
	A	S		AH	-	-	D	-	OFF	4	MIN	M	P	P	-	T	T	RCS usage: 21.6 # /min
LM (unstaged) CSM (1/4 full)	P	R	Thrusting	Auto	77	D	E	1.4	-	-	-	M	M	M	-	-	-	
	A	S		AH	-	-	D	-	OFF	4	MIN	M	P	P	-	T	T	
LM (unstaged) CSM (Empty)	P	R	Thrusting	Auto	77	D	E	1.4	-	-	-	M	M	M	-	-	-	RCS usage: 1.91 # /min
	A	S		AH	-	-	D	-	OFF	4	MIN	M	P	P	-	T	T	RCS usage: 15.62 # /min
LM (unstaged) CM (only)	P	R	Coasting	AH	76	E	-	5*	-	-	-	M	M	M	A	A	A	
	P	S		AH	77	E	-	5	-	-	-	M	M	M	-	-	-	
	P	S		AH	77	E	-	1.4	-	-	-	M	M	M	-	-	-	
	A	S		AH	-	-	D	-	ON	-	MAX	M	M	M	-	-	-	
	A	S		AH	-	-	D	-	OFF	-	MAX	M	M	M	-	-	-	
	A	S		AH	-	-	D	-	ON	-	MAX	P	P	P	A	A	A	
	P	R	Thrusting	Auto	77	D	E	1.4	-	-	-	M	M	M	-	-	-	RCS usage: 2.15 # /min
	A	S		AH	-	-	D	-	OFF	4	MIN	M	P	P	-	A	A	RCS usage: 16.9 # /min
	A	S		AH	-	-	D	-	OFF	4	MIN	M	M	M	-	-	-	RCS usage: 10.2 # /min
	A	U		AH	-	-	E	-	OFF	4	MIN	M	M	M	-	-	-	RCS usage: 21.1 # /min
	P	R	Maneuvering	AH	77	E	-	1.4	-	-	-	M	M	M	A	A	A	
	A	S		AH	-	-	D	-	ON	-	MAX	P	P	P	A	A	A	
	P	U		AH	76	E	-	1.4	-	-	-	M	M	M	A	T	T	Limited control
	A	U		AH	-	-	D	-	OFF	-	MAX	P	P	P	A	A	A	Cross CPLG

① The programmed PTC maneuver used a modification of the program that was developed for re-entry spin-up of the CM on Apollo 13. This modification is such as to develop a rotation rate of 0.5°/sec.

Table 9.2-1. LM - Active Docked Control Matrix (Cont)

Vehicle Configuration	PGNS/AGS	Rating	Maneuver	Mode Sw.	CONTROL CONFIGURATION: DSKY Verb	U-V Jets	GDA's	DAP DB	Bal Cpls	Att/Trans	AGS DB	Axis Att. Cont: Yaw	Pitch	Roll	CONTROL AXIS INPUT: Yaw	Pitch	Roll	Comments
LM (unstaged) CM (only)			PTC															
	P	R		AH	76	E	-	-	-	-	-	M	M	M	A	T	T	
	P	S	Programmed①	AH	77	E	-	1.4	-	-	-	M	M	M	-	-	-	High RCS prop. usage
	A	S	**	AH	-	-	-	-	ON	-	MIN	P	P	P	A	A	A	
LM (staged) CSM (full)			Coasting															
	A	R		AH	-	-	-	-	ON	-	MIN	P	P	P	A	T	T	
	P	S		AH	77	E	-	1.4	-	-	-	M	M	M	-	-	-	
	P	S		AH	77	E	-	5	-	-	-	M	M	M	-	-	-	
	P	U		AH	76	E	-	-	-	-	-	M	M	M	A	A	A	
	A	U		AH	-	-	-	-	ON	-	MAX	M	M	M	-	-	-	
			Maneuvering															
	A	R		AH	-	-	-	-	ON	-	MIN	P	P	P	A	T	T	
	A	S		AH	-	-	-	-	ON	-	MIN	M	M	M	A	A	A	
	P	S		AH	76	E	-	-	-	-	-	M	M	M	A	T	T	
			Thrusting															
	A	R		AH	-	-	-	-	ON	4	MIN	M	P	P	-	T	T	RCS usage: 60.4 # /min
	P	U		Auto/AH	77	-	-	-	-	-	-	-	-	-	-	-	-	
			PTC															
	A	R		AH	-	-	-	-	ON	-	MIN	P	P	P	A	T	T	
	P	S		AH	76	E	-	-	-	-	-	M	M	M	A	T	T	
	P	S	Programmed①	AH	77	E	-	1.4	-	-	-	M	M	M	-	-	-	RCS usage: APS full .568 # / min APS empty - 1.085 # / min
LM (staged) CSM (3/4 full)			Coasting															
	A	R		AH	-	-	-	-	ON	-	MIN	P	P	P	A	T	T	
	A	S		AH	-	-	-	-	ON	-	MAX	M	M	M	-	-	-	Slow settling response
	P	S		AH	77	E	-	5	-	-	-	M	M	M	-	-	-	
	P	S		AH	77	E	-	1.4	-	-	-	M	M	M	-	-	-	
	P	U		AH	76	E	-	-	-	-	-	M	M	M	A	A	A	
			Maneuvering															
	A	R		AH	-	-	-	-	ON	-	MIN	P	P	P	A	T	T	
	A	S		AH	-	-	-	-	ON	-	MIN	M	M	M	A	A	A	
	P	S		AH	76	E	-	-	-	-	-	M	M	M	A	T	T	

① The programmed PTC maneuver used a modification of the program that was developed for re-entry spin-up of the CM on Apollo 13. This modification is such as to develop a rotation rate of 0.5°/sec.

Table 9.2-1. LM - Active Docked Control Matrix (Cont)

Vehicle Configuration	PGNS/ AGS	Rating	Maneuver	CONTROL CONFIGURATION Mode Sw.	DSKY Verb	U-V Jets	GDA's	DAP DB	Bal Cpls	Att/ Trans	Ags DB	Axis Yaw	Att. Pitch	Cont Roll	CONTROL AXIS INPUT Yaw	Pitch	Roll	Comments
LM (staged) CSM (3/4 full) (Cont.)			Thrusting															
	A	R		AH	-	-	-	-	ON	4	MIN	M	P	P	-	T	T	RCS usage: 60.0 # / min
	P	U		Auto/AH	-	-	-	-	-	-	-	-	-	-	-	-	-	
			PTC															
	A	R		AH	-	-	-	-	ON	-	MIN	P	P	P	A	T	T	
	P	S	(1)	AH	76	E	-	-	-	-	-	M	M	M	A	T	T	
	P	S	Programmed	AH	77	E	-	1.4	-	-	-	M	M	M	-	-	-	RCS usage: APS full - .406 # / min APS empty - 1.025 # / min
LM (staged) CSM (1/2 full)			Thrusting															
	A	R		AH	-	-	-	-	ON	4	MIN	M	P	P	-	T	T	RCS usage: 57.3 # / min
	P	U		Auto/AH	-	-	-	-	-	-	-	-	-	-	-	-	-	
LM (staged) CSM (1/4 full)			Thrusting															
	A	R		AH	-	-	-	-	ON	4	MIN	P	D	P	A	A, T	T	RCS usage: 85 # / min
	A	S		AH	-	-	-	-	OFF	4	MIN	P	D	P	A	A, T	T	RCS usage: 91.5 # / min
	P	U		Auto/AH	-	-	-	-	-	-	-	-	-	-	-	-	-	
LM (staged) CSM (empty)			Thrusting															
	A	R		AH	-	-	-	-	ON	4	MIN	D*	P	P	A	A, T	T	Pitch: TTCA full on, ACA 2 or 4 jet assist.
	A	S	**	AH	-	-	-	-	ON	4	MIN	D*	D	P	A	A, T	T	Pitch: TTCA full on, ACA two jet assist.
	A	S	**	AH	-	-	-	-	ON	4	MIN	D*	P	P	A	A, T	T	Pitch: ACA hardover, TTCA assist
	A	S	**	AH	-	-	-	-	ON	4	MIN	D*	D	P	A	A, T	T	Pitch: TTCA full on ACA prop. or HDover assist.
	A	U		AH	-	-	-	-	ON	4	MIN	M	M	M	A	T	T	
	A	U		AH	-	-	-	-	ON	4	MIN	M	P	P	-	T	T	
	P	U		Auto/AH	-	-	-	-	-	-	-	-	-	-	-	-	-	
LM (staged) CM alone			Coasting															
	A	R		AH	-	-	-	-	ON	-	MIN	P	P	P	A	A	A	
	A	S		AH	-	-	-	-	-	-	MAX	M	M	M	-	-	-	
	P	S		AH	76	E	-	-	-	-	-	M	M	M	A	A	A	Best PGNS
	P	S		AH	76	E	-	-	-	-	-	M	M	M	A	T	T	
	P	S		AH	77	E	-	5	-	-	-	M	M	M	-	-	-	
	P	U		AH	77	E	-	1.4	-	-	-	M	M	M	-	-	-	RCS prop. usage very high

(1) The programmed PTC maneuver used a modification of the program that was developed for re-entry spin-up of the CM on Apollo 13. This modification is such as to develop a rotation rate of 0.5°/sec.

Table 9.2-1. LM - Active Docked Control Matrix (Cont)

Vehicle Configuration	PGNS/ AGS	Rating	Maneuver	CONTROL CONFIGURATION											CONTROL AXIS INPUT			Comments
				Mode Sw.	DSKY Verb	U-V Jets	GDA's	DAP DB	Bal Cpls	Att/ Trans	AGS DB	Axis Att. Cont Yaw	Pitch	Roll	Yaw	Pitch	Roll	
LM (staged) CM alone			Maneuvering															
	A	R		AH	-	-	-	-	ON	-	MIN	P	P	P	A	A	A	
	A	S		AH	-	-	-	-	ON	-	MIN	P	P	P	A	T	T	
	P	S		AH	76	E	-	1.4	-	-	-	M	M	M	A	A	A	Best PGNS
	P	S		AH	76	E	-	1.4	-	-	-	M	M	M	A	T	T	
	P	S		AH	77	E	-	1.4	-	-	-	M	M	M	A	A	A	
			Thrusting															
	A	R		AH	-	-	-	-	ON	4	MIN	D*	D	P	A	A, T	T	Pitch: ACA 2 or 4 jet, TTCA assist
	A	S		AH	-	-	-	-	ON	4	MIN	D*	D	P	A	A, T	T	Pitch: TTCA full on ACA two jet assist.
	A	S		AH	-	-	-	-	ON	4	MIN	D*	P	P	A	A, T	T	Pitch: ACA hardover, TTCA assist.
	A	S		AH	-	-	-	-	ON	4	MIN	D*	P	P	A	A, T	T	Pitch: TTCA full on, ACA hardover assist
	A	U		AH	-	-	-	-	ON	4	MIN	M	M	M	A	A	A	
	A	U		AH	-	-	-	-	ON	4	MIN	P	P	P	A	T	T	
	P	U		Auto/AH	-	-	-	-	-	-	-	-	-	-	-	-	-	
	A	U		AH					ON	4	MIN	M	M	M	-	T	-	Satisfactory control but not recommended since TTCA may oppose auto inputs
			PTC															
	A	R		AH	-	-	-	-	ON	-	MIN	P	P	P	A	T	T	
	P	S		AH	76	E	-	-	-	-	-	M	M	M	A	A	A	
	P	U	Programmed (1)	AH	77	E	-	1.4	-	-	-	M	M	M	-	-	-	RCS usage: APS full 1.94 # /min

(1) The programmed PTC maneuver used a modification of the program that was developed for re-entry spin-up of the CM on Apollo 13. This modification is such as to develop a rotation rate of 0.5°/sec.

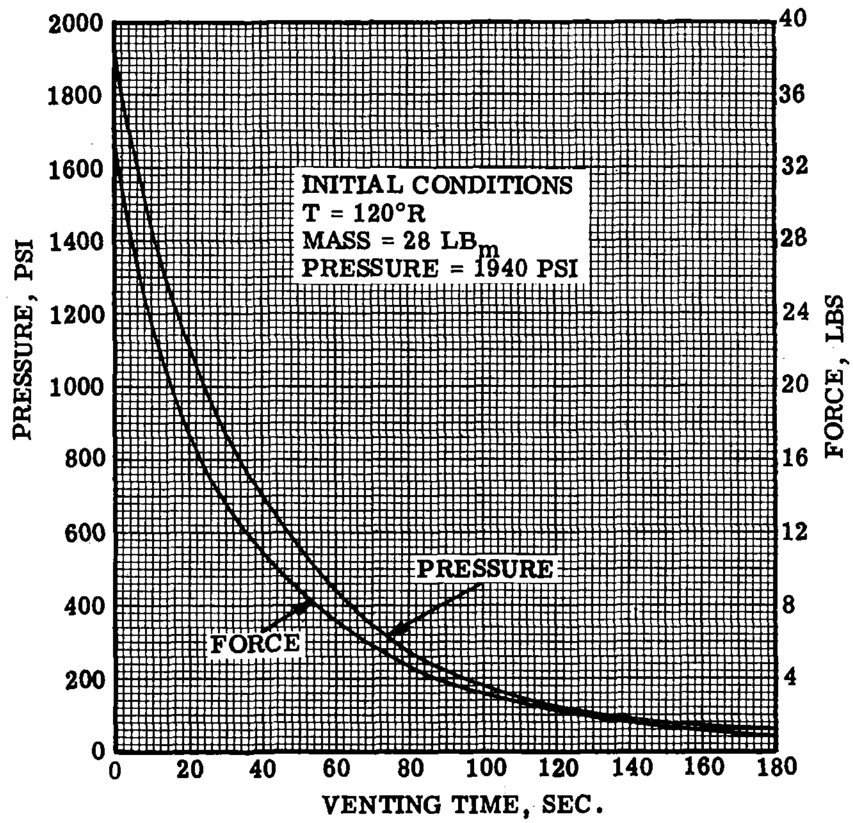

Figure 9.1-1 SHe Tank Venting Pressure and Thrust for 28 Lb Load Through SHe Thrust Neutralizer (See Para. 9.1)

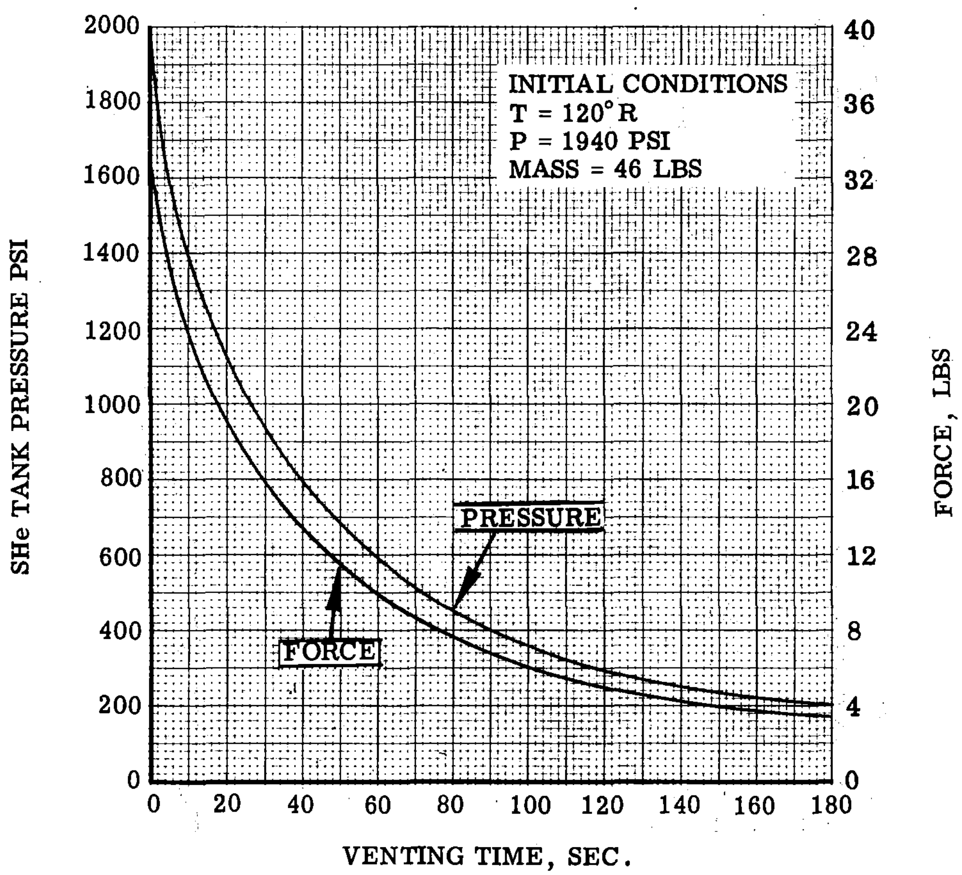

Figure 9.1-2 SHe Tank Venting Pressure and Thrust for 46 Lb Load Through SHe Thrust Neutralizer (See Para. 9.1)

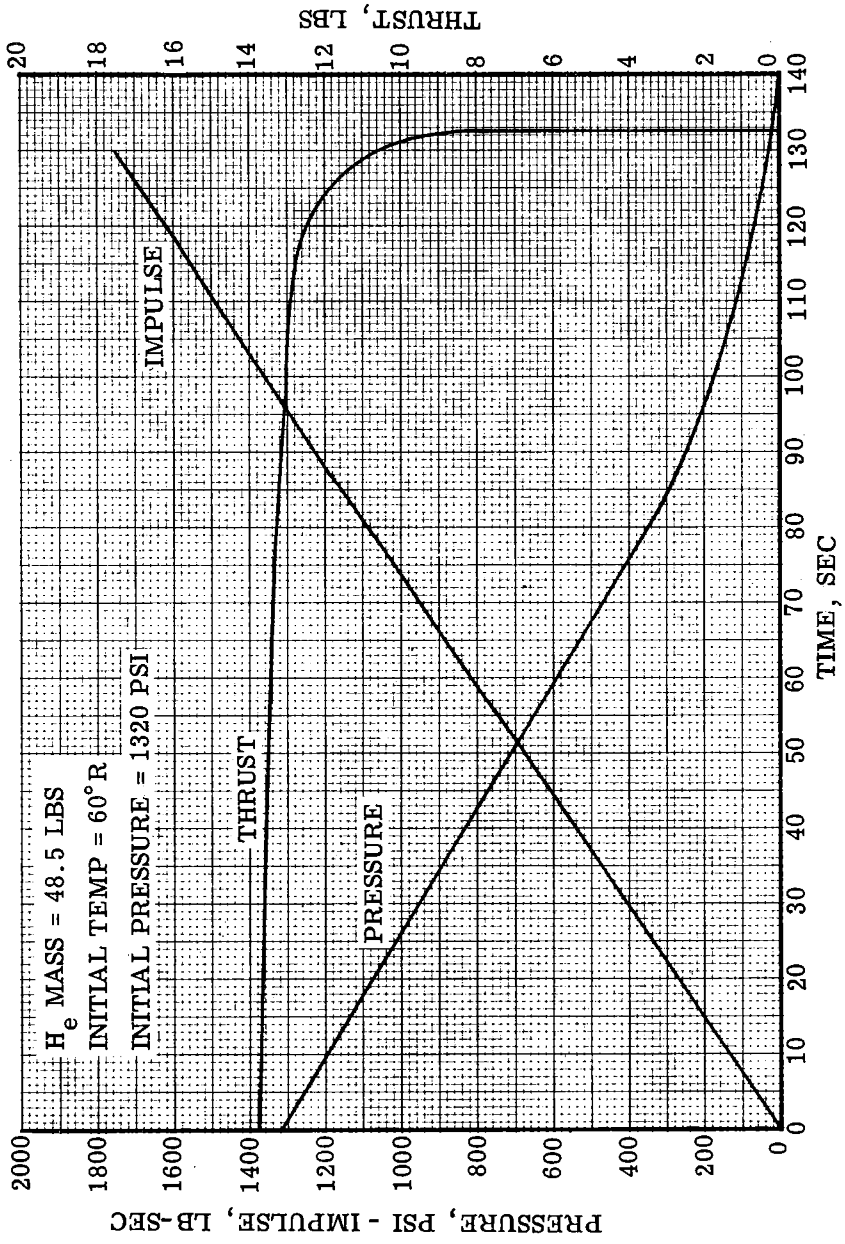

Figure 9.1-3 Helium Vent Through Lunar Dump Valves
(See Para. 9.1)

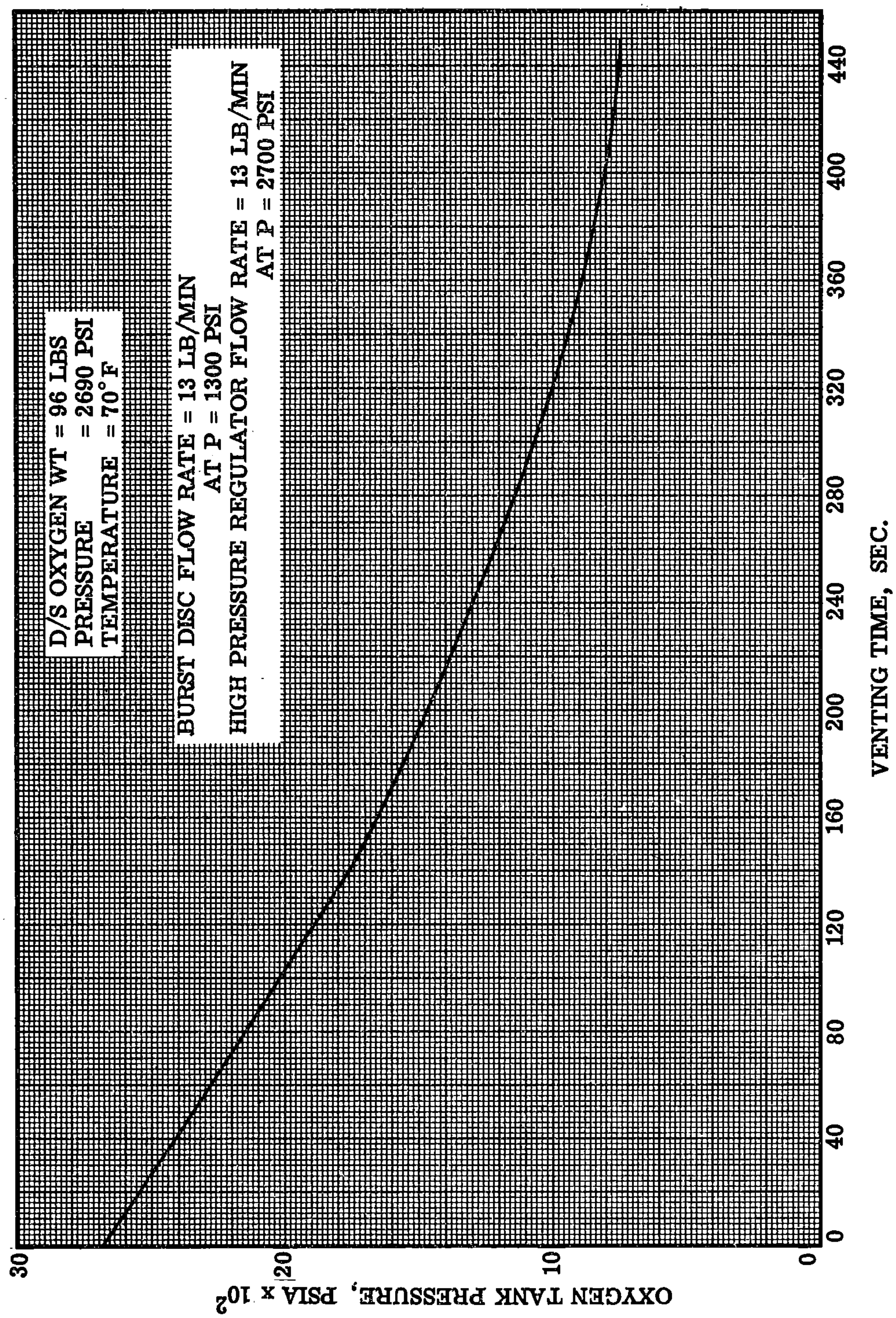

Figure 9. 1-4. D/S Oxygen Tank Pressure as a Function of Time From Burst Disc Rupture

This appendix will not be updated and the data presented are only valid up to the Apollo 12 launch date, 14 November 1969. Consequently, revisions subsequent to the Apollo 12 flight may introduce data into the basic text of the data book that conflicts with the data in this appendix. Maintaining or deleting this appendix for LM-6 in the SODB is entirely at the option of the user.

Volume II LM Data Book
APPENDIX LM-6

TABLE OF CONTENTS

Changes to baseline data specific to LM-6 are included in this appendix.

Volume II LM Data Book
APPENDIX LM-6

TABLE OF CONTENTS

Changes to baseline data specific to LM-6 are included in this appendix.

Volume II LM Data Book
APPENDIX LM-6

TABLE OF CONTENTS

Changes to baseline data specific to LM-6 are included in this appendix.

Volume II LM Data Book
APPENDIX LM-6

TABLE OF CONTENTS

Changes to baseline data specific to LM-6 are included in this appendix.

LM6/3.1 COMMUNICATIONS

OPERATIONAL LIMITATIONS OR PROCEDURE	RATIONALE
LM6/C-5 SM RCS Plume Impingement on Steerable Antenna CSM jets B3 and C4 are not constrained by S-band steerable antenna on LM-6 in light of the 7 seconds maximum allowable plume heating imposed by the LM thermal insulation.	Continuous firing limited per Paragraph 3.8 RCS-5, planned landing site, sun angle, and stay time permit thermal control coating degradation, due to impingement, in excess of amount predicted for nominal mission operations. See Paragraph LM6/4.1.2.8 for additional rationale and affects of plume induced torque.

LM6/3.6 PROPULSION - APS

OPERATIONAL LIMITATION OR PROCEDURE	RATIONALE
LM6/APS-1 Propellant Tank Pressure-Temperature Limit Relationship (NASA DATA SOURCE)	
The propellant tank pressures should not exceed the values given in Figures LM6/3.6.1-1, LM6/3.6.1-2 and LM6/3.6.1-3.	Reliability is reduced below allowable value.
LM6/APS-9 Ambient Helium Storage Tank Pressure	
Helium tank pressure limitations are given in Figure LM6/3.6.1-4.	If maximum is exceeded, reliability is reduced below allowable value. If minimum is exceeded, there will be insufficient helium to complete a lunar mission duty cycle.

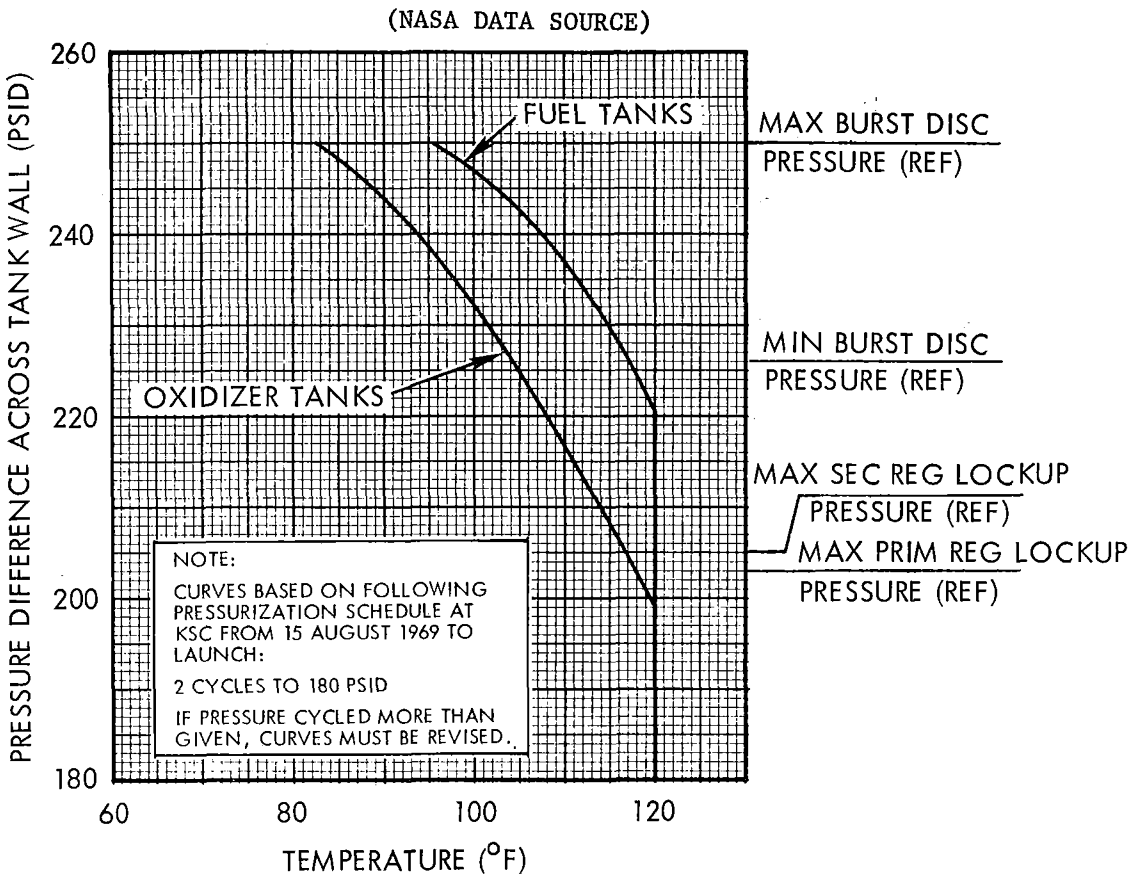

Figure LM6/3.6.1-1. Maximum Allowable Pressure-Temperature Limit Relationship for LM-6 Ascent Stage Propellant Tanks

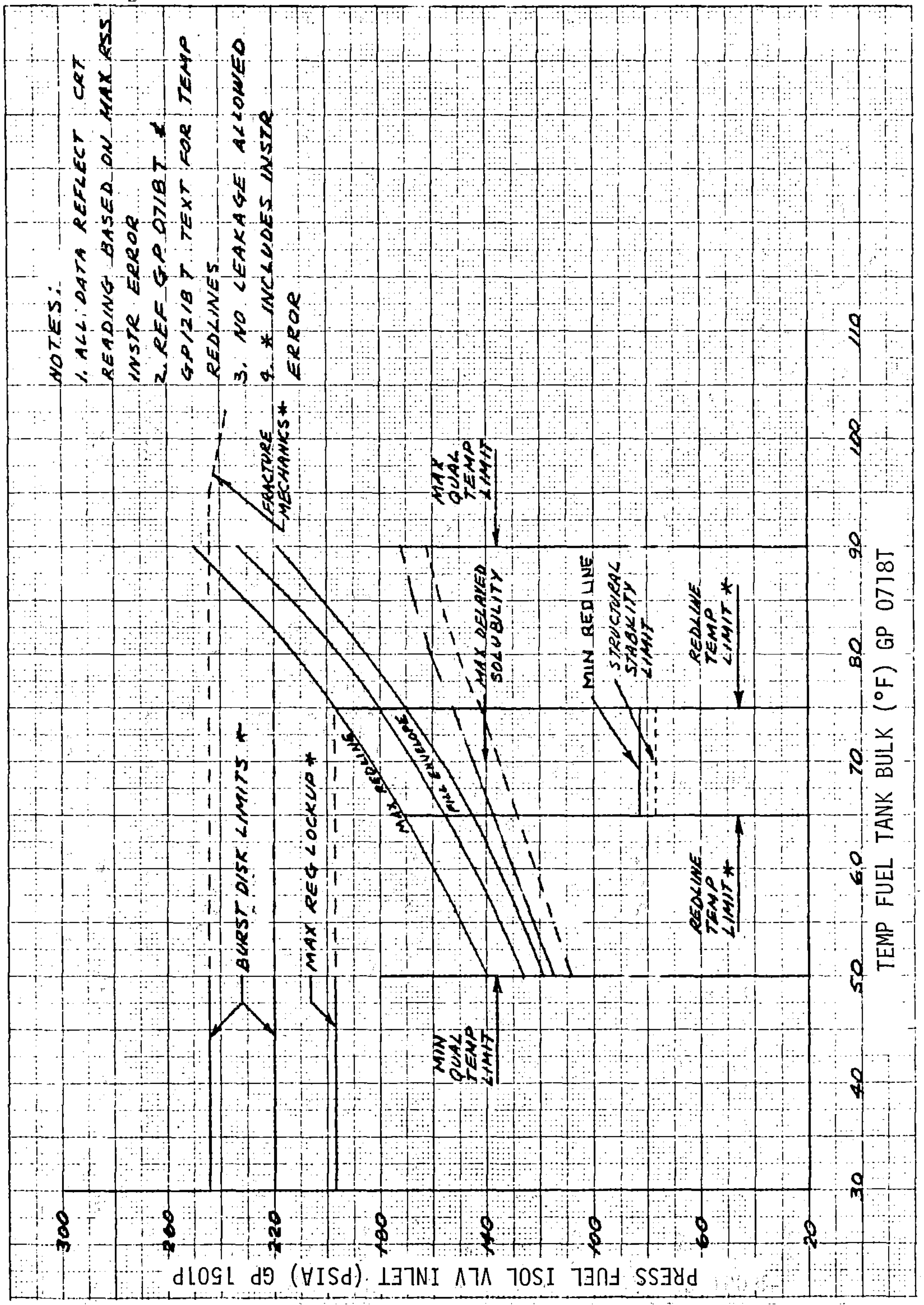

Figure LM6/3.6.1-2. APS Fuel Tank Pressure-Temperature Limitations

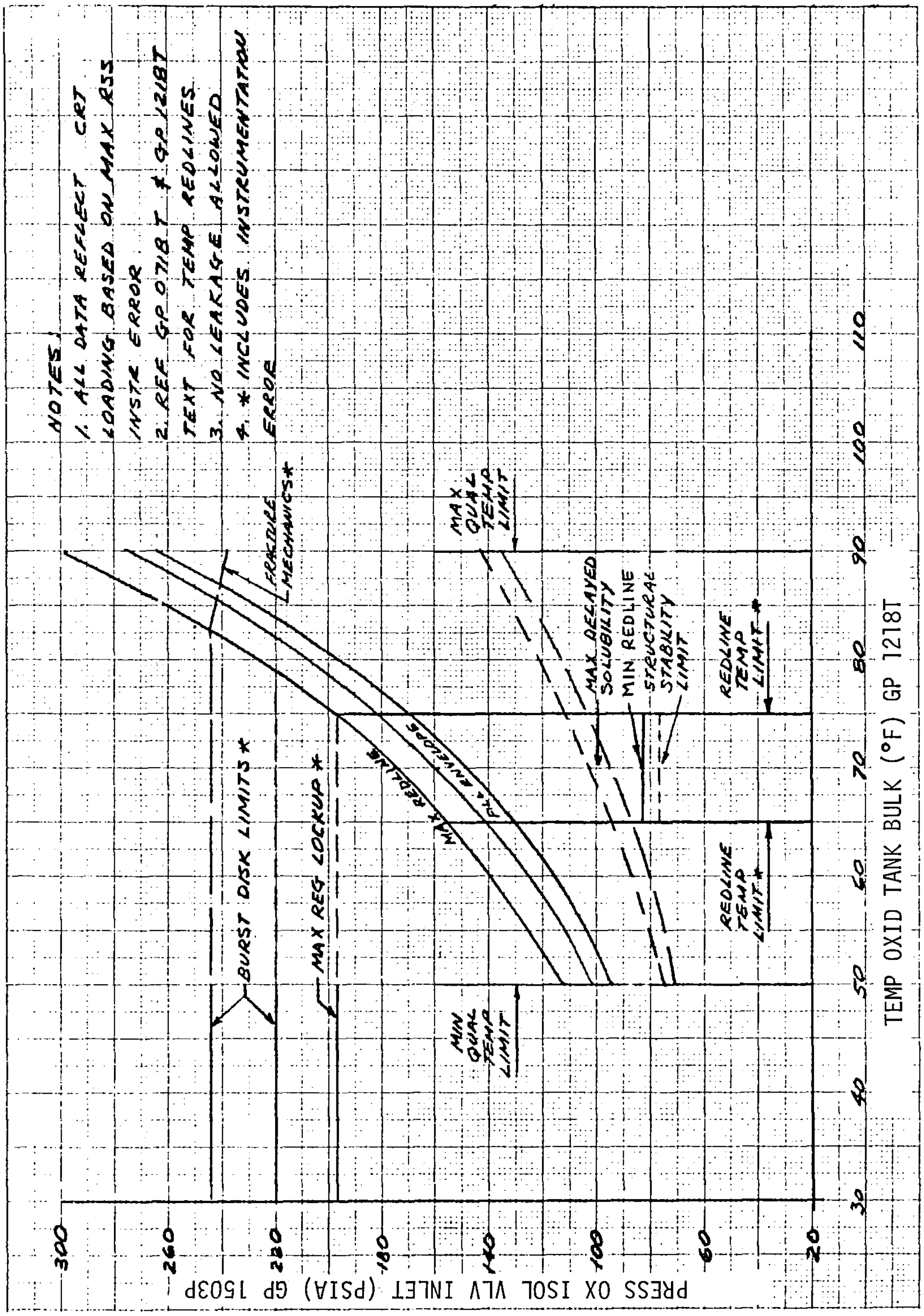

Figure LM6/3.6.1-3. APS Oxidizer Tank Pressure-Temperature Limitations

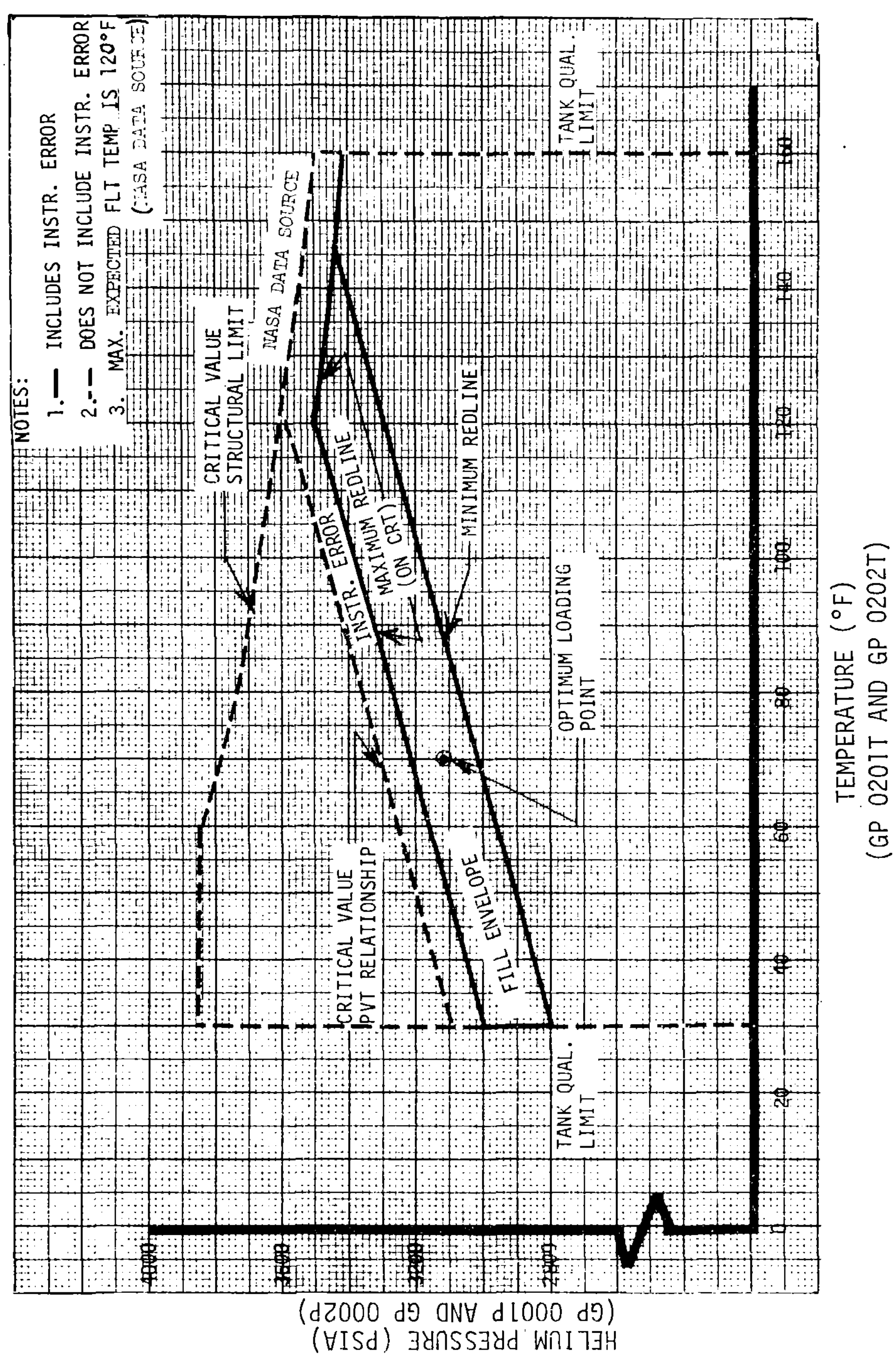

Figure LM6/3.6.1-4. APS Helium Tank Pressure-Temperature Limitations

LED-540-54

LM6/3.7 PROPULSION - DPS

OPERATIONAL LIMITATION OR PROCEDURE	RATIONALE
LM6/DPS-6 Propellant Tank Pressure-Temperature Limit Relationship	
The propellant tank pressures should not exceed the values given in Figures LM6/3.7.1-1, LM6/3.7.1-2 and LM6/3.7.1-3.	Reliability is reduced below the allowable value.
LM6/DPS-8 Non-Throttling Range Engine Operation (NASA DATA SOURCE)	
The maximum allowable burn time in the non-throttling range for the LM-6 DPS engine during the lunar landing duty cycle is 50 seconds.	Off-nominal mixture ratios may result or the thrust chamber may burn through.

LM6/DPS-17 Engine Interface Pressure (Fuel and Oxidizer)

Event	Minimum	Maximum	Rationale
Preburn	30 psia	275 psia	If maximum is exceeded, burst disk pressure will be exceeded and helium supply will be reduced. If below minimum, freezing of fuel in heat exchanger may result.
During Burn	150 psia @ FTP	275 psia	If maximum exceeded, burst disk pressure will be exceeded and helium supply will be reduced.
	120 psia @ 10% to 65% thrust (See Note)		If below minimum, extreme combustion roughness may result, which could cause engine damage.

NOTE: Severe chamber pressure spikes can occur as these limits are approached; therefore, operation near these limits should be minimized.

OPERATIONAL LIMITATION OR PROCEDURE	RATIONALE
LM6/DPS-20 Ambient Helium Storage Tank Pressure-Temperature Limitations	
Ambient helium tank pressure limitations are given in Figure LM6/3.7.1-4.	If the maximum is exceeded, reliability is reduced below allowable value.

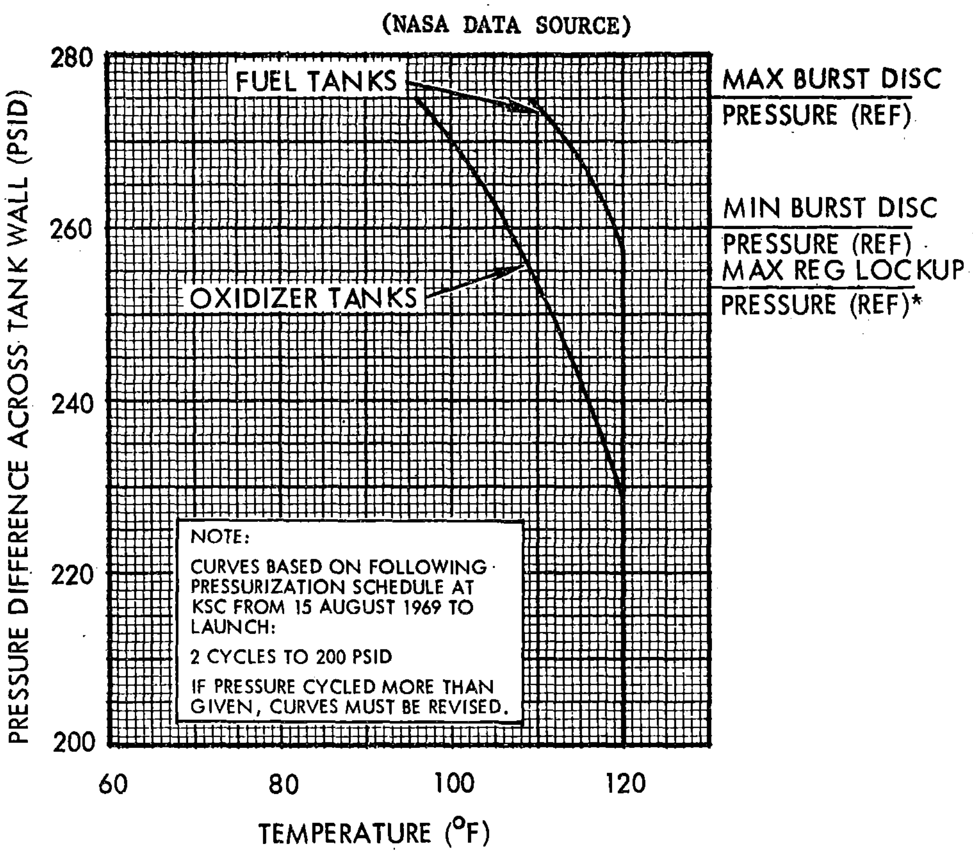

*255 PSIA FOR REG INLET PRESSURE BETWEEN 320 AND 400 PSIA

Figure LM6/3.7.1-1. Maximum Allowable Pressure-Temperature Limit Relationship for LM-6 Descent Stage Propellant Tanks

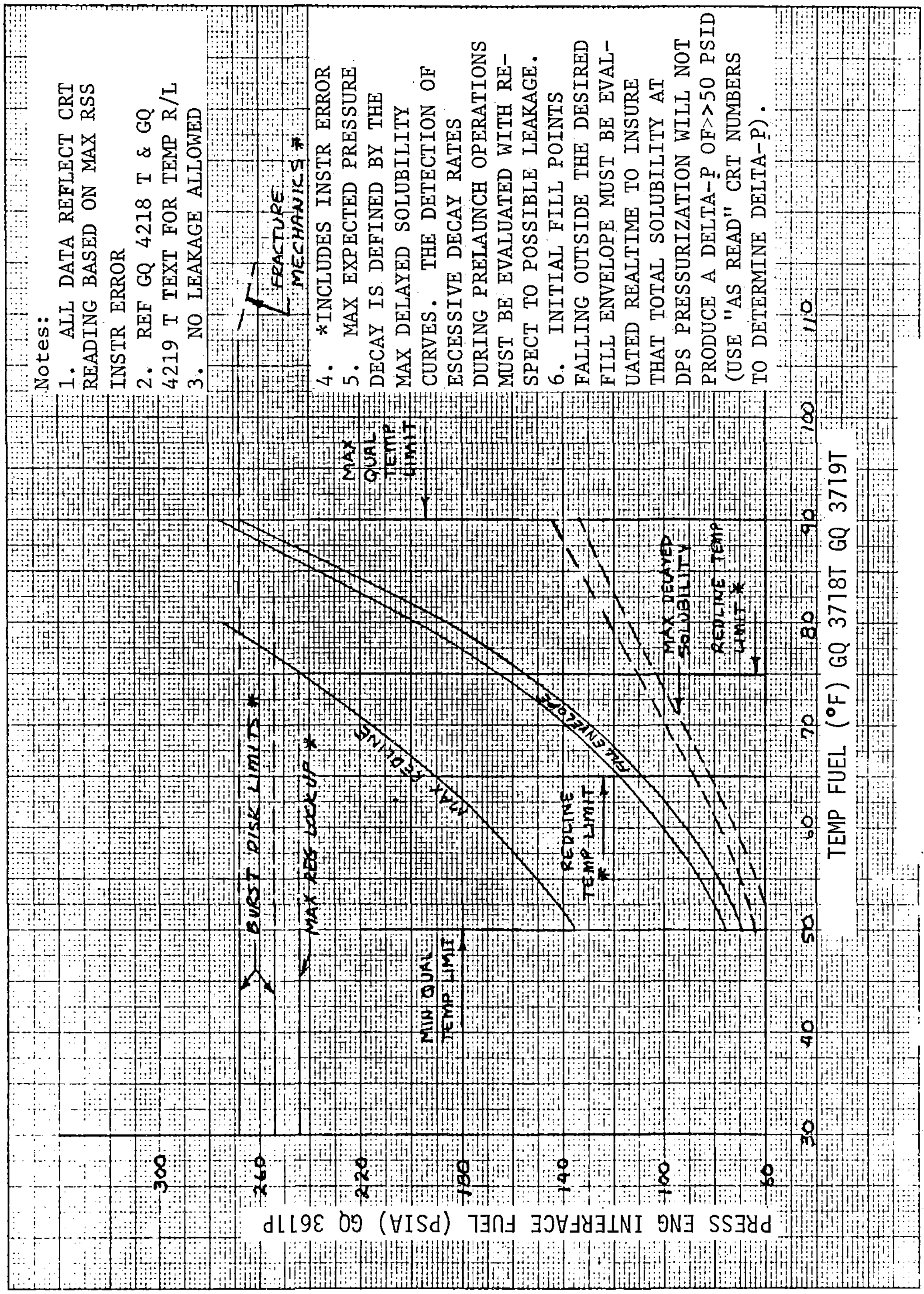

Figure LM6/3.7.1-2. DPS Fuel Tank Pressure-Temperature Limitations

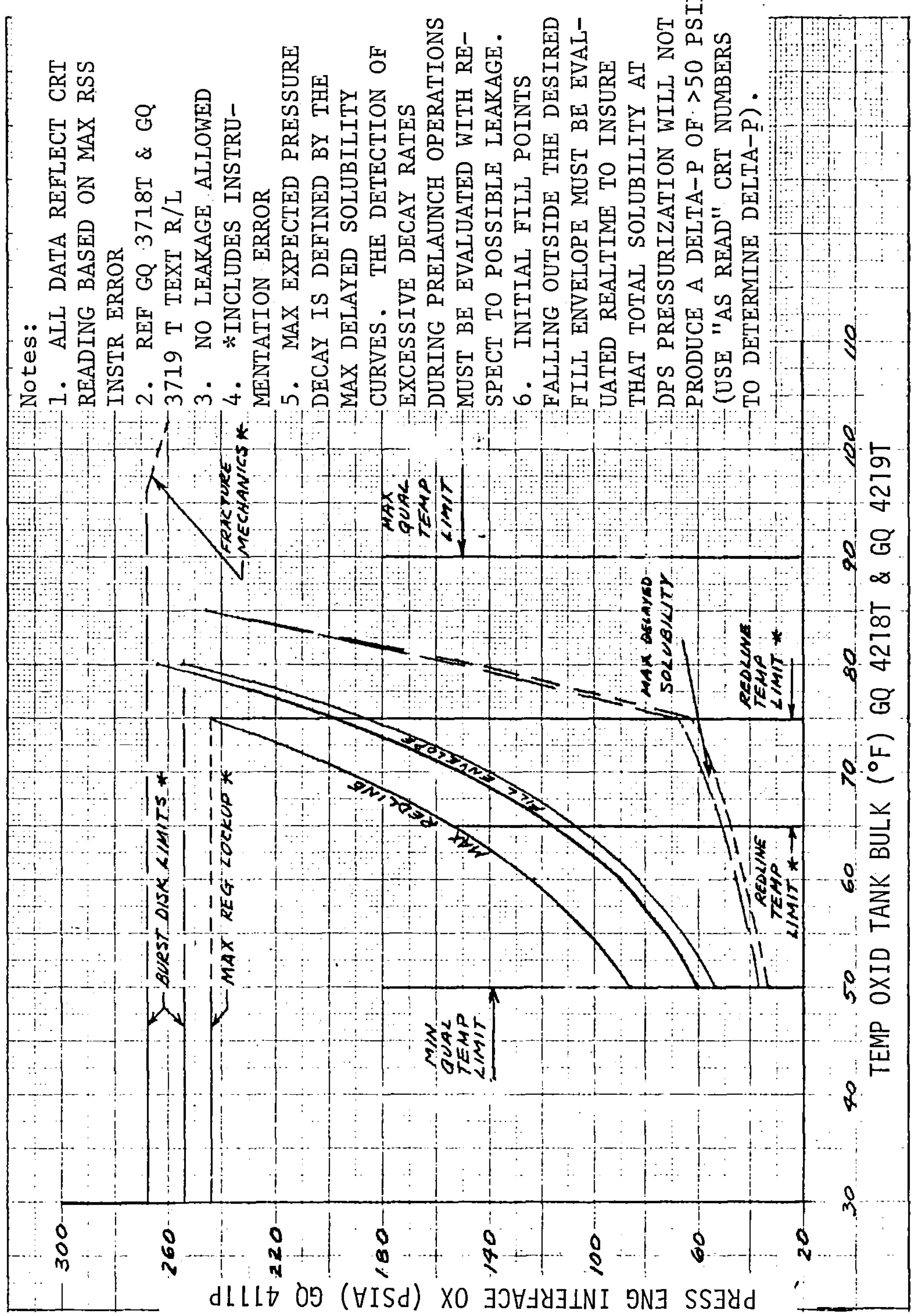

Figure LM6/3.7.1-3. DPS Oxidizer Tank Pressure-Temperature Limitations

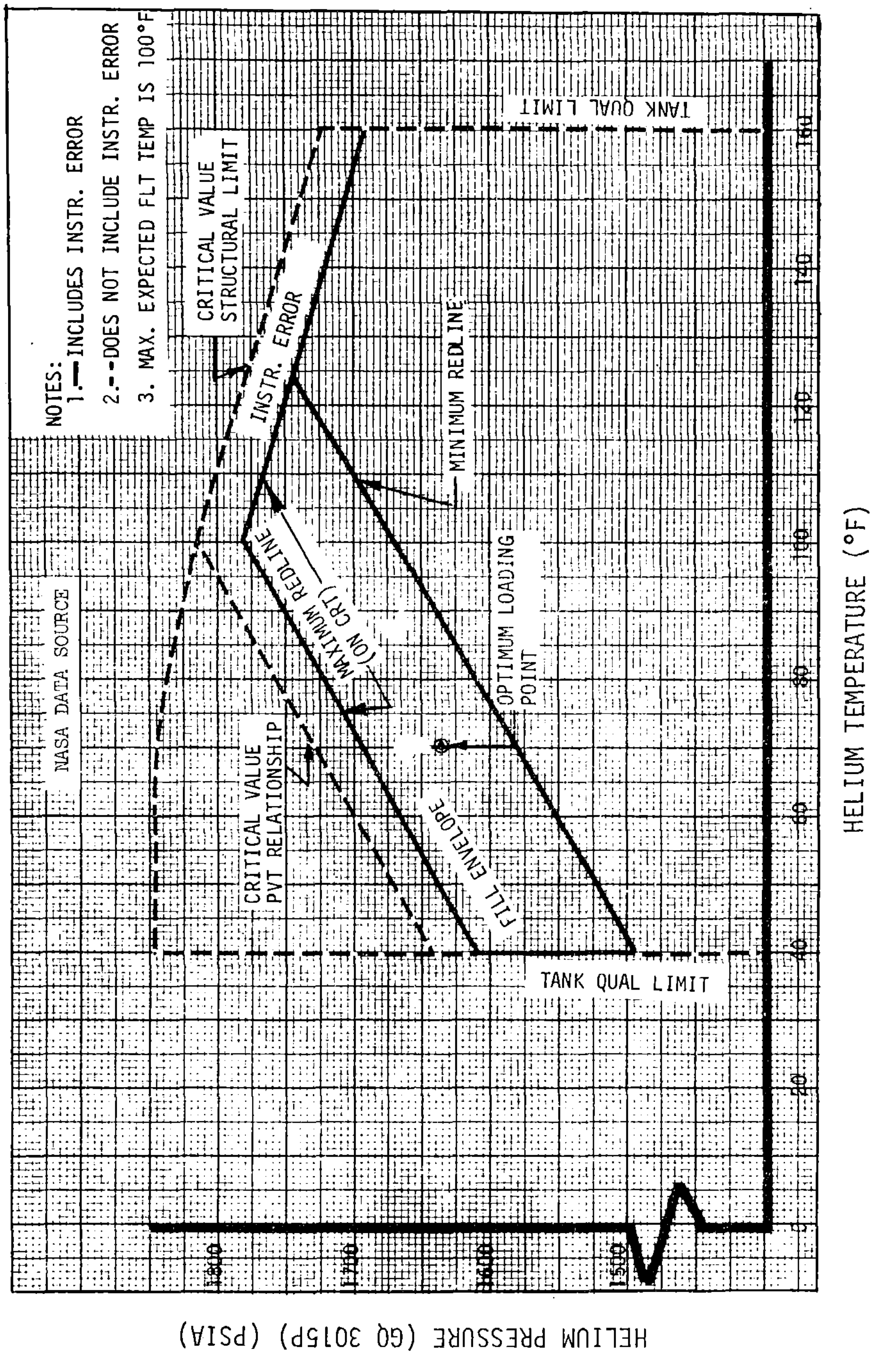

Figure LM6/3.7.1-4. DPS Ambient Helium Tank Pressure-Temperature Limitations

LM6/3.8 REACTION CONTROL SUBSYSTEM

OPERATIONAL LIMITATION OR PROCEDURE	RATIONALE
LM6/RCS-13 Propellant Tank Pressure-Temperature Limit Relationship (NASA DATA SOURCE)	
The propellant tank pressure should not exceed the values given in Figure LM6/3.8.1-1.	Reliability is reduced below the allowable value.
LM6/RCS-17 RCS Helium Bottle Pressure-Temperature Limitations	
RCS helium bottle pressure-temperature limitations are given in Figure LM6/3.8.1-2.	If the maximum is exceeded, reliability is reduced below allowable values.

(NASA DATA SOURCE)

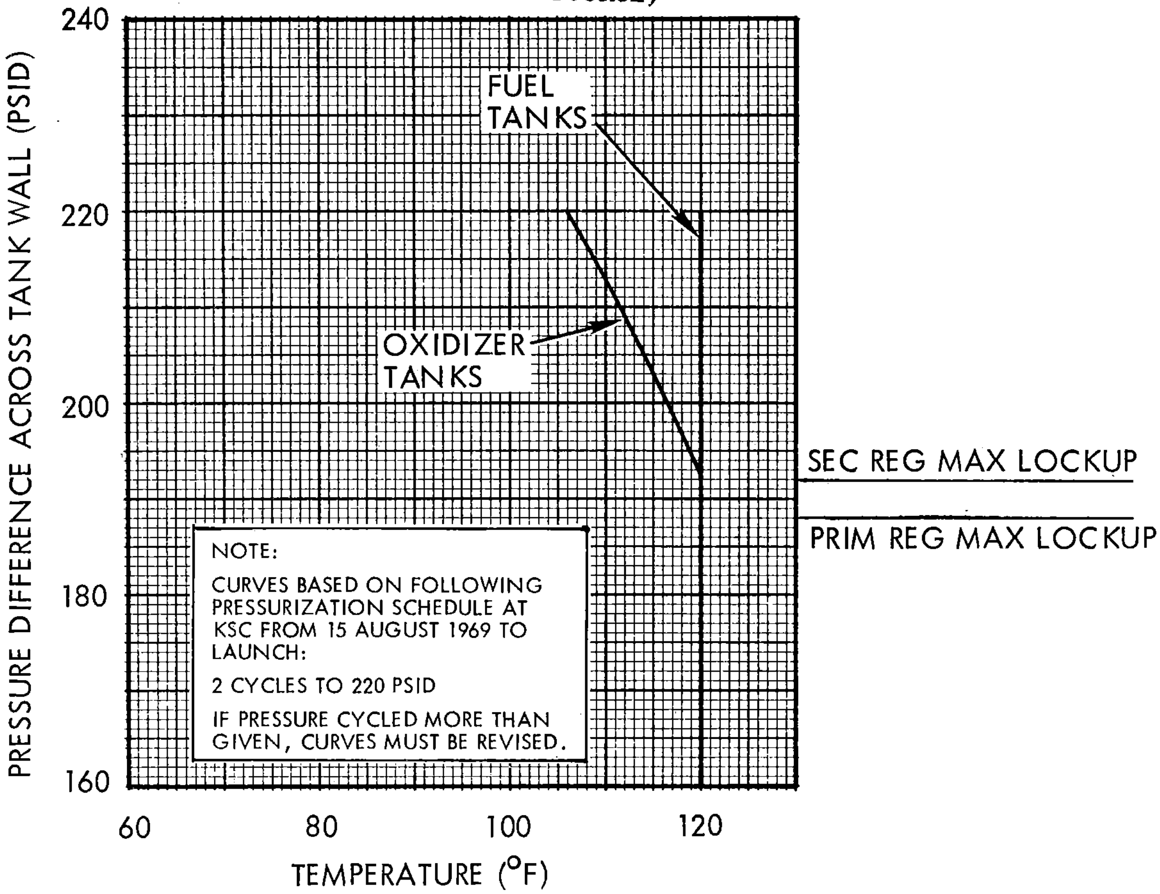

NOTE: RELIEF VALVE SETTING 132 ± 8 PSI

Figure LM6/3.8.1-1. Maximum Allowable Pressure-Temperature Limit Relationships for LM-6 RCS Propellant Tanks

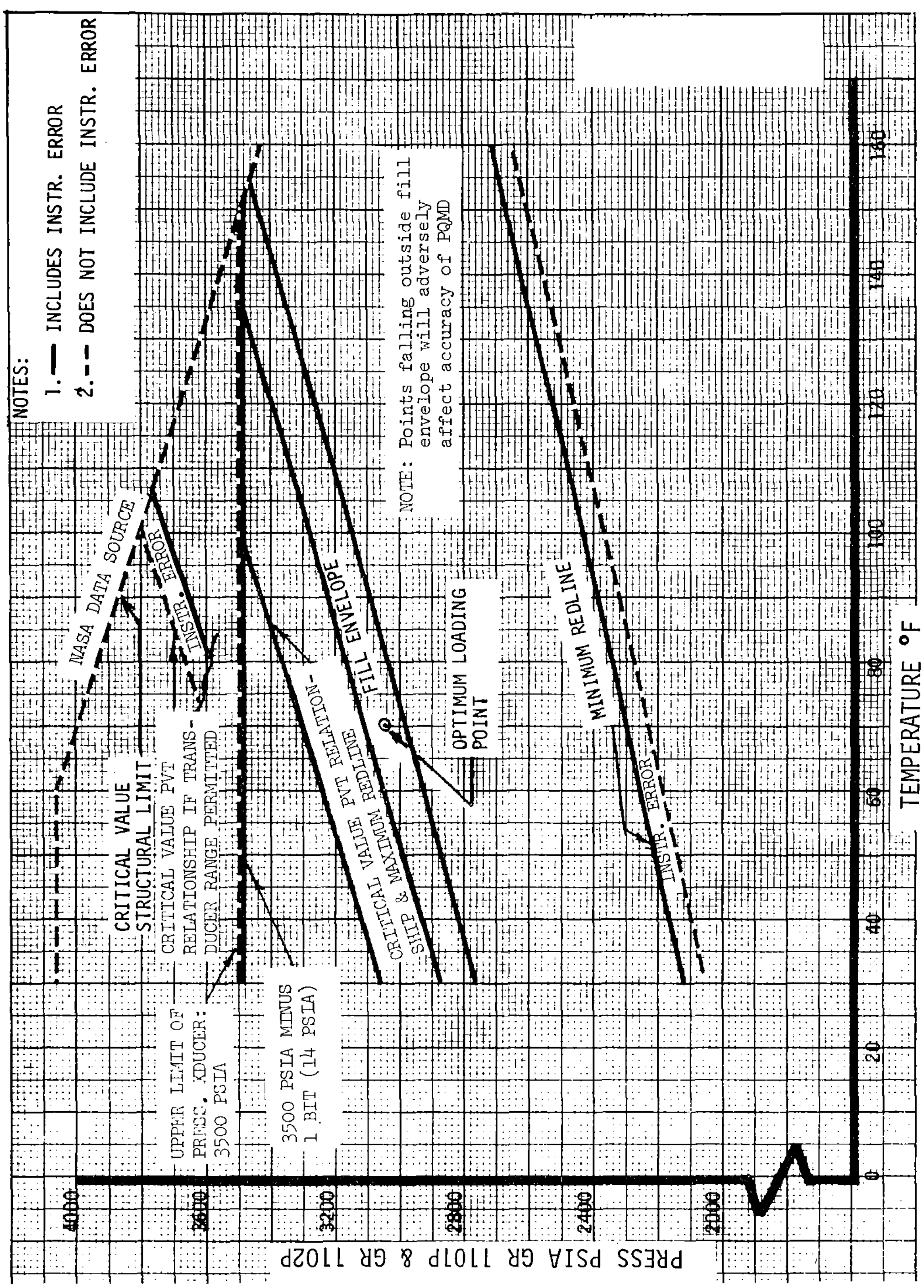

Figure LM6/3.8.1-2. RCS Helium Bottle Pressure-Temperature Limitations

Table LM6/3.10.1-1. Ascent Propulsion Subsystem (APS) Limitations

COMPONENT	TEMPERATURE LIMITS (°F)		LOW LIMIT REASON	HIGH LIMIT REASON	MEASUREMENT	
	LOW	HIGH			NUMBER	LOCATION
Fuel Tank		120		Fracture mechanics. Based upon secondary regulator lockup at 205 psid.	GP0718T	Fuel Tank Bulk
Oxidizer Tank		116			GP1218T	Ox Tank Bulk

NOTES:
1. Measurement number readings are valid only when tanks are at least 75% full.
2. See Figure LM6/3.6.1-1 for APS fracture mechanics pressure-temperature relationship curves.
3. See Table 3.10-5 for other APS temperature limitations.

Table LM6/3.10.1-2. Descent Propulsion Subsystem (DPS) Limitations

COMPONENT	TEMPERATURE LIMITS (°F)		LOW LIMIT REASON	HIGH LIMIT REASON	MEASUREMENT	
	LOW	HIGH			NUMBER	LOCATION
Fuel Tank		109		Fracture mechanics. Based upon burst disc pressure of 275 psid.	GQ3718T GQ3719T	Tank #1 Bulk Tank #2 Bulk
Oxidizer Tank		96			GQ4218T GQ4219T	Tank #1 Bulk Tank #2 Bulk

NOTES:
1. Measurement number readings are valid only when tanks are at least 75% full.
2. See Figure LM6/3.7.1-1 for DPS fracture mechanics pressure-temperature relationship curves.
3. See Table 3.10-6 for other DPS temperature limitations.

Table LM6/3.10.1-3. Reaction Control Subsystem (RCS) Limitations

COMPONENT	TEMPERATURE LIMITS (°F)		LOW LIMIT REASON	HIGH LIMIT REASON	MEASUREMENT	
	LOW	HIGH			NUMBER	LOCATION
Fuel Tank						
System A		100/120		Tank spec. limit and no engine firing experience above 100°F/Fracture mechanics. Based upon secondary regulator lock-up at 192 psid post-LOI.	GR2121T	Fuel Tank Outlet
System B		100/120			GR2122T	Fuel Tank Outlet
Oxidizer Tank						
System A		100/120		Tank spec. limit and no engine firing experience above 100°F/Fracture mechanics. Based upon secondary regulator lock-up at 192 psid post-LOI	GR2121T	Fuel Tank Outlet
System B		100/120			GR2122T	Fuel Tank Outlet

NOTES:
1. See Figure LM6/3.8.1-1 for RCS fracture mechanics pressure-temperature relationship curves.
2. See Table 3.10-7 for other RCS temperature limitations.

LM6/4.1.2 S-Band Communications (NASA DATA SOURCE)

A summary chart giving RF margins at lunar distance for S-band downlink communications is given in Table LM6/4.1.2-1.

LM6/4.1.2.8 RCS Plume Impingement on Steerable Antenna

(a) Maximum Allowable Plume Heating

- 30 seconds continuous LM -X upfiring engines of quads 3 and 4
- 45 seconds continuous CSM -X forward firing engines B3 and C4 (LM/CSM docked, antenna stowed) Also see constraint RCS-5
- 7 seconds continuous CSM -X forward firing engines B3 and C4 (LM/CSM docked, antenna unstowed) (7 seconds is a vehicle thermal insulation constraint; reference constraint RCS-5)

(b) Cumulative Firing

Cumulative firing on the antenna, when pointed outside allowable region (Figure 4.1-2), is not a constraint for LM-6. Proposed landing site (23.45° west) and sun elevation angle at landing (5°) permits thermal control coating degradation in excess of amount possible. (Antenna can withstand approximately 100% degradation in thermal properties ($\alpha = 0.2$ to $\alpha = 0.4$) before overheating. Degradation caused by LM-6 and CSM RCS firings is not expected to exceed 40%; $\alpha = 0.28$).

(c) Plume Induced Torque

Plume torque from CSM RCS may cause antenna to lose lock if firings are 190 milliseconds in duration or greater (reference H-1 mission Revs 11 and 12; antenna positions P+68°, Y+19° and P+86°, Y+12° which are close to worst orientation; worst orientation could cause loss of lock with CSM pulse duration of 150 milliseconds). If the LM-6 antenna angles are to be maintained, it would be advisable to switch from Auto to Manual Slew mode when firings of 190 milliseconds or greater are anticipated. The alternative would be to Auto-Track with the antenna in a more desirable orientation (Pitch angles +165° to +195° and +15° to -15° with yaw angles +0° to +30° are preferred orientations where loss of lock is not anticipated). No structural damage is anticipated if antenna is driven into its mechanical stops. Care should be exercised with respect to in-the-stops operation of the antenna which could cause damage due to overheating; reference SODB constraint C-19.

Table LM6/4.1.2-1 Summary Chart, RF Margins (Nominal) at Lunar Distance, LM S-band Downlink Communications (NASA DATA SOURCE)

Equipment Used Mode	Steerable (LM) 85-ft (MSFN)		Steerable (LM) (a)30-ft (MSFN)		Omni (LM) 85-ft (MSFN)		Omni (LM) (b)210-ft (MSFN)		(c)Erectable (LM) 85-ft (MSFN)		Erectable (LM) (a)30-ft (MSFN)	
	PA on	PA off	PA on	PA off	PA on	PA off	PA on	PA off	PA on	PA off	PA on	PA off
1. Voice/BIO Hi Bit TLM	13.8 13.5	1.6 -10.2	6.7 6.5	-5.5 -17.3	-8.2 -8.5		-0.2 -0.5		22.0 21.7	9.8 -2.0	15.0 14.7	2.8 -9.0
2A. PRN Ranging Voice/BIO Hi Bit TM	30.3 12.7 12.5	13.7 0.6 -11.2	22.7 5.7 5.4	6.1 -6.6 -18.2	6.0 -9.5 -9.8		N/A -1.5 -1.8		38.5 20.9 20.6	22.0 8.8 -3.0	31.4 13.7 13.5	14.8 1.5 -10.0
2B. PRN Ranging Voice/BIO Hi Bit TM	18.3 13.2 13.0	1.8 1.2 -10.6	10.8 6.1 5.9	-5.8 -6.0 -17.7	-5.9 -8.8 -9.0		N/A -0.8 -1.0		26.6 21.4 21.1	10.1 9.2 -2.4	19.5 14.4 14.1	2.9 2.2 -9.5
3. Lo Bit TM	31.4	10.0	24.3	3.0	9.4		17.4	-3.9	39.6	18.3	32.6	11.2
4. BU Voice Lo Bit TM	26.3 30.2	11.7 8.5	19.3 23.2	4.7 1.5	4.4 8.2		12.4 16.2	-2.2 -5.5	34.5 38.4	20.2 17.0	27.5 31.4	12.8 9.6
5. BU Voice	30.5	13.1	23.4	6.0	8.7	-8.6	16.6	-0.7	38.7	21.3	31.6	14.3
6. Emergency Key	51.8	34.0	44.8	26.4	29.0	11.6	37.5	19.6	60.0	42.7	53.0	35.2
7. Voice/Bio Lo Bit TM	13.8 29.5	1.6 5.8	6.7 22.5	-5.4 -1.2	-8.2 7.5		-0.2 15.5		22.0 37.7	9.9 14.1	15.0 30.7	2.8 7.0
8. LM Voice EVA Voice Lo Bit TM Bio EMU (3.9-kHz Channel)	13.0 21.2 28.5 9.4 11.9	0.4 8.5 8.1 -3.9 -1.4	5.9 14.1 21.4 2.3 4.8	-6.5 1.4 1.0 -11.0 -8.5	-8.0 -0.9 6.5 -12.6 -10.1		0.0 7.1 14.5 -4.6 -2.1		21.2 29.4 36.7 17.6 15.1	8.6 16.7 16.3 4.3 6.8	14.1 22.3 29.6 10.6 13.1	1.6 9.7 9.2 -2.7 -0.2
9. LM Voice EVA Voice EMU (3.9-kHz Channel) Hi Bit TM	-5.4 1.2 -3.4 1.2								2.7 9.3 4.8 9.3		-4.4 2.2 -2.3 2.2	
10. LM Voice EVA Voice EMU (3.9-kHz Channel) Hi Bit TM TV (B & W) TV (Color)	-5.4 1.2 -4.4 -0.4 2.1 -6.4								2.6 9.2 3.8 7.6 10.2 1.6		-4.4 2.2 -3.2 0.6 3.1 -5.5	
11A. PRN Ranging	35.7	18.4	28.7	11.4	11.5	-5.8	N/A	N/A	N/A	N/A	N/A	N/A
11B. PRN Ranging	23.7	6.4	16.7	-0.6	-0.3	-17.6	N/A	N/A	N/A	N/A	N/A	N/A

NOTES:

- Range = 215 000 n.mi.; omni gain taken as -3 dB; TM and voice computed for 10^{-3} BER and 70% WI, respectively.
- 2A denotes downlink mode 2 with uplink mode 1 (PRN only); 2B denotes downlink mode 2 with uplink mode 6 (PRN, voice, and updata). Similarly for modes 11A and 11B.
- Worst-case margins are generally 1-2 dB lower than the nominal margins given here.
- Shaded blocks denote that these margins are negative by more than 10 dB for at least one channel or service within the mode.

(a) Results given for cooled-paramp 30-ft stations; uncooled-paramp results are 3.3 dB worse.

(b) Applicable to Goldstone 210-ft station (MARS); Parkes (PSK) 210-ft station is 1.5 dB worse.

(c) Steerable/210-ft combination gives the same margins as the erectable/85-ft.

LM6/4.2.4 Thermal Variations for the MESA

Figures LM6/4.2.4-1 through LM6/4.2.4-4 indicate thermal response for the MESA and temperature sensitive stowed equipment. Data are provided for cold, nominal, and hot conditions. The cold case is for 7.22°F sun angle and 60°F temperature at MESA deployment. Nominal case is for 10.12°F sun angle and 70°F temperature at deployment. Hot case is for 40°F sun angle and 80°F temperature at deployment with sun incident on MESA.

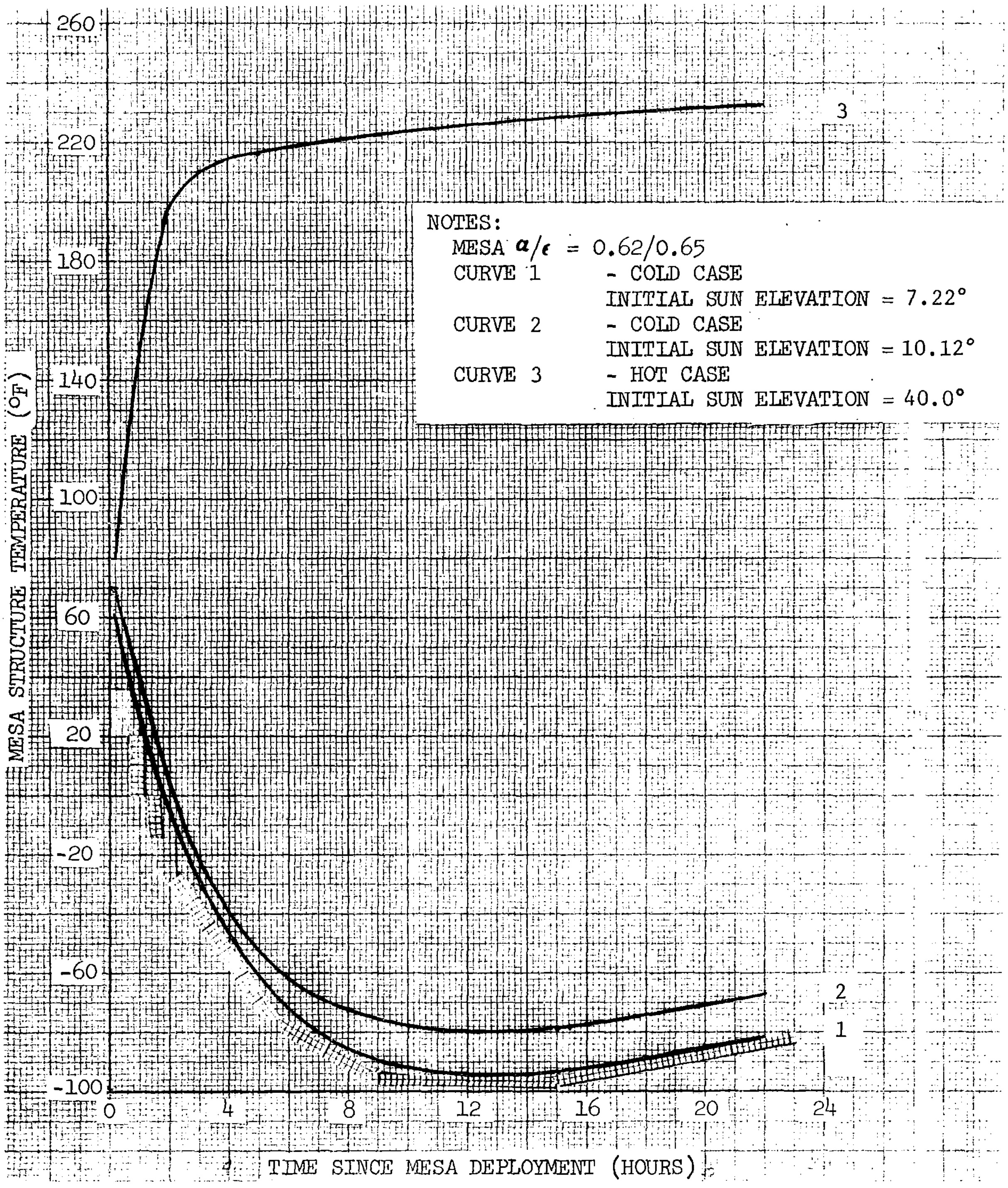

Figure LM6/4.2.4-1. MESA Structure Thermal Response

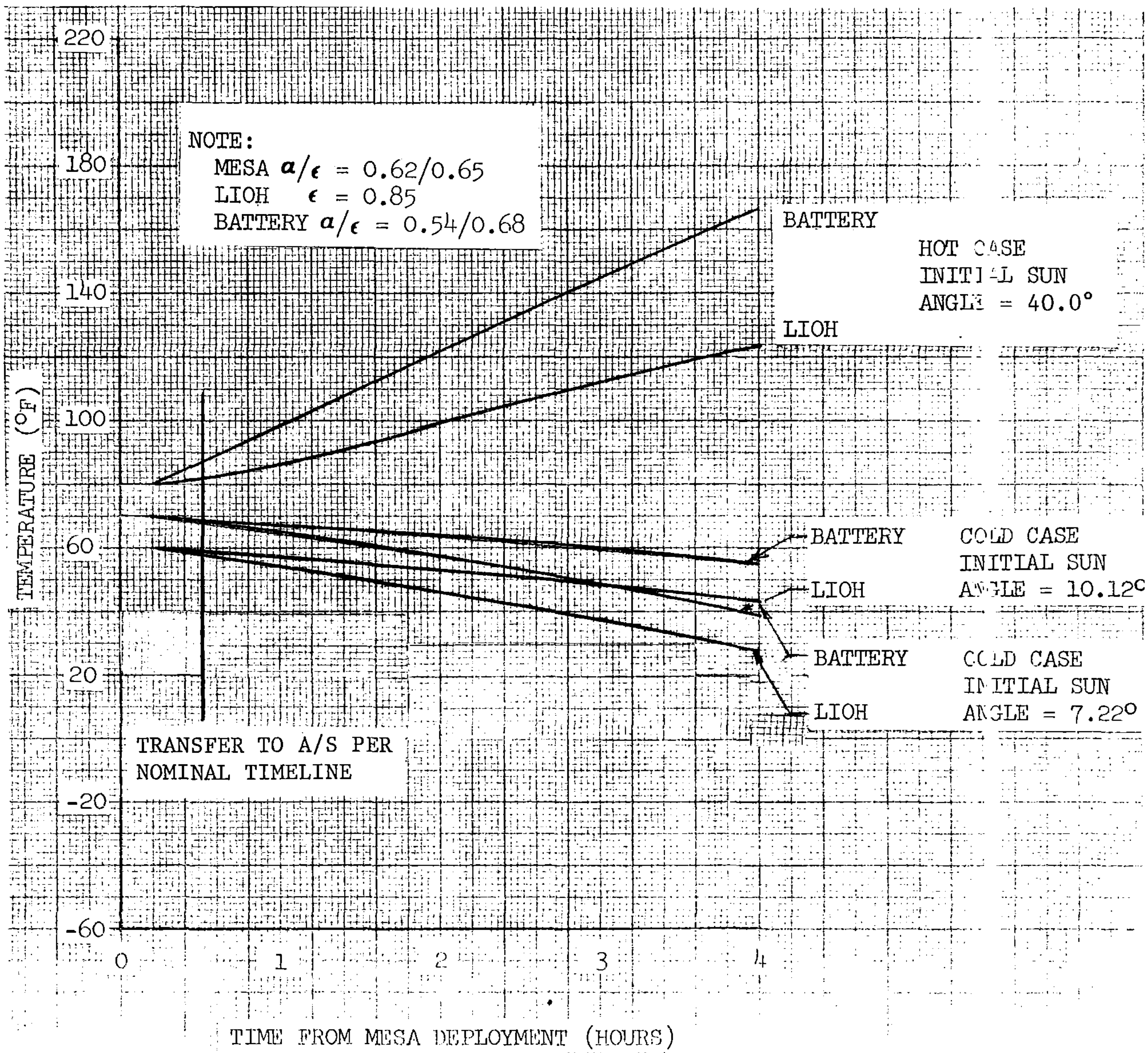

Figure LM6/4.2.4-2. PLSS Consumables Thermal Response

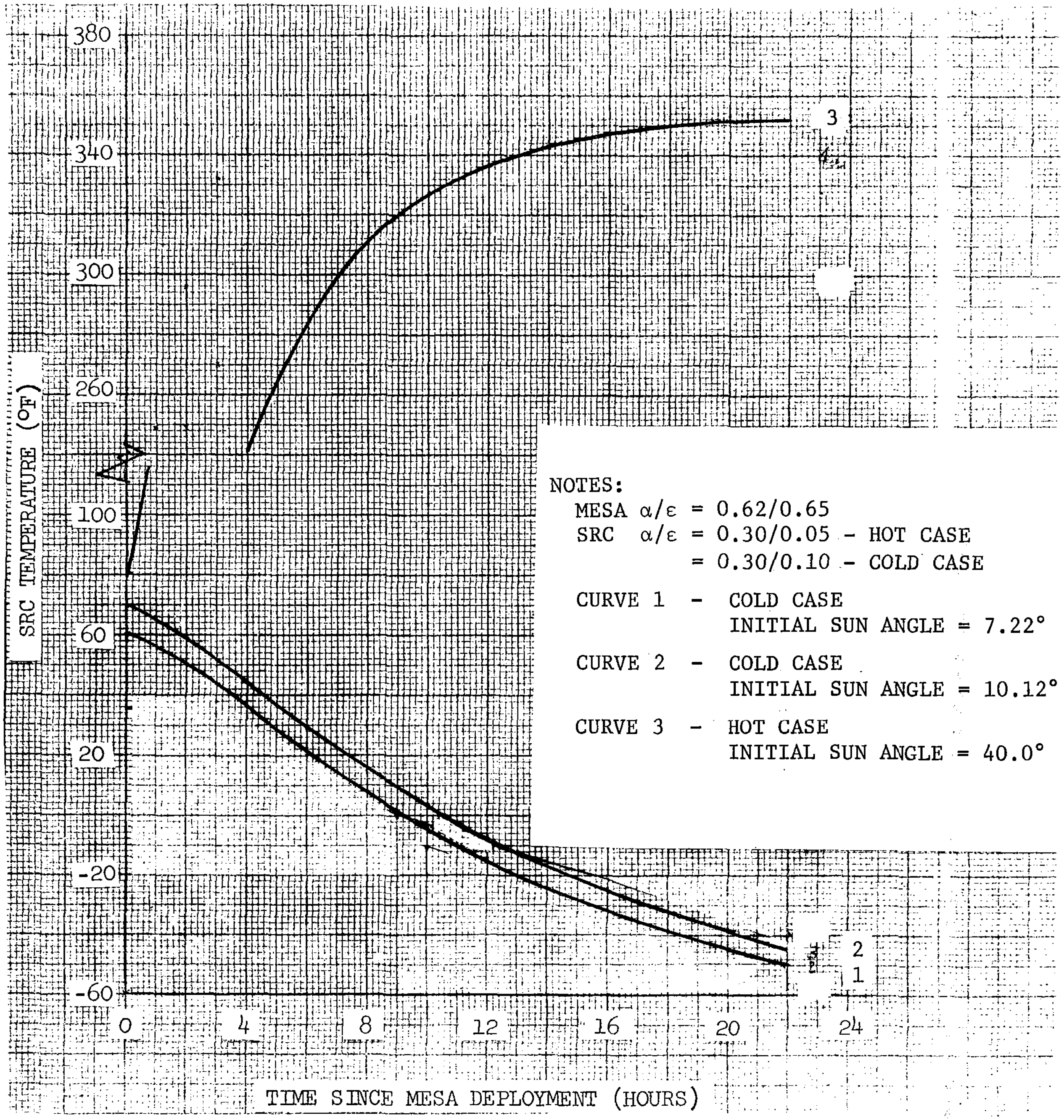

Figure LM6/4.2.4-3. SRC Thermal Response in MESA Well

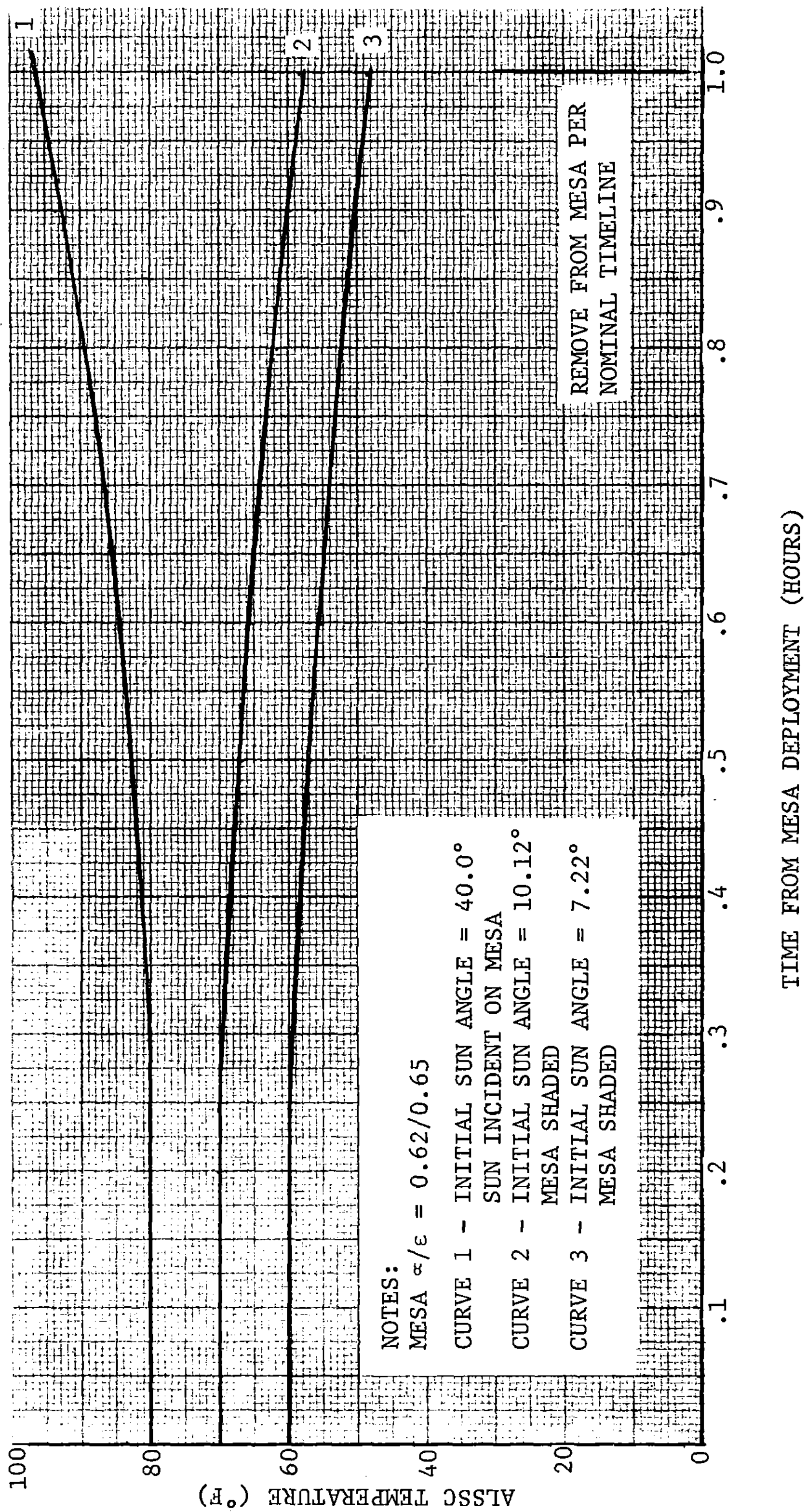

Figure LM6/4.2.4-4. Stereo Camera Thermal Response

LM6/4.3.8 Environmental Control Equipment

LM6/4.3.8.1 Heat Transport Section Water Sublimators

Figures LM6/4.3.8-1 and LM6/4.3.8-2 present glycol outlet temperature as a function of glycol inlet temperature for primary HTS sublimator (209) and secondary HTS sublimator (224), respectively. Figures LM6/4.3.8-3 and LM6/4.3.8-4 represent heat rejection capabilities for primary HTS sublimator (209) and secondary HTS sublimator (224), respectively.

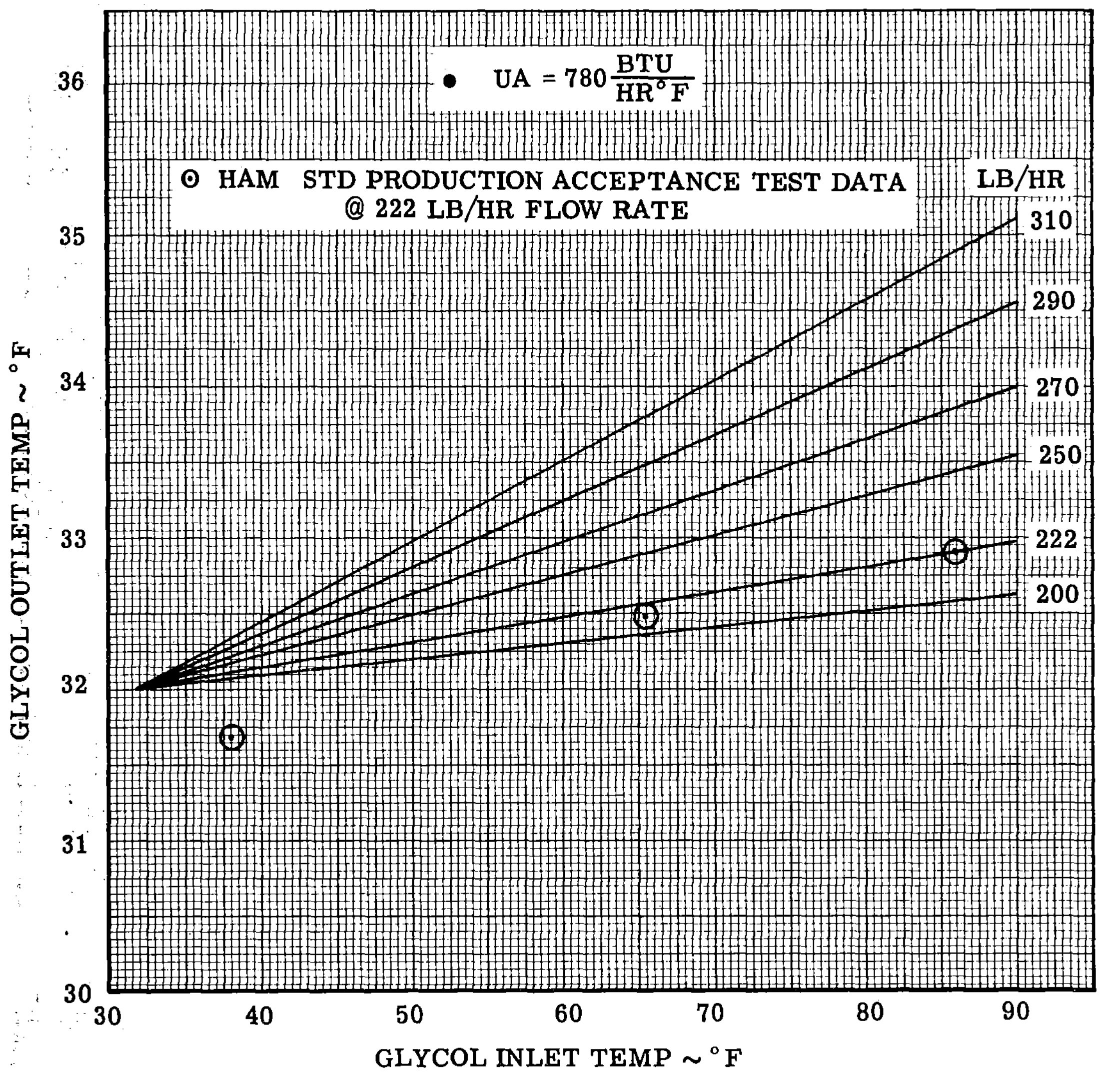

Figure LM6/4.3.8-1. Primary HTS Sublimator (209) LM-6 Acceptance Test Performance (U/N 129)

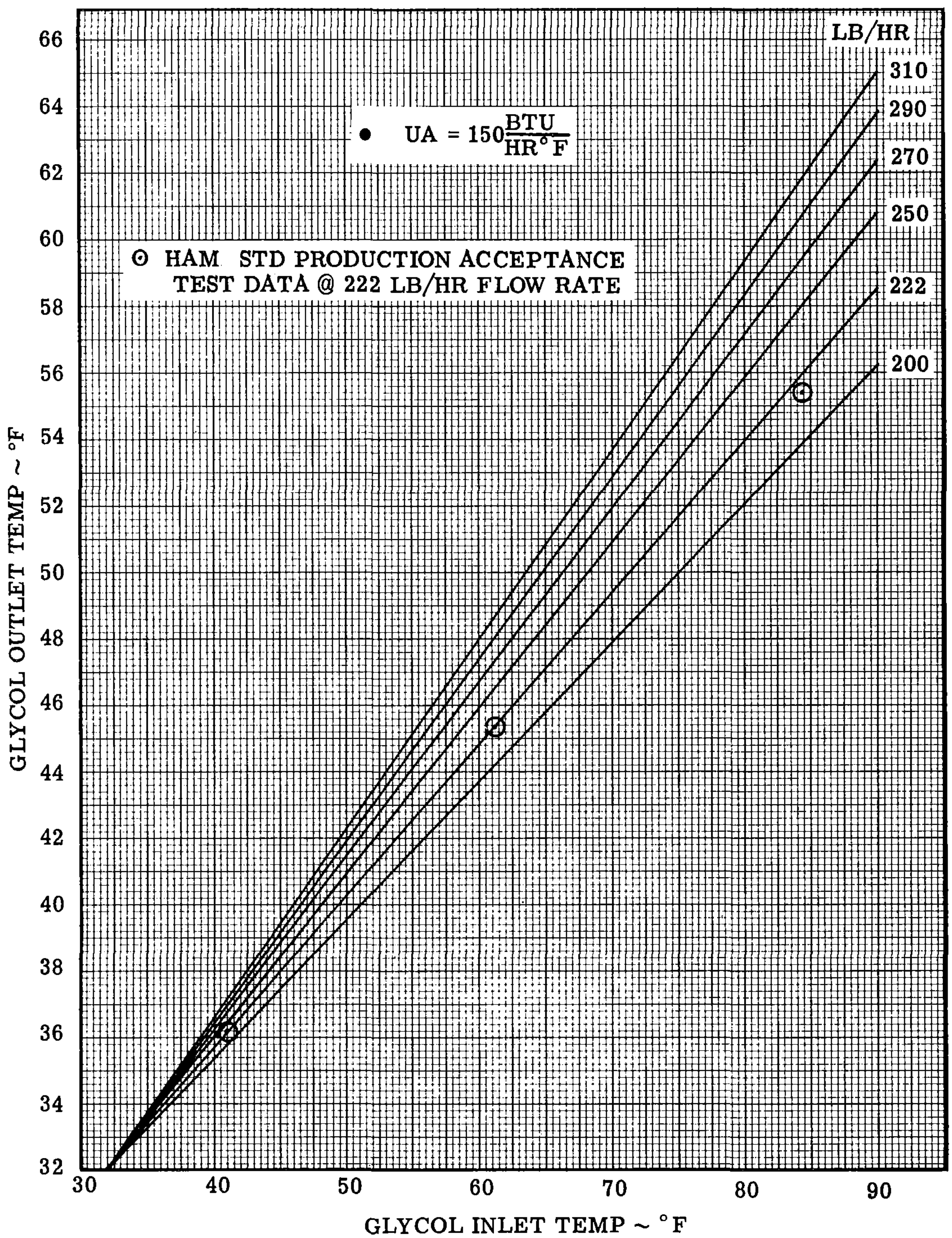

Figure LM6/4.3.8-2. Secondary HTS Sublimator (224) LM-6 Acceptance Test Performance (U/N 144)

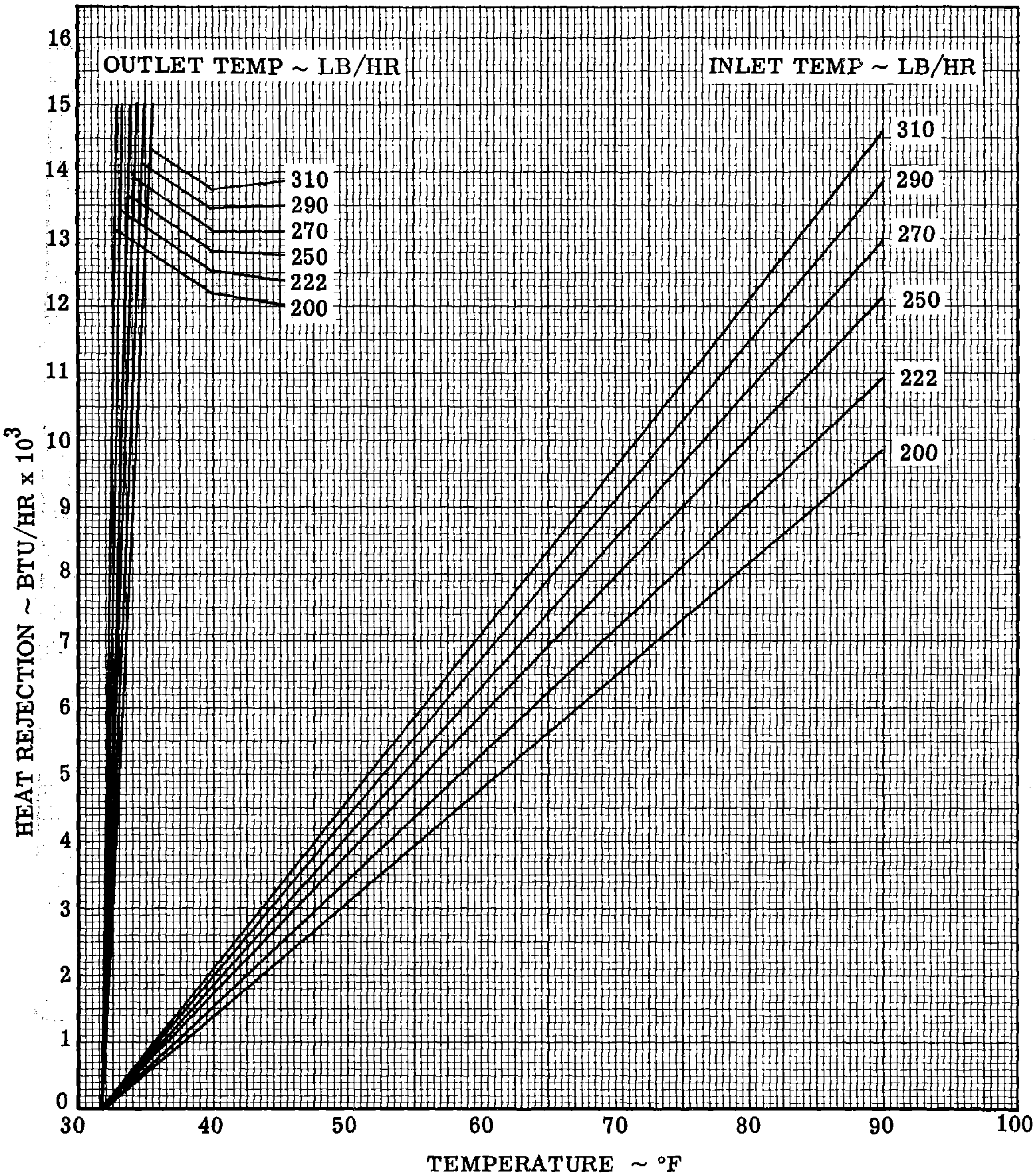

Figure LM6/4.3.8-3. LM-6 Primary HTS Sublimator (209)
Heat Rejection Capability for UA = $780 \frac{BTU}{HR°F}$ (U/N 129)

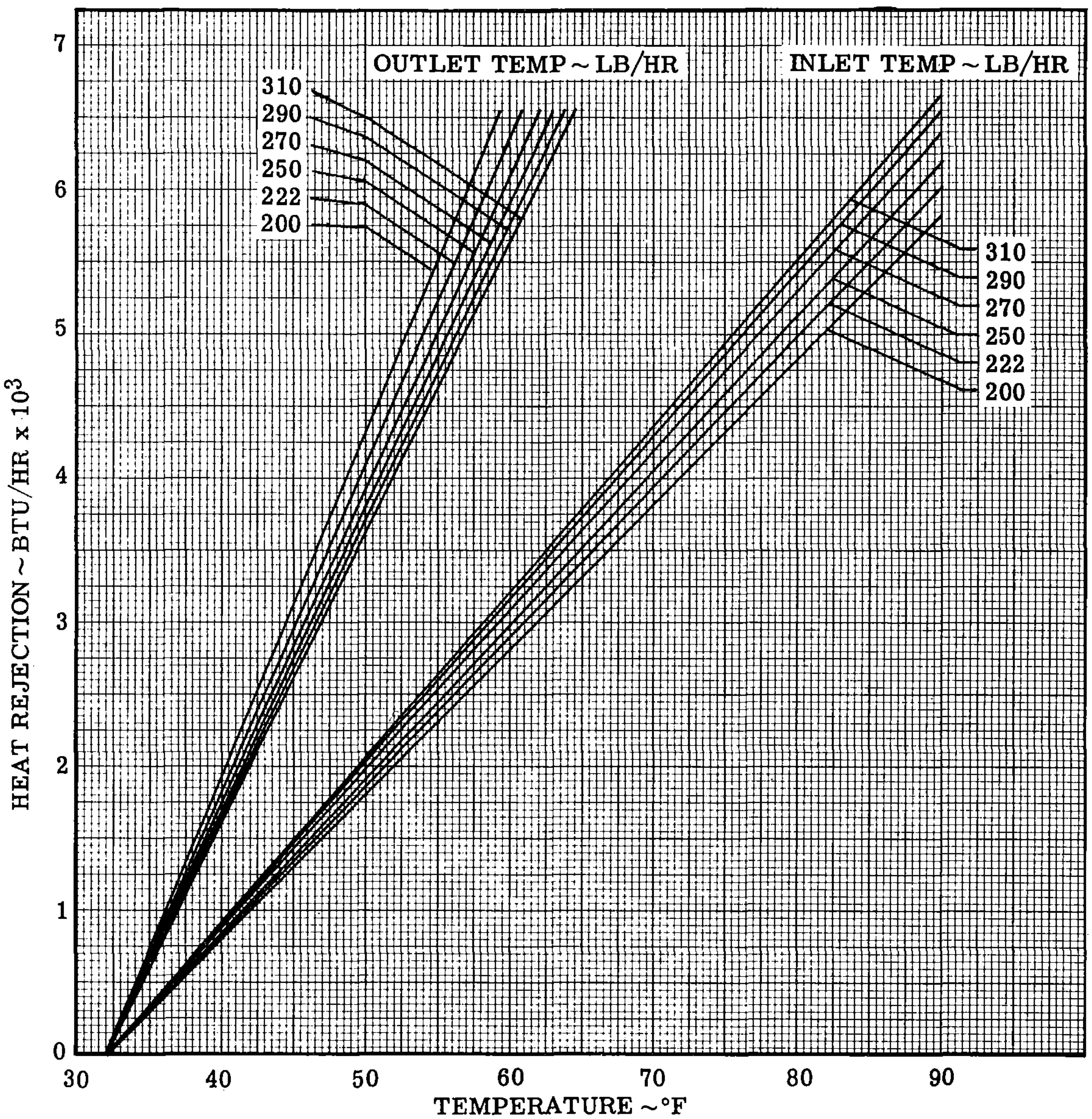

Figure LM6/4.3.8-4. LM-6 Secondary HTS Sublimator (224)

Heat Rejection Capability for UA = 150 $\frac{BTU}{HR°F}$ (U/N 144)

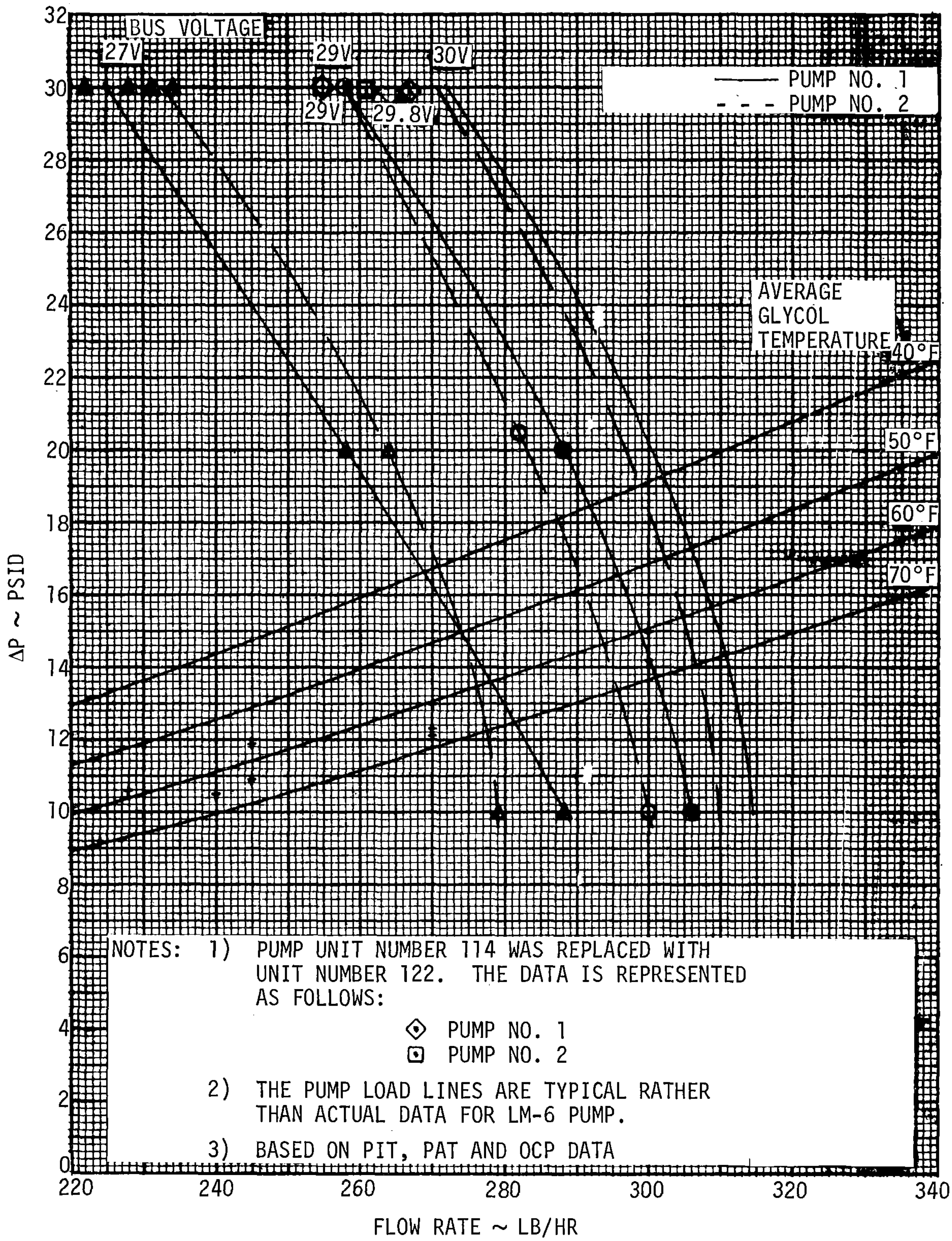

Figure LM6/4.3.8-5. Pump Load Line and HTS ΔP Characteristics

LM6/4.3.11 Duty Cycle of LM Heaters

The estimated average heater powers of the LM Heaters for the LM6/H Mission are presented in Table LM6/4.3.11-1. The mission phases or definable spacecraft operations occur as shown in the headings of the table.

Antenna (S-band Steerable, Rendezvous Radar, Landing Radar) heater requirements were determined from a review and application of the following:

a) Thermal Studies
b) Acceptance and qualification test data
c) LM-3, LM-4, LM-5 flight data

Guidance Equipment (IMU, ASA) heater requirements were determined from a combination of the following:

a) Calculations using vehicle structure and coolant temperatures, when applicable
b) LM-3, LM-4, and LM-5 flight data

Window and AOT heaters are nonthermostatically controlled/constant power devices. Table LM6/4.3.11-1 lists the nominal heater power of these items and indicates worst case usage for the H1 Mission. The window heaters will be energized at the discretion of the crew when fogging is noted.

The RCS Thruster heater requirements were determined from the following:

a) Thermal Studies
b) LM-3, LM-4, and LM-5 flight data

Lunar stay estimates of heater duty cycle for antenna and RCS Thruster heaters were based on a low sun angle at landing (10° to 13°), and did not consider any shadowing or vehicle tilting due to irregular terrain.

Table LM6/4.3.11-1 Average Heater Power During Mission Phases

Heaters	Launch & Boost LM Power -00:30 to 02:37 Watts	Translunar Coast LM Power 02:37 to 03:50 Watts	Translunar Coast CSM Power 03:50 to 73:00 Watts	Lunar Orbit & Descent CSM Power 73:00 to 91:35 Watts	Lunar Orbit & Descent LM Power 91:35 to 98:00 Watts	Lunar Stay LM Power 98:00 to 126:00 Watts	Ascent & Lunar Orbit LM Power 126:00 to 130:50 Watts
S-Band Steer Ant.	2	4	4	2	2 (Note 1)	2	2 (Note 1)
Rend. Radar Ant.	6	8	8	6	8 (Note 1)	10	8 (Note 1)
Land. Radar Ant.	8	20	20	10	10 (Note 1)	-	-
ASA	7	7	7	7	17 (Note 3)	55	17 (Note 3)
IMU	15	15	15	15	14.5 (Note 3)	14.5 (Note 3)	14.5 (Note 3)
Fwd Window (CDR)	0	0	0	0	61.8 (Note 4)	61.8 (Note 4)	61.8 (Note 4)
Fwd Window (SE)	0	0	0	0	61.8 (Note 4)	61.8 (Note 4)	61.8 (Note 4)
Docking Window	0	0	0	0	24.0 (Note 4)	24.0 (Note 4)	24.0 (Note 4)
AOT	0	0	0	0	5.0	5.0	5.0
RCS Thruster	0	0	0	0	(Note 2)	50.0	20.0
Total Average Power/Phase, Watts			54	40			
Average Current at 28 vdc, amps			1.93	1.43			

NOTES:
1) Heater duty cycle estimates are for periods when antennas are de-activated. Duty cycles are estimated to be zero when the antennas are active.
2) 764 watts for 1/2 hour warmup followed by a 140 watt average until undocking and a 20 watt average for the remainder of this phase.
3) Total ASA power is 55 watts; 38 watts instrument power plus 17 watts heater power. Total IMU power is 73.5 watts; 59 watts instrument power plus 14.5 watts heater power.
4) Window heaters are normally zero since they are energized only when fogging is noted.

LM6/4.5.1.4 Guidance Computer Erasable Memory Constants (NASA DATA SOURCE)

The following listings pertain to the LM Guidance Computer (LGC) pad loaded erasable memory constants. Mission time computed constants, such as state vectors, etc., are not included.

Table LM6/4.5.1-1 contains a tabular listing of the erasable load, both mission tape parameters and launch tape parameters. The remarks column contains a short description of the use of the constant.

The "Rev" column denotes the number of revisions to the value of the corresponding parameter that have been incorporated in publications of the Apollo 12 erasable load.

A single or double star (* or **) next to a parameter mnemonic denotes that it is also in the inflight erasable load. These parameters would have to be verified or reloaded in order to completely initialize the LGC in orbit. A single star denotes loading by ground uplink; a double star denotes loading by the astronaut via the DSKY.

Table LM6/4.5.1-1 H PRELAUNCH ERASABLE LOAD (LUMINARY 116) (NASA DATA SOURCE)

MISSION TAPE

REV	MNEMONIC	ADDRESS	VALUE	SF	OCTAL	REMARKS
	FLAGWRD 3	0077	02000 octal	-	02000	
	FLAGWRD 8	0104	00000 octal	-	00000	
	FLGWRD 10	0106	00000 octal	-	00000	
*	E3J22R2M	1347	92.0479047931E15 m^5/cs^2	58.	12160	
*	E32C31RM	1350	13.1289255968E22 m^6/cs^2	80	03363	
*	RADSKAL	1351, 1352	0 LR low scale altitude bits/meter/cs	21	00000,00000	
*	SKALSKAL	1353	0	0	00000	
*	GCOMPSW	1477	0	-	00000	
	TETCSM	1570	37777 octal	-	37777	To inhibit initial P00 integration

Table LM6/4.5.1-1 H PRELAUNCH ERASABLE LOAD (LUMINARY 116) (Continued) (NASA DATA SOURCE)

MISSION TAPE

	REV	MNEMONIC	ADDRESS	VALUE	SF	OCTAL	REMARKS
		TETLEM	1642	37777 octal	-	37777	To inhibit initial P00 integration
*		X789	1700, 1701	0.0 radians	***	00000, 00000	
*		X789+2	1702, 1703	0.0 radians	***	00000, 00000	
*		X789+4	1704, 1705	0.0 radians	***	00000, 00000	
		REFSMMAT	1733, 1734	0.68000001	1	12702, 21730	rev 0 of mission tape
*		RANGEVAR	1770, 1771	$0.1111111111 \times 10^{-4}$	-12	01351, 24734	
*		RATEVAR	1772, 1773	1.877777×10^{-5}	-12	02354, 04750	
*		RVARMIN	1774	66 m^2	12	00410	
*		VVARMIN	1775	0.17445×10^{-5} m^2/cs^2	-12	00165	

***5 for earth; 3 for moon

Table LM6/4.5.1-1 H PRELAUNCH ERASABLE LOAD (LUMINARY 116) (Continued) (NASA DATA SOURCE)

MISSION TAPE

REV	MNEMONIC	ADDRESS	VALUE	SF	OCTAL	REMARKS
*	WRENDPOS	2000	3048 m	14	05750	10,000 ft
*	WRENDVEL	2001	0.03048 m/cs	0	00763	10 ft/sec
*	WSHAFT	2002	0.015 radians	-5	17270	15 m rad
*	WTRUN	2003	0.015 radians	-5	17270	15 m rad
*	RMAX	2004	609.6 m	19	00023	2000 ft
*	VMAX	2005	0.006096 m/cs	7	00001	2 ft/sec
*	WSURFPOS	2006	1524 m	14	02764	5000 ft
*	WSURFVEL	2007	0.01524 m/cs	0	00372	5 ft/sec
*	SHAFTVAR	2010	$1x10^{-6}$ rad^2	-12	00103	1 $(m\ rad)^2$
*	TRUNVAR	2011	$1x10^{-6}$ rad^2	-12	00103	1 $(m\ rad)^2$

Table LM6/4.5.1-1 H PRELAUNCH ERASABLE LOAD (LUMINARY 116) (Continued) (NASA DATA SOURCE)

MISSION TAPE

	REV	MNEMONIC	ADDRESS	VALUE	SF	OCTAL	REMARKS
*		AGSK	2020,2021	32400000 cs	28	03671,21200	90 hr
*		TLAND	2400,2401	39811554.0 cs	28	04575, 34742	110.58765 hrs
*		RBRFG	2402,2403	52.37530800 m	24	00000,01506	171.835 ft
*		RBRFG+2	2404,2405	0.0 m	24	00000,00000	0.0 ft
*		RBRFG+4	2406,2407	-3254.836061 m	24	77774,72222	-10678.596 ft
*		VBRFG	2410,2411	-0.3227100480 m/cs	10	77772,72612	-105.876 ft/sec
*		VBRFG+2	2412,2413	0.0 m/cs	10	00000,00000	0.0 ft/sec
*		VBRFG+4	2414,2415	-0.0031699200 m/cs	10	77777,76300	-1.040 ft/sec
*		ABRFG	2416,2417	0.000019022568 m/cs^2	-4	00004,37445	0.6241 ft/sec^2
*		ABRFG+2	2420,2421	0.0 m/cs^2	-4	00000,00000	0.0 ft/sec^2

Table LM6/4.5.1-1 H PRELAUNCH ERASABLE LOAD (LUMINARY 116) (Continued) (NASA DATA SOURCE)

MISSION TAPE

	REV	MNEMONIC	ADDRESS	VALUE	SF	OCTAL	REMARKS
*		ABRFG+4	2422,2423	-0.000277502112 m/cs^2	-4	77667,50111	-9.1044 ft/sec^2
*		VBRFG*	2424,2425	-0.0570585600 m/cs	13	77777, 74261	-18.72 ft/sec
*		ABRFG*	2426,2427	-0.001665012672 m/cs^2	-4	77113,60670	-54.6264 ft/sec^2
*		JBRFG*	2430,2431	-0.5738399496 x 10^{-8} m/cs^3	-21	77472, 72437	-0.01882677 ft/sec^3
*		GAINBRAK	2432, 2433	1.0	0	37777, 37777	1.0
*		TCGFBRAK	2434	3000 cs	17	00567	30 sec
*		TCGIBRAK	2435	90000 cs	17	25762	900 sec
*		RAPFG	2436, 2437	33.85870800 m	24	00000, 01036	111.085 ft
*		RAPFG+2	2440, 2441	0.0 m	24	00000, 00000	0.0 ft
*		RAPFG+4	2442, 2443	-8.166811200 m	24	77777, 77574	-26.794 ft

Table LM6/4.5.1-1 H PRELAUNCH ERASABLE LOAD (LUMINARY 116) (Continued) (NASA DATA SOURCE)

MISSION TAPE

	REV	MNEMONIC	ADDRESS	VALUE	SF	OCTAL	REMARKS
*		VAPFG	2444, 2445	-0.0152186640 m/cs	10	77777, 70152	-4.993 ft/sec
*		VAPFG+2	2446, 2447	0.0 m/cs	10	00000, 00000	0.0 ft/sec
*		VAPFG+4	2450, 2451	0.0007559040 m/cs	10	00000, 00306	0.248 ft/sec
*		AAPFG	2452, 2453	$-0.07997952 \times 10^{-4}$ m/cs^2	-4	77775, 74720	-0.2624 ft/sec^2
*		AAPFG+2	2454, 2455	0.0 m/cs^2	-4	00000, 00000	0.0 ft/sec^2
*		AAPFG+4	2456, 2457	$-0.1560576 \times 10^{-4}$ m/cs^2	-4	77773, 75055	-0.5120 ft/sec^2
*		VAPFG*	2460, 2461	0.0136062720 m/cs	13	00000, 00676	4.464 ft/sec
*		AAPFG*	2462, 2463	$-0.9363456 \times 10^{-4}$ m/cs^2	-4	77747, 56422	-3.072 ft/sec^2
*		JAPFG*	2464, 2465	$0.5509930560 \times 10^{-9}$ m/cs^3	-21	00022, 35646	0.0018077200 ft/sec^3
*	1	GAINAPPR	2466, 2467	0	0	00000,00000	

Table LM6/4.5.1-1 H PRELAUNCH ERASABLE LOAD (LUMINARY 116) (Continued) (NASA DATA SOURCE)

MISSION TAPE

	REV	MNEMONIC	ADDRESS	VALUE	SF	OCTAL	REMARKS
*		TCGFAPPR	2470	3000 cs	17	00567	30 sec
*		TCGIAPPR	2471	20000 cs	17	04704	200 sec
*		VIGN	2472, 2473	16.90256208 m/cs	10	00416, 16071	5545.46 ft/sec
*		RIGNX	2474, 2475	-39782.453328 m	24	77731, 44630	-130519.86 ft
*		RIGNZ	2476, 2477	-436655.657 m	24	77125, 62404	-1432597.3 ft
*		KIGNX/B4	2500, 2501	-0.617631	4	76607, 61356	
*		KIGNY/B8	2502, 2503	$-2.4770341207 \times 10^{-6}$ m^{-1}	-16	72634, 51602	-0.755×10^{-6} ft/ft^2
*		KIGNV/B4	2504, 2505	-41000 cs	18	72775, 57777	-410 sec
*		LOWCRIT	2506	2124.4 DPS throttle pulses	14	04114	5985 lbf
*		HIGHCRIT	2507	2348.0 DPS throttle pulses	14	04454	6615 lbf

Table LM6/4.5.1-1 H PRELAUNCH ERASABLE LOAD (LUMINARY 116) (Continued) (NASA DATA SOURCE)

MISSION TAPE

	REV	MNEMONIC	ADDRESS	VALUE	SF	OCTAL	REMARKS
*		V2FG	2510, 2511	-0.009144 m/cs	10	77777, 73242	-3.0 ft/sec
*		V2FG+2	2512, 2513	0 m/cs	10	00000, 00000	0
*		V2FG+4	2514, 2515	0 m/cs	10	00000, 00000	0
*		TAUVERT	2516, 2517	1000 cs	14	01750, 00000	10.0 sec
*		DELQFIX	2520, 2521	60.96 m	24	00000, 01717	200 ft
*		LRALPHA	2522	0.0166666667 rev	-1	01042	6.0 deg. stow position
*		LRBETA1	2523	0.0666666667 rev	-1	04211	24.0 deg. Note: These are nominal rather than measures LR
*		LRALPHA2	2524	0.0166666667 rev	-1	01042	6.0 deg. position values hover position
*		LRBETA2	2525	0.0 rev	-1	00000	0.0 deg.
*		LRVMAX	2526	6.096 m/cs	7	01414	2,000 ft/sec

Table LM6/4.5.1-1 H PRELAUNCH ERASABLE LOAD (LUMINARY 116) (Continued) (NASA DATA SOURCE)

MISSION TAPE

REV	MNEMONIC	ADDRESS	VALUE	SF	OCTAL	REMARKS
*	LRVF	2527	0.6096 m/cs	7	00116	200 ft/sec
*	LRWVZ	2530	0.3	0	11463	
*	LRWVY	2531	0.3	0	11463	
*	LRWVX	2532	0.3	0	11463	
*	LRWVFZ	2533	0.2	0	06315	0.2
*	LRWVFY	2534	0.2	0	06315	0.2
*	LRWVFX	2535	0.2	0	06315	0.2
*	LRWVFF	2536	0.1	0	03146	0.1
*	RODSCALE	2537	0.003048 m/cs	-7	14370	1.0 ft/sec
*	TAUROD	2540, 2541	150 cs	9	11300, 00000	1.5 sec

Table LM6/4.5.1-1 H PRELAUNCH ERASABLE LOAD (LUMINARY 116) (Continued) (NASA DATA SOURCE)

MISSION TAPE

	REV	MNEMONIC	ADDRESS	VALUE	SF	OCTAL	REMARKS
*		LAG/TAU	2542, 2543	0.413333	0	15164, 01420	0.413333
*		MINFORCE	2544, 2545	0.4359257183 $\frac{kg\ m}{cs^2}$	12	00001, 27631	980.0 lb
*		MAXFORCE	2546, 2547	2.802379618 $\frac{kg\ m}{cs^2}$	12	00013, 06551	6300.0 lbs
*		J1PARM	2550, 2551	1838791.801 m	23	07007, 14372	6032781.5 ft
*		K1PARM	2552, 2553	-1202676.250 m/rw	23	73323, 40567	-627991.7 ft/rad
*		J2PARM	2554, 2555	1880624.221 m	23	07131, 03007	617008.6 ft
*		K2PARM	2556, 2557	-1129727.418 m/rw	23	73541, 60022	-589900.6 ft/rad
*		THETCRIT	2560, 2561	0.0234444444 rev	0	00600, 03510	8.44 deg
*		RAMIN	2562, 2563	1791455.081 m	24	03325, 16761	5877477.3 ft
*		YLIM	2564, 2565	15186.4 m	24	00016, 32446	8.2 n.mi.
*		ABTRDOT	2566, 2567	0.059436 m/cs	7	00007, 23346	19.5 ft/sec
*		COSTHET1	2570, 2571	0	-8	00000, 00000	
*		COSTHET2	2572, 2573	0.8660254037	+2	06733, 07535	
*		DLAND	2634, 2635	0 m	24	00000, 00000	
*		DLAND+2	2636, 2637	0 m	24	00000, 00000	

Table LM6/4.5.1-1 H PRELAUNCH ERASABLE LOAD (LUMINARY 116) (Continued) (NASA DATA SOURCE)

MISSION TAPE

	REV	MNEMONIC	ADDRESS	VALUE	SF	OCTAL	REMARKS
*		DLAND+4	2640, 2641	0 m	24	00000, 00000	
*		ROLLTIME	3001	2783 cs	14	05337	27.83 sec
*		PITTIME	3002	2338 cs	14	04442	23.38 sec
*		DKTRAP	3003	-0.0038888888 rev/sec	-3	77001	
*		DKOMEGAN	3004	10	14	0012	
*		DKKAOSN	3005	60	14	00074	
*		LMTRAP	3006	-0.0038888888 rev/sec	-3	77001	
*		LMOMEGAN	3007	0	14	00000	
*		LMKAOSN	3010	60	14	00074	
*		DKDB	3011	256 rev^{-1}	15	00200	
*		IGNAOSQ	3012	0.020611111 rev/sec^2	-2	02507	7.42 deg/sec^2
*		IGNAOSR	3013	0.0007777778 rev/sec^2	-2	00063	0.28 deg/sec^2
*		DOWNTORK	3113	0 jet seconds	5	00000	
*		DOWNTORK+1	3114	0 jet seconds	5	00000	
*		DOWNTORK+2	3115	0 jet seconds	5	00000	

Table LM6/4.5.1-1 H PRELAUNCH ERASABLE LOAD (LUMINARY 116) (Continued) (NASA DATA SOURCE)

MISSION TAPE

	REV	MNEMONIC	ADDRESS	VALUE	SF	OCTAL	REMARKS
*		DOWNTORK+3	3116	0 jet seconds	5	00000	
*		DOWNTORK+4	3117	0 jet seconds	5	00000	
*		DOWNTORK+5	3120	0 jet seconds	5	00000	
*		ATIGINC	3400,3401	18000 cs	28	00001,03120	3 min
*		PTIGINC	3402,3403	18000 cs	28	00001,03120	3 min
*		AOTAZ	3404	-0.1656777778 rev	-1	65312	-59.644° (2's comp)
*		AOTAZ+1	3405	+0.0008750000 rev	-1	00035	+0.315° (2's comp)
*		AOTAZ+2	3406	0.167444444 rev	-1	12557	+60.280°
*		AOTAZ+3	3407	0.3343194444 rev	-1	25313	+120.355°
*		AOTAZ+4	3410	-0.4990583333 rev	-1	40036	-179.661°

Table LM6/4.5.1-1 H PRELAUNCH ERASABLE LOAD (LUMINARY 116) (Continued) (NASA DATA SOURCE)

MISSION TAPE

	REV	MNEMONIC	ADDRESS	VALUE	SF	OCTAL	REMARKS
*		AOTAZ+5	3411	-0.3324666667 rev	-1	52561	-119.688° (2's comp)
*		AOTEL	3412	0.1252166667 rev	-1	10007	+45.078°
*		AOTEL+1	3413	0.1252805556 rev	-1	10011	+45.101°
*		AOTEL+2	3414	0.1252750000 rev	-1	10011	+45.099°
*		AOTEL+3	3415	0.1252055556 rev	-1	10007	+45.074°
*		AOTEL+4	3416	0.1251444444 rev	-1	10005	+45.052°
*		AOTEL+5	3417	0.1251472222 rev	-1	10005	+45.053°
*		LRHMAX	3420	15240 m	14	35610	50,000 ft
*		LRWH	3421	0.35	0	13146	
*		ZOOMTIME	3422	2600 cs	14	05050	26 sec

Table LM6/4.5.1-1 H PRELAUNCH ERASABLE LOAD (LUMINARY 116) (Continued) (NASA DATA SOURCE)

MISSION TAPE

	REV	MNEMONIC	ADDRESS	VALUE	SF	OCTAL	REMARKS
*		TENDBRAK	3423	6200 cs	17	01407	62 sec
*		TENDAPPR	3424	1200 cs	17	00226	12 sec
*		DELTTFAP	3425	-11000 cs	17	75240	-110.0 sec
*		LEADTIME	3426	-220 cs	17	77743	2.2 sec (a negative number for coding ease)
*		RPCRTIME	3427	6200 cs	17	01407	62 sec
*		RPCRTQSW	3430	-1	+1	57777	
*		TNEWA	3431, 3432	20000,00000 octal	28	20000, 00000	A large number (about 2 weeks); to prevent re-cycling the Lambert solution.

Table LM6/4.5.1-1 H PRELAUNCH ERASABLE LOAD (LUMINARY 116) (Continued) (NASA DATA SOURCE)

LAUNCH TAPE

	REV	MNEMONIC	ADDRESS	VALUE	SF	OCTAL	REMARKS
		MASS	1243, 1244	15240.48 kg	16	07342, 00000	33599.5 lbs at DOI ignition
**		LEMMASS	1326	15240.48 kg	16	07342	33599.5 lbs at DOI ignition
**		CSMMASS	1327	16562.29 kg	16	10055	36513.6 lbs
*		PBIASX	1452	PIPA counts/cs	-3	76730	cm/sec^2
*		PIPASCFX	1453		-9	65013	ppm
*		PBIASY	1454	PIPA counts/cs	-3	00047	cm/sec^2
*		PIPASCFY	1455		-9	66376	ppm
*		PBIASZ	1456	PIPA counts/cs	-3	01217	cm/sec^2
*		PIPASCFZ	1457		-9	61721	ppm
*		NBDX	1460	gyro pulses/cs	-5	00177	meru

Table LM6/4.5.1-1 H PRELAUNCH ERASABLE LOAD (LUMINARY 116) (Continued) (NASA DATA SOURCE)

LAUNCH TAPE

	REV	MNEMONIC	ADDRESS	VALUE	SF	OCTAL	REMARKS
*		NBDY	1461	gyro pulses/cs	-5	00245	meru
*		NBDZ	1462	gyro pulses/cs	-5	00430	meru
*		ADIAX	1463	$\frac{\text{gyro pulses/cm}}{\text{sec}^2}$	-5	00202	meru/g
*		ADIAY	1464	$\frac{\text{gyro pulses/cm}}{\text{sec}^2}$	-5	77373	meru/g
*		ADIAZ	1465	$\frac{\text{gyro pulses/cm}}{\text{sec}^2}$	-5	00150	meru/g
*		ADSRAX	1466	$\frac{\text{gyro pulses/cm}}{\text{sec}^2}$	-5	77661	meru/g
*		ADSRAY	1467	$\frac{\text{gyro pulses/cm}}{\text{sec}^2}$	-5	00064	meru/g
*		ADSRAZ	1470	$\frac{\text{gyro pulses/cm}}{\text{sec}^2}$	-5	00234	meru/g

Table LM6/4.5.1-1 H PRELAUNCH ERASABLE LOAD (LUMINARY 116) (Continued) (NASA DATA SOURCE)

LAUNCH TAPE

	REV	MNEMONIC	ADDRESS	VALUE	SF	OCTAL	REMARKS
*		TEPHEM	1706-1710	1180932000 cs	42	00004, 14616 13640	For launch on November 14 at 16:22 GMT in 1969
		AZO	1711, 1712	0.7746576443 rev	0	30623, 37552	
*		-AYO	1713, 1714		0	77777, 73551	
*		AXO	1715, 1716		0	00000, 26073	
		REFSMMAT+2	1735, 1736	0.11141622	1	01620, 27060	TEPHEM for November 14 = 16:22 GMT
*		504LM	2012, 2013		0	77775, 44333	
*		504LM+2	2014, 2015		0	77767, 67526	
*		504LM+4	2016, 2017		0	77771, 55324	
*	1	RLS	2022, 2023	1.590504497E6m	27	00302, 04721	-2.942400008 deg lat SITE 7
*	1	RLS+2	2024, 2025	-6,896999955E05m	27	77653, 71667	-2.344329983 deg long SITE 7
*	1	RLS+4	2026, 2027	-8.910649896E04m	27	77765, 43732	-1.185205176 n.mi. SITE 7
*		HIASCENT	3000	4945.3 kg	16	02324	10.902.5 lbs

LM6/4.5.1.5.2 Assembly Alignment Data of Spacecraft Docking Mating Surfaces to the Navigation Base.

Angular Alignment of the Docking Ring Seal Surface Relative to the Navigation Base Axes	
About Z	About Y
-0° 1' 8"	-0° 1' 10"

Sign Convention for Docking Ring Surface Plane Tilt

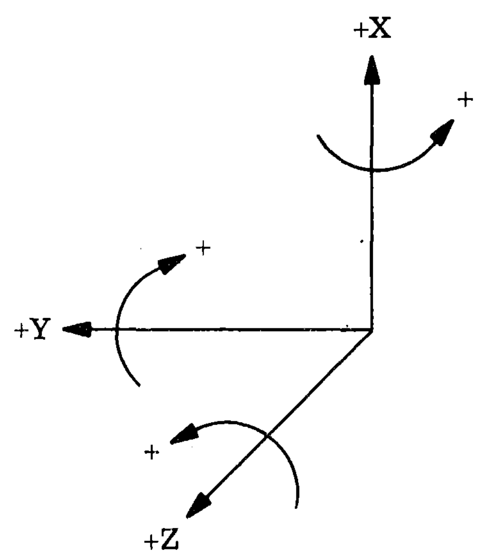

(Right Hand Rule)

Note: All data shown is for an unpressurized LM at ambient conditions. (REF: LAV-566-109 Dated August 8, 1968)

LM6/4.5.1.5.3 AOT Alignment Data

The azimuth and elevation angles for the rear right, rear left and the close (rear) detent positions of the AOT (relative to the AOT mounting surface) are tabulated below for LM-6 (AOT Designation 613 , Serial No. 19). These rear detent angles have been calculated using measured azimuth and elevation angles of the front detent positions. The uncertainty associated with these calculated angles is ±2 arc minutes.

The front 3 detent angles are measured, relative to the AOT mounting surface, at Kollsman Instrument Corporation and have a measurement uncertainty of ±30 arc seconds. For information, these measured angles are included in the tabulation. To verify these measured values, an AOT functional test has been performed on the spacecraft.

LM-6 AOT DETENT DATA

	Front (Measured)		
Data	L	F	R
Azim. (Deg)	300.356	0.315	60.280
Elev. (Deg)	45.078	45.101	45.099

	Rear (Calculated)		
Data	R_R	C_L	L_R
Azim. (Deg)	120.355	180.339	240.312
Elev. (Deg)	45.074	45.052	45.053

The above data is for an unpressurized vehicle at ambient conditions.

LM6/4.5.1.5.4 COAS Alignment Data

The alignments of the COAS at the forward and overhead locations were performed with a cabin pressure of 5 psig at ambient temperature. The following is the data:

Location	Alignment (Vehicle Axis)
COAS Forward Position (Relative LM NAV Base Gage)	Pitch (Y): 0°0'0" Yaw (X): 0°0'0" Roll (Z): 0°0'0"
COAS Overhead Position (Relative to the Centerline of the Docking Tunnel)	Parallel to LM "X" axis within ± 30 min. Yaw (about X) not measured.

Note: Use right hand rule to establish sign.

LM6/4.5.2.1 Abort Sensor Assembly

The LM-6 ASA Set Point Temperature, as read by T/M #GI-3301, is T_{Set} = 121.7°F (Standby and Operate Modes). The nominal temperature reading in the "OFF" mode is 121.0°F. The temperature maintenace limits are specified in Paragraph 4.5.2.1.

LM6/4.5.2.1.2 AGS Angular Mounting Error

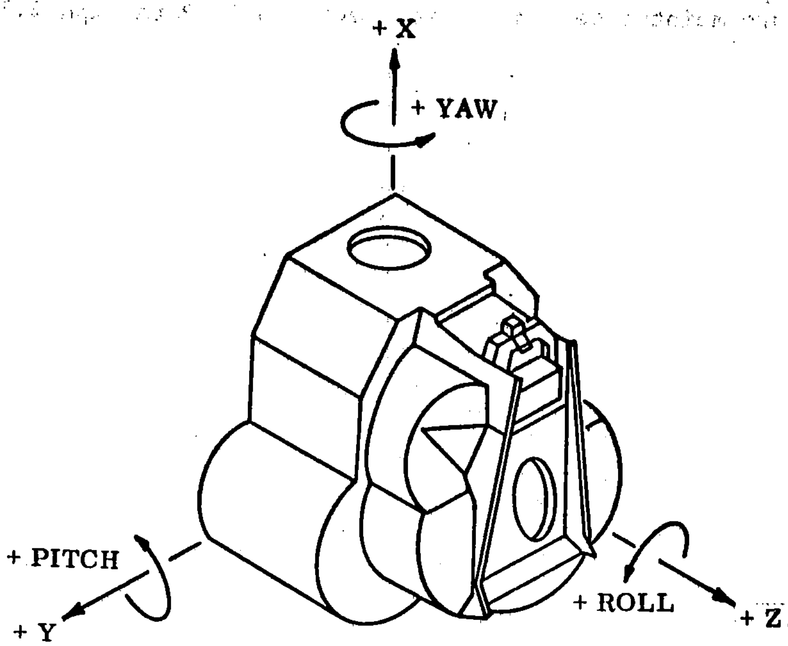

The measured mechanical alignment error of the ASA mounting surface as compared to the NAV. Base Gage (Vehicle Coordinate System) and to the IMU is shown below:

	ASA/NAV. Base	IMU/NAV. Base	ASA/IMU
Pitch:	-00° 02' 40"	-00° 01' 27"	-00° 01' 13"
Roll:	-00° 00' 54"	-00° 01' 42"	+00° 00' 48"
Yaw:	-00° 01' 28"	-00° 02' 00"	+00° 00' 32"

(Ref.: LDW 280-51067, dated 25 June 1968)

LM6/4.5.2.2 Abort Electronics Assembly (NASA DATA SOURCE)

The following listings pertain to the Abort Electronics Assembly Memory Constants.

Table LM6/4.5.2-1 contains a glossary of the constants.

Table LM6/4.5.2-2 contains the current values in both octal and decimal, with units.

An asterisk by the name of the constants indicates that these constants are dependent on the hardware to be used during a mission.

Table LM6/4.5.2-1. Glossary of AGS Constants

(NASA DATA SOURCE)

NAME	DESCRIPTION OF LMDAP INPUT	INTERNAL AEA UNITS	LMDAP INPUT UNITS
1J	Desired TPI time for CSI computation	SEC	MIN
4J	Time increment from node to TPF (in TPI mode)	SEC	MIN
17J	Radar range rate	FPS	FPS
18J	Radar range	FT	FT
25J	DEDA altitude update	FT	FT
28J1	Component of External V input in $\underline{V}_1$ Direction	FPS	FPS
28J2	Component of External V input in $\underline{W}_1$ Direction	FPS	FPS
28J3	Component of External V input in $\underline{U}_1$ Direction	FPS	FPS
1J1	LM Update State Vector - X Inertial Position	FT	FT
1J2	Y Inertial Position	FT	FT
1J3	Z Inertial Position	FT	FT
1J4	X Inertial Velocity	FPS	FPS
1J5	Y Inertial Velocity	FPS	FPS
1J6	Z Inertial Velocity	FPS	FPS
1J7	LM Update State Vector Epoch Time	SEC	MIN
2J1	CSM Update State Vector - X Inertial Position	FT	FT
2J2	Y Inertial Position	FT	FT
2J3	Z Inertial Position	FT	FT
2J4	X Inertial Velocity	FPS	FPS
2J5	Y Inertial Velocity	FPS	FPS
2J6	Z Inertial Velocity	FPS	FPS
2J7	CSM Update State Vector Epoch Time	SEC	MIN

Table LM6/4.5.2-1. Glossary of AGS Constants (Continued)

(NASA DATA SOURCE)

NAME	DESCRIPTION OF LMDAP INPUT	INTERNAL AEA UNITS	LMDAP INPUT UNITS
1K1P*	X axis gyro drift bias	RAD/20MS (Compen.)	DEG/HR (Bias)
1K6P*	Y axis gyro drift bias	RAD/20MS (Compen.)	DEG/HR (Bias)
1K11P*	Z axis gyro drift bias	RAD/20MS (Compen.)	DEG/HR (Bias)
	A positive gyro drift bias causes a gyro output of more than 32 pulses per millisecond (640 pulses per 20 milliseconds) for no ASA rotation. The range of each of the biases is ± 10 deg/hr.		
1K3*	X axis gyro scale factor deviation	NO-UNITS(Deviation)	NO-UNITS (Deviation)
1K8*	Y axis gyro scale factor deviation	NO-UNITS(Deviation)	NO-UNITS (Deviation)
1K13*	Z axis gyro scale factor deviation	NO-UNITS(Deviation)	NO-UNITS (Deviation)
	A positive scale factor deviation exists when a gyro's scale factor is greater than 2^{-16} radians per pulse. The range of each deviation is ± .78 percent.		
1K14*	Compensation constant for X gyro spin axis mass unbalance drift	RAD/FPS	DEG/HR/G
	A positive gyro spin axis mass unbalance exists when a positive ASA acceleration in the direction of the X gyro input axis results in a negative X gyro output (less than 640 pulses per 20 milliseconds) with no rotation. The range of the bias is ± 10 deg/hr/g.		

*These constants are dependent on the hardware to be used during a mission.

Table LM6/4.5.2-1. Glossary of AGS Constants (Continued)

(NASA DATA SOURCE)

NAME	DESCRIPTION OF LMDAP INPUT	INTERNAL AEA UNITS	LMDAP INPUT UNITS
1K18P*	X asis accelerometer scale factor deviation	FPS/PULSE (Scale Factors)	NO-UNITS (Deviation)
1K20P*	Y axis accelerometer scale factor deviation	FPS/PULSE	NO-UNITS (Deviation)
1K22P*	Z axis accelerometer scale factor deviation	FPS/PULSE	NO-UNITS (Deviation)
	A positive accelerometer scale factor deviation exists when the measured accelerometer's scale factor is greater than the nominal value of + .003125 fps/pulse. The range of this input is ± 24 percent.		
1K19P*	X axis accelerometer bias	FPS/20MS(Compen.)	MICRO G (Bias)
1K21P*	Y axis accelerometer bias	FPS/20MS(Compen.)	MICRO G (Bias)
1K23P*	Z axis accelerometer bias	FPS/20MS(Compen.)	MICRO G (Bias)
	A positive accelerometer bias results in an accelerometer output of more than 32 pulses per millisecond (640 pulses per 20 milliseconds). The range of each of these biases is ± 2000 μg.		
1K26	X axis azimuth alignment gain constant (lunar align)	NO-UNITS	NO-UNITS
1K27	Lunar align leveling alignment constant	RAD/FPS	RAD/FPS
1K28	Lunar align leveling alignment constant	NO-UNITS	NO-UNITS
1K29	Lunar align stop error criterion	RAD	RAD
1K30	Gyro calibrate time	2-SEC	2-SEC
1K33	Gyro calibration gain constant	NO-UNITS	NO-UNITS
1K34	Gyro calibration gain constant	1/20MS	1/20MS
1K35	Navigation sensed velocity threshold	FT/SEC	FT/SEC
1K36	Accelerometer calibration gain constant	NO-UNITS	NO-UNITS

*These constants are dependent on the hardware to be used during a mission.

Table LM6/4.5.2-1. Glossary of AGS Constants (Continued)

(NASA DATA SOURCE)

NAME	DESCRIPTION OF LMDAP INPUT	INTERNAL AEA UNITS	LMDAP INPUT UNITS
1K37	Accelerometer calibration time	2-SEC	2-SEC
6K2	Radar filter initialization value of P_{11} and P_{22}	FT^2	FT^2
6K4	Radar filter initialization value of P_{33} and P_{44}	$(FPS)^2$	$(FPS)^2$
6K5	Radar filter factor in r_y update	NO-UNITS	NO-UNITS
6K6	Radar filter factor in V_y update	NO-UNITS	NO-UNITS
6K8	Radar filter term in q_{11}	$(FT/SEC)^2$	$(FT/SEC)^2$
6K9	Radar filter factor in q_{11} and q_{22}	$(RAD)^2$	$(RAD)^2$
6K10	Radar filter factor in q_{11} and q_{22}	FT^2	FT^2

Table LM6/4.5.2-1. Glossary of AGS Constants (Continued)

(NASA DATA SOURCE)

NAME	DESCRIPTION OF LMDAP INPUT	INTERNAL AEA UNITS	LMDAP INPUT UNITS
1K9	Ullage counter limit	COUNTS	COUNTS
4K2	Coefficient in T_B computation	SEC/FT	SEC/FT
4K3	Coefficient in T_B computation	$(SEC/FT)^2$	$(SEC/FT)^2$
4K7	Cant angle of engine about Y-axis	RAD	RAD
4K8	Cant angle of engine about Z-axis	RAD	RAD
4K21	Limit on body attitude errors	RAD	RAD
4K23	Time to maintain attitude hold momentarily after staging	40-MSEC	40-MSEC
4K25	Ascent engine cutoff impulse compensation	FPS	FPS
4K26	V_G threshold for engine cutoff	FPS	FPS
4K27	Hover Abort overflow protection	FPS	FPS
4K34	Lower limit on a_T	FT/SEC^2	FT/SEC^2
4K35	Ullage threshold	FT/SEC^2	FT/SEC^2

Table LM6/4.5.2-1. Glossary of AGS Constants (Continued)

(NASA DATA SOURCE)

NAME	DESCRIPTION OF LMDAP INPUT	INTERNAL AEA UNITS	LMDAP INPUT UNITS
1K4	Altitude/Altitude rate interpolation factor	NO-UNITS	NO-UNITS
2K1	Lunar gravitational constant	FT^3/SEC^2	FT^3/SEC^2
2K2	Reciprocal of 2K1	SEC^2/FT^3	SEC^2/FT^3
2K4	$-2K1\ \Delta T$ ($\Delta T = 2$ sec)	FT^3/SEC	FT^3/SEC
3K4	Sine of central angle limit in TPI	NO-UNITS	NO-UNITS
4K4	Coefficient in linear expression for $\dot{r}_f$	1/SEC	1/SEC
4K5	Quantity in linear expression for $\dot{r}_f$	FT	FT
4K6	Upper limit on $\dot{r}_f$	FPS	FPS
4K10	Factor in LM desired semi-major axis α_L (O.I.)	FT/RAD	FT/RAD
4K12	Acceleration check for lower limit of $\dddot{r}_d$	FT/SEC^2	FT/SEC^2
5K14	Upper limit on $\dddot{r}_d$	FT/SEC^3	FT/SEC^3
5K16	Upper limit on $\dddot{y}_d$	FT/SEC^3	FT/SEC^3
5K17	Lower limit on $\dddot{y}_d$	FT/SEC^3	FT/SEC^3
5K18	Lower limit on $\dddot{r}_d$	FT/SEC^3	FT/SEC^3
5K20	Lower limit on $\dddot{r}_d$	FT/SEC^3	FT/SEC^3
5K26	Velocity-to-be-gained threshold	FPS	FPS
K55	Scale factor for $\dot{r}$ display	NO-UNITS	NO-UNITS
WBX	X component of unit vector for guidance steering	NO-UNITS	NO-UNITS
WBY	Y component of unit vector for guidance steering	NO-UNITS	NO-UNITS
WBZ	Z component of unit vector for guidance steering	NO-UNITS	NO-UNITS
2J	Cotangent of desired LOS angle at TPI for CSI computation	NO-UNITS	NO-UNITS

Table LM6/4.5.2-1. Glossary of AGS Constants (Continued)

(NASA DATA SOURCE)

NAME	DESCRIPTION OF LMDAP INPUT	INTERNAL AEA UNITS	LMDAP INPUT UNITS
3J	Rendezvous offset time for TPI computation	SEC	MIN
5J	Landing site radius	FT	FT
6J	Desired LM transfer time for TPI routine	SEC	MIN
7J	Term in LM desired semi-major axis α_L (O.I.)	FT	FT
8J	Lower limit of α_L (O. I.)	FT	FT
9J	Upper limit of α_L (O. I.)	FT	FT
16J	Orbit insertion targeted injection altitude	FT	FT
21J	Vertical pitch steering altitude threshold	FT	FT
22J	Vertical pitch steering altitude rate threshold	FPS	FPS
23J	Orbit insertion targeted injection radial rate	FPS	FPS
29J	Radar filter update time initialization value	SEC	MIN

Table LM6/4.5.2-1. Glossary of AGS Constants (Continued)

(NASA DATA SOURCE)

NAME	DESCRIPTION OF LMDAP INPUT	INTERNAL AEA UNITS	LMDAP INPUT UNITS
1K24	FDAI computation singularity region	NO-UNITS	NO-UNITS
1K56	Negative of lunar rotation rate times .02 sec	RAD	RAD
2K3	q value set if overflow occurs in e^2 computation of LM orbit parameters	FT	FT
2K11	Set value of V_T if no valid TPI solution	FPS	FPS
2K14	Initial p perturbation	FT	FT
2K17	Number of p-iteration minus 3	COUNTS	COUNTS
2K18	Partial derivative protector in p-iterator routine	SEC	SEC
2K19	Δ_p limiter	FT	FT
2K20	p-iterator convergence check	SEC	SEC

Table LM6/4.5.2-1. Glossary of AGS Constants (Continued)

(NASA DATA SOURCE)

NAME	DESCRIPTION OF LMDAP INPUT
BACCSF	Convert .001 ft/sec^2 to fps/20 msec at B1
BM13SF	Convert .01°/hr to rad/20 msec at B13
B23SF	Convert 100 ft to ft at B23
B18SF	Convert .1 min to sec at B18
B13VSF	Convert .1 fps to fps at B13
B3SF	Convert .01° to rad at B3
B23RSF	Convert .1 nmi to ft at B23
B13SF	Convert .01 min to sec at B13

Table LM6/4.5.2-2. AGS Constants
(NASA DATA SOURCE)

NAME	LOC.	CONVERSION FACTOR	AEA OCT.	AEA VALUE (ENGINEERING VALUE)	UNITS
1J	0275	.60000 02	000000	.00000000 00	MIN
4J	0306	.60000 02	000000	.00000000 00	MIN
17J	0503	.10000 01	000000	.00000000 00	FPS
18J	0316	.10000 01	000000	.00000000 00	FT
25J	0223	.10000 01	000000	.00000000 00	FT
28J1	0450	.10000 01	000000	.00000000 00	FPS
28J2	0451	.10000 01	000000	.00000000 00	FPS
28J3	0452	.10000 01	000000	.00000000 00	FPS
1J1	0240	.10000 01	000000	.00000000 00	FT
1J2	0241	.10000 01	000000	.00000000 00	FT
1J3	0242	.10000 01	000000	.00000000 00	FT
1J4	0260	.10000 01	000000	.00000000 00	FPS
1J5	0261	.10000 01	000000	.00000000 00	FPS
1J6	0262	.10000 01	000000	.00000000 00	FPS
1J7	0254	.60000 02	000000	.00000000 00	MIN
2J1	0244	.10000 01	000000	.00000000 00	FT
2J2	0245	.10000 01	000000	.00000000 00	FT
2J3	0246	.10000 01	000000	.00000000 00	FT

Table LM6/4.5.2-2. AGS Constants (Continued)
(NASA DATA SOURCE)

	NAME	LOC.	CONVERSION FACTOR	AEA OCT.	AEA VALUE (ENGINEERING VALUE)	UNITS
	2J4	0264	.10000 01	000000	.00000000 00	FPS
	2J5	0265	.10000 01	000000	.00000000 00	FPS
	2J6	0266	.10000 01	000000	.00000000 00	FPS
	2J7	0272	.60000 02	000000	.00000000 00	MIN
*	1K1P	0544	-.96963-07	777772	.57629721-01	DEG/HR
*	1K6P	0545	-.96963-07	000021	-.16328421 00	DEG/HR
*	1K11P	0546	-.96963-07	000007	-.67234674-01	DEG/HR
*	1K3	0550	.10000 01	024116	.61500073-03	NO-UNITS
*	1K8	0551	.10000 01	153740	.32939911-02	NO-UNITS
*	1K13	0552	.10000 01	140276	.29410124-02	NO-UNITS
*	1K14	0537	.15091-06	000012	.30856887-01	DEG/HR/G
*	1K18P	0534	.31250-02	315040	.12817383-02	NO-UNITS
*	1K20P	0535	.31250-02	314356	-.16365051-02	NO-UNITS
*	1K22P	0536	.31250-02	314247	-.23136139-02	NO-UNITS
*	1K19P	0540	-.64254-06	777755	.45120725 03	MICRO-G
*	1K21P	0541	-.64254-06	777773	.11873875 03	MICRO-G
*	1K23P	0542	-.64254-06	000003	-.71243251 02	MICRO-G
	1K26	0626	.10000 01	561111	-.14285742 03	NO-UNITS

Table LM6/4.5.2-2. AGS Constants (Continued)
(NASA DATA SOURCE)

NAME	LOC.	C.F.	CONVERSION FACTOR	AEA VALUE (ENGINEERING VALUE)	UNITS
1K27	0627	.10000 01	262132	.43499947-01	RAD/FPS
* 1K28	0630	.10000 01	327211	.10763379 03	NO-UNITS
1K29	0631	.10000 01	004061	.99992752-03	RAD
1K30	0617	.10000 01	000226	.15000000 03	2-SEC
1K33	0632	.10000 01	243656	.79999924-01	NO-UNITS
1K34	0633	.10000 01	247613	.19999919-04	1/20MS
1K35	0634	.10000 01	000400	.25000000 00	FT/SEC
1K36	0635	.10000 01	777651	-.66375733-03	NO-UNITS
1K37	0621	.10000 01	000017	.15000000 02	2-SEC
6K2	0457	.10000 01	027657	.99999744 08	FT2
6K4	0456	.10000 01	031000	.10000000 03	FT2/SEC2
6K5	0656	.10000 01	505075	-.73000336 00	NO-UNITS
6K6	0522	.10000 01	777605	-.24023437 00	NO-UNITS
6K8	0304	.10000 01	000034	.21875000 00	FT2/SEC2
6K9	0611	.10000 01	376057	.30290103-04	NO-UNITS
6K10	0517	.10000 01	005754	.62504960 07	FT2
* 1K9	0616	.10000 01	000005	.50000000 01	COUNTS
* 4K2	0654	.10000 01	713267	-.50203875-04	SEC/FT

Table LM6/4.5.2-2. AGS Constants (Continued)
(NASA DATA SOURCE)

	NAME	LOC.	CONVERSION FACTOR	AEA OCT.	AEA VALUE (ENGINEERING VALUE)	UNITS
*	4K3	0655	.10000 01	016336	.16802915-08	SEC2/FT2
*	4K7	0566	.10000 01	006547	.26176453-01	RAD
*	4K8	0602	.10000 01	000000	.00000000 00	RAD
	4K21	0666	.10000 01	020603	.26181030 00	RAD
*	4K23	0622	.10000 01	000076	.62000000 02	40MSEC
*	4K25	0657	.10000 01	000066	.33750000 01	FPS
*	4K26	0454	.10000 01	002140	.70000000 02	FPS
*	4K27	0473	.10000 01	406000	-.80000000 04	FPS
	4K34	0660	.10000 01	002000	.10000000 01	FT/SEC2
	4K35	0661	.10000 01	000146	.99609375-01	FT/SEC2
	1K4	0624	.10000 01	031463	.99998474-01	NO-UNITS
	2K1	0636	.10000 01	235407	.17318811 15	FT3/SEC2
	2K2	0637	.10000 01	320020	.57740271-14	SEC2/FT3
	2K4	0674	.10000 01	542371	-.34637623 15	FT3/SEC
	3K4	0613	.10000 01	026164	.17364502 00	NO-UNITS
	4K4	0565	.10000 01	203045	.40000081-02	1/SEC
*	4K5	0662	.10000 01	257014	.57351680 07	FT
	4K6	0527	.10000 01	002400	.80000000 02	FPS

Table LM6/4.5.2-2. AGS Constants (Continued)

(NASA DATA SOURCE)

	NAME	LOC.	CONVERSION FACTOR	AEA OCT.	AEA VALUE (ENGINEERING VALUE)	UNITS
*	4K10	0227	.10000 01	546670	-.62726400 06	FT/RAD
	4K12	0506	.10000 01	012000	.50000000 01	FT/SEC2
	5K14	0560	.10000 01	000000	.00000000 00	FT/SEC3
*	5K16	0561	.10000 01	012173	.10000229-01	FT/SEC3
*	5K17	0601	.10000 01	765605	-.10000229-01	FT/SEC3
	5K18	0564	.10000 01	631463	-.10000038 00	FT/SEC3
	5K20	0523	.10000 01	000000	.00000000 00	FT/SEC3
	5K26	0466	.10000 01	000360	.15000000 02	FPS
	K55	0607	.10000 01	377777	.99999237 00	NO UNITS
*	WBX	0514	.10000 01	724161	-.34202576 00	NO-UNITS
*	WBY	0515	.10000 01	607560	-.93969726 00	NO-UNITS
	WBZ	0516	.10000 01	000000	.00000000 00	NO-UNITS
	2J	0605	.10000 01	003775	.19970703 01	NO-UNITS
	3J	0312	.60000 02	000000	.00000000 00	MIN
*	5J	0231	.10000 01	255633	.56951680 07	FT
*	6J	0307	.60000 02	120235	.42830208 02	MIN
*	7J	0224	.10000 01	270063	.60325760 07	FT
*	8J	0225	.10000 01	261367	.58157440 07	FT

Table LM6/4.5.2-2. AGS Constants (Continued)
(NASA DATA SOURCE)

NAME	LOC.	CONVERSION FACTOR	AEA OCT.	AEA VALUE (ENGINEERING VALUE)	UNITS
9J	0226	.10000 01	326447	.70312320 07	FT
16J	0232	.10000 01	001652	.60032000 05	FT
21J	0233	.10000 01	000607	.25024000 05	FT
22J	0464	.10000 01	001440	.50000000 02	FPS
* 23J	0465	.10000 01	000470	.19500000 02	FPS
* 29J	0274	.60000 02	756330	-.30000000 03	MIN
1K24	0625	.10000 01	000071	.86975098-03	NO-UNITS
1K56	0673	.10000 01	777616	-.53085387-07	RAD
2K3	0216	.10000 01	040000	.10485760 07	FT
2K11	0526	.10000 01	273400	.60000000 04	FPS
2K14	0217	.10000 01	001415	.49984000 05	FT
2K17	0620	.10000 01	000005	.50000000 01	COUNTS
2K18	0447	.10000 01	000360	.15000000 02	SEC
2K19	0230	.10000 01	017205	.50003200 06	FT
2K20	0453	.10000 01	000040	.20000000 01	SEC
BM13SF	0676	.10000 01	365706	.96049499 00	
B23SF	0677	.10000 01	243656	.63999939 00	
B18SF	0700	.10000 01	125253	.33333588 00	

Table LM6/4.5.2-2. AGS Constants (Continued)
(NASA DATA SOURCE)

NAME	LOC.	CONVERSION FACTOR	AEA OCT.	AEA VALUE (ENGINEERING VALUE)	UNITS
B13VSF	0701	.10000 01	240000	.62500000 00	
B3SF	0702	.10000 01	131415	.34970856 00	
B23RSF	0703	.10000 01	032756	.10533142 00	
B13SF	0704	.10000 01	032525	.10416412 00	
BACCSF	0446	.10000 01	303240	.76293945 00	

113 CONSTANTS ANALYZED

LM6/4.5.4.2 Rendezvous Radar Angular Mounting Error

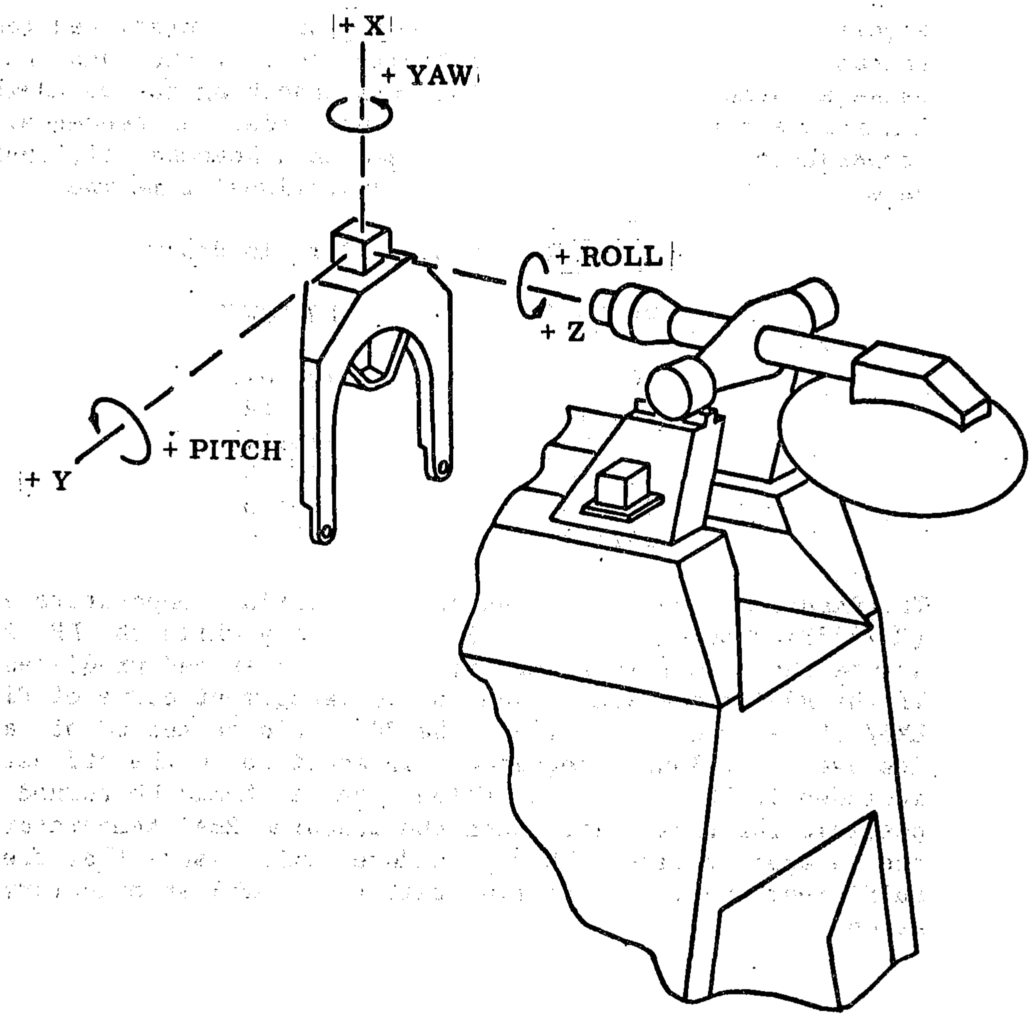

The angular installation error between the LM-6 NAV. Base Gage (Vehicle Coordinate System) and the RR alignment gage is shown below:

Pitch:	+00° 02' 38"
Roll:	-00° 00' 46"
Yaw:	+00° 00' 56"
RSS:	2' 56"

These errors are well within the RSS 3-axis specification error of 15.5'.

(Ref.: LMO-566-121, dated 3 February 1969)

LM6/4.5.4.3 RR Timeline Operation

Figures LM6/4.5.4-9 and LM6/4.5.4-10 show the predicted temperature response of the high power multiplier chain (HPMC) and the gyro package during the LM-6 mission from undocking to touchdown and from lunar ascent to the completion of the rendezvous sequence. The temperature profiles shown are based on a November 14, 1969 launch date trajectory and the following operational timeline:

MISSION H-1 RR TIMELINE (Time in Hrs:Min G.E.T.)

RR "ON"	RR "OFF"
107:00	107:07
108:40	108:48
109:50	110:11
112:10	112:35
139:40	140:10
142:22	145:35

The Rendezvous Radar Antenna Assembly (RRAA) temperature sensor (GN7723T) should be monitored continuously while the RR is on to assure that the temperature rise does not exceed predicted values. If the RRAA temperature exceeds the management curve of Figures LM6/4.5.4-9 and LM6/4.5.4-10 the RR should be turned off as soon as its use is no longer required. In addition to the off periods included in the present timeline, the RR should be turned off whenever possible for those times when the measured RRAA temperature exceeds the management line. This procedure will assure that there is sufficient in-limit operating time to accomplish mandatory RR operation.

LM6/4.5.4.4.11 RR and T AGC Voltage Versus Range

Figure LM6/4.5.4-6 shows the expected AGC voltage levels versus range and signal level for RR No. 23 with T No. 23. The use of curves instead on nomographs permits a better visualization of the interaction of the variables and also avoids the difficulty of trying to design a nomograph to fit empirical data on non-linearly interrelated variables.

LM6/4.5.4.4.11.1 RR and T AGC Voltage Versus Range and LOS Angle

Figures LM6/4.5.4-7 and LM6/4.5.4-8 show RR AGC readings at several ranges between 0.2 n mi and 400 n mi, as a function of the angle between the LOS and the antenna boresight. The data are shown for angles out to ±10° in both the shaft and trunnion axes, except where very low signal levels would produce low AGC readings which would be of little value.

LM6/4.5.4.4.12 Rendezvous Radar Self Test

Figure LM6/4.5.4-1 shows the effects of environment on the RR Self Test parameters of range and range rate.

LM6/4.5.4.4.16 Allowable Vehicle Accelerations During RR Power Off Periods

Figures LM6/4.5.4-2 through LM6/4.5.4-5 show the maximum allowable LM body accelerations for any angular position of the RR antenna trunnion and shaft axes under which the antenna will not move from a fixed position with no power applied to the RR. The effect of varying the antenna temperatures is also indicated in the figures.

The antenna shaft axis will always be parallel to the LM Y-axis. Therefore, LM body accelerations about the LM Y-axis can be used directly. However, as the shaft axis rotates, the trunnion axis will be parallel to the LM X-axis at 0° shaft position and parallel to the LM Z-axis at -90° shaft position. For other shaft positions, the allowable LM acceleration about the LM axes must be converted to the acceleration about the trunnion axis at the appropriate shaft position.

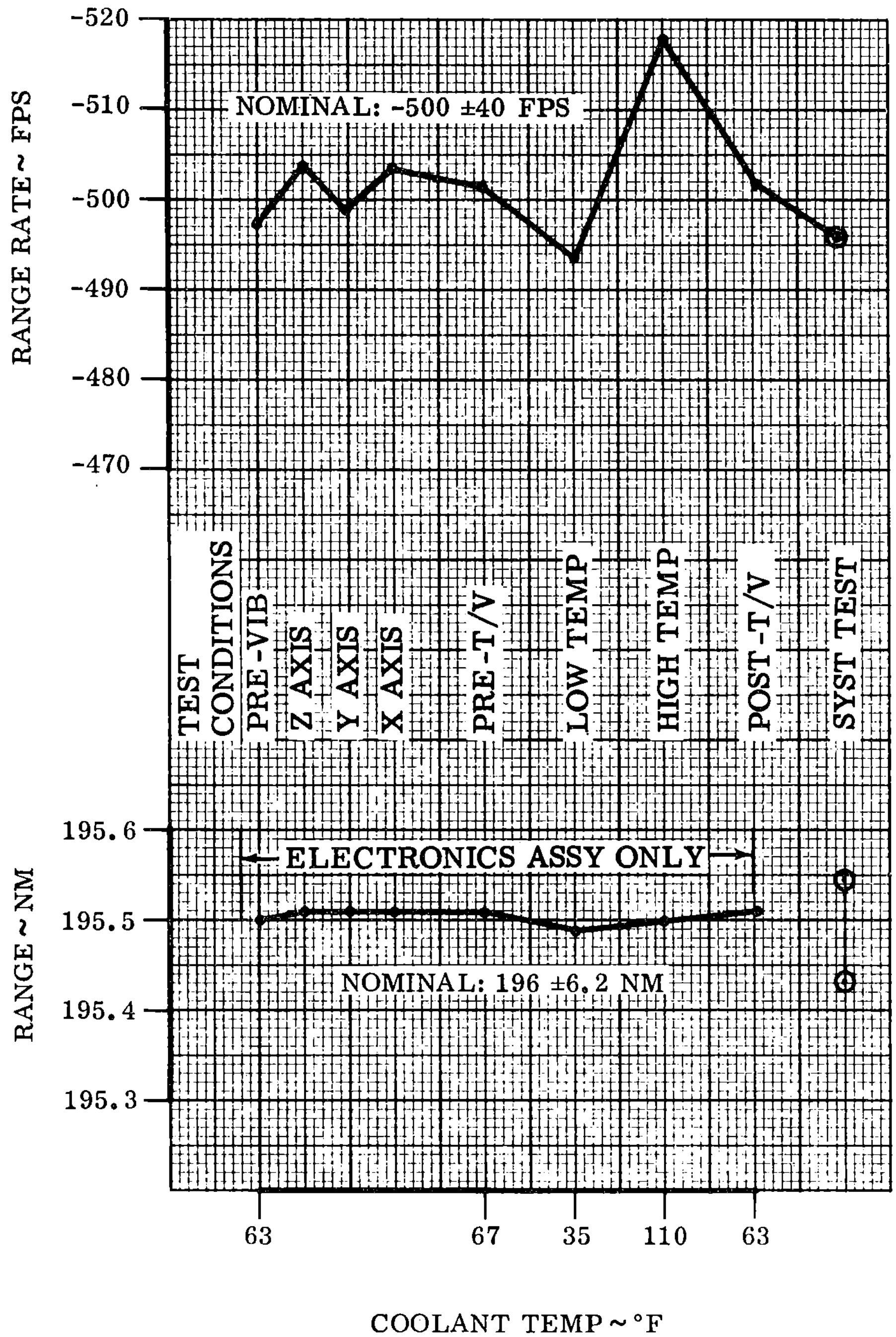

Figure LM6/4.5.4-1. Environmental Effects on RR Self Test Parameters
(See Para. 4.5.4.4.12)

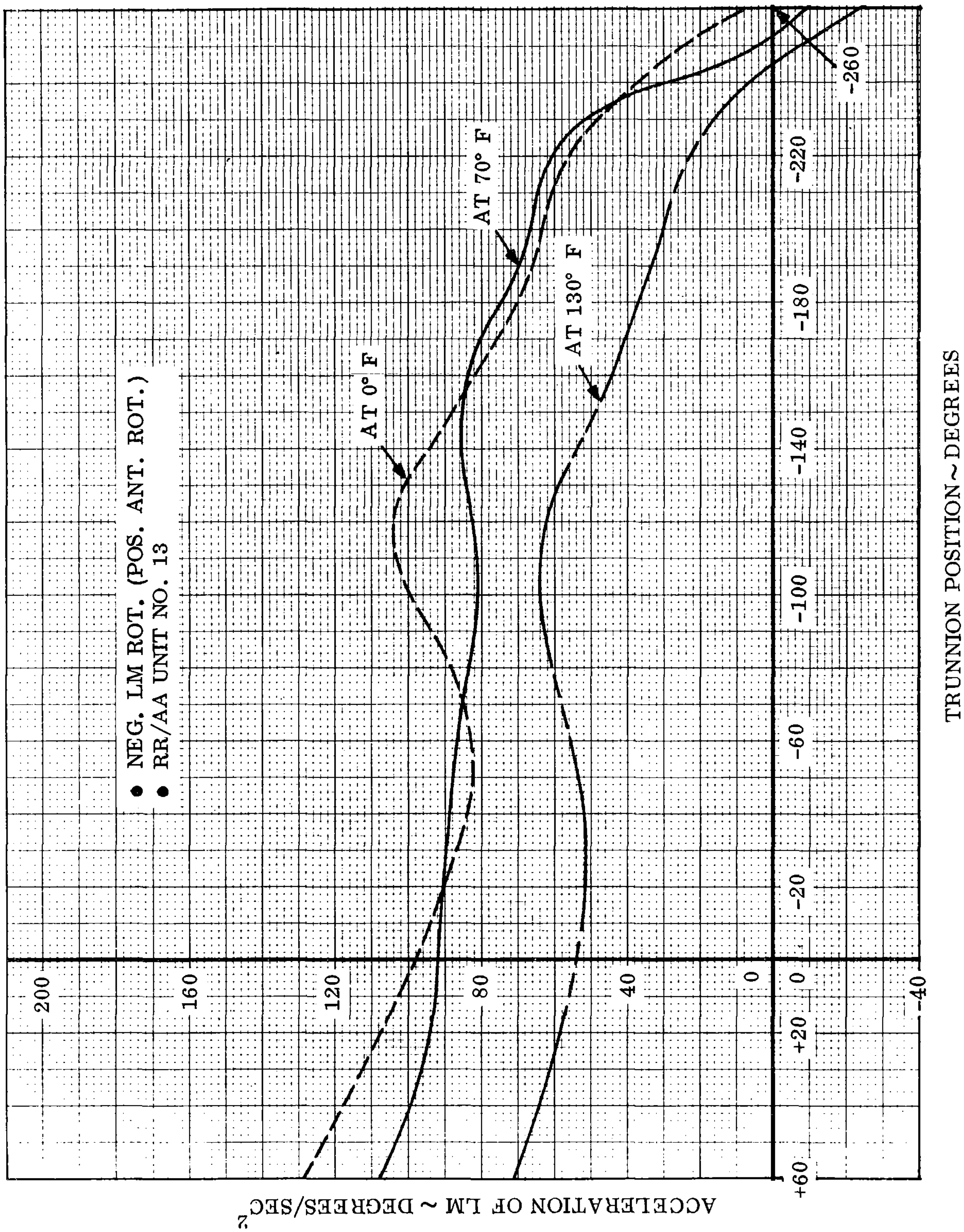

Figure LM6/4.5.4-2. Allowable Acceleration Trunnion Axis
(See Para. 4.5.4.4.16)

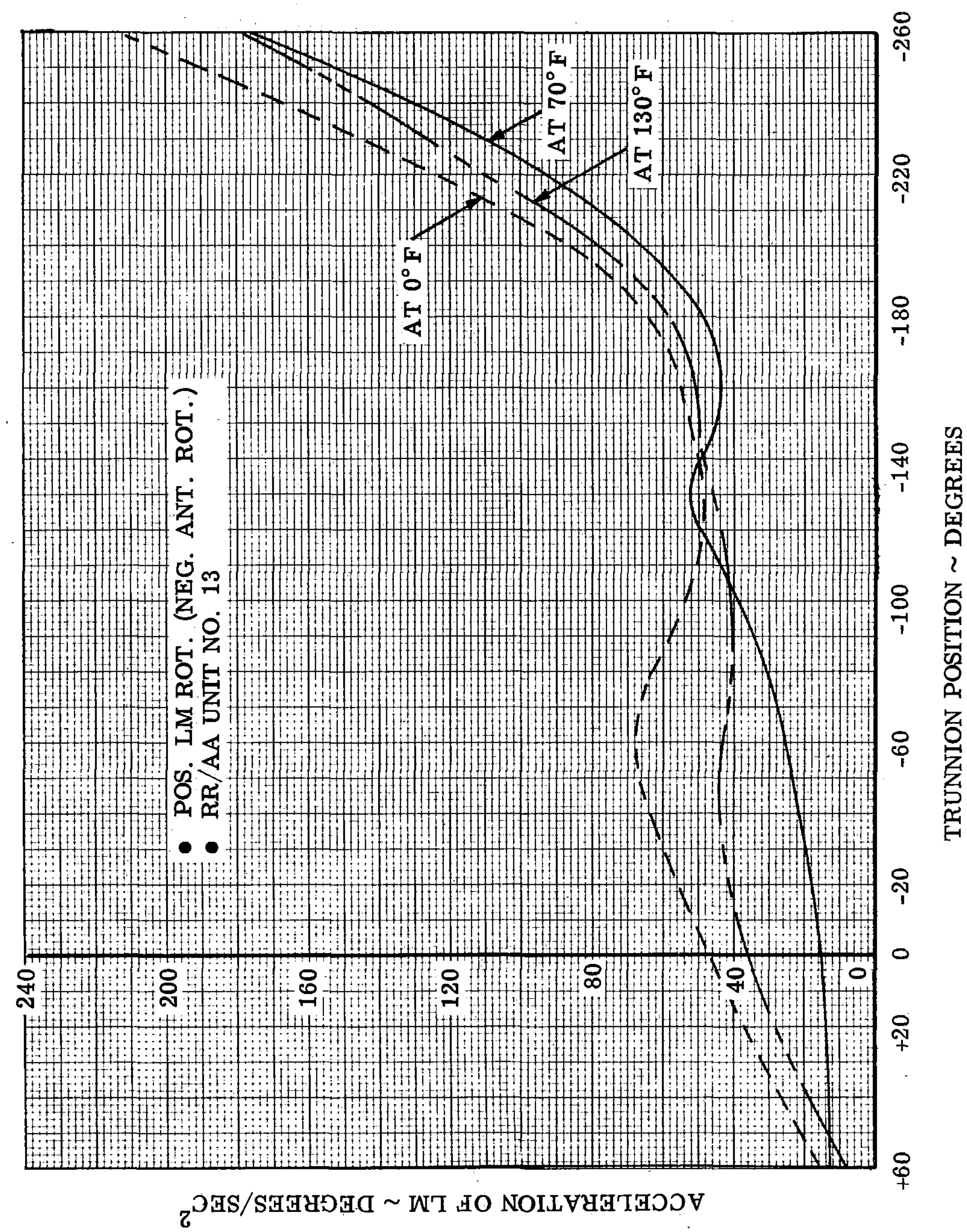

Figure LM6/4.5.4-3. Allowable Acceleration Trunnion Axis

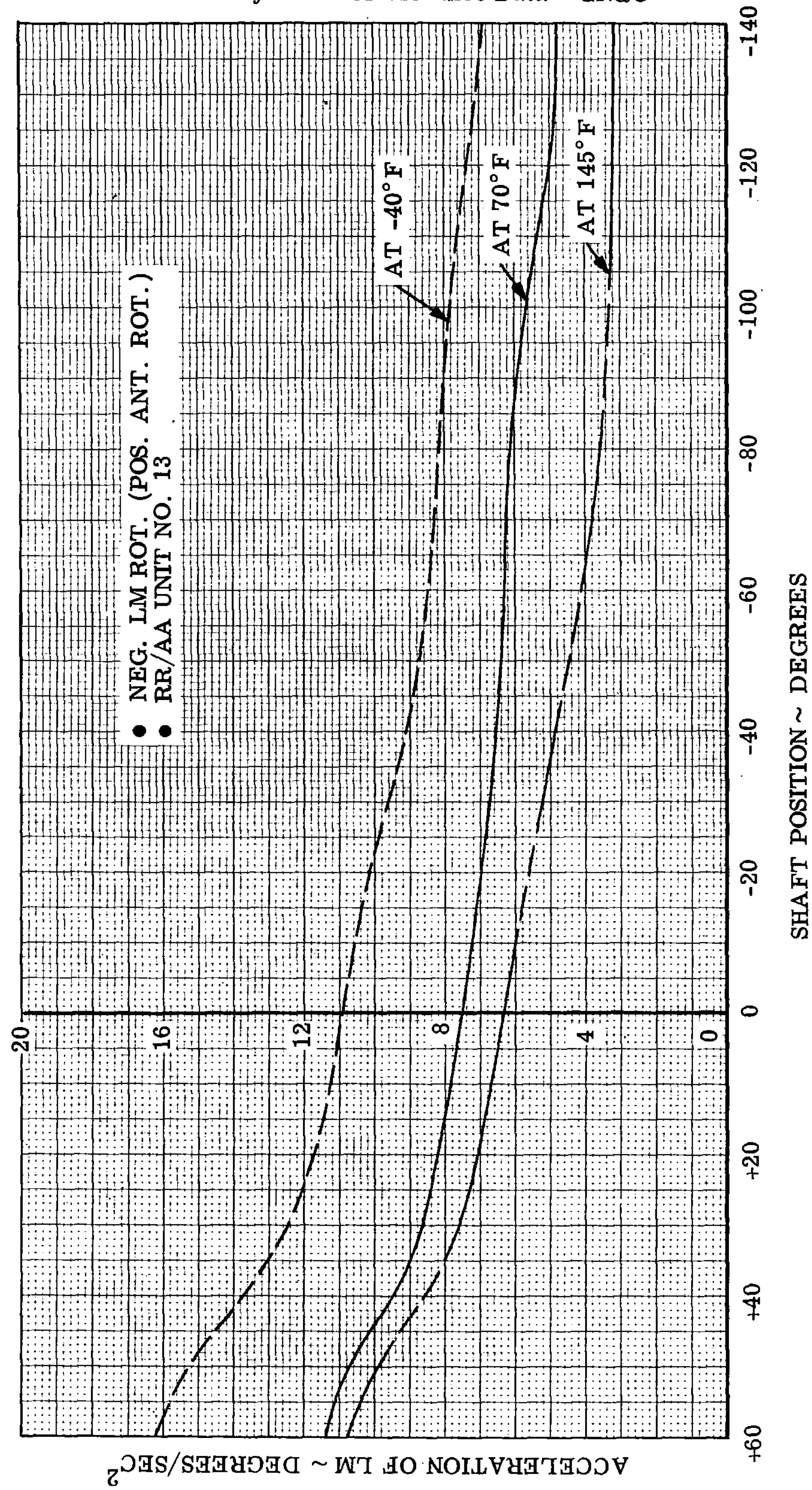

Figure LM6/4.5.4-4. Allowable Acceleration Shaft Axis

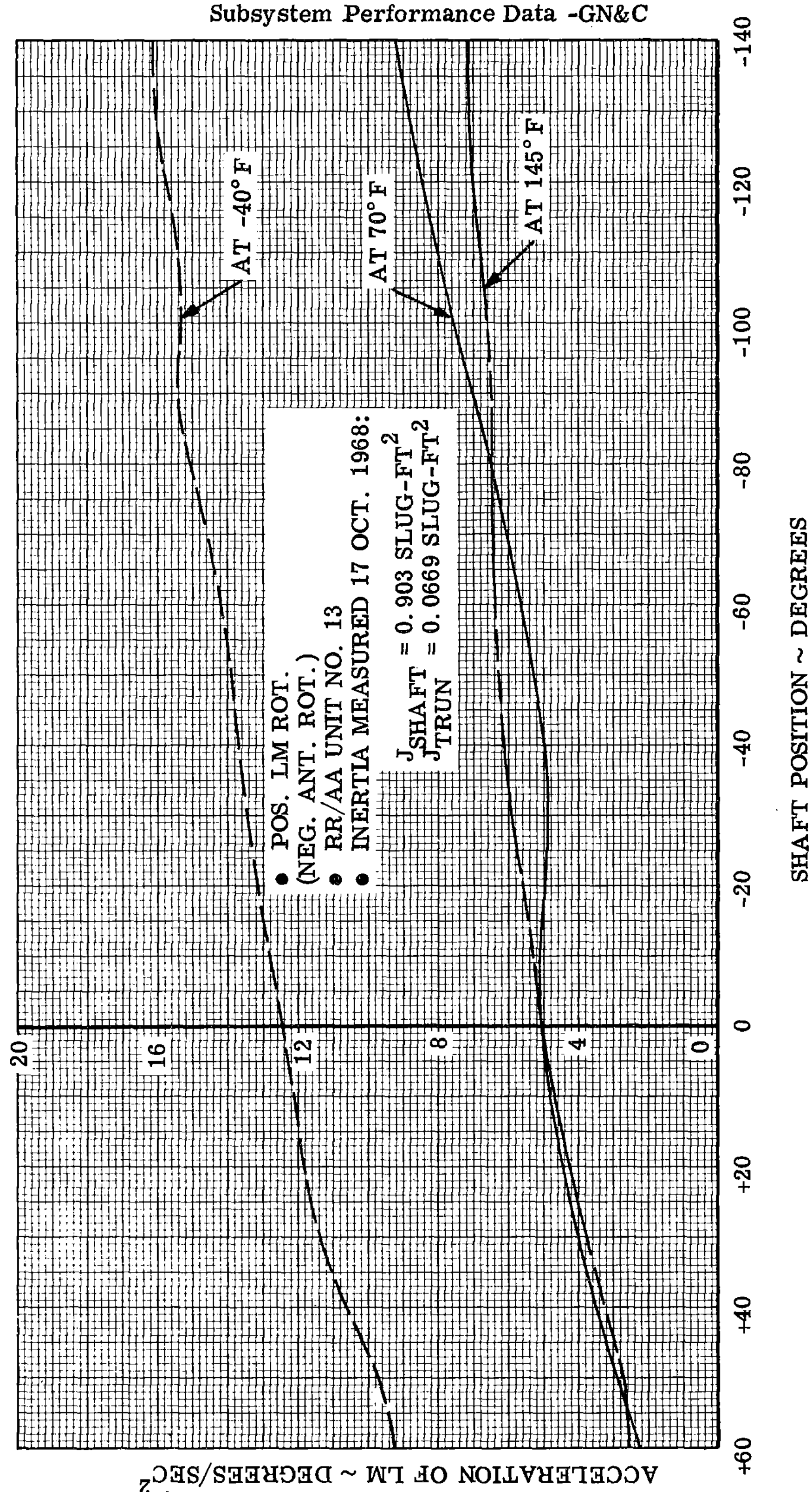

Figure LM6/4.5.4-5. Allowable Acceleration Shaft Axis

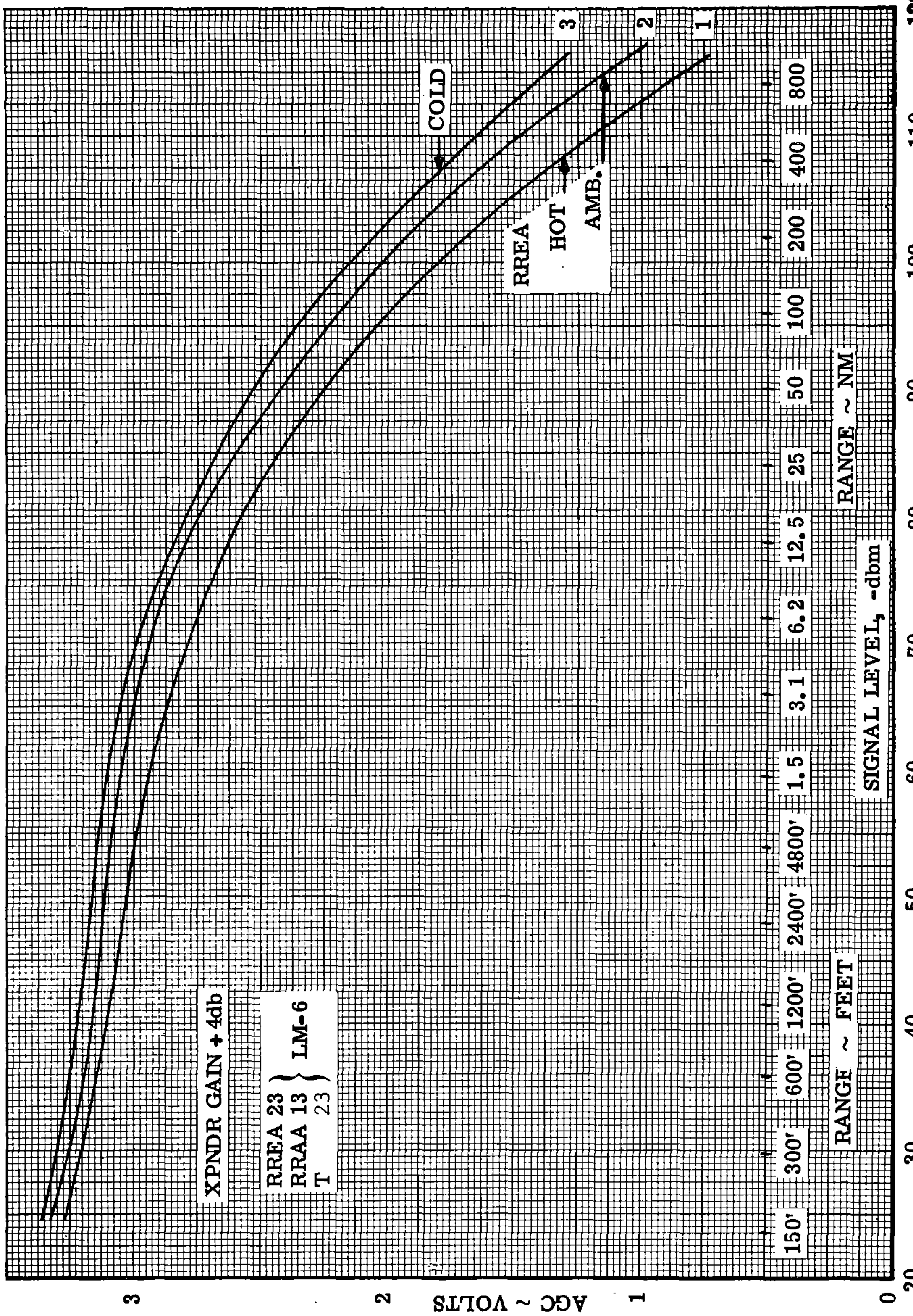

Figure LM6/4.5.4-6. LM6RR AGC Versus Signal Level and Range With T No. 23
(See Para. 4.5.4.4.11)

- ALL DATA ROUNDED OFF TO NEAREST TENTH

1. 400 NM RANGE
2. 100 NM RANGE
3. 50 NM RANGE
4. 1.5 NM RANGE
5. 1200 FT RANGE

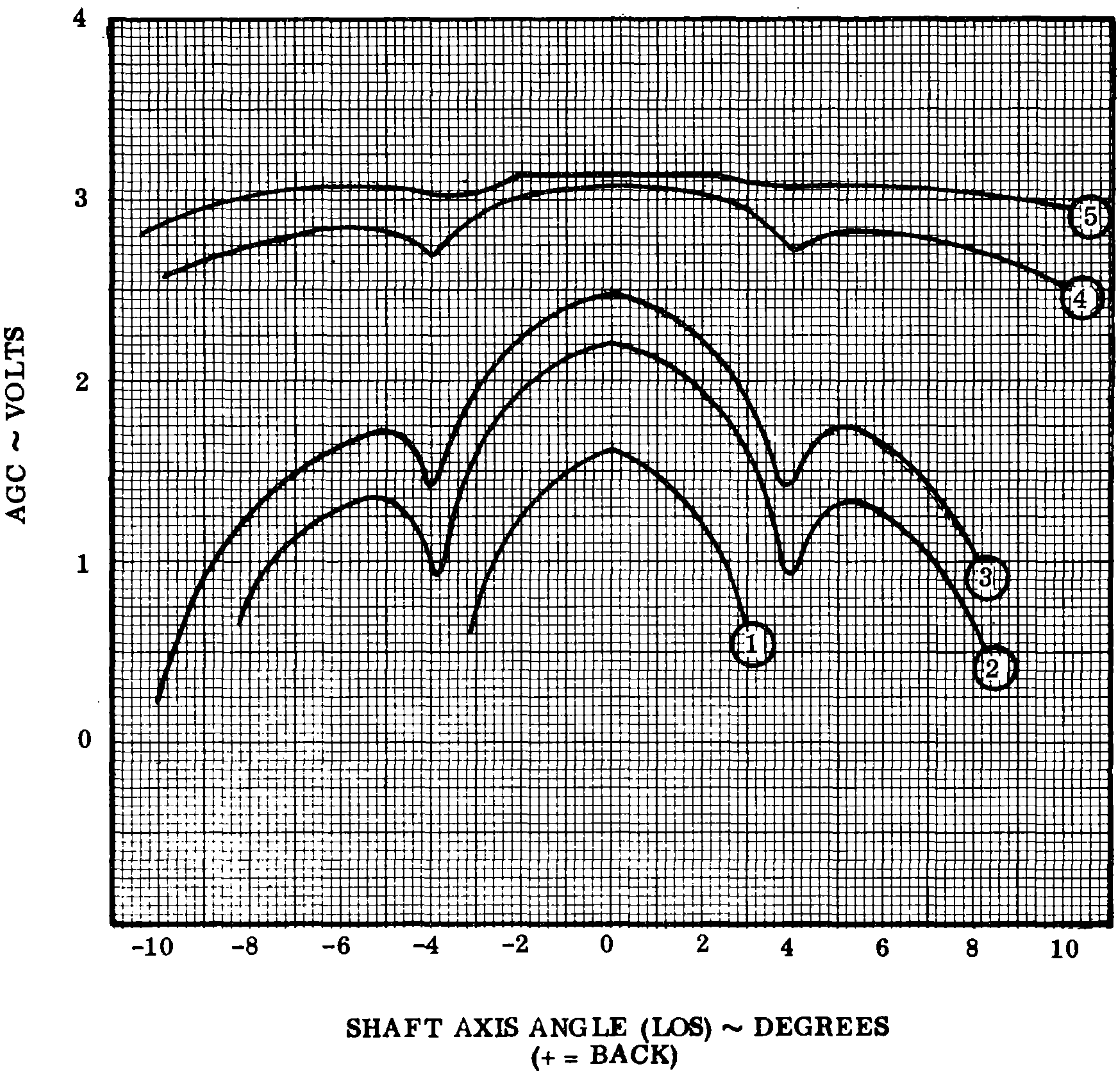

Figure LM6/4.5.4-7. AGC Versus Shaft Axis Angles
(See Para. 4.5.4.4.11.1)

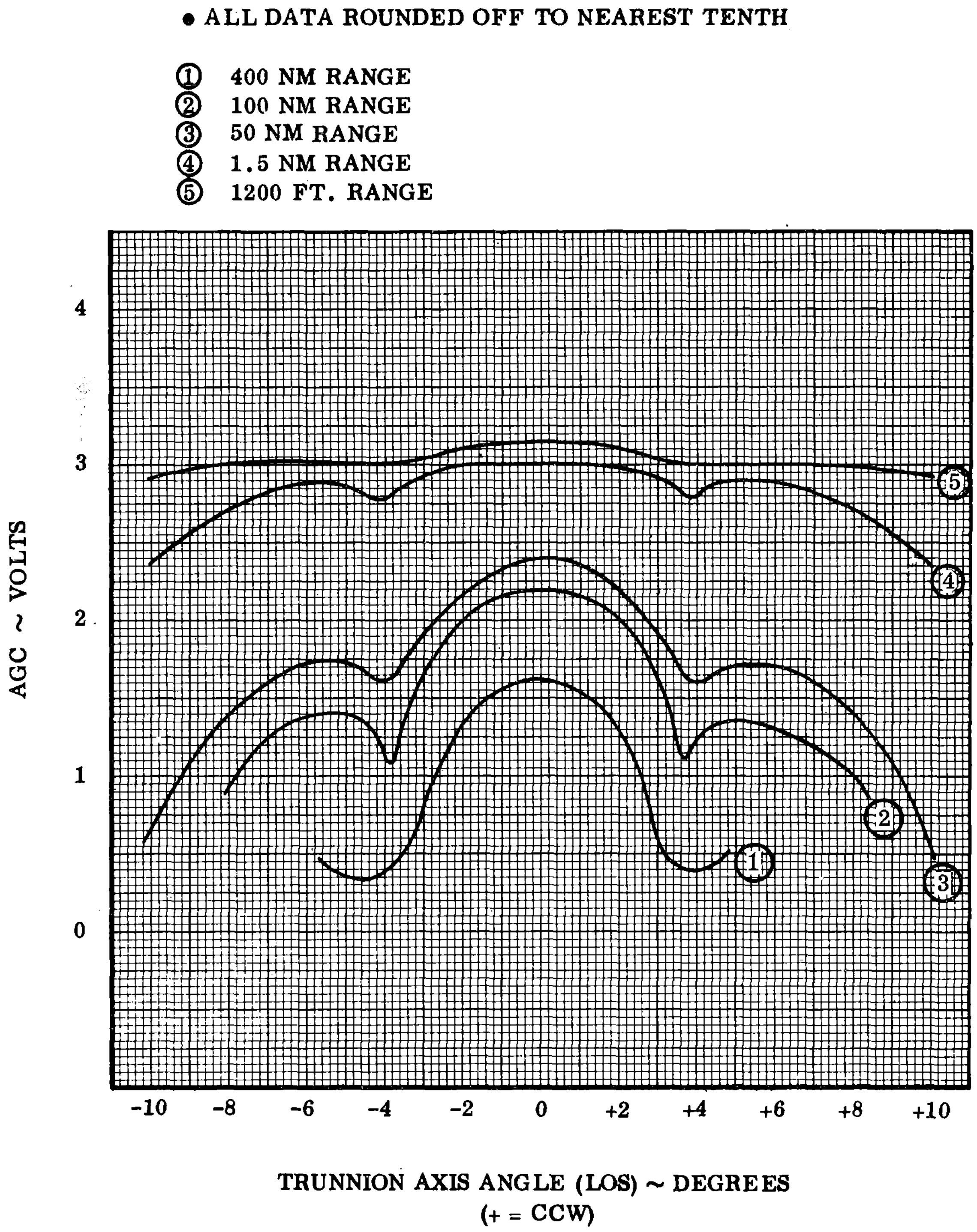

Figure LM6/4.5.4.-8. AGC Versus Trunnion Axis Angle
(See Para. 4.5.4.4.11.1)

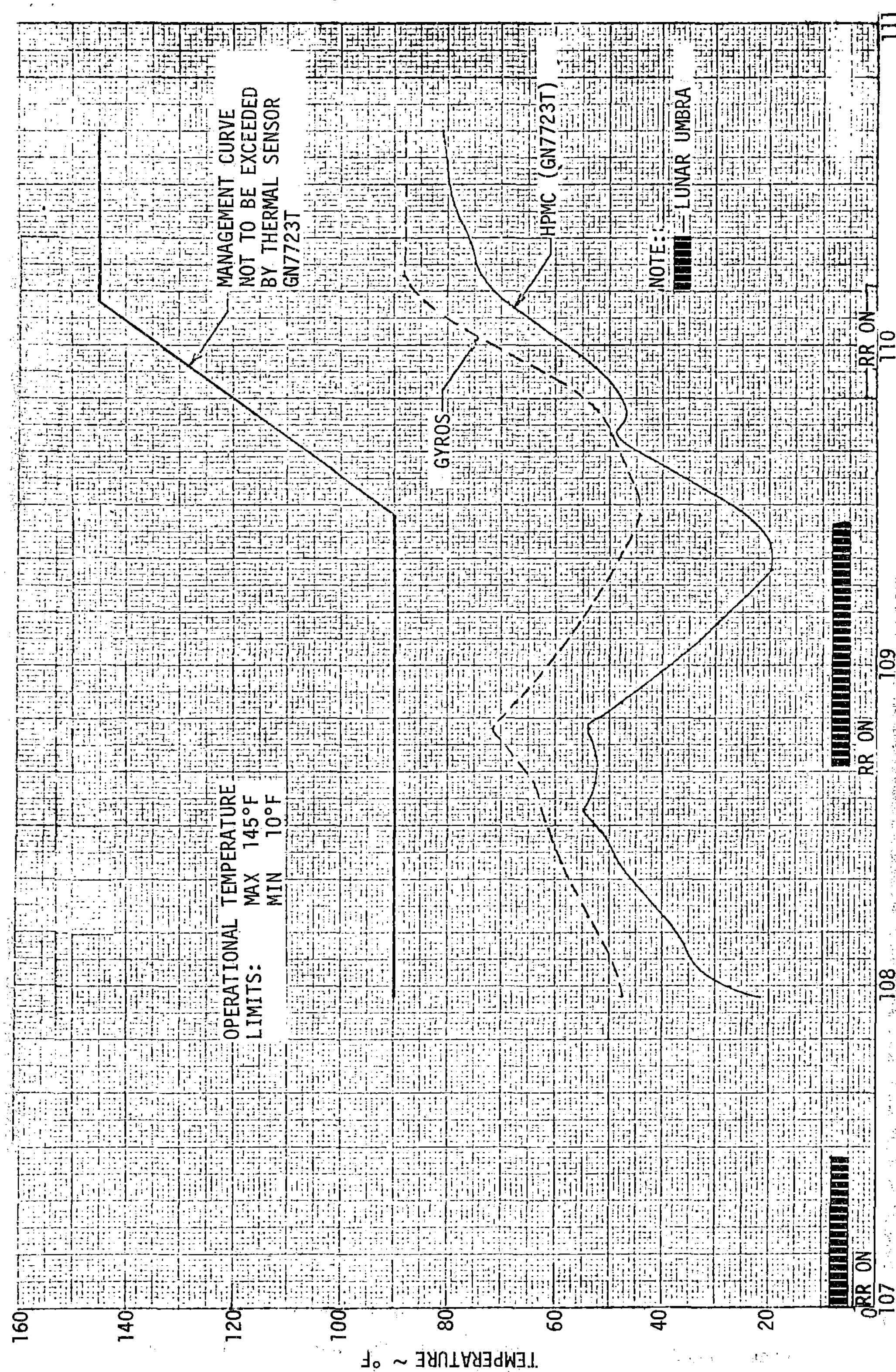

Figure LM6/4.5.4-9. Predicted RR HPMC and Gyro Temperature Profile for Final Flight Plan Timeline (Undocking to Touchdown)

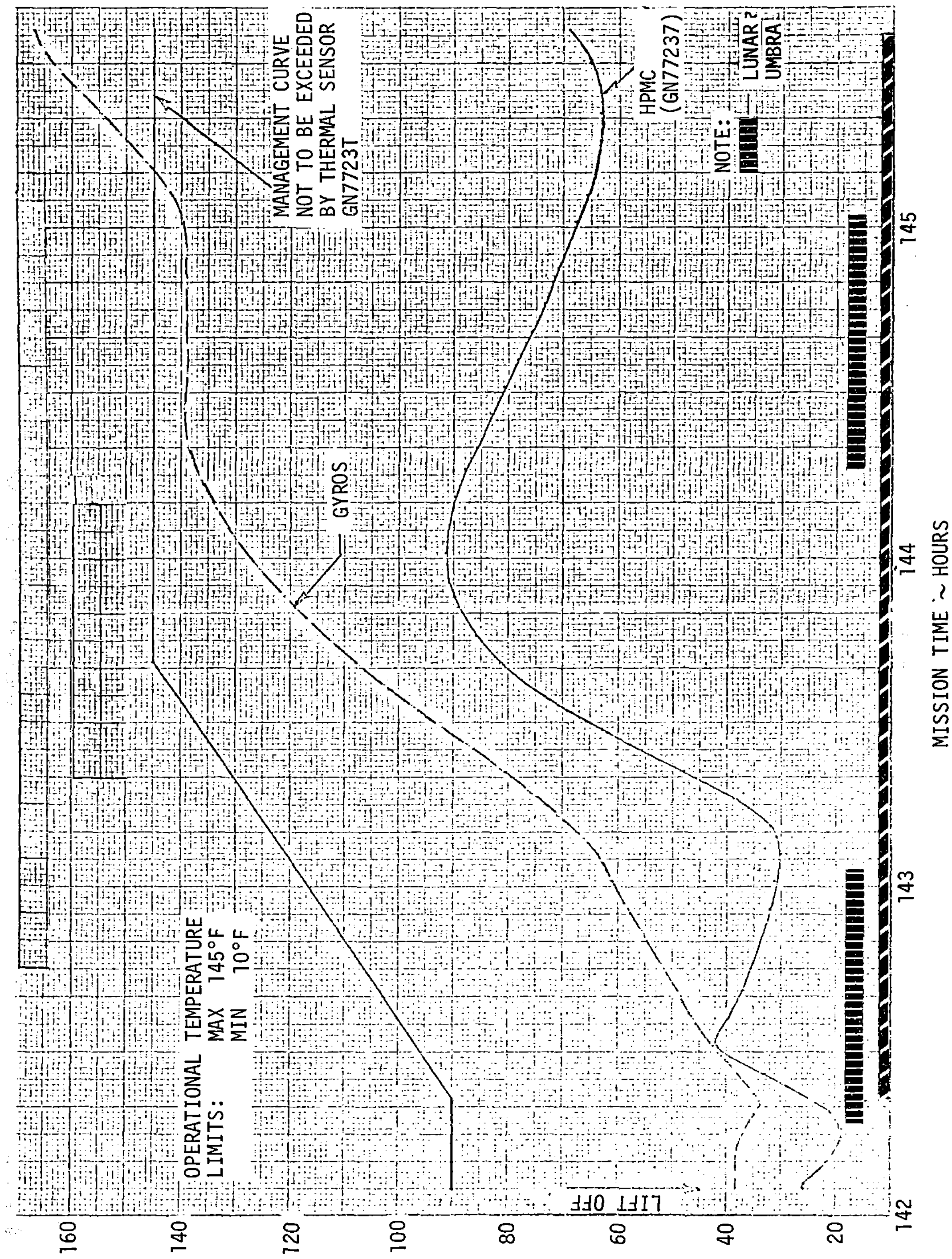

Figure LM6/4.5.4-10. Predicted RR HPMC and Gyro Temperature Profile for Final Flight Plan Timeline (ASCENT TO DOCKING)

LM6/4.5.5.1.16 LR Power Monitor

The following is a calibration of the R. F. Power Monitor Meter with LR P-46.

Transmitter	Power (dBm)	Power (MW)	Monitor (VDC)	Calibration
Velocity	25.4	347	3.26	9.4×10^{-3} V/MW
Altimeter	24.6	288	3.23	11.2×10^{-3} V/MW

Note: The power in milliwatts is at the output of the multiplier chain and does include losses in the antenna assembly.

LM6/4.5.5.1.17 Loss of LR Lock as a Function of Vehicle Pitch and Roll for an Apollo 11 Type Trajectory

Figures LM6/4.5.5-1 through LM6/4.5.5-4 describe the LR loss of lock as a function of vehicle pitch and roll for the nominal descent trajectory for antenna positions 1 and 2, respectively.

LM6/4.5.5.1.18 Expected Altitude of LR Velocity and Range Initial "Data Good" Indication

Figure LM6/4.5.5-5 describes the signal-to-noise (S/N) ratio as a function of altitude for LR beams 1, 2 and 3 (i.e., the velocity beams). The minimum S/N threshold required for lock-on and the range sweep limit are also indicated. Figure LM6/4.5.5-6 includes the same data for beam 4 (the range beam).

Altimeter lock-on ("Data Good") is achieved when beams 1, 2 and 4 are locked-on. Velocity lock-on is achieved when beams 1, 2 and 3 are locked-on.

Note: The band on range acquisition altitude is due to variations in the following items:

a) Radar temperature
b) Signal-to-noise (S/N) uncertainties

LM6/4.5.5.1.21 LR Predicted Accuracy

Figure LM6/4.5.5-7 shows the predicted LR accuracy as a function of time from ignition and of altitude, for an Apollo 11 type descent trajectory.

LM6/4.5.5.2 Landing Radar Temperature Profile

Figure LM6/4.5.5-8 presents the Landing Radar Antenna Assembly typical high temperature and low temperature profiles for LM6/Mission H-1.

LM6/4.5.5.3 Landing Radar Mechanical Alignment

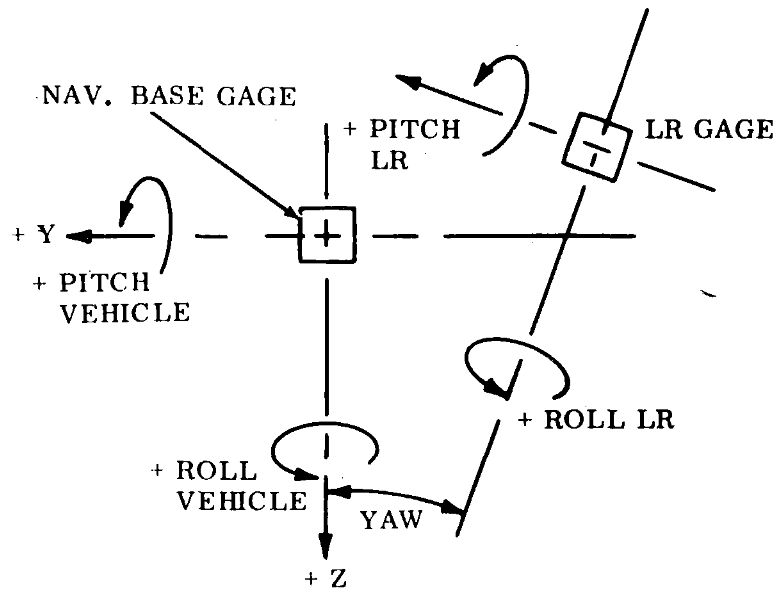

The Landing Radar Antenna Assembly alignment for LM-6 with respect to the Vehicle Coordinate System (Nav. Base Gage) is shown below:

	Position #1	Position #2
Pitch:	-24° 02' 27"	+00° 01' 17"
Roll:	-00° 03' 57"	-00° 03' 06"
Yaw:	-06° 07' 33"	-06° 06' 13"

(Ref.: LMO-566-215, dated Sept. 1969)

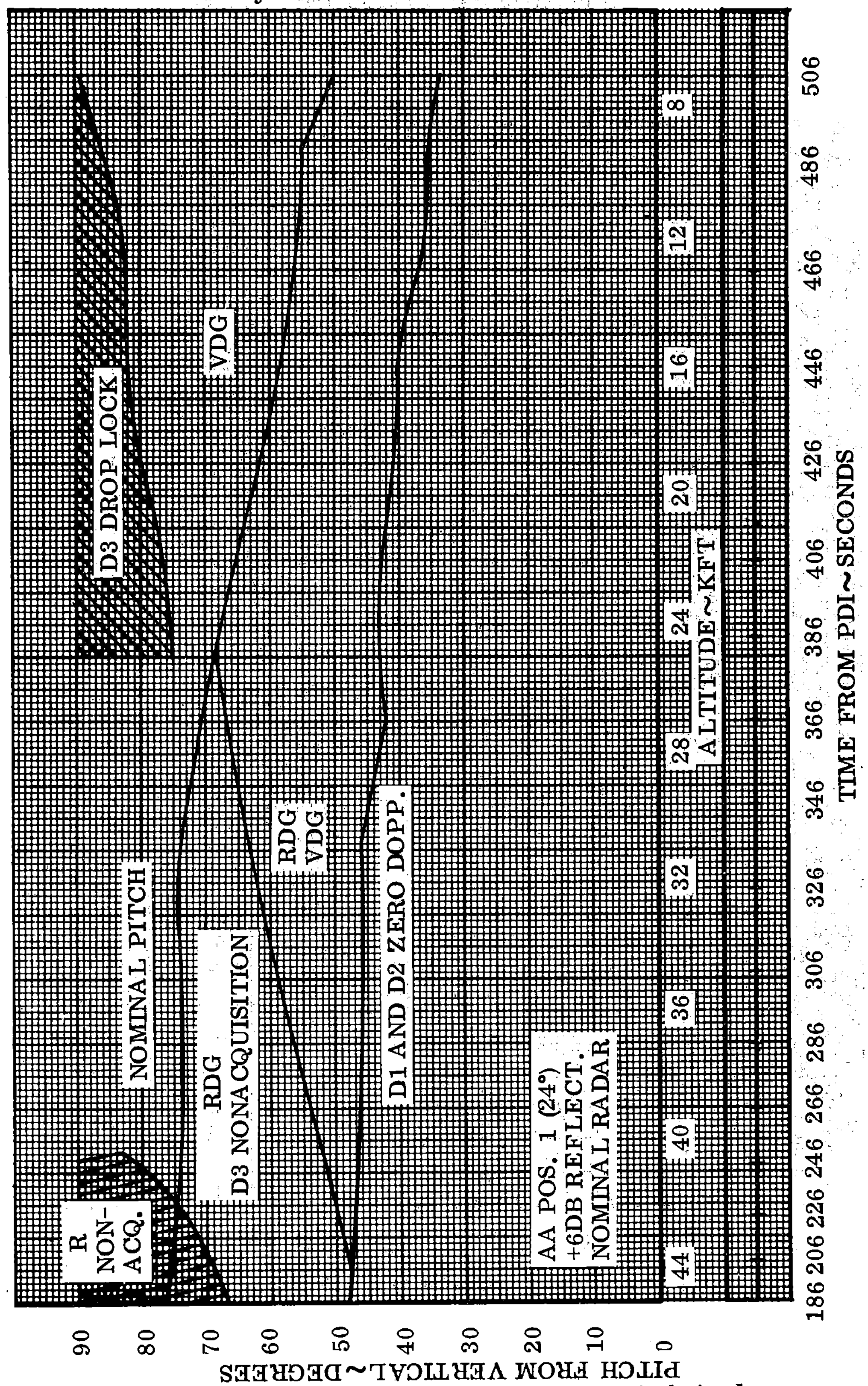

Figure LM6/4.5.5-1. LR Loss of Lock versus Pitch Angle

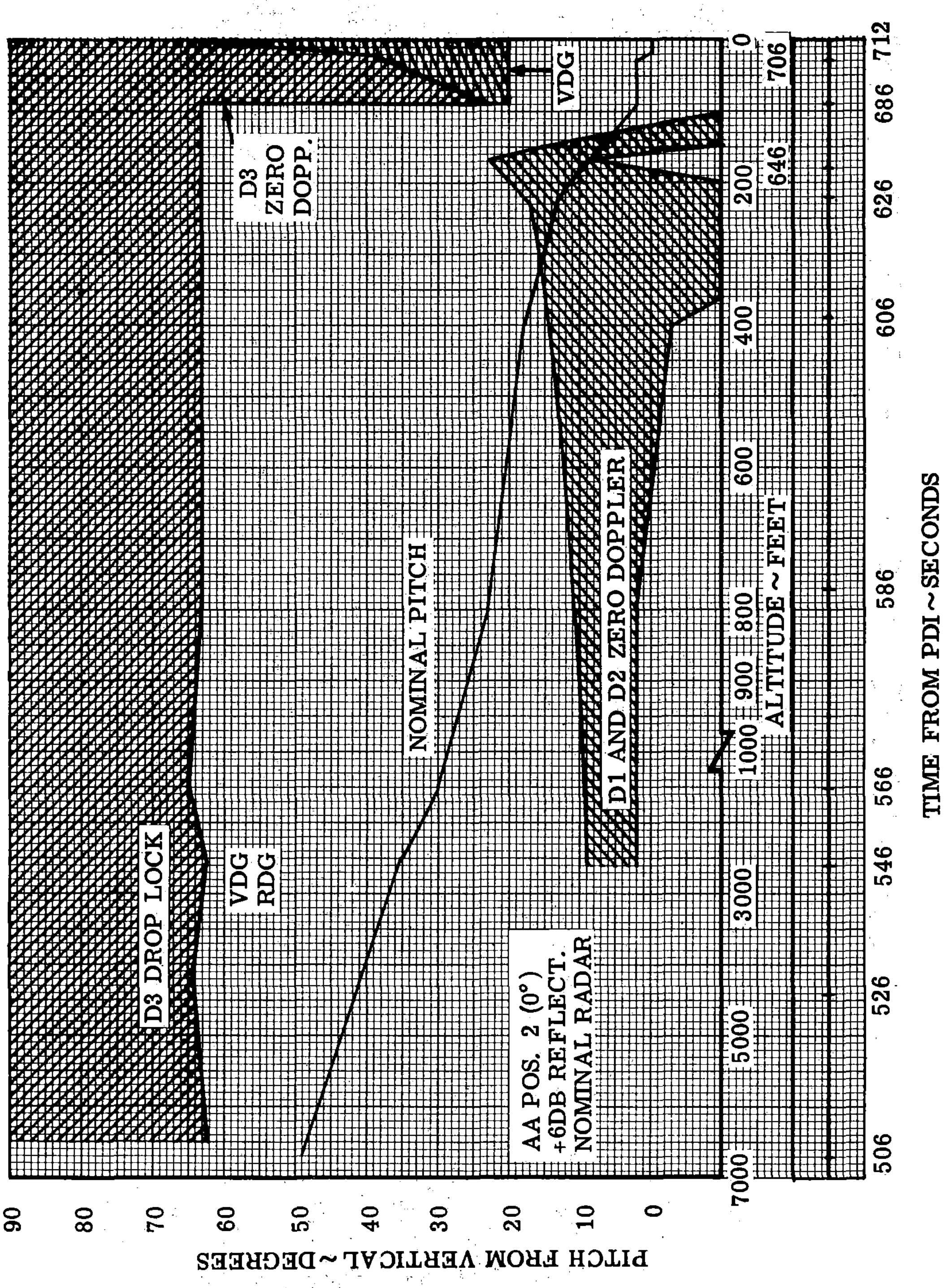

Figure LM6/4.5.5-2. LR Loss of Lock versus Pitch Angle

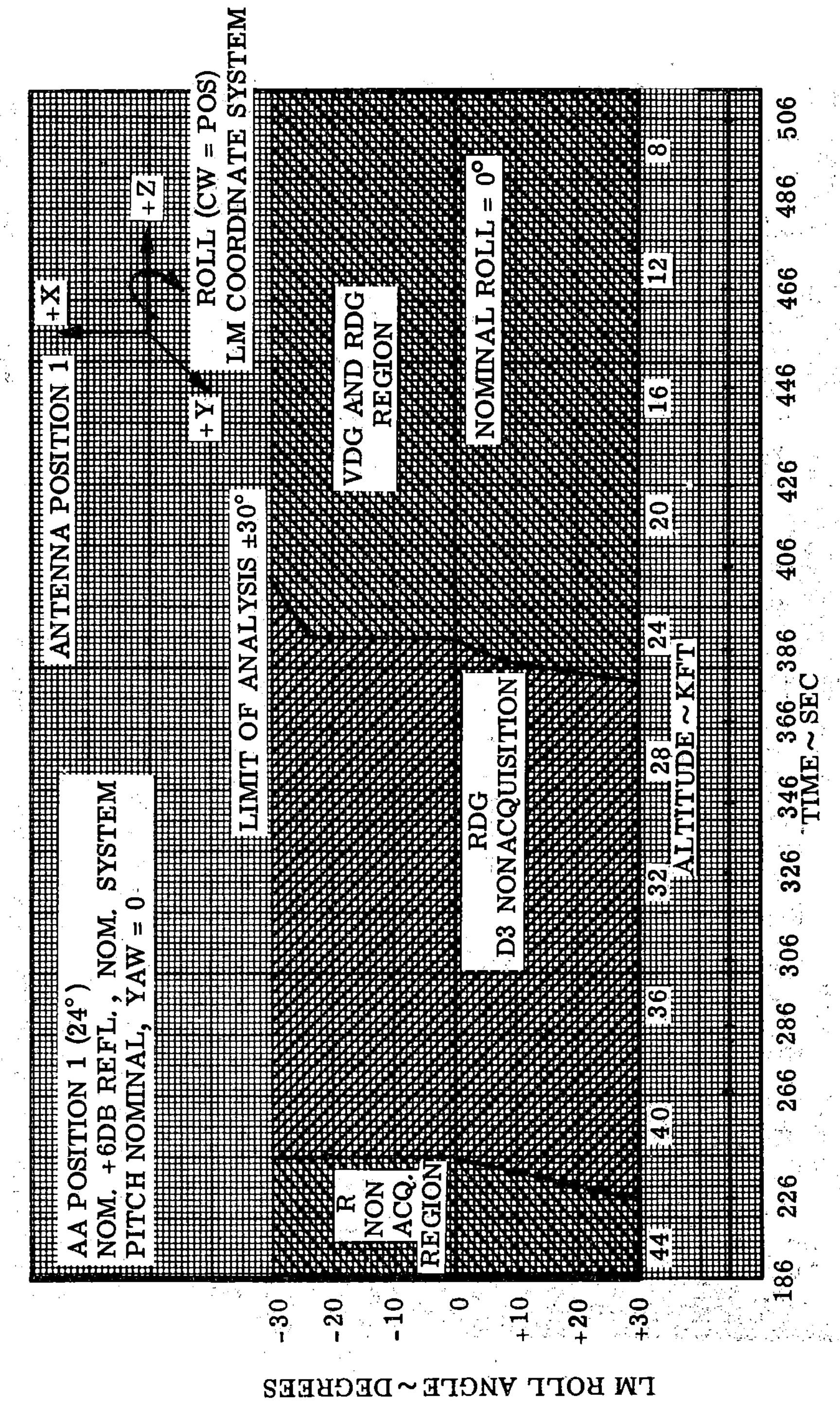

Figure LM6/4.5.5-3. LR Loss of Lock versus Roll Angle

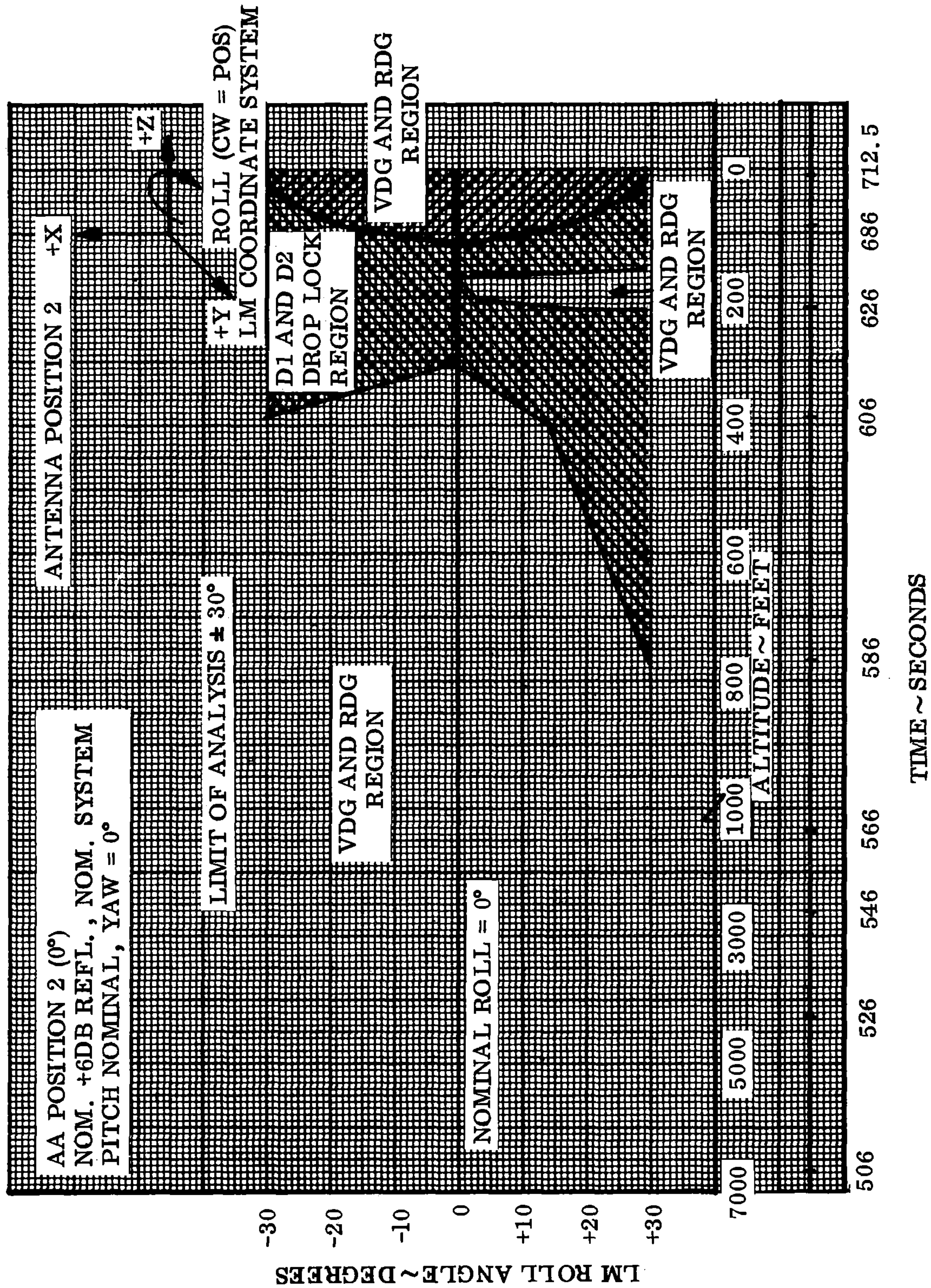

Figure LM6/4.5.5-4. LR Loss of Lock versus Roll Angle

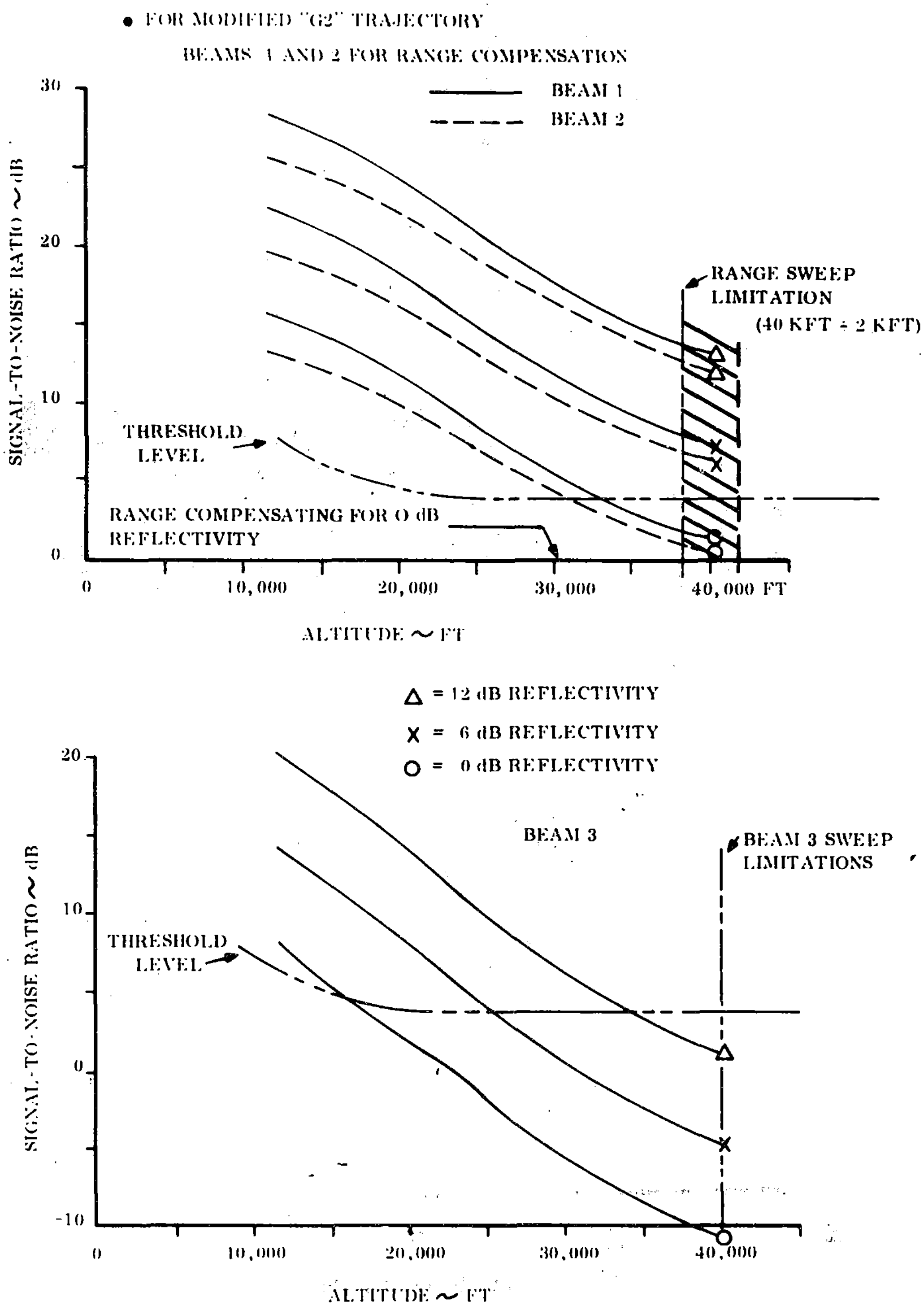

Figure LM6/4.5.5-5. Landing Radar Lock-on Capability - Velocity Beams

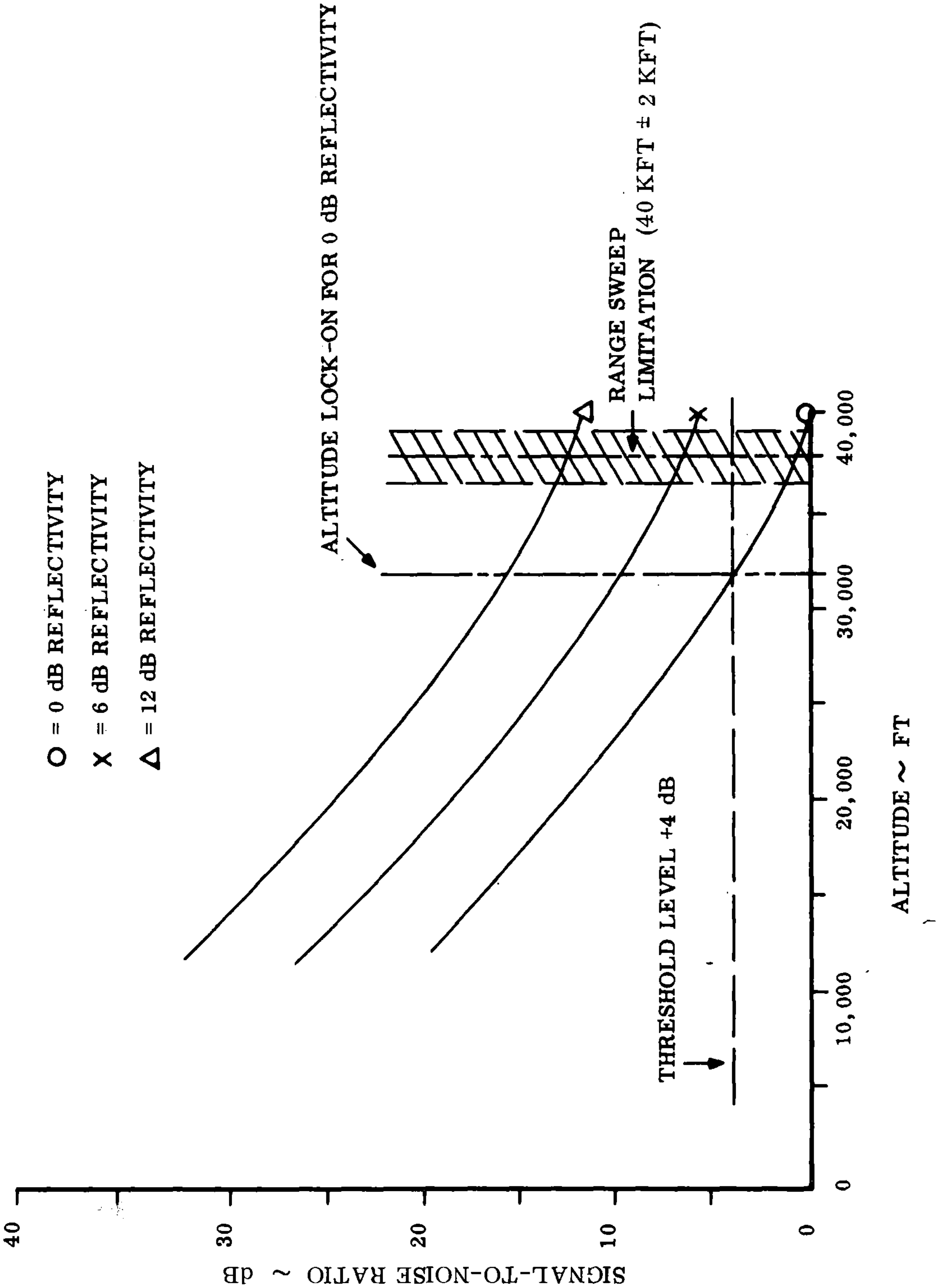

Figure LM6/4.5.5-6. Landing Radar Lock-on Capability - Range Beam

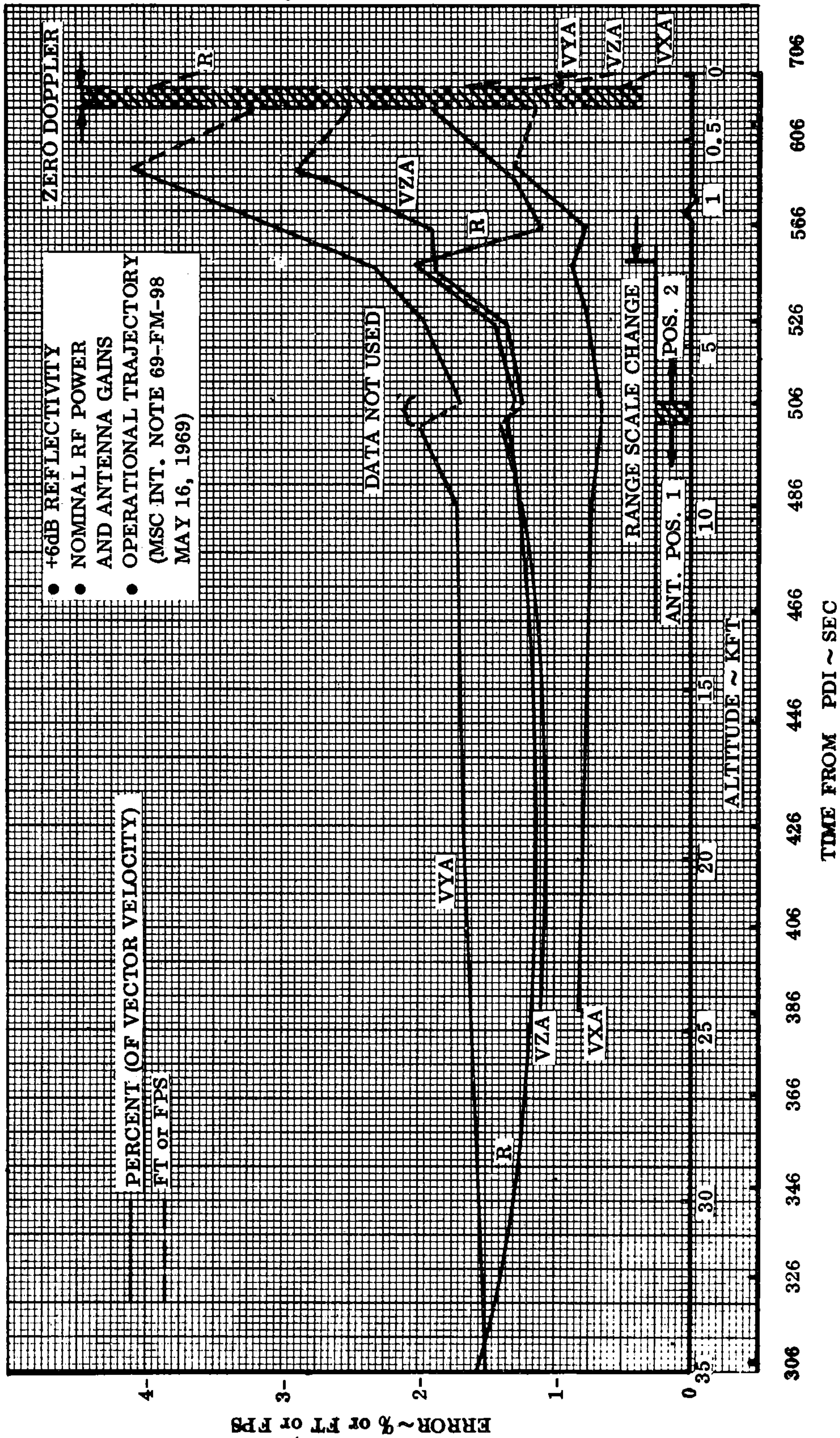

Figure LM6/4. 5. 5-7. Landing Radar Accuracy

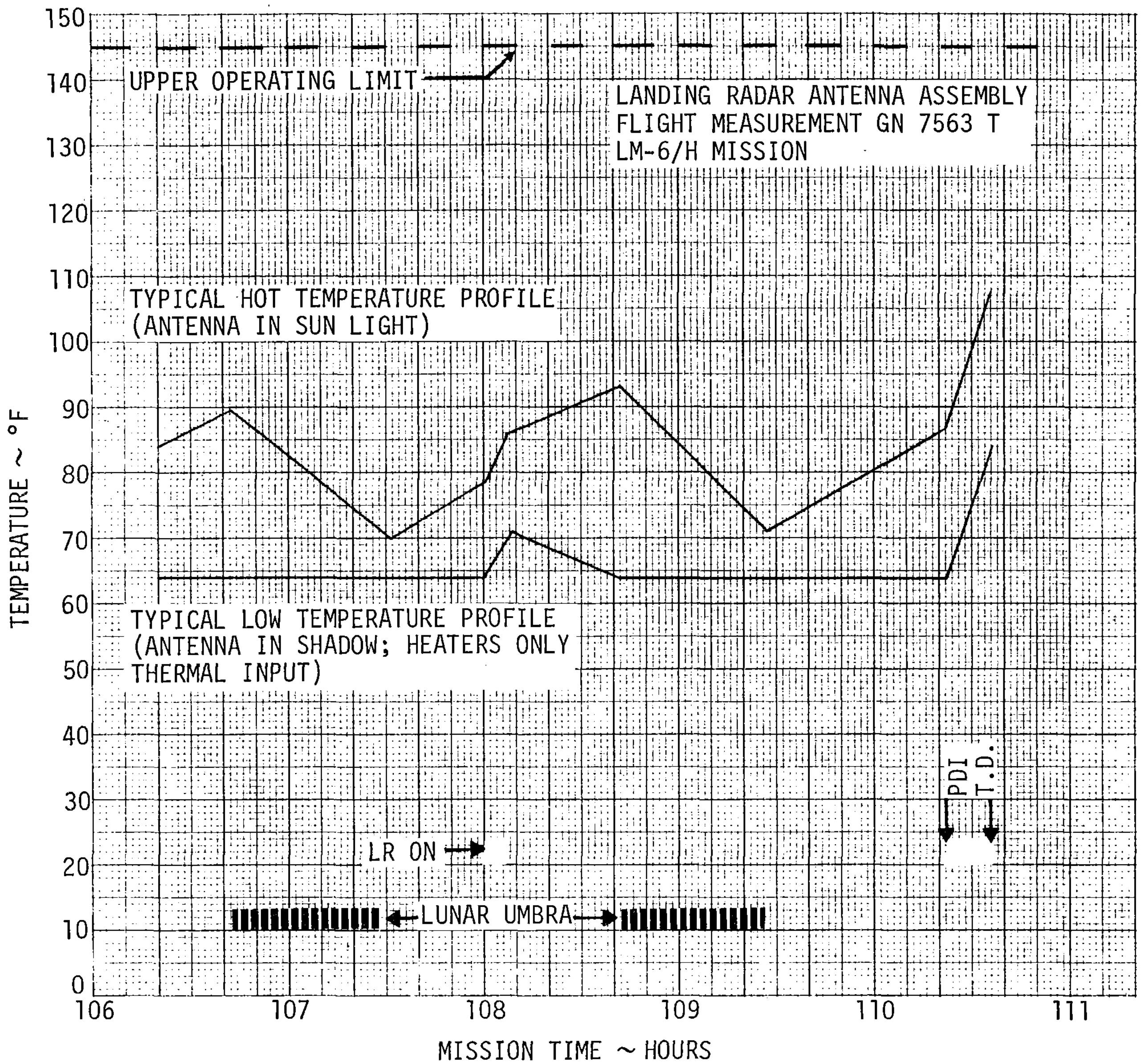

Figure LM6/4.5.5-8. Landing Radar Antenna Assembly Temperature Profile

LM6/4.6.1 Mission H1 (LM-6) APS Preflight Analysis

The APS mission duty cycle used in the following analysis is as follows:

Event	Duration
APS Lunar Liftoff	To Depletion

The planned APS mission duty cycle will be a manned burn initiated from the lunar surface and of a duration to achieve the required ΔV of approximately 6090 fps.

The vehicle weight characteristics and loaded propellant quantities were obtained from Reference 1. Table LM6/4.6.1-1 is a summary of the LM-6 APS physical characteristics.

It should be noted that the effect of the Reaction Control System on APS performance has been neglected in this analysis. The RCS will affect APS performance in the following manner:

1) RCS propellant consumption (APS/RCS interconnect closed) will alter vehicle weight;

2) RCS propellant consumption through the APS/RCS interconnect will decrease the propellant available to the APS and thus shorten the APS burn time available and decrease the ΔV capability. Also, since the RCS operates at a mixture ratio different from that of the APS, the mixture ratio from the APS tanks will be changed. (The mixture ratio of the ascent engine will not be significantly changed.)

The engine performance characterization consists of C* (characteristic exhaust velocity), C_f (thrust coefficient), A_t (throat area), and interface-to-chamber fluid flow resistances defined as functions, where applicable, of P_c (chamber pressure), μ (mixture ratio), T (propellant temperature), t_b (engine burn time), t_{acc} (accumulated time on chamber), and helium saturation into the propellants.

The helium regulator characterization used was the nominal Class I - primary regulator expected performance.

The nominal mixture ratio of 1.605 is for nonsaturated propellant conditions prior to ignition. If the tanks are pressurized earlier than is now planned and, therefore, cause helium saturation of the propellants, the mixture ratio will shift to 1.599.

LM6/4.6.1 (Continued)

The liquid propellant bulk temperatures at the start of the first APS burn were assumed to be 70°F for oxidizer and fuel.

Plots from the simulation of the LM-6 APS nominal performance under the assumptions and conditions discussed previously are presented in Figures LM6/4.6.1-1 through LM6/4.6.1-9. Figure LM6/4.6.1-2 presents the predicted ablative chamber throat area as a function of burn time. The time-varying characteristic of this parameter is included because of its influence in imparting a time-varying character to other propulsion parameters.

APS performance data at three time points have been tabulated and are presented in Table LM6/4.6.1-2. The burnout time presented in this table is the burn time available assuming no RCS usage of APS propellant through the interconnect.

An uncertainty propagation dispersion analysis was conducted using root-sum-squaring techniques to determine APS performance dispersions. The uncertainties associated with the basic parameters defining propulsion system operation are listed in Table LM6/4.6.1-3. The values given in Table LM6/4.6.1-3 have been derived from Rocketdyne and Grumman data by the methods discussed in Reference 2. These values express the uncertainty of the various parameters as 1-sigma at a 50 percent confidence level. These values were used as input to establish the performance dispersions included as part of Table LM6/4.6.1-2. Also presented in Table LM6/4.6.1-2 are average values of the various parameters taken over the duty cycle. The column labeled "Total Standard Deviation" is the standard deviation which must be used in conjunction with the given average values. This total standard deviation is the result of combining the error associated with predicting the parameter (as in Table LM6/4.6.1-2, column labeled "Dispersions/Standard Deviation") with the error resulting from use of a constant (average) value.

The data presented herein are valid for nominal system conditions. The values of propulsion system parameters presented herein do not represent boundary conditions of operation for the system and, therefore, should not be used as limit values.

The recommended values of mixture ratio shift resulting from APS malfunctions are: -0.018; +0.010 mixture ratio units from the nominal.

Volume II LM Data Book
Subsystem Performance Data - Propulsion - APS

References

1. CSM/LM Spacecraft Operational Data Book, Volume III, Mass Properties, SNA-8-D-027(III) REV 1, Amendment 62, 6 June 1969.

2. "Propulsion Systems Dispersion Analysis and Optimum Propellant Management," TRW Technical Report 11176-H060-R0-00, R. K. M. Seto, 28 October 1968.

Table LM6/4.6.1-1

LM-6 APS Engine and Feed System Physical Characteristics

<u>Engine</u>[1]	
Engine No.	Rocketdyne S/N 0001C
Injector No.	Rocketdyne S/N 4097716
Initial Chamber Throat Area (in^2)	16.358
Nozzle Exit Area (in^2)	748.959
Initial Expansion Ratio	45.785
Injector Resistance (lb_f-sec^2/lb_m-ft^5)@ time zero and 70°F	
Oxidizer	12832.
Fuel	20646.
<u>Feed System</u>	
Total Volume (Pressurized, Check Valves to engine interface)(ft^3) [2]	
Oxidizer	36.94
Fuel	37.02
Resistance, Tank Bottom to Engine Interface (lb_f-sec^2/lb_m-ft^5) at 70°F[3]	
Oxidizer	2396.
Fuel	4008.

[1] Rocketdyne Log Book, "Acceptance Test Data Package for Rocket Engine Assembly-Ascent LM-Part No. RS000580-001-00, Serial No. 0001," 30 August 1968.

(2) Per telecon P. E. Cota, MSC Propulsion, 1 August 1969.

(3) Per telecon L. Rothenberg, GAC Propulsion, 24 July 1969.

Table LM6/4.6.1-2 Mission H1 APS Preflight Performance Prediction Summary

PARAMETER	NOMINAL PERFORMANCE			DISPERSION	AVERAGE VALUES	
	Start of Burn T = 10 secs	"Mid-Tank" T = 222 secs	End of Burn T = 461.8 secs	Standard Deviation (1σ)	Integrated Average	Total Standard Deviation (1)
Specific Impulse (ISP), lb_f-sec/lb_m	309.5	309.7	309.1	1.213	309.5	1.28
Thrust (FVAC), lb_f	3495.	3465.	3461.	38.3	3470.	40.25
Mixture Ratio (MR)	1.611	1.605	1.600	.0094	1.605	.0100
Chamber Pressure (PC), psia	123.0	123.5	122.1	--	123.2	--
Oxidizer Flowrate (WDTOE), lb_m/sec	6.968	6.894	6.891	--	6.907	--
Fuel Flowrate (WDTFE), lb_m/sec	4.326	4.295	4.308	--	4.303	--
Usable Oxidizer (WOX), lb_m	3154.	1686.	0.	--	--	--
Usable Fuel (WFL), lb_m	1969.	1056.	10.	--	--	--
ΔV (DVTP), ft/sec	106.	2655.	6617.	--	--	--

(1) Note that the dispersions in this column are for the average values only.

TABLE LM6/4.6.1-3

LM-6 APS UNCERTAINTY DISPERSIONS

PARAMETER	STANDARD DEVIATION	STANDARD DEVIATION (%)
Characteristic Exhaust Velocity (C*), ft/sec	20.55	0.36
Specific Impulse(I_{sp})*, lb_f-sec/lb_m	1.209	0.39
Mixture Ratio *	0.0089	0.55
Propellant Feed System Oxidizer Resistance, lb_f-sec^2/lb_m-ft^5	9.79	0.35
Propellant Feed System Fuel Resistance, lb_f-sec^2/lb-ft^5	12.80	0.29
Propellant Tank Ullage Pressures, psia	1.3	0.72
Propellant Tank Ullage ΔP, psia	0.167	----
Propellant Bulk Temperatures, °F	1.7	2.43
Propellant Bulk ΔT, °F	0.5	----
Ablative Engine Throat Area, in^2	0.222	1.35

*Engine parameters at standard interface conditions

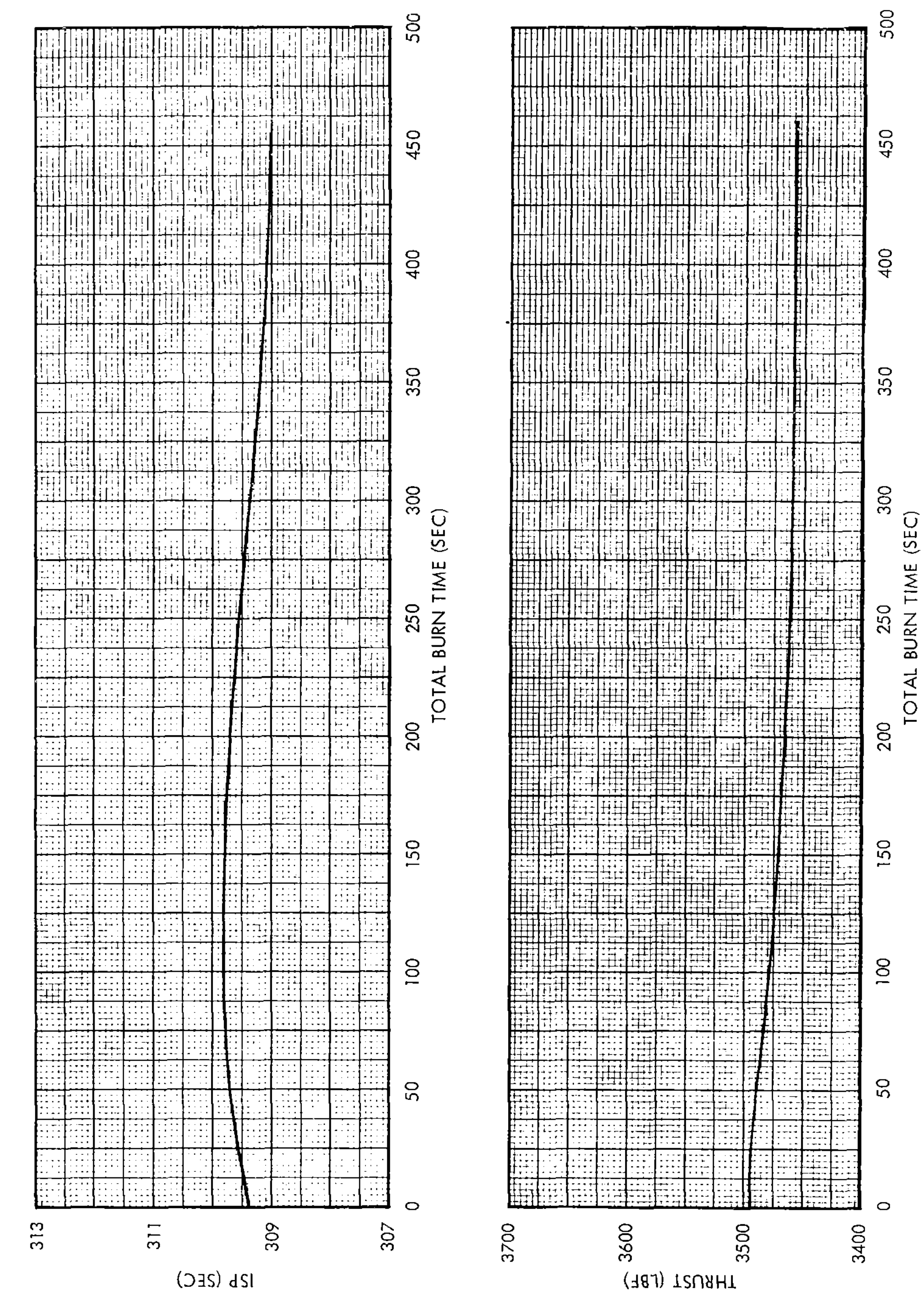

Figure LM6/4.6.1-1 Mission H1 APS Preflight Per‑formance Prediction - Thrust and Specific Impulse Vs. Time

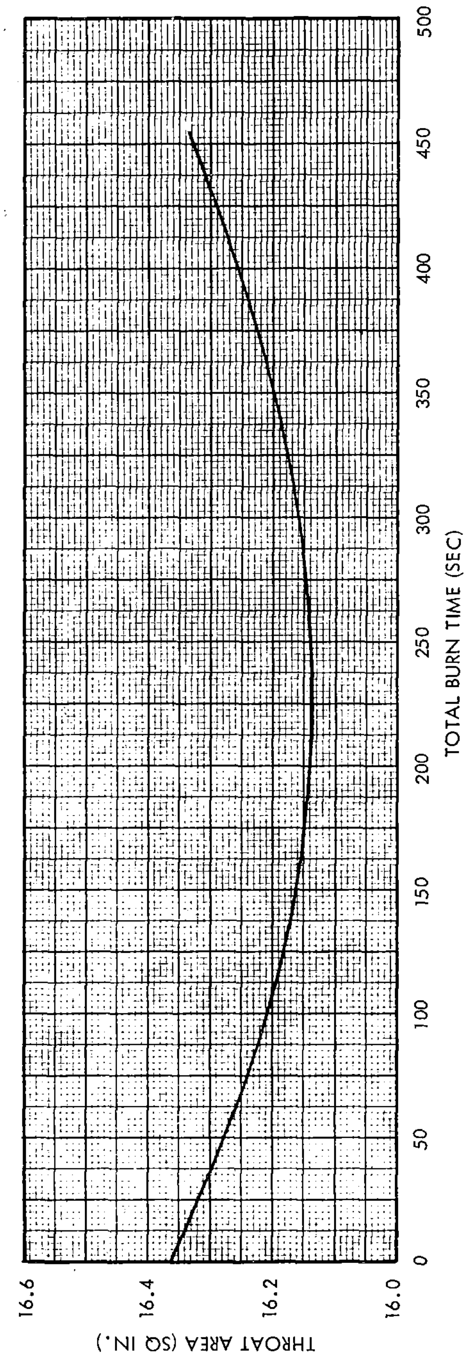

Figure LM6/4.6.1-2 Mission H1 APS Preflight Performance Prediction - Throat Area Vs. Time

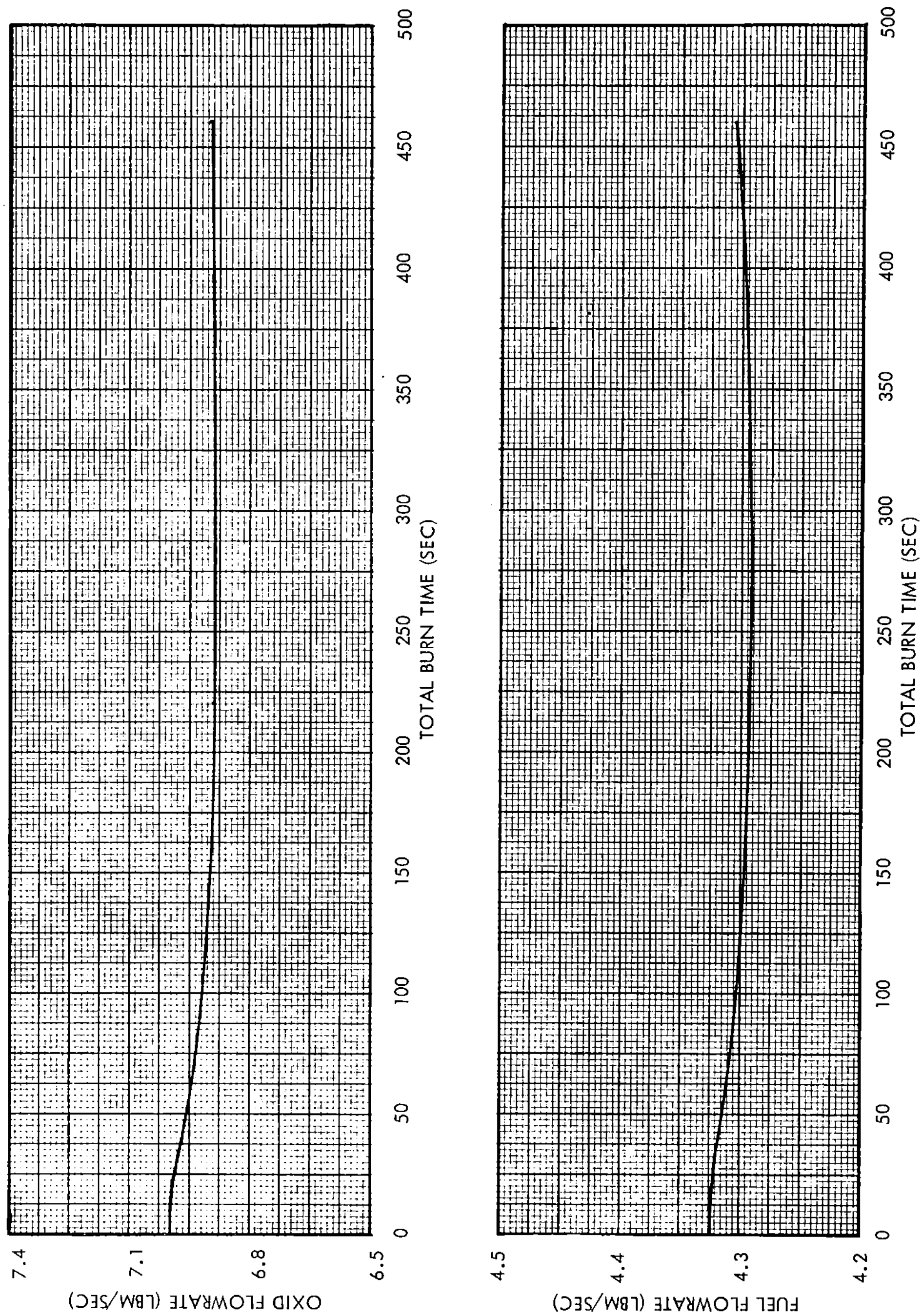

Figure LM6/4.6.1-3 Mission H1 APS Preflight Performance Prediction - Oxidizer and Fuel Flowrates Vs. Time

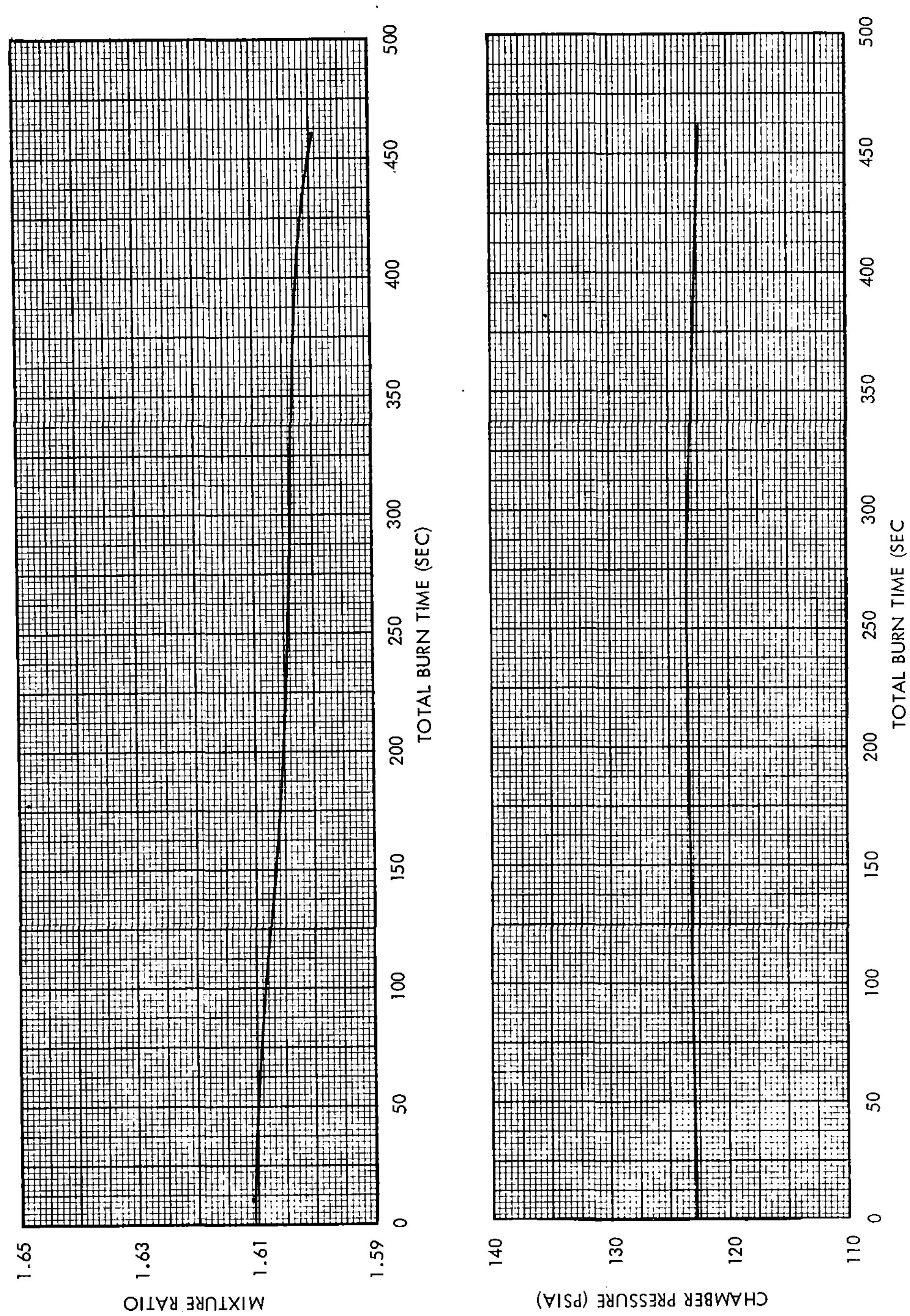

Figure LM6/4.6.1-4 Mission H1 APS Preflight Performance Prediction - Chamber Pressure and Mixture Ratio Vs. Time

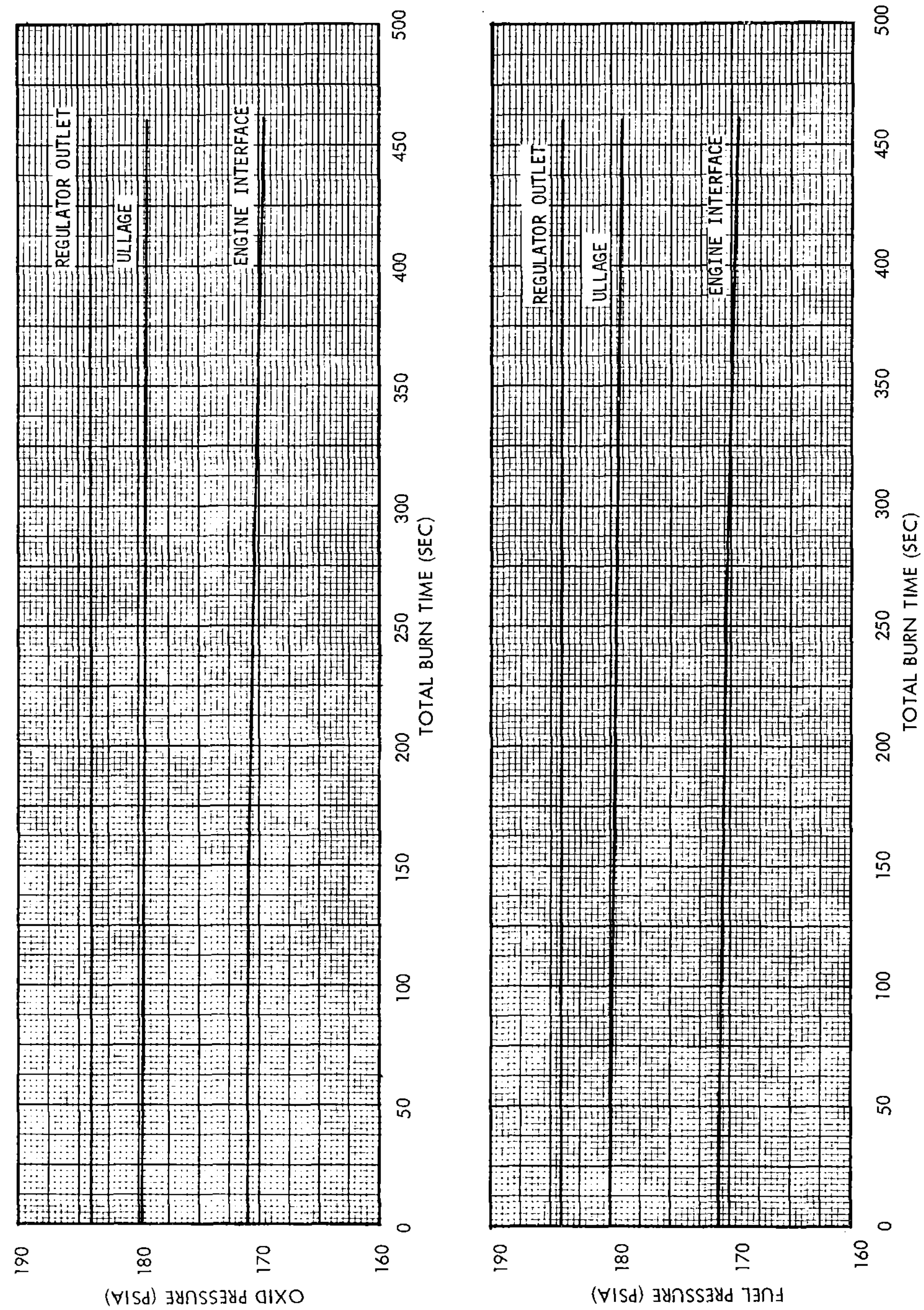

Figure LM6/4.6.1-5 Mission H1 APS Preflight Performance Prediction - Fuel and Oxidizer System Pressures Vs. Time

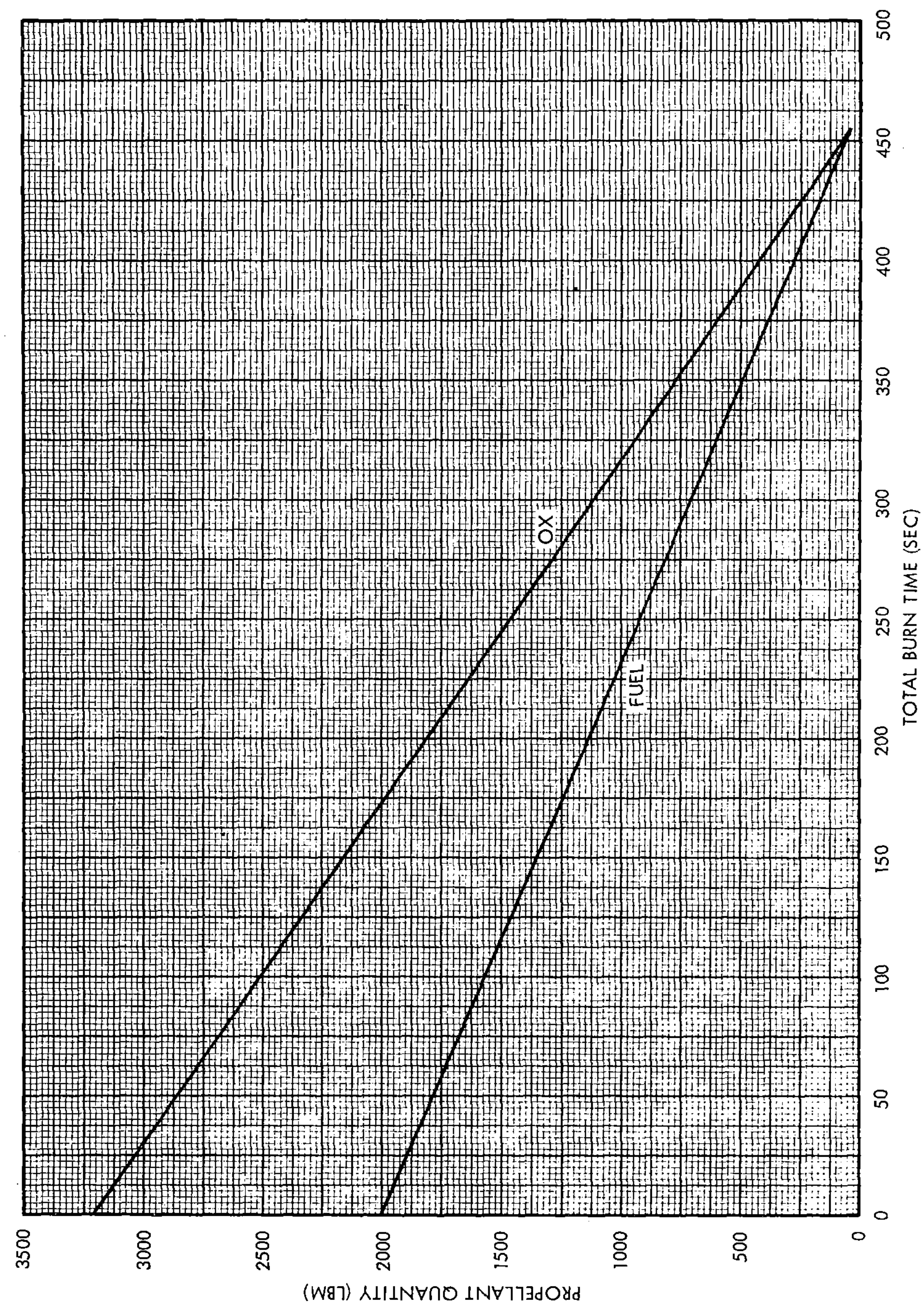

Figure LM6/4.6.1-6 Mission H1 APS Preflight Performance Prediction - Propellant Quantities Vs. Time

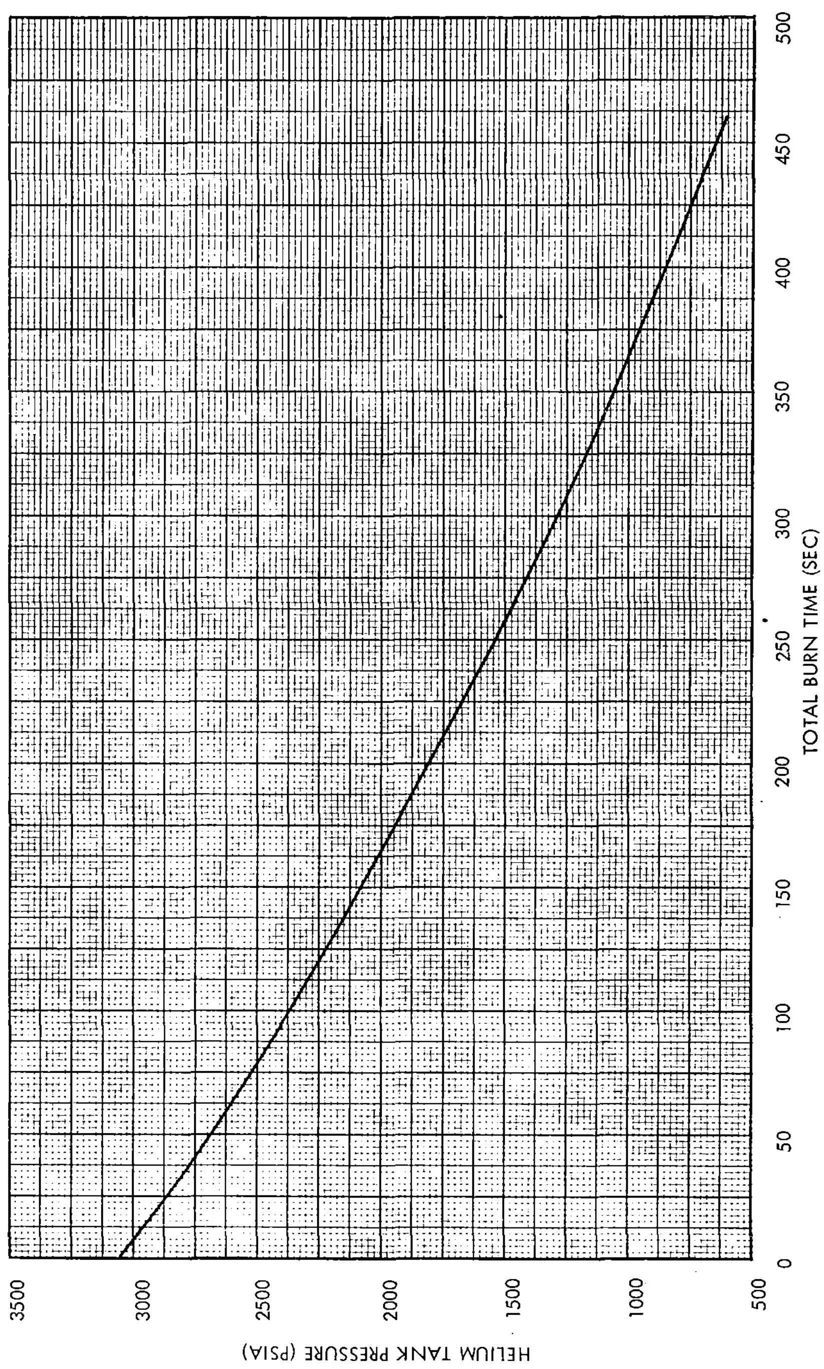

Figrue LM6/4.6.1-7 Mission H1 APS Preflight Performance Prediction - Helium Tank Pressure Vs. Time

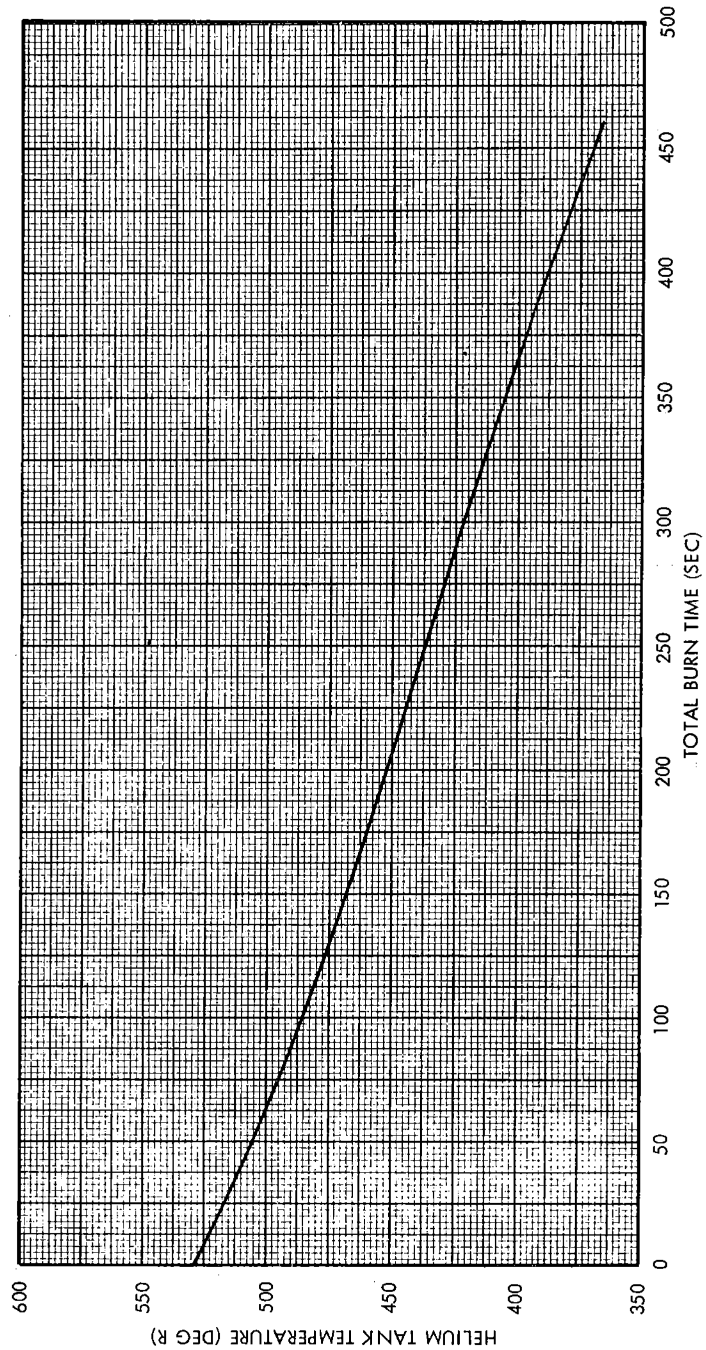

Figure LM6/4.6.1-8 Mission H1 APS Preflight Performance Prediction - Helium Tank Temperature Vs. Time

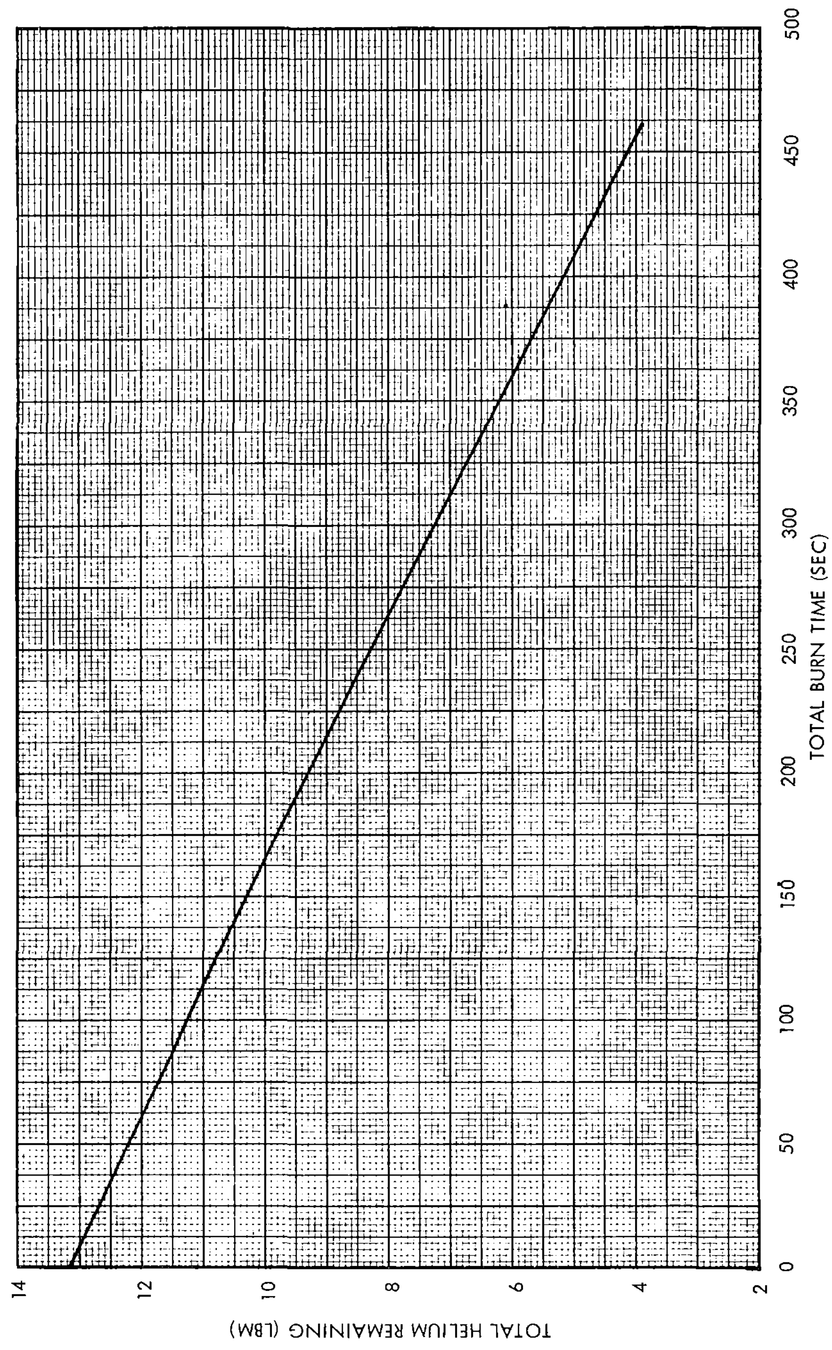

Figure LM6/4.6.1-9 Mission H1 APS Preflight Performance Prediction - Total Helium Remaining Vs. Time

LM6/4.6.8 Thrust Vector Change With Burn Time

The initial thrust vector displacement on engine serial number 0001C is Z = -0.029 inches, Y = -0.025 inches.

LM6/4.6.9 Preflight Thermal Analysis of APS

Figures LM6/4.6.9-1 through LM6/4.6.9-6 document the LM-6 preflight thermal analysis of the APS. Figures LM6/4.6.9-1 through LM6/4.6.9-3 give the predicted temperature response of the APS engine mounts, valve package and injector, respectively. Figures LM6/4.6.9-4 and LM6/4.6.9-5 give the pressure and temperature response of the APS helium bottle as a function of time after an APS burn. Finally, Figures LM6/4.6.9-6 and LM6/4.6.9-7 give the bulk fuel and oxidizer temperature as a function of elapsed time during the mission.

Propellant valve temperature is based on analysis with very little experimental verification. It is recommended that a 25 percent margin, (based upon the delta between start temperature and any point on the curve) for uncertainties in the analysis, be added to the temperature rise shown in Figure LM6/4.6.9-2.

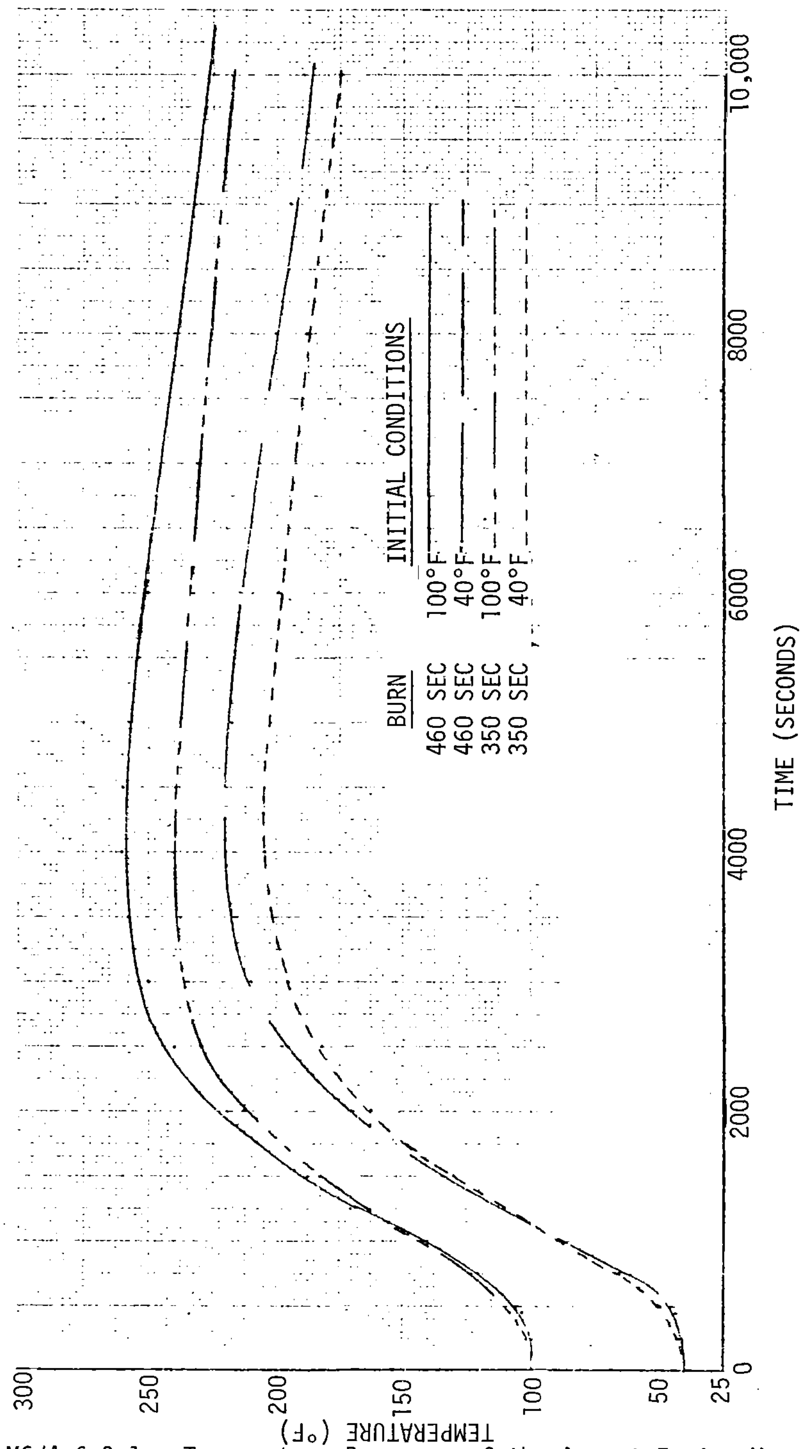

Figure LM6/4.6.9-1. Temperature Response of the Ascent Engine Mounts as a Function of Time Past Engine Ignition

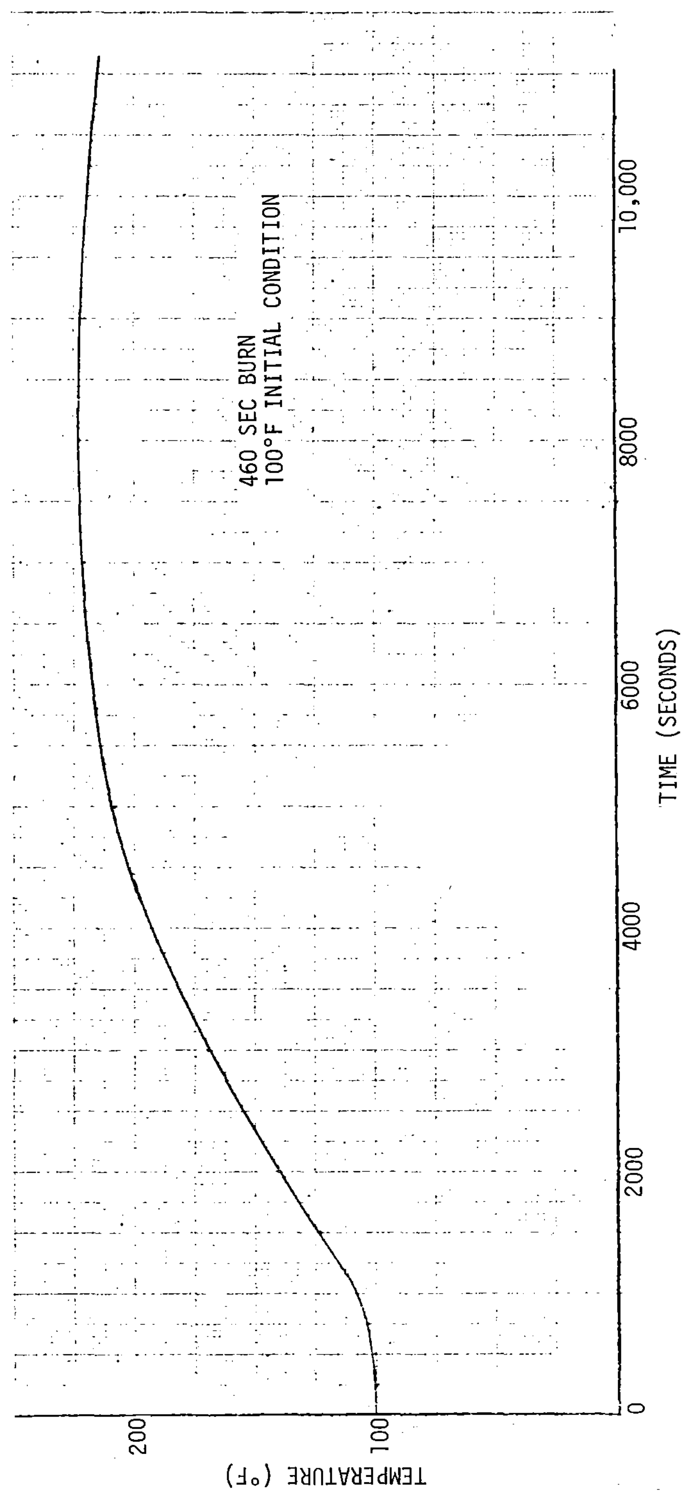

Figure LM6/4.6.9-2. Temperature Response of the Ascent Engine Valve Package as a Function of Time Past Engine Ignition

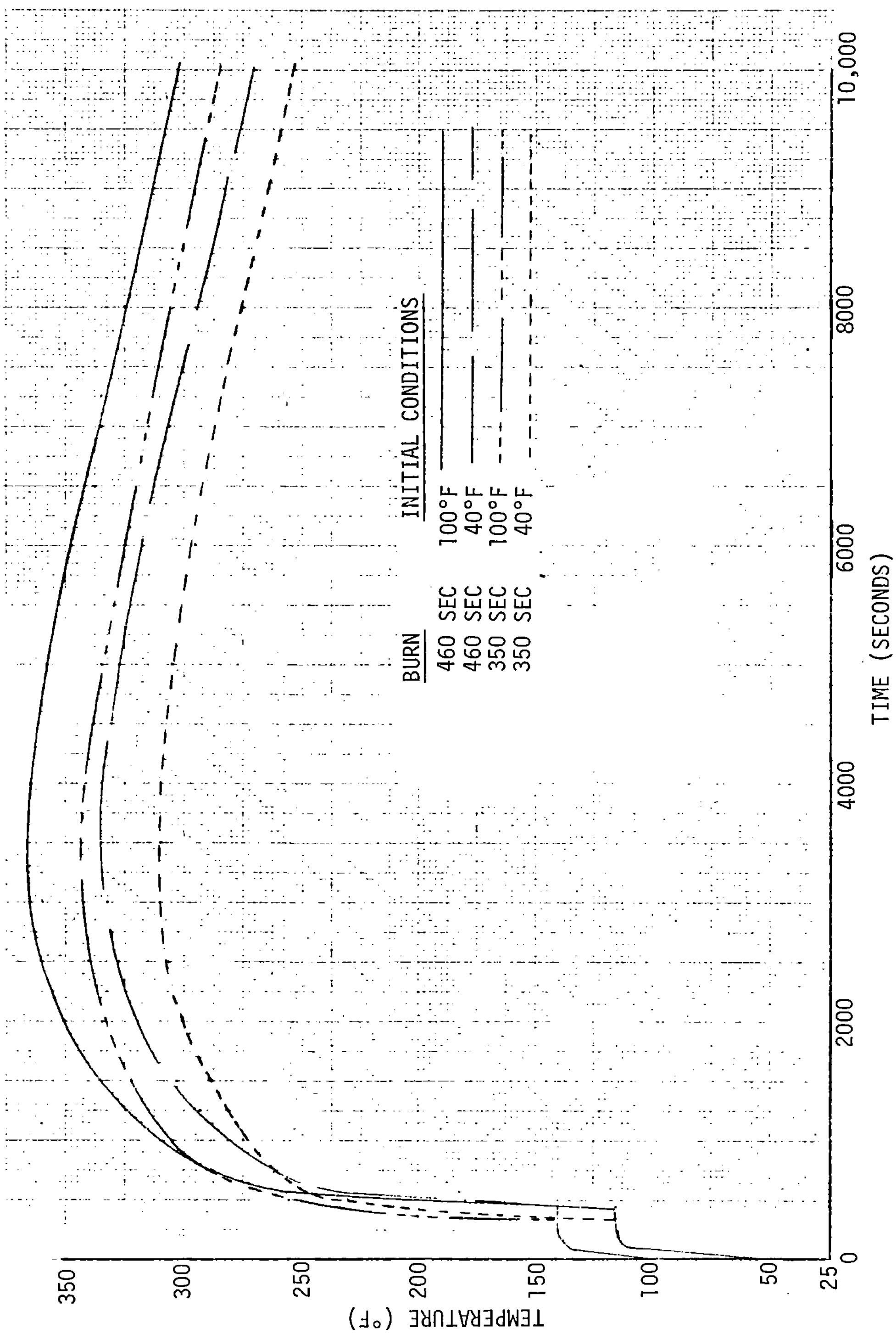

Figure LM6/4.6.9-3. Temperature of Ascent Engine Injector as a Function of Time Past Engine Ignition

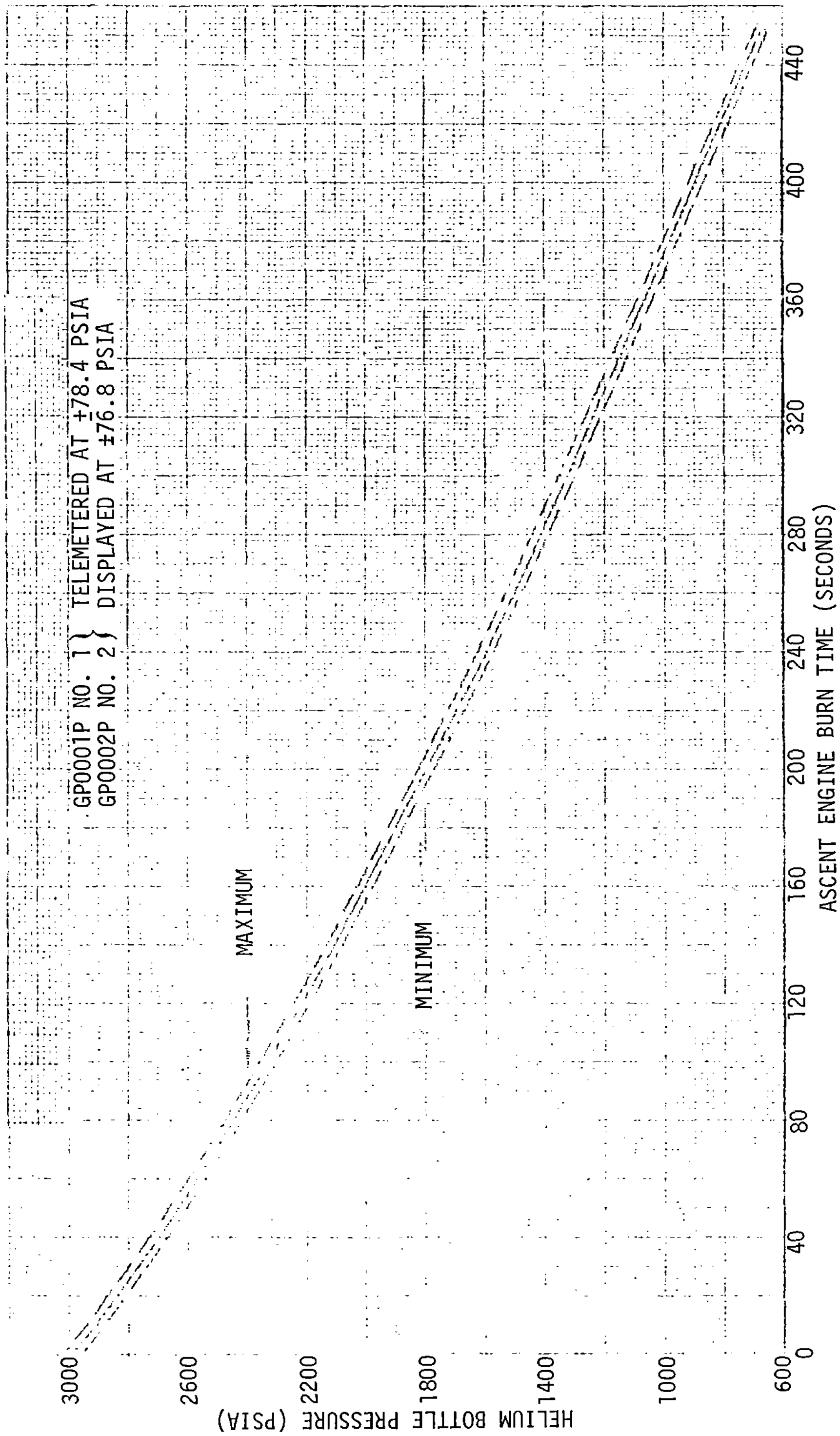

Figure LM6/4.6.9-4 APS Helium Bottle Pressure Vs. Ascent Engine Burn Time

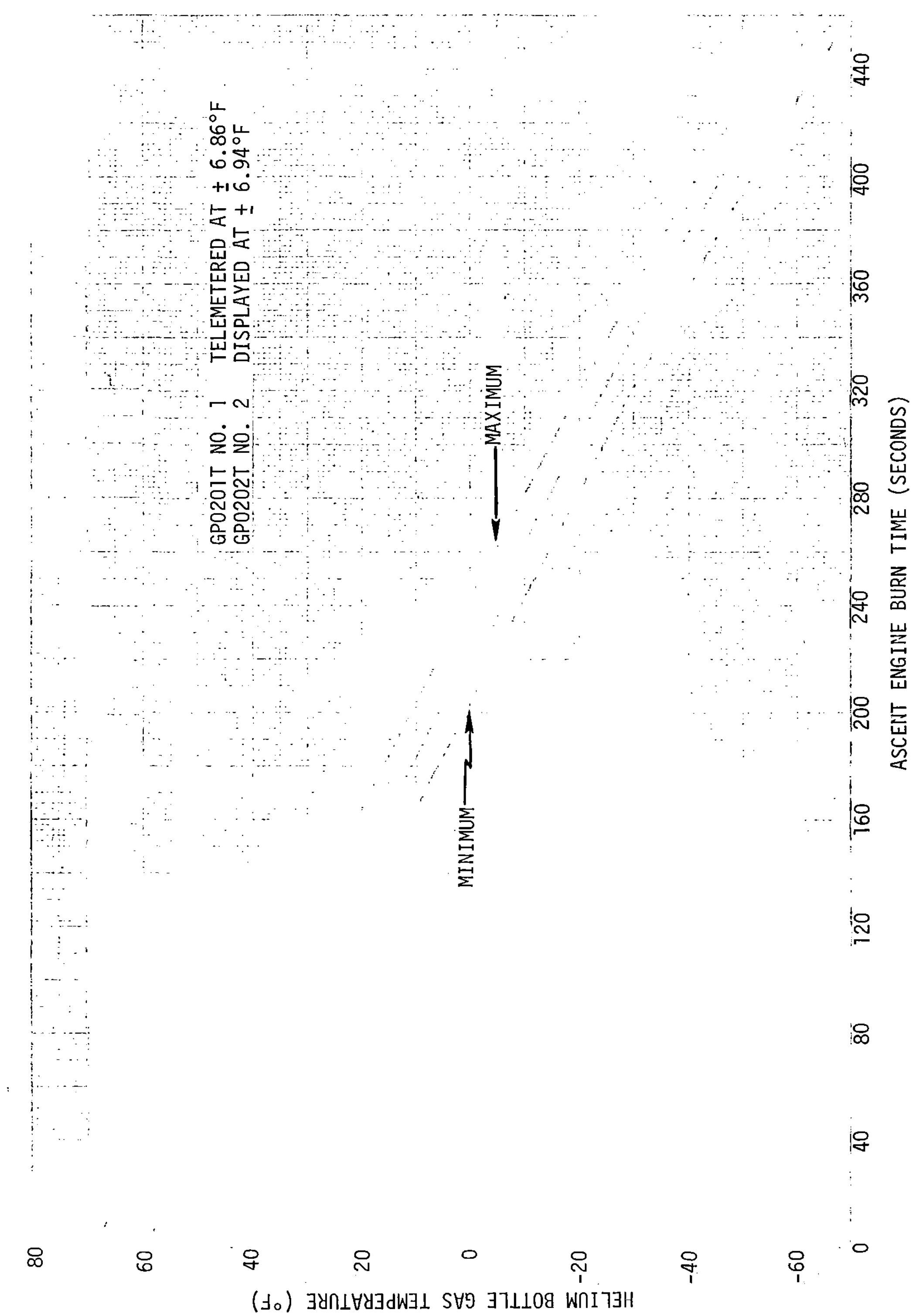

Figure LM6/4.6.9-5. APS Helium Bottle Gas Temperature Vs Ascent Engine Burn Time

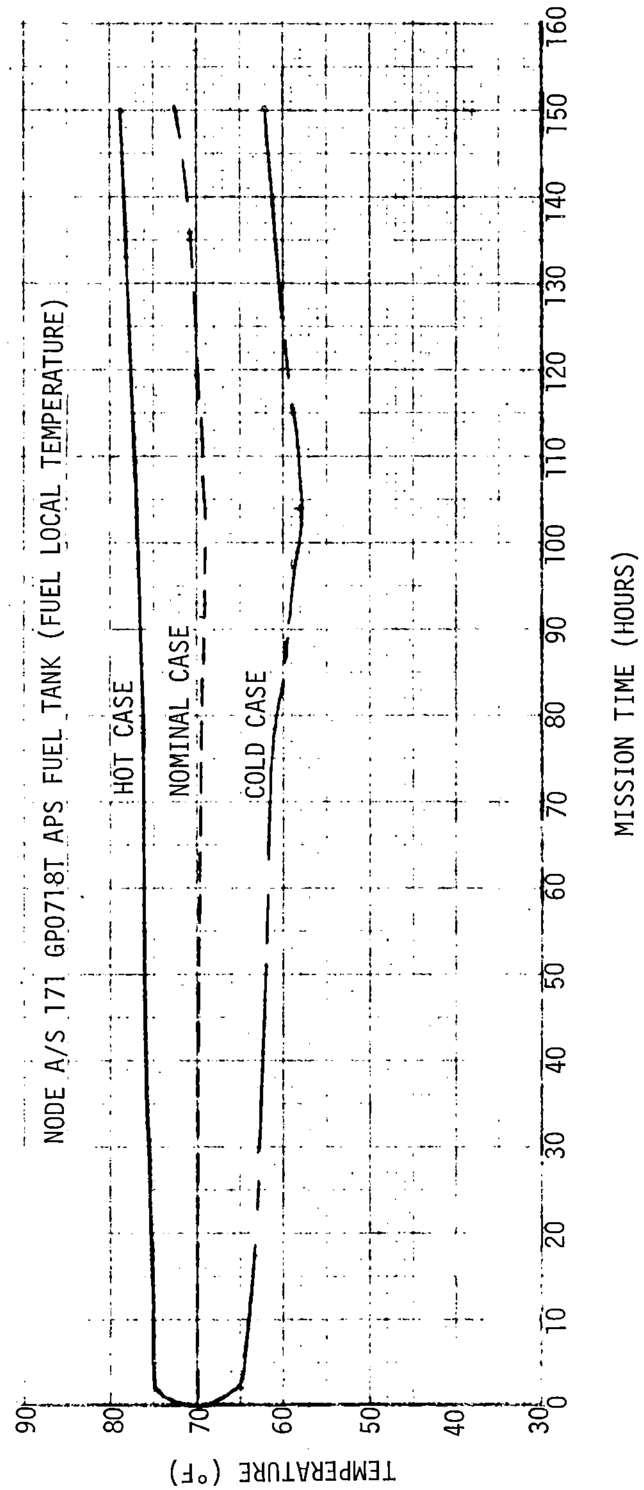

Figure LM6/4.6.9-6. Mission H Predicted Thermocouple Response
Ascent Stage/Descent Stage

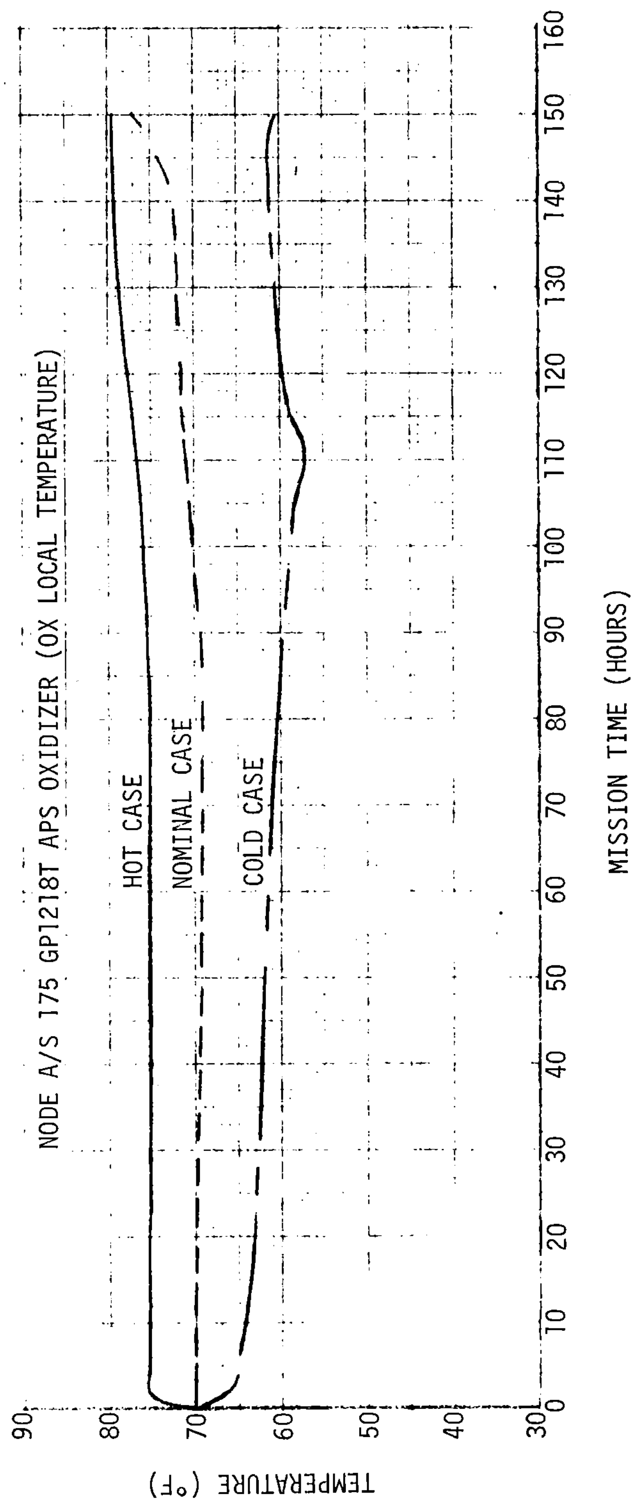

Figure LM6/4.6.9-7. Mission H Predicted Thermocouple Response Ascent Stage/Descent Stage

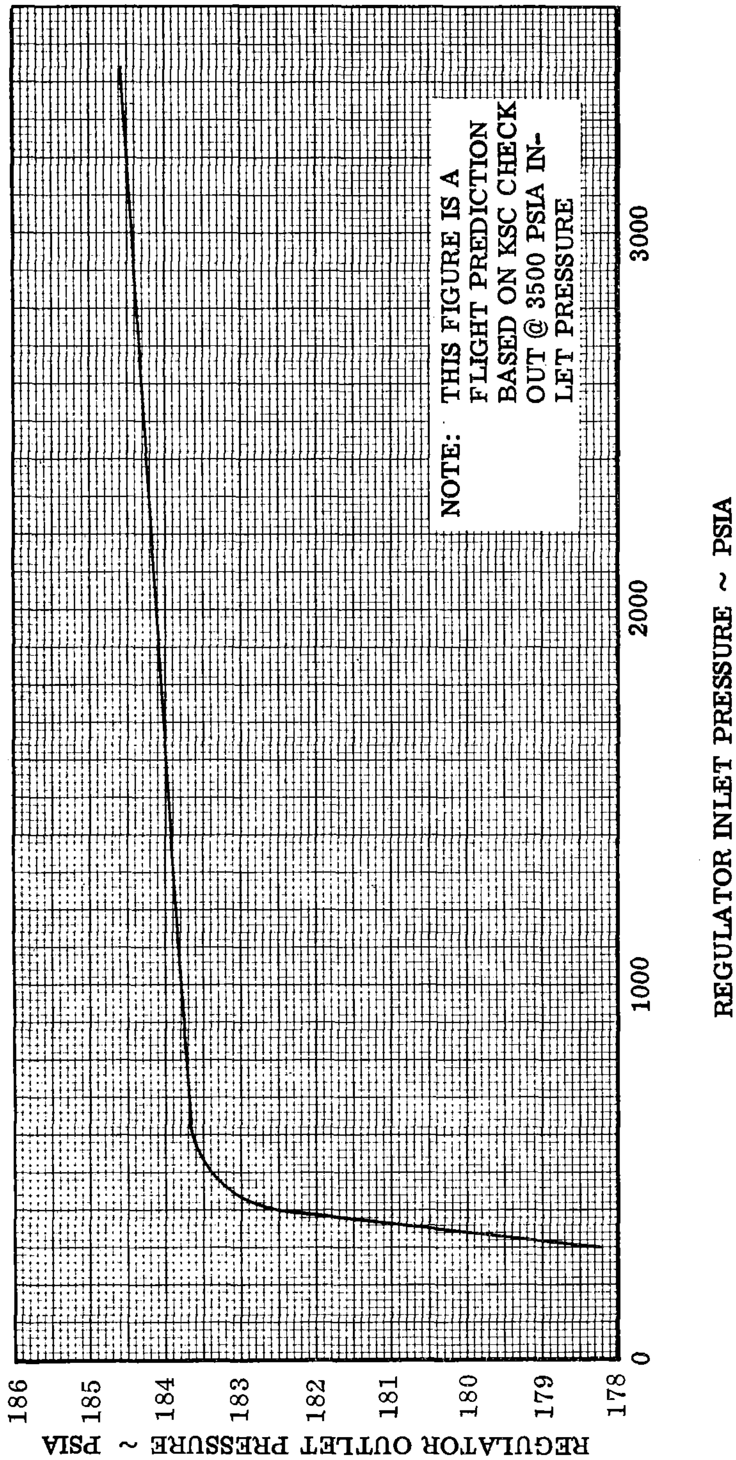

Figure LM6/4.6.12-1. Ascent Engine Regulator Performance

LM6/4.7.1 Mission H-1 (LM-6) DPS Preflight Analysis (NASA DATA SOURCE)

The data presented herein are valid only for the system at nominal conditions and do not represent the boundary conditions of operation for the system. Therefore, these values should not be used as limit values.

The nominal mission duty cycle for the Mission H-1/LM-6 DPS is presented in Figure LM6/4.7.1-1. The spacecraft weight and propellant loading used in the simulation are given in Table LM6/4.7.1-1. Descent engine and feed system physical characteristics are shown in Table LM6/4.7.1-2.

It should be noted that all performance parameters presented are for DPS operation only, and do not include RCS contributions to thrust or velocity gain. The predicted RCS propellant usage was simulated during the burns as a weight change.

The helium regulator characteristics used to establish the DPS propellant tank ullage pressures were derived from GAEC PIT data. Propellant temperatures measured during Missions F and G were assumed to be representative of those to be expected during Mission H-1.

A summary of the Mission H-1 (LM-6) performance prediction is given in Table LM6/4.7.1-3 and Figures LM6/4.7.1-1 through LM6/4.7.1-9. Figures LM6/4.7.1-10 and LM6/4.7.1-11 present the vehicle and engine related effective specific impulse as functions of burn time. A prediction of the supercritical helium tank pressure profile is presented in Figure LM6/4.7.1-12. The dispersions associated with thrust, specific impulse, and mixture ratio are given in Figures LM6/4.7.1-13 through LM6/4.7.1-15, respectively.

The vehicle effective specific impulse for the descent burn was 300.5 seconds. This value includes the effect of approximately 87 lbm of consumables which are expelled from the spacecraft during the time from PDI to lunar touchdown. The value of the engine effective specific impulse which does not include the effect of the consumables other than propellant was 302.6 seconds. It should be noted that the effective specific impulse is not only a function of engine performance but is dependent on vehicle initial mass, mass changes with time, and velocity requirements. Substantial deviations from the conditions of the simulation will invalidate the use of this effective specific impulse. The 1-sigma variation in effective engine specific impulse is ± 1.97 seconds for the simulation. The effective vehicle mixture ratio is 1.593 and the 1-sigma variation is ± 0.0075.

The LM-6 DPS shutoff valve malfunction characterization data are as follows: an AB valve malfunction will result in shifts of +0.020, -0.93 seconds, and -274 lbf for mixture ratio, specific

LM6/4.7.1 (Continued)

impulse, and thrust, respectively; while a CD valve malfunction will result in shifts of -0.021, -0.78 seconds, and -235 lbf, respectively, for the given parameters. These data are applicable to FTP operation only.

During the nominal mission, the low level sensor should not be activated prior to the nominal touchdown time (680 seconds after descent burn ignition). If the vehicle is hovering the oxidizer low level sensor should be activated at approximately 719 ±3 seconds (assuming nominal CG shifts-see Table LM6/4.7.1-1). The approximate hover time from the low level signal to oxidizer depletion is predicted to be 113 ±3 seconds or 832 ±3 seconds after engine ignition. The dispersion in time is based on the dispersion in the oxidizer level at low level sensor activation (see paragraph LM6/4.7.5).

A docked LM-6 Descent Propulsion System (DPS) burn to propellant depletion simulation was made using the Descent Ascent Monte Carlo Program (DAMP).

The data presented herein are valid only for the systems at nominal conditions and do not represent the boundary conditions of operation for the system. Therefore, these values should not be used as limit values.

It was assumed that at engine ignition, the LM was docked with the CSM. The mission duty cycle consisted of a minimum throttle (approximately 12.2% of full thrust) segment of 26 seconds with the remainder of the burn at the Fixed Throttle Position (FTP). The burn was terminated when either the usable oxidizer or fuel was depleted.

The initial spacecraft weight was assumed to be 70,007 lbm with 11,148.0 lbm and 6,943.9 lbm of tanked oxidizer and fuel, respectively. Depletion occurs when the tanked quantities reach 108 lbm for oxidizer or 15 lbm for fuel.

At 573.0 seconds after ignition, fuel depletion occurred with approximately 1.4 lbm of usable oxidizer remaining. The velocity change for the burn was 2905.2 ft/sec. The effective engine specific impulse, which neglects consumables other than propellants that are expelled from the spacecraft during the burn, was 302.64 seconds. The effective vehicle specific impulse was 301.32 seconds. The average mixture ratio was 1.593.

Figures LM6/4.7.1-16 through LM6/4.7.1-24 present DPS engine parameters for the burn.

Chamber pressure versus commanded thrust for zero, nominal, and maximum throat erosion is shown in Figure LM6/4.7.1-25. Chamber pressure versus time for zero, nominal, and maximum throat erosion over the LM-6 duty cycle is shown in Figures LM6/4.7.1-26 through LM6/4.7.1-28, respectively.

LM-6 DESCENT PROPULSION SYSTEM

WEIGHT CHARACTERISTICS[1]

SPACECRAFT WEIGHTS (lbm)

DPS Stage Inert		4604.2
Loaded Propellant		18429.2
DPS Oxidizer	11350.9	
DPS Fuel	7078.3	
Loaded APS Stage and Crew		10933.1
LM Weight at Separation		33966.5

UNUSABLE PROPELLANTS

	Oxidizer	Fuel
TRAPPED PROPELLANT	(60.4)	(35.2)
Fill Lines	0.2	0.1
Engine	12.2	6.4
Balance Lines	11.3	7.3
Branch Lines	17.0	8.0
Common Lines	19.0	8.1
Isolation SQ Bypass and Miscellaneous	0.7	0.7
Heat Exchanger	0.0	4.6
LOST PROPELLANT	(5.2)	(5.7)
Start Transient (Two cycles)	2.6	2.0
Shutdown Transient (Two cycles)	2.6	3.7
RESIDUALS IN TANKS	(120.6)	(23.4)
Tank Wetting	2.0	2.0
Zero-G Can	8.6	5.2
Center of Gravity (Thrust Vector)	75.0	3.0
Unporting Prevention	16.0	10.7
Propellant Vapor	19.0	2.5
PROPELLANT USABLE FOR BURN TO DEPLETION	(-27.5)	(-16.7)
Lines	-27.5	-12.1
Heat Exchange	0.0	-4.6
TOTAL UNUSABLES	158.7	47.6
	206.3	

Note: Unusables are defined as that propellant which is physically unavailable to the engine.

[1]These mass properties were used for the purpose of this analysis. Reference should be made to Volume III, Spacecraft Operational Data Book, for current official mass properties data.

Table LM6/4.7.1-2

LM-6 Descent Propulsion Engine and Feed System Physical Characteristics

ENGINE	
Engine Number	1040
Chamber Throat Area, In^2	54.197[1]
Nozzle Exit Area, In^2	2569.7[4]
Nozzle Expansion Ratio	47.7[4]
Oxidizer Interface to Chamber Resistance at FTP $\frac{lbm\text{-}sec^2}{lbf\text{-}ft^5}$	3960.0[3]
Fuel Interface to Chamber Resistance at FTP $\frac{lbm\text{-}sec^2}{lbf\text{-}ft^5}$	6325.2
Fuel Film Coolant Tapoff Point to Combustion Chamber $\frac{lbm\text{-}sec^2}{lbf\text{-}ft^5}$	465069
FEED SYSTEM	
Oxidizer Propellant Tanks, Total Ambient Volume, Ft^3	126.0[4]
Fuel Propellant Tanks, Total Ambient Volume, Ft^3	126.0[4]
Oxidizer Tank to Interface Resistance, $\frac{lbm\text{-}sec^2}{lbf\text{-}ft^5}$	427.03[2]
Fuel Tank to Interface Resistance, $\frac{lbm\text{-}sec^2}{lbf\text{-}ft^5}$	674.53[2]

[1]TRW No. 01827-6173-R000, TRW LM Descent Engine Serial No. 1040 Acceptance Test Performance Report, Paragraph 6.9, 19 July 1968.

[2]GAEC Cold Flow Tests

[3]TRW No. 4721.3.69-63, LM-6, Engine Serial No. 1040 Descent Engine Characteristic Equations, March 1969

[4]Approximate values.

Table LM6/4.7.1-3. Mission H1 Final DPS Preflight Performance Prediction Summary

Parameter	15 seconds of first burn	Start of second burn	36 seconds of second burn				356 seconds of second burn				396 seconds of second burn	520 seconds of second burn	680 seconds Touchdown
	Nominal Performance	Nominal Performance	Nominal Performance	Standard Deviation (1σ)	Standard Deviation (%)	3σ Minimum	Nominal Performance	Standard Deviation (1σ)	Standard Deviation (%)	3σ Minimum	Nominal Performance	Nominal Performance	Nominal Performance
Throttle Position %	40.68	12.24*	FTP	FTP	FTP	FTP	FTP	FTP	FTP	FTP	56.42	53.78	26.85
ISP	299.82	296.15	304.60	1.345	0.442	300.57	302.33	1.345	0.445	298.30	302.31	301.15	295.13
F	4271	1285	9854	41.8	0.424	9729	9948	45.122	0.454	9813	5924	5647	2819
MR	1.5957	1.6150	1.5940	0.0045	0.282	1.5805	1.5929	0.0045	0.283	1.5794	1.5869	1.5879	1.6032
Pc	45.39	13.65	104.25				99.18				58.84	55.58	27.10
$\dot{W}_O$	8.757	2.679	19.879	0.124	0.624	19.507	20.215	0.135	0.668	19.81	12.021	11.521	5.883
$\dot{W}_F$	5.488	1.659	12.471	0.079	0.633	12.473	12.691	0.083	0.654	12.44	7.576	7.256	3.670
WO	11257	11135	10875	11.83	0.109	10840	4455	47.08	1.057	4314	3714	2200	957
WF	7023	6946	6783	7.38	0.109	6761	2755	29.77	1.081	2666	2289	1334	556

*Throttle Command Voltage = 2.600 VDC

Table LM6/4.7.1-3. (Continued)
Mission H1 Final DPS Preflight Performance Prediction Summary (Performance During Hover-To-Depletion)

Parameter	756 seconds of second burn	832 seconds Depletion (Ox)
	Nominal Performance	Nominal Performance
Throttle Position %	25.70	24.60
ISP	294.68	294.24
F	2698	2583
MR	1.6039	1.6046
Pc	25.58	24.16
$\dot{W}o$	5.639	5.408
$\dot{W}f$	3.516	3.370
WO	515.64	95.69
WF	281.15	19.38

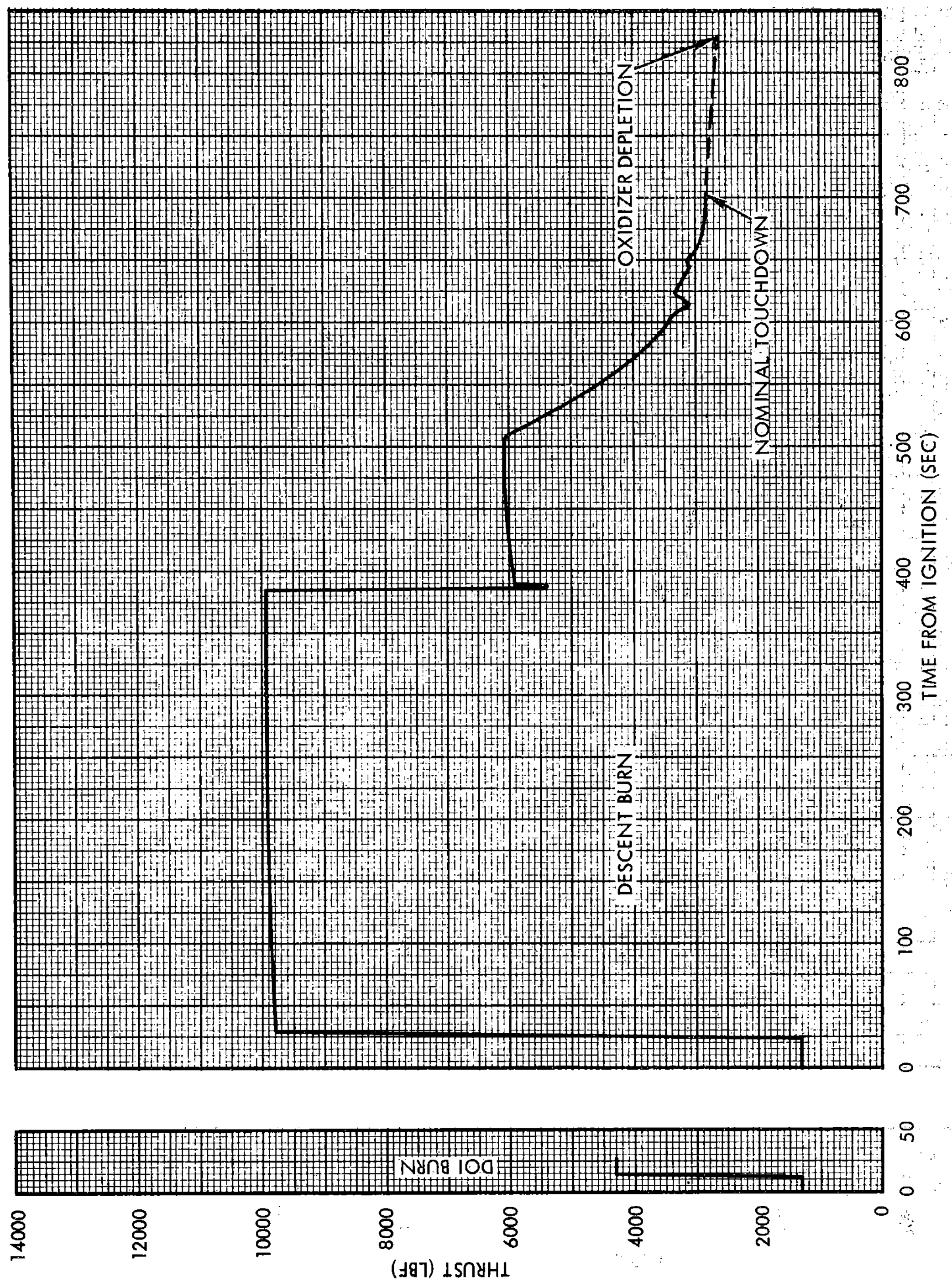

Figure LM6/4.7.1-1. Mission H1 Final DPS Preflight Performance Prediction-Thrust Vs. Time

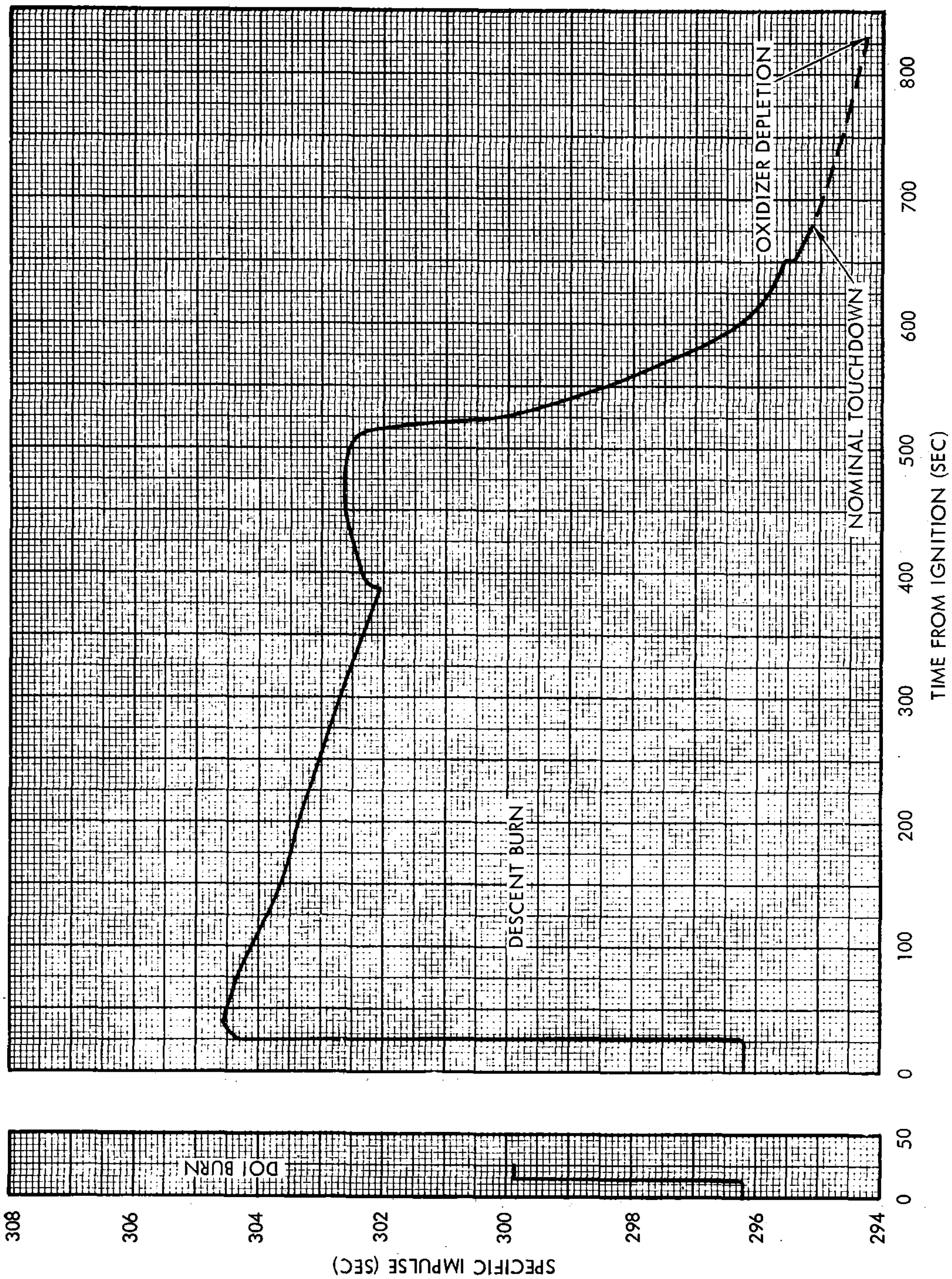

Figure LM6/4.7.1-2. Mission H1 Final DPS Preflight Performance Prediction-Specific Impulse Vs. Time

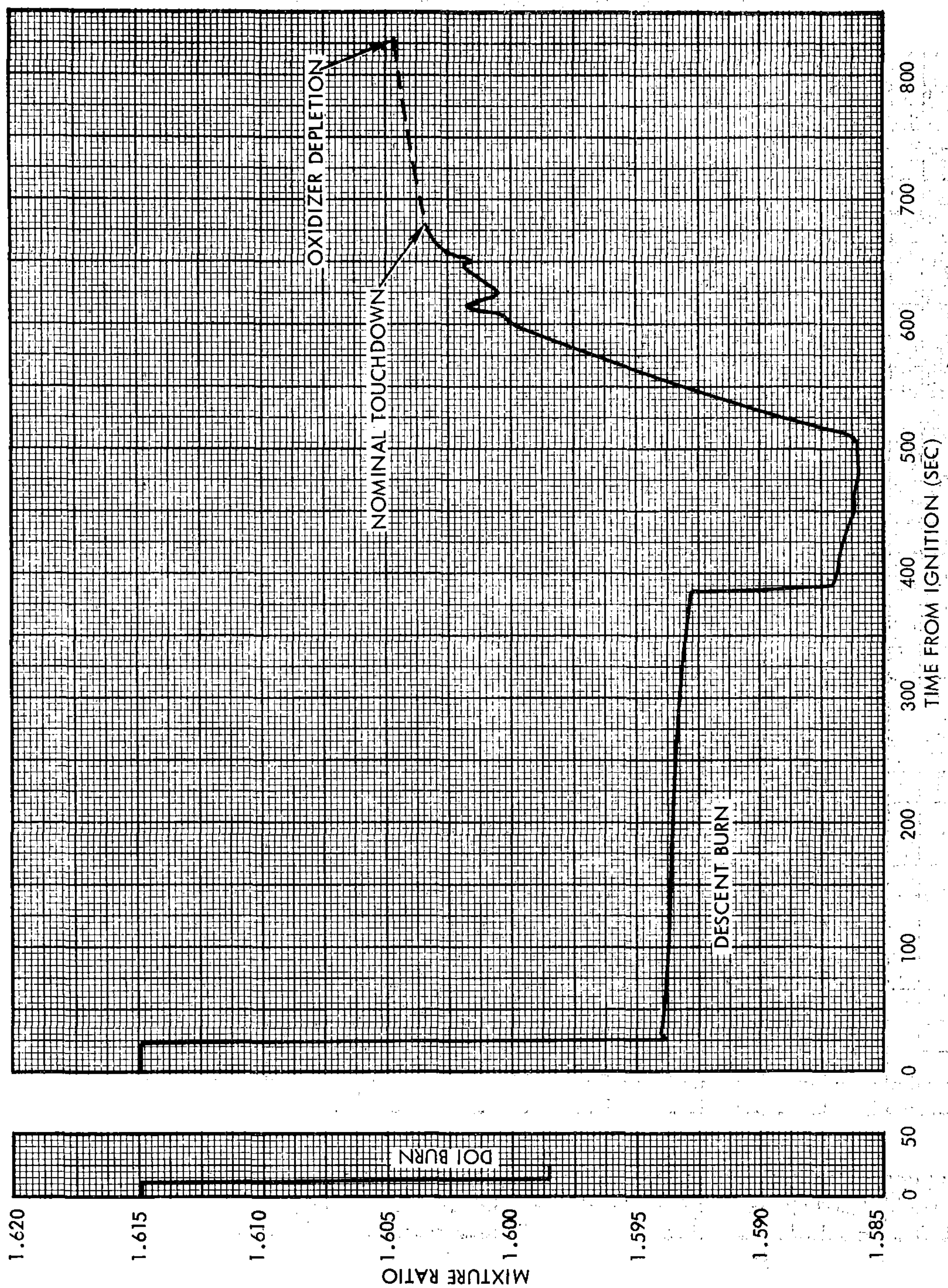

Figure LM6/4.7.1-3. Mission H1 Final DPS Preflight Performance Prediction-Mixture Ratio Vs. Time

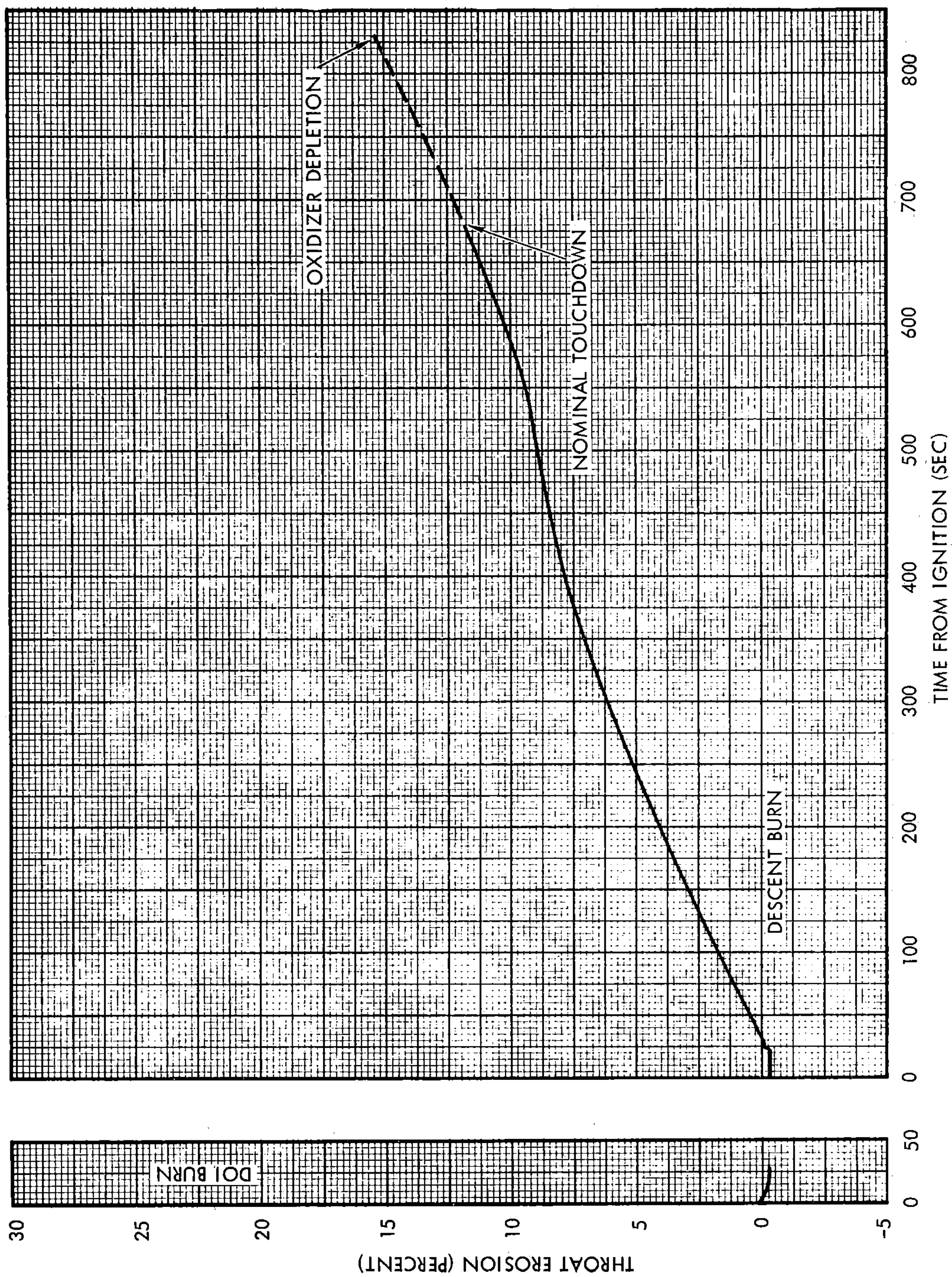

Figure LM6/4.7.1-4. Mission H1 Final DPS Preflight Performance Prediction-Throat Erosion Vs. Time

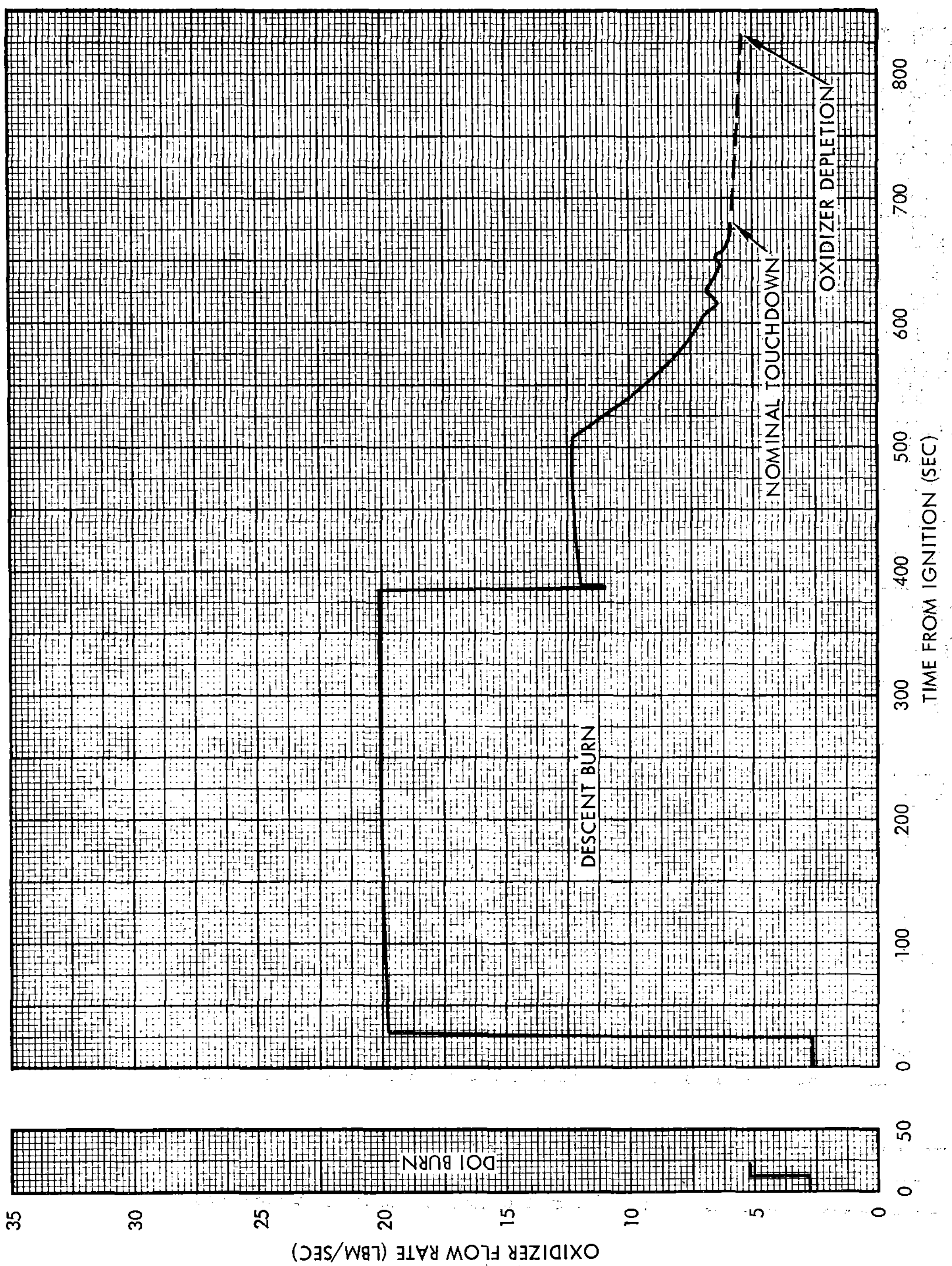

Figure LM6/4.7.1-5. Mission H1 Final DPS Preflight Performance Prediction-Oxidizer Flow Rate Vs. Time

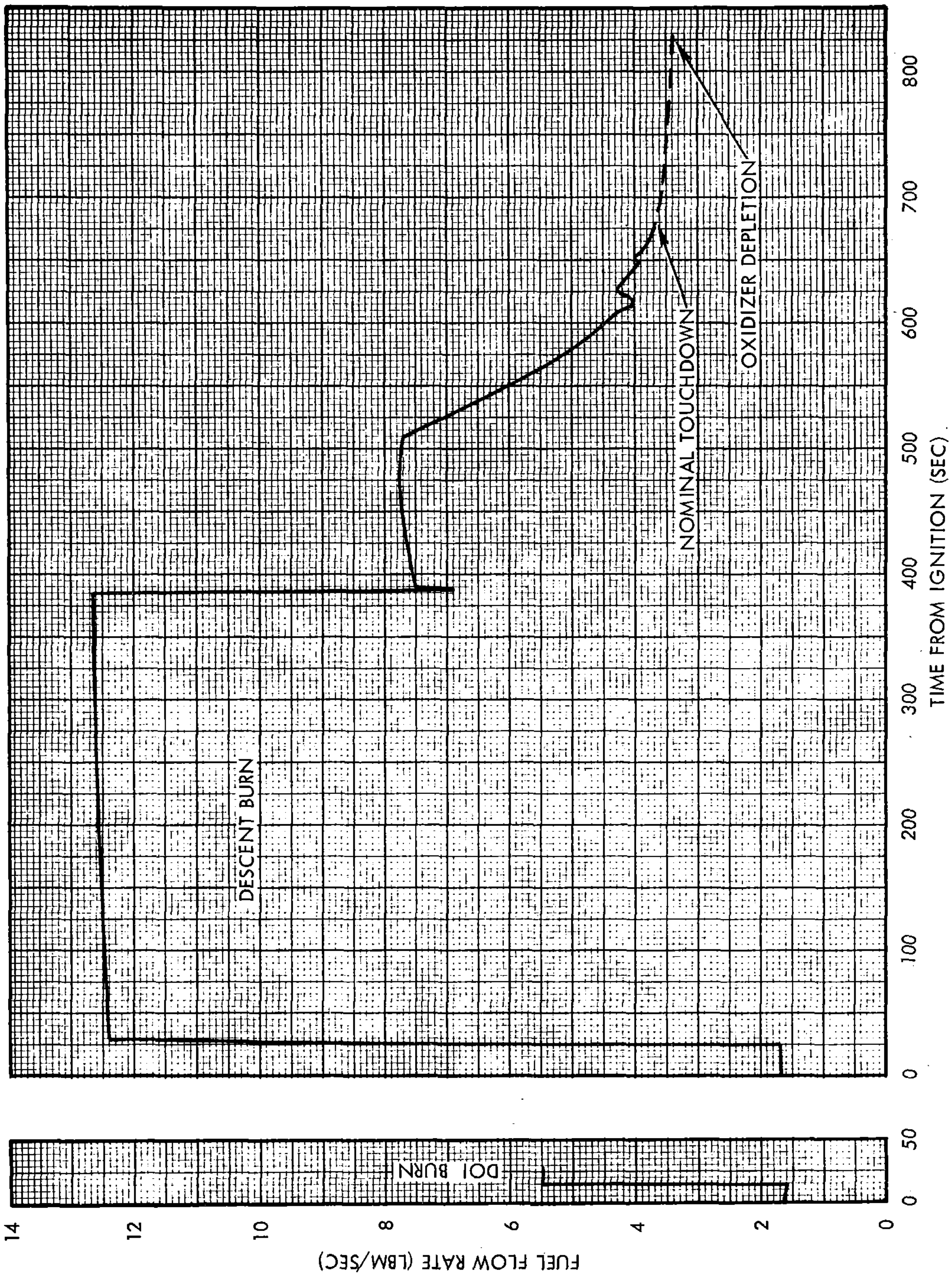

Figure LM6/4.7.1-6. Mission H1 Final DPS Preflight Performance Prediction-Fuel Flow Rate Vs. Time

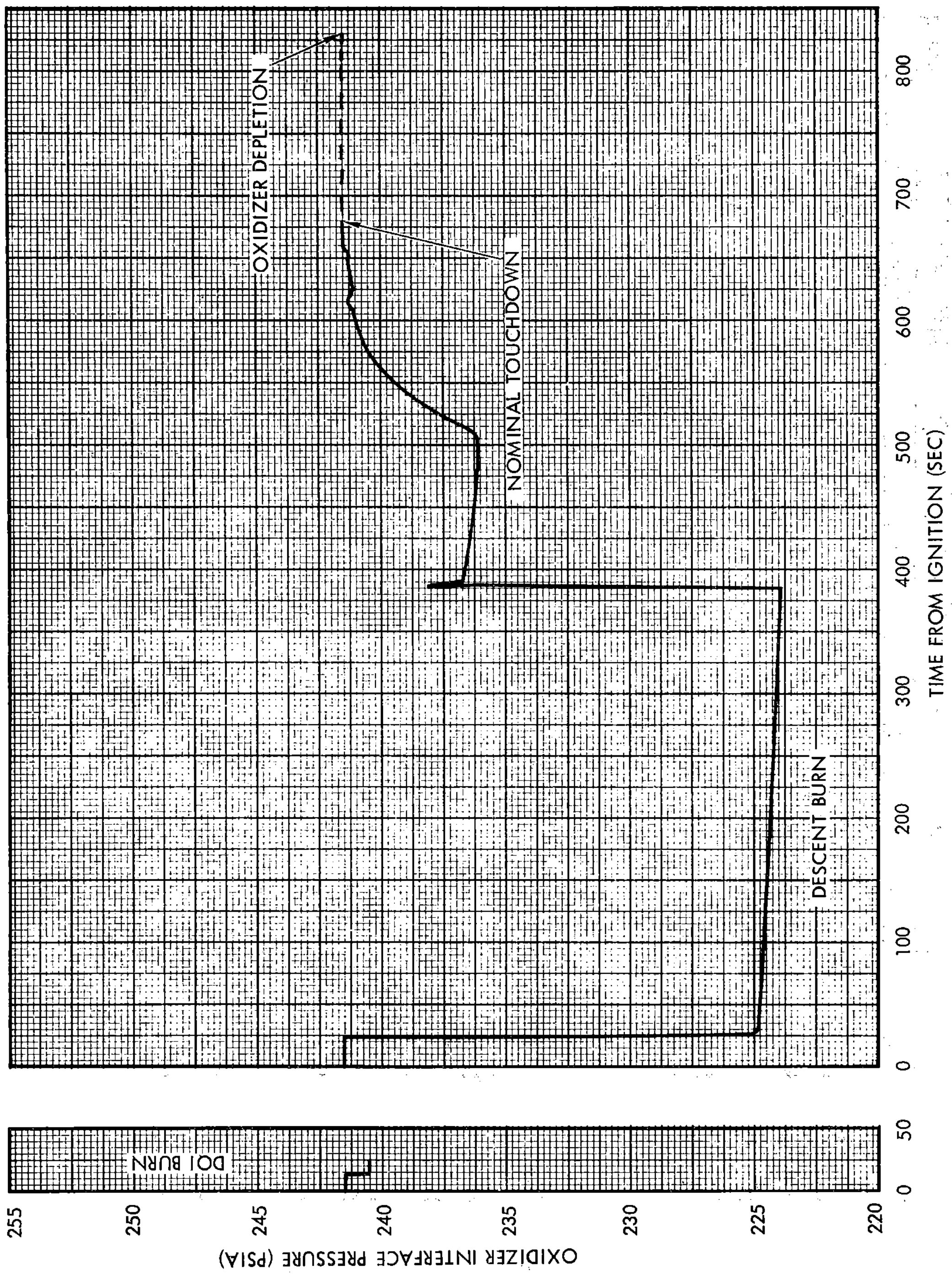

Figure LM6/4.7.1-7. Mission H1 Final DPS Preflight Performance Prediction-Oxidizer Interface Pressure Vs. Time

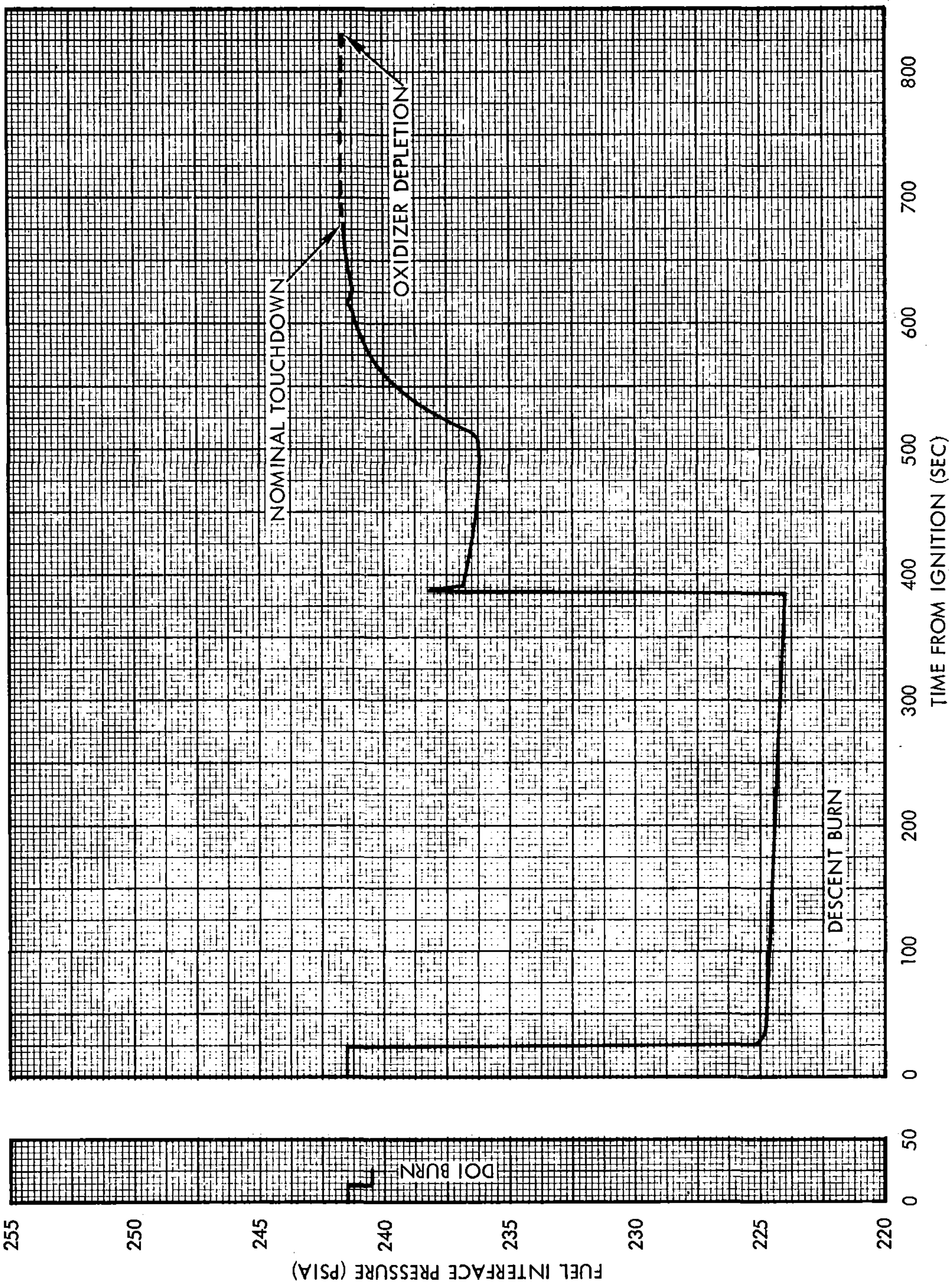

Figure LM6/4.7.1-8. Mission H1 Final DPS Preflight Performance Prediction-Fuel Interface Pressure Vs. Time

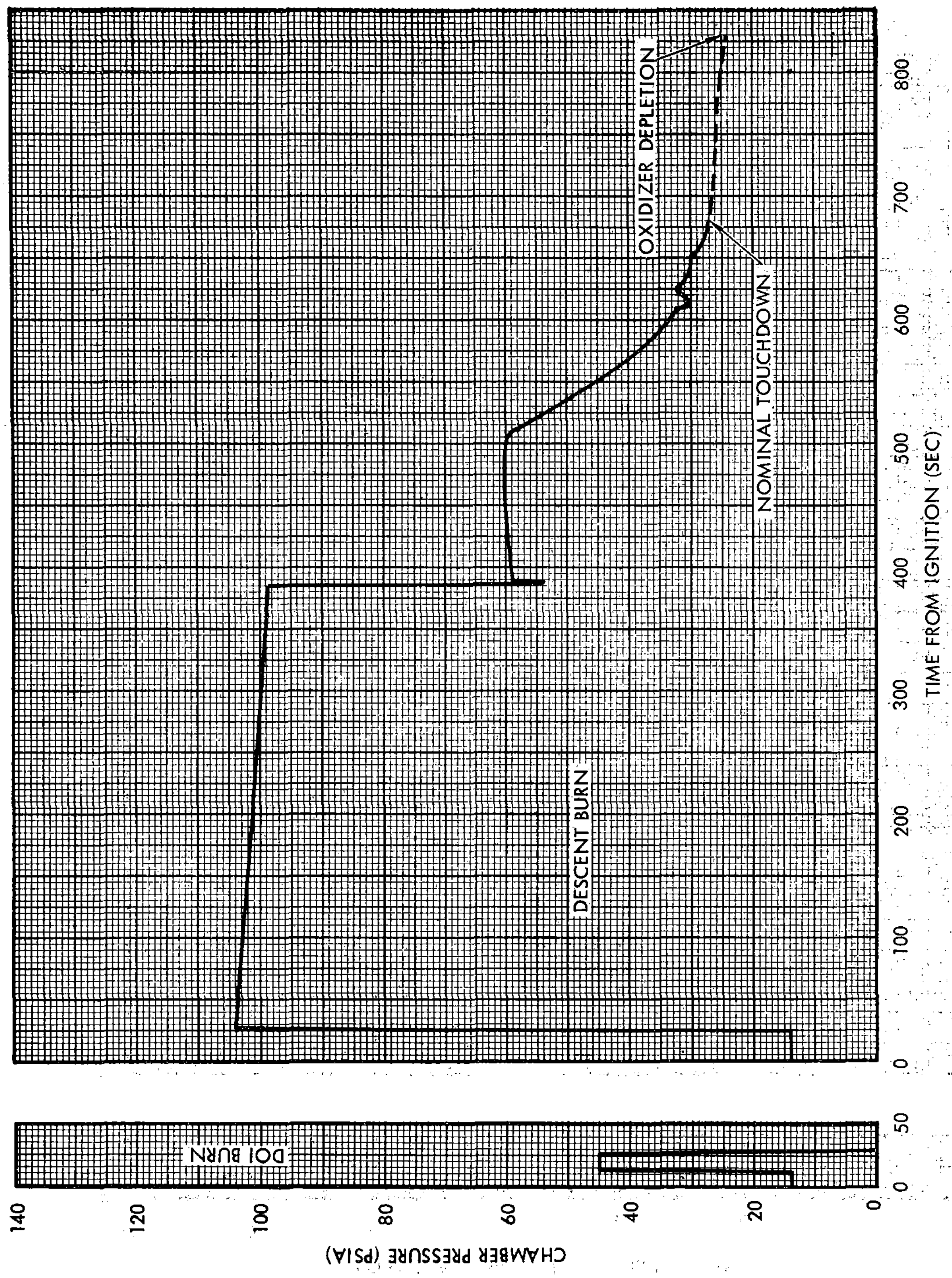

Figure LM6/4.7.1-9. Mission H1 Final DPS Preflight Performance Prediction-
Chamber Pressure Vs. Time

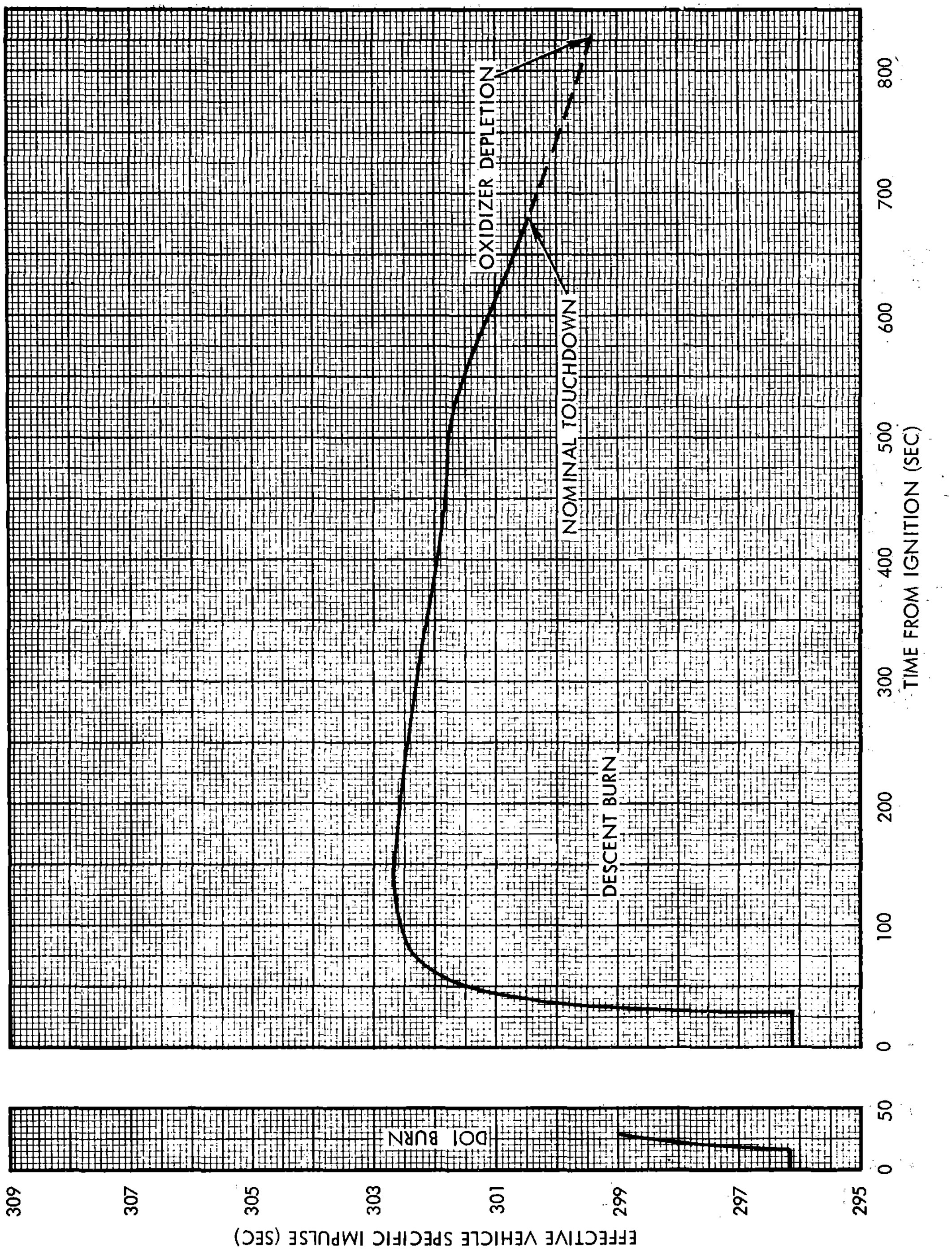

Figure LM6/4.7.1-10. Mission H1 Final DPS Preflight Performance Prediction-Effective Vehicle Specific Impulse Vs. Time

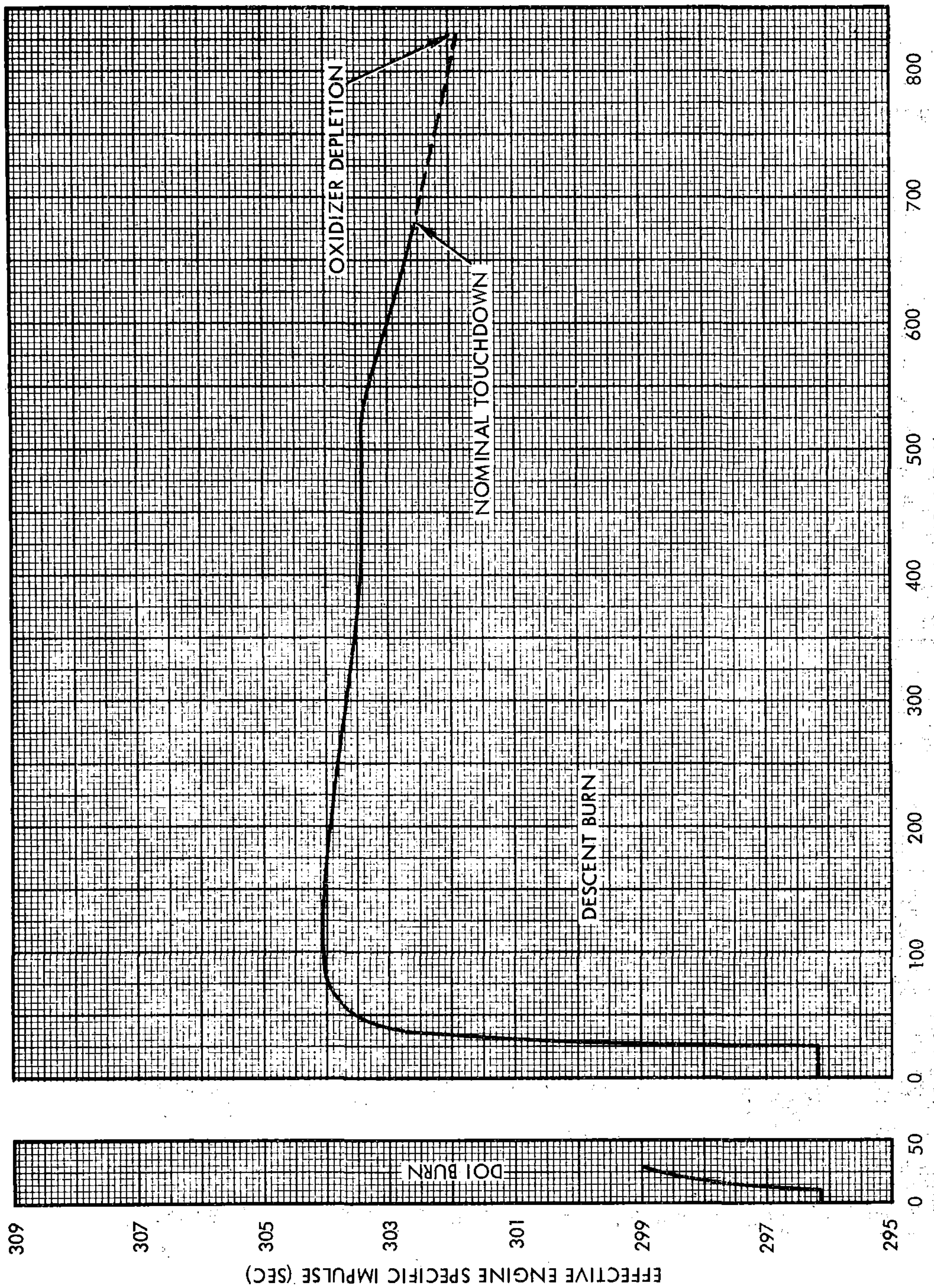

Figure LM6/4.7.1-11. Mission H1 Final DPS Preflight Performance Prediction-Effective Engine Specific Impulse Vs. Time

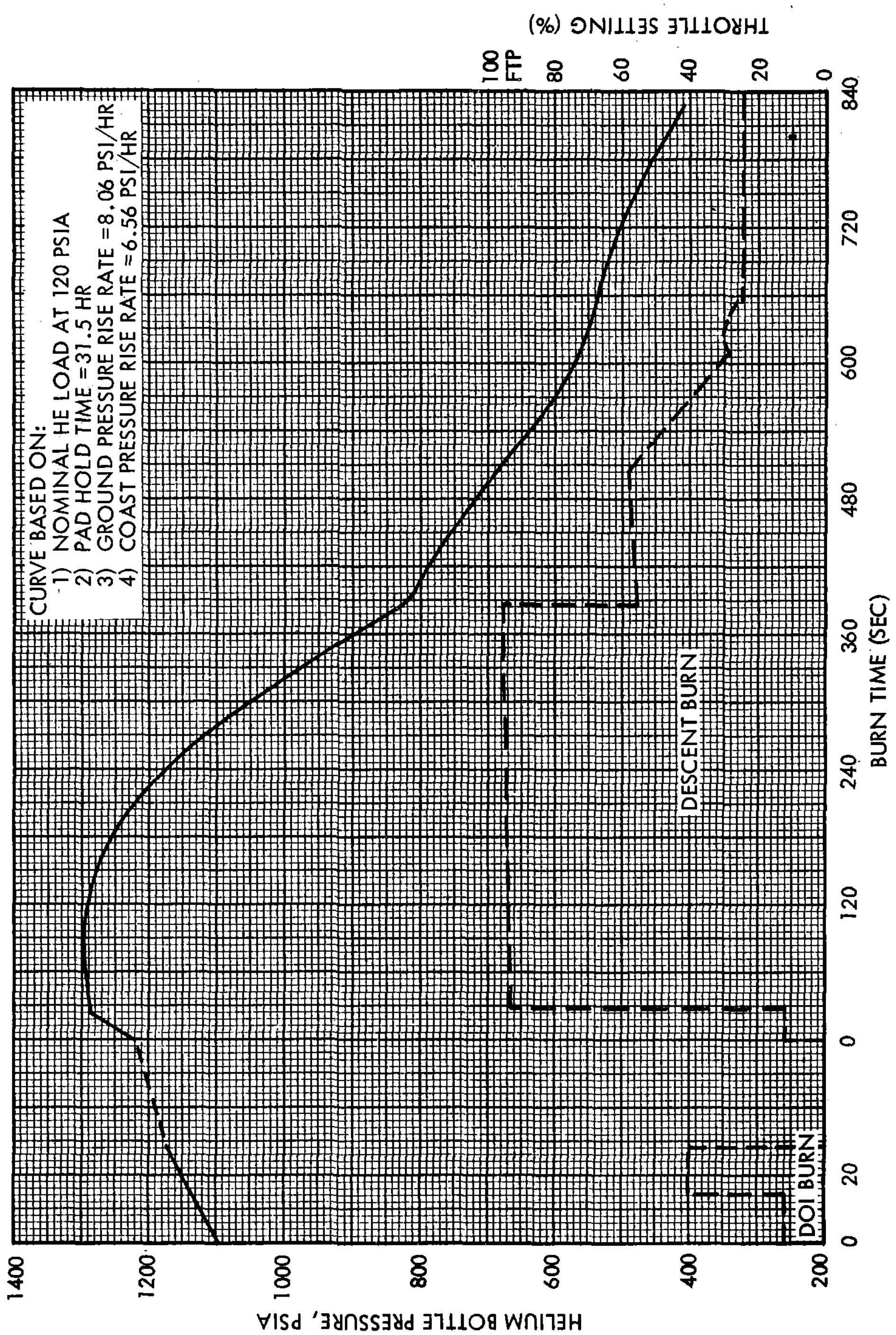

Figure LM6/4.7.1-12. Mission H1 Final DPS Preflight Performance Prediction-Supercritical Helium Bottle Pressure Vs. Time

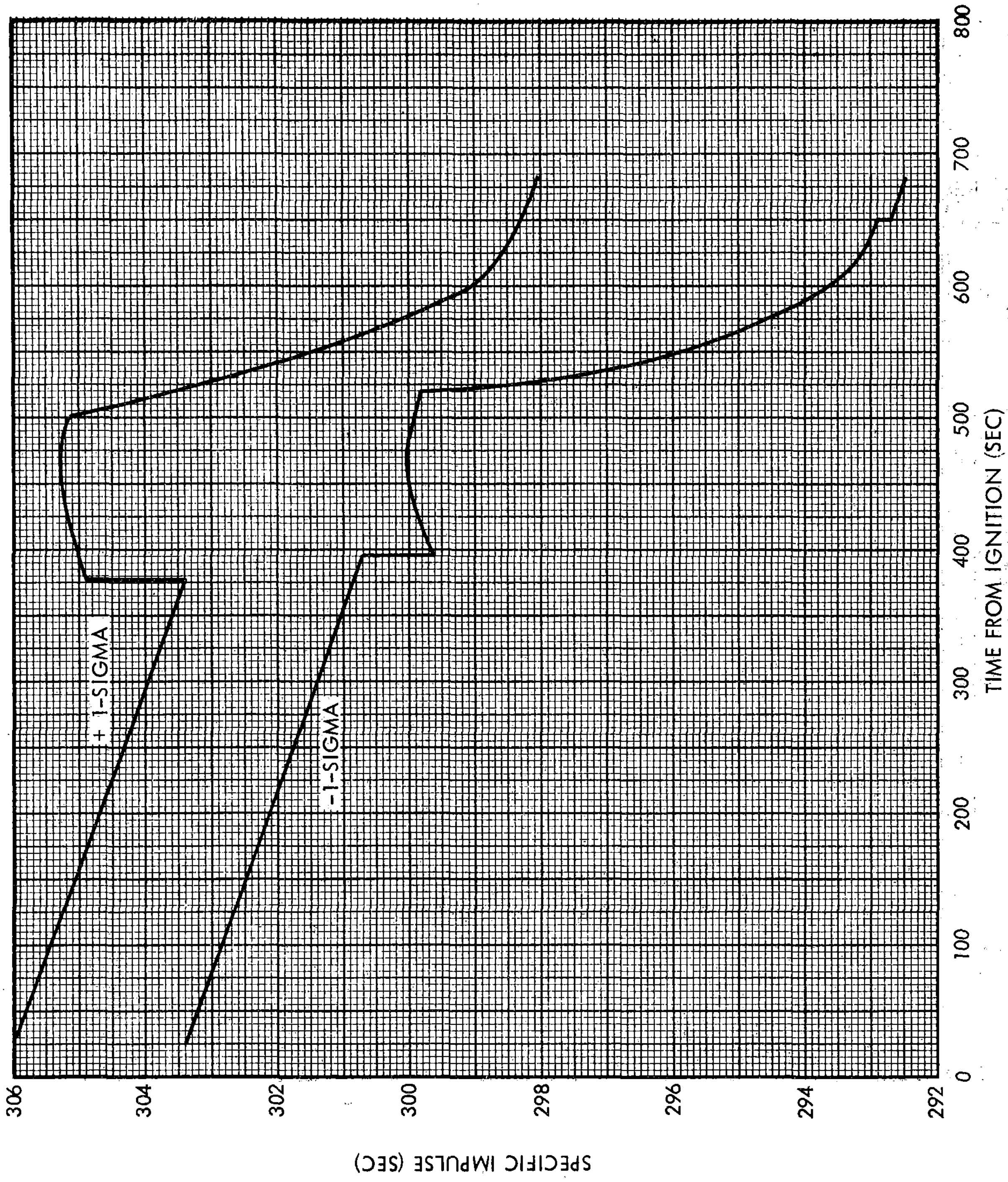

Figure LM6/4.7.1-13. Mission H1 Final DPS Preflight Performance Prediction-Specific Impulse Dispersion Vs. Time

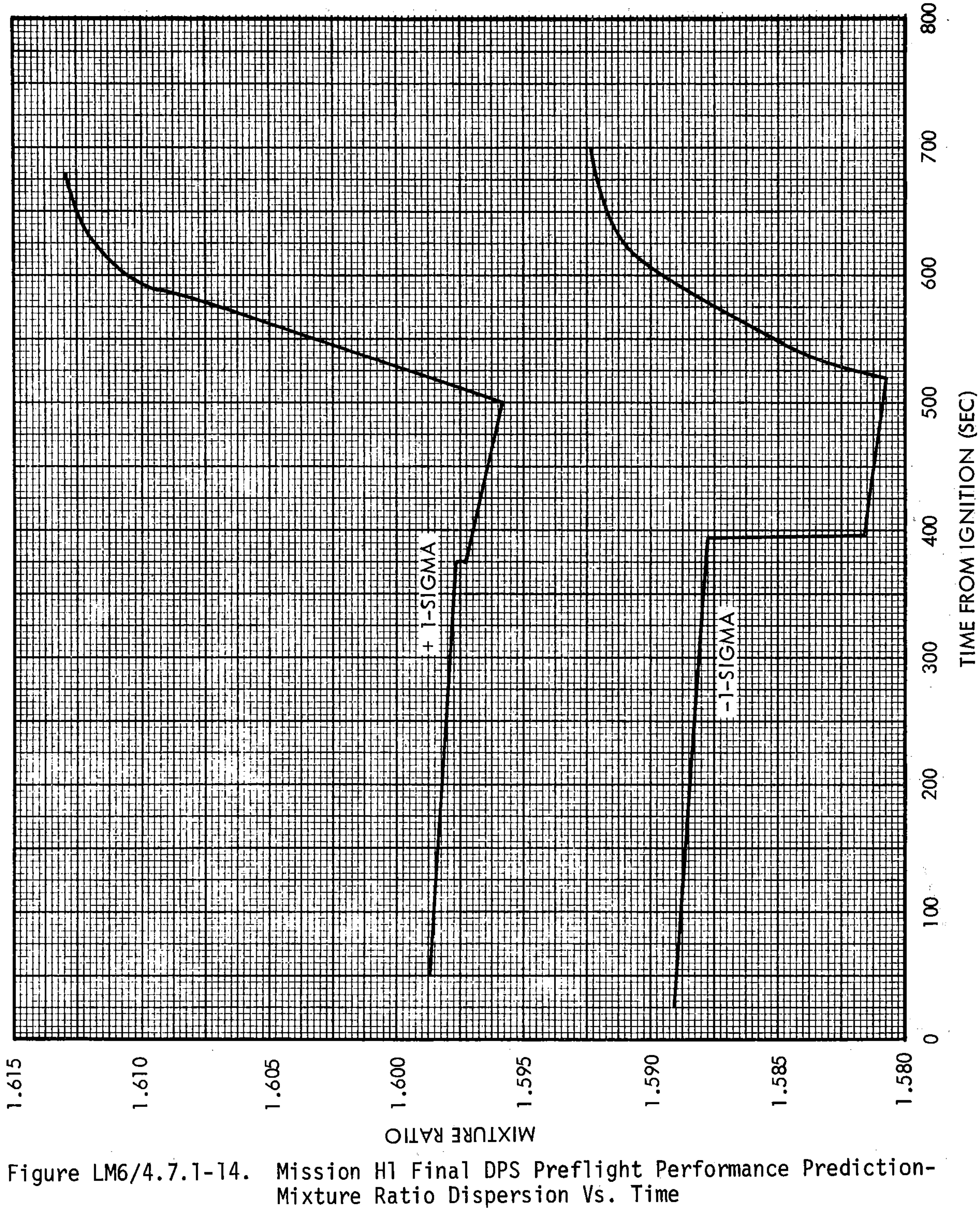

Figure LM6/4.7.1-14. Mission H1 Final DPS Preflight Performance Prediction-Mixture Ratio Dispersion Vs. Time

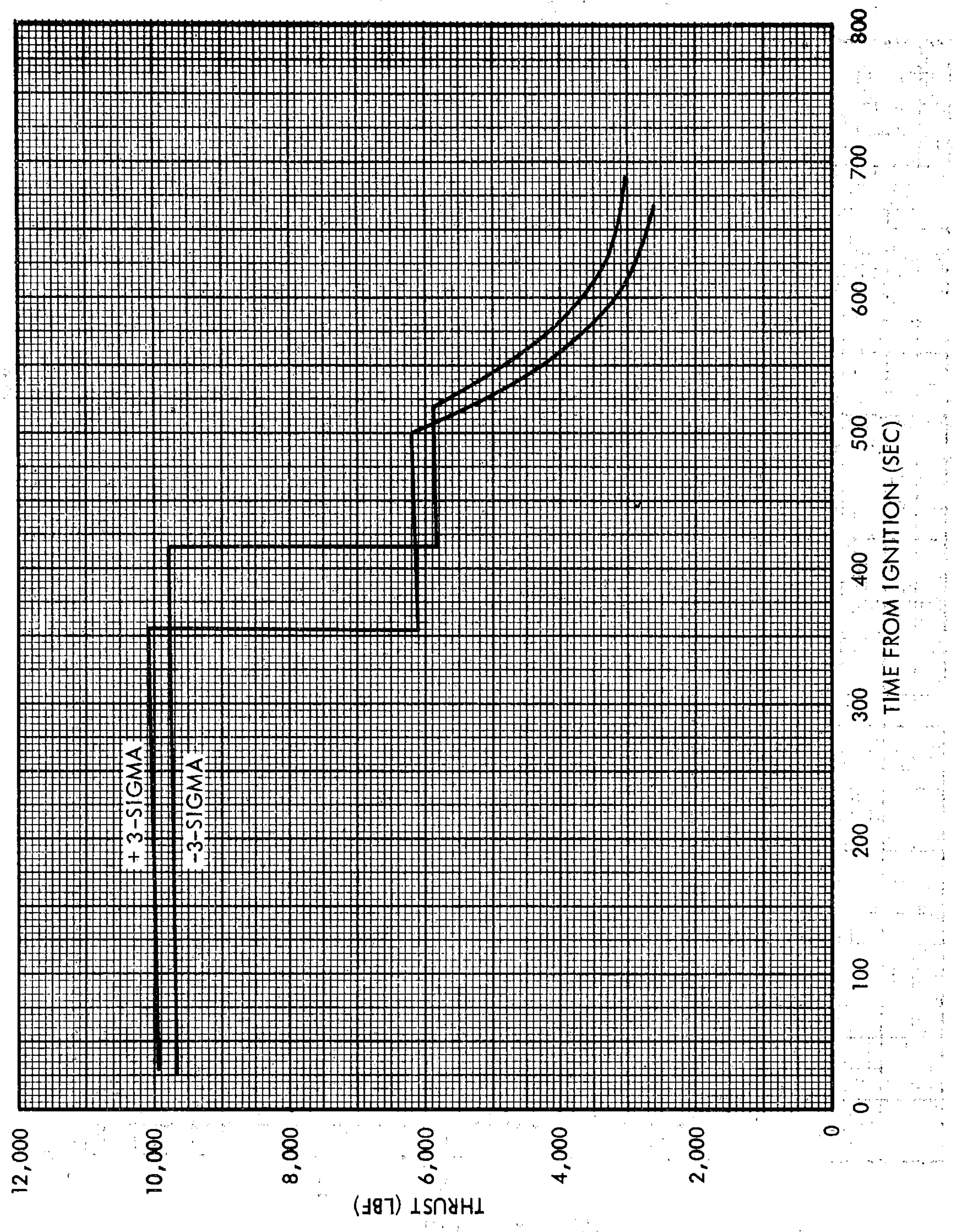

Figure LM6/4.7.1-15. Mission H1 Final DPS Preflight Performance Prediction-Thrust Dispersion Vs. Time

(NASA DATA SOURCE)

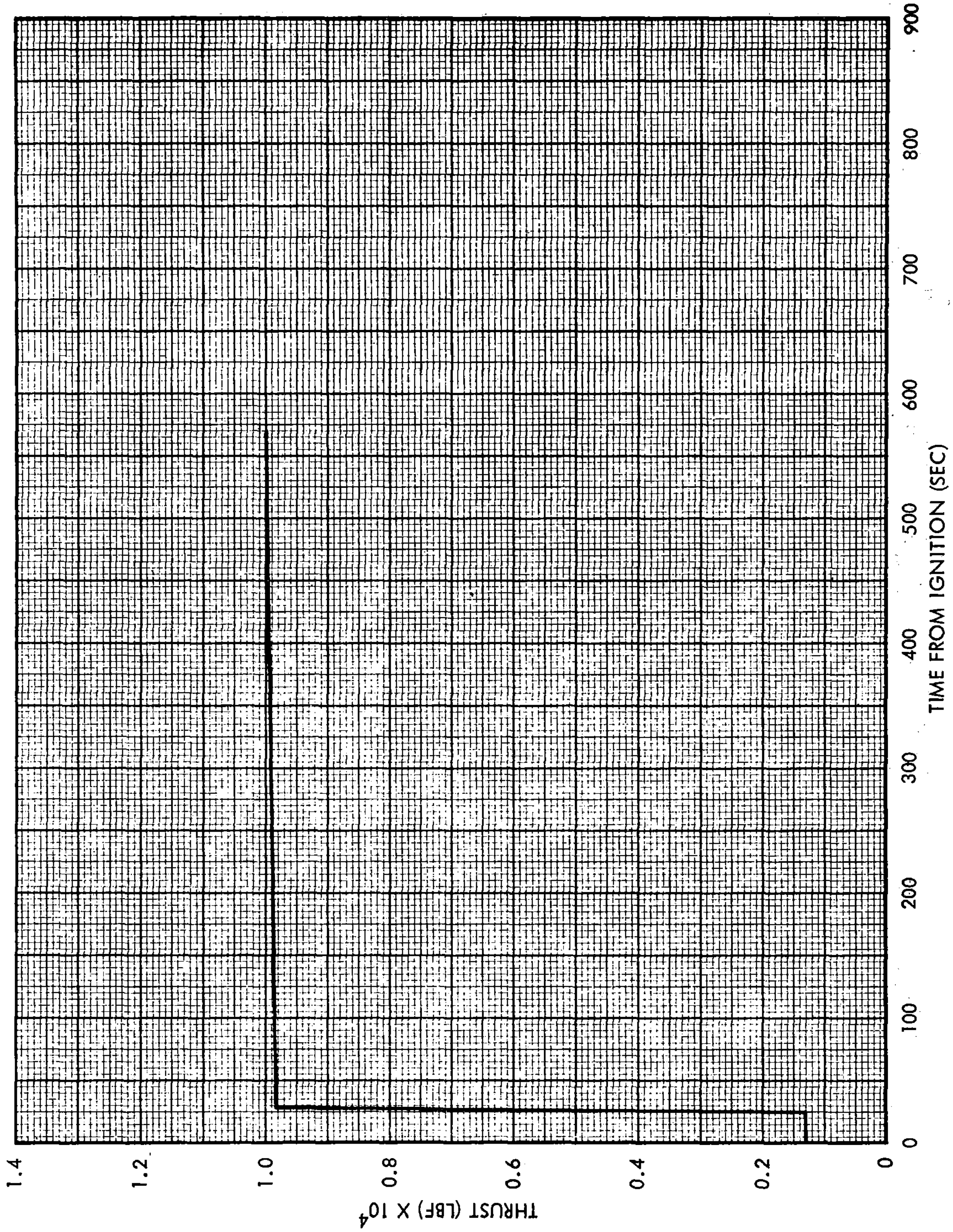

Figure LM6/4.7.1-16. Mission H-1 DPS Preflight Performance Prediction-Docked FTP Burn to Depletion-Thrust Vs Time

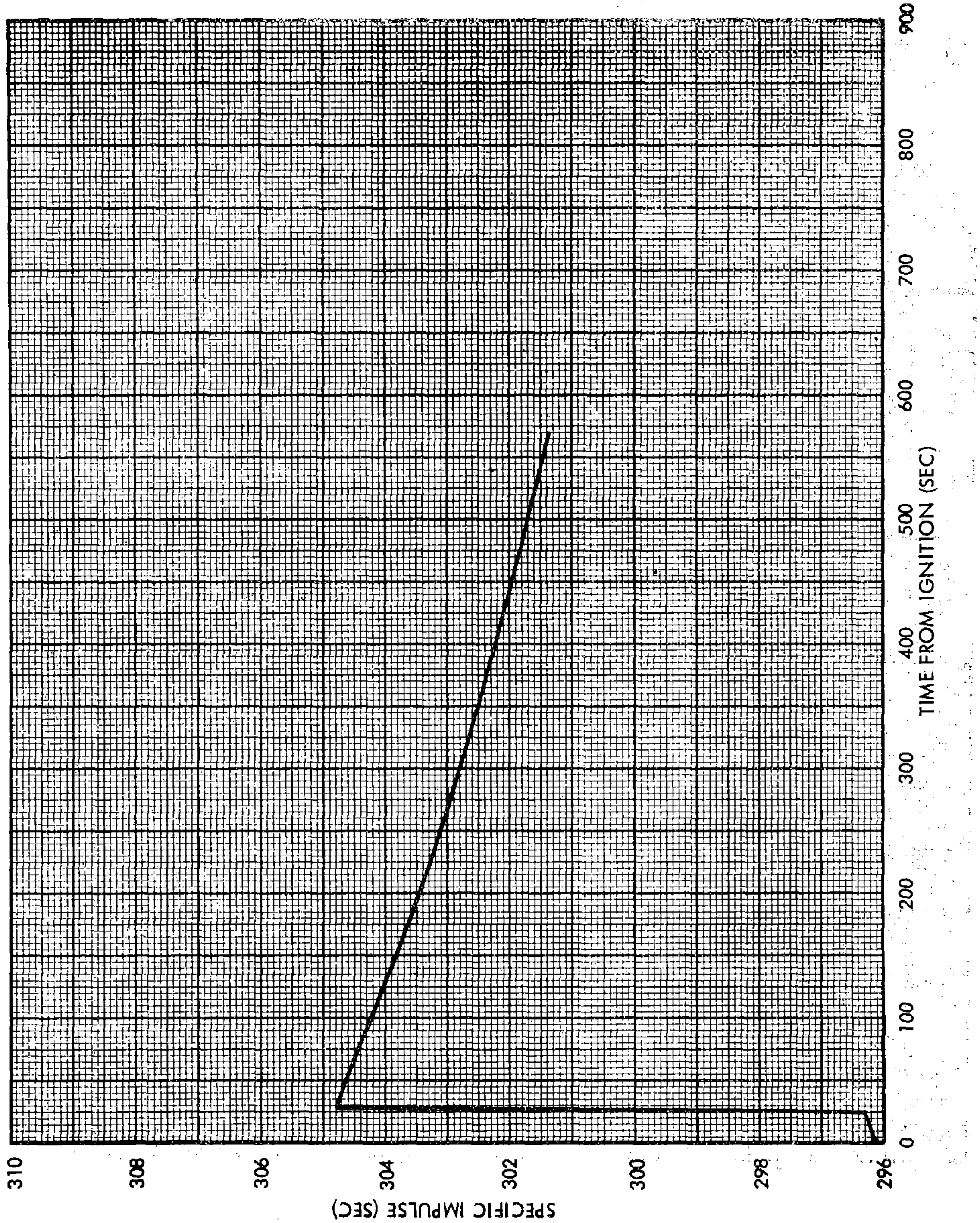

Figure LM6/4.7.1-17. Mission H-1 DPS Preflight Performance Prediction-Docked FTP Burn to Depletion-Specific Impulse Vs Time

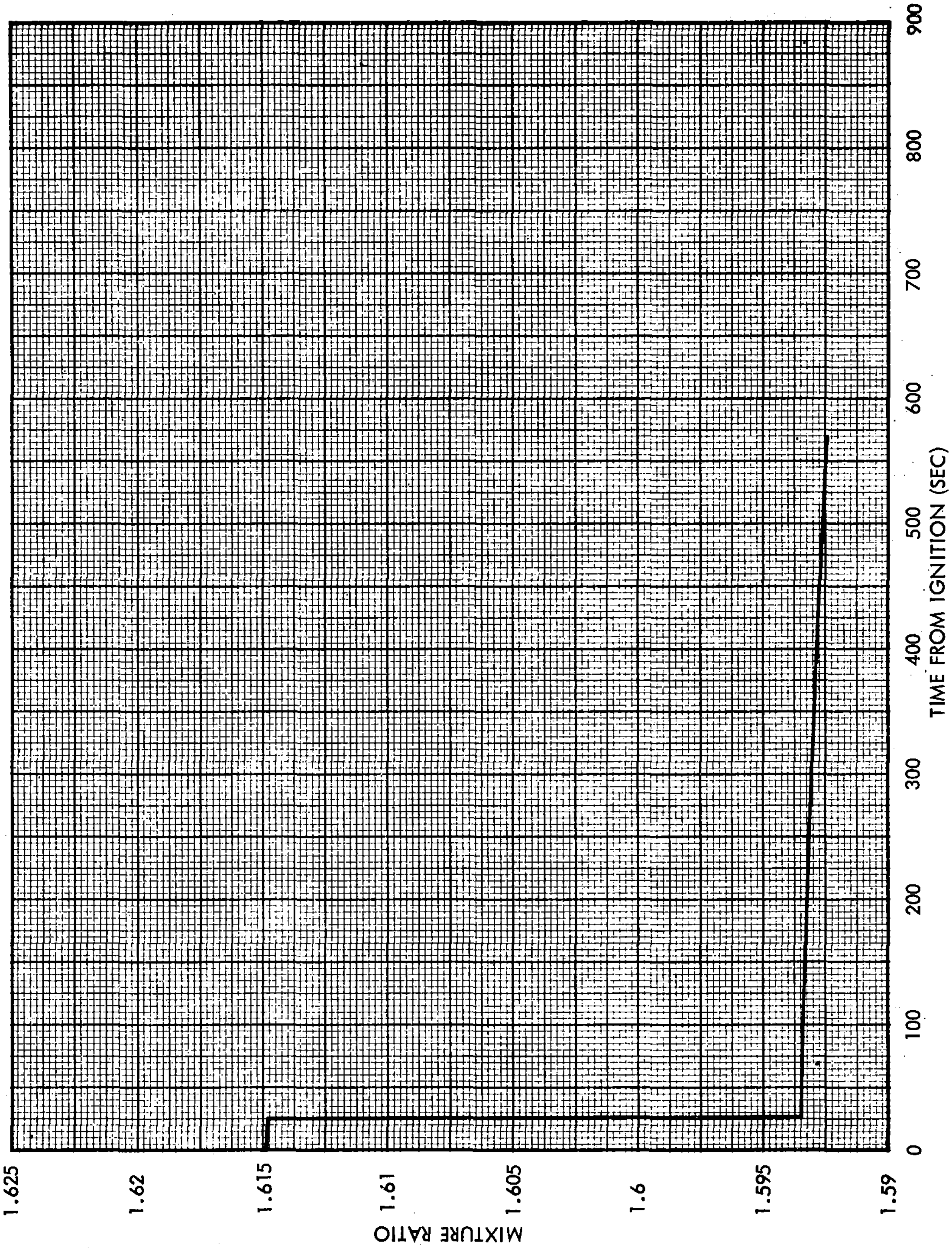

Figure LM6/4.7.1-18. Mission H-1 DPS Preflight Performance Prediction-Docked FTP Burn to Depletion-Mixture Ratio Vs Time

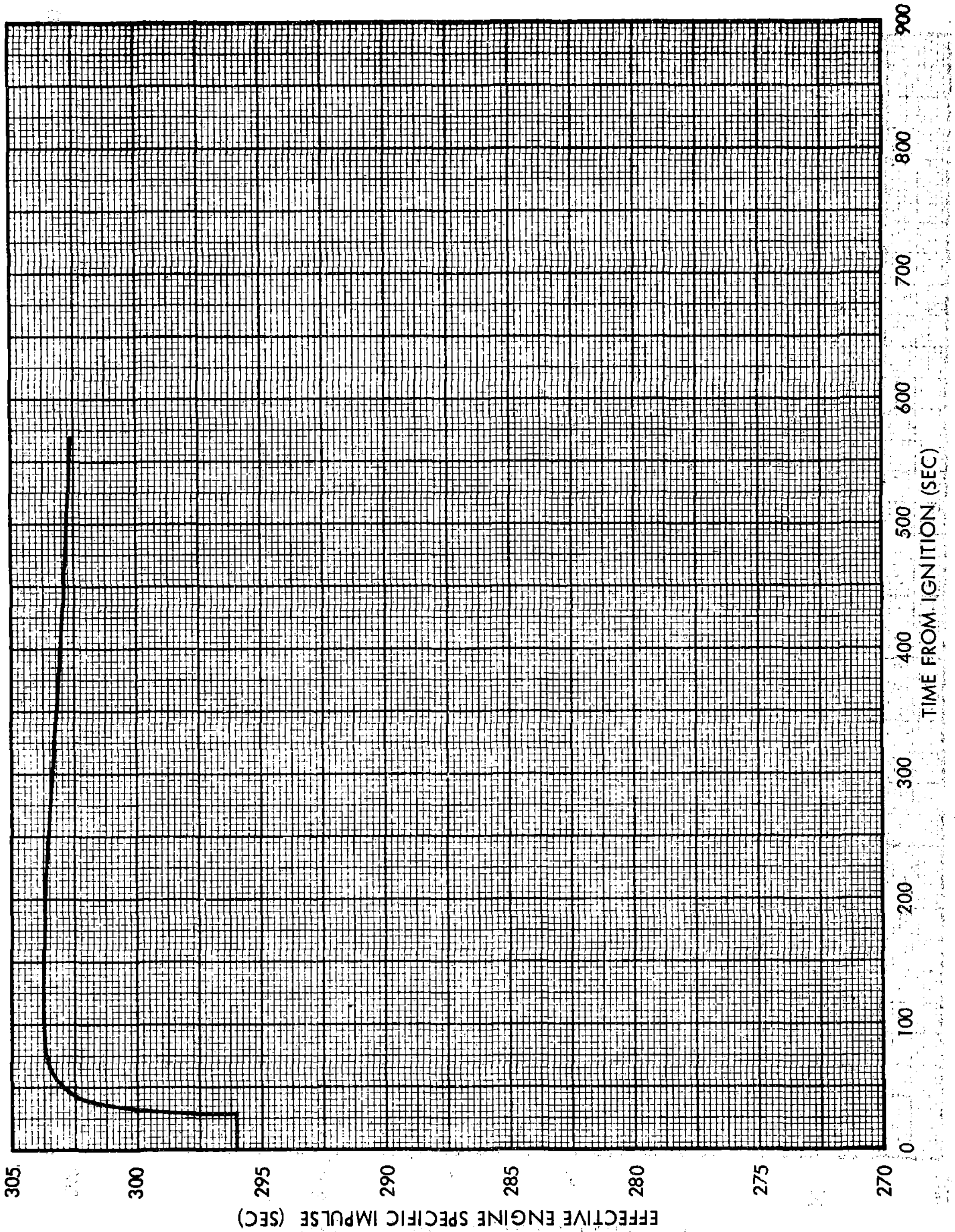

Figure LM6/4.7.1-19. Mission H-1 DPS Preflight Performance Prediction-Docked FTP Burn to Depletion-Effective Engine Isp Vs Time

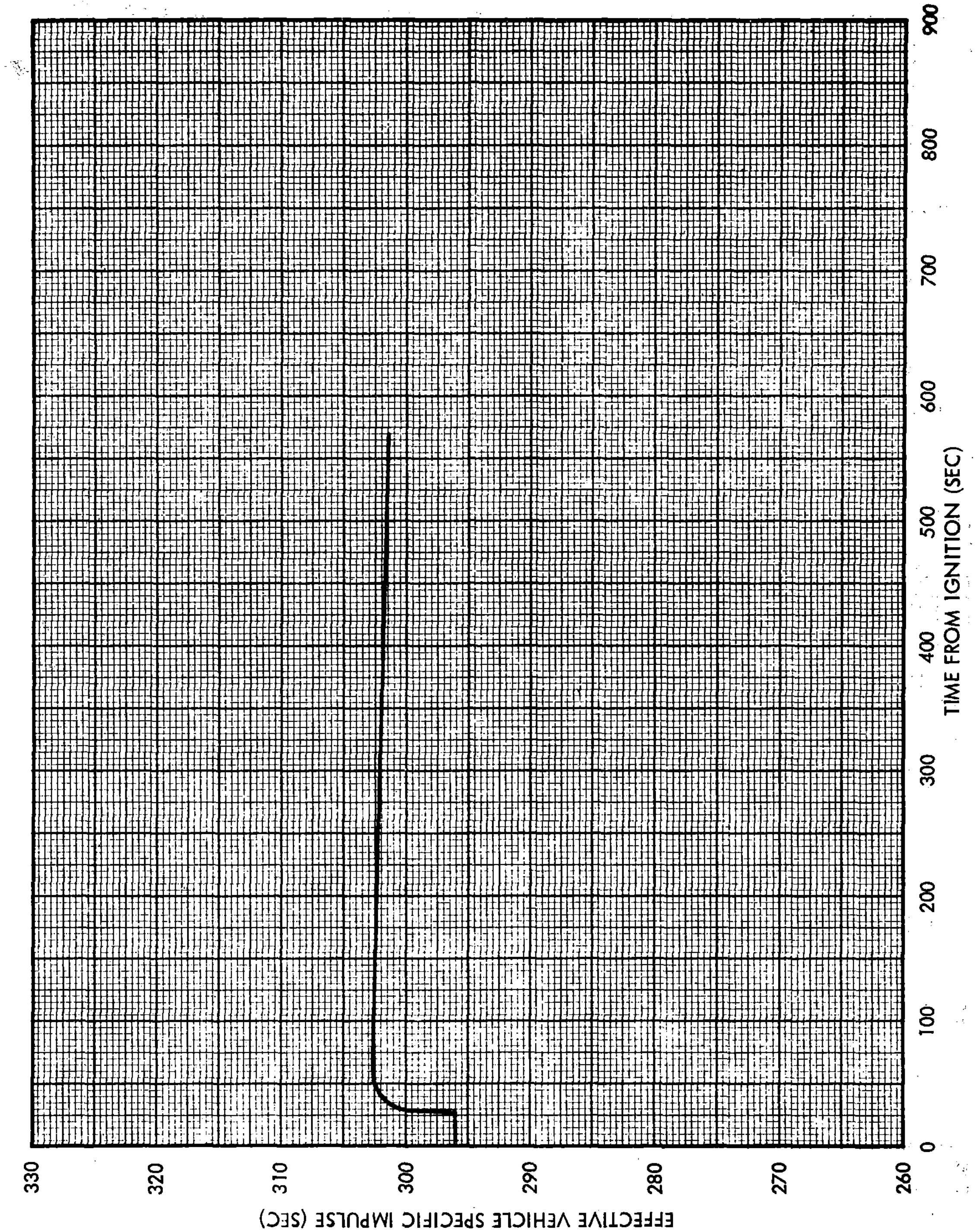

Figure LM6/4.7.1-20. Mission H-1 DPS Preflight Performance Prediction-Docked FTP Burn to Depletion-Effective Vehicle Isp Vs Time

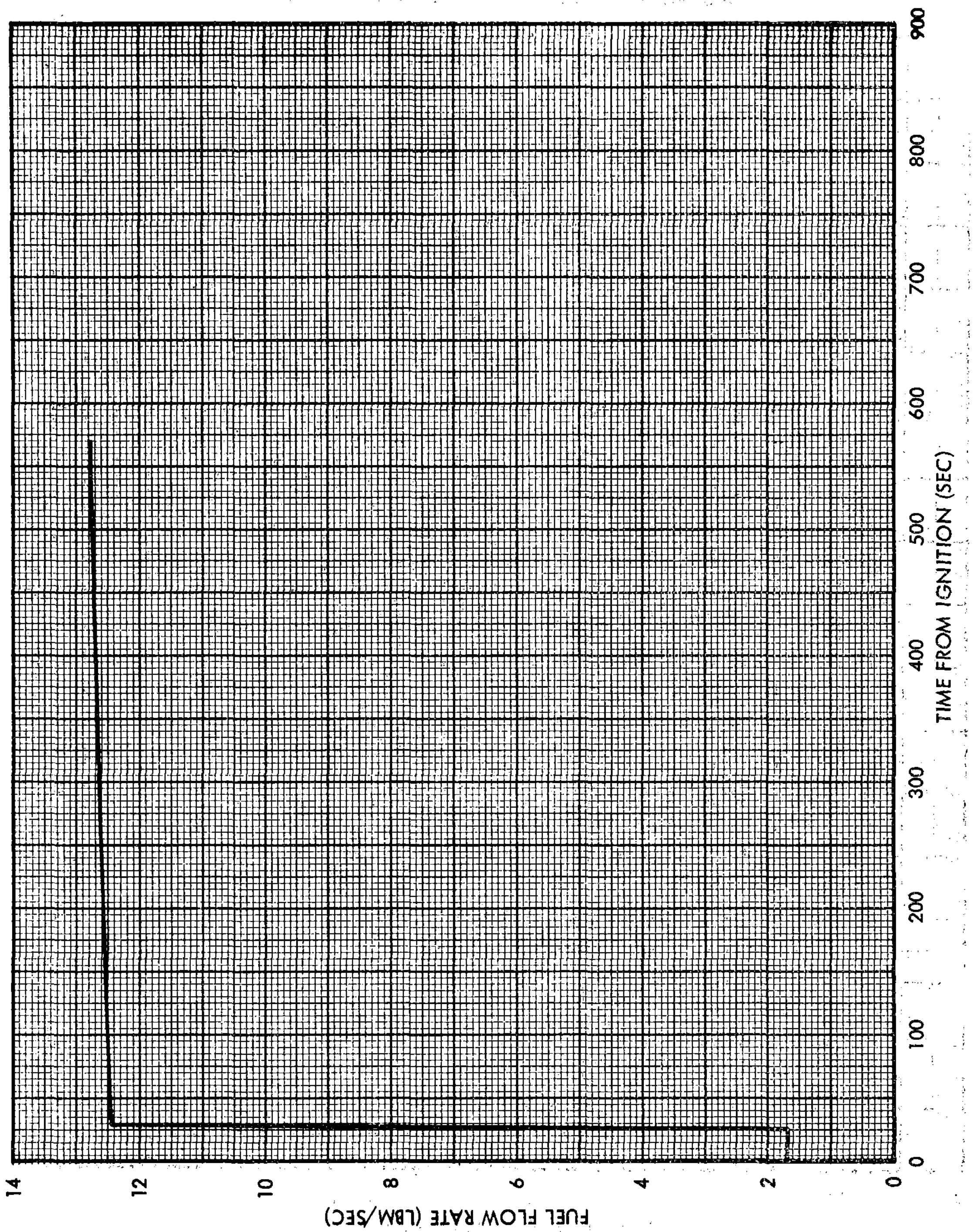

Figure LM6/4.7.1-21. Mission H-1 DPS Preflight Performance Prediction-Docked FTP Burn to Depletion-Fuel Flow Rate Vs Time

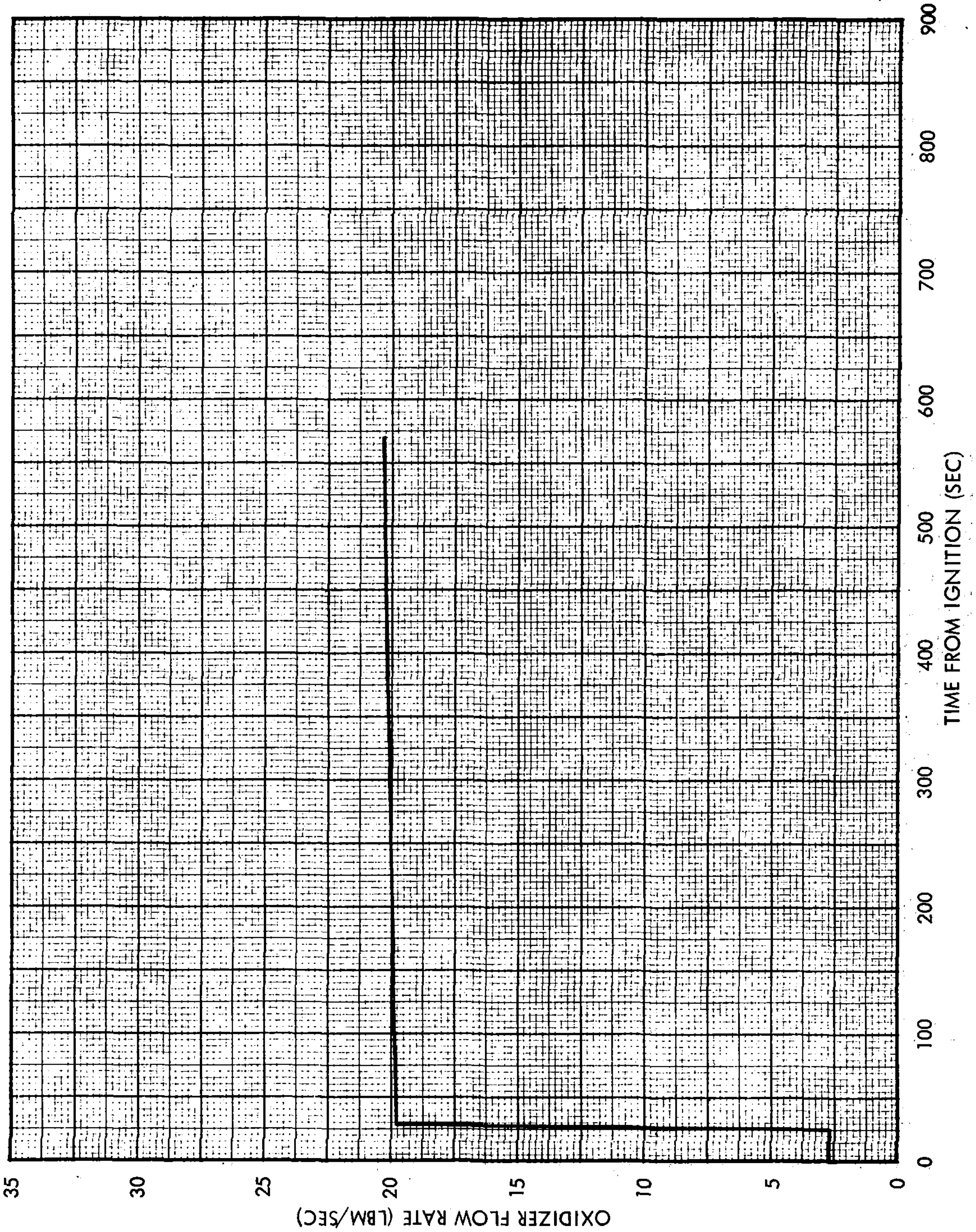

Figure LM6/4.7.1-22. Mission H-1 DPS Preflight Performance Prediction-Docked FTP Burn to Depletion-Oxidizer Flow Rate Vs Time

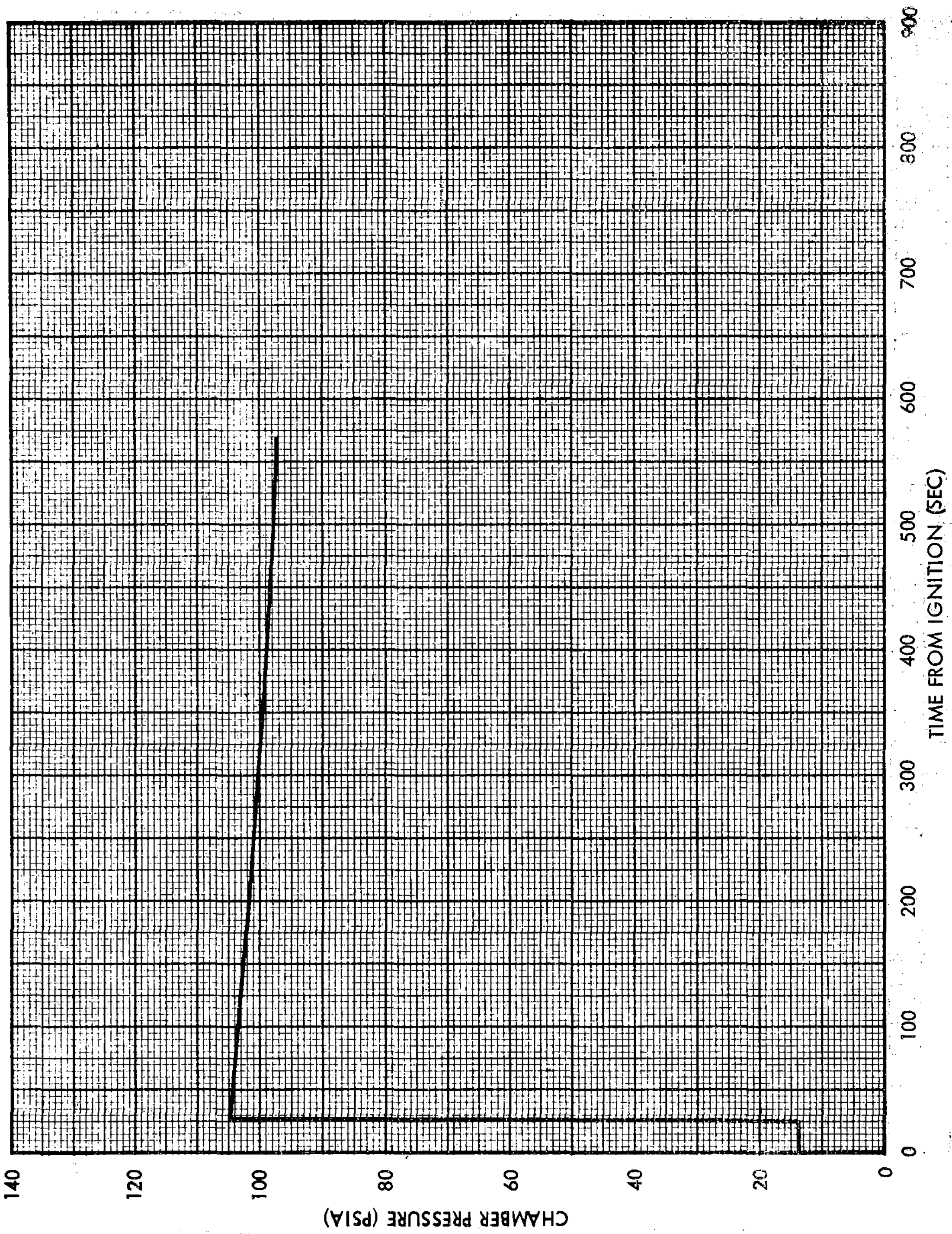

Figure LM6/4.7.1-23. Mission H-1 DPS Preflight Performance Prediction-Docked FTP Burn to Depletion-Chamber Pressure Vs Time

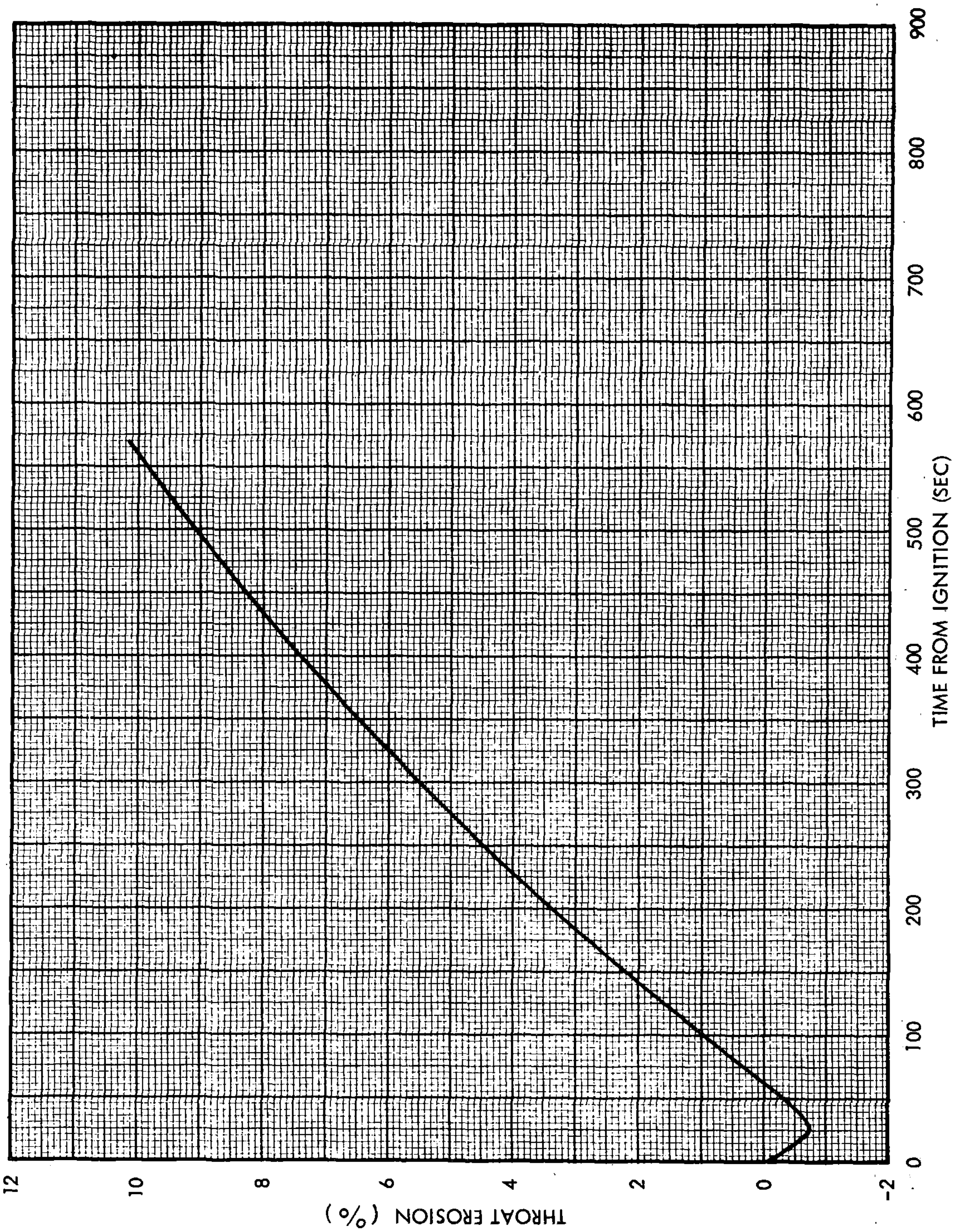

Figure LM6/4.7.1-24. Mission H-1 DPS Preflight Performance Prediction-Docked FTP Burn to Depletion-Throat Erosion Vs Time

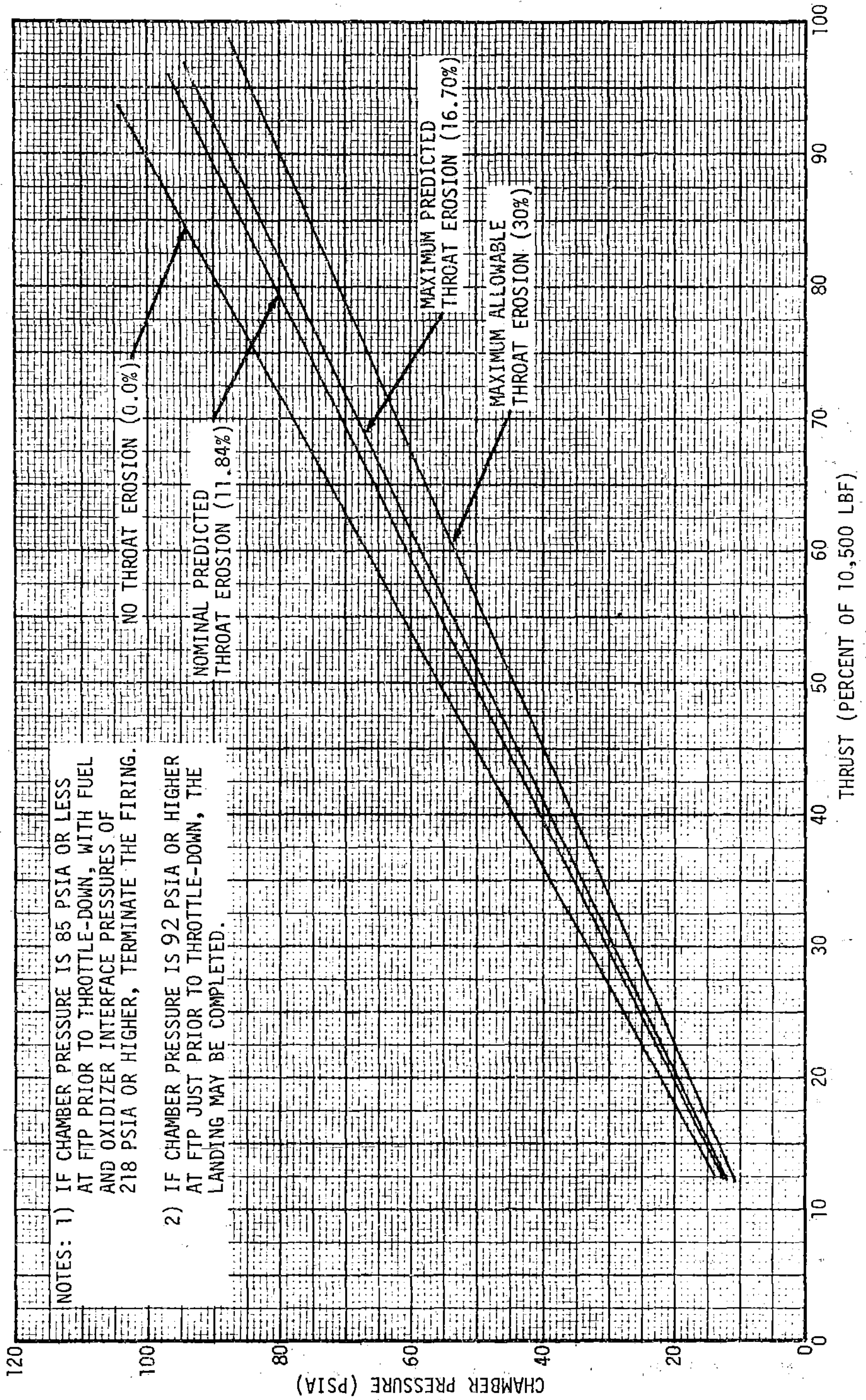

Figure LM6/4.7.1-25. Mission H-1 DPS Preflight Performance Prediction-Chamber Pressure Vs. Commanded Thrust for Zero, Nominal, Maximum Predicted and Maximum Allowable Throat Erosion

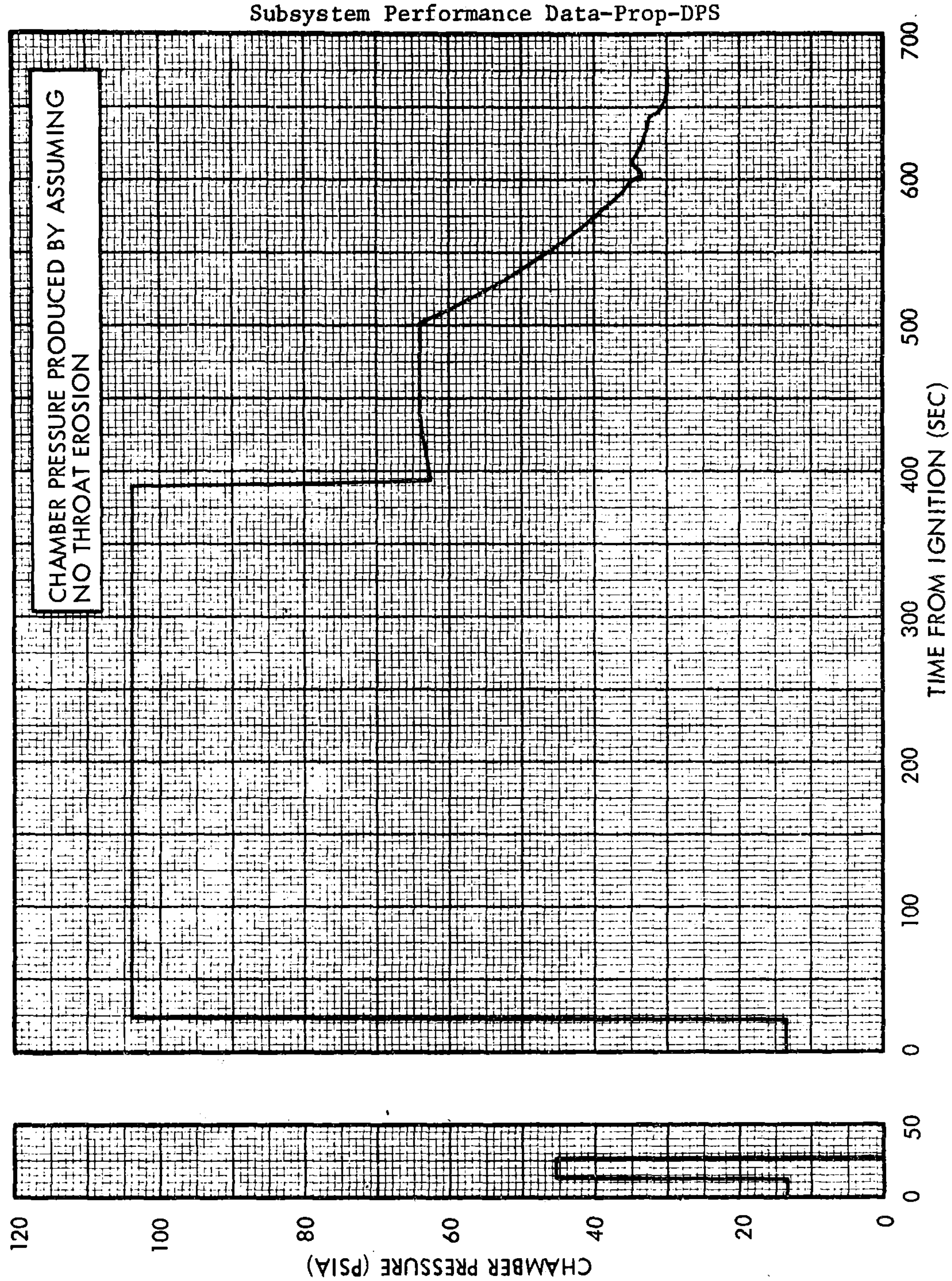

Figure LM6/4.7.1-26. Mission H-1 DPS Preflight Performance Prediction-Chamber Pressure Vs Time for Zero Throat Erosion

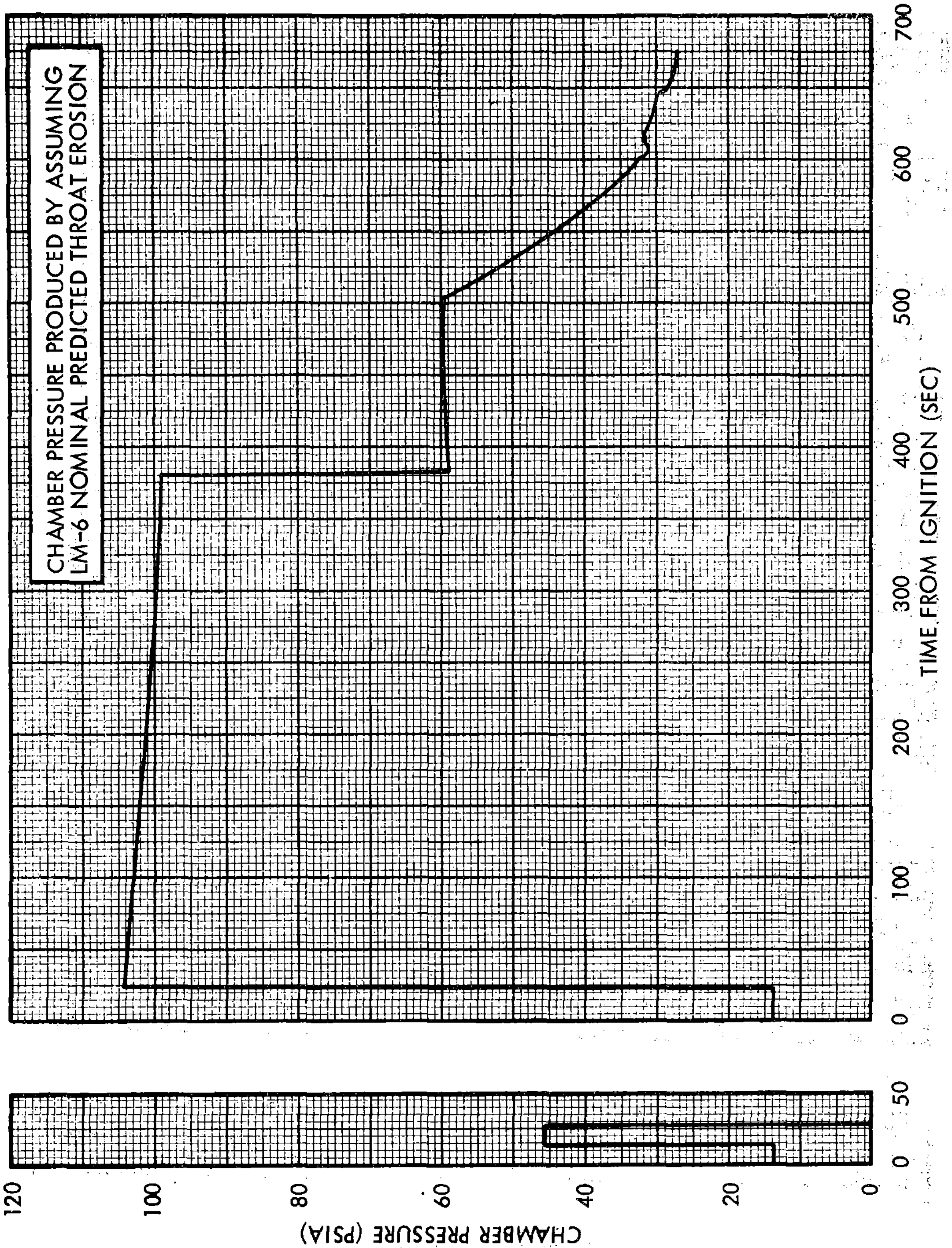

Figure LM6/4.7.1-27. Mission H-1 DPS Preflight Performance Prediction-Chamber Pressure Vs Time for Nominal Throat Erosion

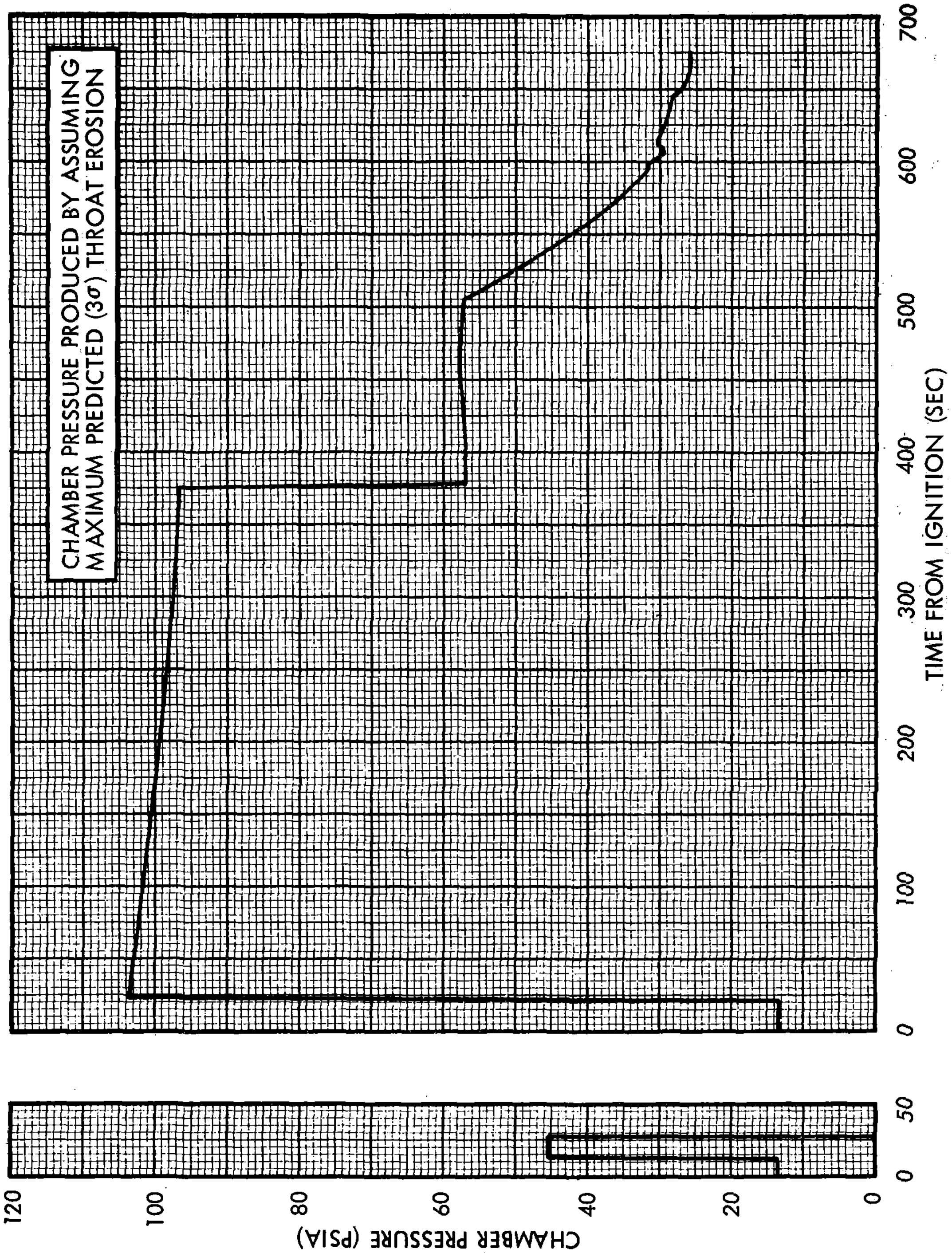

Figure LM6/4.7.1-28. Mission H-1 DPS Preflight Performance Prediction-Chamber Pressure Vs Time for Maximum Predicted Throat Erosion

LM6/4.7.2 Supercritical Helium Tank Pressure (NASA DATA SOURCE)

The predicted heat leak pressure rise rate for the LM-6 supercritical helium tank is 8.55 psi/hr. This prediction is based upon an analysis of the heat leak performance measured on the specific tanks for LM-6 in cold-flow tests at GAEC, Bethpage, and vendor acceptance tests. The above prediction includes a measurement uncertainty of 0.35 psi/hr.

The above value of the heat leak pressure rise rate is the best value currently available. It will be updated with data from the countdown demonstration test as those data become available.

LM6/4.7.5 DPS Propellant Tank Low Level Sensor Operation

Data from GAC give the propellant quantities remaining in the DPS tanks (at 70°F) at the time of low level sensor actuation as:

Tank	Quantity
Fuel	202±9.9 lbm per tank
Oxidizer	322±13.4 lbm per tank

The propellants in the feed lines and heat exchanger should be added and the propellants in the zero-g can and for unporting prevention should be deducted from the above quantities. Values for these are taken from the Spacecraft Operational Data Book, Volume III, Rev 2, 20 August 1969, Section 5.6:

Component	Fuel, lbm	Oxidizer, lbm
Feed Lines	+12.1	+27.5
Heat Exchanger	+ 4.6	-0-
Zero-G Can	- 5.2	- 8.6
Unporting Prevention	-10.7	-16.0
Total	+ 0.8	+ 2.9

The propellant quantity corrections tabulated above should be applied regardless of whether depletion occurs from a single tank or both tanks of a pair simultaneously. This is so because in both cases the trapped quantities will be used or not used identically (helium ingestion upon depletion of a single tank effectively shuts off the undepleted tank). Also, since at the time of low level sensor actuation it is not possible to determine whether or not both tanks of a pair are at the same propellant level (they both could be at the high or at the low level), the single tank dispersions should be summed to arrive at the dispersions for both tanks of a pair taken together.

Based upon the above statements and data the propellant quantities available after low level sensor actuation are as follows:

Fuel	404.8±19.8 lbm
Oxidizer	646.9±26.8 lbm

The mean values of fuel and oxidizer flow rate during hover from low level sensor actuation to depletion were calculated to be:

Fuel Flow Rate:	3.482 lbm/sec
Oxidizer Flow Rate:	5.585 lbm/sec

(Spacecraft Operational Data Book, Volume II, Rev. 2, 1 September 1969, Para. LM6/4.7.1).

Using the above flow rates and propellant quantities the burn time from low level sensor actuation to depletion was calculated to be 116.3 seconds for fuel and 115.8 seconds for oxidizer. Both the burn times given above are slightly on the conservative side in as much as use of a mean flow rate is conservative by approximately 1.6 seconds compared to integrating along a thrust-time curve.

The dispersions associated with the burn times given above are ±5.7 seconds for fuel and ±4.8 seconds for oxidizer. Therefore, the minimum burn times from low level sensor actuation to depletion were calculated to be 110.6 seconds for fuel and 111.0 seconds for oxidizer.

Because there are two fuel and two oxidizer tanks, each with a low level sensor with the dispersion given in the first paragraph, the RSS dispersion for the two tanks of a pair represents a more likely case than the maximum dispersion case given immediately above. The RSS dispersions for the total fuel and total oxidizer available at low level sensor activation were calculated to be ±14.0 and ±19.0 lbm, respectively. The burn time dispersions associated with these quantities are ±4.0 seconds for fuel and ±3.4 seconds for oxidizer. Thus, the RSS minimum burn times were calculated to be 112.3 seconds for fuel and 112.4 seconds for oxidizer.

The above burn time calculations do not take into account the uncertainty about the nominal predicted flow rates.

LM6/4.7.6.1 DPS Engine Thrust Vector Alignment

The gimbal trim angles for the DPS engine may be calculated using the equations provided in Paragraph 4.7.6.1. The thrust vector angles of the DPS engine at the start of the DOI burn are given in the Spacecraft Operational Data Book, Volume III, Mass Properties, Revision 2, as:

$$\delta\theta_T = -0.660 \text{ degrees}$$

$$\delta\psi_T = -0- \text{ degrees}$$

These values, together with a startup thrust of 1268 pounds, were then used to calculate the gimbal trim angles:

$$\delta\theta = -0.718 \text{ degrees}$$

$$\delta\psi = +0.058 \text{ degrees}$$

These are the recommended launch pad settings for the DPS gimbal trim angles at the start of the DOI burn.

The trim angles are set using the LM Guidance Computer (LGC), and must be expressed referenced to the positive gimbal stops. To accomplish this, 6.05 degrees were added to the trim angles above.

This results in

$$\delta\theta' = 5.332 \text{ degrees}$$

$$\delta\psi' = 6.108 \text{ degrees}$$

both referred to the positive gimbal stops.

The LGC has a nominal drive rate of 0.2000 degrees/second hard-wired into it. Therefore, all actual gimbal angles must be converted to equivalent angles based on the hard-wired drive rate using the actual gimbal drive rates in both pitch and roll. Where entered via the LGC erasable memory load, the angles must be expressed as drive times (from the positive stops). Where entered or displayed on the DSKY the equivalent angles must be expressed as degrees of arc.

LM6/4.7.6.1 DPS Engine Thrust Vector Alignment (Continued)

The GDA drive rates are listed below.

Functional Axis	Drive Rate
Pitch (X-Z plane)	0.2116 deg/sec
Roll (X-Y plane)	0.2122 deg/sec

The gimbal trim data to be entered in the LGC erasable memory load are then obtained as follows:

$$\text{PITTIME} = \frac{\delta\theta'}{0.2116} = 25.19 \text{ seconds}$$

$$\text{ROLLTIME} = \frac{\delta\psi'}{0.2122} = 28.79 \text{ seconds}$$

The corresponding angles to be entered or read from the DSKY are obtained as follows:

$$\text{P-TRIM} = \delta\theta' \left(\frac{0.2000}{0.2116}\right) = 5.038 \text{ degrees}$$

$$\text{R-TRIM} = \delta\psi' \left(\frac{0.2000}{0.2122}\right) = 5.758 \text{ degrees}$$

LM6/4.7.6.2 GDA Drive Rates

Measurement	Data	
Time of Travel	- pitch 57.17 sec - roll 57.03 sec	These times are the average of 3 measurements made on LM-6 at Bethpage and KSC.
Angular Rate	- pitch 0.2116 °/sec - roll 0.2122 °/sec	

NOTE: Computed Angle of Travel = 12.1° (in either axis)

LM6/4.7.8 Preflight Thermal Analysis of DPS

Figures LM6/4.7.8-1 through LM6/4.7.8-14 document the preflight thermal analysis of the LM-6 DPS. Figures LM6/4.7.8-1 and LM6/4.7.8-2 show the SHe tank temperature and pressure response during a DPS burn. Figure LM6/4.7.8-3 gives the outlet temperature of the external heat exchanger, while Figure LM6/4.7.8-4 shows the fuel temperature drop across the heat exchanger as a function of fuel flow rate.

Figures LM6/4.7.8-5 and LM6/4.7.8-6 show the internal heat exchanger inlet and outlet temperatures as a function of engine burn time. Figure LM6/4.7.8-7 gives the temperature of the fuel line at the engine interface and at just upstream of the flow control valves. Likewise, Figures LM6/4.7.8-8 through LM6/4.7.8-10 show temperature response of the injector manifold, fuel shutoff valve, and fuel flow control valve for the DPS. Temperatures of the corresponding component in the oxidizer feed system are expected to be similar. Finally, Figures LM6/4.7.8-11 through LM6/4.7.8-14 show the bulk propellant temperatures as a function of mission elapsed time.

Propellant valve and line temperatures are based on analysis. It is recommended that a 25 percent margin (based upon the difference between the start temperature and any point on the curve) for uncertainty in the analysis, be added to the temperature rises in Figures LM6/4.7.8-7 through LM6/4.7.8-10.

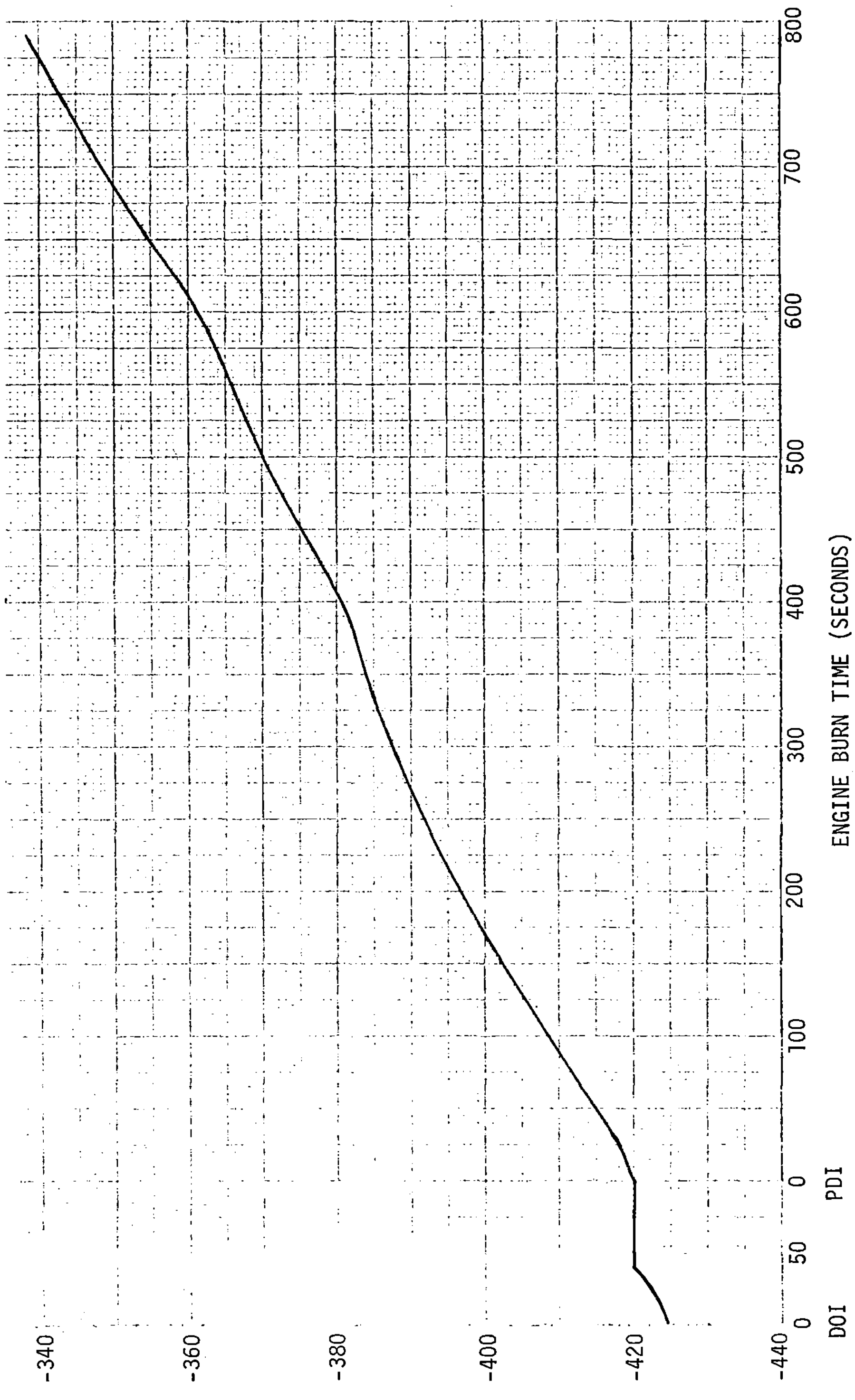

Figure LM6/4.7.8-1. Supercritical Helium Tank Temperature Vs. Engine Burn Time

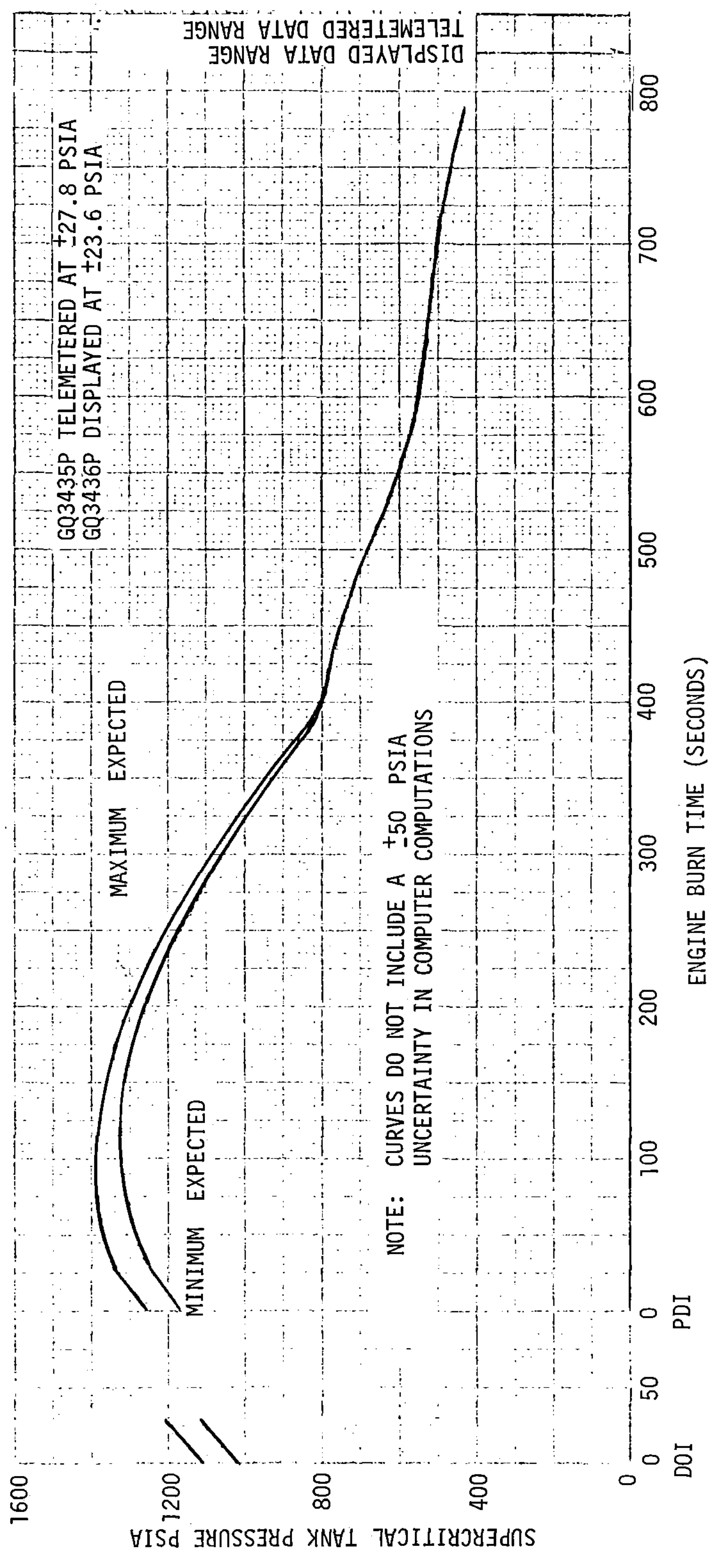

Figure LM6/4.7.8-2. Supercritical Helium Tank Pressure Vs. Engine Burn Time

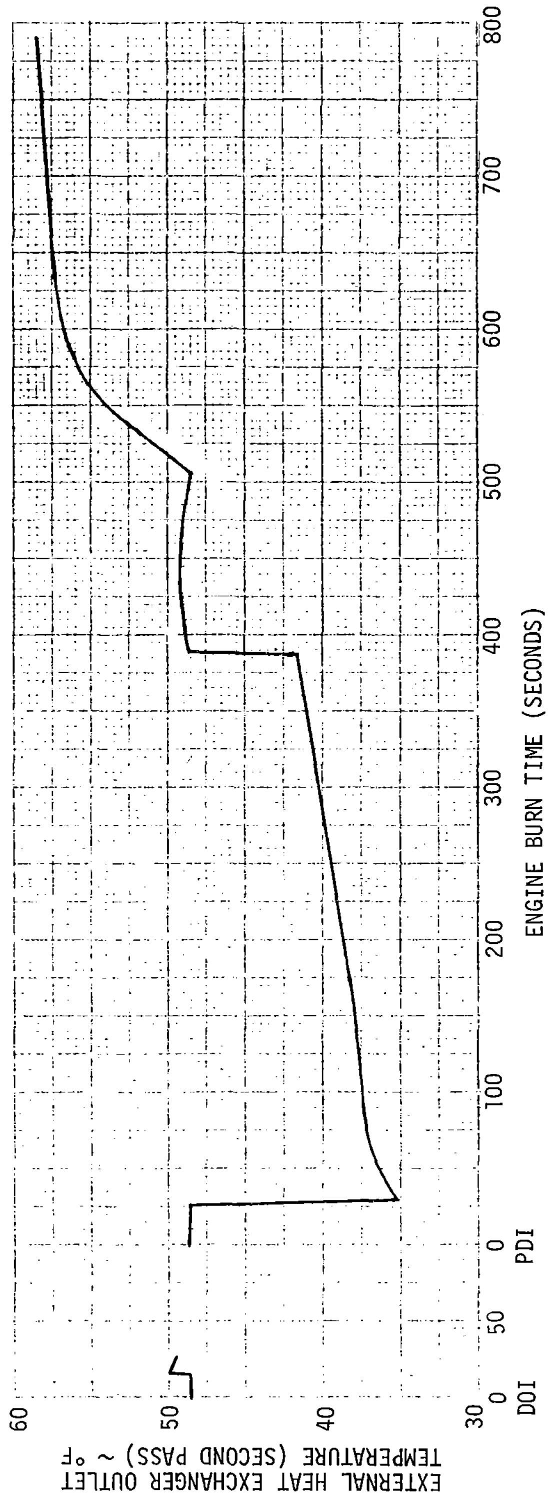

Figure LM6/4.7.8-3. External Heat Exchanger Outlet Temperature (Second Pass) Vs. Engine Burn Time

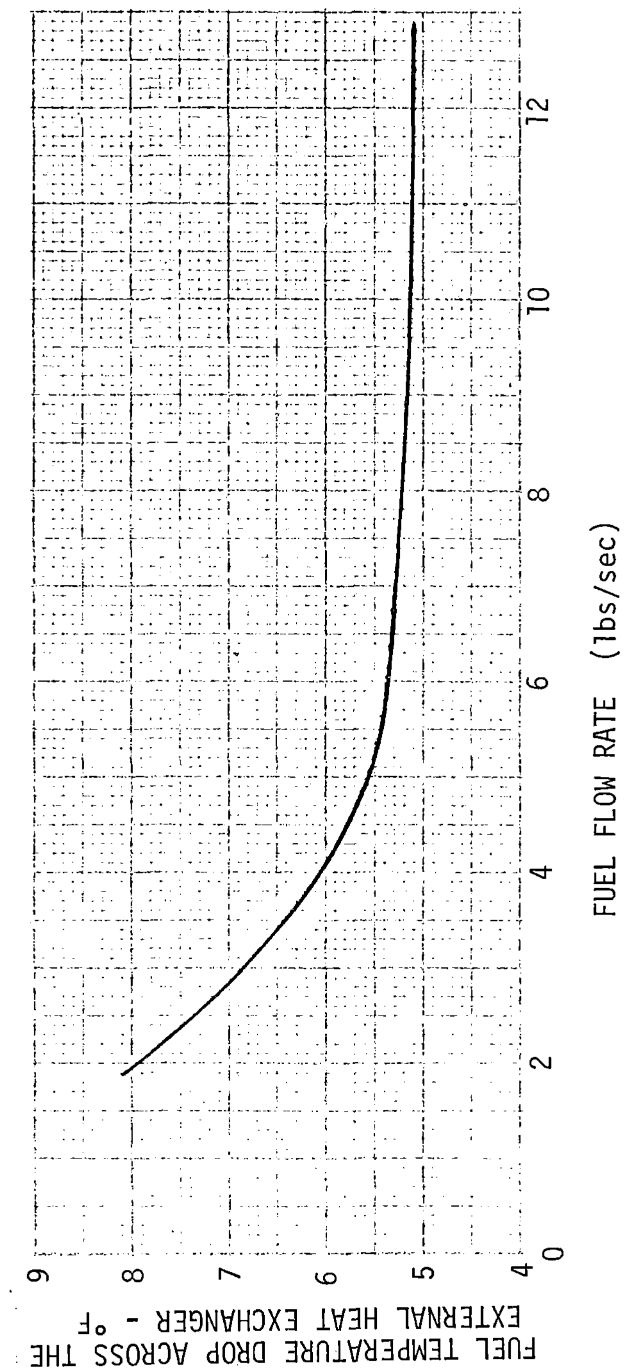

Figure LM6/4.7.8-4. Fuel Temperature Drop Across the External Heat Exchanger Vs. Fuel Flow Rate

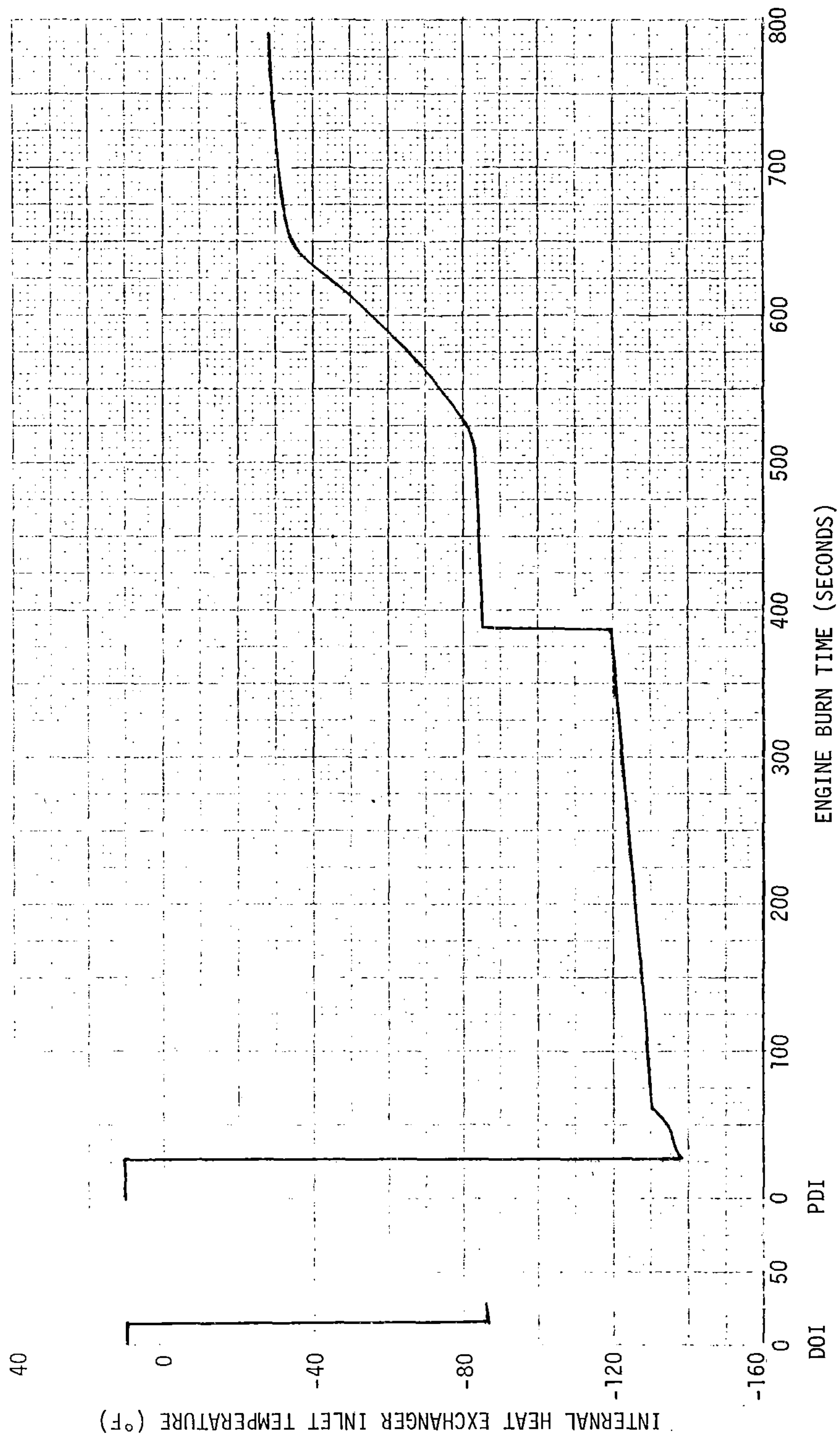

Figure LM6/4.7.8-5. Internal Heat Exchanger Inlet Temperature Vs. Engine Burn Time

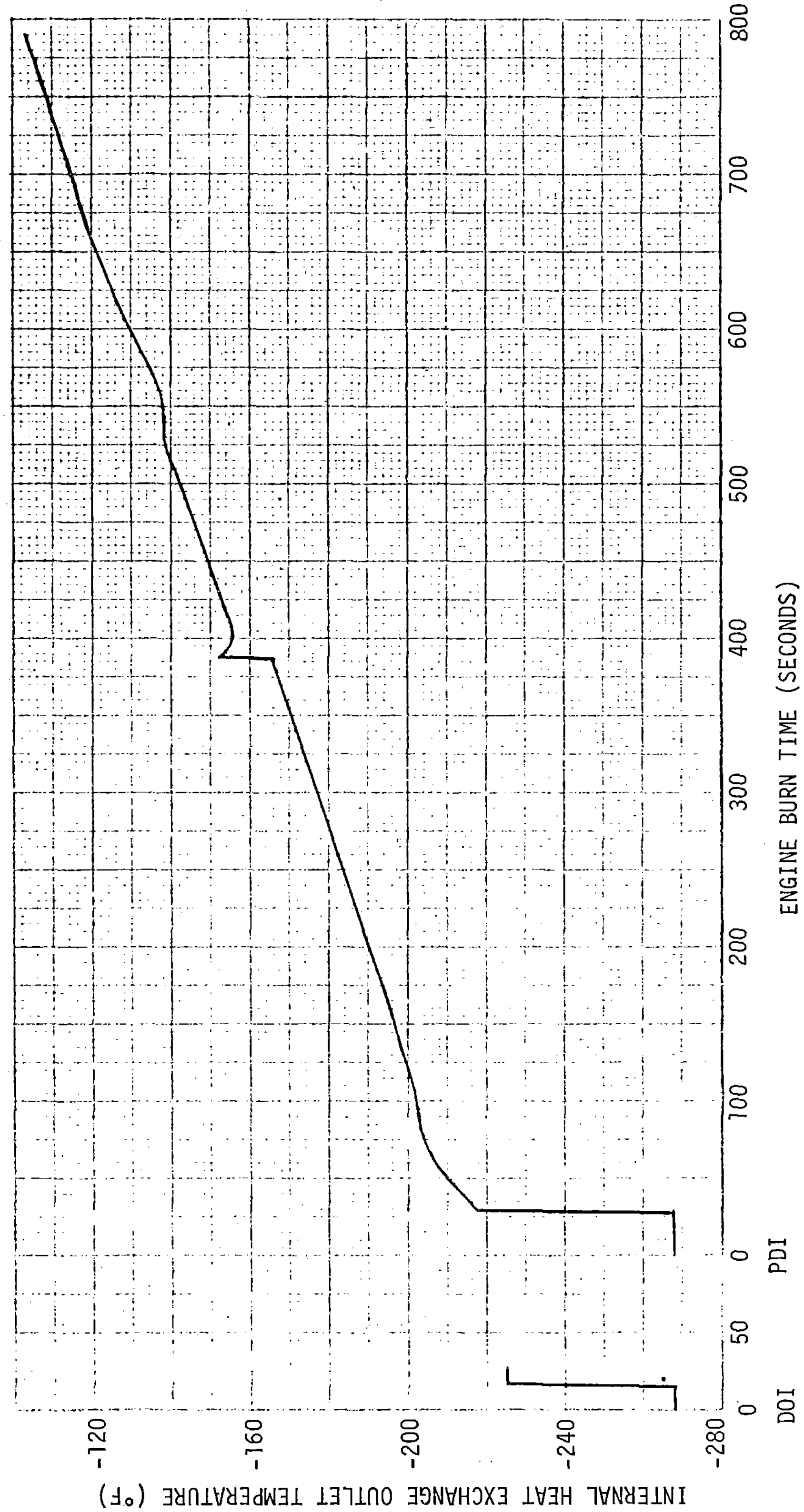

LM6/4.7.8-6. Internal Heat Exchanger Outlet Temperature Vs. Engine Burn Time

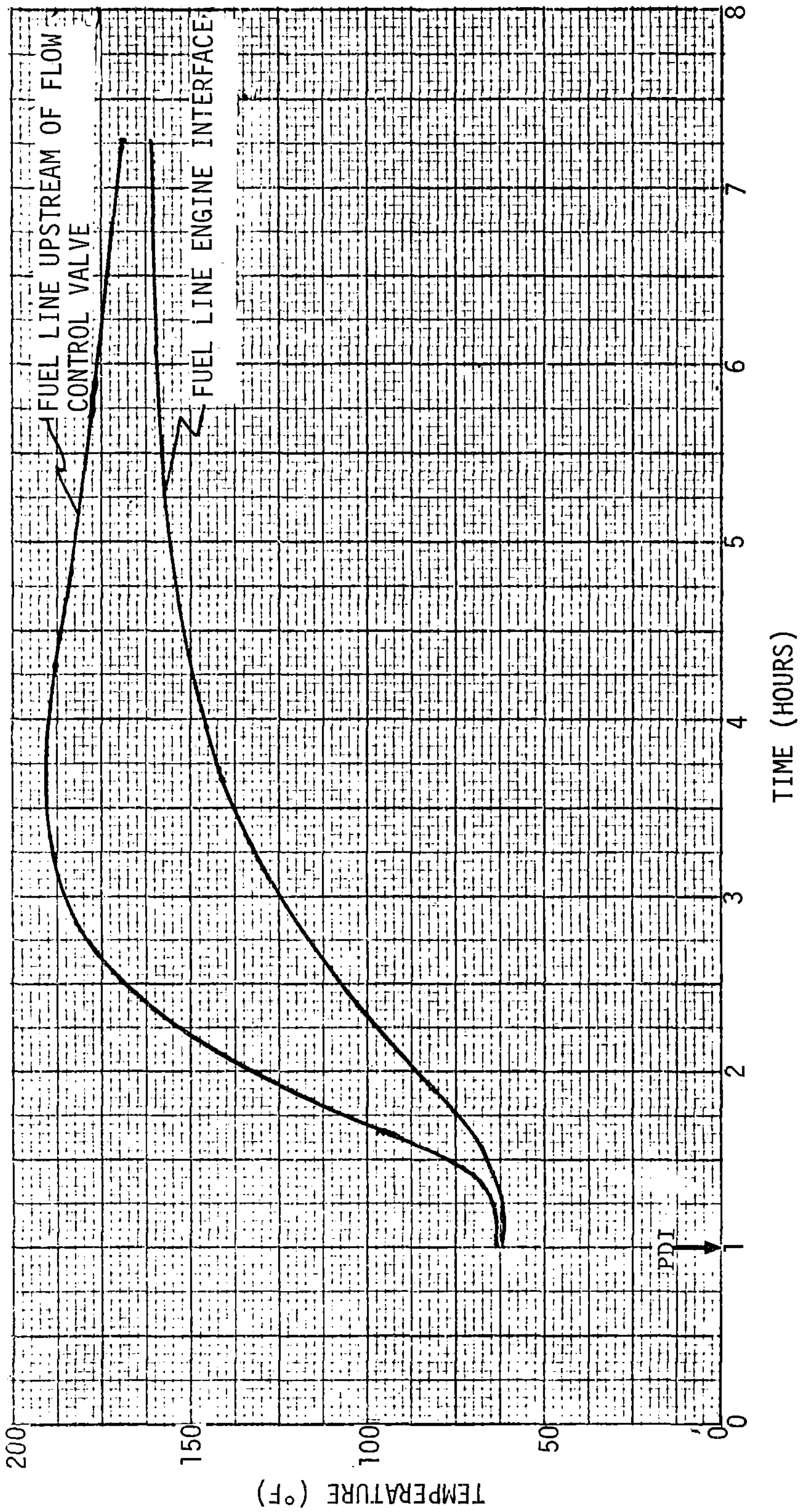

Figure LM6/4.7.8-7. Fuel Line Temperature Vs Time

TO BE SUPPLIED

Figure LM6/4.7.8-8. Temperature Response of DPS Injector Vs Elapsed Time Past Ignition

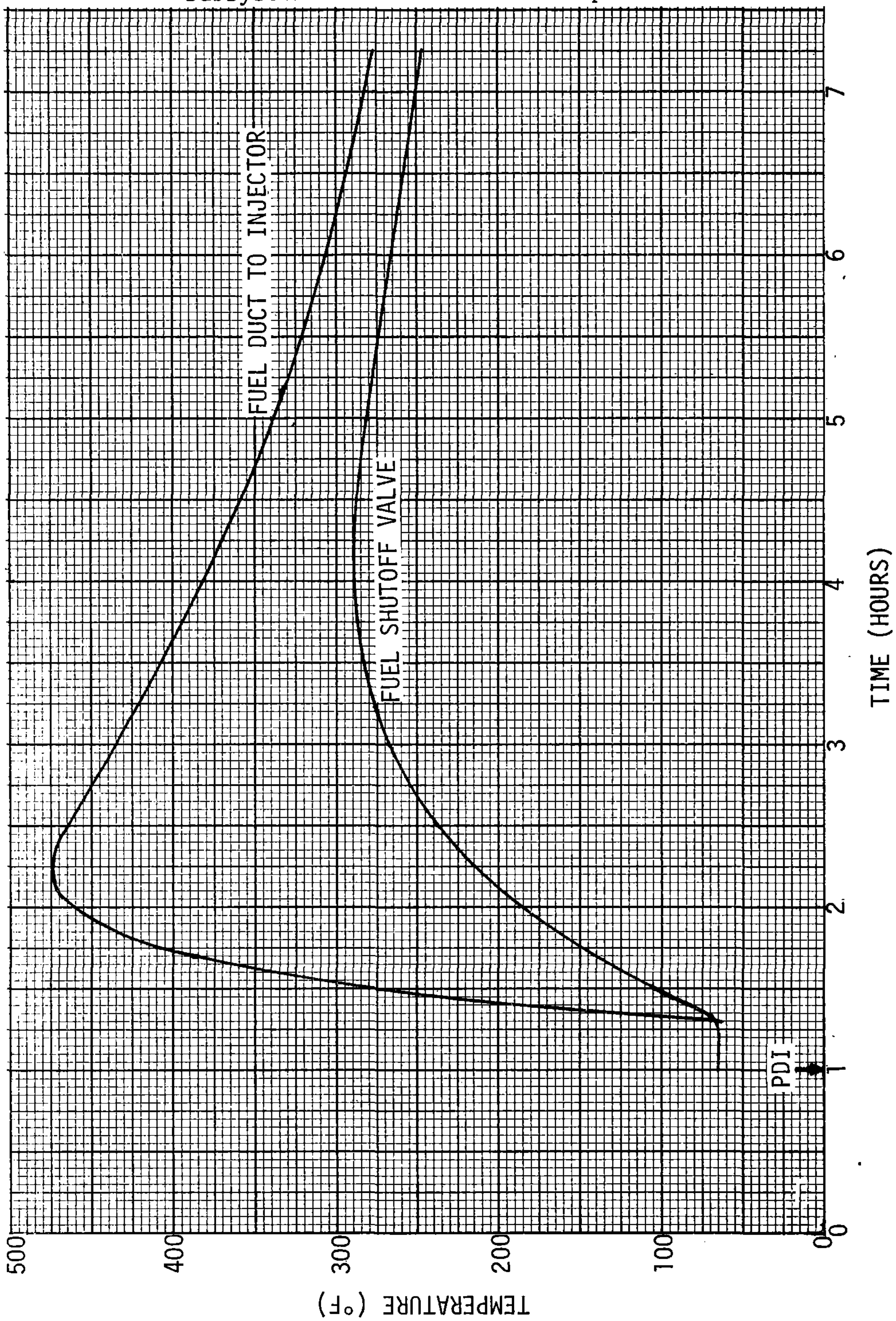

Figure LM6/4.7.8-9. Temperature of Fuel Duct to Injector and Fuel Shutoff Valve Vs Time

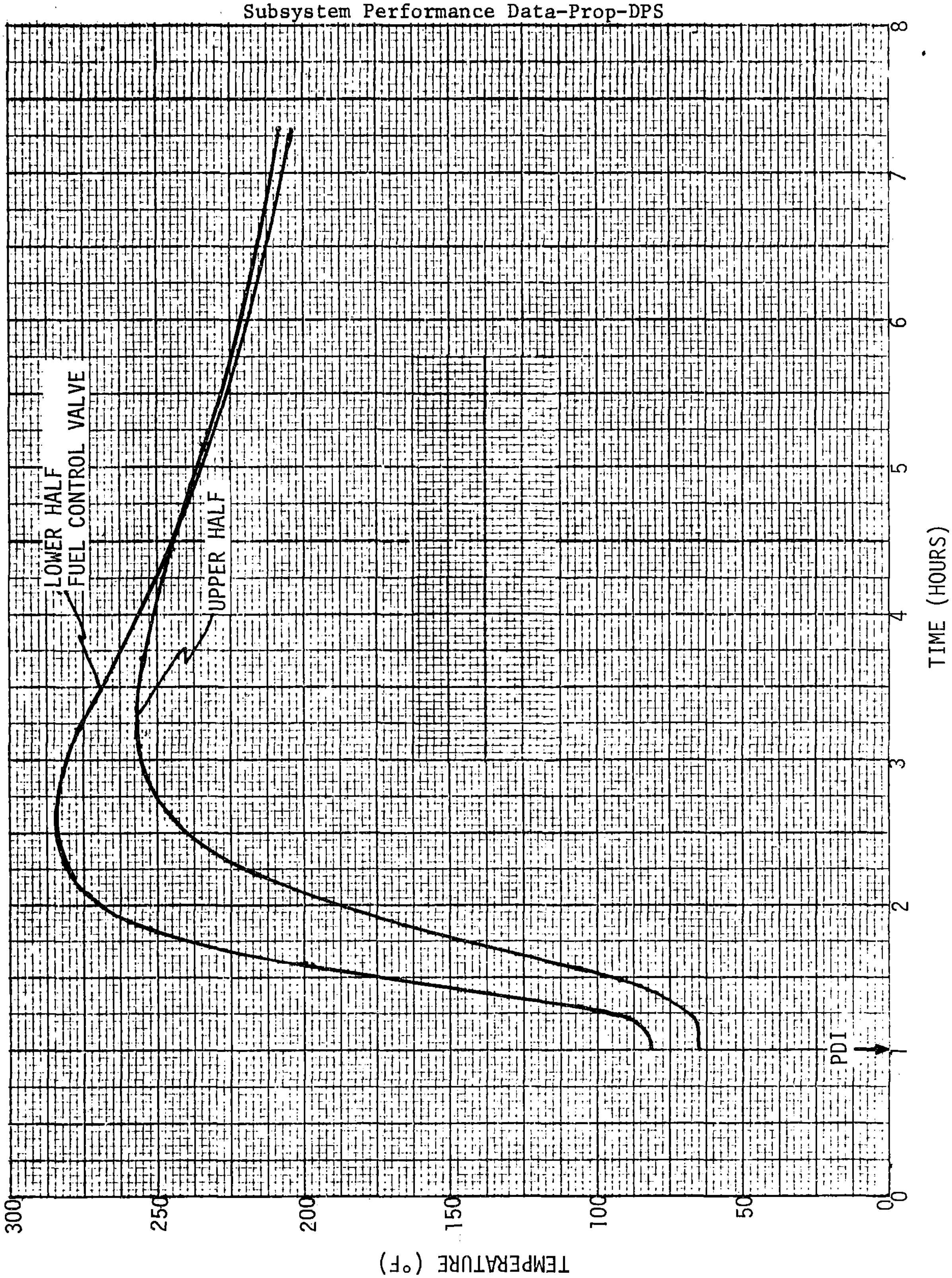

Figure LM6/4.7.8-10. Fuel Flow Control Valve Temperature Vs Time

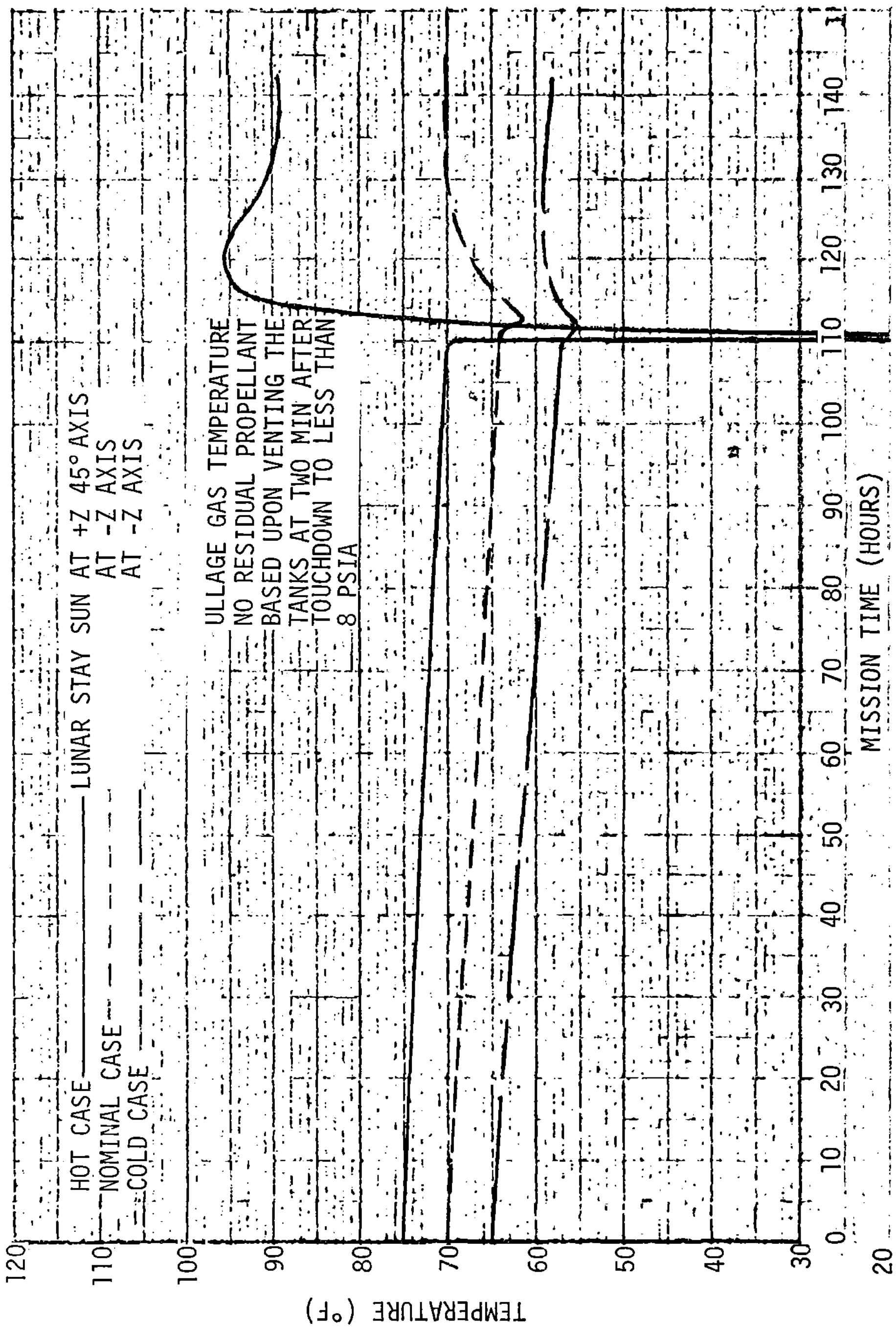

Figure LM6/4.7.8-11. Mission H Predicted Thermocouple Response-
Descent Engine GQ3718T +Y Tank

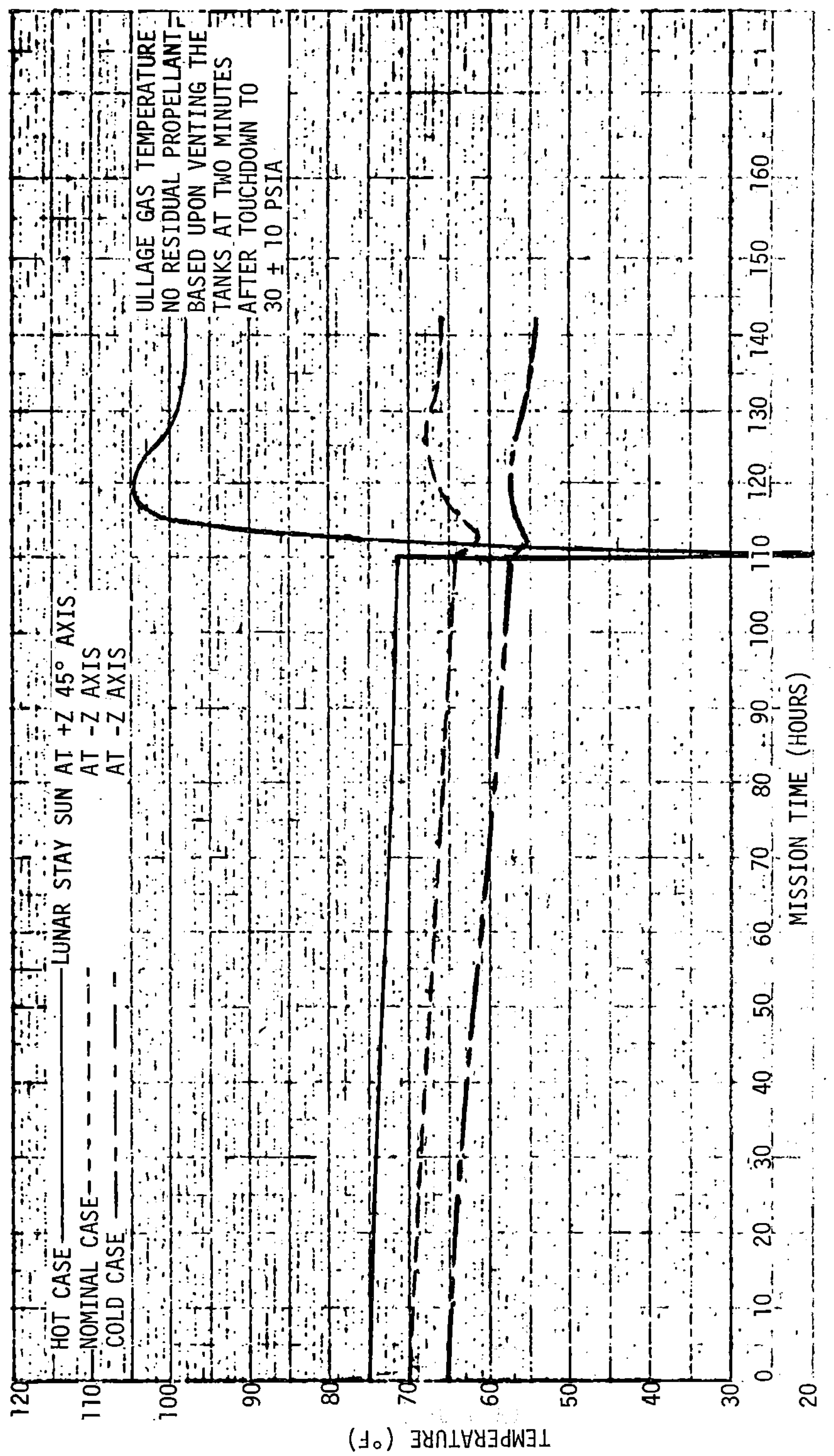

Figure LM6/4.7.8-12. Mission H Predicted Thermocouple Response-Descent Stage GQ4219T +Z Tank

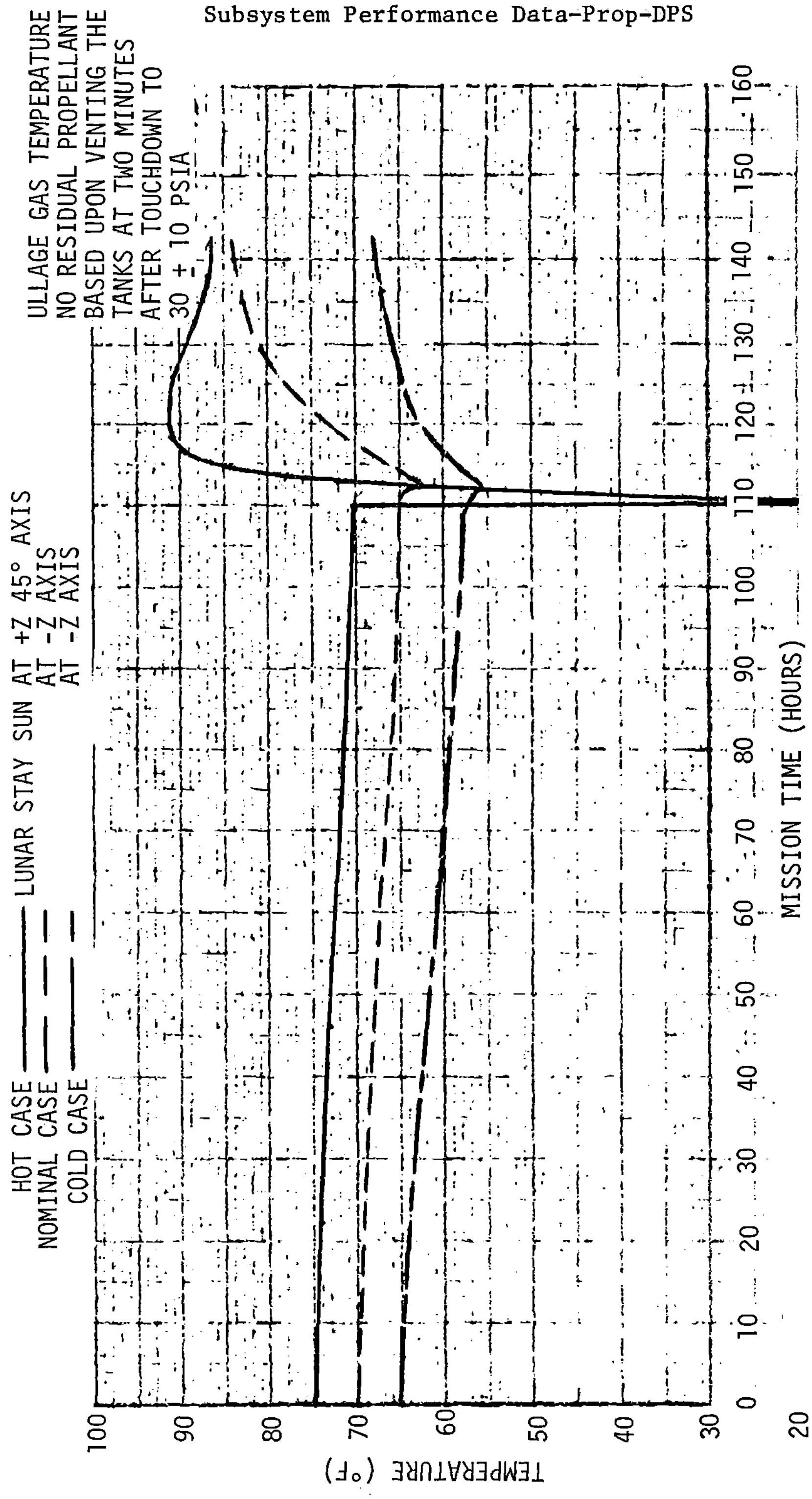

Figure LM6/4.7.8-13. Mission H Predicted Thermocouple Response-
Descent Stage GQ4218T -Z Tank

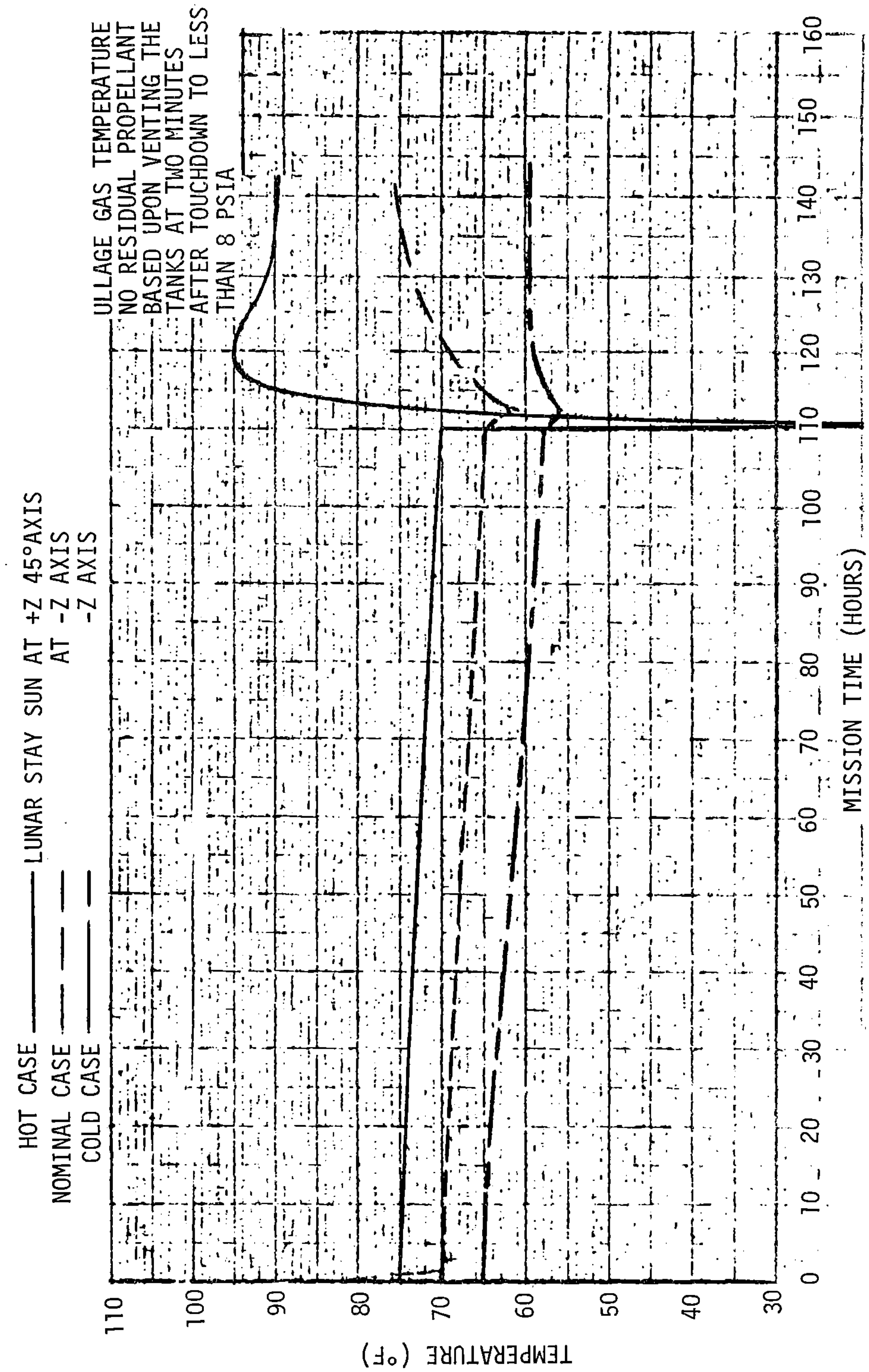

Figure LM6/4.7.8-14. Mission H Predicted Thermocouple Response-
Descent Stage GQ3719T -Y Tank

LM6/4.7.12.1 DPS Propellant Tank Venting for Lunar Landing Mission

The thermal profile for the DPS propellant tanks is dependent upon engine burn time and quantity of residual propellant in the specific tank. The fracture mechanics limits are dependent upon the pressurization history of each tank and the burst disc pressure (measured value of 265 psid for the LM-6 tanks).

In the event of failure of the LM-6 DPS oxidizer tanks to vent, abort is not necessary if the propellant remaining in each oxidizer tank is at least 150 pounds. If the propellant remaining in any oxidizer tank is less than 150 pounds, in excess of two hours is required for temperatures to increase to a point such that the fracture mechanics may be reached.

These results are based on a DPS bulk propellant temperature of 70°F at the time of the main engine firing, and a fracture mechanics limit of 103°F at 265 psid. For a DPS bulk temperature of 75°F at the time of the main engine firing, the limiting propellant quantity increases from 150 pounds to 220 pounds.

In the event of failure of the LM-6 DPS fuel tanks to vent, abort is not necessary to avoid fracture mechanics limits.

* Graphs of ullage pressure versus time after touchdown, showing the maximum allowable pressure from fracture mechanics for various quantities of residual oxidizer, are given in Figures LM6/4.7.12-1 and LM6/4.7.12-2. These are for the nominal and hot landing cases, respectively.

*NASA DATA SOURCE

NOTE: NOMINAL LANDING CASE - 6 IN. LANDING GEAR STROKE, EXHAUST NOZZLE 12 IN. ABOVE SURFACE, BASE HEAT SHIELD 38 IN. ABOVE SURFACE.

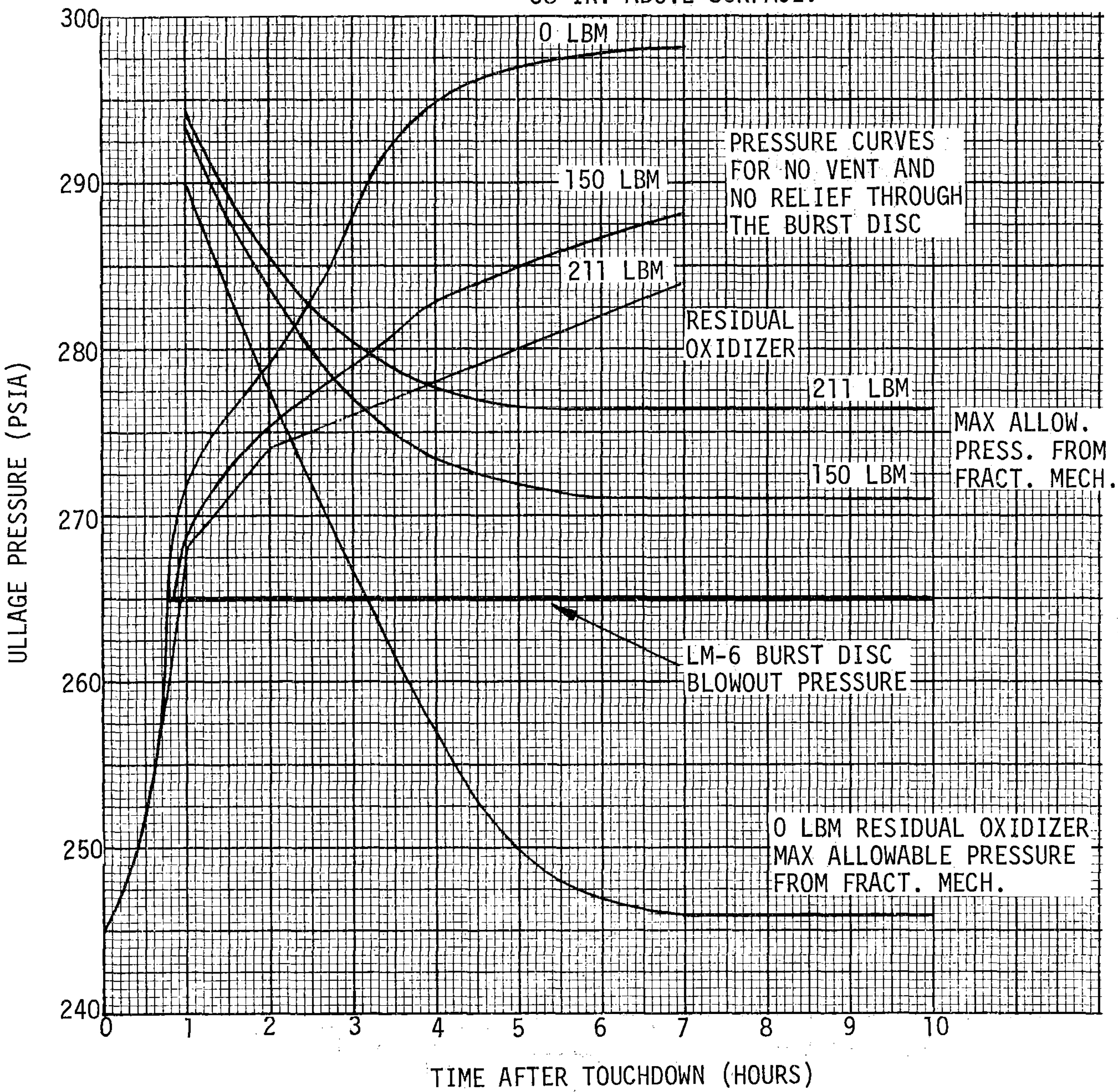

Figure LM6/4.7.12-1. Ullage Pressure Vs Time After Touchdown for Failure of the Oxidizer Tanks to Vent - Nominal Landing Case

NOTE: HOT LANDING CASE - MAXIMUM LANDING GEAR STROKE, BURIED EXHAUST NOZZLE, BASE HEAT SHIELD 9 IN. ABOVE LUNAR SURFACE.

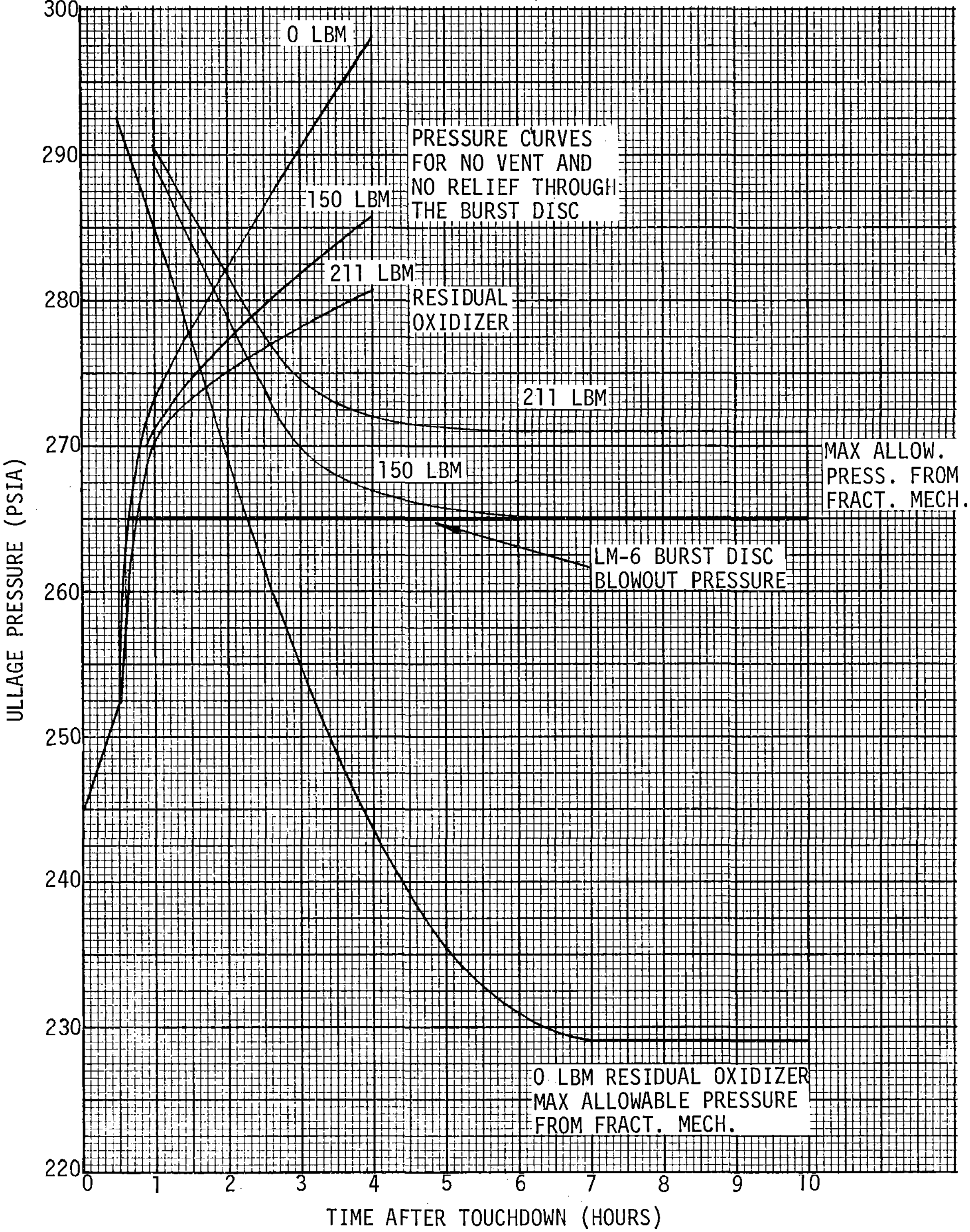

Figure LM6/4.7.12-2. Ullage Pressure Vs Time after Touchdown for Failure of the Oxidizer Tanks to Vent - Hot Landing Case

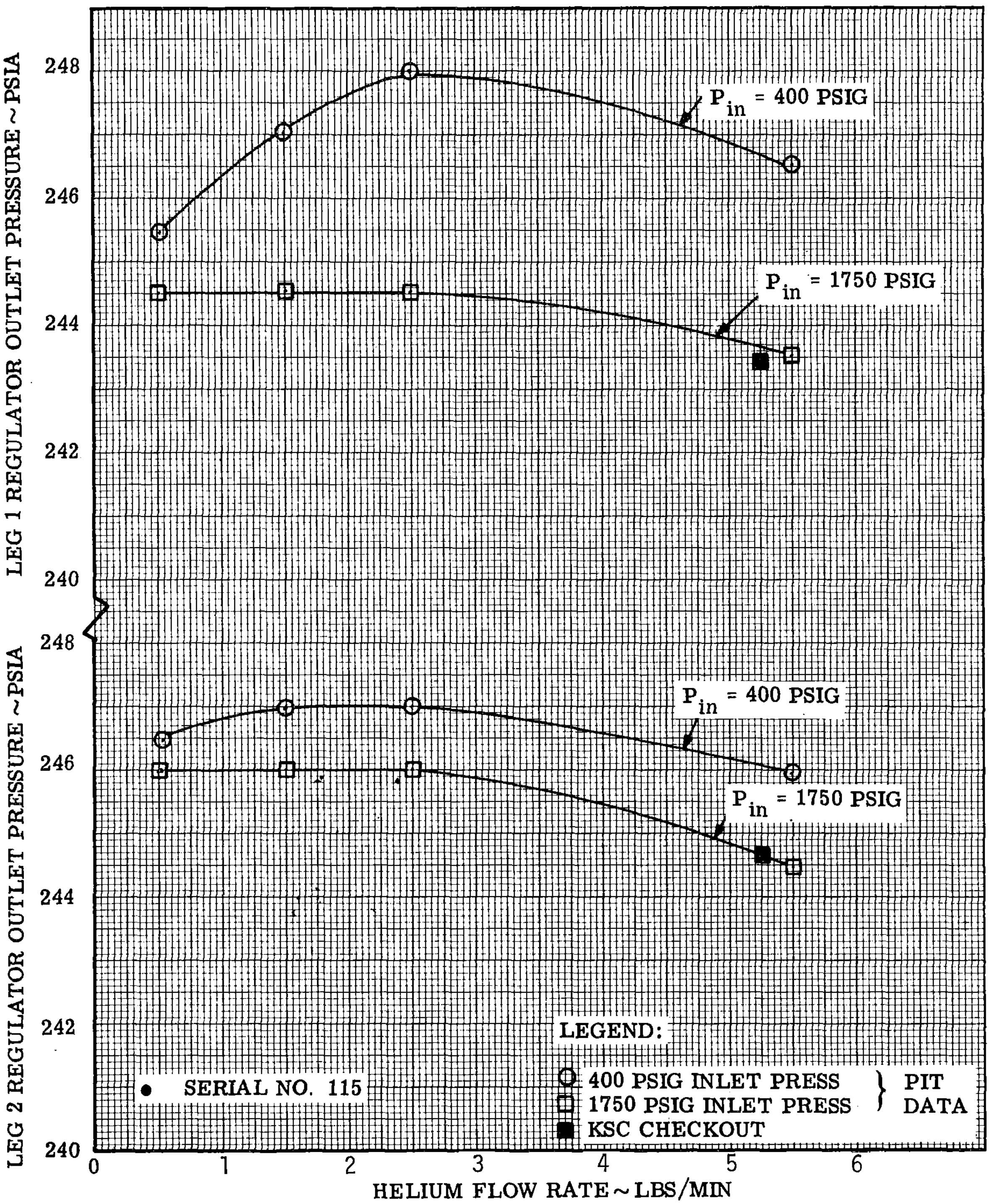

Figure LM6/4.7.15-1. Descent Engine Regulator Performance

LM6/4.8.6.1 Multiple Steady State Firings Heating Effects

Figure LM6/4.8.6-1 shows the plume impingement limits of the +X and -X RCS thrusters in terms of allowable thruster activity at various duty cycles, as a function of elapsed time. The primary +X firing constraint curves represent the attainment of maximum allowable S-Band antenna electronic parts temperature assuming 75°F and 35°F start temperatures, as well as the effective Mission G antenna positioning. Also shown is the constraint curve for the EVA antenna. The primary -X firing constraint curve is a combination of plume impingement capabilities of RCS plume deflectors, the front of the scientific equipment bay and side of quad 3; or plume deflectors and the landing gear secondary strut end fitting and the deploy truss end fitting. Exceeding these limits will cause potential loss of the item involved.

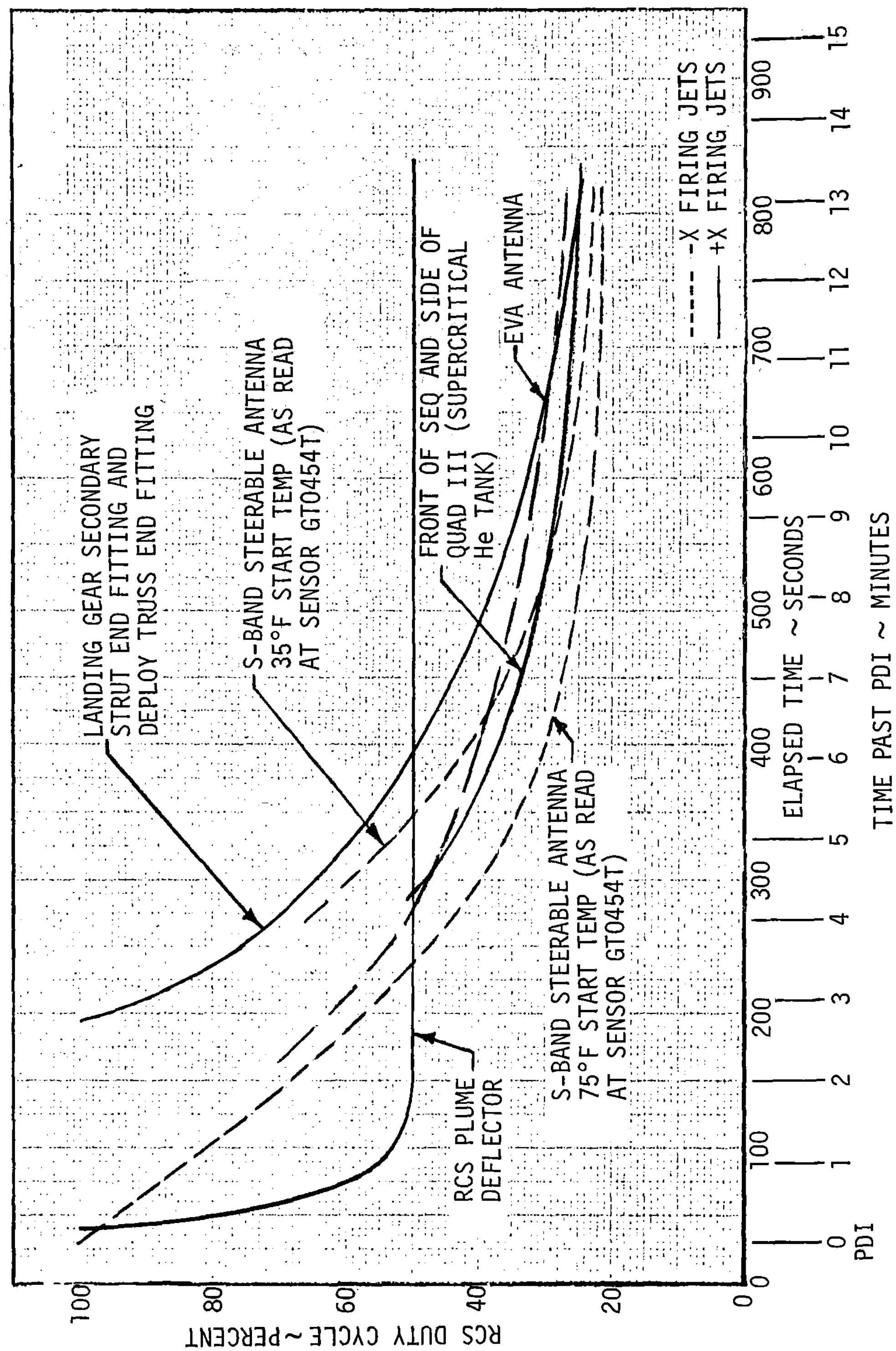

Figure LM6/4.8.6-1. Plume Impingement Capability - Unstaged

LM6/4.8.14 RCS Plume Impingement Constraints as a Result of Gimbal Drive Actuator (± Pitch or ± Roll) Failure During a DPS Burn in PGNS Mode

Figure LM6/4.8.14-1 shows the maximum allowable offset angles as limited by the RCS impingement constraints for the affected vehicle hardware. These curves were developed from the LM-6 RCS plume impingement capability curve (See Figure LM6/4.8.6-1).

In event of a GDA Failure during powered descent, RCS plume impingement may constrain the mission. Figure LM6/4.8.14-2 represents the maximum allowable accumulated RCS firing time at any juncture during powered descent, for GDA Failure at several different times. The curves reflect duty cycles which cause failure of the plume deflectors or landing gear fittings.

Figures LM6/4.8.14-3 and LM6/4.8.14-4 show the nominal descent engine gimbal angles (pitch and roll, respectively) for the Mission H-1 profile. Further, they also show the maximum allowable GDA offset angle at failure during PDI, for RCS fuel consumption and controllability constraints.

Figures LM6/4.8.14-5 and LM6/4.8.14-6 present the maximum allowable delta from nominal, GDA roll and pitch angles at failure, with respect to fuel consumption and controllability (See Figure LM6/4.8.14-1). This should facilitate real time evaluation of the feasibility of continuing powered descent once a failure has occurred.

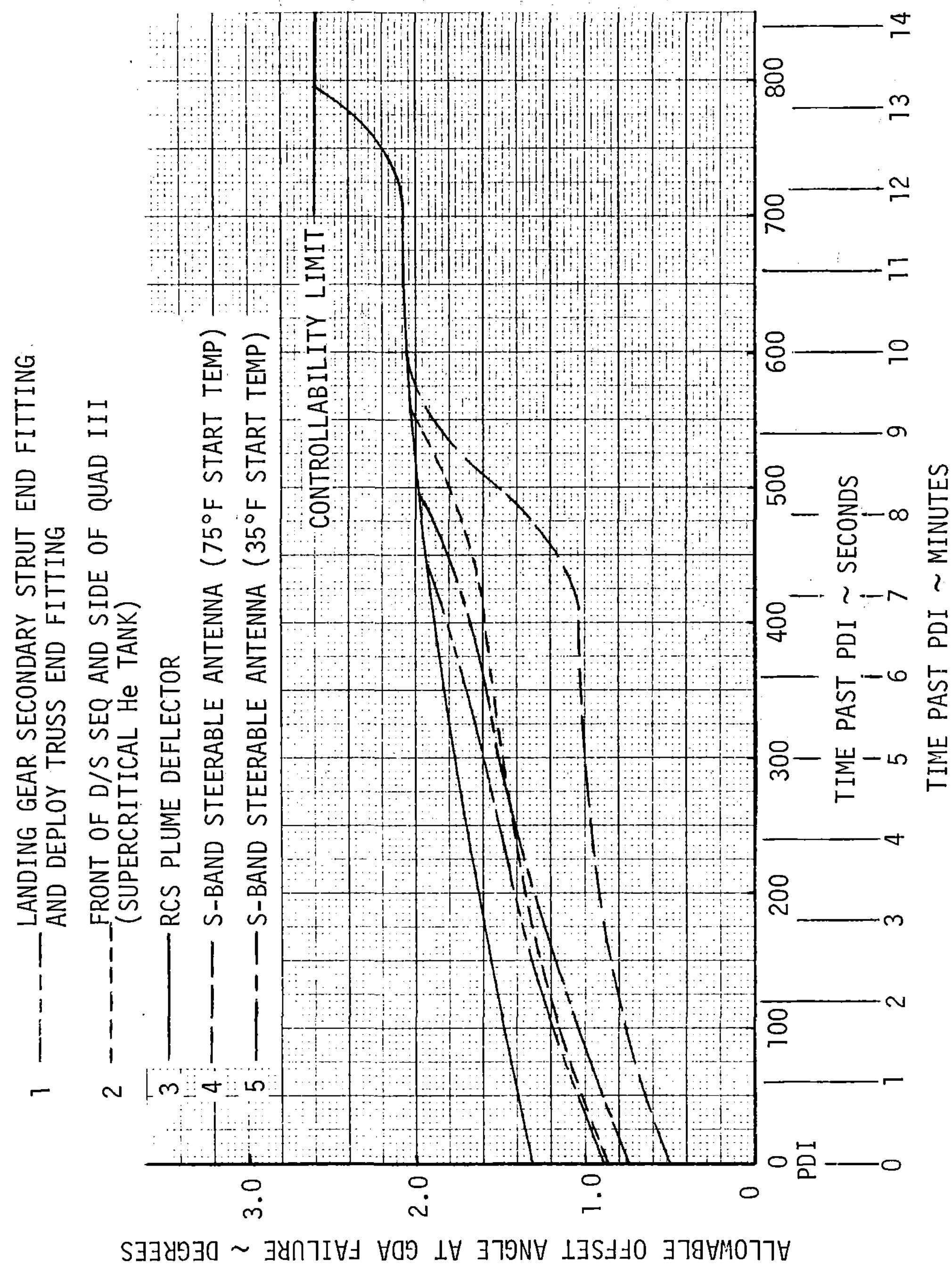

Figure LM6/4.8.14-1. Maximum Allowable GDA Offset Angle at the Time of GDA Failure Vs Time During a DPS Firing

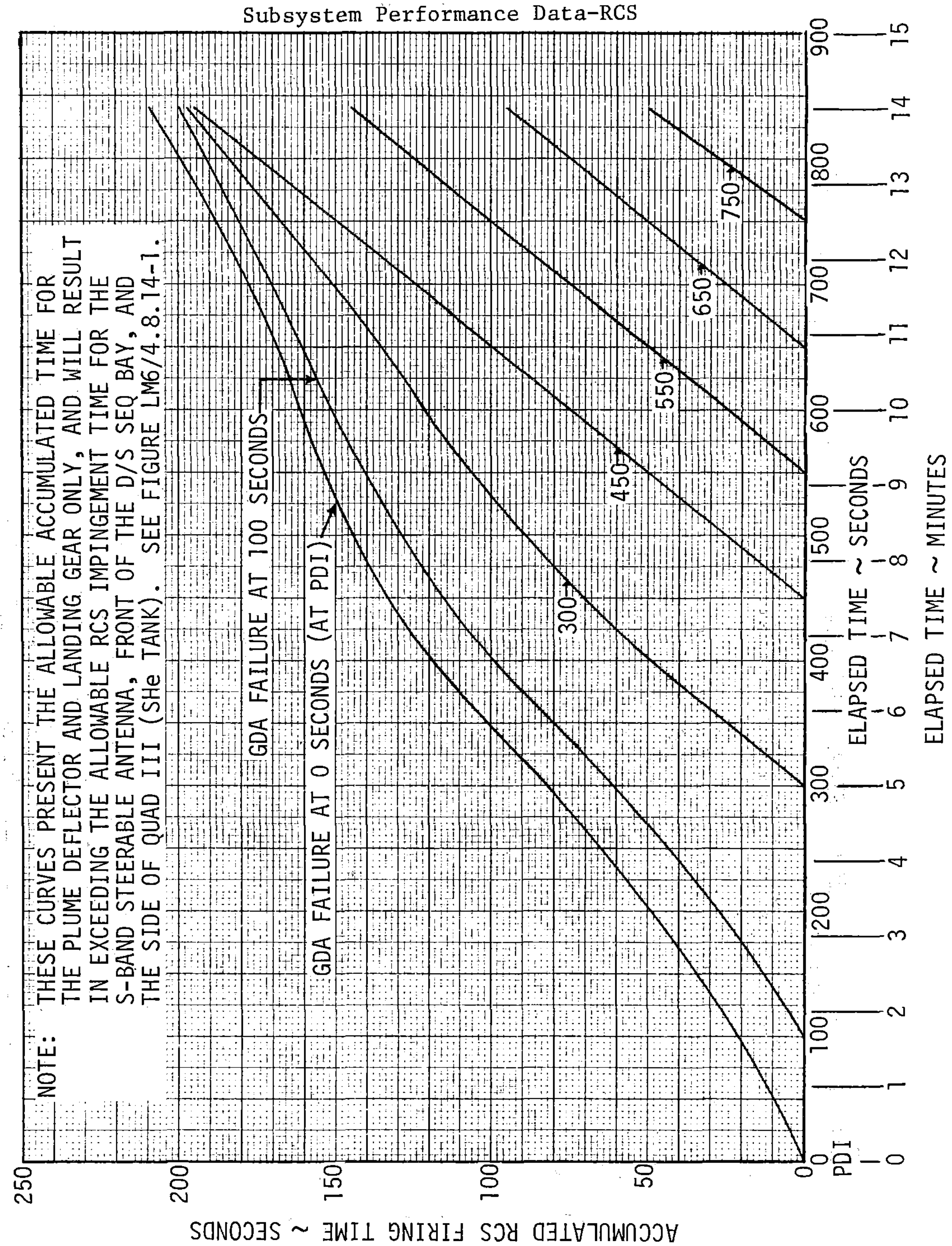

Figure LM6/4.8.14-2. Maximum Allowable Accumulated RCS Firing Time Per -X or +X RCS Engine Vs Elapsed Time Past PDI for Plume Deflector and Landing Gear

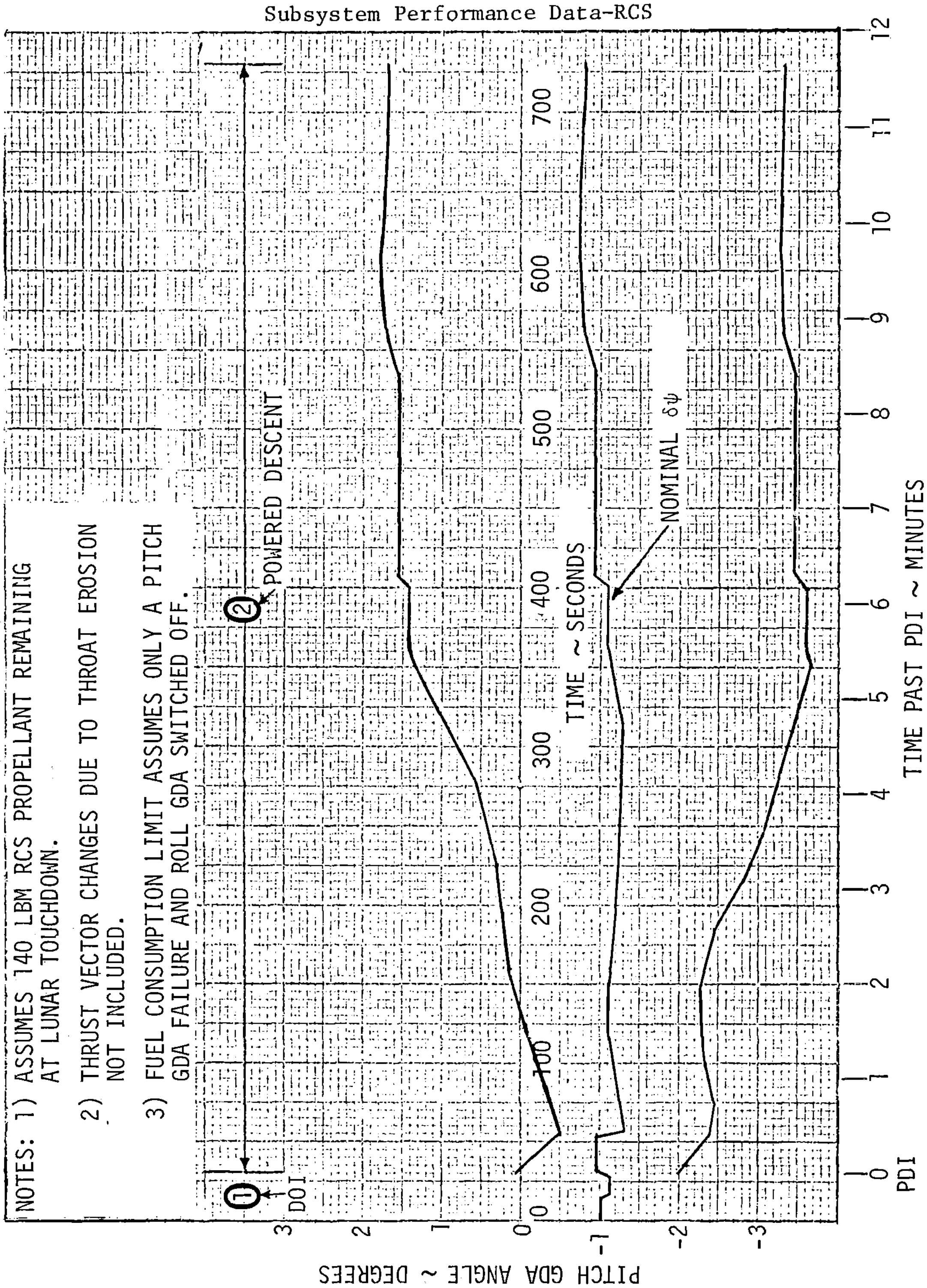

Figure LM6/4.8.14-3. Mission H-1 Nominal Expected Pitch GDA Angle ($\delta\psi$ - FMES Notation) and Maximum Allowable Deviations for RCS Propellant and Controllability Red Lines as a Function of Elapsed Burn Time

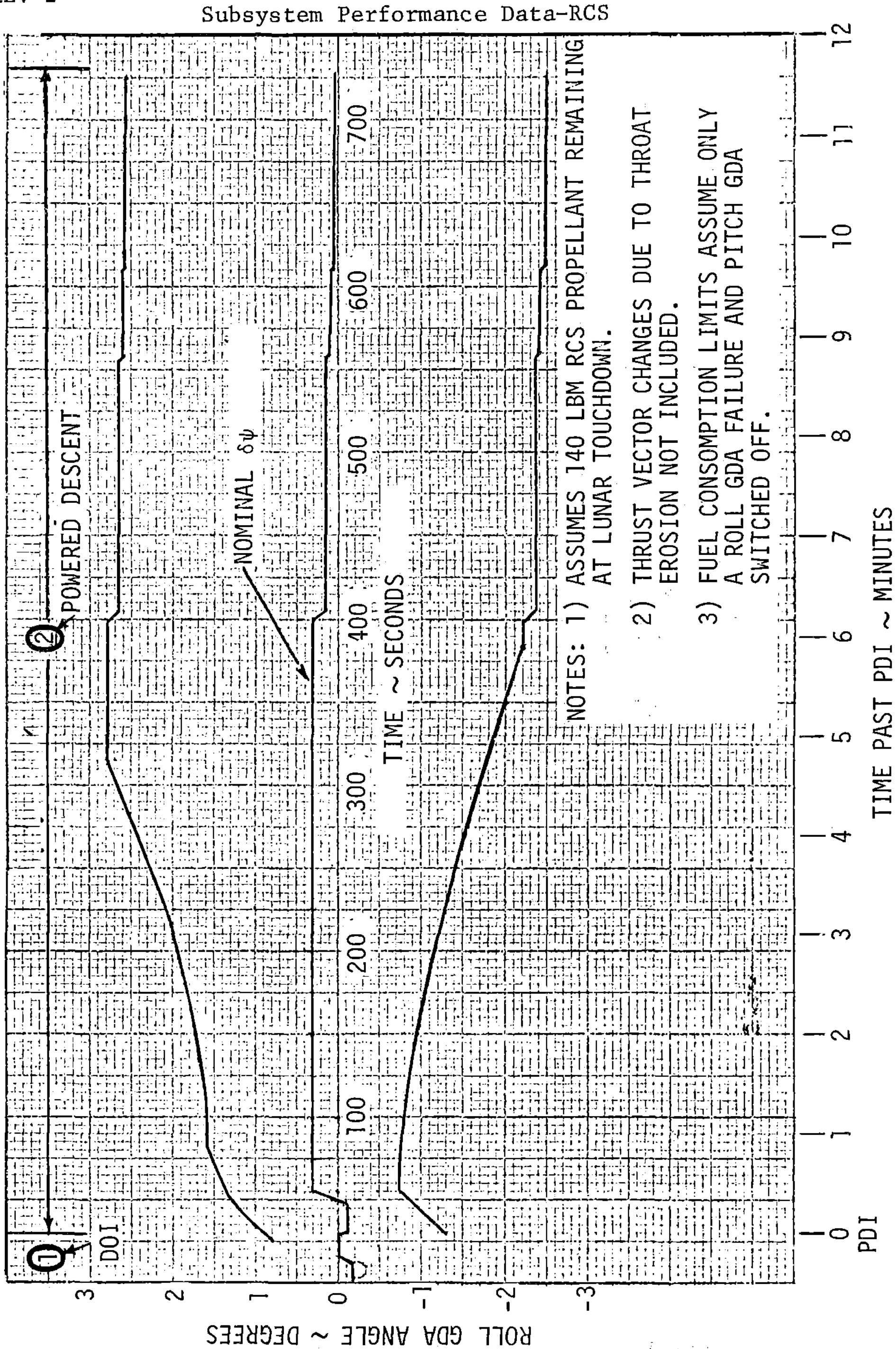

Figure LM6/4.8.14-4. Mission H-1 Nominal Expected Roll GDA Angle ($\delta\psi$ - FMES Notation) and Maximum Allowable Deviations for RCS Propellant and Controllability Redlines as a Function of Elapsed Burn Time

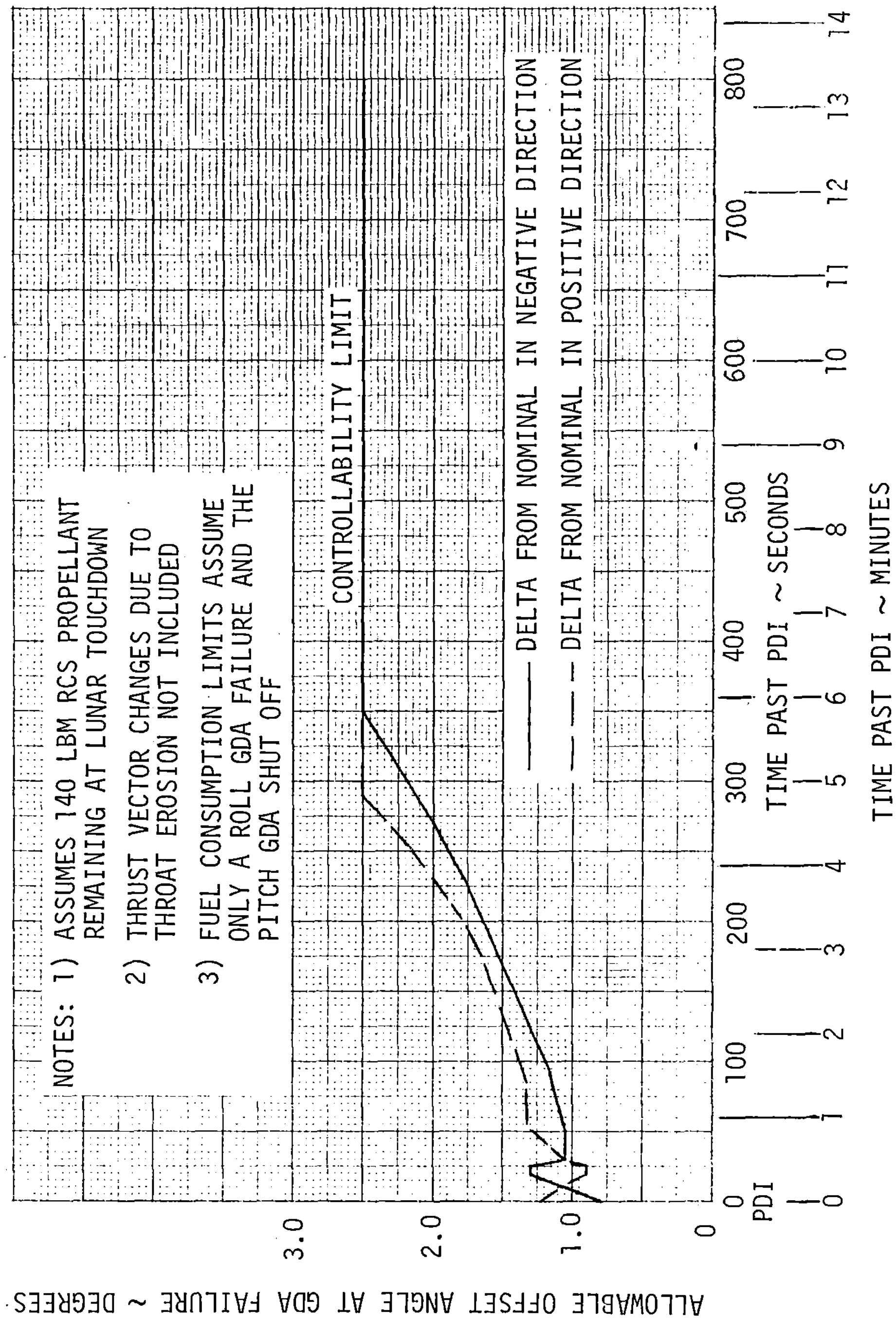

Figure LM6/4.8.14-5. Maximum Allowable Roll GDA Offset Angle at the Time of GDA Failure Vs Time During a DPS Firing (PDI)

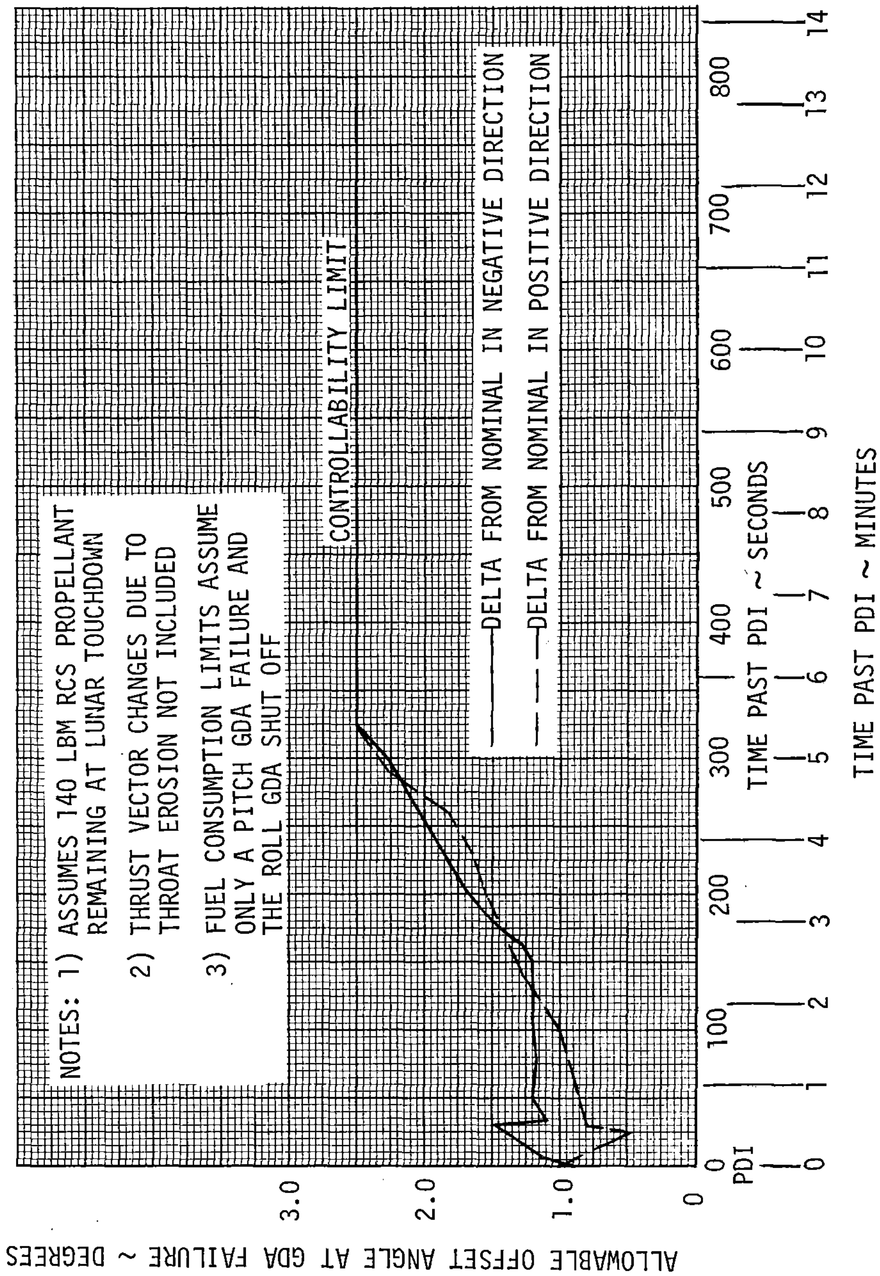

Figure LM6/4.8.14-6. Maximum Allowable Pitch GDA Angle at the Time of GDA Failure Vs Time During a DPS Firing